FINITE ELEMENT MODELLING OF SHEAR CONNECTION FOR STEEL-CONCRETE COMPOSITE GIRDERS

By

EHAB ABD EL-FATTAH MOHAMED EL-LOBODY

B.Sc., M.Sc.

Submitted in accordance with the requirements for the degree of

Doctor of Philosophy

The University of Leeds

Department of Civil Engineering

November, 2002

The candidate confirms that the work submitted is his own and that appropriate credit has been given where reference has been made to the work of others.

ACKNOWLEDGEMENTS

First words and foremost thanks to Allah, the most beneficent and merciful.

I would like to express my sincere appreciation and thanks to my supervisors, Dr. Dennis Lam and Professor Andrew Beeby for their guidance, generous help, continued encouragement and support throughout the whole period of this research for which I am greatly indebted.

I would like to express my gratitude to University of Leeds for providing the experimental, computing and other facilities.

I would like to acknowledge the Egyptian Government for providing the financial support for this research. Further thanks are due to my home Institution, Faculty of Engineering; Tanta University for the study leave provided for the course of research.

I feel thankfulness to Mr. T.F. Nip, research associate; University of Leeds, for providing his help with my testing. Further I thank the staff at Test and Casting Labs, School of Civil Engineering; University of Leeds, for all their help with the fabrication and casting of the specimens especially Mr. Richard Bell and Mr. Peter Flatt. Thanks also due to all technical staff in the Department for their assistance.

I would like to thank Mrs. Dorothy A Carr Senior Clerk, Civil Engineering Department for her help and support. Further thanks are due to my colleagues in the department Mahmoud, Ahmed, Suprapto and Jian Yang.

Finally, thanks are due to my parents and my wife Lobna for their patience, support and encouragement throughout the duration of research. It would have been impossible for me to complete this thesis in such a manner without my wife support, encouragement and taking care of my daughter Yara and my twin sons Yousef and Hazem.

Declaration

I declare that this thesis is the result of my own work. No part of this thesis has been submitted to another University or other educational establishment for a degree, Diploma or other qualification.

Ehab El-lobody

(Ehab El-lobody)

ABSTRACT

The main objective of this thesis is to develop effective 3-dimensional finite element models to trace the behaviour of headed stud shear connectors in composite girders with solid slabs and precast hollow core slabs. The finite element package ABAQUS was used to conduct the analysis. Push-off tests with both types of slabs were simulated taking into consideration all material nonlinearities of the components. The models are able to predict the headed shear stud capacity, the load-slip characteristic of the shear connection and modes of failure. The results obtained show good agreement with specified data from Codes of practice and results of available numerical and experimental literature. Parametric studies were carried out using both models to investigate the effects of the change in different parameters on the behaviour of shear connections.

Full-scale push-off tests with solid and precast hollow core slabs have been carried out to verify the finite element models. The shear connection capacity, load-slip curves and modes of failure were detected from experimental investigation. Both numerical and experimental results were compared and good agreement has been achieved. The comparison has shown that the model is able to predict accurately the behaviour of headed studs in composite girders with both types of slabs.

The non-linear load-slip characteristics of the headed shear stud connector obtained from FE models of push-off tests were used in modelling the structural behaviour of composite steel-solid slab concrete and steel-precast hollow core slab girders. A finite element model has been developed for the analysis of each type. The models took into account the non-linear behaviour of concrete slab, steel beam and shear connectors. The accuracy and efficiency of the models have been demonstrated by comparing finite element results with available published experimental and numerical research. An effective parametric study for the evaluation of the effective width for steel-precast concrete slab composite girders is presented.

TABLE OF CONTENTS

LIST OF FIGURES

Chapter4

Chapter 5

Chapter 6

Chapter 7

LIST OF TABLES

NOTATIONS

A_s	Cross-sectional area of stud
A_{steel}	The cross sectional area of the steel beam
b	Slab width
[B]	Shape function matrix
b_{eff}	Effective width
bs	Bar size
C	Concrete grade
d	Stud diameter
[d]	Displacement matrix
[D]	Material property matrix
d_{sh}	Stud shaft diameter
E_c	Static Young's modulus of elasticity of concrete
E_{co}	Initial Young's modulus for concrete
E_{cp}	Average value of elastic modulus of the in-situ and pr-cast concrete
E_s	Young's modulus of steel
F	External forces
[F]	Load matrix
F_{conc}	The resistance of the concrete flange
F_{con}	The resistance force of the shear connectors
F_{steel}	The resistance of the steel beam
F_{flange}	The axial capacity of one steel flange
f_c	Concrete cylinder compressive strength
f_{cp}	Average concrete cylinder strength of the in-situ and pre-cast concrete
f_{cu}	Cube strength of concrete
f_u	Ultimate tensile strength of the headed stud material
f_{yc}	Yield stress of concrete
f_{ys}	Yield stress of steel
FEM	Finite element method
g	Transverse gap width

h	Overall length of stud
h_{sh}	Stud shaft height
HCU	Hollow core unit
K	Reduction factor
[k]	Stiffness matrix
$[K_e]$	Element stiffness matrix
L	Beam span
L_o	Distance between the points of zero bending moment
M_{comp}	The ultimate moment capacity of the composite beam
M_s	The plastic moment capacity of the steel beam section
N_f	Number of shear connectors required for complete interaction
N_r	Number of connectors
u	Displacements
UB	Universal beam
UC	Universal column
P	Load
P_r	Resistance of a stud in a trough
P_{RD}	Resistance of shear stud
Q_K	Characteristic shear force resistance
Q_u	Ultimate shear force resistance
t	Concrete slab thickness
T	Test specimen
w	Width of hollow concrete unit
Z_{pl}	The plastic modulus of steel beam section
γ_v	Partial safety factor
ϕ	Diameter of reinforcement high tensile steel bar
β	Factor which takes into account the gap width
ε	Factor which takes into account the diameter of transverse high tensile steel
ω	Transverse joint factor
σ_x	Longitudinal axial stress
σ_{max}	Peak value of the longitudinal axial stress

1. Introduction

1.1 Introduction

Composite steel-concrete construction is used extensively in the construction of modern buildings and highway bridges owing to its advantages in terms of saving in weight of steel, increasing load capacity and reduction in construction depth. In composite beam design, headed stud shear connectors are commonly used to transfer longitudinal shear forces across the steel-concrete interface. The shear strength of the stud and the resistance of the concrete slab against longitudinal cracking are the main factors affecting the shear stiffness and strength of the shear connection. Calculation of the structural behaviour of composite beams depends on how much slip is assumed to occur at the interface between concrete and steel. Up to now, experimental push-off tests are the traditional source of knowledge about the load-slip behaviour and the shear capacity of the shear stud in composite beams. All current equations governing the behaviour of the headed shear stud connectors are empirical formulae based on the statistical analysis of test results.

Since full-scale push-off tests remain costly and time-consuming, analytical procedures that can predict the non-linear response and the ultimate load capacity of the push-off test are developed. To replace most of the experiments, the verification of the analytical method should be established by comparing with selective, well-controlled experimental results. Due to the complexity of the three-dimensional stress-strain state and interaction between shear connector and concrete, there has so far been little success in mathematical modelling of the push-off test.

Although the experimental measures of strain and displacements with increasing load provide valuable insight into the push-off test, in many cases important load effects cannot be measured with the necessary accuracy. This is due to the fact that the necessary measuring process is either not feasible or is too expensive. Numerical studies using the finite element method (FEM) thus provide a cost-effective alternative. Also the number of geometric and mechanical parameters which can reasonably be expected to influence the shear connection behaviour is significant. In such cases numerical

modelling is a very effective method for including more variables than could be contained in the limited scope of an experimental program.

Composite construction of steel beams with profiled steel decking to support floor slabs eliminated the use of traditional timber temporary forms and false work. In this type of construction headed stud connectors are welded through the steel sheeting on the top flange of the steel beam and profiled steel sheeting is used as a working platform to support construction loads as well as a permanent form-work for the concrete. Although this type of construction is now common in multi-storey steel frame construction, it has some disadvantages in terms of high costs of weld, expensive labour, time and the need of internal propping if the sheet width is exceeded without addition of framing. Recent studies have shown that composite construction of steel beams with precast hollow core units (HCU) can eliminate these problems and give the edge of this type of construction over the composite construction with profiled steel sheeting in special design and environmental situations.

The use of hollow-cored precast concrete flooring is common in multistory construction where there is no composite action between the steel beam and the HC flooring, see figure 1.1. It enables the designers to get the maximum structural strength with minimum weight, covers a wide range of spans up to 15m without propping, takes less erection time, does not require a structural screed to carry diaphragm forces and gives clear span to depth ratios around 35 for office loading. Composite construction with precast HCU is relatively new in the commercial building sector in the UK. In this type of construction, pre-welded mechanical shear connectors on the top flange of the steel beam are used to connect the steel beam with precast HCU flooring. The interaction between the steel beam and the HCU flooring offers additional advantages in terms of increasing the structural strength, reducing construction depth and consequently lowering the construction costs.

The recent finite element models found in the literature simulate briefly the behaviour of shear connector in steel-solid slab push-off test and with limited success. No detailed or even simplified numerical models simulating the behaviour of individual shear connectors embedded in steel-precast HCU slab push-off test have been published. Although the published experimental push-off tests in composite girders with precast

HCU slabs has paved the way towards real understanding of this new area, the number of published tests is limited and still in progress. Extensive experimental parametric studies will require huge number of push-off tests to be carried out. These tests should be carried out at full-scale due to the nature of precast HCU slabs. Taking this into consideration will make it more difficult to study all parameters affecting the behaviour of the shear connector in these tests. Numerical modelling is thus the only way to reduce the number of push-off tests needed to cover all problem variables.

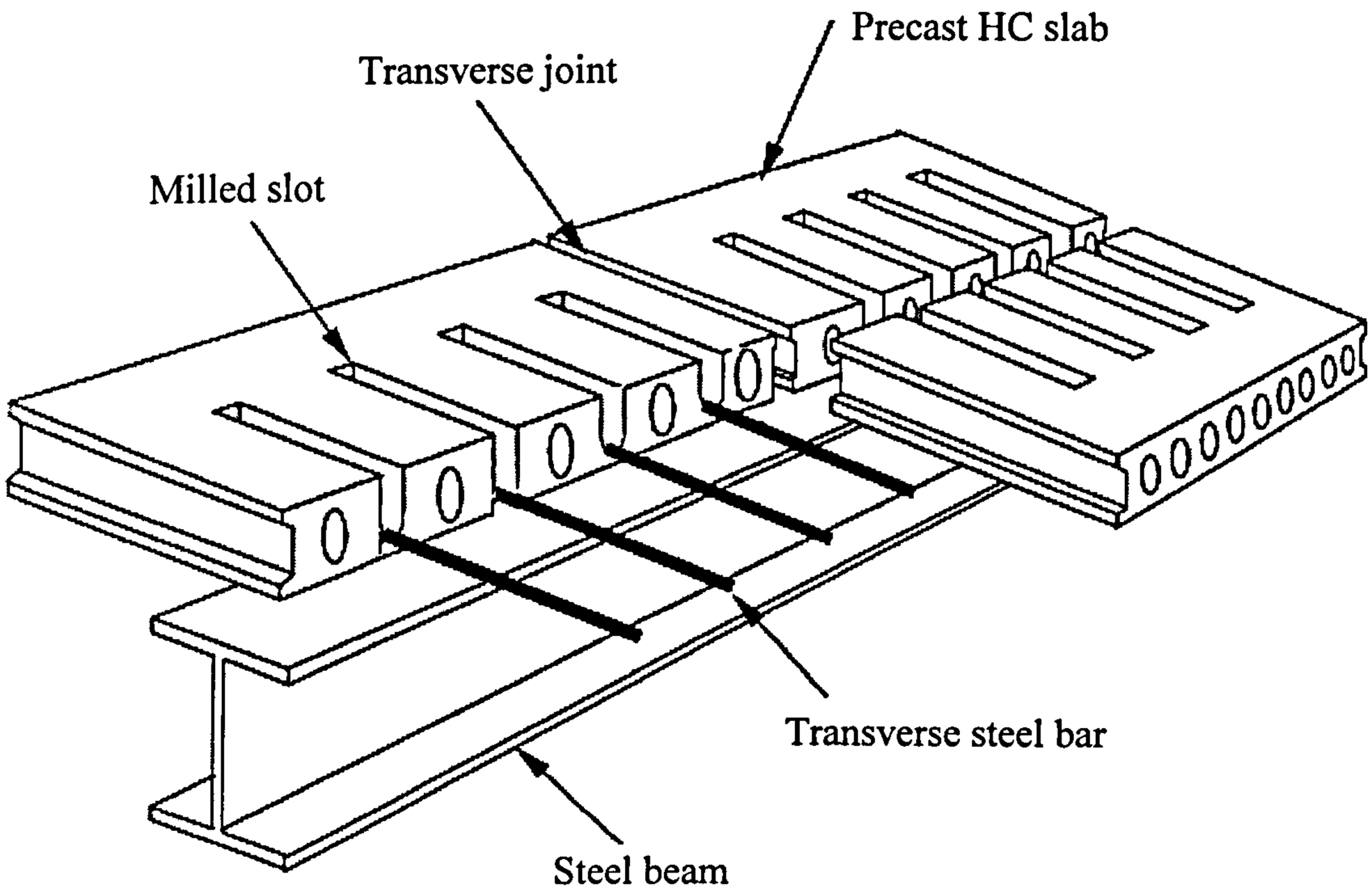

Figure 1.1 Precast HCU's rest on steel beam with no composite action

However, good progress has been achieved in simulating the structural behaviour of composite girders using the FEM, most of the published research has concentrated on steel-solid slab composite girders. The FE modelling of composite girders with precast HCU slabs is new and the only FE model found in this area is that by Lam, Elliott and Nethercot[1]. The detailed FE study of the stress distribution along the length and across the width of these composite girders is needed to add better understanding for its

structural behaviour. Also, it provides designers with useful information about the ultimate load capacities, effective width and the load-deflection curves of these composite girders.

1.2 Objectives of the research

The main objective of this research is to develop two effective 3-D numerical models using the FEM to simulate the behaviour of headed stud shear connectors in steel-solid slab and steel-precast HCU slab push-off tests. The FE package ABAQUS[2] will be used in the analysis. All material nonlinearities of the push-off test components will be taken into consideration. Both models will be validated against test results and compared with available data given in current Codes of Practice to demonstrate the accuracy of the models used. Parametric studies using both models will be performed to investigate variations of different variables affecting the behaviour of headed stud shear connector in both models. The failure modes, the load-slip characteristic of the stud and ultimate shear strength of both connections will be investigated.

The results obtained from both models will be used in simulating the structural behaviour of composite steel-solid slab and steel-precast HCU slab girders. Two FE models are developed to trace the longitudinal structural behaviour of these girders. Both models take into account the non-linear behaviour of concrete, steel beam and shear connectors. The non-linear load-slip relationship of the shear stud is taken from the previous models of steel-solid slab and steel-precast HCU slab push-off tests. The accuracy and efficiency of both models will be demonstrated by comparing the present finite element (FE) results with available published experimental and numerical researches. An effective parametric study for the evaluation of the effective width of steel-precast HCU slab composite girders will be presented. The ultimate load capacity of the composite girders will be obtained and the load-deflection curves will be plotted.

1.3 Scope of the thesis

In order to develop a better understanding of the shear interaction behaviour, the theoretical background of shear interaction and a survey of available design equations in Codes of practices are presented in chapter 2. Also, discussions of the available previous

experimental and numerical researches dealing with the behaviour of the headed studs in steel-solid slab and steel HCU slab push-off tests and composite girders are shown in the same chapter.

Chapter 3 describes the FE procedures used to build the model that simulates the behaviour of headed stud shear connectors in steel-solid slab push-off tests. Description of the model, numerical applications, comparisons with available data in Code of practices and parametric studies are presented. Results of the shear stud capacity, load-slip curves and failure modes are also investigated.

A description of the FE model simulating the behaviour of headed stud shear connectors in steel-precast HC slab push-off tests is found in chapter 4. This is shown together with numerical applications and parametric studies discussing different parameters affecting the behaviour of the stud connector in this connection.

In order to validate the two FE models explained in chapters 3 and 4, experimental push-off tests with solid slabs and precast HC slabs are investigated in chapter 5. Descriptions of both push-off test specimens, devices used and test procedures are presented.

Chapter 6 contains comparisons between the results from the present FE models and the experimental investigations. This is in order to check the validity and accuracy of the FE element models.

The analysis of the structural behaviour of composite girders is shown in chapter 7. Two FE models simulating the behaviour of steel-solid slab and steel-precast HC slab composite girders are explained. Numerical applications and parametric studies to evaluate the effective width of steel-precast HC slab are presented.

The summary of the conclusions reached from the present research is finally presented in chapter 8 and suggestions on possible future areas of interest are given.

2. Literature review

2.1 Introduction

In this chapter, the review of relevant previous research work is divided into three parts:

1. Review of research concerning the shear connection in steel-solid slab and steel-precast hollow core slab composite girders. Also, the general background to shear connection and a survey of present design equations used to evaluate the shear strength of headed stud connectors are presented.
2. Review of research concerning the numerical modelling of push-off tests.
3. Review of the relevant research dealing with the numerical modelling of steel-solid slab and steel-precast HC slab composite girders.

2.2 Shear connection between steel and concrete

2.2.1 General background

Structural designers have long been aware of the advantages of composite construction, such as the savings of steel, reduction in overall structural depth, and the increase in floor stiffness and load capacity. Up to the early 1950's steel beams were designed to act as composite beams with solid concrete slabs of various thickness, and connected to them using a variety of different types of mechanical shear connectors. However, during this period, composite construction in buildings was generally uneconomical. This was due to the significant amount of form-work and propping required for the concrete slabs, along with the costly process in terms of time, of having the shear connectors welded to the steel beams.

In a composite steel-concrete beam, the floor slab tends to slide along the flange of the steel beam and the importance of the shear connectors arises from preventing this slippage. The structural behaviour of a composite beam is affected by the slip at the steel-slab interface. Practically, the assumption that this slip may be completely eliminated can't be ensured. So, accurate calculation methods of the structural behaviour of composite girders must take into consideration the effects of this slip. Push-off tests provide a convenient way to study the behaviour of shear connector without carrying an

expensive full bending test. Initially, the evaluation of the shear capacity of connectors was the main output of these tests. After that, researchers realised that the load-slip behaviour of the connector was also of equal importance. The slip at the steel-concrete interface depends on many factors such as type of connector, size of shear connector, spacing between connectors, type of floor slab and concrete strength of slab. To evaluate the load-slip behaviour of the connector taking into account all parameters that affect the shear connection, an unlimited number of expensive push-off tests would need to be carried out. Numerical modelling of push-off tests can be used in carrying out extensive parametric studies to evaluate the load-slip behaviour of the shear connector much more cheaply. This can be achieved once the approach has been validated against existing data from previous push-off tests.

The development of the electric drawn arc stud welding apparatus in 1954 allowed a type of shear connector known as the *Headed Stud Connector*, (see figure 2.1), to be rapidly fastened to the top flange of the steel beams in situ. Due to its advantages over other forms of shear connection, such as rapid installation and the fact that they were equally strong and stiff in shear in all directions normal to the axis of the stud, the stud connector became one of the most popular types of connector used in composite construction.

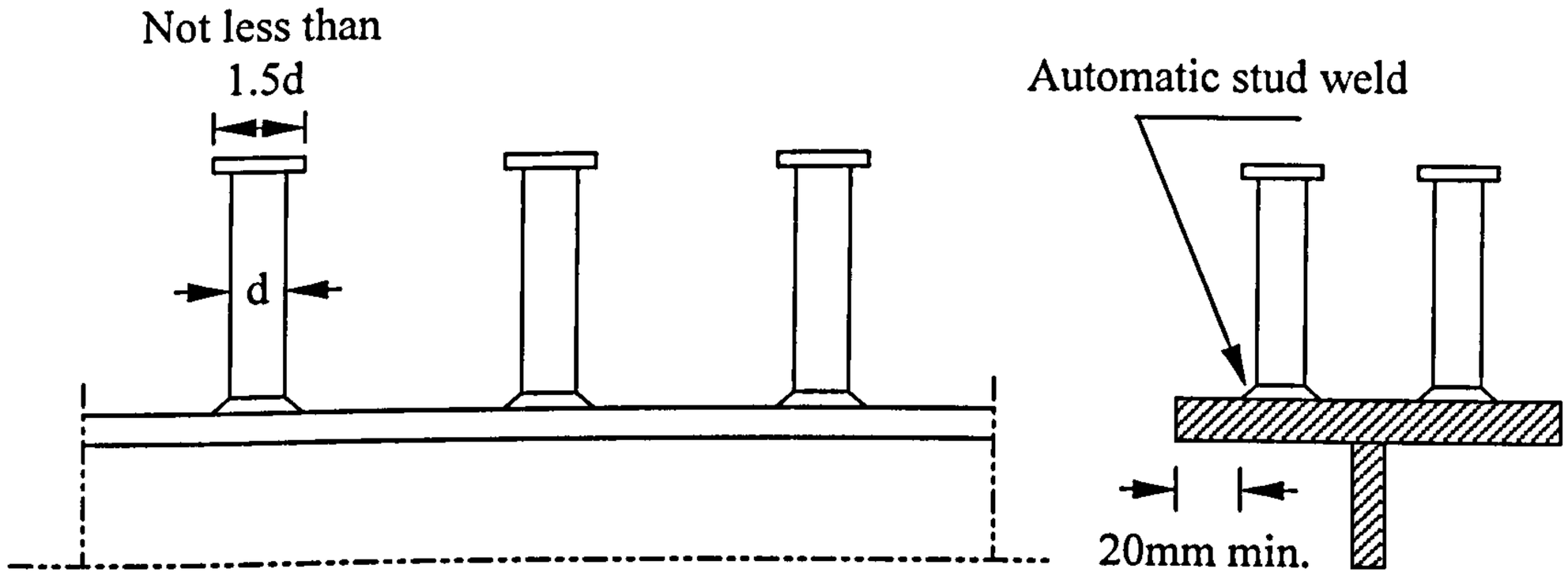

Figure 2.1 Headed stud shear connector

Studies of stud connectors did not begin until 1956. Push-off tests on stud connectors were first carried out at the University of Illinois by Viest[3]. The study used straight studs

with an upset head of diameter ranging from 0.5 in. to 1.25 in. Fatigue and static tests were also performed by Thurlimann[4] at Lehigh University in 1958. These push-off studies used 0.5in. diameter bent studs and, to a lesser extent, 0.75 in. diameter straight studs with an upset head. All the push-off tests showed that steel studs are suitable for use as shear connectors and that the behaviour of a stud connector is similar to that of a flexible channel connector. The shear capacity was found to be a function of the diameter and height of the stud and of the strength of the concrete.

During the latter half of the 1950's, profiled steel sheeting (decking) was introduced in the North American steel construction market that eliminated the use of traditional timber temporary forms. Initially the new decking system served only as a replacement for the timber form-work due to its advantages of serving as a working platform to support the construction loads, as well as a permanent form-work for the concrete. Once the sheets had their surfaces suitably embossed with small indentations to ensure reliable bond with the concrete, it became an integral structural element of the slab by providing all or part of the main tension reinforcement and it was eventually incorporated into the overall composite floor and framing system. Since the decking created a barrier between the concrete slab and the steel beam, holes were initially cut or punched into the deck for the welding of the stud shear connectors, but it soon became possible to weld these connectors through the decking. Composite construction of steel frames with profiled steel decking to support the floor slabs is now common in multi-storey steel frame construction. The disadvantages are associated with the operation and cost of welding the connectors through the decking on site, limitations to maximum spans to about 3.5m without propping or the addition of framing, and a 'wet-trade' is involved for pouring the concrete floor that prevents a dry construction environment.

The use of precast concrete hollow core units (HCU) in conjunction with the steel frame to provide composite action is relatively new. Precast concrete HCU floors are already used extensively in long span steel framed buildings. The precast HCU is considered in isolation from the beam and no composite action is assumed. Tie steel is placed on site into the milled slots made at the top of the hollow cores, which are filled with grade C25 (minimum) in-situ concrete. The slab rests directly on the top of the flange of the steel beam as shown in Fig. 2.2 and there is no mechanical connection to the beam. Figure 2.3

shows the details of the precast-in-situ joint in a composite beam with HCU. The longitudinal and transverse joints between the HCU's are filled with in-situ concrete so that horizontal compressive membrane forces can be transferred through the slab.

Figure 2.2 Composite beam with tapered-end hollow core slabs during construction

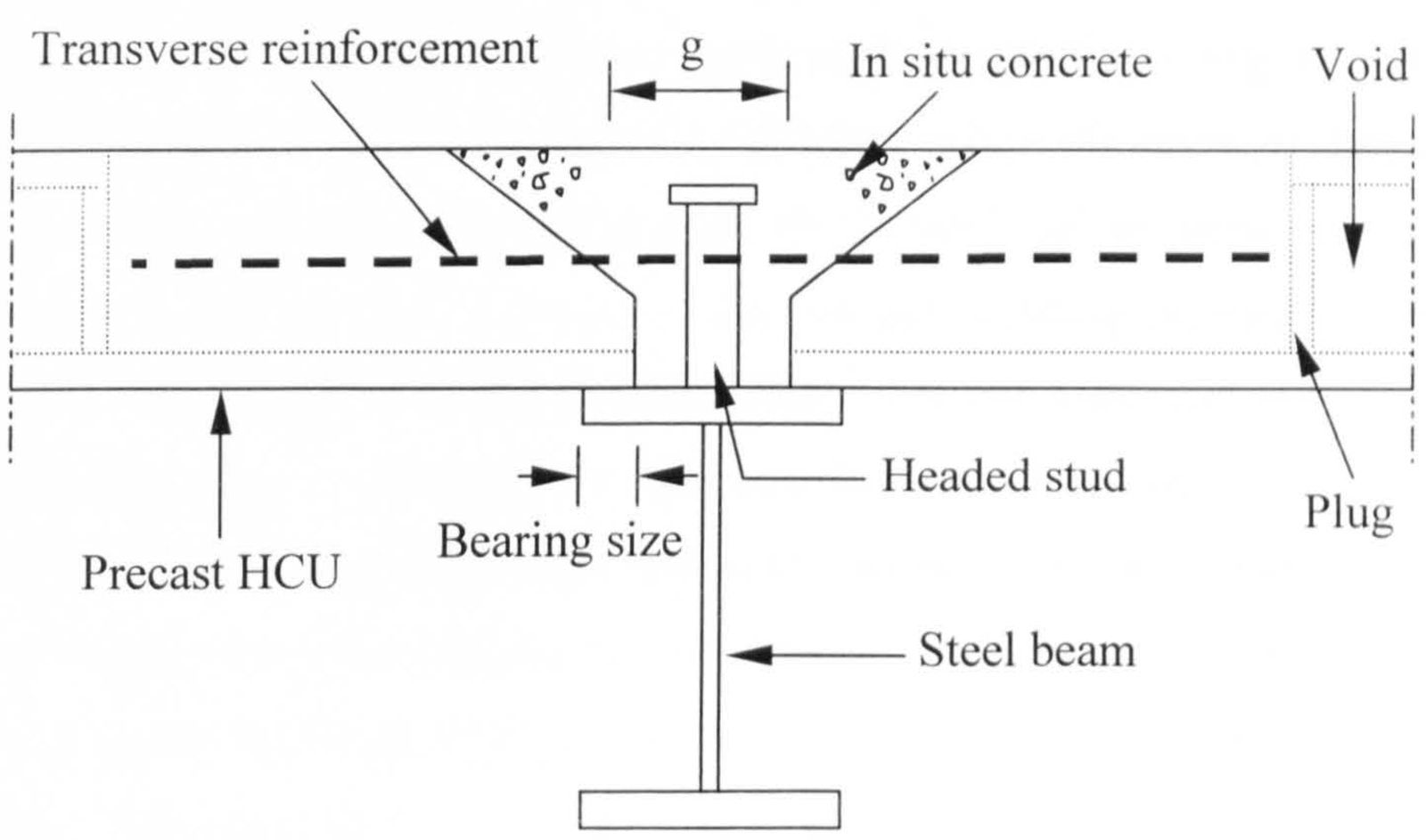

Figure 2.3 Details of the precast-in-situ joint of composite beam with tapered end HCU

Composite construction incorporating HCU's is intended to complement the now traditional steel frame/steel decking method and to offer advantages where, for reasons of design or environmental considerations, a steel decking system may be precluded. The main advantages of this form of construction are that the precast concrete slabs can

span up to 15m without propping. The erection of 1.2m wide precast concrete units is simple and quick. Shear studs are pre-welded on beams before delivery to site, thereby offering additional savings associated with shorter construction times.

2.2.2 Shear connectors

In steel-to-concrete composite construction, longitudinal shear forces are transferred across the steel-concrete interface by the mechanical action of the shear connectors. The problem associated with this connection is that it is a region of severe and complex stress. The methods of connection have been developed empirically and verified by tests. These tests show that at low loads, most of the longitudinal shear is transferred by bond at the interface. This bond breaks down at higher loads, and once broken it can not be restored. So in design calculations, bond strength is taken as zero. Also greasing the steel flange before the concrete is cast destroys the bond between it and the concrete slab. The design of the connectors to ensure an adequate degree of interaction is specified in the codes of practice CP 117 Part 1[5] (1965) and CP 117 Part 2[6] (1967).

The most widely used type of connector is the headed stud shown in Fig. 2.1 The current British code of practice[7] (1990) requires the steel from which the studs are manufactured to have an ultimate tensile strength of at least 450 N/mm^2 and an elongation of at least 15%. The advantages of stud connectors are that the welding process is rapid, they provide little obstruction to reinforcement in the concrete slab, and they are equally strong and stiff in shear in all directions normal to the axis of the stud.

The property of a shear connector most relevant to design is the relationship between the longitudinal shear force transmitted, P, and the slip at the interface, S. This load-slip curve should ideally be found from tests on composite beams. However, most of the data on connectors have been obtained from various types of "push-off" test. The flanges of a short length of steel-I section are connected to two small concrete slabs. The details of the "standard push test" given in Eurocode 4[8] (1994) is shown in Figure 2.4. The slabs are bedded onto the lower platen of a compression-testing machine or frame, and the load is applied to the upper end of the steel section. Slip between the steel member and the two slabs is measured at several points, and the average slip is plotted against the load per connector.

The test must be specified in detail, for the load-slip relationship is influenced by many variables, including:

1. number of connectors in the test specimen,
2. mean longitudinal stress in the concrete slab surrounding the connectors,
3. size, arrangement, and strength of slab reinforcement,
4. thickness of concrete surrounding the connectors,
5. freedom of the base of each slab to move laterally,
6. bond at the steel-concrete interface,
7. strength of the concrete slab, and
8. degree of compaction of the concrete surrounding the base of each connector.

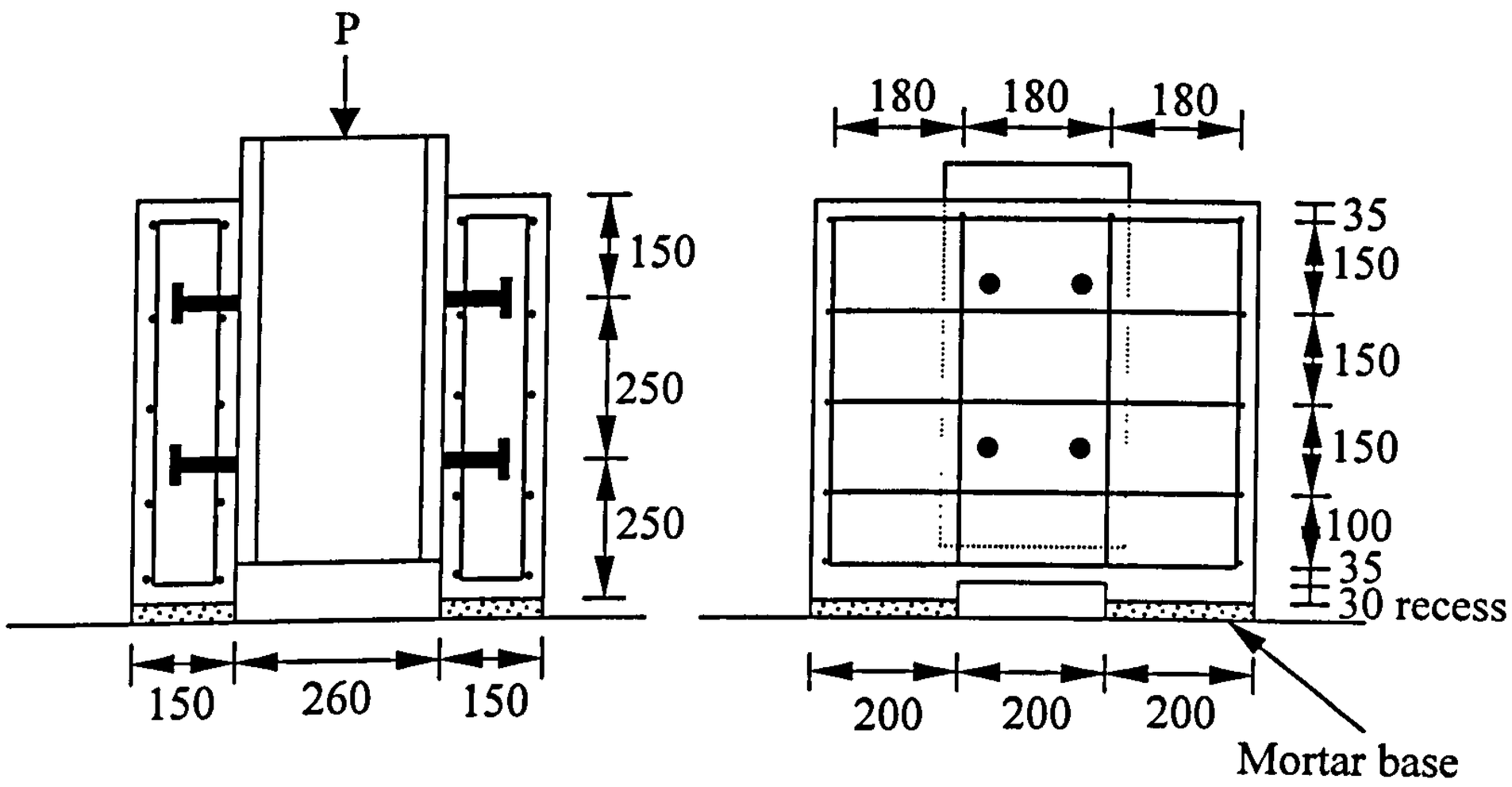

Figure 2.4 Standard push-off test specimen according to Eurocode 4

The details shown in Figure 2.4 include requirements relevant to items 1 to 6. The amount of reinforcement specified and the size of the slabs are greater than that of the British standard test[9] (1979) shown in Figure 2.5. Eurocode 4 gives results that are less influenced by splitting of the slabs and so give better predictions of the behaviour of connectors in beams as mentioned by Johnson[10,11].

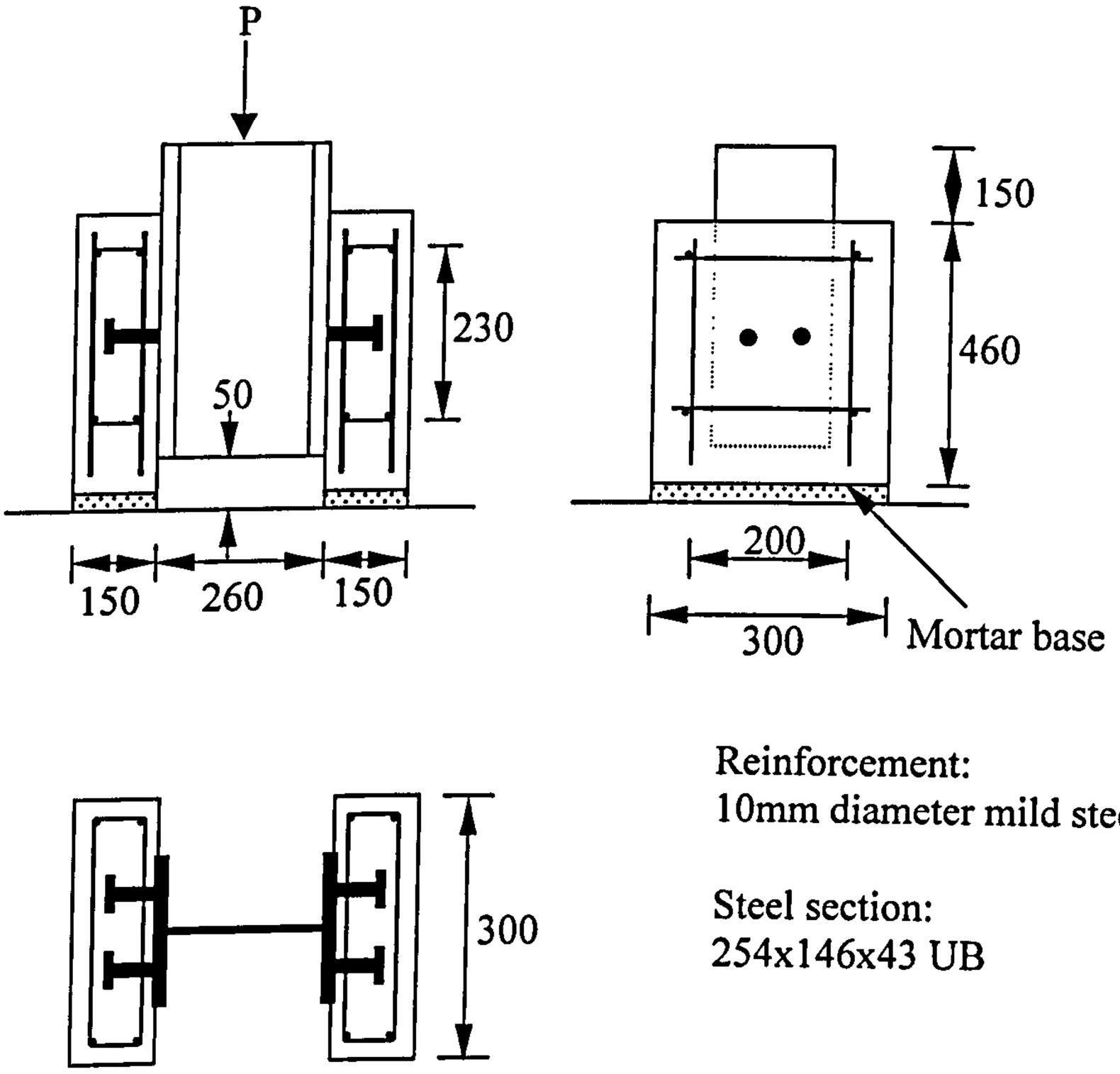

Figure 2.5 Standard push-off test specimen according to BS 5400

2.2.3 Complete and partial shear concoction

A very important aspect of the design of composite beams is the design of shear connectors. The connection between the steel beam and the concrete slab is called "complete" in the sense that the slip and uplift at the interface of the two elements are negligible. Shear connection in composite beams is identified[12,13] as complete when the beam has a bending strength that would not be increased by the addition of further

connectors. On the other hand, the connection between steel beam and concrete is called partial when fewer connectors are used than are required for the complete shear connection. The term "partial connection" should not be considered to imply unsatisfactory shear connectors but rather a connection resulting in non-negligible slip at the steel beam-concrete slab interface. This slip has a great influence on both the strength and the deformations of the composite beam. Significant contributions have been made in this scientific area[14] where the influence of the slip on the ultimate plastic strength of the composite beam has been studied.

The accurate analysis of the behaviour of composite beams with partial connection is very important since the slip between steel and concrete may be big enough to cause fracture of some connectors at serviceability state. Appropriate ductility of the shear connectors is the only way to sustain the likely big slip deformations without fracture.

2.2.4 Design equations for the evaluation of shear stud capacities

The design standards for shear studs in solid concrete slabs are covered in Great Britain by BS 5950[7] and Eurocode 4[8]. The development of design equations used in evaluating shear stud capacities will be discussed in the next paragraphs. The capacities depend on the type of the concrete slab used with the steel beam to form the composite interaction.

2.2.4.1 Solid reinforced concrete slabs

The strength of shear studs in solid reinforced concrete slab was first determined in 1971 by Ollgarrd et al.[15], and was presented in terms of an empirical formula after carrying out 48 push-off tests. The ultimate shear force resistance Q_u (in N units) of the headed studs was given as follows:

$$Q_u=0.5A_s(f_cE_c)^{1/2} \qquad \text{.....(2.1)}$$

where:

A_s is the cross-sectional area of the stud diameter 'd' (mm^2 units)

f_c is the concrete cylinder compressive strength (N/mm^2)

E_c is the static modulus of elasticity of the concrete(N/mm^2)

This equation, which was adopted in CP 117, assumes concrete crushing failure rather than a shear failure of the headed stud.

Later, in BS 5950[7], data presented by Menzies[16] were used to develop the characteristic shear force resistance Q_K. There is no theoretical basis to these data and values given in table 5 in this code reflect only the size of the stud and strength of the concrete.

In Eurocode 4[8] the resistance P_{RD} is defined in clause 6.3.2.1 using two equations: the first representing concrete failure and the second corresponding the failure of the stud at its collar. The lower of the following values should be used in design:

$$P_{RD}=0.29\alpha d^2(f_{cK}E_c)^{1/2}/\gamma_v \qquad \text{.....(2.2)}$$

$$P_{RD}=0.8f_u*\pi d^2/4\gamma_v \qquad \text{.....(2.3)}$$

where:

$\alpha=0.2(h/d+1) < 1.0$

h is the overall length of stud

f_{cK} is the concrete cylinder compressive strength (N/mm^2) specified in Table 3.1 of EC4[8].

f_u is the ultimate tensile strength of the headed stud material

γ_v is the partial safety factor taken as 1.25 for the ultimate condition.

2.2.4.2 Stud connectors used with profiled steel sheeting

Where profiled sheeting is used, stud connectors are located within concrete ribs that have a haunch shape. The sheeting normally run either transverse or parallel with the span of the beam. The following parameters[17,18] affect the behaviour of stud in composite beams with profiled sheeting in addition to geometrical data shown in Fig. 2.6:

1. The compressive strength and density of concrete.
2. The ultimate tensile strength of stud.
3. The location of stud within the concrete rib, in relation to the direction of sheeting.

4. The shape of the steel profile, and whether the studs are welded through it or through holes in it.
5. The size, spacing and level of any reinforcement in the slab.

Tests show that the shear resistance of connectors is sometimes lower than it is in a solid slab, for materials of the same strength, because of local failure of the concrete rib. For this reason Eurocode 4[8] specifies reduction factors, applied to the resistance P_{RD} as follows:

$$P_r = kP_{RD} \qquad \text{.....(2.4)}$$

where 'P_r' is resistance of a stud in a trough, and 'k' is the reduction factor which depends on the direction of sheeting.

For sheeting with ribs parallel to the beam, the factor (k_l) is

$$k_l = 0.6(b_o/h_p)(h/h_p - 1) \leq 1.0 \qquad \text{.....(2.5)}$$

where the dimensions b_o, h_p and h are illustrated in Fig.2.6, and h is taken as not greater than 'h_p+75'mm.

The Eurocode 4 rules are discussed by Johnson and Anderson[11].

Systematic theoretical and finite-element studies since 1981, mainly by Oehlers[19] and initially for solid and haunched slabs, have been extended to parallel sheeting.

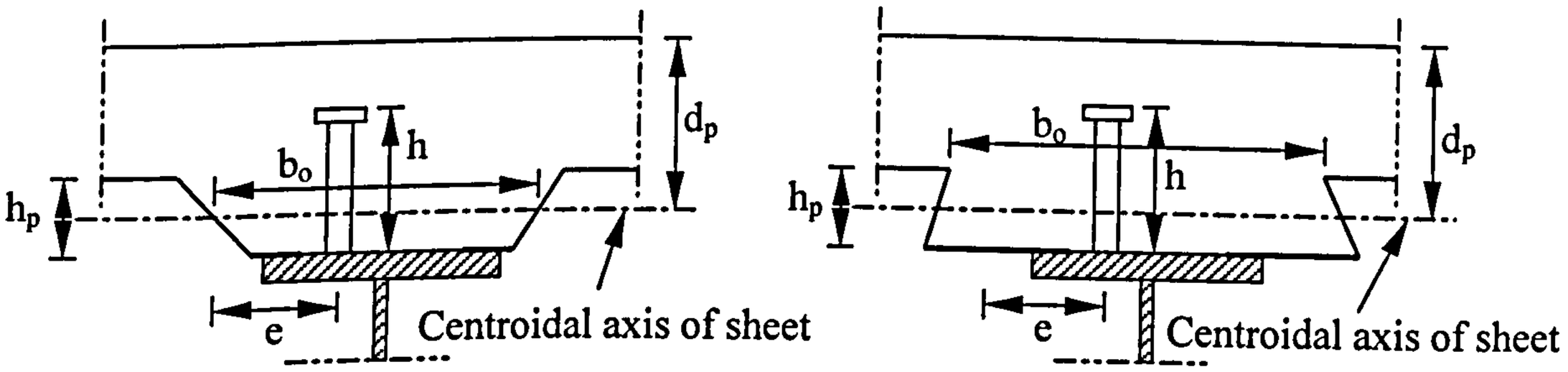

Figure 2.6 Composite beam and composite slab spanning the same direction

For sheeting with ribs transverse to the beam, the factor (k_t) is

$$k_t=[0.7/(N_r)^{1/2}](b_o/h_p)(h/h_p-1) \leq 1.0 \quad \text{.....(2.6)}$$

where N_r is the number of connectors in one rib where it crosses a beam, not to be taken greater than 2 in calculations.

It was recommended that off-centre studs should be placed on alternative sides of the trough, but no other account was taken of the important influence of dimension "e" in Fig. 2.6.

The reinforcement in a composite slab is usually a light welded mesh. Tests[18] show that when placed below the heads of the studs, the mesh can increase the shear resistance of the studs. In practice, the control of its level is poor and its detailing is not related to that of the shear connection.

Johnson and Yuan[20,21] considered results of 269 push tests in a study of existing design rules for the static shear resistance of stud connectors in profiled steel sheeting. It was found[22] that test data were scarce for:

1. the influence of the thickness of the profiled sheeting "t" and of light weight aggregate.
2. the influence of the position of the studs in each trough.
3. values of "b_o" less than "$2h_p$".
4. parallel sheeting.

So, the results for 34 push tests were reported and seven distinct modes of failure were found. The design rules for the static shear resistance of stud connectors in profiled sheeting were studied and it is found that they are limited in case of studs placed off-centre in the steel troughs. Developed equations based on theoretical models were obtained for seven observed modes of failure. The modes are shown to give good performance when compared with reported test results.

2.2.4.3 Stud connectors used with hollow-cored floor slabs

Present knowledge of determining the capacity of the connectors in a composite beam consisting of pre-cast concrete hollow-cored floor slabs arises from the work of Lam, Elliott and Nethercot[23]. 12 full-scale push-off tests were carried out to study the effects of the size of the gap between the ends of the pre-cast slabs, the amount of tie steel placed transversely across the joint, and the strength of concrete in-fill on the capacity of the shear stud. The following design equation, modified from the Eurocode 4[8] 'equation 2', was given and there was no modification in equation 3 as the strength of the shear stud is thought not to be influenced by the pre-cast construction.

$$P_{RD}=0.29\alpha\beta\varepsilon d^2(\omega f_{cp}E_{cp})^{1/2}/\gamma_v \qquad \text{.....(2.7)}$$

where:

β is a factor which takes into account the gap width "g" (mm), see figure 2.3, and is given as $0.5(g/70+1) \leq 1.0$, and $g > 30$ mm

ε is a factor which takes into account the diameter "ϕ" of transverse high tensile steel (grade 460) and is given by $0.5(\phi/20+1) \leq 1.0$, and $\phi \geq 8$ mm

ω is the transverse joint factor $=0.5(w/600+1)$, "w" is the width of hollow concrete units

f_{cp} is the average concrete cylinder strength = 0.8×average cube strength of the in-situ and pre-cast concrete

E_{cp} is the average value of elastic modulus of the in-situ and pre-cast concrete.

All other terms are as for Eq. 2.2.

2.2.5 Previous studies of shear connection in steel-solid slab composite beams

In 1967, Davies[24] showed that the ultimate capacity of a stud connector in a push-off test depends to a large extent upon the pattern and spacing of the connectors. It was observed that if the studs were oriented parallel to the direction of the load, its ultimate capacity was reduced. Also, a decrease in the longitudinal stud spacing resulted in a decrease in ultimate strength. A further study by Davies[25] showed that when transverse reinforcement is provided in a solid concrete slab, the cracking resistance of the slab is improved. The longitudinal cracks only develop when the yield stress of the

reinforcement is reached. Therefore, a certain minimum amount of transverse reinforcement has to be used, to achieve the maximum load-carrying capacity of a composite beam.

In 1971, Johnson[10] found that the concrete strength influences the mode of failure of shear connection between steel and concrete, as well as the failure load. It was also found by Menzies[16], when comparing the strengths of shear connectors given in CP 117 Part 1[5] and Part[6] with his results of push-out tests made at the building research station, that:

1- CP 117 part 1 assumes linear relationships between the static strength of shear connectors and the concrete strength.

2- CP 117 part 2 assumes that the variation of fatigue strength of stud connectors with concrete strength was inside limited range of concrete strengths.

So, experimental work was conducted on 34 push-out specimens to investigate the effect of concrete strength and density on the static and fatigue strength of connectors.

This was done over a wide range of concrete strengths. Different types of connectors, studs, channels and bars were used and the maximum load per connector, the mode of failure and the slab in which the failure occurred were given. The maximum static loads per connector were plotted against the compressive strength of both water-stored and air-stored concrete cubes. The slip in the static tests, i.e. the vertical movement of the slab relative to the steel beam, was plotted for each specimen against the load. The maximum and minimum values of the cyclic load per connector, the fatigue life, and the mode of failure were given. It was concluded that:

1- Modification of specified strengths of shear connector given in CP 117 is desirable for a larger range of concrete strengths.
2- Distinction should be made in design between connectors embedded in normal density concrete and lightweight concrete.
3- The static strengths of studs in normal density concrete are over estimated in CP 117.
4- When the density of the lightweight concrete is below 1400 kg/m^3 (87 lb/ft^3) there may be difficulty in ensuring adequate connection strength and an adequate degree of interaction in a composite beam.

5- The specification in CP 117 of the fatigue strength of stud connectors based on percentages of static strength is confirmed when embedded in normal-density concrete.

In 1987, Jayas and Hosain[26] conducted tests on 18 full-size push-out specimens and four pull-out specimens. The objective of the project was mainly to study the behaviour of headed studs in composite beams with ribbed metal decks perpendicular and parallel to the steel beam but five of the push-out specimens had solid concrete slabs. These five push-out specimens were similar to those tested by Ollgaard et al.[15] (1968). The used stud has a diameter of 16mm and a height of 76mm. They found that when the studs were spaced sufficiently far apart, the mode of failure is likely to be because of shearing off of studs. On the other hand, concrete failure was observed in specimens when the studs were closely spaced (longitudinal spacing less than six times the stud diameter) and this led to a reduction in the stud strength by 7%.

In 1989 Oehlers[27] investigated the longitudinal shear flow in composite steel-concrete beams across the steel-flange/concrete-slab interface by the action of individual connectors. They have shown that shear connectors in steel-concrete composite beams act as steel dowels embedded in a concrete medium. These shear connectors are generally assumed to fail when the steel component fractures, which may be a consequence of the gradual reduction in strength and stiffness of the concrete in the bearing zone of high tri-axial compressive stress (Oehlers and Johnson 1987[28]). Oehlers has stated that the concentrated load P that a connector applies to a slab can induce three distinct modes of cracking of the slab shown in his figure 2.7. The modes of cracking are:

1. The lateral cracks extending from the sides of the connector and caused by the ripping action of the concentrated load on the slab. These cracks are assumed to have little effect on the connector strength since they occur away from the high tri-axial compression bearing zone.
2. Shear cracks that occurs near the compressive zone and hence and hence may affect the tri-axial restraint.

3. Splitting cracks that occur in front of the tri-axial compression zone due to the concentrated load induced by the shear connector. These large lateral tensile stresses propagate and induce splitting behind the shear connector and also relieve the tri-axial restraint to the bearing zone leading to connector failure through compressive failure of concrete.

Oehlers found that splitting cracks reduce the strength of the shear connection to less than 20% of its theoretical shear connector strength. Also, fully anchored transverse reinforcement placed in front of a heavily loaded single connector did not increase the splitting strength of the slab nor increase the strength after splitting. However, the transverse reinforcement was found to limit the strength of the split and allow a general gradual reduction in the shear load after splitting.

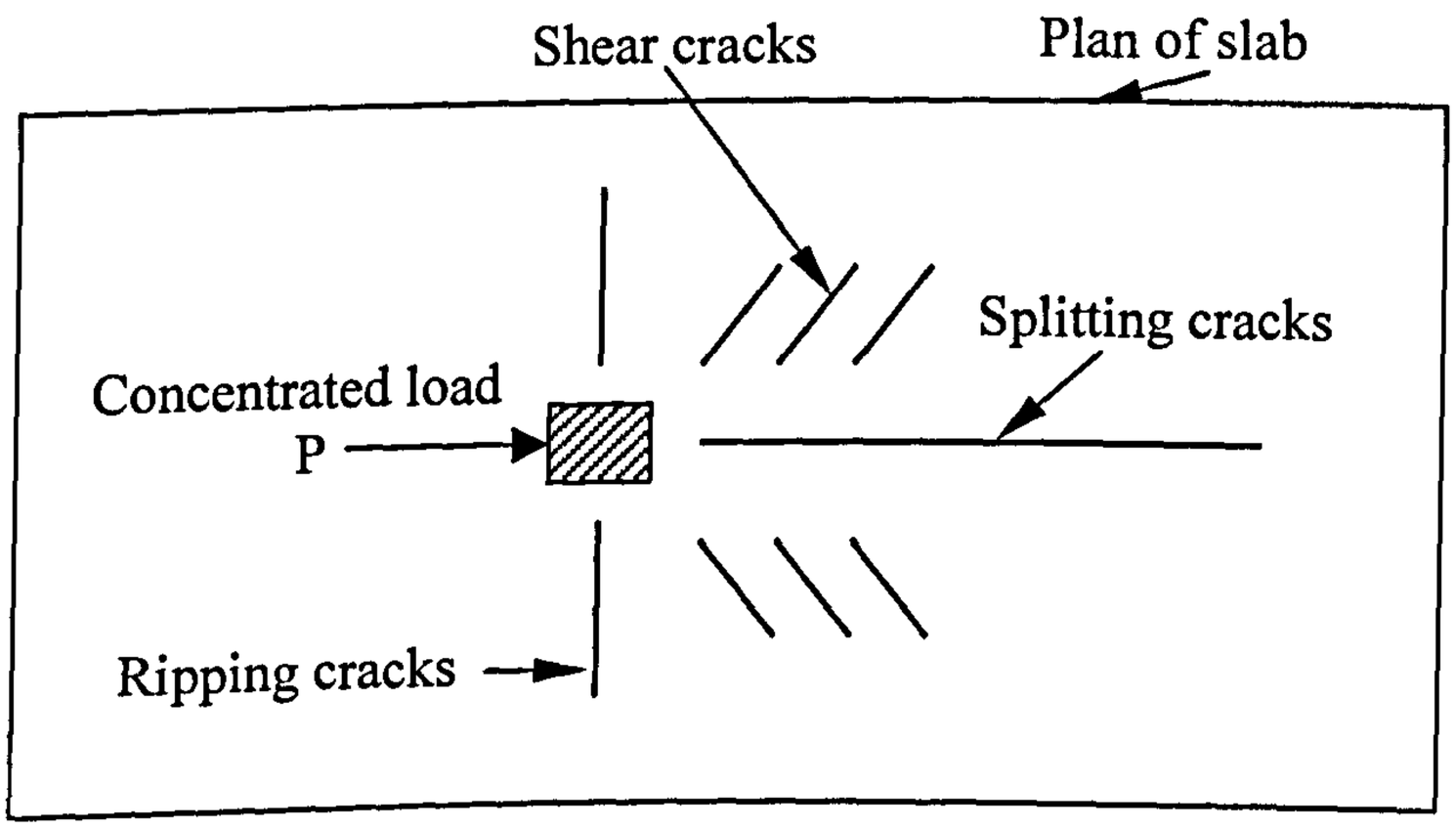

Figure 2.7 Crack formation of slabs in composite girders

In 1994, Oehlers and Park[29] found that composite steel-concrete connections that incorporate a haunch are prone to splitting failure. This is because the shear connectors have to transfer high concentrations of load into the concrete slab in the region of the haunch where the side cover to the connectors is limited. The experimental tests were on stud shear connectors encased in haunches with sloping sides. A similar study, done by Johnson[30] (1972), to determine the splitting resistance for haunches with vertical sides. They obtained the load-slip curves of the connectors for different haunch slopes. It was concluded that these results can be used to design composite slabs made with steel

decking when the ribs of the steel decking are parallel to the steel section of composite beam.

Push-out tests on studs in high strength and normal strength concrete have been carried out by Li and Krister[31] (1996). Eight push-out specimens were divided into four pairs, according to the concrete strength and the amount of reinforcement in concrete slabs. The authors found that the concrete compressive strength significantly affects the strength of the shear connections. The increase in the maximum shear load was about 34% when the cylinder compressive strength of the concrete increased from 30-81 MPa. The tests showed that the amount of slip at the maximum load was of the same level for both normal strength and high strength concrete. However, ductile behaviour of the studs was observed for the normal strength specimen after the maximum load. The descending branch of the load-slip curves for the high strength concrete was short and steep. The reinforcement in the concrete slabs negligible influence on the capacity of normal strength concrete (the increase was about 6%), but confined the concrete surrounding the studs. A negligible effect of reinforcement on the capacity of the shear connection was observed in high strength concrete specimen.

2.2.6 Previous studies of shear connection in steel-precast HC slab composite beams

Limited published literature on composite construction incorporating steel beams-precast HCU slabs were found. Some researches dealing with composite construction incorporating steel beams-precast solid slabs were found and there will be discussed in this section as well.

In 1996 Moy and Tayler[32] carried out 27 push-off tests to evaluate the shear strength of headed studs in solid precast concrete planks. The precast planks were used as permanent shutters for the in situ concrete. The precast planks had a depth of 65mm and a bearing width of 50mm on the steel beam flange. A 533mm depth by 210mm width by 92kg steel beam was used with two studs welded on each flange. The diameter of the headed stud used was 19mm and different lengths ranging from 95-120mm were used. The rest of the 150mm depth of the slab was made with in situ concrete. Figure 2.8 shows the details of Moy and Tayler push-off test specimen. A typical load-slip curve of the 19mm stud was obtained and the results showed a reduction in strength of

connection as the volume of in situ concrete decreases. It was recommended that the width of the in situ concrete on the flange be a minimum of 100mm. It was also recommended that two layers of reinforcement must be used in the slab to avoid concrete splitting.

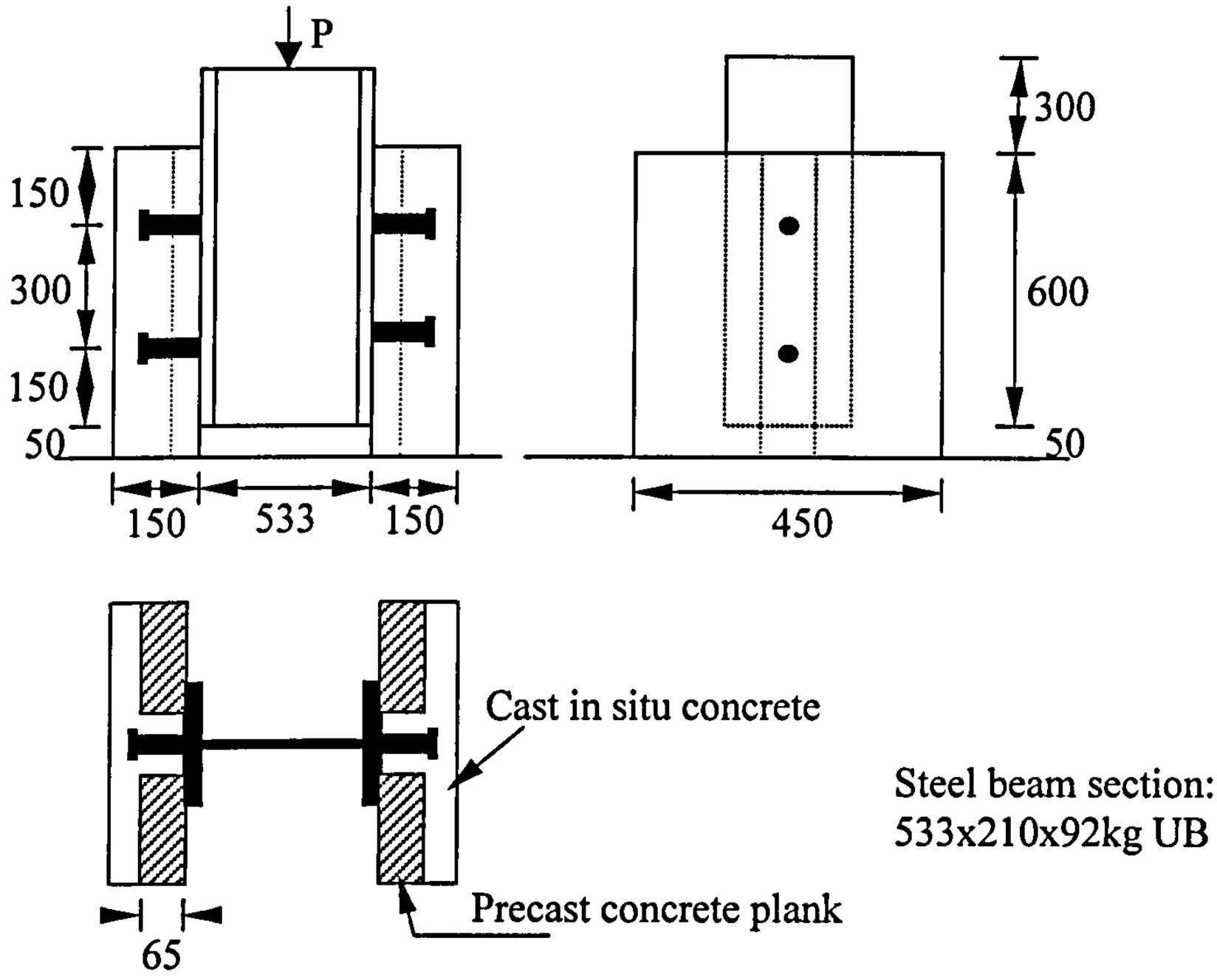

Figure 2.8 Details of push-off test specimen conducted by Moy and Tayler

Push-off tests on headed studs in precast HC slabs were published first by Lam, Elliott and Nethercot[23] (1998). The authors carried out 12 full-scale push-off tests (10 tests on headed studs used with tapered end precast HCU slabs and 2 on headed studs used with reinforced solid concrete slabs). The tests were carried out horizontally as shown in figure 2.9 with the same cross section shown in figure 2.3. The tests were carried out for different gap sizes 'g' (40, 65 and 120mm) between the ends of the precast slabs. Also different transverse reinforcement sizes (8, 16 and 25mm) were used. Two of the 10 tests consisted of two 1200mm widex150mm deep HCUs where others consisted of four 600mm wide x 150mm deep HCUs. The HCUs were connected to grade 43 steel 356x171 UB with pre-welded headed studs at 150mm centers. Milled slots

approximately 500mm long were made in the second cores from the edges of the units. The characteristic cube strength for the precast concrete was taken as 50 N/mm^2. All studs were 19mm diameter x 125mm height (TRW-Nelson headed studs). The authors found that the capacity of the stud is reduced compared with that in a solid reinforced concrete slab. A reduction formula for the precast effect was derived, refer to section 2.2.4.3 from this thesis, and the load-slip curves of the studs were plotted for the 12 push-off tests.

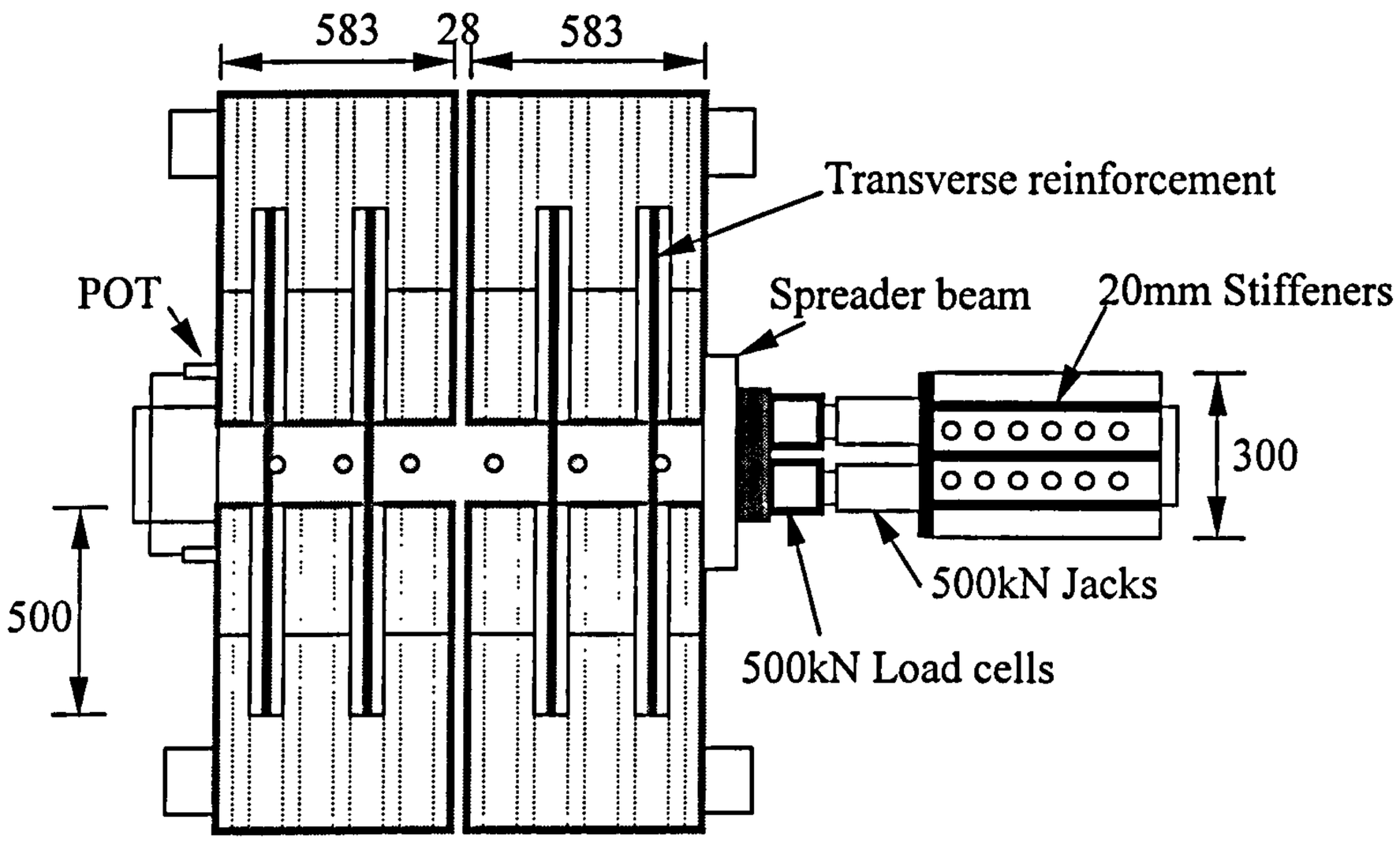

Figure 2.9 Horizontal push-off testing as carried by Lam, Elliott and Nethercot

The behaviour of shear connections in a composite beam with a full-depth precast slab was investigated by Shim et al.[33] (2000). 18 push-out tests were performed with variations of the stud shank diameter and the compressive strength of the mortar. Figure 2.10 shows the push-off test specimen used by the authors to evaluate the shear stud properties in a composite beam with a full-depth precast slab. Different stud diameters (13, 16, 19 and 22mm) were used with a stud height of 150mm. The push-out tests were similar to BS 5400[9], but it had shear pockets for stud shear connectors and a bedding mortar layer 20mm thick between the precast slab and the steel beam. The load-slip

curves of the stud were obtained and the relationship between the shear stud capacity and the stud diameters was plotted. From the experimental work, the authors observed that the deformations of the stud in a full-depth precast slab were greater than its deformations in a cast-in-place slab. The static strengths of the shear connections agree approximately with those evaluated from the tensile strength of the stud shear connectors. Also, an empirical equation for the initial shear stiffness of a shear connection was proposed.

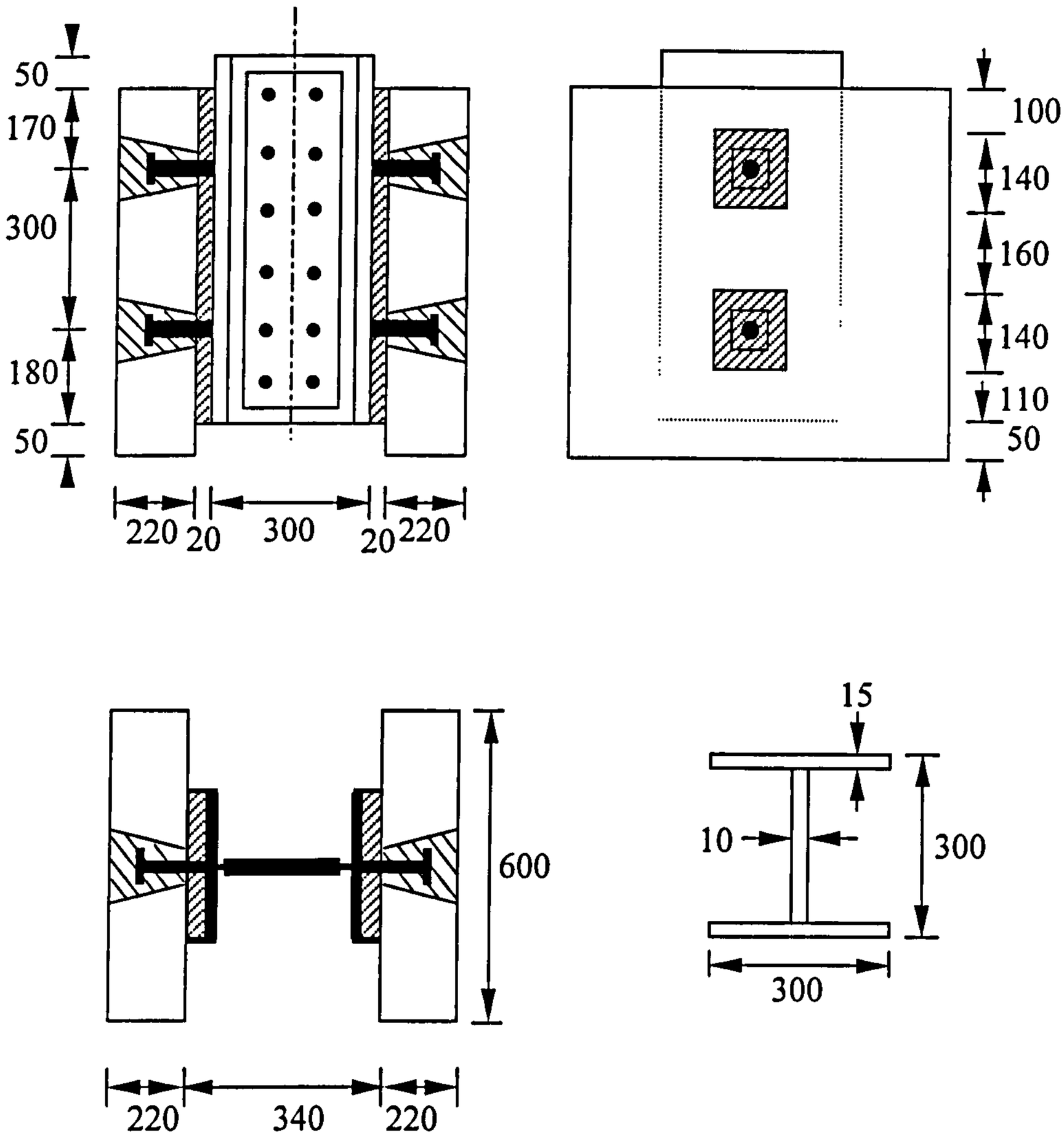

Figure 2.10 Details of push-out test specimen used by Shim et al.

In 2001, Nip and Lam[34] investigated the effect of end conditions of hollow core slabs on longitudinal shear capacity of composite beams. The published work was an extension for Lam et al.[23] and mainly concerned about push-off tests with precast HCU slab of square ends, see figure 2.11 that shows some of theses units on top of steel beam as shown by the authors. 18 push-off tests (12 push-off tests with precast HCU slab of square ends, 2 push-off tests with precast HCU slab of tapered ends and 4 push-off tests with solid slab) were carried out by the authors. The same horizontal push-off testing approach used by Lam. et al.[23] was used. The headed studs used had 19mm diameter and 100mm height. The precast floor specimens consisted of four 600mm wide hollow core units connected to a 254 x 254 x 73 UC. Each beam had six pre-welded studs at 150mm centers. The effects of transverse reinforcement size, gap width and in situ concrete strength were discussed by the authors. The authors concluded that 100mm height headed studs with square-end HC slabs performed as well as the 125mm height headed studs with tapered end HC slabs. It is also concluded that the optimum in situ gap width that should be used for square end HC slab is 80mm and 16mm diameter high tensile bars are recommended to be used as transverse reinforcement to ensure a slip ductility of 6mm at the maximum load.

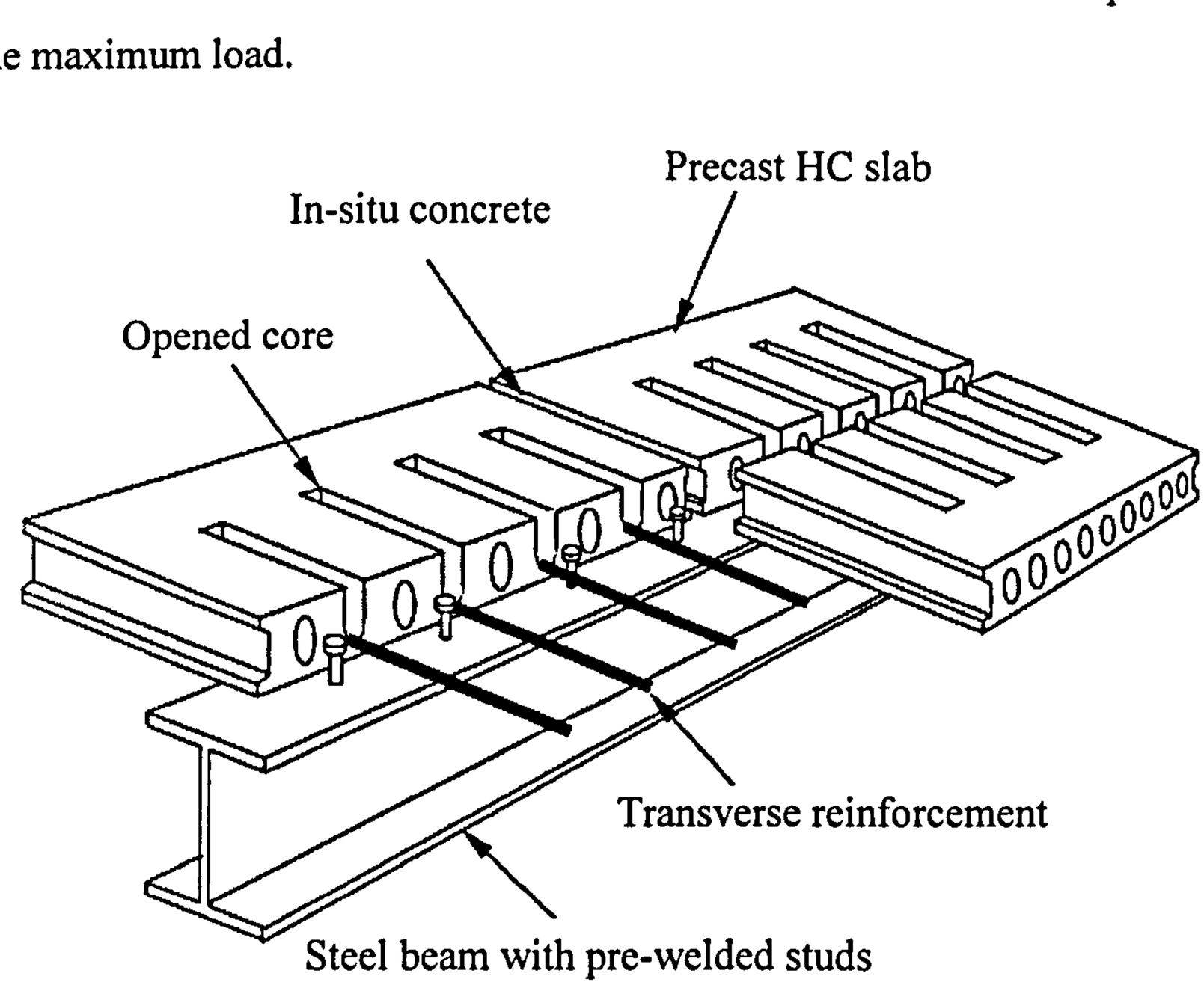

Figure 2.11 Composite beam with HC slabs of square ends studied by Nip and Lam

2.3 Previous studies on numerical modelling of push-off tests

It is evident from the previous literature review that the experimental work is mostly used in order to obtain the shear stud capacity and the full load-slip curve of the shear connector. It is also shown that most of the push-off tests carried out were concentrated on headed studs used with solid slabs and limited researches were found on headed studs used with precast hollow core slabs and precast solid slabs.

Recent studies like that one investigated by Nethercot[35] (2001) have shown the importance of combining experimental and numerical study in advancing structural engineering understanding. The author mentioned that there is a lack in the detailed numerical studies dealing with the behaviour of the individual connector. It is also mentioned that the absence of experimental/numerical approach means that the real understanding is lacking and design expressions are very limited.

Limited number of numerical models have been found in the literature for push-off tests with solid slabs and full precast solid slabs and will be discussed in the next paragraphs. No numerical models have been found for push-off tests with precast HC slabs except that one published by Lam et al.[36] (2001) which is a part of this study.

Initially, Johnson and Oehlers[37] (1981) used a simplified purpose-written program, developed originally by Oehlers[38], in their parametric study to predict the shank failure loads of headed stud in steel-solid slab push-off test and the influence of weld collar on forces acting on the stud. The program performed a step-by-step plane stress elastic analysis using triangular finite elements. Initially, one stud and one slab of a push-off test specimen were modeled. The stud shank and the weld collar were assumed to be of square cross-section. The program took into account two types of local failure, cracking due to tensile stress and cracking due to tensile strain caused by normal compressive stress. The program was used in two modes, linear elastic analysis of isotropic materials with and without the provision for concrete to fail in tension. In both modes the shear connection was assumed to have reached its maximum strength when the maximum stress in the shank of the stud reached the measured ultimate tensile strength of the shank. The failure of concrete in compression was not modeled in this study. The authors found that a weld collar less than 5mm high attracts 70% of the total shear and

reduces the bending moment at the base of the stud to one third of the value found for a stud without a collar.

The inelastic behaviour of shear connections was investigated by Kalfas et al.[39] in 1997. The authors used the FEM to model the behaviour of shear connectors in a steel-solid slab push-off test. The results were compared with series of push-off tests performed in the steel-structures laboratory of Democritus University of Thrace. The model simulated the linear and non-linear behaviour of the materials (bi-linear stress-strain curves were used for concrete and headed stud shear connector). The three components of a push-off test were simulated with different types of standard finite elements. The concrete slab was modeled by non-linear volume elements, the steel beam by a rigid bar element and the shear connectors by non-linear beam elements as shown in Fig. 2.12. The finite element package COSMOS was used in the analysis. The load-slip curve obtained from the FE solution was compared with experimental results and the maximum deviation between the results was about 14% as shown in Fig. 2.13. Although the concrete slab was modeled with 1920 elements, the results obtained were inaccurate and this may be attributed to the incompatibility of the FE elements used. The predicted shear stud capacity is considerably higher than that tabulated in BS 5950 and Eurocode 4 and the mode of failure was not investigated. The authors suggested to improve the material models by including the strain hardening of steel, contribution of concrete rebars and small tensile branch of the stress-strain diagram of concrete to reduce the deviation between experimental and FE solution.

The behaviour of headed shear stud connector in a steel-full-depth precast slab push-off test was modeled numerically by Shim et al.[33] (2000) using the FE method. The push-off test specimen shown in figure 2.10, previously discussed, was constructed using the standard FE package ABAQUS[40]. The purpose of the model was to investigate the initial stress distribution of the shear stud connector in the push-off test under consideration. The distributions of flexural and shear stresses along the stud shank were given. The stresses were concentrated around the root of the stud shank below a height of 20mm. The authors found that the flexural deformation of the stud shear connector was greater than that in the case of cast in place slabs which can resist the splitting force better through adequate reinforcement. The study was based on linear-elastic material

properties to investigate initial stresses only. The load-slip curves of the stud, shear stud capacity and modes of failure were not obtained from this FE study.

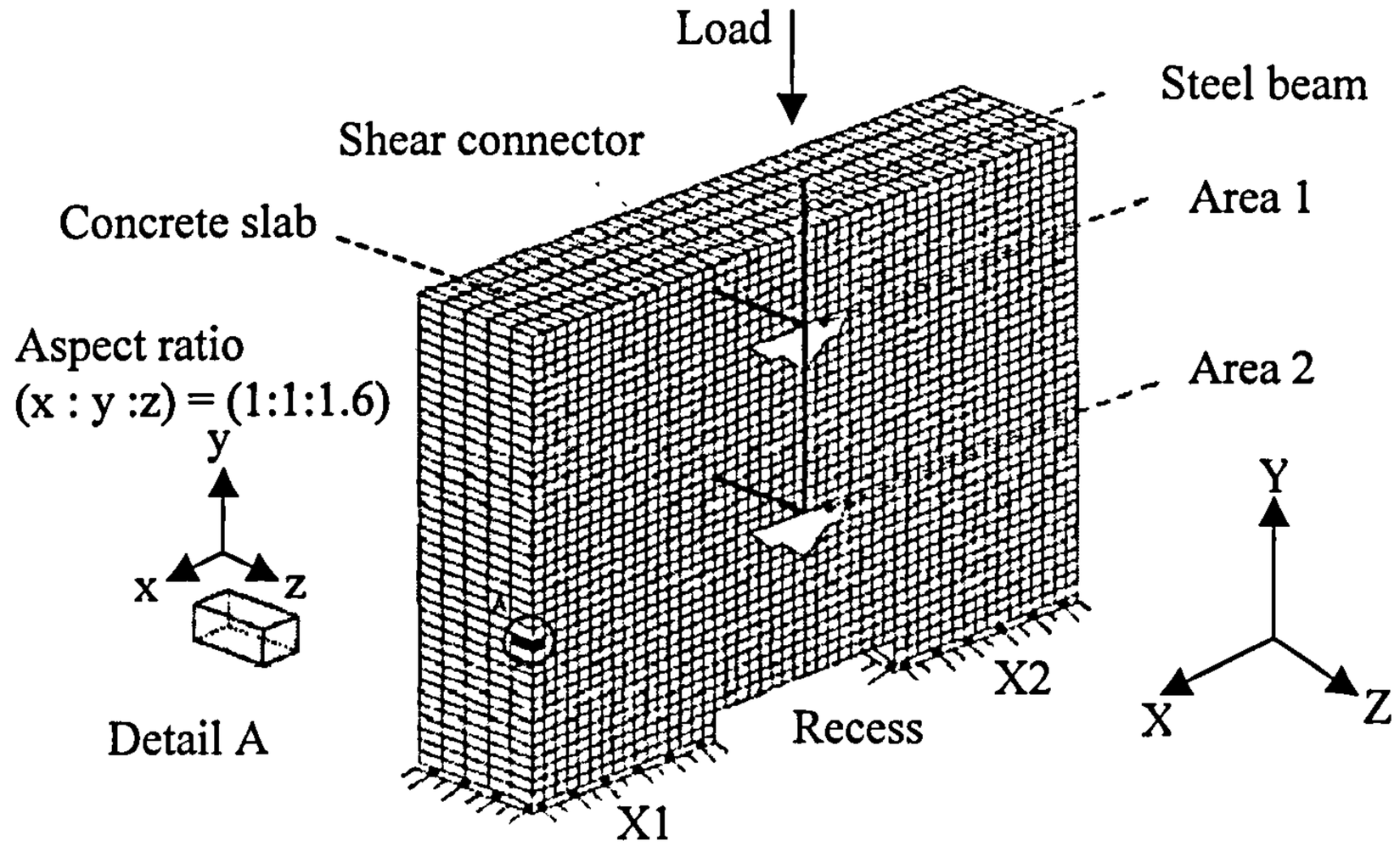

Figure 2.12 FE representation of push-off test specimen modeled by Kalfas et al.[39]

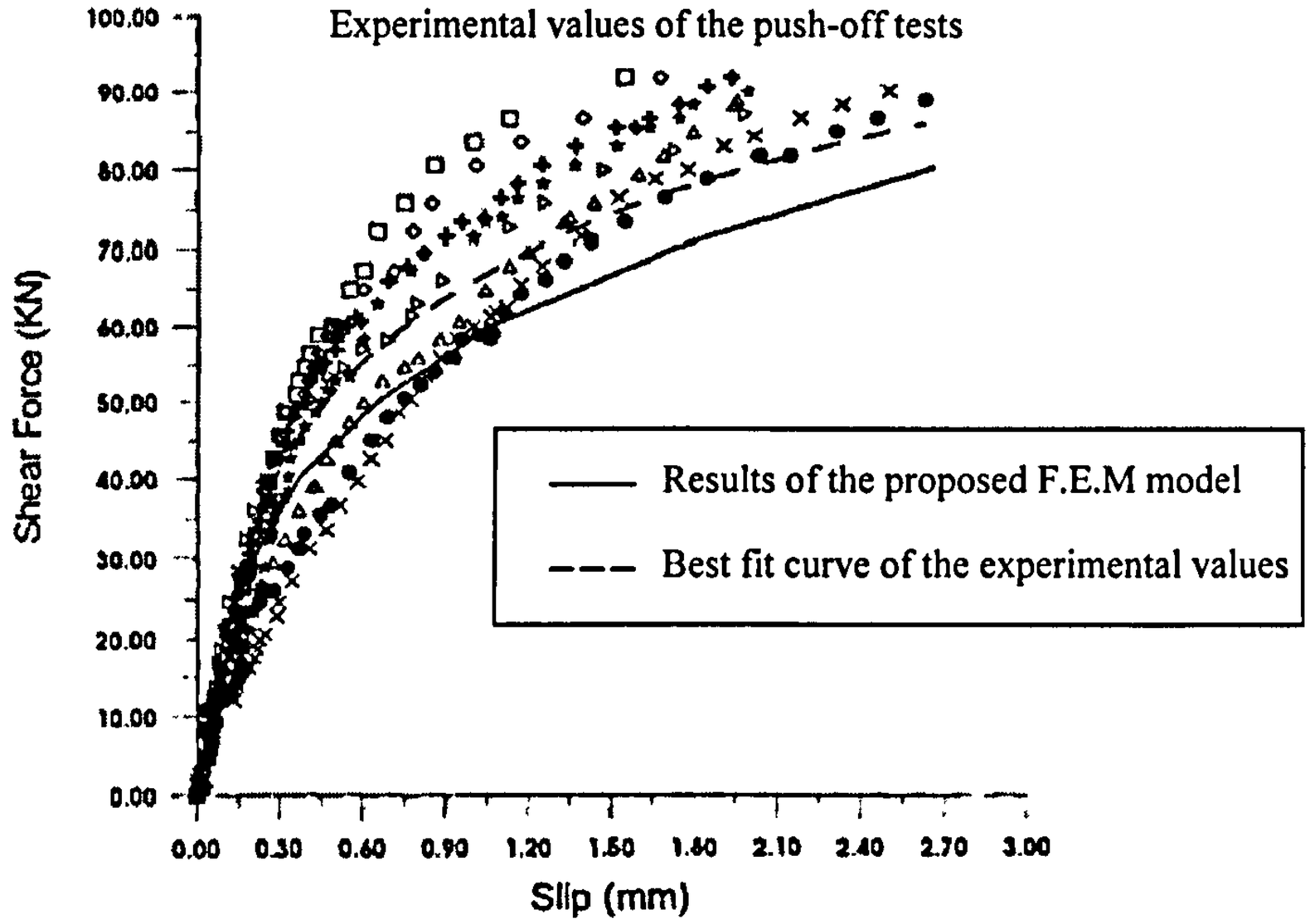

Figure 2.13 Comparison of experimental and FEM results given by Kalfas et al.[39]

2.4 Numerical modelling of composite girders

Many experimental and numerical studies have been carried out to investigate the structural behaviour of composite steel-concrete girders. Most of these studies were concentrated on composite steel-solid slabs girders and very few dealt with steel-precast HC slab. Steel-concrete composite beam behaviour is generally influenced by the shear connection flexibility. In this research, the results obtained from the modelling of shear connections (push-off tests) in steel-solid slab and steel-precast HC slab will be used in modelling the longitudinal behaviour of both composite girders.

There is no intention to survey most of research that has been carried out on composite girders in general in this thesis. The review will be concentrated only on how other researchers numerically simulated the different components of a composite girder including the shear connection between these components. Among those surveyed researches in this study, researches deal with the evaluation of the effective width, ultimate load capacity and load-deflection curves of composite girders.

2.4.1 Numerical modelling of steel-solid slab composite girders

Initially, Ansourian[41] (1975) used the FE method in analyzing composite steel-solid slab floor systems. The author studied the full composite action between concrete slabs and steel joists in the elastic range. The principal variable of the study was the ratio of the flexural stiffness of the joist and slab. Two different methods of FE models were investigated. In the first model, the slab was represented by a combination of 16-node and 8-node solid three-dimensional prismatic elements and the joist was represented by plane stress elements. At a section of the structure, each steel beam flange was represented by one element and the web was represented by two elements. The authors found satisfactory convergence with this method but the preparation of data and analysis of output were time consuming. In the second model, the slab was represented by thin plate elements built up from the superposition of linear curvature triangles for the flexural stresses and linear strain triangles for the membrane stresses and the joist was represented by beam elements. The author found that the second model gives applicable output of bending moments and plane stresses.

Mofatt et al.[42] (1978) introduced a numerical study of the elastic longitudinal bending behaviour of composite box girder bridges in which the use of flexible shear connectors results in incomplete interaction between the slab and girder components. They used the finite element method in their analysis and the buckling and the inelastic behaviour were not considered. Some preliminary investigations were carried out to determine suitable finite element meshes for use in analysing the girders. The box girders, the slab and the reinforcement were represented by shell elements. The shear connectors were represented by linkage elements that allowed slip in the plane of the concrete-steel interface. It was assumed that the shear connection would be provided by 19 mm x 100 mm headed studs. On the basis of information given in Reference[43] (1963), the authors used constant slip modulus of the studs as $0.4x10^6$ N/mm. The authors highlighted the need for Codes of Practice to include design information on the stiffness and distribution requirements of the connectors in composite girders.

The load carrying capacity of composite beams under partial shear interaction was investigated theoretically by Dabaon et al.[44] (1993). The effect of the non-linear behaviour of the shear stud connector has been taken into consideration. Different ranges of shear interaction were used and both elastic and plastic load carrying capacities were calculated. A computer program was developed to carry out the analysis and the authors found good agreement between previous experimental and theoretical investigations. The authors stressed the importance of including the actual degree of interaction in order to get accurate results from the analysis of composite girders.

In 1994, Mistakidis et al.[45] introduced a numerical method taking into consideration the nonlinearities introduced in the analysis of long span composite girders. The authors have stated that the experimental data shows a non-linear behaviour for the load-deformation curve of the shear connectors joining the steel beam with the concrete slab. The influence of the behaviour of the connectors has been demonstrated through the analysis of a long span composite girder spanning 30.0m. The finite element method was used in modelling the composite girder. Bending finite elements with axial deformation possibility representing the concrete slab and the steel beam were used. Spring elements of zero length which can bear only shear force and obey the load-deformation law of the shear connectors were used to connect steel and concrete. The authors have concluded

that consideration of the actual load-deformation diagram of studs in the design of composite girders is needed and increases the safety of the beam at the serviceability limit-state.

In 1997, studies carried out by Oehlers et al[46] and by Oven et al.[47] investigated numerically the behaviour of composite steel-solid slab beams. Oehlers et al.[46] found that the maximum flexural capacity of composite beams in buildings, where the axial strength of the concrete section is usually much larger than that of the steel section, partial interaction has virtually no effect on the strength. Conversely, partial interaction can reduce the strength of composite beams with very strong steel sections, where the axial strength of the steel section is much greater than that of the concrete section. Also, it has been found that the greatest effect of partial interaction is to reduce the strain in the steel element and hence limit the beneficial effects of strain hardening. The work of the authors was part of an ongoing study and a computer model has been developed to carry out the parametric study.

Oven et al.[47] derived a two-dimensional non-linear inelastic finite element model for the structural analysis of steel-solid slab composite beams with flexible shear connection. The effects of slip between the steel beam and the concrete slab and the non-linear nature of force-slip characteristics of the shear connectors were included. The model was based on a two dimensional non-linear FE analysis program INSTAF, developed originally for steel frames by El-Zanaty[48]. The program used a line element with four degrees of freedom at each node to represent the steel I-section and the concrete slab. The material nonlinearities of the composite girder components have been incorporated. The author concluded that the model can be used to predict the load-deflection behaviour and the slip distribution along the length of the beam and the model has been validated by comparing the results with published test data.

Cai[49] (1998), in his analysis of cable stayed composite bridges, used a finite element model to represent the shear connection between a steel beam and a concrete slab. A two dimensional finite element was used in their analysis to model the steel beam and the concrete slab. The two elements are then connected via rigid links to model the shear connectors and hence they eliminated slip at the steel-concrete interface.

The composite connection between steel beam and solid concrete slab was modelled by Youn and Chang[50] (1998) using three-dimensional finite elements. The model consists of two layers of solid elements and three dimensional beam elements. Like Cai[46], rigid links were used between the concrete slab and the girders. Orthotropic reinforcing bars in the concrete slab were modelled by four layered elements as a smeared layer with constant thickness. The thickness of the smeared layer was equal to the area of each bar divided by the bar spacing. The finite element programme 'ABAQUS'[51] was used to analyse this model. The use of rigid links assumes that the interaction between the steel beam and concrete slab is complete and there is no slip between the shear connectors, which is not true and has been rejected by many researchers.

In 1999, Gattesco[52] studied numerically the non-linear behaviour of composite steel-solid slab beams with deformable shear connection. The numerical procedure accounted for the non-linear behaviour of concrete, steel and shear connector. The finite element package COBENA was used in the analysis. The steel beam and the concrete slab were modelled by using beam-type elements that have four nodal points with three degrees of freedom per node (horizontal and vertical displacements and rotation in the x-y plane). The interface between the steel beam and the concrete slab was modelled by two horizontal springs. The uplift of the concrete slab with respect to the steel beam and the buckling effects of the steel beam were neglected. The model was verified by comparing the finite element solutions with the experimental work of Chapman and Balakrishnan at Imperial College, London[53]. The author found good agreement between numerical and experimental results and concluded that this model can be used for extensive parametric studies on composite beams with complete or partial shear connection.

Kwak and Seo[54] (2000) modelled the behaviour of composite girder numerically using the finite element method. The aim of the study was to predict the long-term behaviour of composite steel-solid slab girders in bridges. A two-dimensional beam element that has three degrees of freedom (two translations and one rotation) has been used in the analysis to represent the steel beam and the concrete slab. Material nonlinearities have been taken into consideration. The elements were divided into imaginary layers to describe the material properties with the assumption that plane sections remain plane to represent the linearity in the strain distribution on any section at any time. The load-slip

characteristic of the stud has been neglected in the analysis and perfect interaction has been assumed between the steel beam and the concrete slab.

The finite element method had been used in the numerical modelling of steel-solid composite beams curved in plane by Thevendran et al.[55] (2000). The numerical model was used to verify the experimental testing aimed by the authors to study the ultimate load behaviour of these composite girders. The finite element software, ABAQUS, has been used in the analysis. Full composite action between steel beam and concrete slab was assumed Figure 2.14 Shows a typical finite element mesh with 1257 elements used by the authors in the analysis.

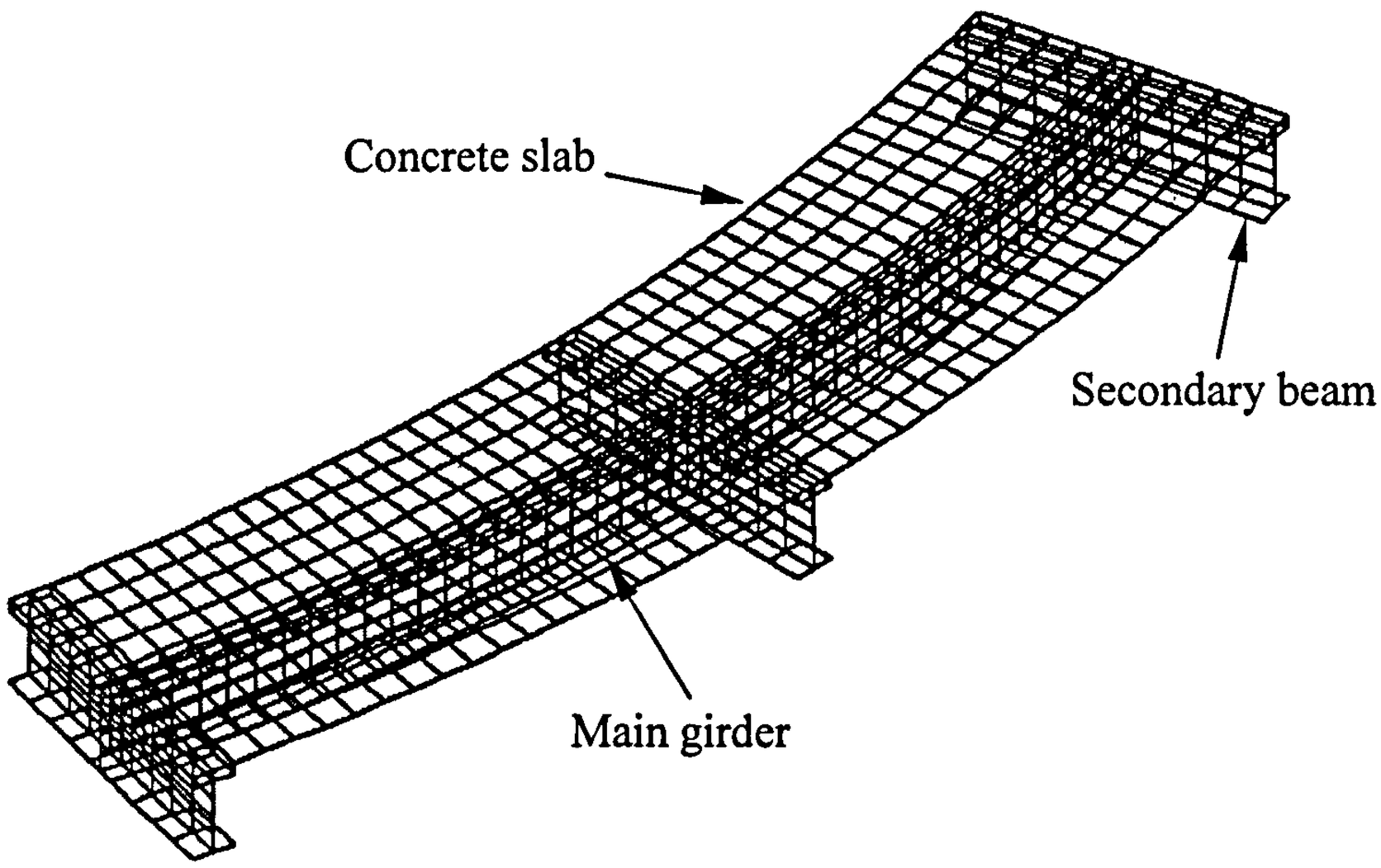

Figure 2.14 FE model of the composite beam modelled by Thevendran et al.[55]

Thevendran et al.[55] used three-dimensional finite elements to build his model. In the finite element model, the concrete slab was modelled by four-node isoparametric thick shell elements with the coupling of bending stiffness while the steel flanges and web were modelled by four-node isoparametric thin elements with the coupling of bending and stiffness. The shear connectors between concrete slab and steel flange were modelled by rigid beam elements. Rigid connection beam elements were used to model the shear studs based on the assumption that no slip occurs between the concrete slab and the steel girder. The material nonlinearities of the steel beam and the concrete slab

were accounted in the analysis. The authors found good agreement between experimental and numerical results in most of the cases. The observed discrepancies in some of the results between the values predicted numerically and that predicted experimentally is attributed to neglecting the slip at the steel-concrete interface by using rigid elements to represent the studs.

In 2002, Amadio and Fragiacomo[56] used the finite element method to model steel-solid slab composite girders. The model was used in studying the evaluation of effective width for serviceability and ultimate analysis. The ABAQUS[57] software was used in the parametric study carried out by the authors. In the model, the shell elements were used in modelling both the steel beam and the concrete slab. A non-linear elastic law represented the behaviour of the shear connection. The effects of steel and concrete material nonlinearities were taken into consideration. Although this research was applied on cantilever beams, the authors concluded that the numerical study demonstrated that the connection deformability affected the evaluation of the effective width of steel-solid slab composite beams.

A displacement-based finite element model for the analysis of steel-solid slab composite girders with flexible shear connection was developed by Faella et al.[58]. The model originally developed by improving the two-node one-dimensional displacement-based finite element. The research is still in press and the authors suggested that the model might be used in the accurate simulation of the behaviour of composite girders.

2.4.2 Numerical modelling of steel-precast HC slab composite girders

Only one numerical model has been found in the literature for simulating the behaviour of composite girders with precast hollow core slabs. This model was developed by Lam[59] (1998) to verify the experimental testing of composite steel-precast HC slab girders published later by Lam et al.[60] (2000). The finite element software ABAQUS[61] was used in the analysis. In the model, the concrete slab was modelled by using two-dimensional 8-node plane stress elements while the steel beam was modelled by using two-dimensional 4-node plane stress elements. Figure 2.15 shows the FE mesh used by Lam. The transverse reinforcement was not modelled as a separate element due to the limitation of the two-dimensional element used but its effect was taken indirectly into

account in simulating the shear connection behaviour. Both the precast HC slab and in-situ concrete were modelled as a single concrete element that had a breadth equals to the thickness of the precast HCU and with combined material properties. The shear connectors were modelled by using spring elements that obeyed the load-slip characteristic of the shear stud connector used. Lam concluded that, although the composite precast hollow core beam was modelled in a simplified way, the results obtained from the model showed good agreement with the experimental results. The model was used in carrying out extensive parametric studies that took into account the different parameters affecting the behaviour of composite steel-precast HC slab girders. This parametric study on composite girders with precast hollow core slabs has been published by Lam, Elliott and Nethercott[1] (2000). Also, from the results of the parametric study, design charts have been developed for initial sizing of composite girders by the authors[62] (2000).

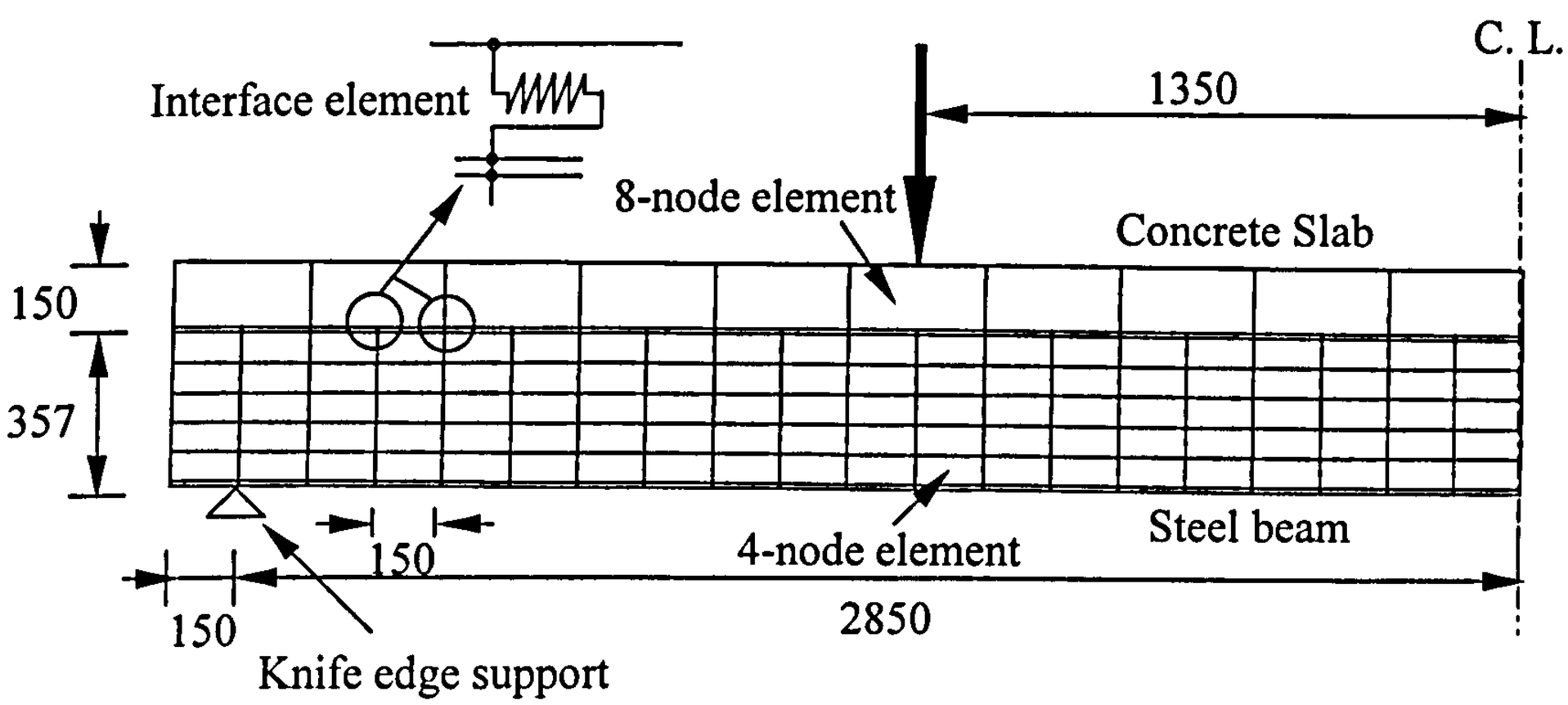

Figure 2.15 Finite element mesh of the composite beam used by Lam

Another simplified model has been developed for the numerical simulation of the shear connection in composite girders but with full depth precast decks. The numerical model was developed by Shim et al.[63] (2001) as a part of a study carried out to investigate design considerations of the shear connection in steel-concrete composite bridges with

full depth precast decks. The authors assumed that the shear connection was continuous and uniform along the beam and no separation took place at the interface. The finite element method has been used in the analysis and a composite beam element that has 12 degrees of freedom was developed. The shear stiffness of the shear connection was evaluated from linear elastic analysis and this in addition to the assumption of full interaction between steel beam and concrete slab limit the use of this model in an accurate finite element analysis.

3.3 Summary

The review of previous research presented in this chapter has indicated some conclusions that are summarized as follows:

1. The experimental work, represented by push-off tests, is mostly used in order to obtain the full load-slip curve and the failure load of shear connectors.
2. There is no closed-form analytical solution of the shear connection between steel and concrete.
3. The published experimental work dealing with steel-precast hollow-core slab push-off tests was very limited and most of the research concentrated on steel-solid slab push-off tests.
4. The finite element method has been used by many researchers in the numerical simulation for the behaviour of shear connectors in push-off tests and in composite girders and some of the researchers used the ABAQUS package in their analysis.
5. No work was found on simulating the behaviour of shear connector in steel-precast hollow-core slab push-off tests.
6. Some of the finite element models used with composite steel-concrete girders assume complete interaction between steel and concrete and represent the studs with rigid links. Other researches that took into consideration the actual behaviour of the shear connector were concentrated on composite steel-solid slab girders and only one model has been found dealing with steel-precast hollow-core slab girders.
7. Published research has shown that the consideration of the actual load-slip characteristic of the shear connector is of significance and increases the safety of composite girders at serviceability state.

In this research two accurate finite element models are developed to simulate the behaviour of headed stud shear connectors in steel-solid slab and steel-precast hollow-core slab push-off tests in details. The FE package ABAQUS[2] is used in the analysis and the FE results are compared with new experimental push-off tests with solid and precast hollow-core slabs. The obtained properties of the headed shear stud connector from both FE models are used in modelling the longitudinal behaviour of composite steel-solid slab and composite steel-precast hollow-core slab girders.

3. Finite Element Modelling of Headed Stud in Composite Steel Beams with Solid Slabs

3.1 Introduction

In this chapter a 3-D finite element model is developed using ABAQUS[2] to simulate the behaviour of headed shear stud connectors in composite girders with solid slabs. The model is validated against existing published experimental work and compared with data given in the current Code of Practices, which both demonstrate the accuracy of the model used. Also, the model will be validated against test results presented in chapter 5. Parametric studies using this model are performed to investigate variations in concrete strength and shear stud diameter on the shear connection behaviour. Discussion of the different modes of failure of headed stud shear connector in steel-solid slab push-off tests is presented.

3.2 Push-off test

The properties of shear connector most relevant to composite design are the shear capacity and the load-slip characteristic at the interface. The load-slip curve should ideally be found from tests on full-scale composite beams, but in practice, a simpler push-off test is adopted. Before going through FE modelling details, a description of the push-off test specimen is necessary since the main objective is to develop a finite element model that faithfully represents all aspects of the physical behaviour of the shear connection that have been observed in the push-off tests.

3.2.1 Description of push-off test specimen

A push-off test specimen is formed from a short length of steel beam that is connected to two small concrete slabs by means of shear connectors as shown in Figure 3.1. The slabs are then conventionally bedded down on mortar directly onto the reaction floor with load being applied to the upper end of the steel member. Slip between the steel member and the two slabs is measured at specified load or displacement increments, and the average slip is typically plotted against the load per connector. This push-off test specimen is similar to the standard push-off test specimen according to CP 117[5], but only one stud is connected to each flange since it

is assumed that the load is transferred equally from the steel beam to each shear connector. The predicted shear capacity will be independent of the number of shear connectors used in the experimental work and it can be obtained for different stud diameters by adjusting the finite element mesh only and without changing the concrete dimensions.

The push-off test specimen shown in Figure 3.1 consists of a 254x254x73UC and two concrete slabs attached to the flanges of the steel beam with dimensions of 619mm long, 469mm wide, and 150mm thickness for each slab. One stud connector is attached to each flange with a shank diameter of 19mm and 100 mm in height. The distance from the connector to the concrete edges, in the direction of loading, is taken 200 mm with a concrete recess over the steel beam equal to 50 mm similar to CP117[5]. In the perpendicular direction, it is taken as 300mm with total length of concrete slab 619mm similar to Eurocode 4[8].

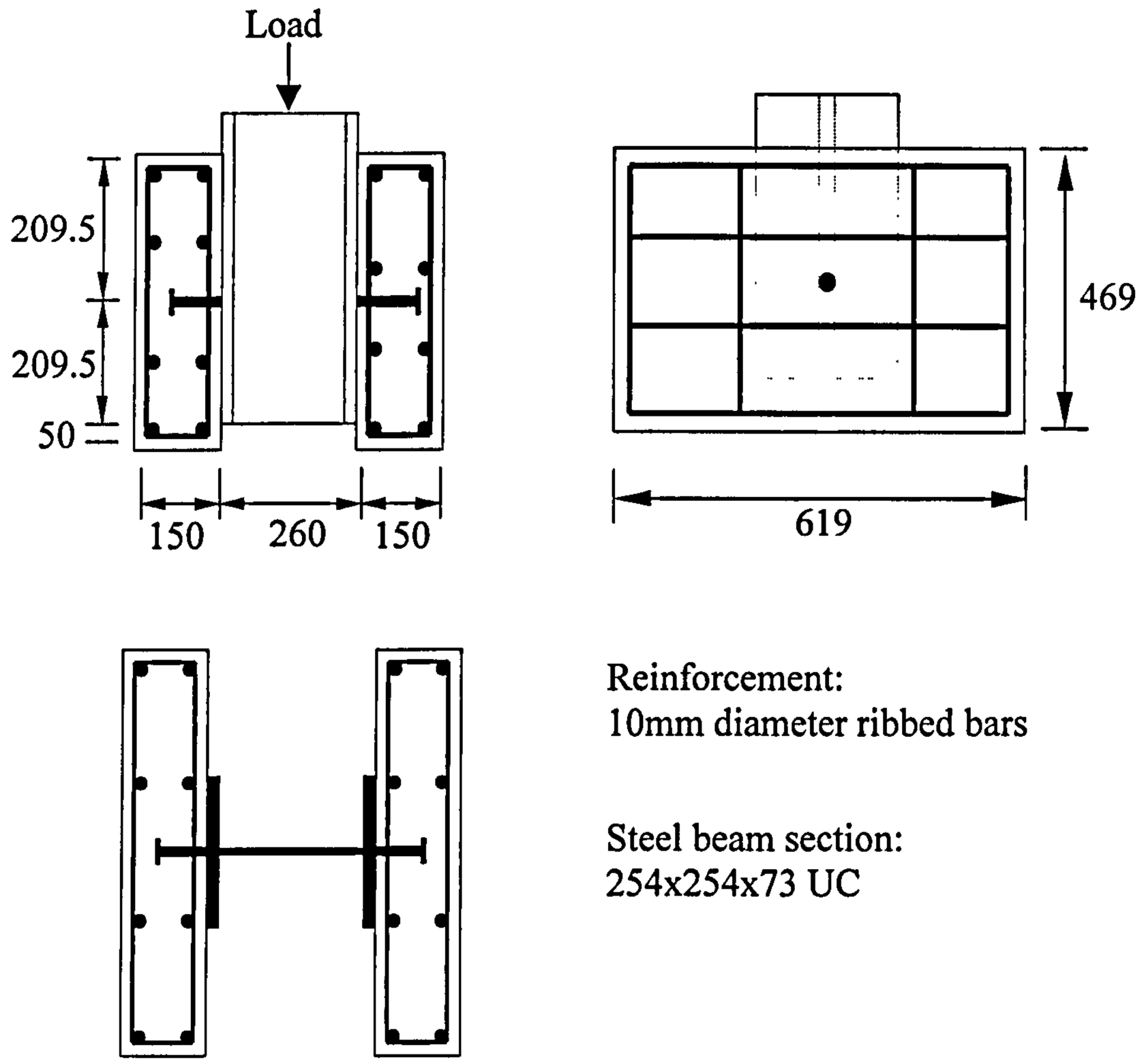

Figure 3.1 Details of push-off test specimen

3.3 Finite element modelling

In the next sections, brief description of the finite element method in general terms is given. The finite elements and other aspects of modelling that will be used in this study will be presented as well.

3.3.1 Finite element method

The finite element method is a numerical technique for analysing structures in which the structure is divided into small (finite) elements. The behaviour of the variables in each type of element is defined by a suitable shape function. From the shape function for each element, the stiffness matrix [k] is developed. Then the stiffness matrices are assembled into the global stiffness matrix. The applied load is arranged in a matrix known as the load matrix [F] expressed as follows:

$$[F]= \Sigma[K[[d] \qquad \text{.....(3.1)}$$

Then the displacement [d] at every nodal point is calculated. From the displacements, element stresses and strains are calculated.

3.3.2 Non-linear finite element analysis

In the linear analysis, it is assumed that the displacements of the finite element assemblage are infinitesimally small and the material is linearly elastic. In addition, it is assumed that the nature of the boundary conditions remain unchanged during the application of the load. If that condition is not satisfied, the problem is called non-linear. Non-linear problems may be due to finite deformation or/and due to the non-linear of material properties. Problems involving deformations of the order of the thickness are called geometrically non-linear problems. Problems involving non-linear stress-strain relation are classified as materially non-linear problems.

In linear problems, the overall stiffness matrix [K] is a function of geometry and material properties. Therefore the element matrix $[K_e]$ remains constant for linear problems, and hence is calculated once as:

$$[K_e]=_v\int[B]^T[D][B]dv \qquad \text{.....(3.2)}$$

where:

[D] is the material property matrix

[B] is the shape function matrix

In non-linear problems, the overall stiffness matrix [K] is a function of the current state of stress and strain. Therefore $[K_e]$ must be updated to take into account the changing material properties and/or the geometry with the current stress and strain. For non-linear problems, $[K_e]$ can be written as:

$$[K_e]=f(F,U) \qquad \text{.....(3.3)}$$

where:

F is the external forces

U is the displacement

Fig. 3.2 shows the basic effect of variation of the stiffness matrix in linear and non-linear problems.

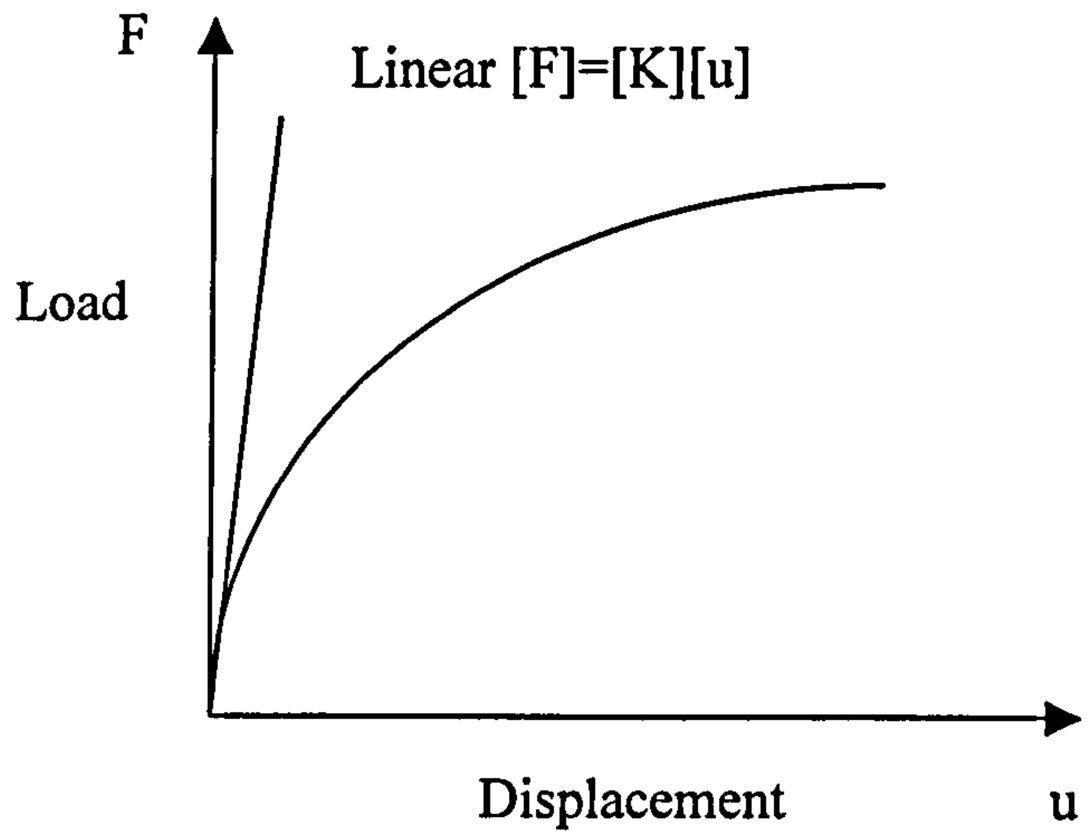

Figure 3.2 Stiffness matrix in non-linear problems

3.3.3 Numerical procedure in non-linear problems

There are two solutions techniques for non-linear problems:

1. The incremental procedure
2. The iterative procedure

In the incremental procedure the total load is divided into small increments and for each increment a new [K] is used. In the iterative procedure a constant [K] is used in

all increments. At first the full load is applied and iterations are performed to check that equilibrium is satisfied. After each iteration, the 'unbalanced' portion of the external force is estimated and applied in the next increment. The finite element software ABAQUS[2] used in this study uses a combination of these two methods. In addition it allows the use of modified RIKS method which assists in obtaining a solution for potentially numerically unstable cases, that are associated with buckling and/or yielding.

3.3.4 ABAQUS steps in creating and analysing a finite element analysis

The finite element package, ABAQUS, is a general purpose finite element program which offers linear and non-linear analysis capability for static, dynamic, heat transfer, soil consolidation and other problems. It is widely used in structural analysis, for which it provides a comprehensive element library and also provides a comprehensive material library allowing linear, non-linear elastic and elastic-plastic material modelling. Different loading procedures can be chosen to ensure efficient computation for a diverse range of problems. Input data are controlled by option blocks and modification of various features can be performed easily. To develop the model it is necessary to define the geometry of the model, material properties, boundary conditions, the load and request the results of interest.

3.3.4.1 Developing the model geometry

To construct the geometry of the model, all the nodes must first be defined by giving each node a number and then identifying the co-ordinates of the node. But it is not essential to write down all the nodes and their co-ordinates, since it is possible to give the co-ordinates of the principal nodes and their numbers and then to generate the intermediate nodes through some special commands (*NGEN, NFILL, NCOPY). After the node definition the next step is to define the elements. To define the elements, the required input is the element number, type of the element and the numbers of the nodes forming the element. As in the case of generating nodes, elements can also be generated from the master element, through special commands (*ELCOPY, * ELGEN). When using these special commands, the numbering of the nodes and elements must be maintained in a regular fashion.

3.3.4.2 Material properties

To define the properties of the materials, it is essential to divide the elements into specific sets. Then for each set of elements it is possible to assign individual material properties. Material properties for modelling purposes can be obtained from coupon tests of the material. From the test it is possible to obtain Young's modulus of elasticity, Poisson's ratio and the stress-strain curve. To define the ultimate static strength, the user must provide elastic and plastic yield strength and can also define the strain hardening properties. All properties come from the material's uni-axial δ-ε curve.

3.3.4.3 Boundary conditions

To define the support condition or to establish symmetry, appropriate restraints on nodes or node sets are required. Nodes can be restrained for any/all displacements or any/all rotations, or for both.

3.3.4.4 Loads

The magnitude, type (distributed, concentrated, line etc.), direction and the node number or the node set or element over which load acts must be given. It is also possible to define the initial values of applied load. The condition for terminating the analysis can also be defined (at a certain displacement/rotation at certain node, load magnitude etc.).

3.3.4.5 Output request

After defining the model geometry, material properties, boundary conditions, and loads, the results from the analysis can be obtained in different formats. Outputs can be created in TEXT format (.DAT) or in ASC II format (.FIL, .RES) which can be post processed. Through the use of the (*RESRART) option, it is possible to create a graphic results file (.RES) for any required results (displaced shape, rotation contour, stress contour etc.).

3.3.5 Mesh fineness

It is possible to make a few initial runs to decide how fine the mesh should be. Results from each run can be compared and a mesh density can be identified, beyond

which making a finer mesh will not affect the results of the analysis. The mesh should be finer at the location of points of interest and stress concentrations, elsewhere it can be made gradually coarser. In this study the area which includes the stud connector in the concrete slab and steel beam had a finer mesh and gradually the element size was increased away from it. To produce accurate results it is good practice to keep the aspect ratio of the elements (for shell elements the ratio of the length to width, for solids the ratio of the largest and smallest dimension) close to unity. Usually if the aspect ratio is larger than five, in the region of interest, the results may be inaccurate.

3.3.6 Main elements in use

There are different elements available in the ABAQUS manual. The aim of this section is to describe these elements to choose the most appropriate ones for modelling the shear interaction connection aimed by this study.

3.3.6.1 Shell elements

These elements can be used to model composite girders. Their use requires a smaller number of nodes to model the different components. These elements generally have five degrees of freedom per node; if the in-plane rotation is considered, they become six. The elements are divided into five layers through their thickness and only one node is required through the thickness. The structure of the shell finite element is shown in Figure 3.3. Several types of shell element are available with the ABAQUS suite including four, eight and nine node quadrilateral elements and various forms of triangular elements see Figure 3.4. The main advantage of these elements appears in problems involving bending stresses of initially curved structures and buckling analysis.

- Nodes

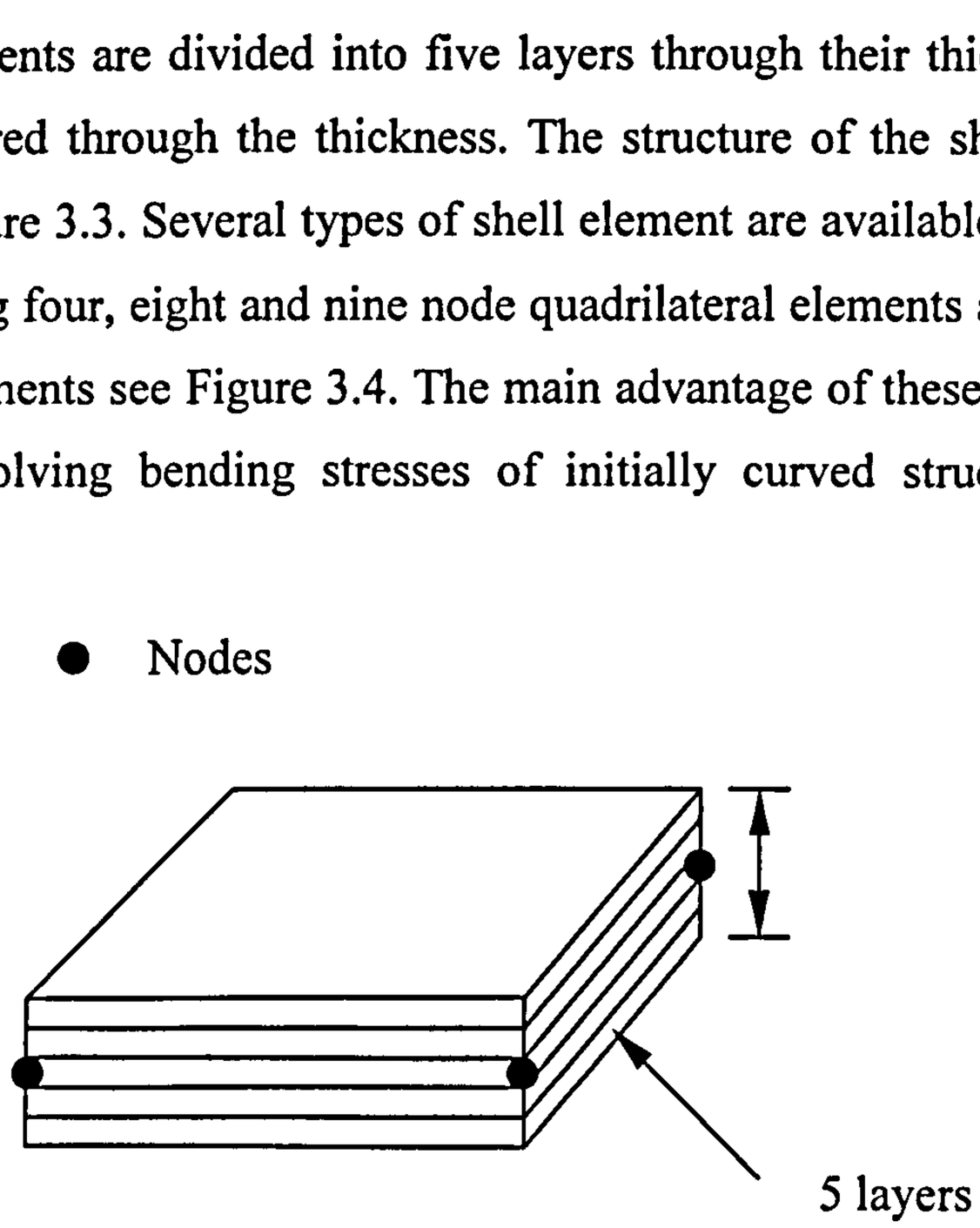

Figure 3.3 Structure of a shell finite element

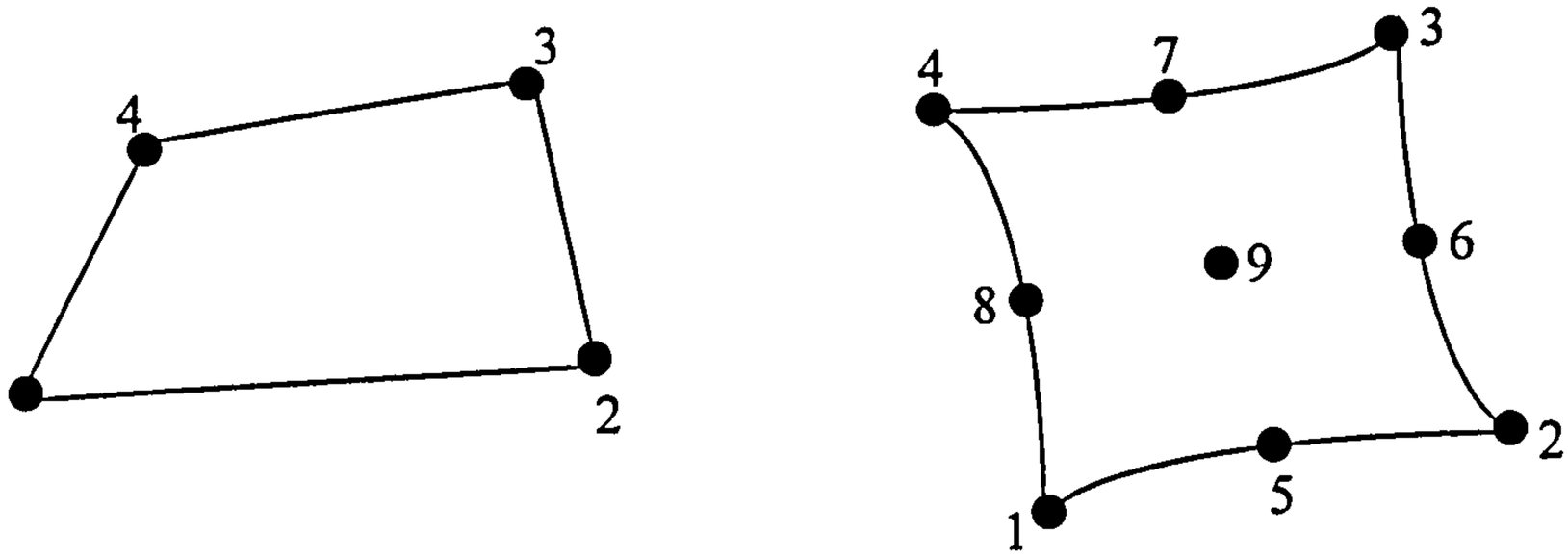

4-Node element　　9-Node element

Figure 3.4 Configuration of four-node and nine-node shell elements

3.3.6.2 Beam elements

These elements allow for bending and stretching actions. They are available in two different formats, in the ABAQUS software, in plane (two displacements and in-plane rotation per node), and three-dimensional (six degrees of freedom active at each node). They can be of various cross sections, i.e. rectangular, circular, I-section, L-section, and general section. The linear and quadratic beam elements include transverse shear deformation and it is ignored in cubic beams.

3.3.6.3 Flexible elements

There are two important elements provided in the ABAQUS. First of them is JOINTIC element which is provided to model the interaction between two nodes which are almost coincident geometrically and which represent a joint which has internal stiffness. The other element is the SPRING element which is used to model the interaction between a node and ground, two nodes in a fixed direction and two nodes with its line of action being the line joining the two nodes. The spring behaviour may be linear or non-linear. The JOINTC elements will be used in simulating the behaviour of studs in the analysis of composite girder explained in chapter 7.

3.3.6.4 Three-dimensional solid elements

There are different types of three-dimensional solid elements available in the ABAQUS. The name of the element depends on the number of nodes that the element contain for example, element C3D4 has four nodes and element C3D8 has

eight nodes and so on. Figure 3.5 shows some types of these elements and node ordering which must be taken into consideration when defining these elements. There are three active translational degrees of freedom at each node. These elements provide accurate results in general cases with fine meshing. Solid elements are provided with first-order (linear) and second order (quadratic) interpolation. Standard first-order elements are essentially constant strain elements but second-order elements are capable of representing all possible linear strain fields. Solid elements provide the most locations at which some components of the gradient of the solution can be discontinuous (such as element edges). In this study, combinations of 3-D solid elements shown in figure 3.5 are chosen to model the behaviour of headed stud shear connector in composite girders because of the following reasons:

1. Three-dimensional elements gave adequate accuracy with less solution time in modelling shear interaction problem.
2. It can represent all different components of composite girder with compatible pattern.
3. It defines accurately the boundaries of the composite girder components with less number of interface elements usually needed to connect the model.

3.4 Present finite element model of steel-solid slab push-off test

To obtain an accurate result from the finite element analysis, it is necessary to make the test set-up and the finite element comparable. This means that the model in the finite element analysis should represent the experimental procedure used in the laboratory as closely as possible.

3.4.1 Finite Element Mesh of the model

Combinations of three-dimensional solid elements, which are available in the ABAQUS[2] software, are used to represent the push out specimen. These combinations are the three-dimensional eight-node element (C3D8), the three-dimensional fifteen-node element (C3D15), and the three-dimensional twenty-node element (C3D20) shown in Figure 3.5. In the modelling of the concrete slab around the stud, C3D15 elements are used and C3D8 elements are used elsewhere. The shank of the stud consists of C3D15 elements and the stud head consists of both C3D15 and C3D20 elements. The width of the head is 1.5 the stud diameter and its thickness is 0.5 the diameter.

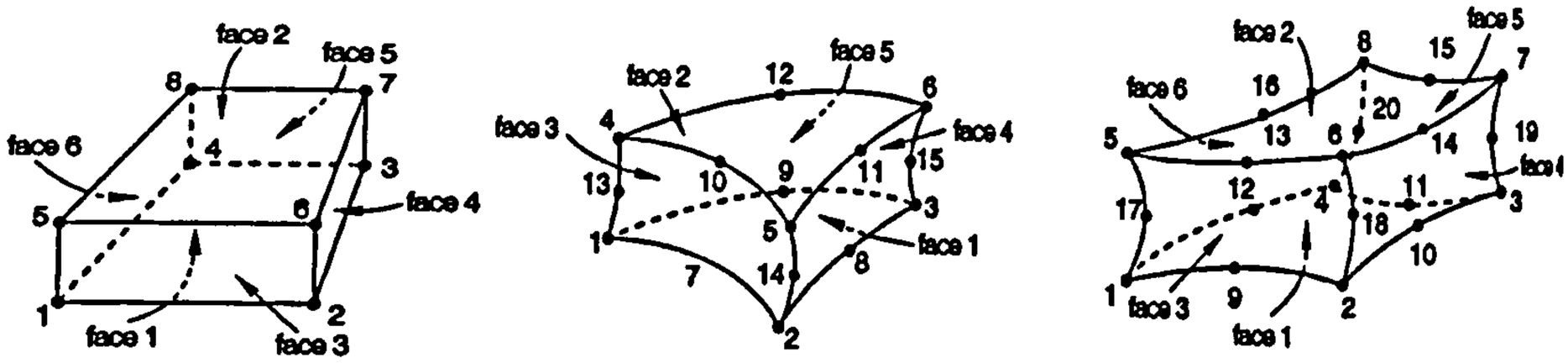

C3D8 element C3D15 element C3D20 element

Figure 3.5 Three-dimensional solid elements

Figure 3.6 shows the finite element FE mesh used to represent the shear interaction between the steel beam and the concrete slab using 19mm x 100mm stud. At the beginning different FE meshes are examined to choose the most appropriate one that gives adequately accurate results and takes less time in the solution process. Because of symmetry, only quarter of the push out arrangement is modelled. The half of the concrete slab is divided into 22 elements along X-direction, 16 elements along Y-direction and 3 elements along Z-direction. The half of the shank of the shear connector consists of one C3D15 element in X-direction, one element in Y-direction and two elements along Z-direction. The half of the stud connector consists of one C3D15 element and two C3D20 elements along X-direction and one element in Y-direction and one element in Z-direction. The mesh is fine and the aspect ratio satisfies the limits of the three dimensional solid elements. The flange half of the steel beam is divided into 4 elements along X-direction, 2 elements along Y-direction and one element in Z-direction. The web quarter of the steel beam is divided into 6 elements along X-direction, 1 element in Y-direction and one element in Z-direction. Push off tests carried by Jayas[26] explained that separation of the concrete behind the shear connector occurred at low load level. This is attributed to the failure of the bond between the stud and the concrete slab behind. According to this observation, only the nodes in front of the stud, in the direction of loading, are connected with the surrounding concrete nodes and other nodes of the stud are detached from that of surrounding concrete. The same approach has been used by Kalfas et al.[39] to eliminate additional stiffness added at the area behind the stud and to avoid the use of interface elements needed to model the behaviour of the bond between the stud and the concrete behind. In addition, the use of interface elements creates difficulties in terms of convergence.

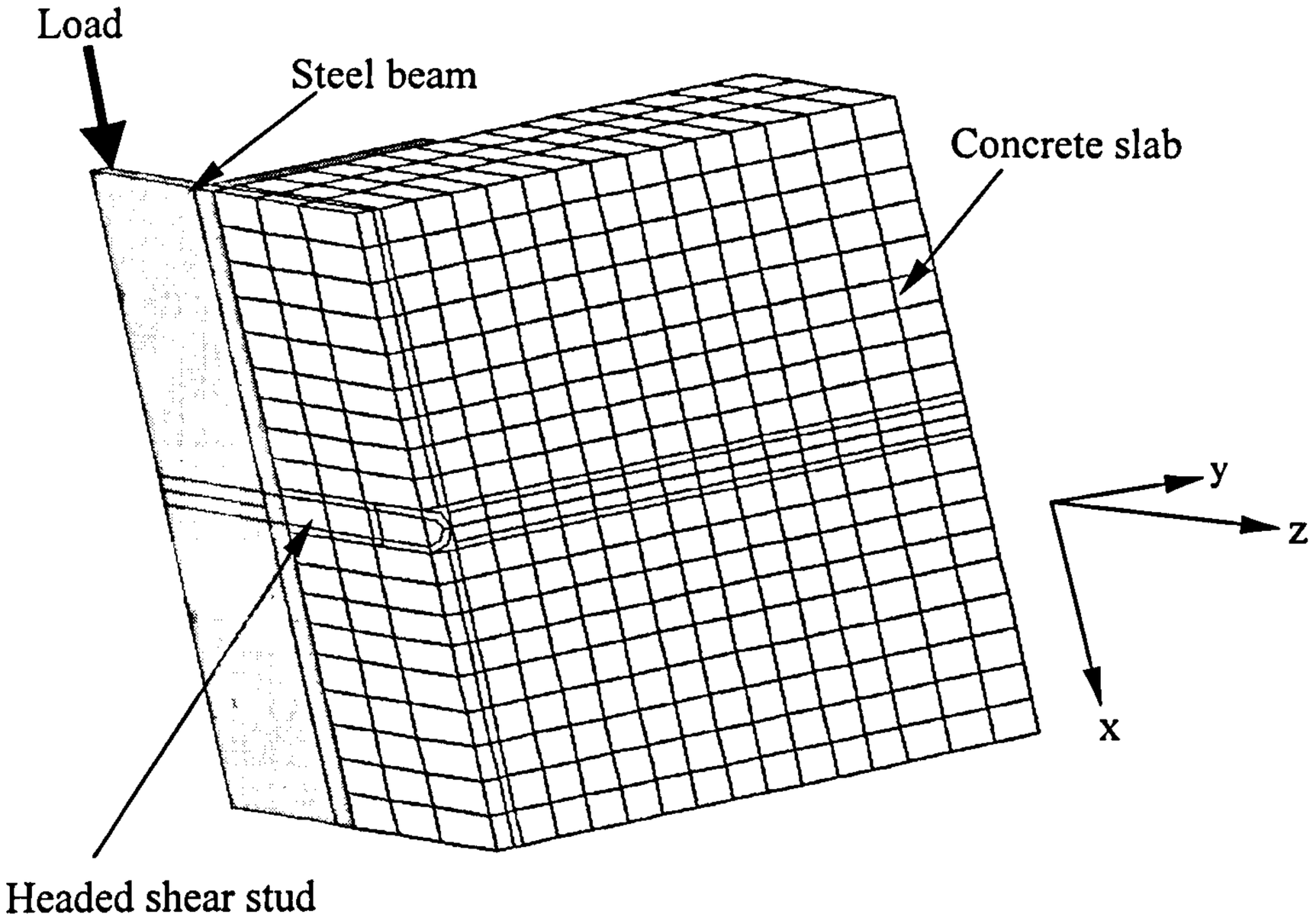

Figure 3.6 Finite element mesh of the model

3.4.2 Boundary conditions

For the application of the support conditions, all nodes of concrete slab in the opposite direction of loading (surface 1) are restricted to move in X-direction to resist the compression load. All nodes along the middle of steel beam web (surface 2) are restricted to move in Z-direction due to symmetry. All concrete nodes, stud nodes, steel beam flange nodes, and steel beam web nodes which lie on the other symmetry surface (surface 3) are restricted to move in Y-direction because of symmetry as shown in Figure 3.7.

3.4.3 Application of load

A static concentrated load is applied at the centre of the steel web as shown in Figure 3.7. This load is applied using the modified RIKS method available in the ABAQUS[2] software. The basic algorithm of this method is the Newton method in which, the solution is obtained as a series of increments with iterations to obtain equilibrium within each increment. The RIKS method is generally used to predict unstable and non-linear collapse of a structure. It uses the load magnitude as an additional unknown and solves simultaneously for loads and displacements. Therefore, another quantity must be used to measure the progress of the solution. ABAQUS uses the arc

length along the static equilibrium path in load-displacement space. An initial increment of displacement is given on the data line and the initial load proportionality factor is equal to this initial increment using the automatic incremental scheme. This initial increment will be adjusted if the increment fails to converge. From then on, the value of load after each increment is computed automatically. The solution ends either by specifying the maximum value of the load or a maximum displacement value at a specified degree of freedom.

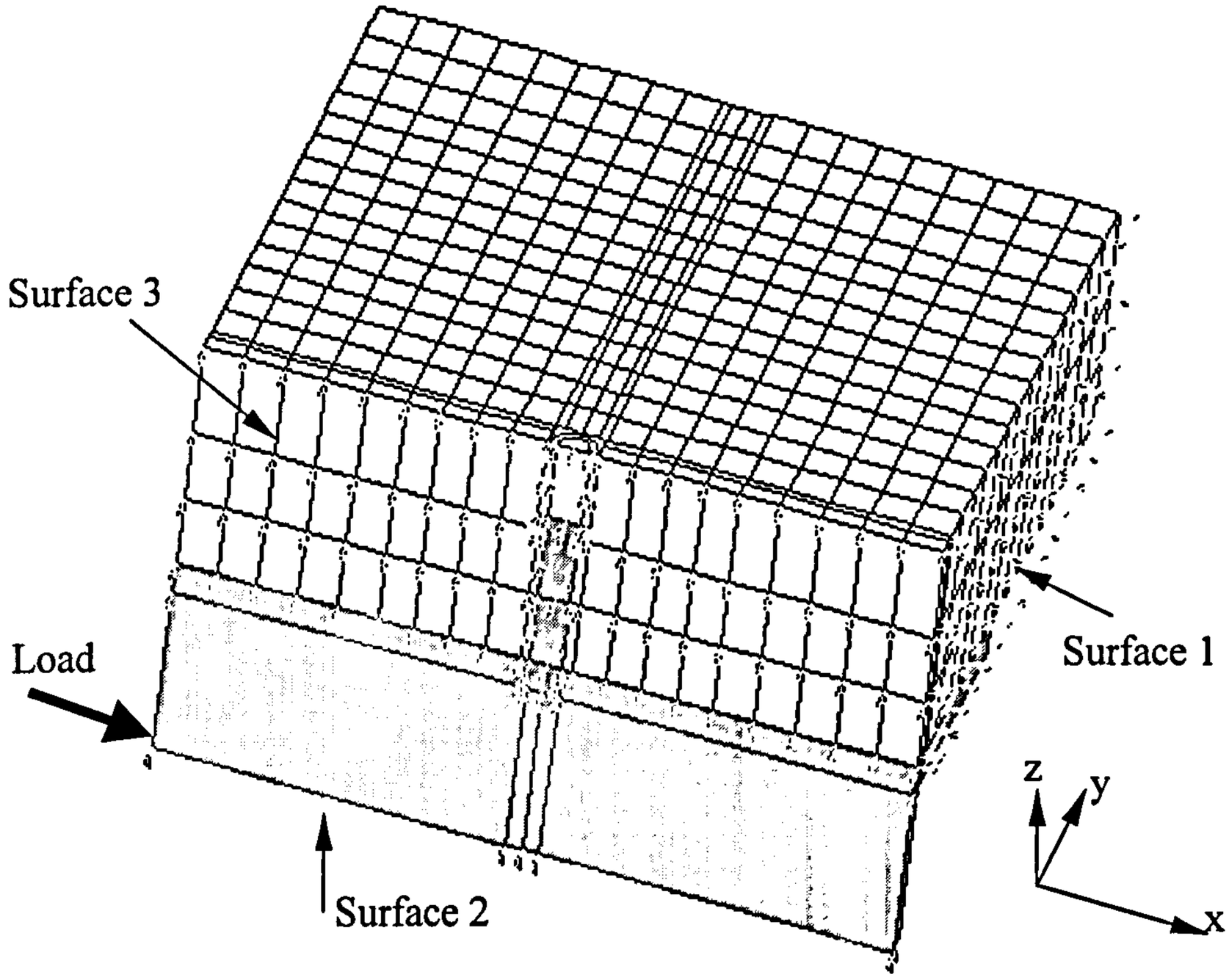

Figure 3.7 Finite element model of push-off test specimen

3.4.4 Material model of concrete

In a push-off test, the concrete slab is subjected mainly to compression stresses associated with tensile splitting stresses. Initially, the ABAQUS concrete model was used in which the concrete is simulated close to its actual behaviour. This resulted in premature failure due to tensile splitting of concrete. To avoid this problem concrete is treated as an elastic-plastic material as shown in figure 3.8. The model assumes that the reinforcement bars are smeared within the concrete elements, to prevent tensile splitting, and are not modelled separately. The option (*PLASTIC) is used to specify the plastic part of the material model for elastic-plastic materials that use the

Mises yield surface. It is assumed that the concrete behaves as a linear-elastic material up to the yield stress. Perfect plasticity is obtained when reaching the yield stress. For the elastic part of the stress-strain curve, it is required to identify both Young's modulus and Poisson's ratio for concrete. For the plastic part of the stress-strain curve, it is required to identify the yield stress. Following the BS 8110[65], average values of yield strain, Young's modulus of concrete and the yield stress can be calculated from the following relations:

$$\varepsilon_{yc} = .00024 \sqrt{f_{cu}} \quad \text{.....(3.4)}$$

$$f_{yc} = 0.8\, f_{cu} \quad \text{.....(3.5)}$$

$$E_c = f_{yc}/\varepsilon_{yc} \quad \text{.....(3.6)}$$

where:

E_c : Young's modulus of concrete

f_{cu} : the cube strength of concrete

f_{yc} : the yield stress of concrete

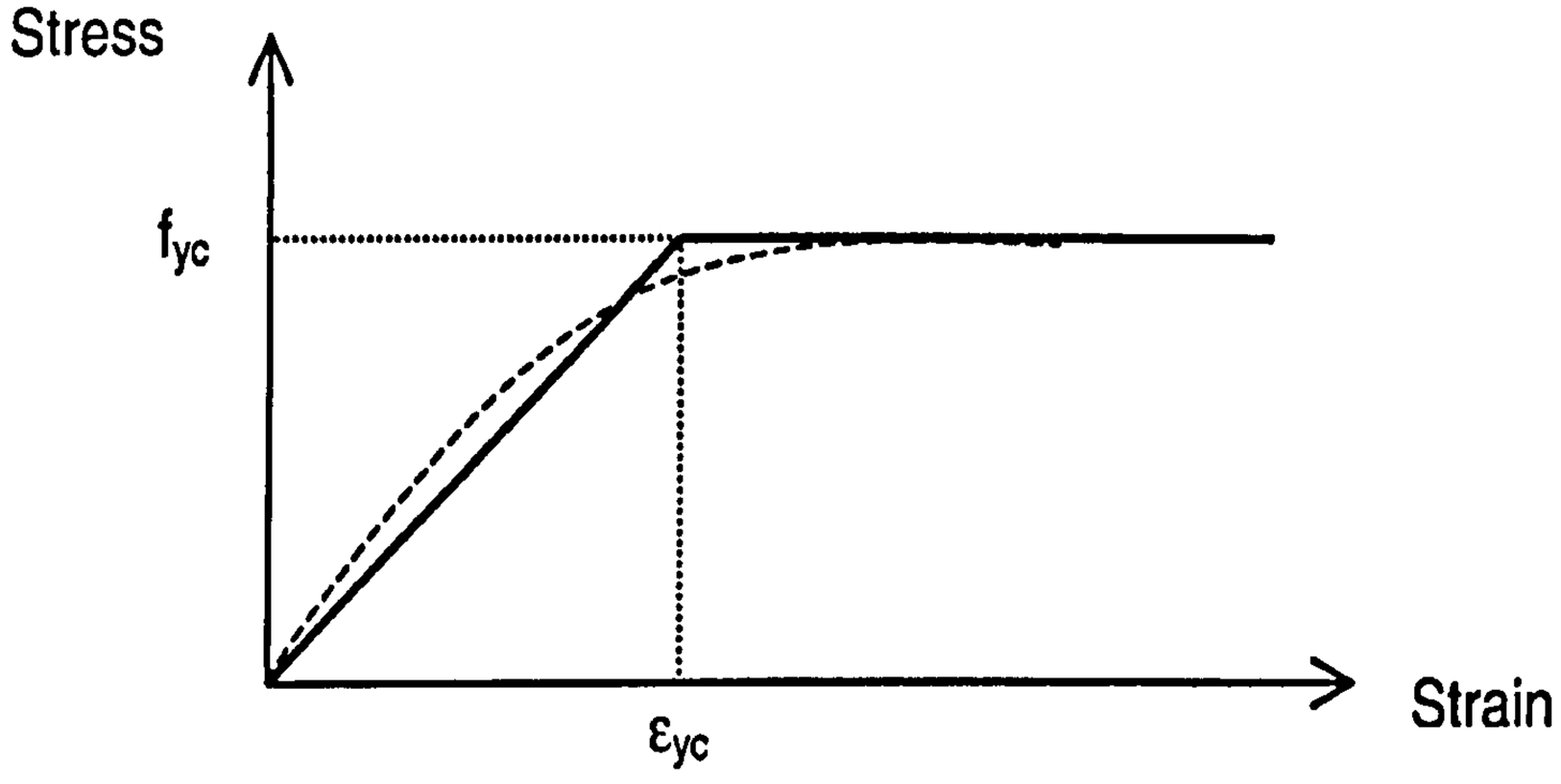

Figure 3.8 Bilinear stress-strain curve for the concrete model

3.4.5 Material model of headed shear stud

The shear stud material is of great importance in modelling the shear interaction between steel and concrete since the region around the stud is a region of severe and complex stresses. The shear forces are transferred across the steel-concrete interface by the mechanical action of shear connectors. To determine the mechanical properties of the stud material, three coupons were machined from the headed studs.

The average of the three coupon tests was 470.8 N/mm^2. This average is taken as the maximum allowed yield stress, f_{ys}, in simulating the stud material. The stress-strain curve of headed stud is shown in Figure 3.9 together with the simulated bilinear stress-strain model. The stud material model behaved as linear elastic material with Young's modulus E_s up to the yield stress of stud, f_{ys}. After this stage, it becomes fully plastic. In the present study, the following values are used for the stud material.

E_s : 200000 N/mm^2

f_{ys} : 470.8 N/mm^2

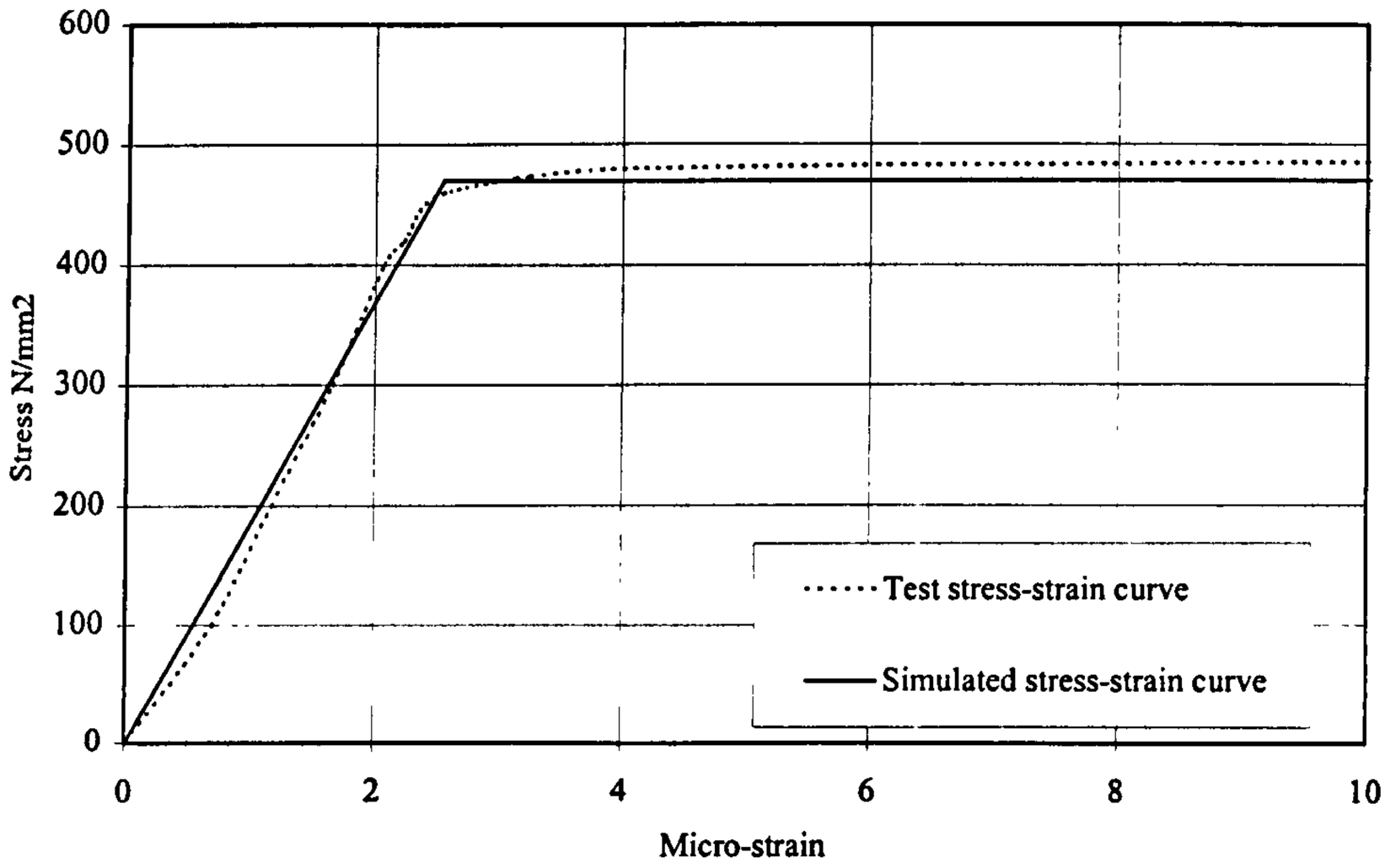

Figure 3.9 Bilinear stress-strain curve for the headed stud

3.4.6 Material modelling of steel beam

The steel beam is modelled with yield stress of 275N/mm^2 in this study using the same bilinear curve shown in Figure 3.9. It is believed that the effect of the steel beam is insignificant in a push-off test. Its function is to allow for the transmission of applied load to the connectors and hence the characteristic load-slip characteristic in the steel-concrete interface can be studied.

3.5 Modes of failure

In experimental test, the ultimate capacity of the shear connector is determined when the maximum load from the push-off test is observed. Although the push-off

measured strain and displacement with increasing load provide a valuable insight into the problem, it is very difficult to determine the exact failure mode of the specimen. Generally, three modes of failure were observed from the push-off test. The first mode of failure is the concrete cone failure where no stud failure is observed. For this mode of failure, the concrete around the stud started to fail before the stud yielded, the failure progresses through the thickness of the concrete forming a conical shape around the stud as shown experimentally by MacMackin et al.[64]. The conical failure planes are shown in Figure 3.10.

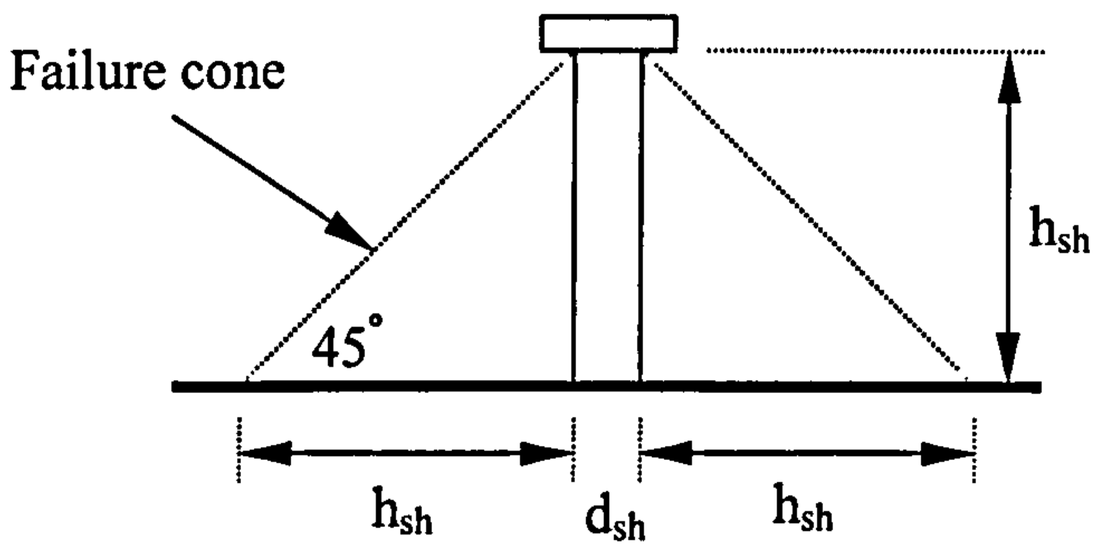

Figure 3.10 Conical failure planes

The second mode of failure is that the stud connector was fully yielded and no concrete failure is observed. This mode of failure is identified as stud failure mode where the yield stress is reached by the stud element while full yielding of the concrete elements around the stud is not reached.

Finally, the third mode of failure is the combined failure of stud and concrete slab when maximum stresses are reached in stud and concrete elements. All three modes of failure were observed in the experimental push-off tests.

By using the ABAQUS post-processing package, it is possible to follow the stress distribution across the stud and the concrete slab of the finite element model at each load increment. In addition, from data files, the load at each increment can be obtained. Therefore, the modes of failure can be easily observed and failure capacity can be determined.

3.6 FE model results from simulating present push-off tests

Four push-off test specimens were simulated using the present FE model. Each of these tests will be discussed separately in the next paragraphs. All the simulated push

off tests had 19mm diameter x 100mm height headed studs. The main variable in these tests was the concrete cube strength. The maximum failure load, the load-slip characteristic of the 19mm diameter x100mm height and the distribution of stresses at each load increment were obtained.

3.6.1 Test S1

Figure 3.11 shows the load-slip curve of the stud obtained by the finite element model. The simulated test specimen had concrete cube strength of 50N/mm^2. The maximum load obtained by the finite element solution was 133.4kN at a slip of 9.26mm. The cause of failure was due to yielding of the stud.

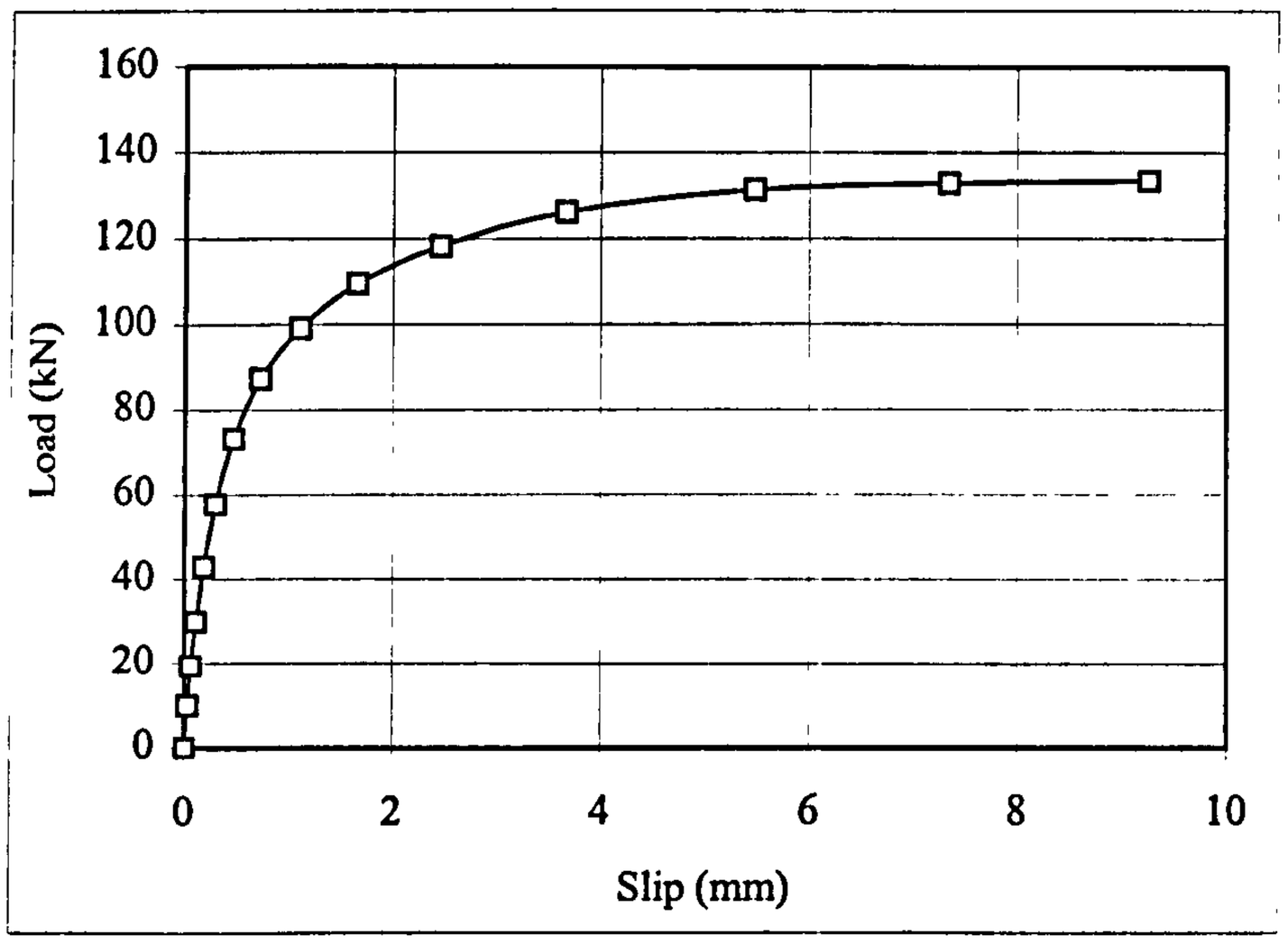

Figure 3.11 Load vs. slip curve of the stud for push-off test S1

The stress contour and deformed shape is plotted in figure 3.12 by using the ABAUS post processing at different load levels. It can be seen that, because of higher concrete strength the upper surface remains unstressed and the conical failure explained previously is not reached while the stud had already yielded when looking through the data files. It is also shown that, the concrete around the headed stud was intact and double curvature bending of the stud was noted.

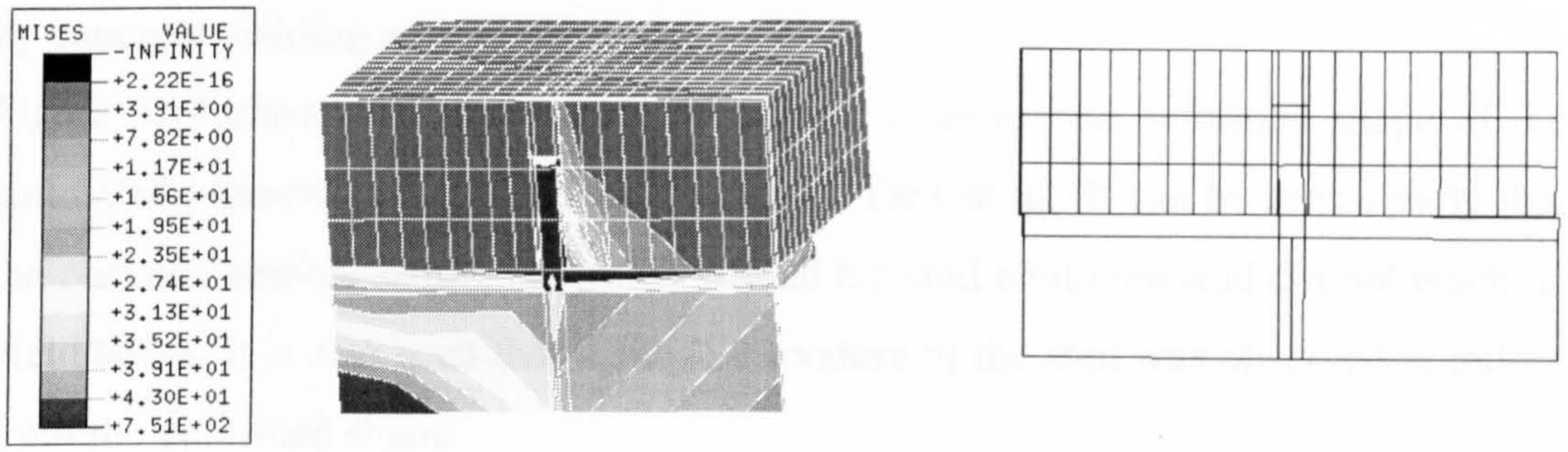

Figure 3.12.a Load level of 58kN

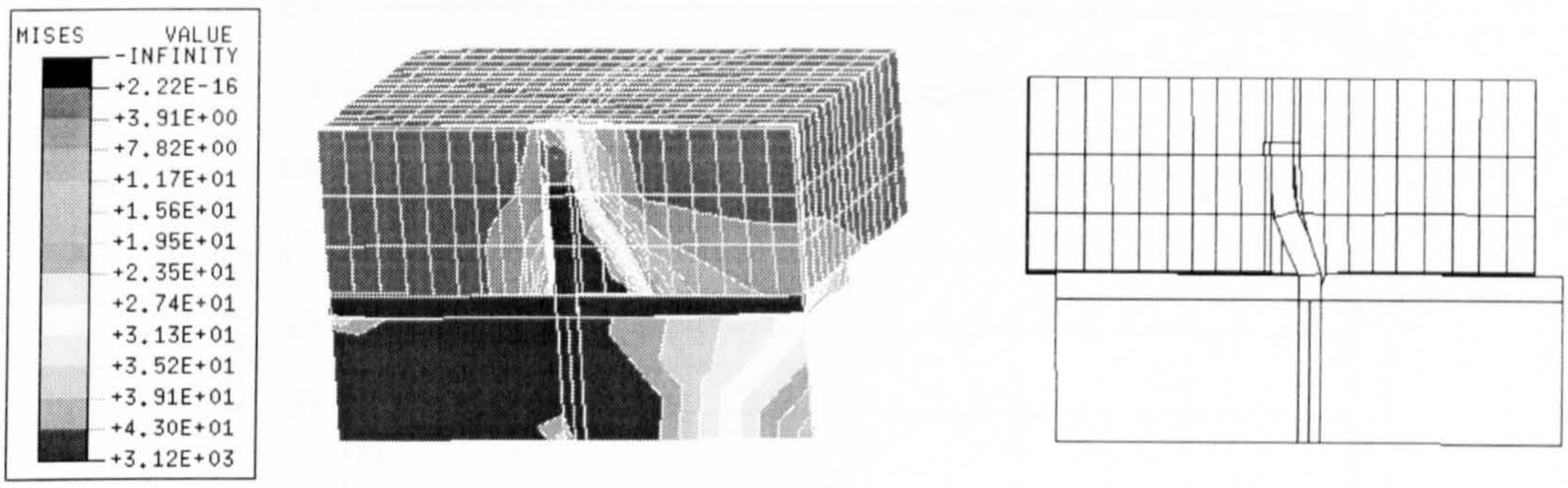

Figure 3.12.b Load level of 118kN

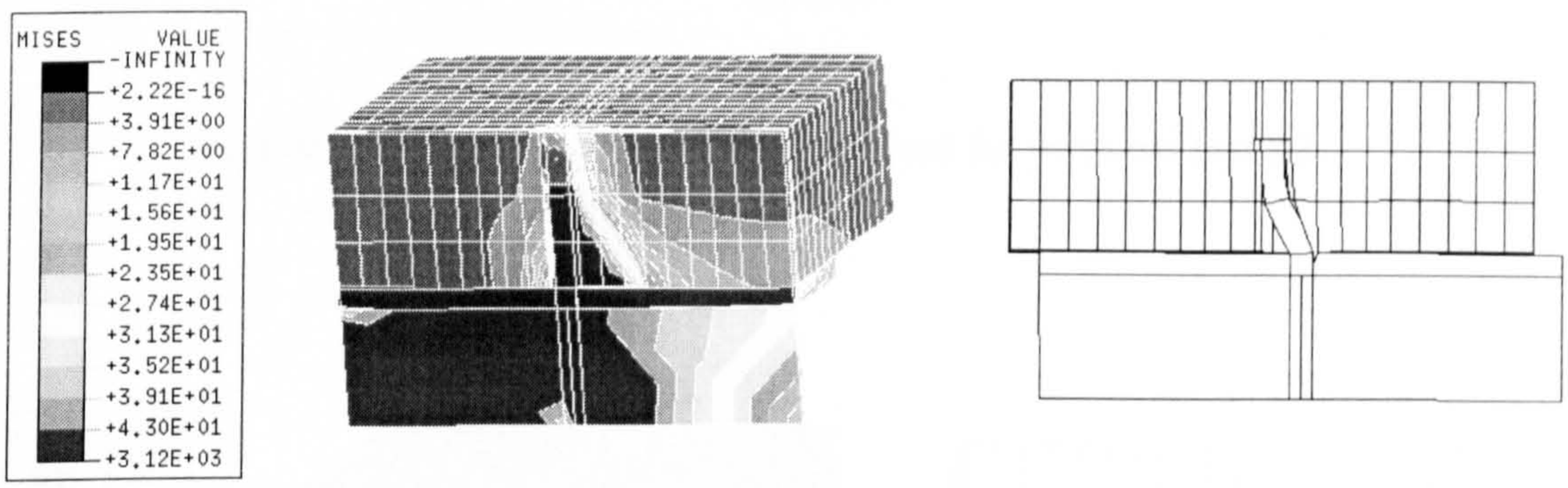

Figure 3.12.c Load level of 133kN

Figure 3.12 Stress contour and deformed shape of FE-S1

3.6.2 Test S2

In this simulated push-off test specimen, the concrete has cube strength of 20N/mm^2 and the same 19mm-diameter x 100mm-height stud is used. Load vs. slip for test S2

is shown in figure in figure 3.13. The maximum failure load obtained from present finite element model was 73.1kN at a slip of 5.2mm. The failure is mainly obtained by concrete yielding around the stud.

Figure 3.14 shows the distribution of contour stresses and deformed shape of the simulated push-off test at different load levels for test S2. It can be seen clearly that the concrete conical failure is formed around the stud while the stud did not reach its yield stress. It is also seen that a single curvature of the stud was observed at failure from the deformed shape.

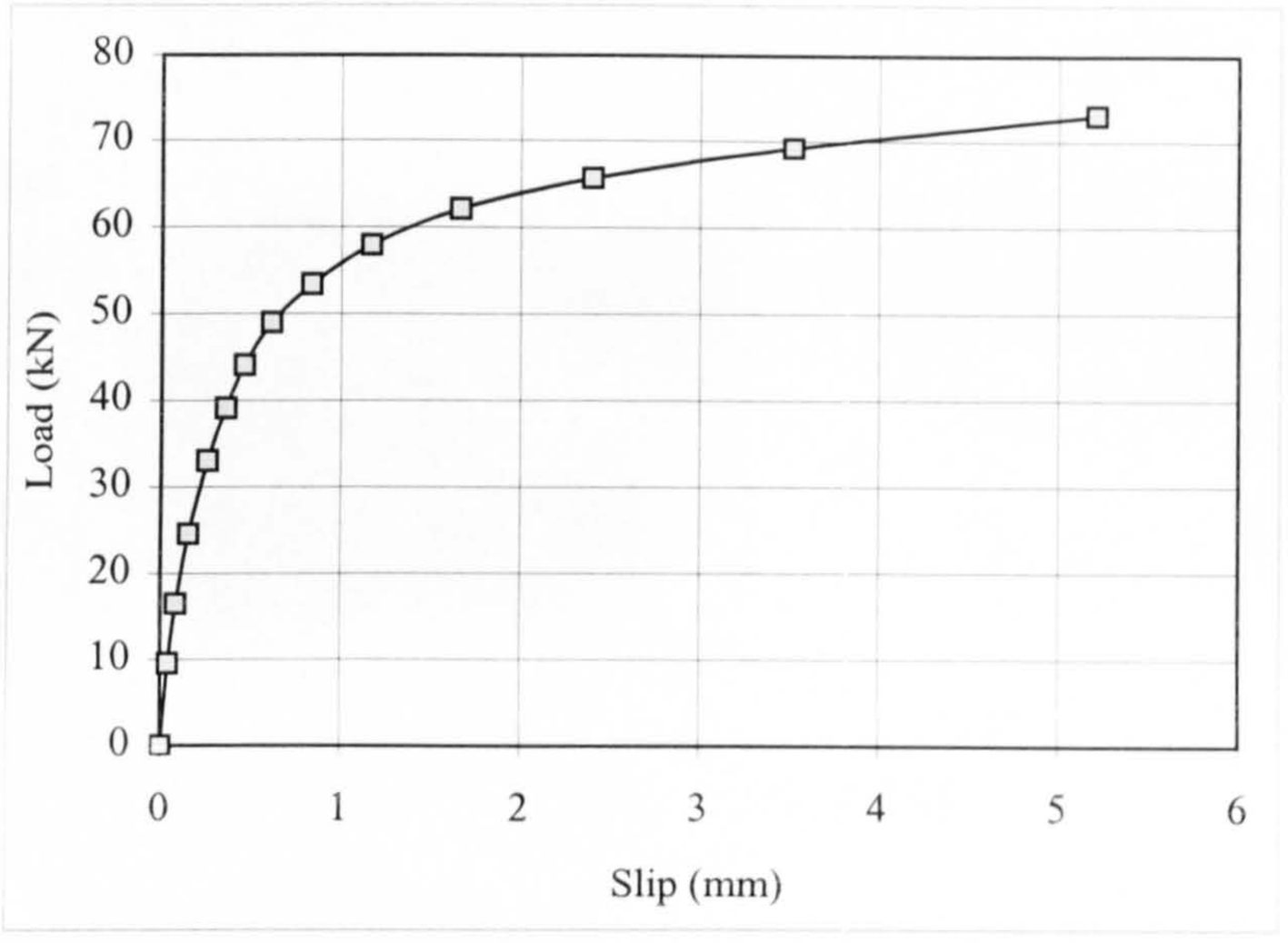

Figure 3.13 Load vs. slip curve of the stud for push-off test S2

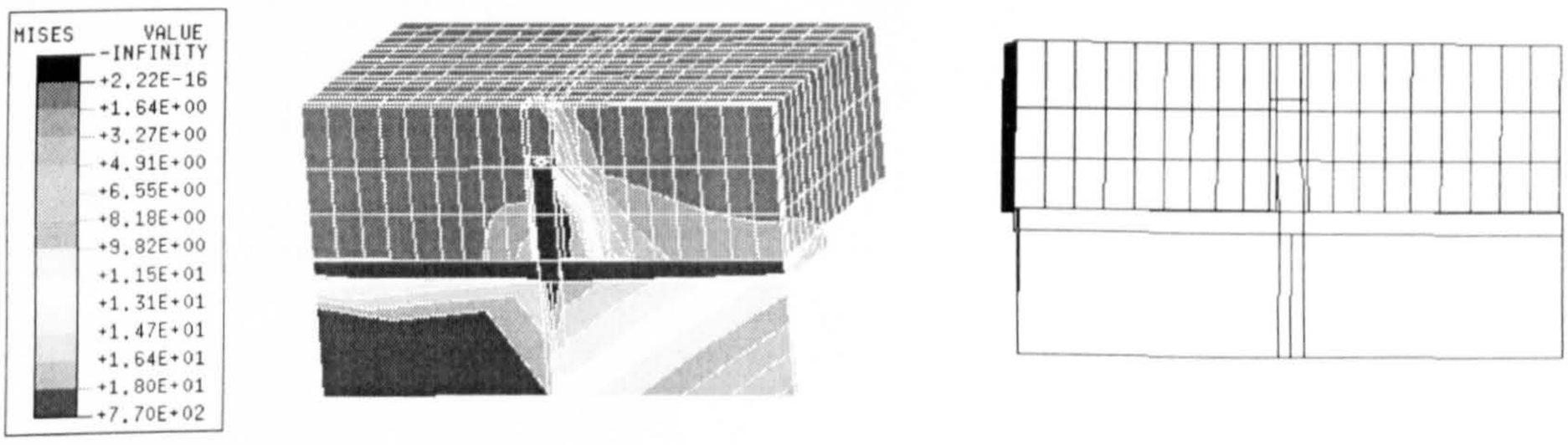

Figure 3.14.a Load level of 39kN

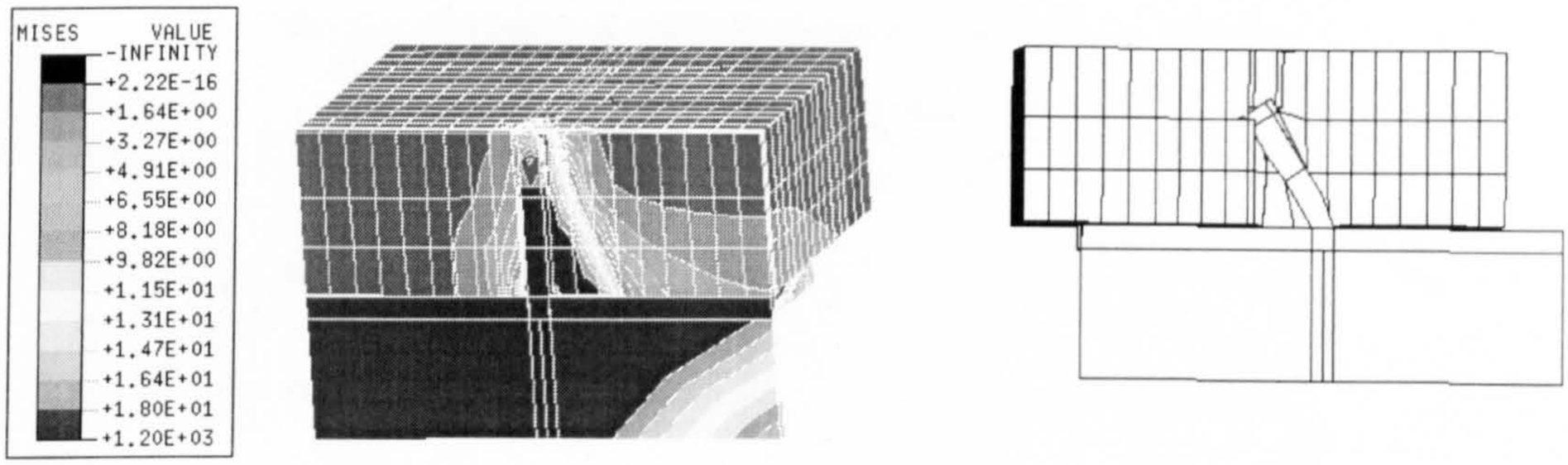

Figure 3.14.b Load level of 58kN

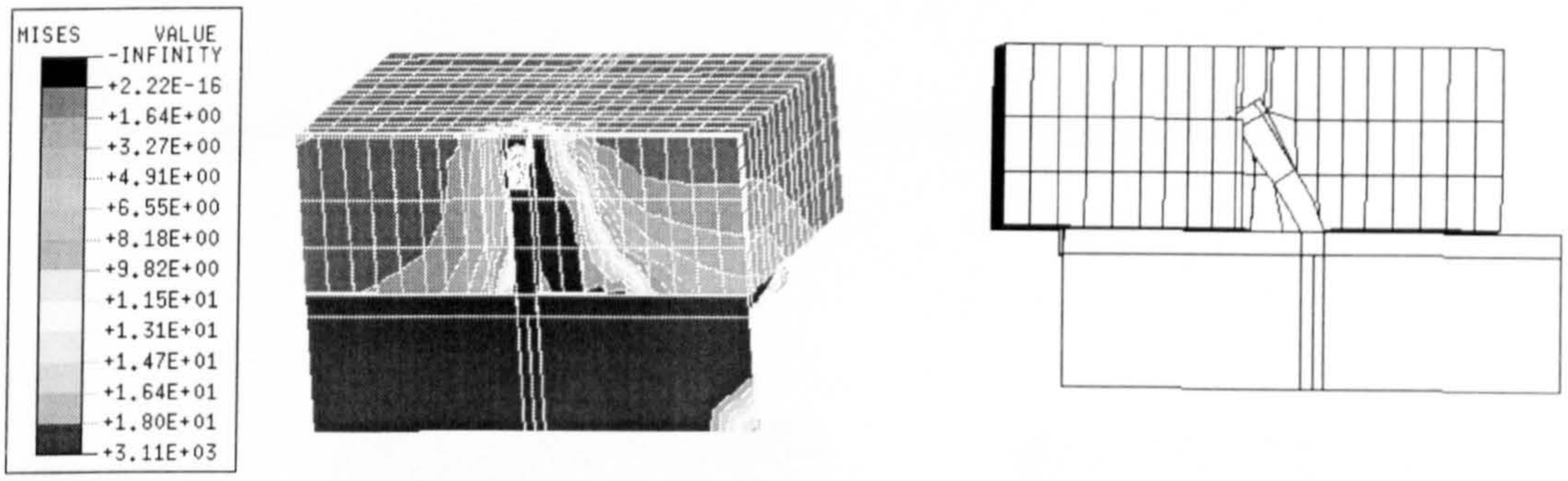

Figure 3.14.c Load level of 73kN

Figure 3.14 Stress contour and deformed shape of FE-S2

3.6.3 Test S3

Figure 3.15 shows the load-slip curve of the stud for test specimen S3 that has concrete cube strength of 30N/mm^2. The maximum failure load was 90kN at a slip of 5.05mm and the failure was reached by combined yielding of stud and concrete elements. This can be seen from following the distribution of contour stresses and deformed shapes at different load levels shown in figure 3.16. The concrete elements around the stud have yielded forming a conical failure shape at maximum load. Also, yielding of the stud element near the stud collar followed the failure of the concrete by yielding due to reaching maximum compressive stresses. The stud yielded in a curvature mode lies between the single and the double modes as seen from the deformed shape shown in figure 3.16.c.

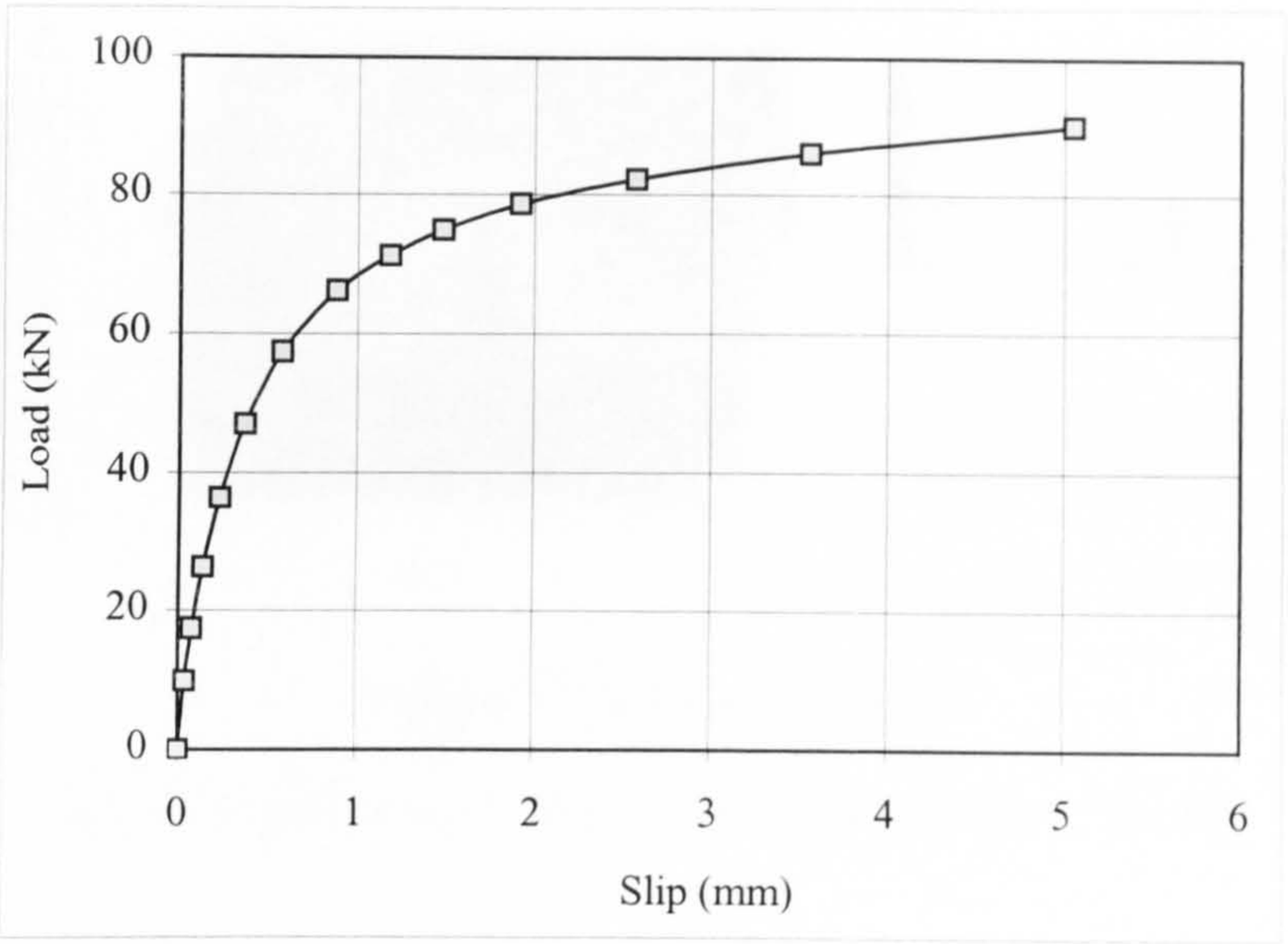

Figure 3.15 Load vs. slip curve of the stud for push-off test S3

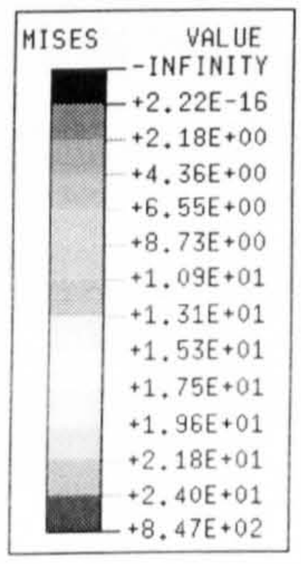

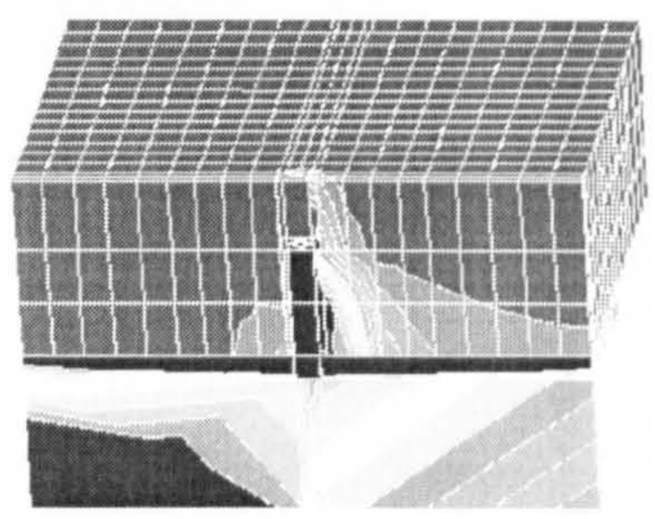

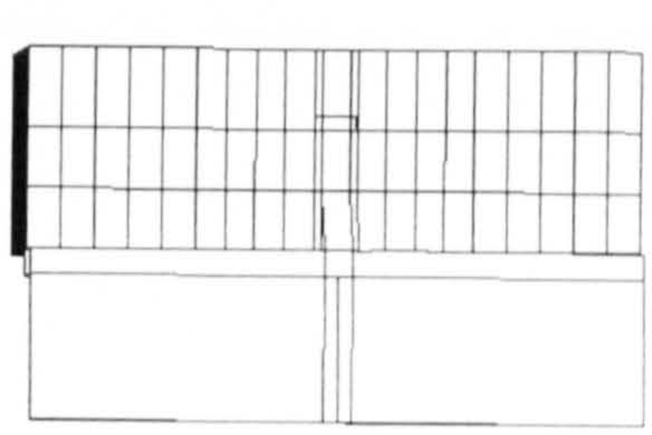

Figure 3.16.a Load of 47kN

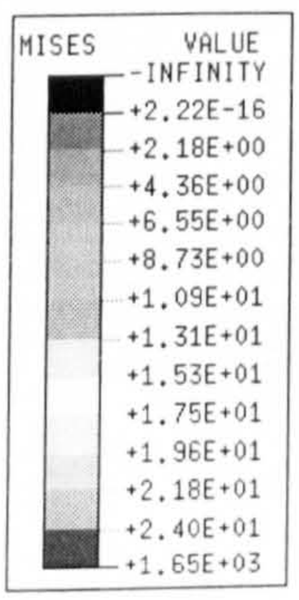

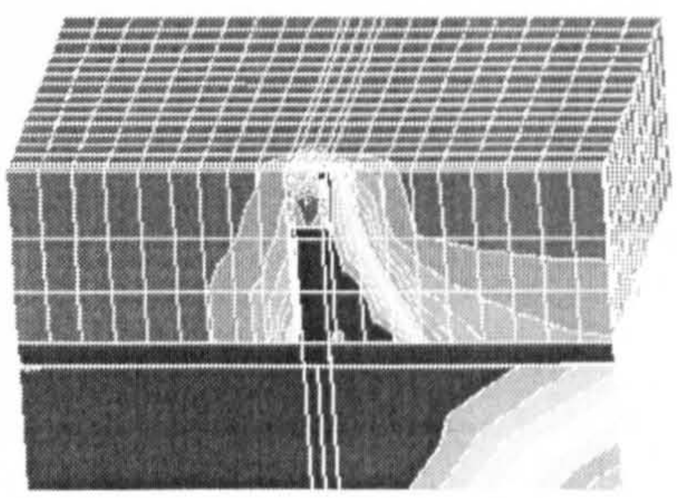

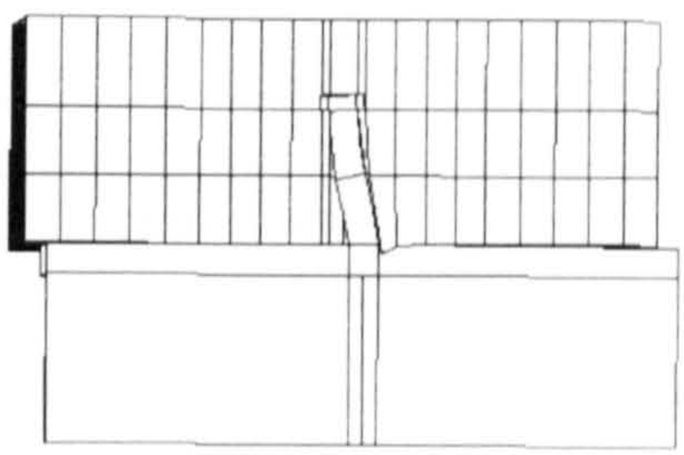

Figure 3.16.b Load of 75kN

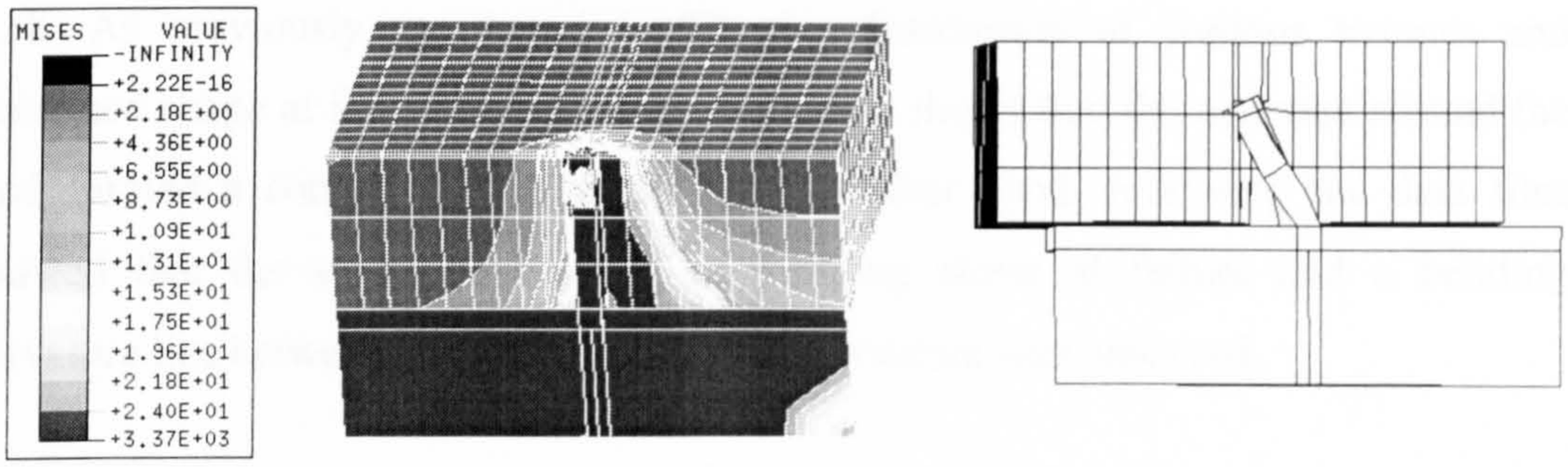

Figure 3.16.c Load of 90kN

Figure 3.16 Stress contour and deformed shape of FE-S3

3.6.4 Test S4

The load-slip characteristic of the stud in the simulated push-off test S4 that has concrete a concrete cube strength of 35N/mm^2 is shown in figure 3.17. The maximum failure load was 100.2kN at a slip of 4.76mm. The cause of failure was combined yielding of concrete elements around the stud and yielding of the stud element at the collar.

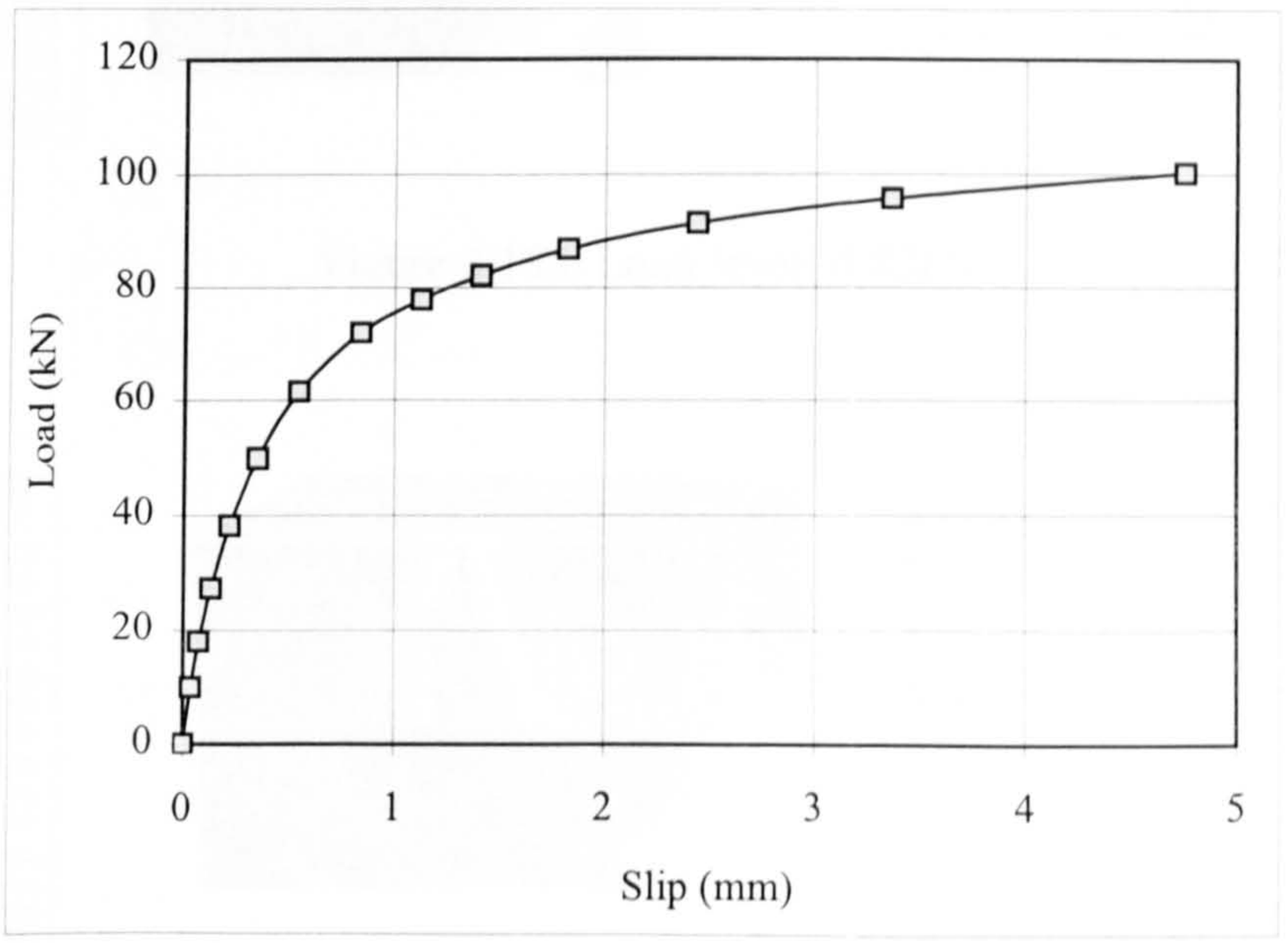

Figure 3.17 Load vs. slip curve of the stud for push-off test S4

The distribution of contour stresses and deformed shape of test S4 is shown in figure 3.18. As previously mentioned in S3, the distribution of contour stresses and deformed shape at failure shown in figure 3.18.c shows that the concrete around the stud formed a conical failure shape. On the other hand, following the data files showed that the stud also reached its yielding stress at failure and a bending curvature lies between the single and double curvature was observed.

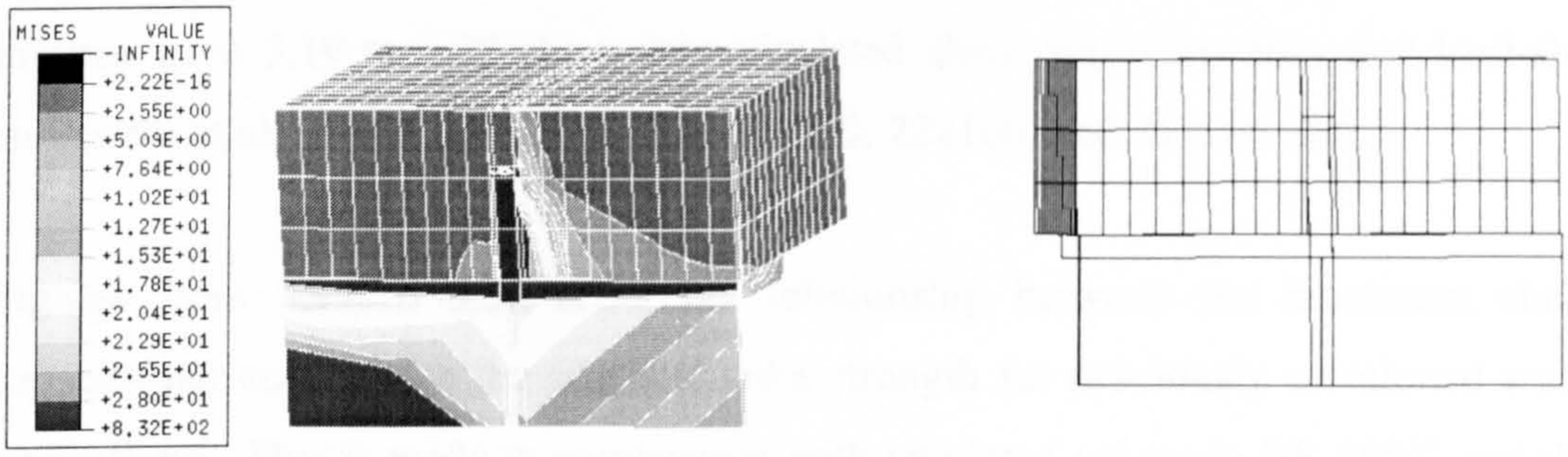

Figure 3.18.a Load level of 50kN

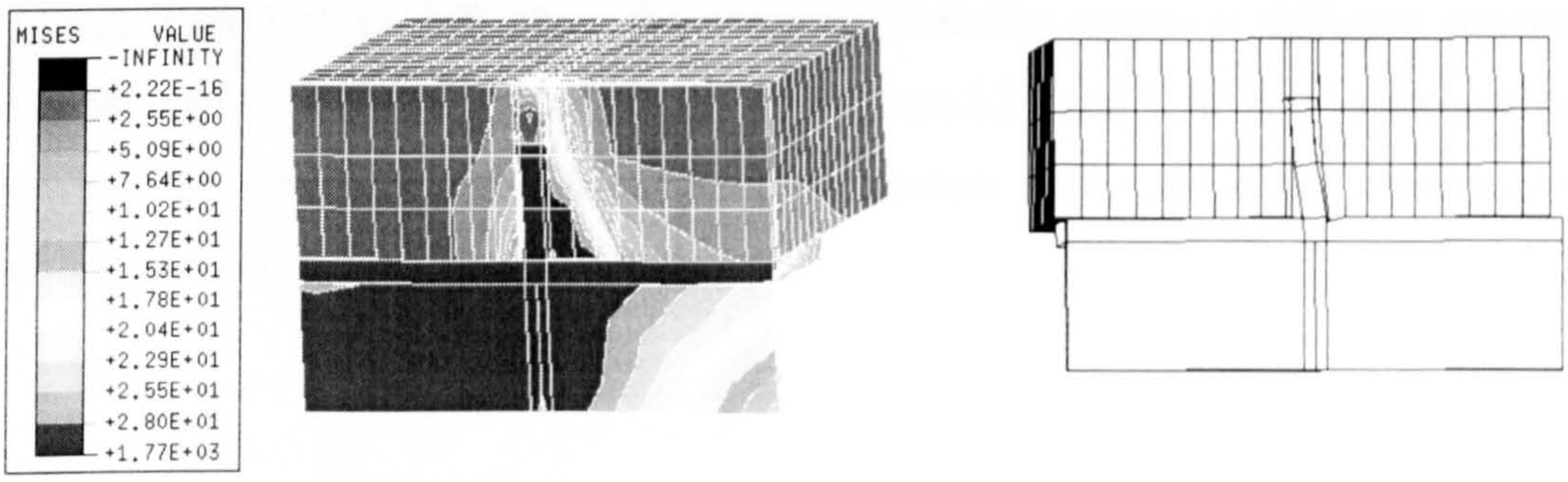

Figure 3.18.b Load level of 82kN

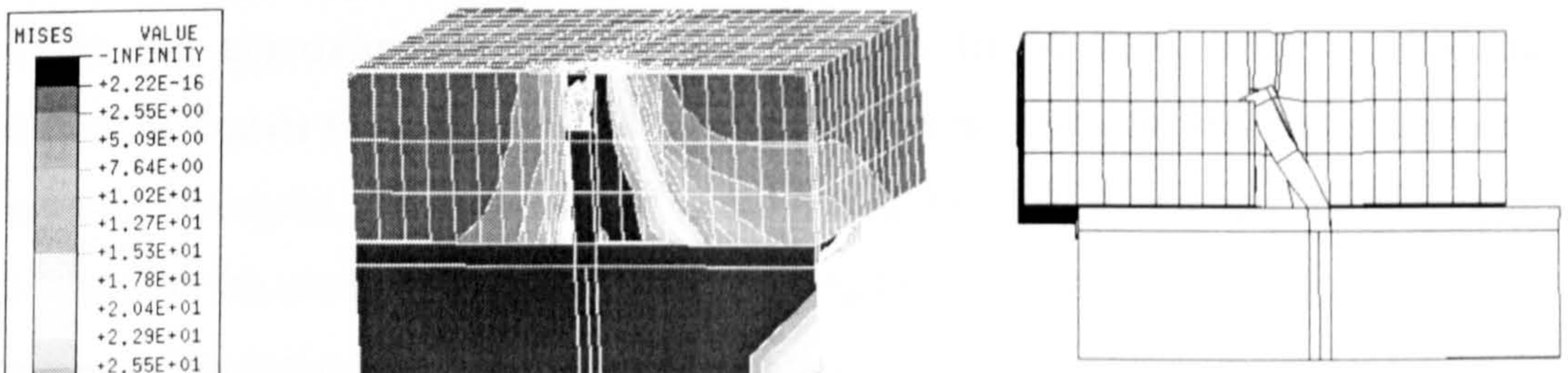

Figure 3.18.c Load level of 100.2kN

Figure 3.18 Stress contour and deformed shape of FE-S4

3.7 Parametric study

A parametric study was conducted using the FE model for 13mm, 16mm, 19mm, 22mm and 25mm diameter headed studs with various concrete strength of 25, 30, 35 and 40 N/mm^2. The results were used to compare with the tabulated values specified in BS 5950 and the calculated value obtained from the equations given by Eurocode 4.

Figures from 3.19 to 3.28 show the calculated shear stud capacities and load-slip curves for studs 13x65, 16x75, 19x75, 19x100, 22x100, and 25x100 mm.

Figures from 3.19 to 3.24 show the relationship between the maximum shear capacity per stud versus the concrete cube strength for previously mentioned studs respectively. This is made in comparison with tabulated values in BS 5950[4] and the smaller value calculated from equations 3.1, 3.2 given by Eurocode 4[8].

Figures from 3.25 to 3.28 show the obtained load-slip curves at different concrete cube strengths for the same stud diameters. Figures 3.29 and 3.30 show a comparison between the obtained load-slip curves from present study and other experimental published work.

3.7.1 Results and discussion

Figure 3.19 shows that the maximum load carried by stud diameter 13x65 mm is increased with the increase of the concrete cube strength. The obtained results from present study lie between the tabulated values in mentioned codes of practice. The results are approximately parallel and close to EC 4 curve with a maximum difference equals to 1.9% of EC 4 results at concrete strength 25 N/mm^2. At lower concrete strengths, the failure load is governed by earlier concrete failure before yielding of the stud. At higher concrete strengths, the failure load is governed with steel yielding rather than concrete failure especially for the 13mm diameter stud.

Figure 3.20 shows the relationship between the maximum load per stud and the concrete cube strength obtained for the 16mm diameter x 75mm height headed stud. The relationship is again close to EC 4 curve. The tabulated values in BS 5950 are remarkably higher than the other values especially at lower concrete strengths.

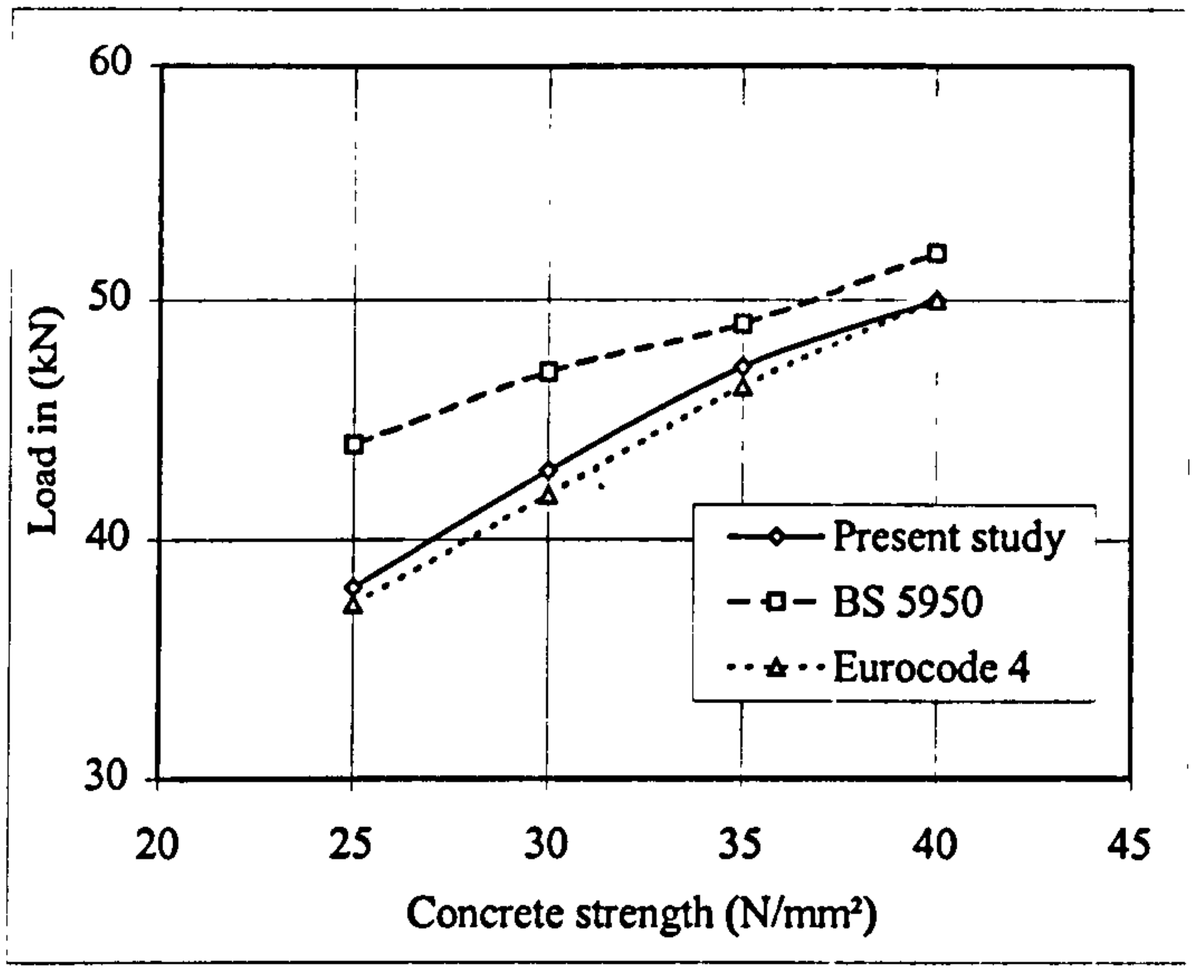

Figure 3.19 Shear capacity for 13 x 65mm headed shear stud

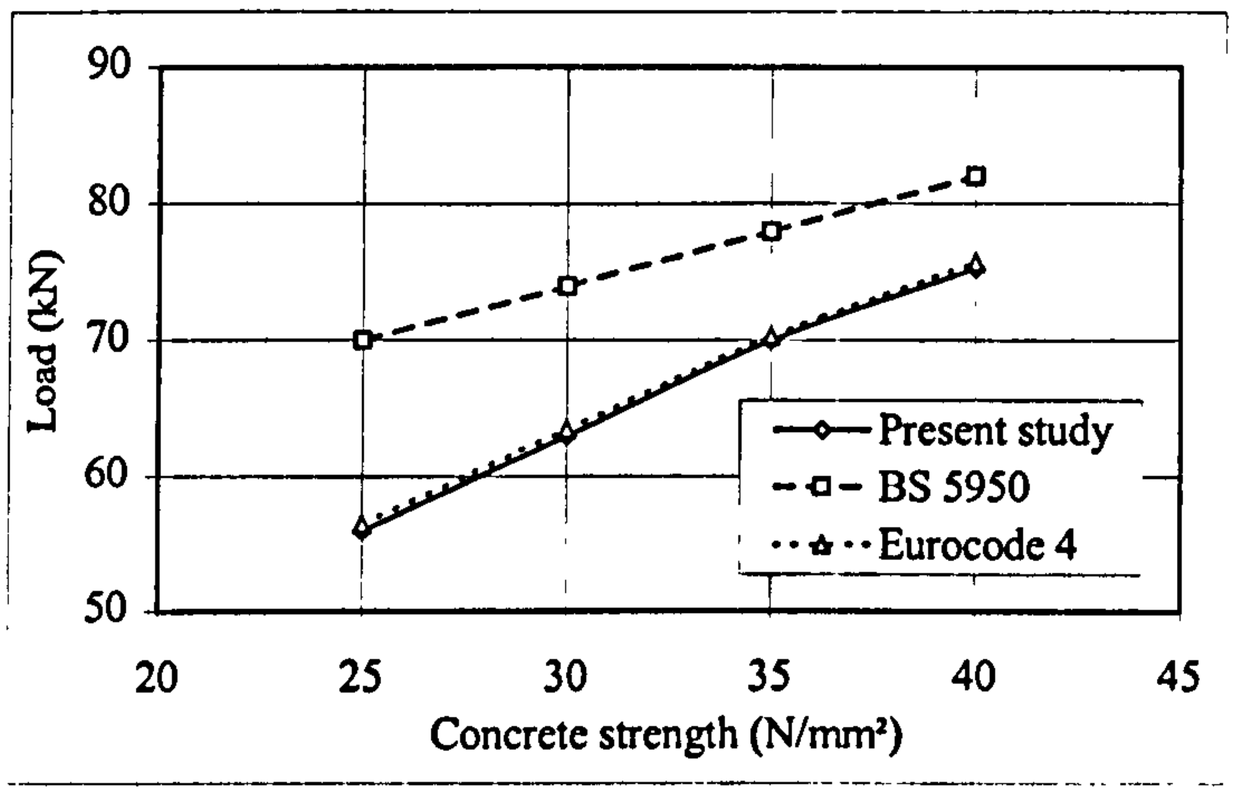

Figure 3.20 Shear capacity for 16 x 75mm headed shear stud

Figures 3.21 and 3.22 show the shear stud capacity vs. concrete cube strength curve for 19mm diameter x 75mm height and 19mm diameter x 100mm height headed studs respectively. The curves are plotted in comparison with tabulated values of the BS 5950[7] and EC 4[8]. In BS 5950[7], there are 16% and 14% differences in the stud strength obtained for 75mm and 100mm heights at concrete strengths 25 and 40 N/mm^2 respectively. On the other hand, both stud strength values are the same when using EC 4 equations since the reduction factor α calculated in Equation 2.2 for height 75 mm is equal to 0.989 (~ 1.0 the same as that for height 100 mm). The

present study shows that the stud capacity of the 19x100 mm is increased by 12.7 % and 11.5 % of that capacity of 19x75 mm at concrete strengths 25 and 40 N/mm^2 respectively. This agrees with the results obtained from finite element analysis carried by Johnson and Oehlers[37]. On the other hand the load v. concrete strength curve obtained from present study is very close to that one of EC 4 for stud 19x100 mm. This means that a modification of the factor (α) is needed by the EC 4 code to account for the effect of the change in stud height.

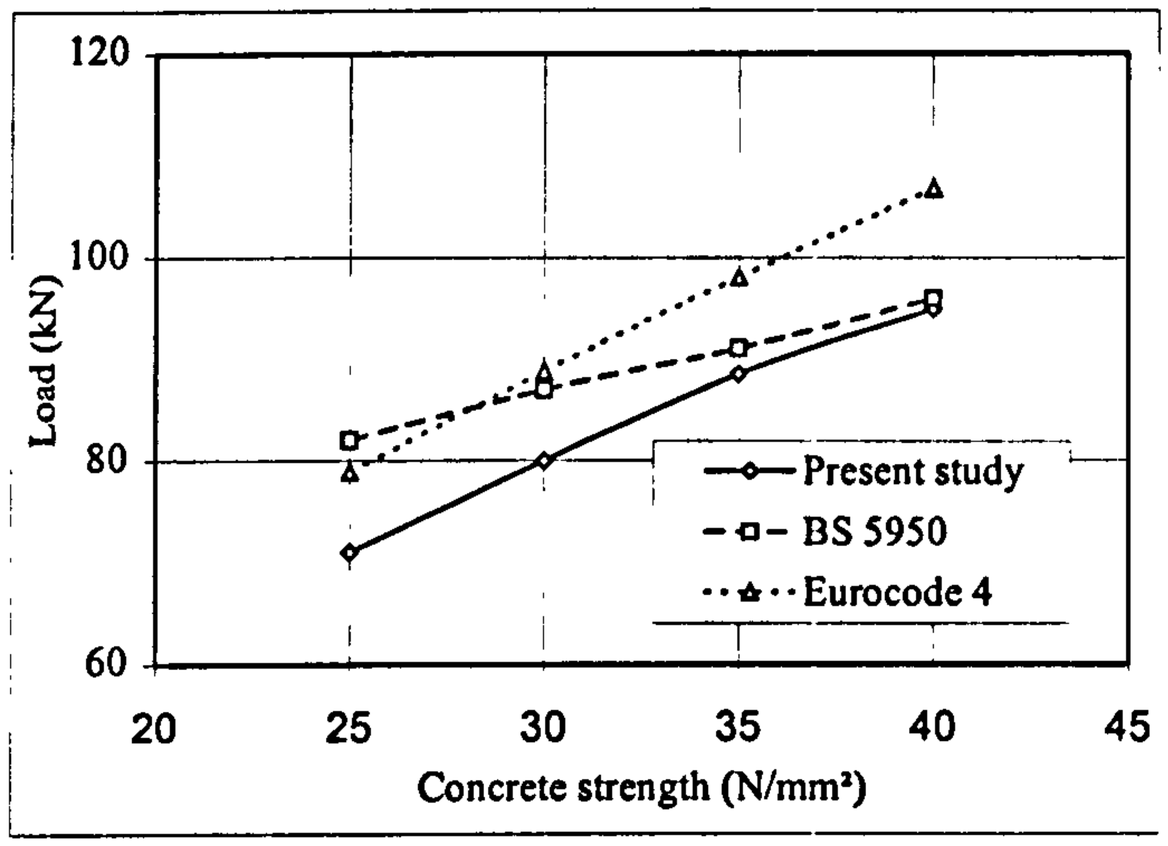

Figure 3.21 Shear capacity for 19 x 75mm headed shear stud

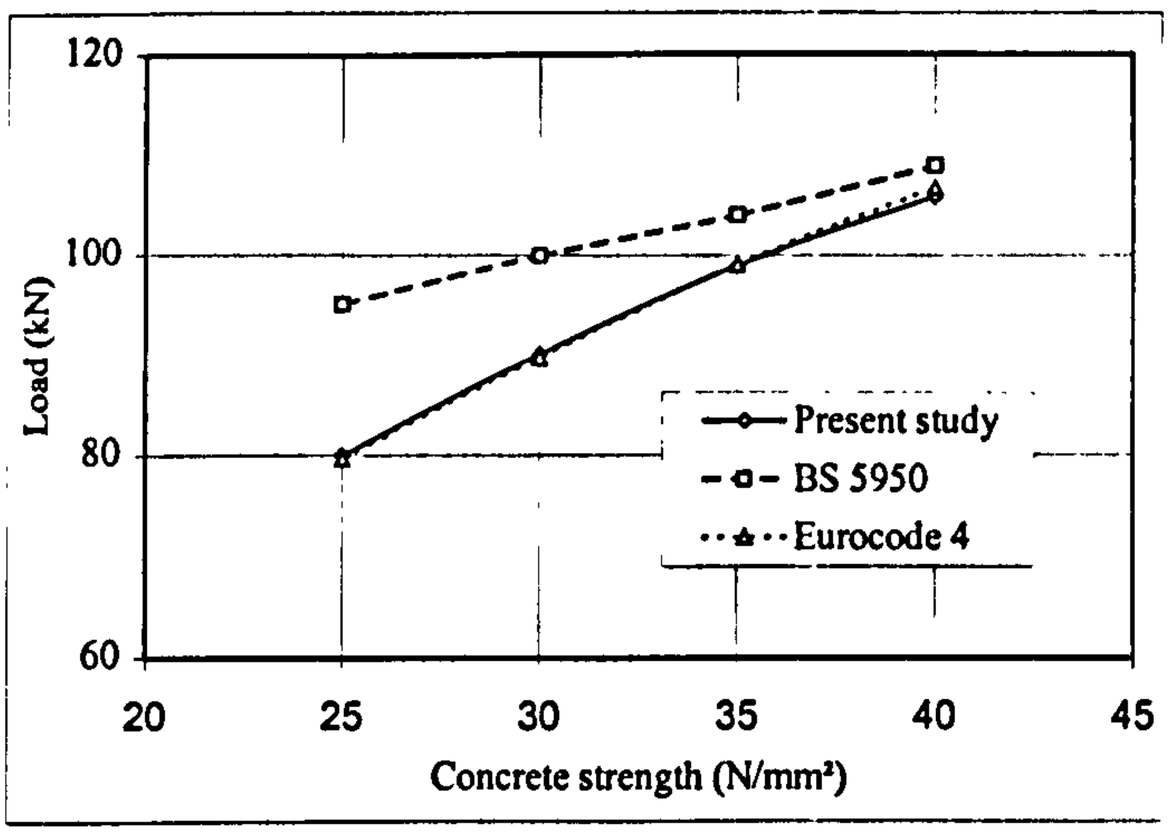

Figure 3.22 Shear capacity for 19 x 100mm headed shear stud

Figures 3.23 and 3.24 show the results obtained from the present study lie below both results of BS and EC 4. This is attributed to the lack of push-out tests carried

out on these diameters. The failure load of these high diameters is governed by the failure of concrete around the stud where the higher concentrations of stresses, except higher values of concrete strengths.

A remark should be noted that for all diameters, the BS 5950 gives stud strengths higher than that results obtained using both EC 4 and present finite element study results at low concrete strengths. The need for modification of the factor α specified in Eq. 1 of the EC 4 clause 6.3.2.1, which takes into consideration the effect of change in stud heights, to adjust the values obtained for 19x75 mm. Also it is recommended to carry more experimental work to modify stud strengths tabulated in both BS and EC 4 codes for diameters 22 and 25 mm.

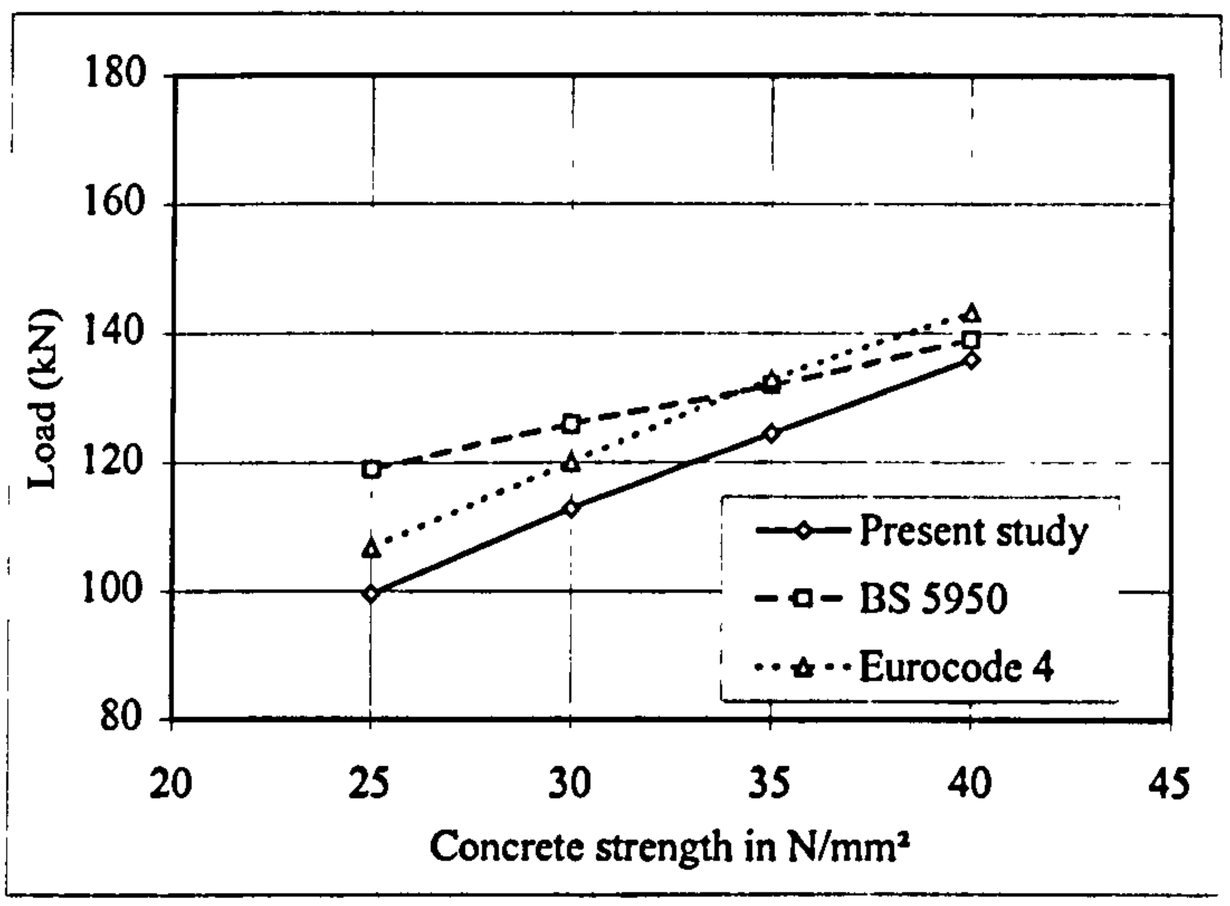

Figure 3.23 Shear capacity for 22 x 100mm headed shear stud

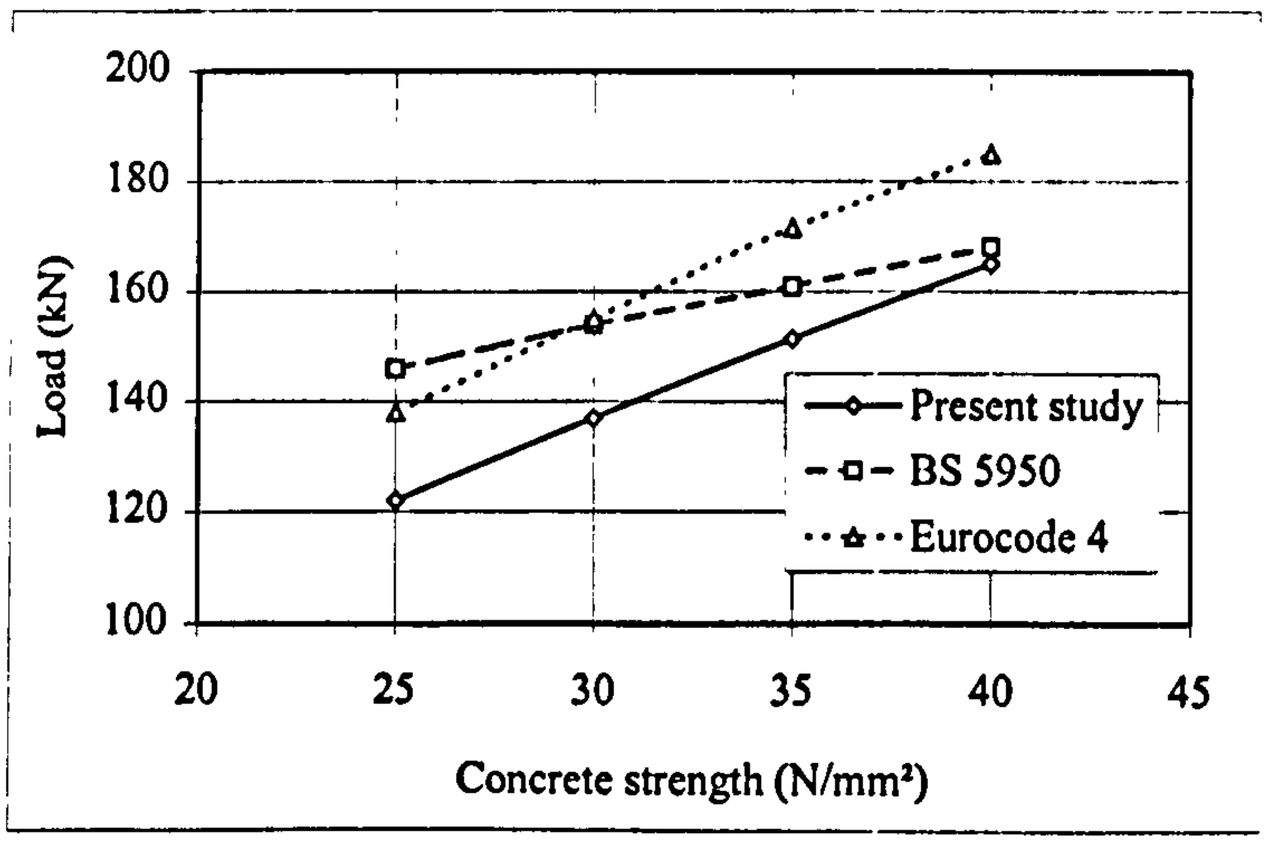

Figure 3.24 Shear capacity for 25 x 100mm headed shear stud

Figures from 3.25 to 3.28 show the relationship between the load carried by the stud and the slip of the steel relative to the concrete slab. The curves become horizontal slightly after reaching the ultimate strength of connection due to the use of bilinear steel and concrete material models since it is assumed that the yield stress remains constant. The last slip represents the maximum slip that can be reached up to the beginning of failure. It can be seen that the ultimate strength of connection is increased either with the increase of stud diameters or the increase in height for a given diameter. The stiffness of stud (slope of tangent of load-displacement curve taken from origin) is increased as well with the increase of stud diameter. The lower the stud diameter the greater deformation undergone before reaching the ultimate strength of connection.

It is noticed that the load-slip curves of studs 19x100 and 19x75 are approximately identical at lower load levels. At higher load levels the stud 19x75 mm starts to yield first before stud 19x100 mm.

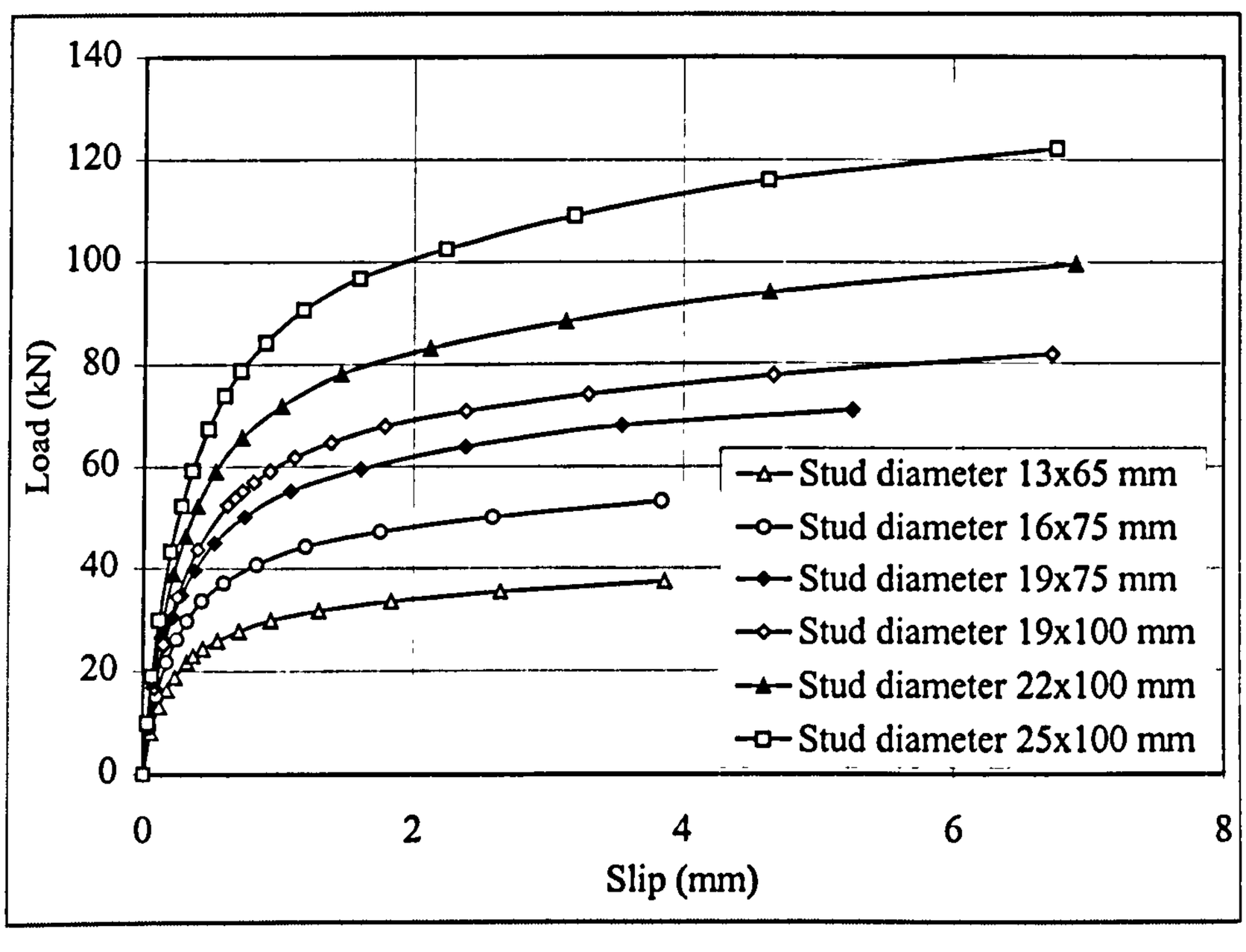

Figure 3.25 Load v. slip curve for concrete strength 25N/mm^2

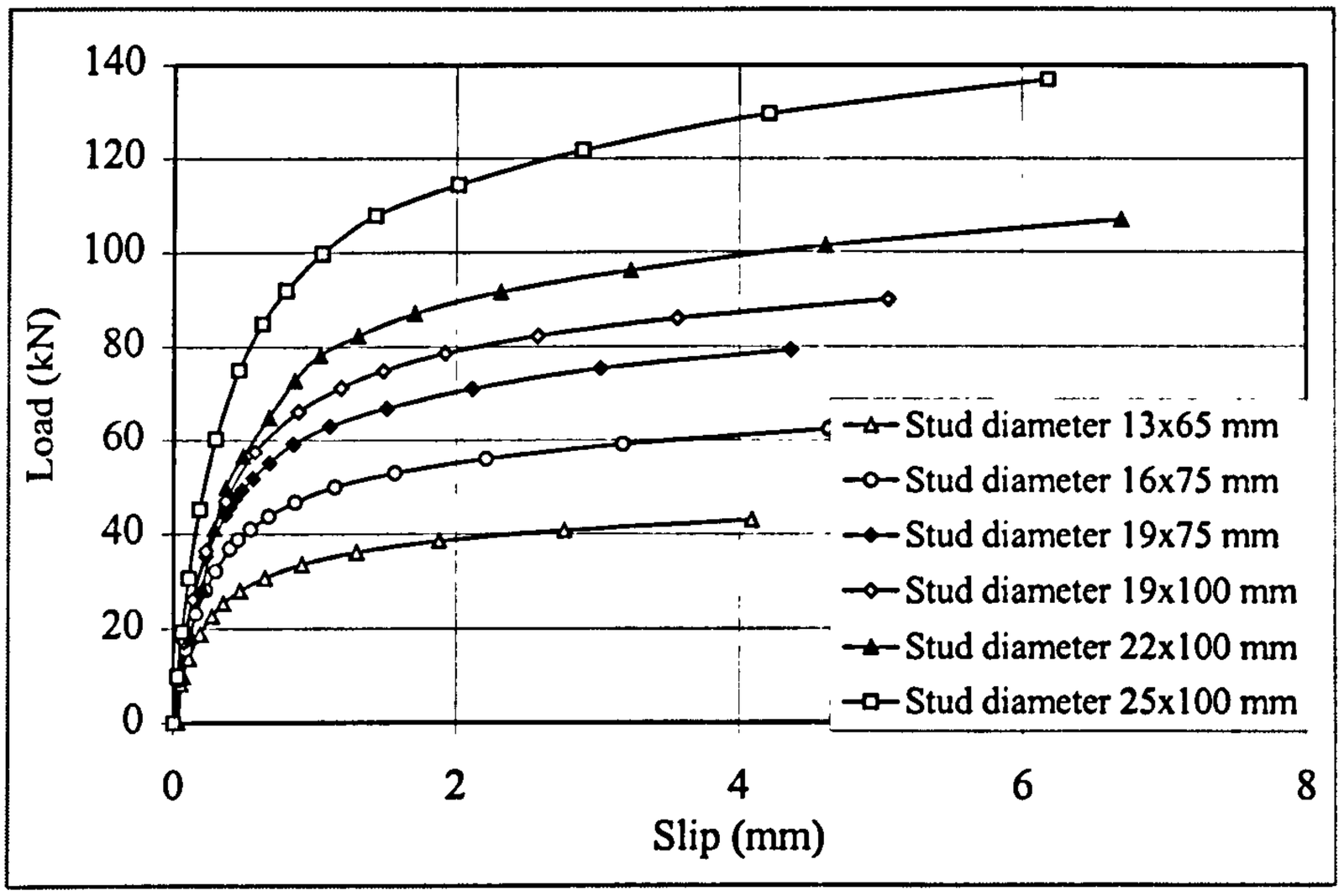

Figure 3.26 Load v. slip curve for concrete strength 30N/mm^2

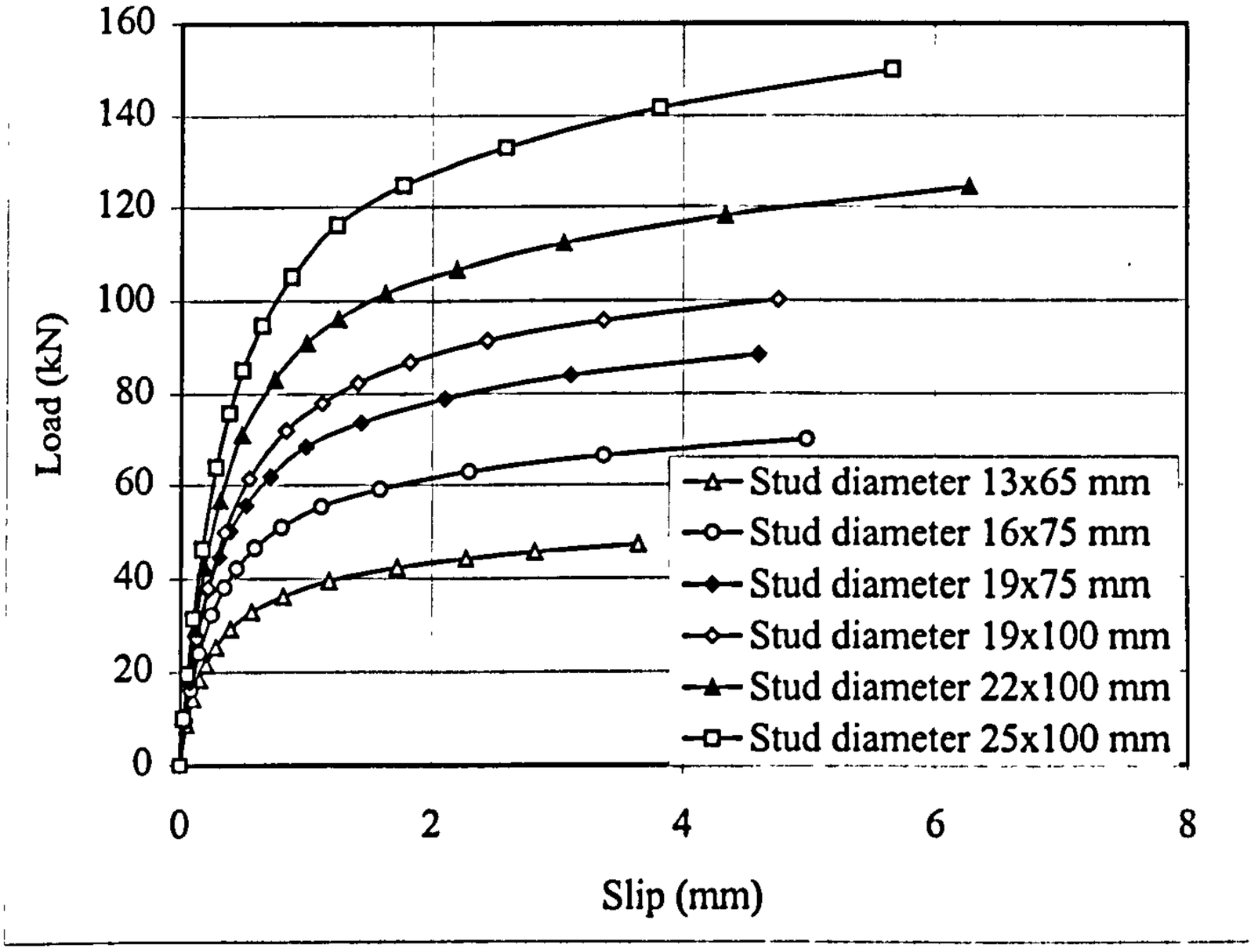

Figure 3.27 Load v. slip curve for concrete strength 35N/mm^2

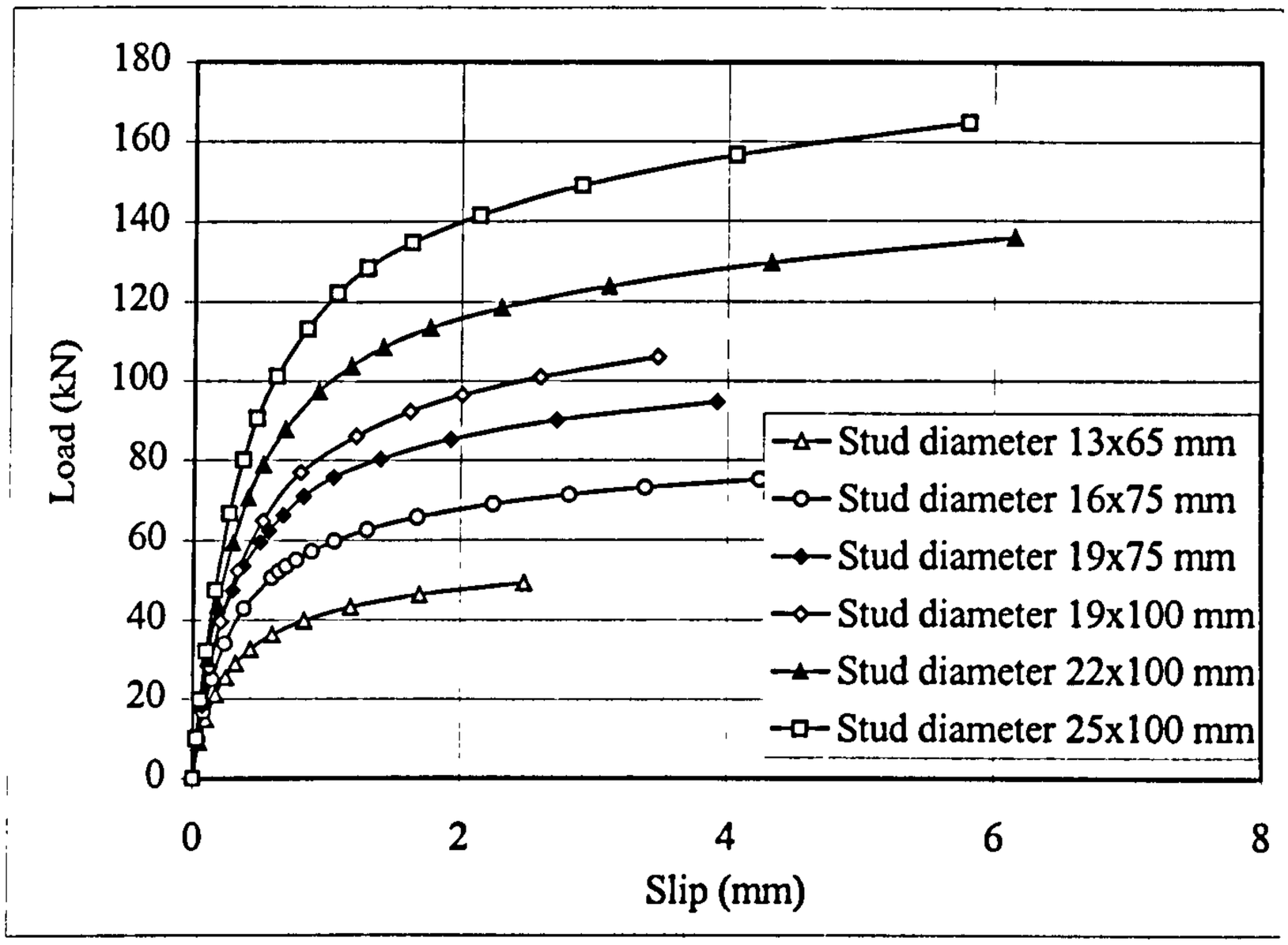

Figure 3.28 Load v. slip curve for concrete strength 40 N/mm^2

3.8 Comparison of present FE solution with available literatures

A further study is conducted to compare the FE-solution with the available push-off test results. Figure 3.29 shows the comparison of FE-solution and push-off test results by Menzies[16] and Lam et al.[23]. The headed stud shear connector used was the 19mm diameter x 100mm height headed stud. The concrete slab thickness was 150mm and has concrete cube strength at the time of testing of 40N/mm^2. Menzies presented his push-off test results as percentage of the maximum load per stud against slip at the interface between steel beam and concrete slab. Figure 3.29 shows the load-slip characteristic of 19mm diameter x 100mm height headed stud observed in push-off tests with 40 N/mm^2 normal density concrete. The figure shows good agreement between the experimental results and the present finite element solution. The output data files from ABAQUS have shown that both the headed stud collar elements and the concrete slab around the stud reached their yield stress at failure. The mode of failure was a combined failure mode.

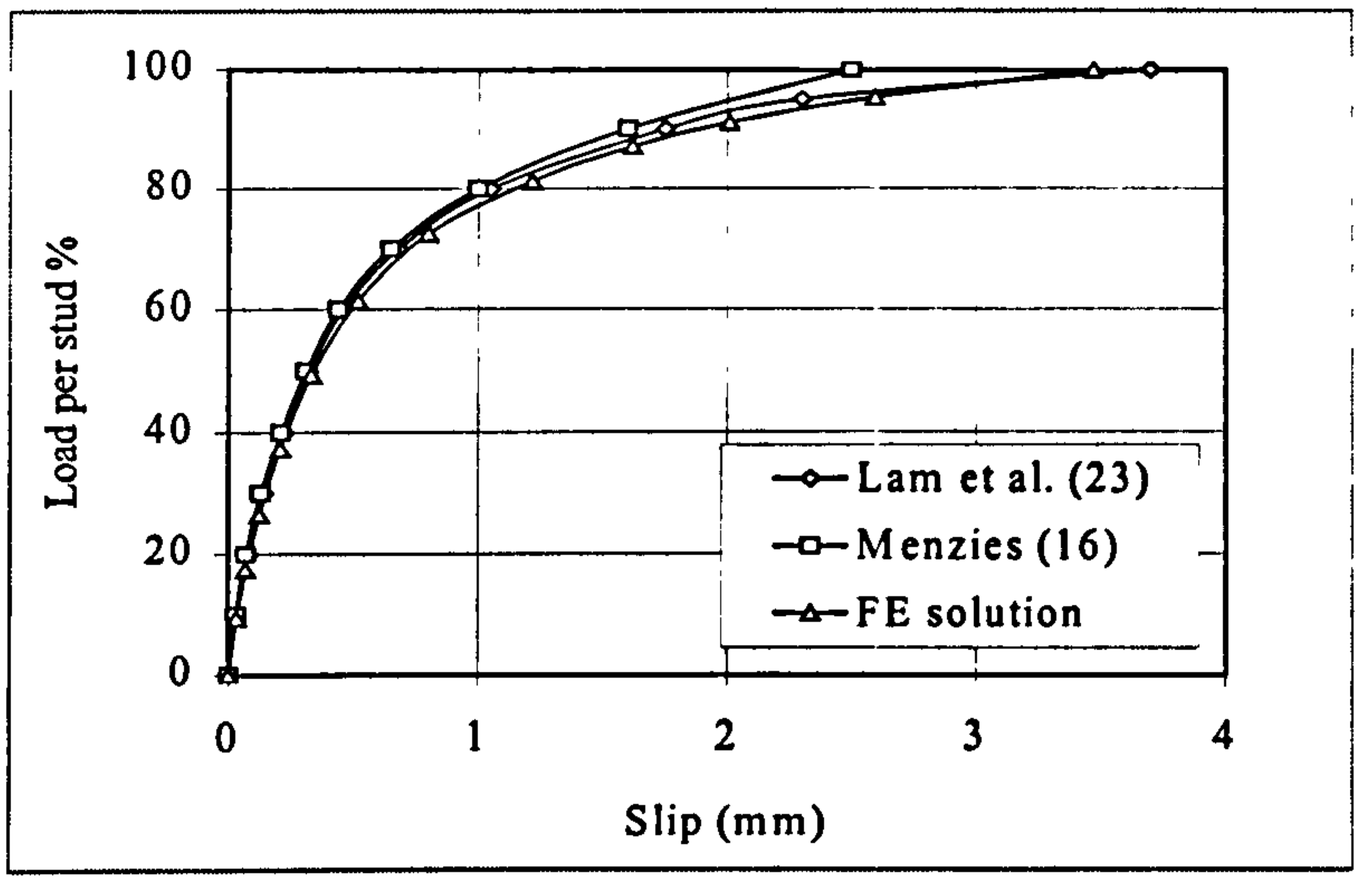

Figure 3.29 Load per stud in percentage vs. slip for 19mm diameter x 100mm height headed stud in 40N/mm^2 concrete

Figure 3.30 shows the comparison of load-slip behaviour of 19mm diameter x 75mm height headed stud in 40N/mm^2 concrete, the load is expressed as a percentage of the maximum load per stud. The FE-solution obtained from this study is compared with that obtained experimentally by Li and Krister[31]. Once again, the FE-solution shows good agreement with the experimental result.

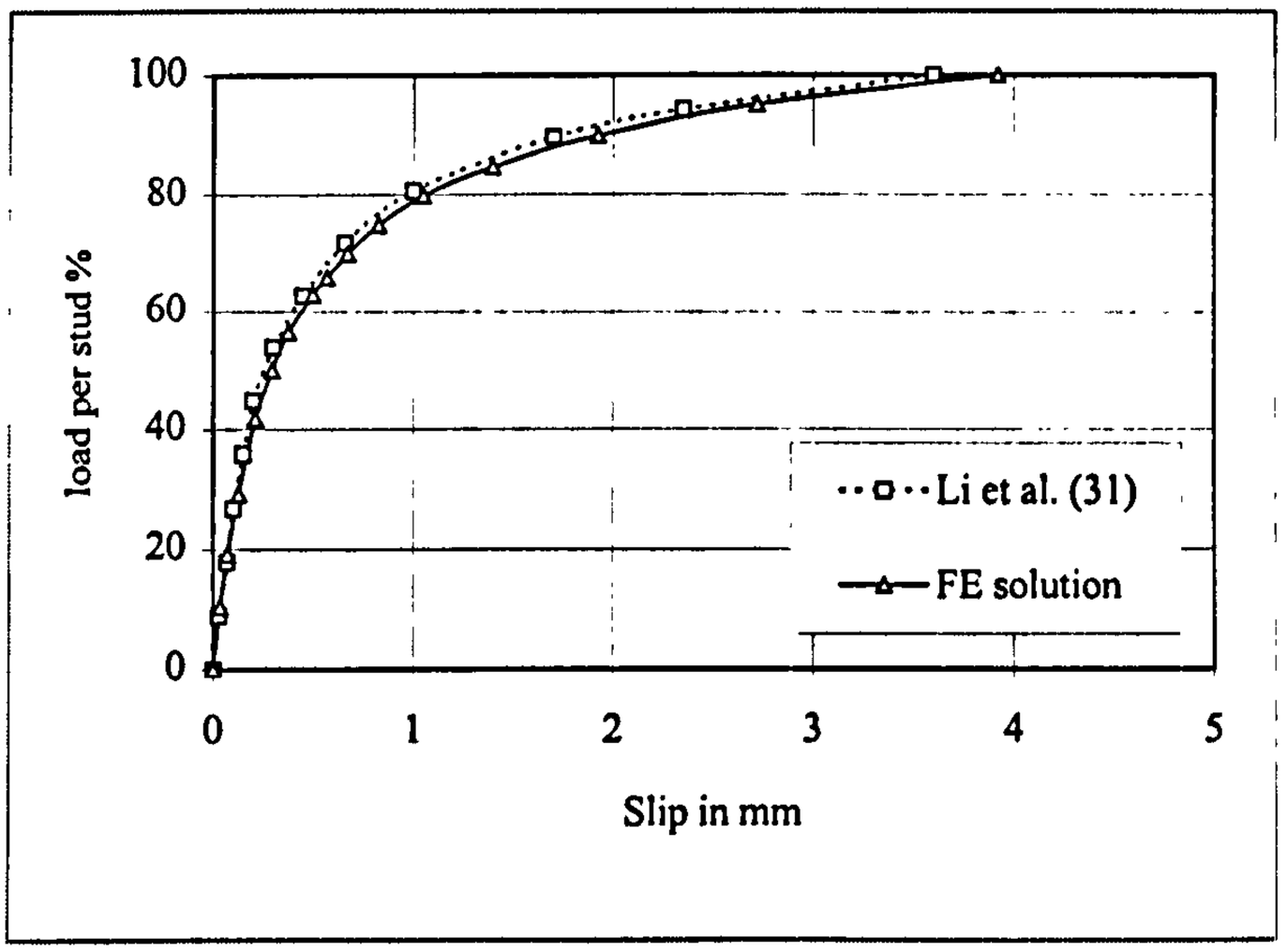

Figure 3.30 Load per stud in percentage vs. slip for 19mm diameter x 75mm height headed stud in 40N/mm^2 concrete

3.9 Summary

The numerical model described in chapter 3 was used to simulate the behaviour of headed stud shear connectors in push-off tests with solid slabs.

Finite element analyses have shown that the concrete cube strength significantly affects load-slip behaviour of headed stud, shear connection capacity, and modes of failure. Specimens with strong concrete have shown higher ductility in terms of the load-slip behaviour of the stud than that of weak concrete. The concrete strength around the stud may be high enough to cause yielding of the stud elements at its collar where the stress concentration is high leading to stud failure mode. Specimens with weak concrete, like specimen S2 that has concrete cube strength of 20N/mm^2, formed concrete cone failure around the stud leading to concrete failure mode. As a general conclusion, the increase in concrete strength increases the shear capacity of headed studs in push-off tests with solid slab till the yielding of the stud element at collar is reached. After this stage, the shear connection capacity is governed by the strength of the headed stud.

It is also observed from the parametric studies that the height of the stud affects the shear connection capacity in addition to its diameter. The shear connection capacity of specimen with 19mm diameter x 75mm height was less than that of 19mm diameter x 100mm height by 12%. Although, there is good agreement between the present finite element results with that predicted from Eurocode 4[8] equations, the reduction in shear connection strength due to the reduction in stud height seems to be ignored by the factor (α) calculated in Equation 2.2. A suggested modification for that factor based on the present finite element modelling to include the effect of the stud height on the shear connection capacity may be given as follows:

$$\alpha = 0.2(h/d+0.5) < 1.0 \qquad \text{.....(3.7)}$$

where h is the overall height of stud and d is the diameter.

Although, a further finite element study may be required to investigate the effect of stud height on the shear connection capacity, Equation 3.7 at least ensures good representation of Eurocode 4[8] shear stud capacity for the studs tabulated in BS 5950[7].

It is observed from the finite element analyses that BS 5950[7] over-estimated the shear capacity of the headed studs. Also, the review of previous experimental research on push-off tests with solid slabs, presented in chapter 2, has shown the lack of push-off tests carried out on headed studs with 22mm diameter x 100mm height and headed studs with 25mm diameter x 100mm height. This suggests that the predicted shear stud capacity from the present finite element solutions are more accurate than that tabulated in BS 5950 and in Eurocode 4 for the 22mm diameter and 25mm diameter headed studs.

The general conclusion to be drawn from all of these studies reported herein is that since finite element modelling can accurately represent all the main features of the behaviour of headed stud in push-off tests with solid slabs, it offers a reliable and very cost-effective alternative to laboratory testing as a way of generating results. Also comparison of FE results with previous experimental research and with values of current codes of practice indicated that the use of the shear stud capacities summarised in Table 3.1 are more reliable than that tabulated in BS 5950[7].

Stud diameter (mm)	Stud Height (mm)	Concrete cube strength			
		C25	C30	C35	C40
13	65	38 (44)	43 (47)	47 (49)	50 (52)
16	75	56 (70)	63 (74)	70 (78)	75 (82)
19	75	71 (82)	80 (87)	89 (91)	95 (96)
19	100	80 (95)	90 (100)	99 (104)	106 (109)
22	100	100 (119)	113 (126)	124 (132)	136 (139)
25	100	122 (146)	137 (154)	151 (161)	165 (168)

( ) BS 5950[7] values

Table 3.1 Ultimate shear capacity (kN) of headed studs in push-off tests with solid slab

4. Finite Element Modelling of Headed stud in Composite Steel Beams with Precast Hollow Core Slabs

4.1 Introduction

In this chapter, a finite element model to simulate the structural behaviour of shear stud connection in steel-precast concrete composite beam is described. Three-dimensional solid elements are used in the analysis and the model takes into account linear and non-linear behaviour of the materials. The model will be validated against test results explained in detail in chapter 5 and both results will be compared in chapter 6. Parametric studies using the model were performed to investigate variations in concrete strength, amount of tie reinforcement placed transversely across the joint and gap size between the ends of precast slabs.

4.2 Push-off test

The behaviour of the headed stud in composite girders with precast hollow core slabs is also investigated experimentally by carrying out push-off tests. To accurately model a steel-precast HC slab push-off test, a detailed description of the push-off test specimen is necessary. The test procedures together with the details of the present push-off tests with HC slabs will presented in chapter 5.

4.2.1 Description of push-off test specimen

The push-off specimen was prepared and carried out horizontally similar to the tests conducted by Lam et al.[23]. It consists of four 600mm wide x 150mm deep x 800mm long prestressed HCU's, see figure 4.1 which shows some of these units. These units result from dividing the typical 1200mm wide x 150mm deep x 800mm long unit shown in figure 4.2 into two parts. The HCU 600mm width was chosen instead of the more common 1200mm wide unit so that the effect of the edge joint was included in a test length of 1200mm. The HCU's are connected to a grade 43 steel 254X254x73 UC with a single row of pre-welded headed studs at 150mm centres. The studs were 19mm diameter x 100mm long (TRW-Nelson Headed Studs) and were attached to the UC by using an automatic fusion welding process.

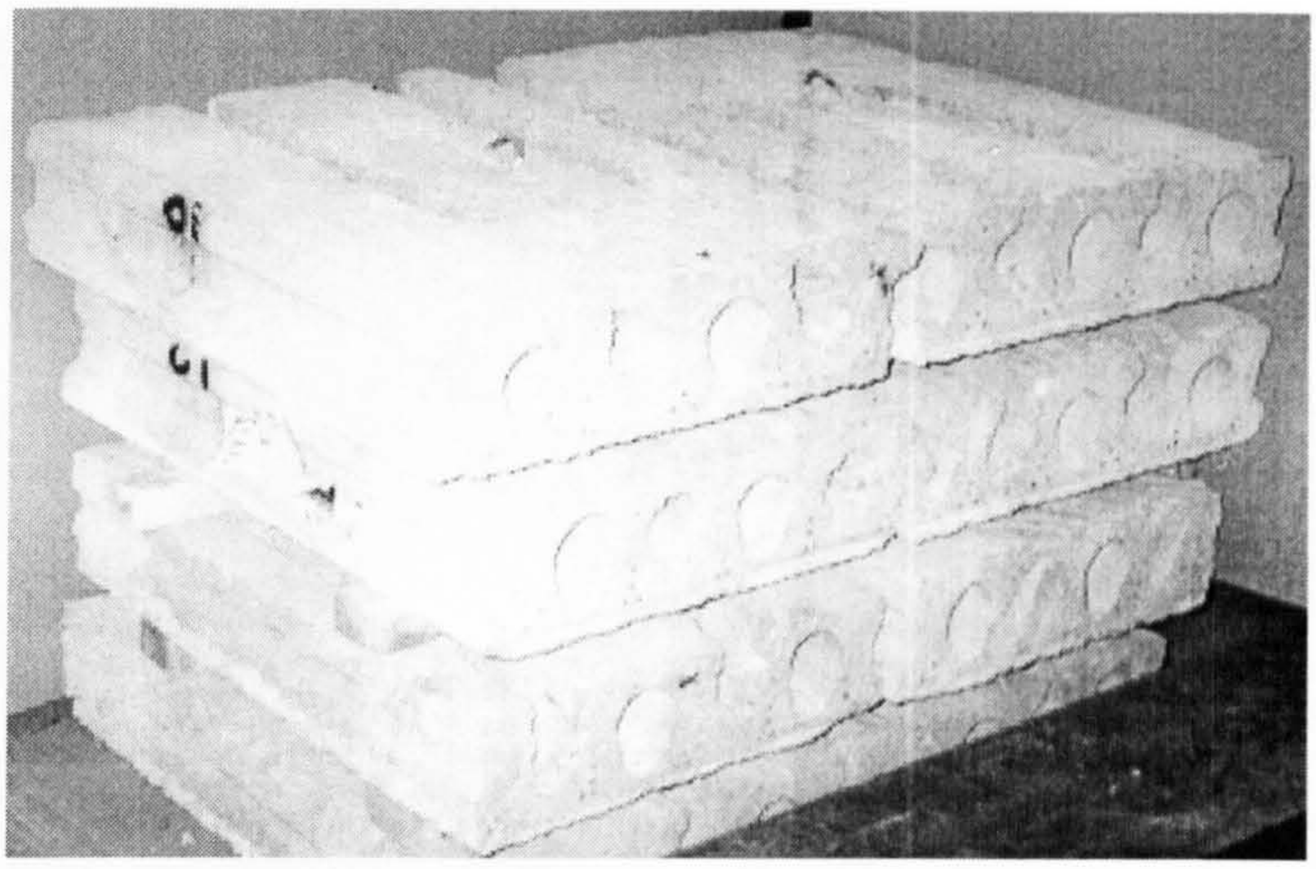

Figure 4.1 General details of 600mm precast hollow core floor units

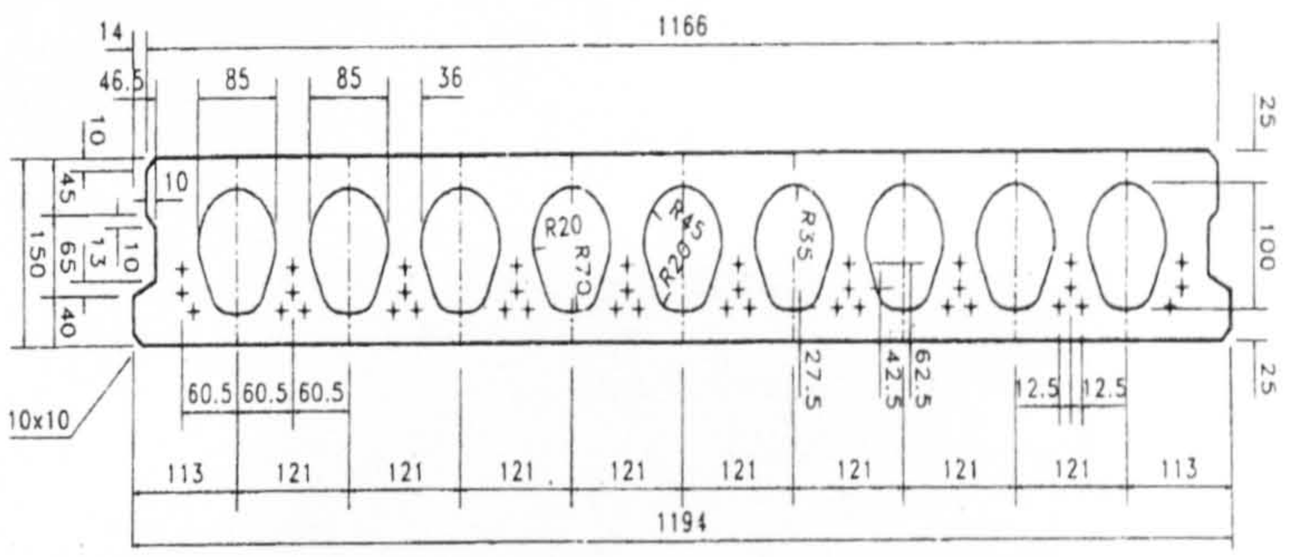

Figure 4.2 Details of a typical 1200mm HCU

The characteristic cube strength for the precast concrete was 50N/mm^2. Slots of 500mm long were made (two slots per 600mm unit) to allow for the placement of transverse reinforcement. The top cover to the transverse reinforcement was 50mm. The gap between the longitudinal edges of the HCU's, the joints between the lateral edges of the HCU's and the slots were filled with in-situ concrete. Figure 4.3 shows the layout of a test specimen before casting of in-situ concrete. Strain gauges were fixed to each transverse reinforcement bar, and covered with plastic tubing, for protection against concrete leaking onto the gauges, to monitor the strain as shown in figure 4.4. Figure 4.5 shows the general arrangement and instrumentation of the push-off test.

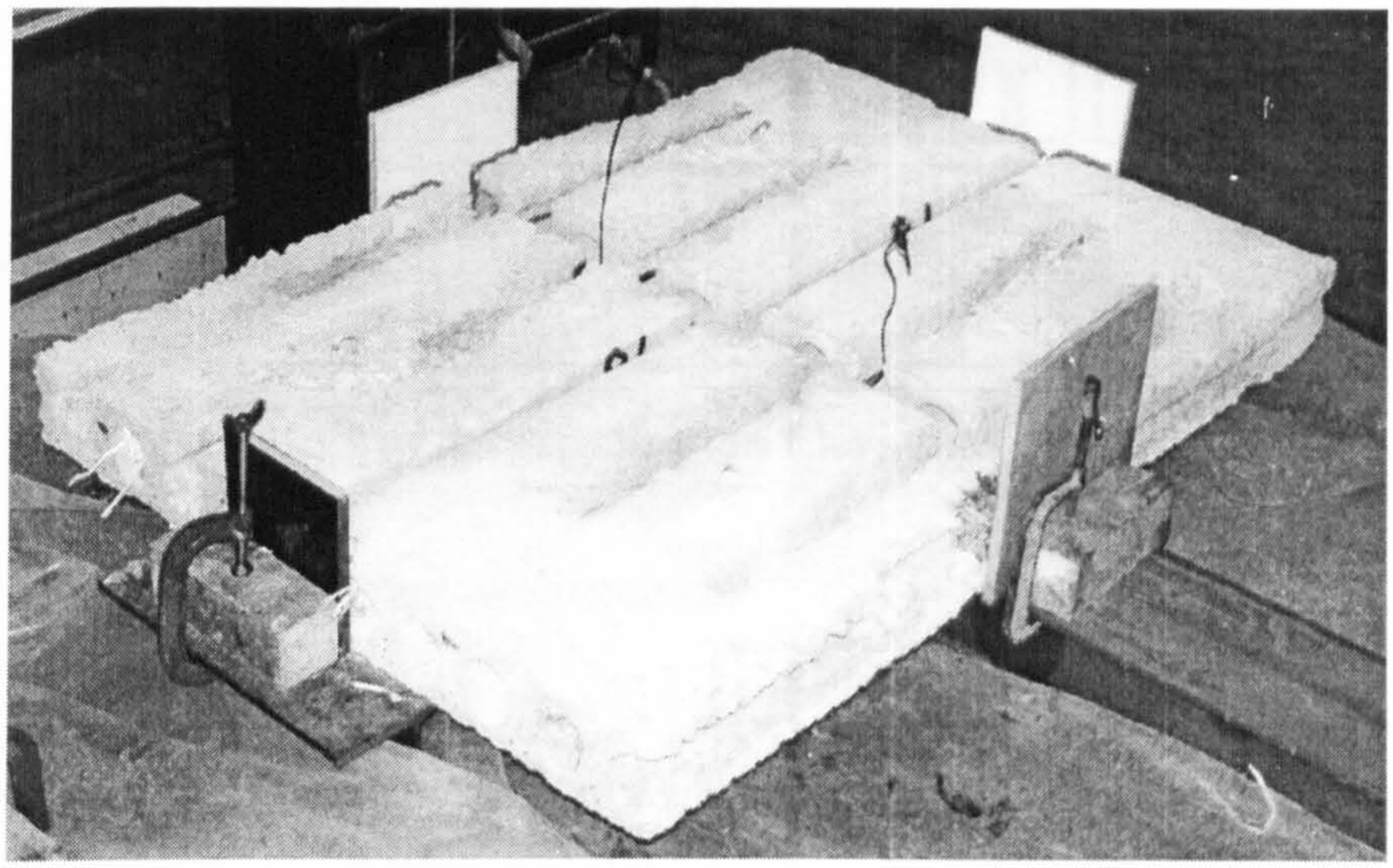

Figure 4.3 General arrangement of test specimen before casting of in-situ concrete

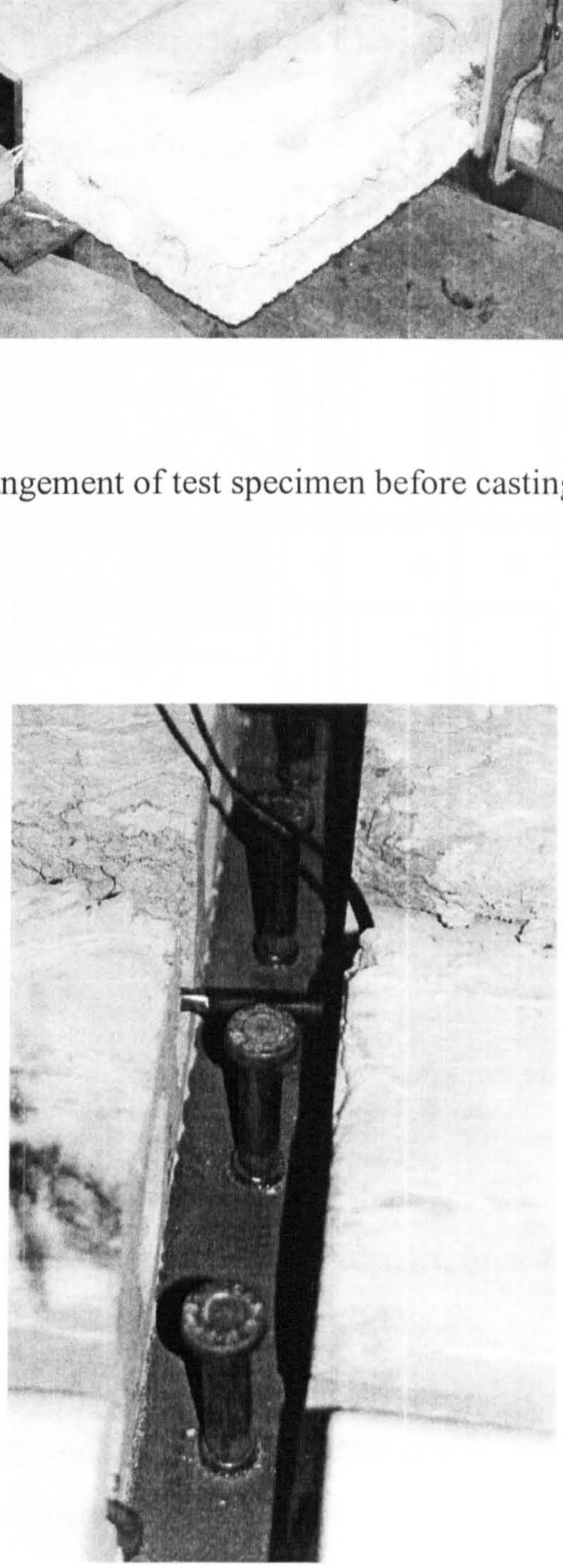

Figure 4.4 Details of headed studs and reinforcement bars within the gap

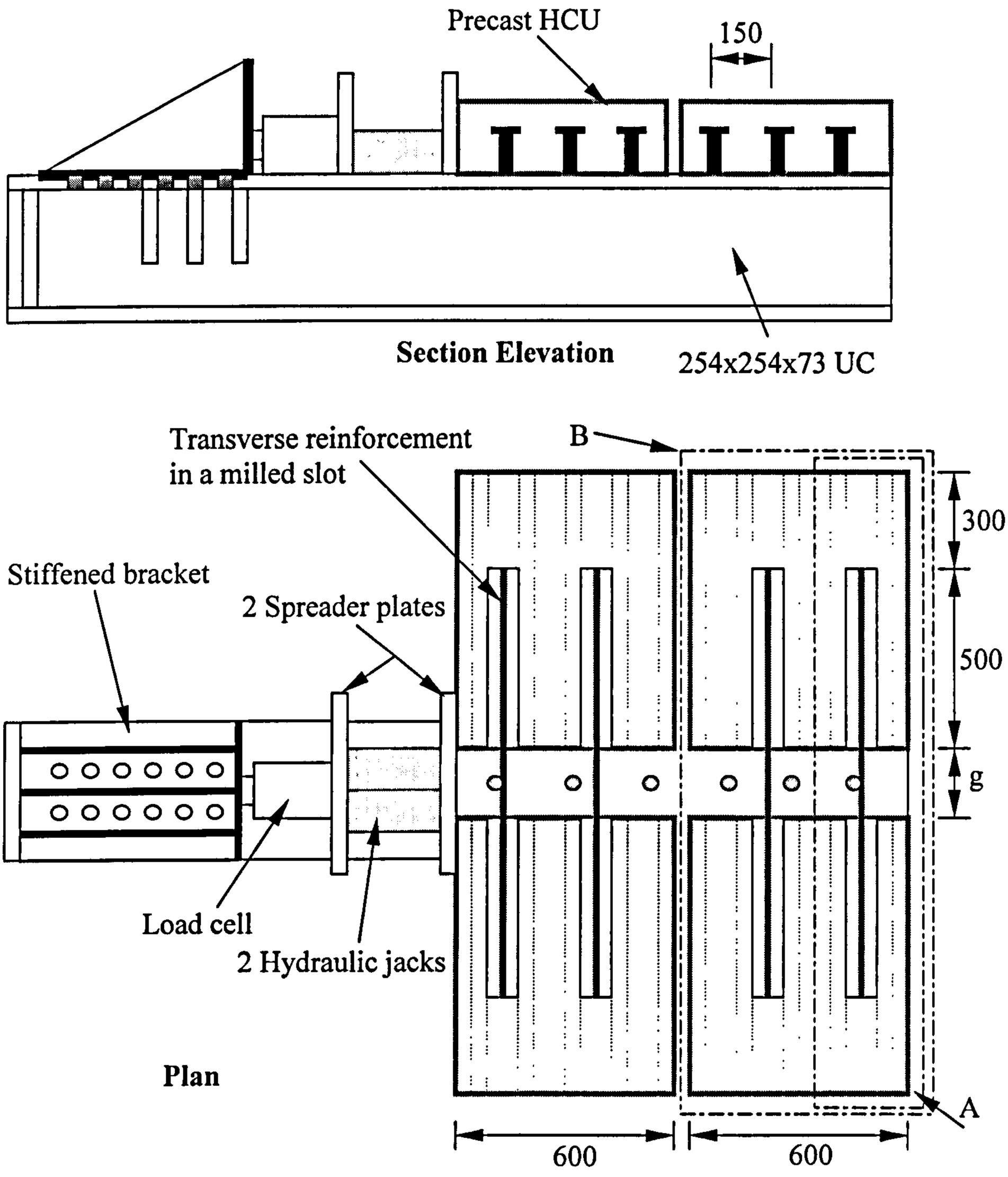

Figure 4.5 General arrangement and instrumentation for push-off test

4.2.2 Simulation of the push-off test for FE modelling

Since it is assumed that the load is transmitted equally from the steel beam to each connector, it decided to simulate (using the FEM) the strip highlighted by the rectangle 'A' in Figure 4.5. Another strip of a full HCU 600mm width containing three studs, highlighted by the rectangle B shown in Figure 4.5, will be modelled later on and a comparison between the obtained results from both models will be presented.

The width of strip 'A', the distance between centres of two hollow cores adjacent to the milled slot one, is equal to 240mm. The distance from the stud to the concrete

edges, in the direction of load, is equal to 120 mm similar to that used in the Eurocode 4[8]. In the test specimen, shown in Figure 4.5, the load is applied as distributed load to the concrete edge by using of a spreader plate and the steel beam is restrained. In this simulated one, the load is applied as concentrated load on the steel beam and the concrete is restrained to avoid local failure of concrete in the finite element model. One transverse reinforcing bar is placed in each side. The cross section area of this bar is taken as an equivalent square area of the circular one and calculated so that the reinforcement ratio is the same as it in the test specimen.

4.3 Finite element modelling

The same FE modelling procedures explained, in chapter 3, for modelling steel-solid slab push-off tests was used in modelling steel-precast HCU slab tests. So, in this chapter, explanation of the FE model used will be presented.

4.3.1 Finite element mesh of the model

Combinations of three-dimensional solid elements, which are available in the ABAQUS[2] software, are used to represent the push out specimen. These combinations are the three-dimensional eight-node element (C3D8), the three-dimensional fifteen-node element (C3D15), and the three-dimensional twenty-node element (C3D20). In the modelling of the cast in situ concrete slab around and above the stud, C3D15 and C3D20 elements are used and C3D8 elements are used elsewhere. The shank of the stud consists of C3D15 elements and the stud head consists of both C3D15 and C3D20 elements.

Figure 4.6.a and Figure 4.6.b show the finite element FE mesh used to represent the shear interaction between the steel beam and the cast-precast concrete slab using stud diameter 19x100mm. Initially, different FE meshes are examined to choose the most appropriate one that gives adequately accurate results and takes less time in the solution process. Because of symmetry, only one quarter of the push out arrangement is modelled. Each precast concrete unit is divided into 10 elements along X-direction, 7 elements along Y-direction and 3 elements along Z-direction. This mesh for the precast unit is slightly coarse since it has high strength that makes the whole precast assemblage rigid in comparison with the cast one. The half of the cast in situ concrete is modelled with 10 elements in X-direction, 2 elements in Y-direction, and 5 elements in Z-direction. The half of the shank of the shear connector consists of one C3D15 element in X-direction, one element in Y-direction and two elements

along Z-direction. The half of the stud connector head consists of one C3D15 element and two C3D20 elements along X-direction and one element in Y-direction and one element in Z-direction. The mesh is fine in the areas where the stress concentration is high and the aspect ratio satisfies the limits of the three dimensional solid elements. The flange half of the steel beam is divided into 3 elements along X-direction, 2 elements along Y-direction and one element in Z-direction. The web quarter of the steel beam is divided into 4 elements along X-direction, 1 element in Y-direction and one element in Z-direction. Also is steel beam mesh is fine since it is very rigid compared to the other components. The half of each transverse reinforcement bar is divided into one element along X-direction, 7 elements along Y-direction and one element along Z-direction.

As explained in chapter 3, only the nodes in front of the stud, in the direction of loading, are merged with the surrounding concrete nodes and other nodes of the stud are detached from that of surrounding concrete. Also, only the nodes of the cast in situ concrete inside the milled slot are merged with the precast one while other nodes, along the contact surface in the direction of load, are detached. This is because the bond between them is destroyed at lower load levels due to the presence of the hollow cores along the contact surface and the change in their concrete strengths.

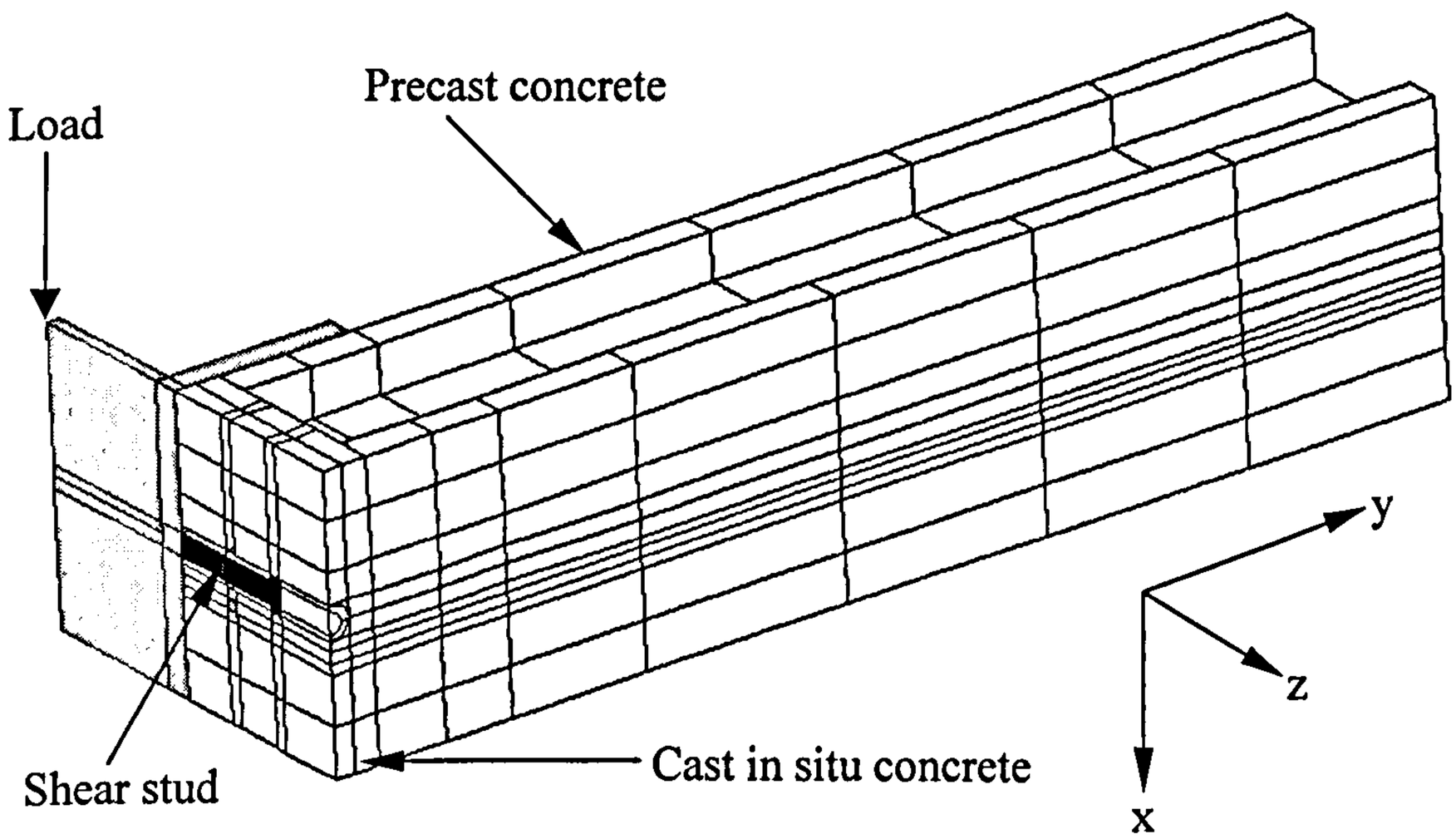

Figure 4.6.a Finite element mesh of the model

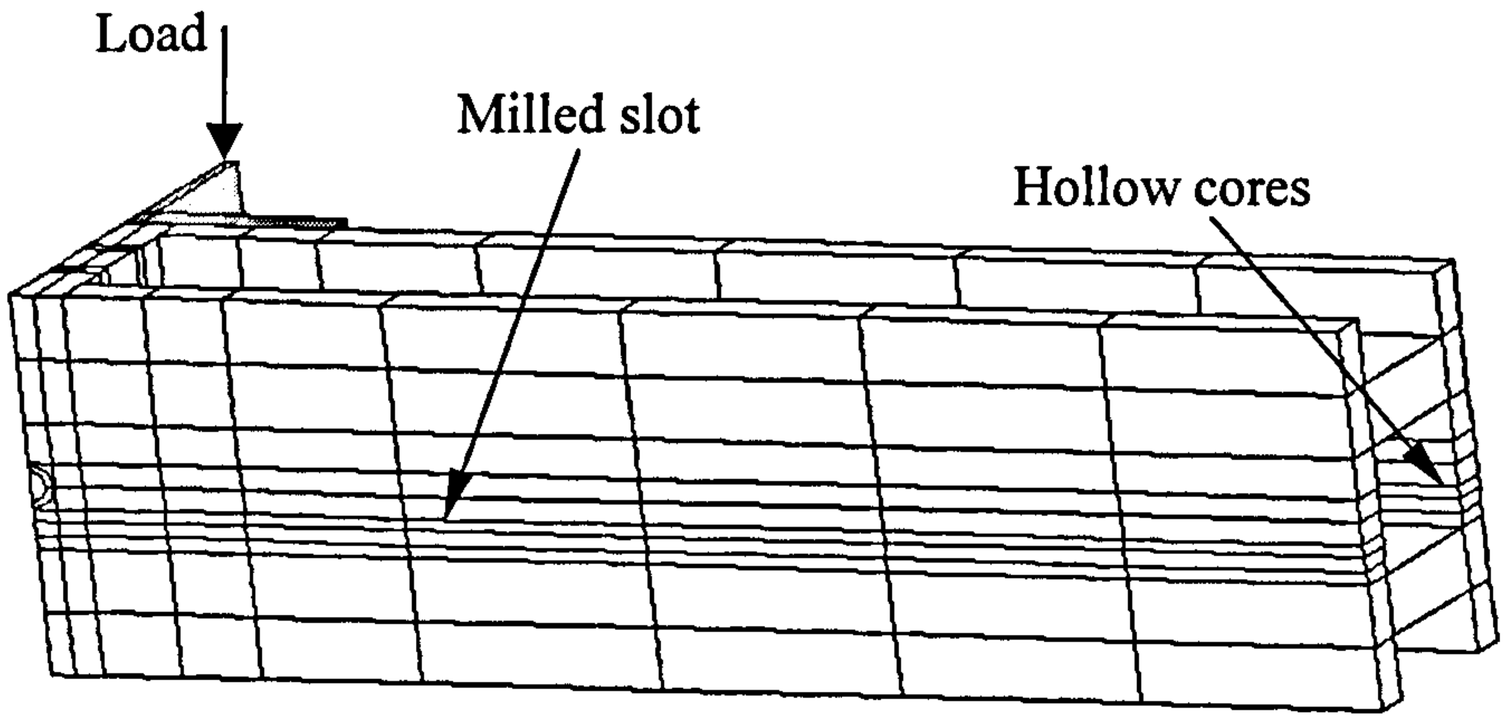

Figure 4.6.b Finite element mesh of the model

4.3.2 Boundary conditions

For the application of the support conditions, all nodes of cast and precast concrete slab in the opposite direction of loading (surface 1) are restricted to move in X-direction to resist the compression load. All nodes along the middle of steel beam web (surface 2) are restricted to move in Y-direction due to symmetry. All concrete nodes, stud nodes, steel beam flange nodes, and steel beam web nodes which lie on the other symmetry surface (surface 3) are restricted to move in Z-direction because of symmetry as shown in Figure 4.7.

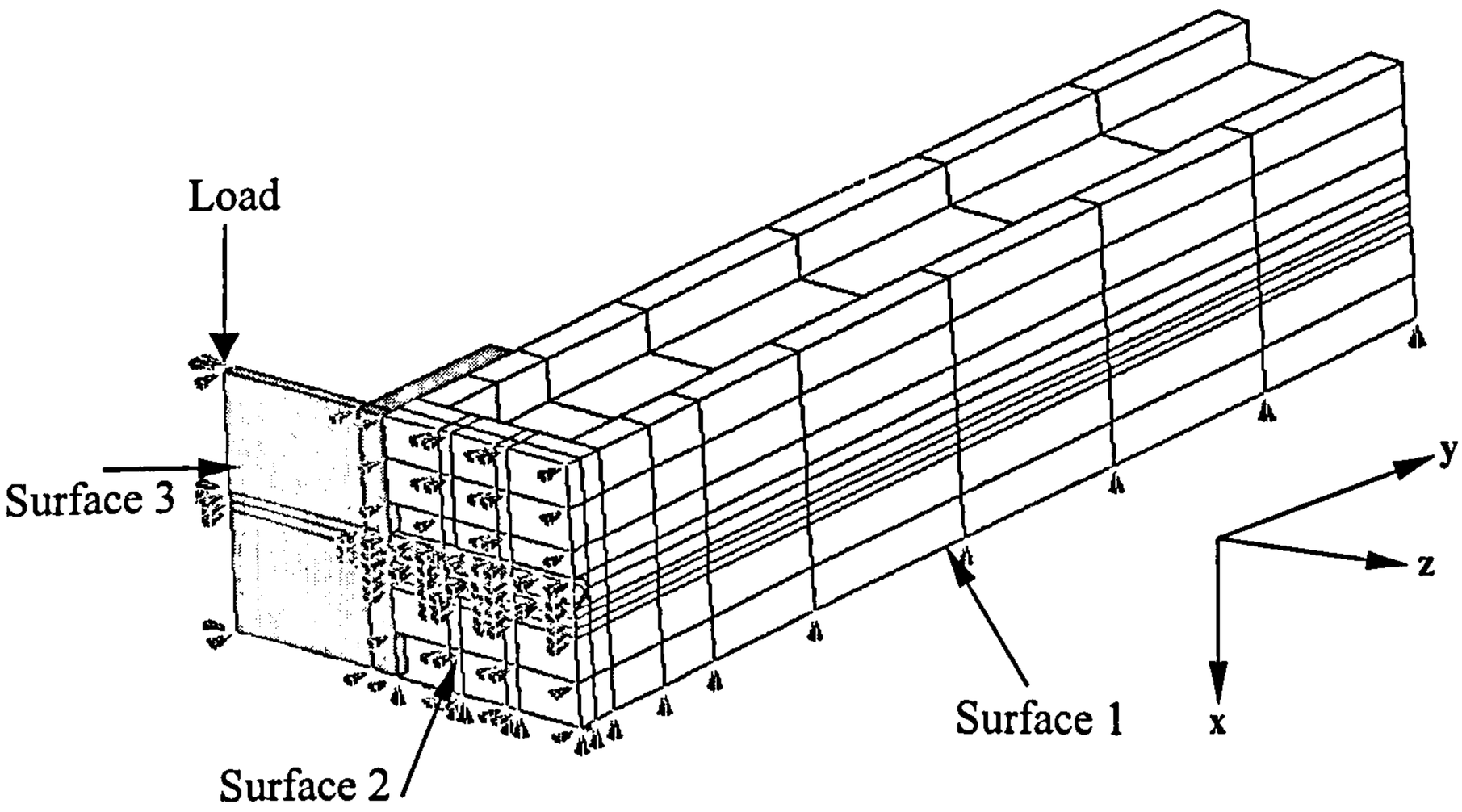

Figure 4.7 Application of load and boundary conditions

4.3.3 Application of load

A concentrated load is applied at the centre of the steel web as shown in Figure 4.7. As explained previously in section 3.4.3, the modified RIKS method available in the ABAQUS[2] software is used to analyse the model from zero load until the maximum load is reached.

4.4 Material modelling of the push-off test specimen components

Modelling of shear connection between steel and precast HC concrete slab requires the successful representation of all different components associated with the connection. To model a component properly it is essential to choose a proper element type, size and to correctly represent all the key material properties. In a shear connection, the following major components must be considered.

1. Cast in situ concrete slab.
2. Precast hollow-cored concrete unit.
3. Steel beam.
4. Shear studs.
5. Transverse reinforcement bar.

4.4.1 Material modelling of a cast in situ and precast concrete

To develop the model for the behaviour of concrete either the cast in situ or the precast one in the composite connection, the bilinear stress-strain curve will be used. This model treats the concrete as elastic-plastic material.

4.4.1.1 Elastic-plastic material model of precast and cast in-situ concrete

This model takes into account the inelastic behaviour of the concrete material. The option (*PLASTIC) is used to specify the plastic part of the material model for elastic-plastic materials that use the Mises yield surface. It is assumed that the concrete behaves as a linear-elastic material up to the yield stress. Perfect plasticity is obtained when reaching the yield stress. For the elastic part of the stress-strain curve, it is required to identify both of Young's modulus and Poisson's ratio for concrete. The same relations used in section 3.4.4 will be used for both precast and in-situ concrete in this chapter. The only difference is the supplied precast concrete unit has concrete strength of 50 N/mm^2 while the cast in situ strength may vary according to the mix proportions.

4.4.2 Material modelling of shear stud and transverse reinforcement bar

The bilinear model used to model the headed shear stud in section 3.4.5 is used in this chapter to model the transverse reinforcement bar. To establish the mechanical properties of the reinforcement bars, tensile tests were conducted to evaluate the yield stress f_{ys} and Young's modulus E_s of the bar.

4.4.3 Material modelling of steel beam

Also, the same bilinear model of steel beam used in section 3.4.6 is used in this chapter to model the steel beam in steel-precast HC slab push-off test.

4.5 FE model results from simulating present push-off tests

Four push-off test specimens were analysed using the present FE model. The test specimens were given a reference of the following format T bs-C-t-g where:

T: test specimen, bs: bar size, C: grade of insitu concrete, t: the concrete slab thickness and g: the gap size. So, T 10-C25-150-65 is a test specimen that has 10mm transverse reinforcement diameter, concrete cube strength of 25N/mm^2, concrete slab thickness of 150mm and a gap size of 65mm.

4.5.1 Test T 10-C25-150-65

The present finite element model is used to analyse a push-off test specimen of 10mm transverse reinforcement bar, 25N/mm^2 cube strength of in-situ concrete, 150mm precast unit and 65mm gap width. Figure 4.8 shows the load-slip curve obtained from FE modelling. The maximum failure load was 67.9kN at 3.16mm slip.

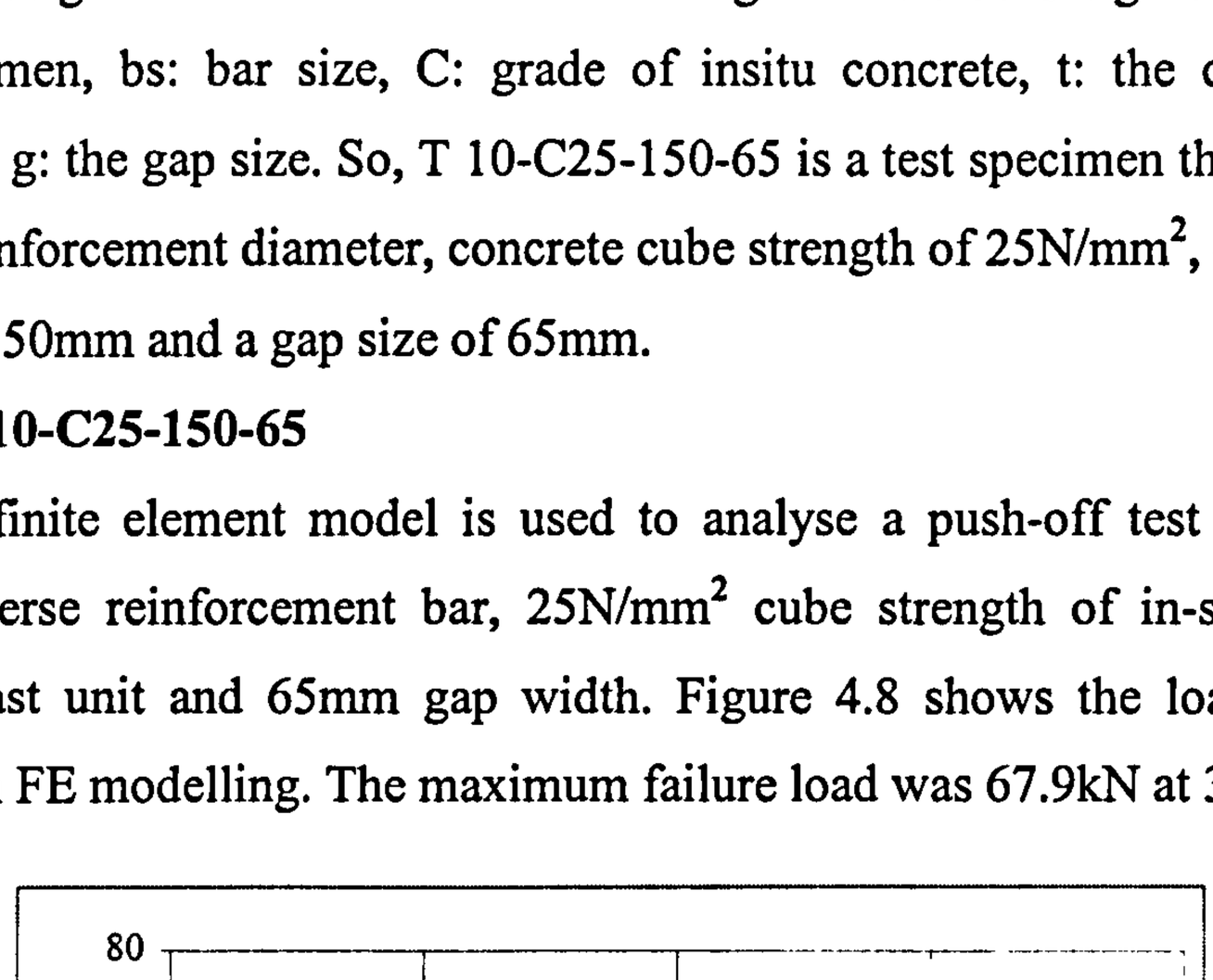

Figure 4.8 Load vs. slip curve of the stud for push-off test T 10-C25-150-65

For lower reinforcement size (10mm), the transverse reinforcement failure mode is likely to occur. The reinforcement bar yields first leading to concrete failure around the stud that has not reached its full yielding yet. Figure 4.9 shows the load-strain curve of the transverse reinforcement bar. It can be seen that the reinforcement bar reached its ultimate strain and consequently ultimate stress at failure.

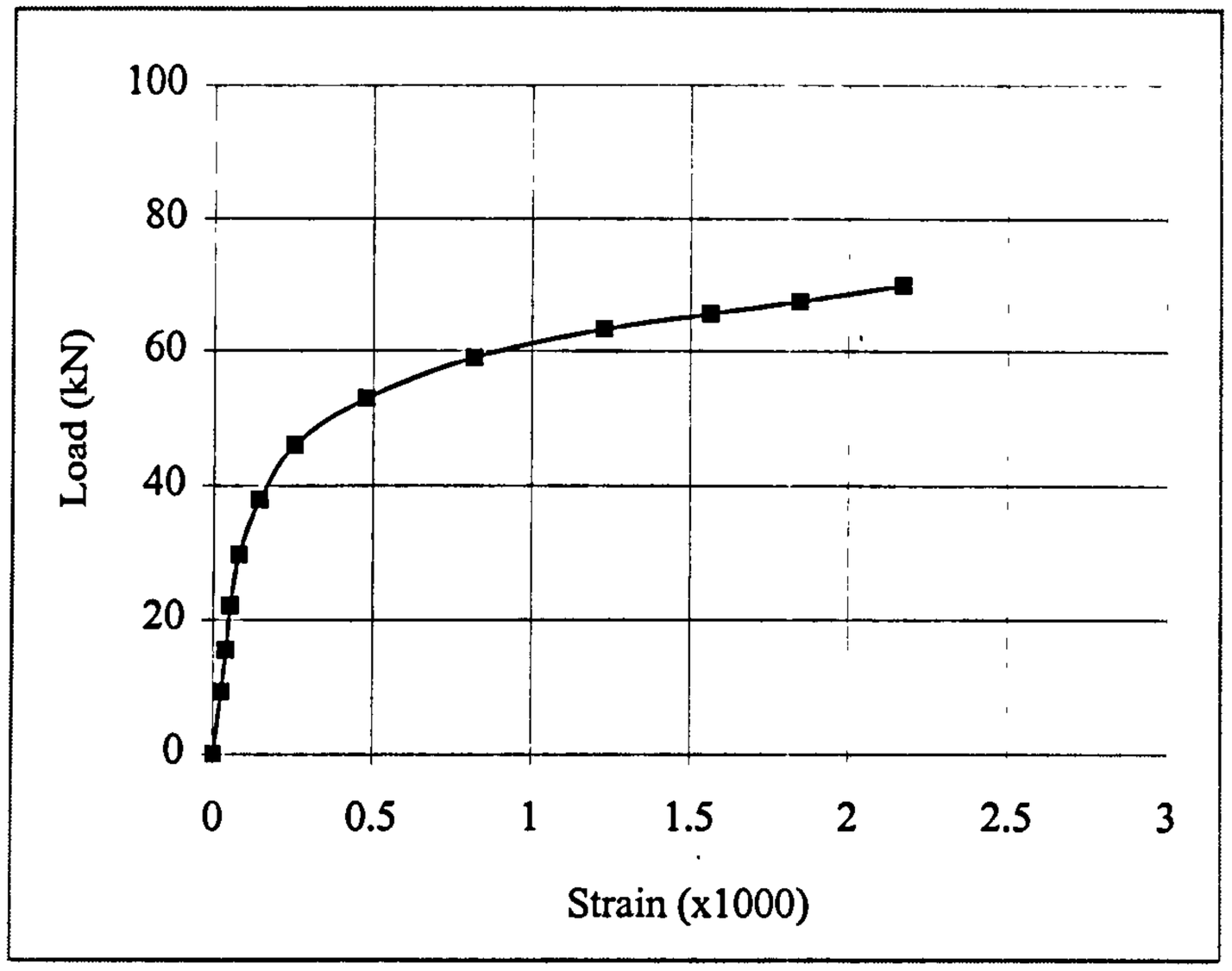

Figure 4.9 Load-strain curve of transverse reinforcement for test T 10-C25-150-65

Figure 4.10 shows the contour stress distribution and deformed shape of T 10-C25-150-65mm at different load levels obtained by post ABAQUS processing. At a load level of 22kN, the concrete elements in front of the stud collar started to yield forming a small failure cone. By continuing loading up to failure the size of the failure cone increased. It can be seen that at failure a full conical concrete failure was obtained and the reinforcement bar yielded at the same time. The failure mode has been explained in chapter 3 but the size of the failure cone is slightly reduced due to the presence of the reinforcement bar that reduces the stress on the concrete around. The conical failure is extended along the in-situ concrete and reached the upper surface.

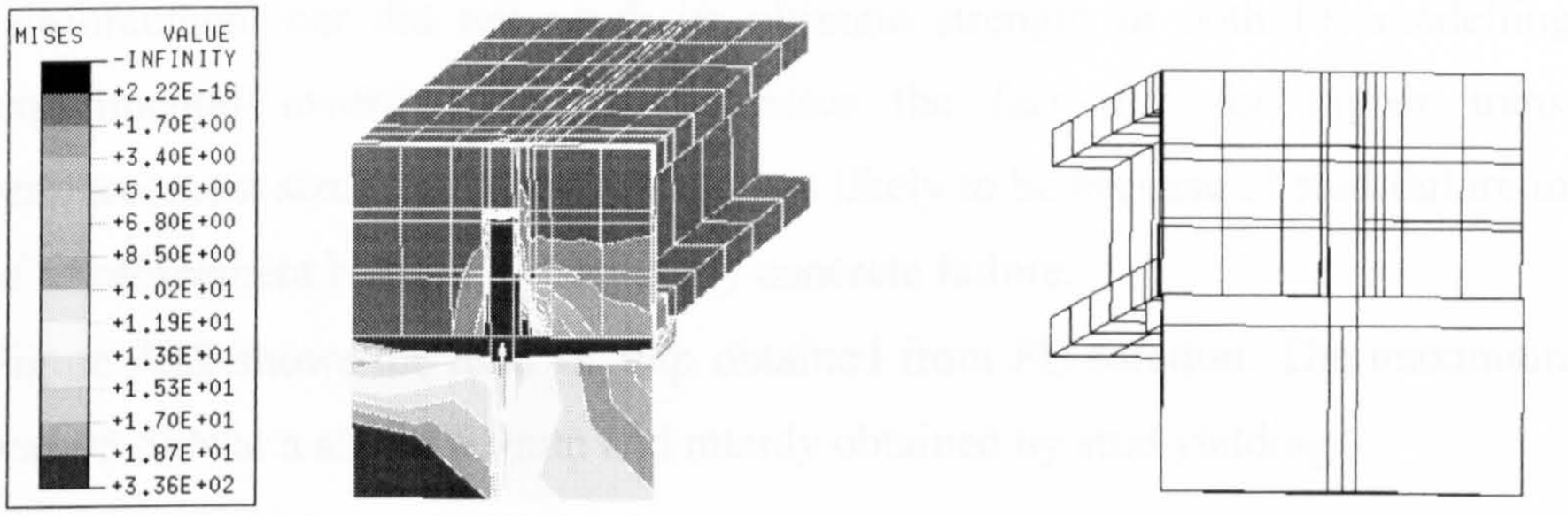

Fig. 4.10.a Load level of 22kN

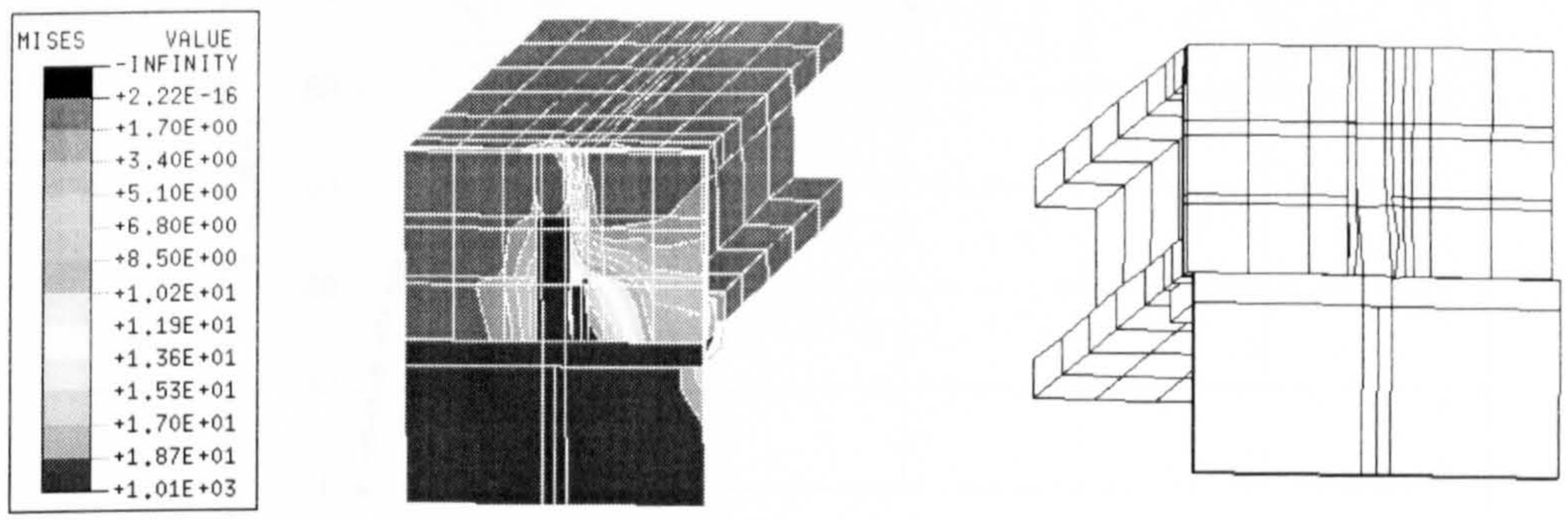

Fig. 4.10.b Load level 46kN

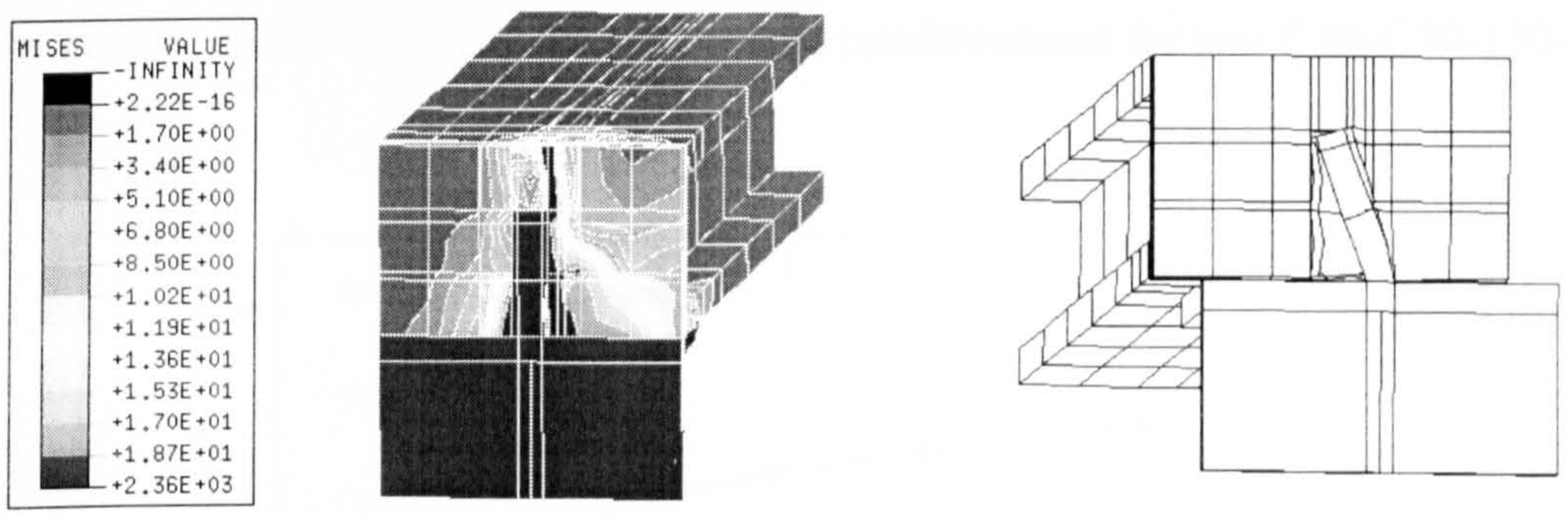

Fig. 4.10.c Load level of 68kN

Figure 4.10 Stress contours and deformed shapes of T10-C25-150-65 at various load levels

4.5.2 Test T 16-C30-150-80

The load vs. strain curve is plotted in figure 4.11 for T 16-C30-150-80 which has larger transverse reinforcement bar diameter (16mm) compared with (10mm) diameter in the previous test. It can be seen that although failure has occurred and

four studs have already sheared off for this push-off test specimen, the transverse reinforcement bar did not reach its ultimate strength in both FE modelling and experimental investigation. This stresses the fact that for higher transverse reinforcement sizes, the mode of failure is likely to be because of stud failure instead of reinforcement bar and consequently concrete failure.

Figure 4.12 shows the load vs. slip obtained from FE solution. The maximum load was 95.5kN at a slip of 6.9mm and mainly obtained by stud yielding.

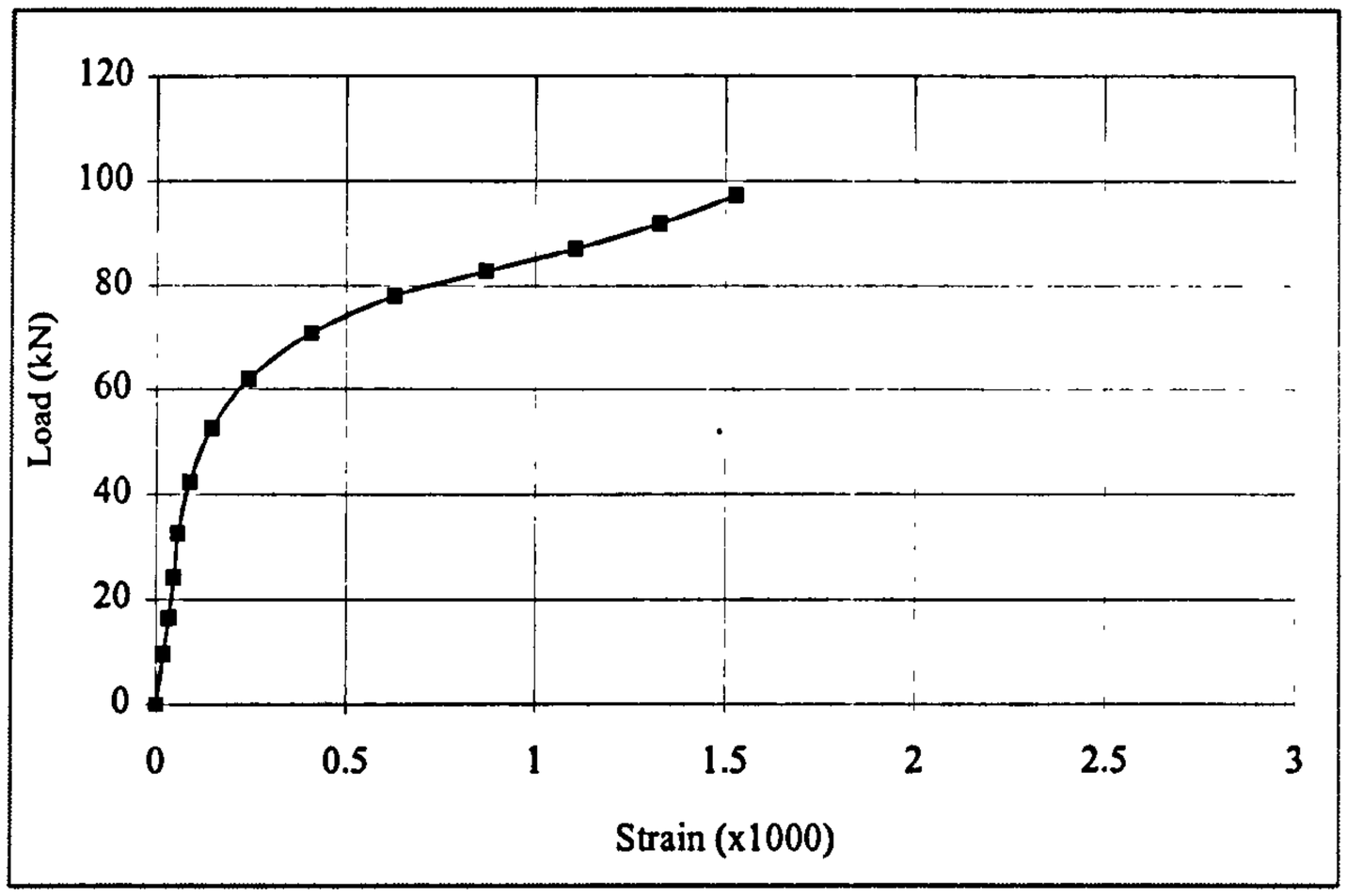

Figure 4.11 Load-strain curve of transverse reinforcement for test T 16-C30-150-80

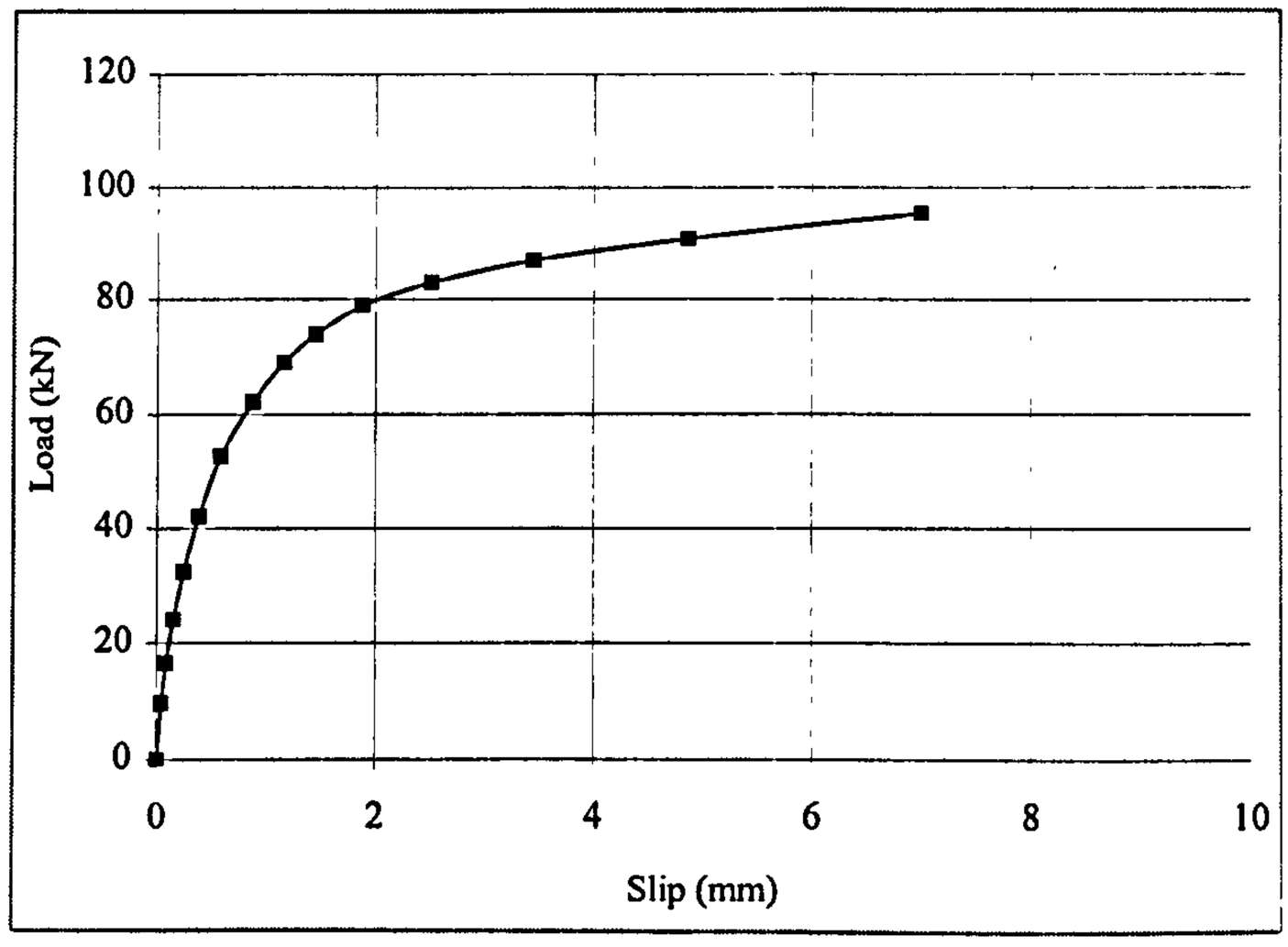

Figure 4.12 Load vs. slip curve of the stud for push-off test T 16-C30-150-80

The distribution of stresses and deformed shapes over the T 16-C30-150-80 test is plotted in figure 4.13 at different load levels. It can be seen that, although the conical failure is reached the failure occurred because of the stud failure since the reinforcement bar can still carry the stresses induced after the concrete failure. The conical failure is extended along the in-situ concrete and reached the upper surface.

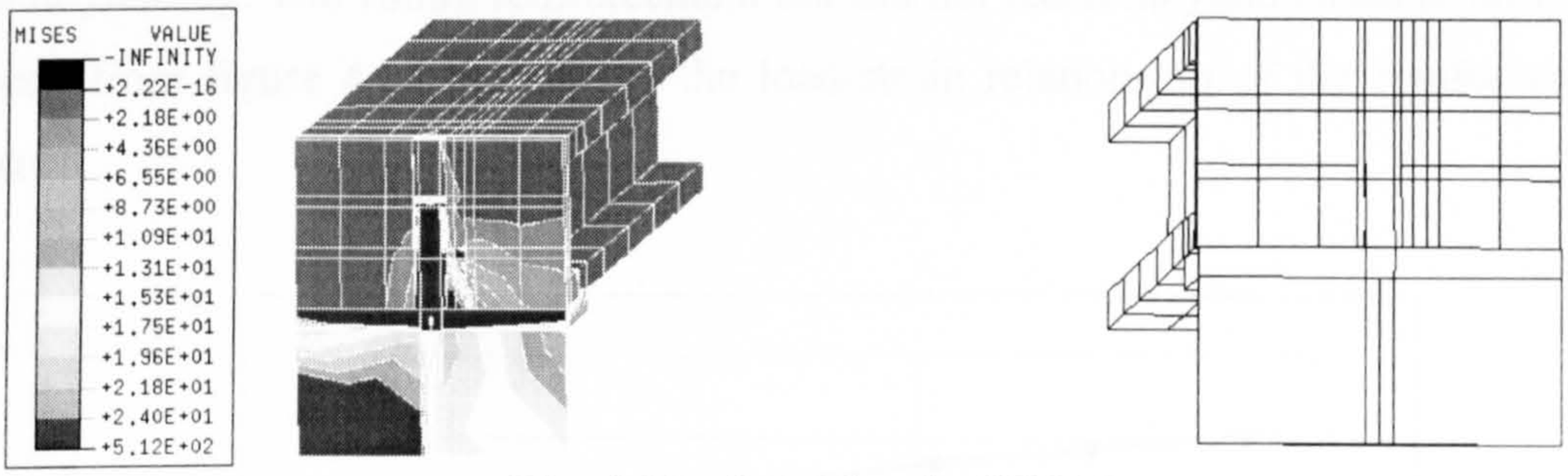

Fig. 4.13.a Load level of 32kN

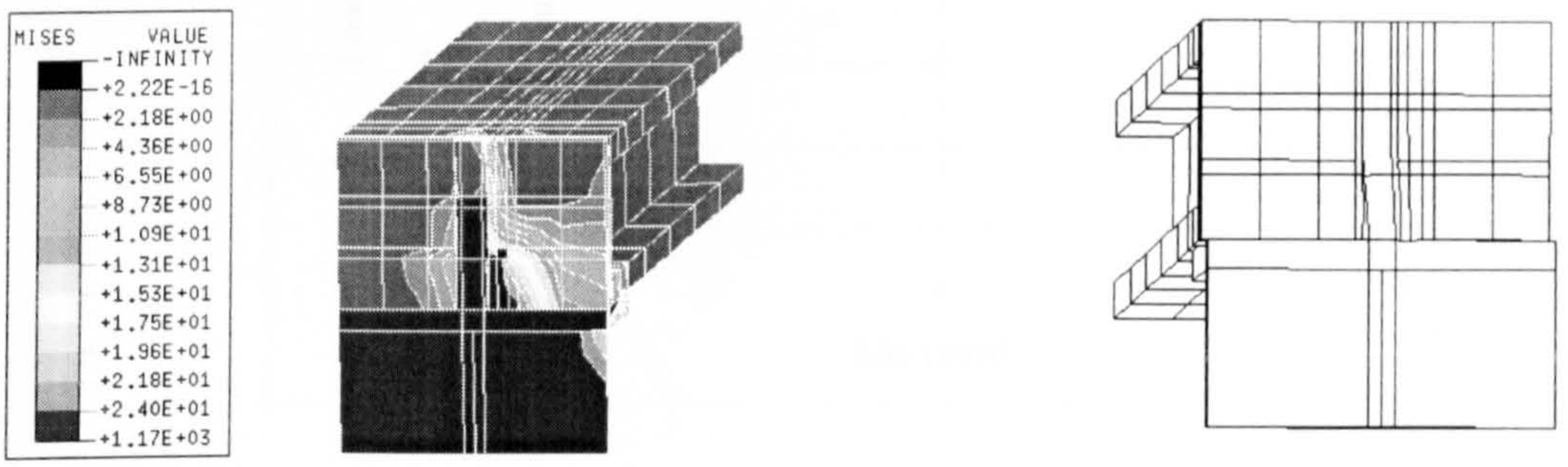

Fig. 4.13.b Load level of 62kN

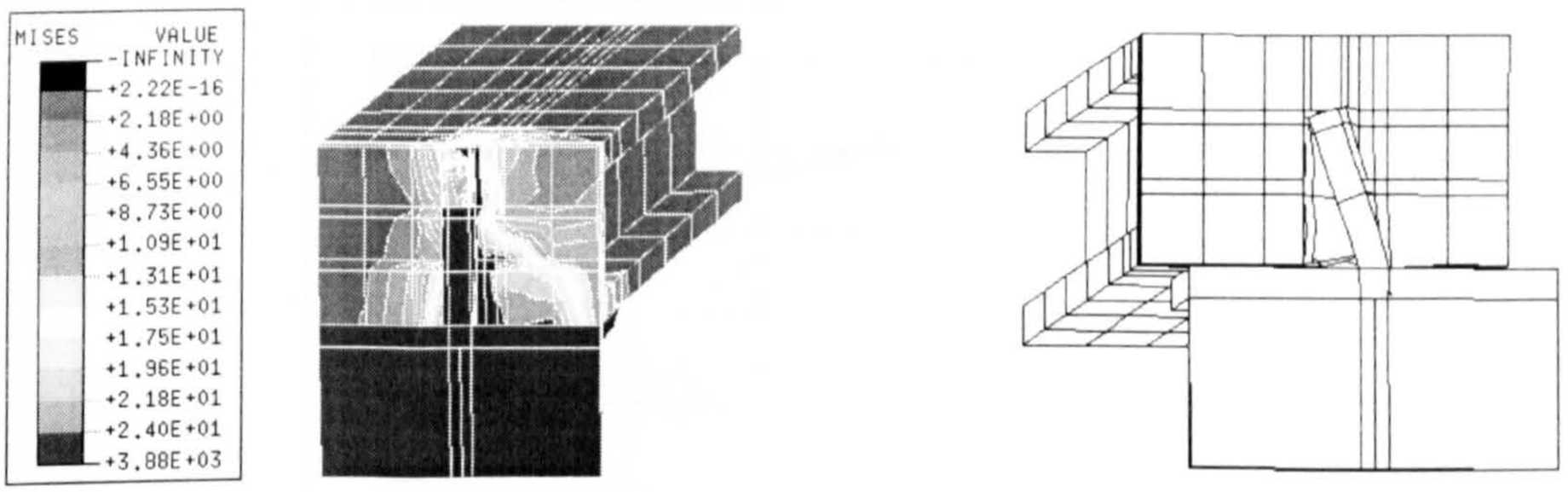

Fig. 13.c Load level of 96kN

Figure 4.13 Stress contours and deformed shapes of T16-C30-150-80 at various load levels

4.5.3 Test T 16-C30-200-80

Figure 4.14 shows the load-slip behaviour of the stud for push-off test T 16-C30-200-80. The specimen has transverse reinforcement bar of 16mm, cast in situ concrete cube strength of 30N/mm^2, precast hollow concrete depth of 200mm and gap size of 80mm. A slight change in the model is needed to keep the aspect ratio in the ABAQUS limits after the increase in depth from 150mm to 200mm. The failure occurred at a load of 100.3kN at a slip of 6.85mm and the cause of failure was the stud yielding. The 16mm reinforcement bar did not reach its yield stress at failure as seen from figure 4.15 that shows the load-strain relationship of the reinforcement bar.

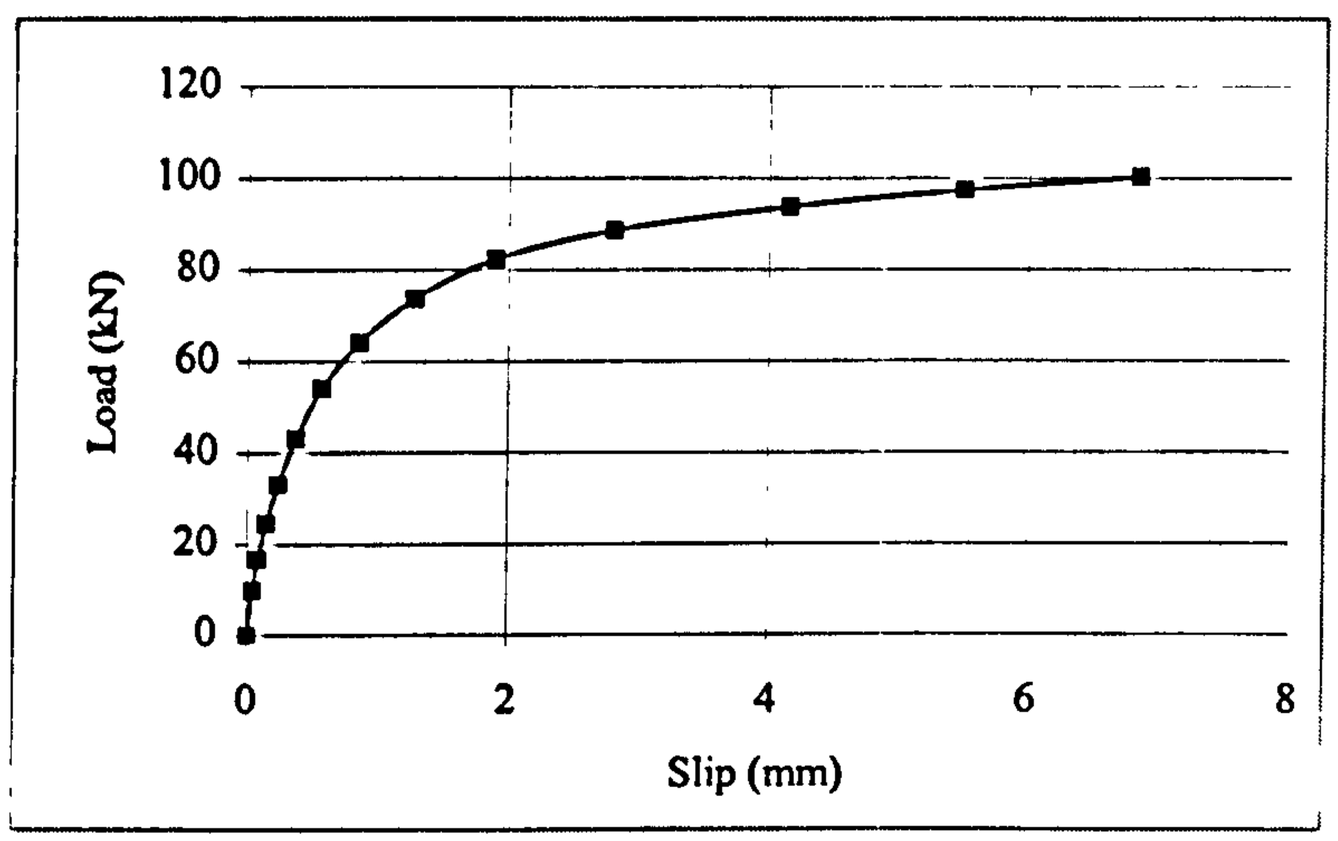

Figure 4.14 Load vs. slip curve of the stud for push-off test T 16-C30-200-80

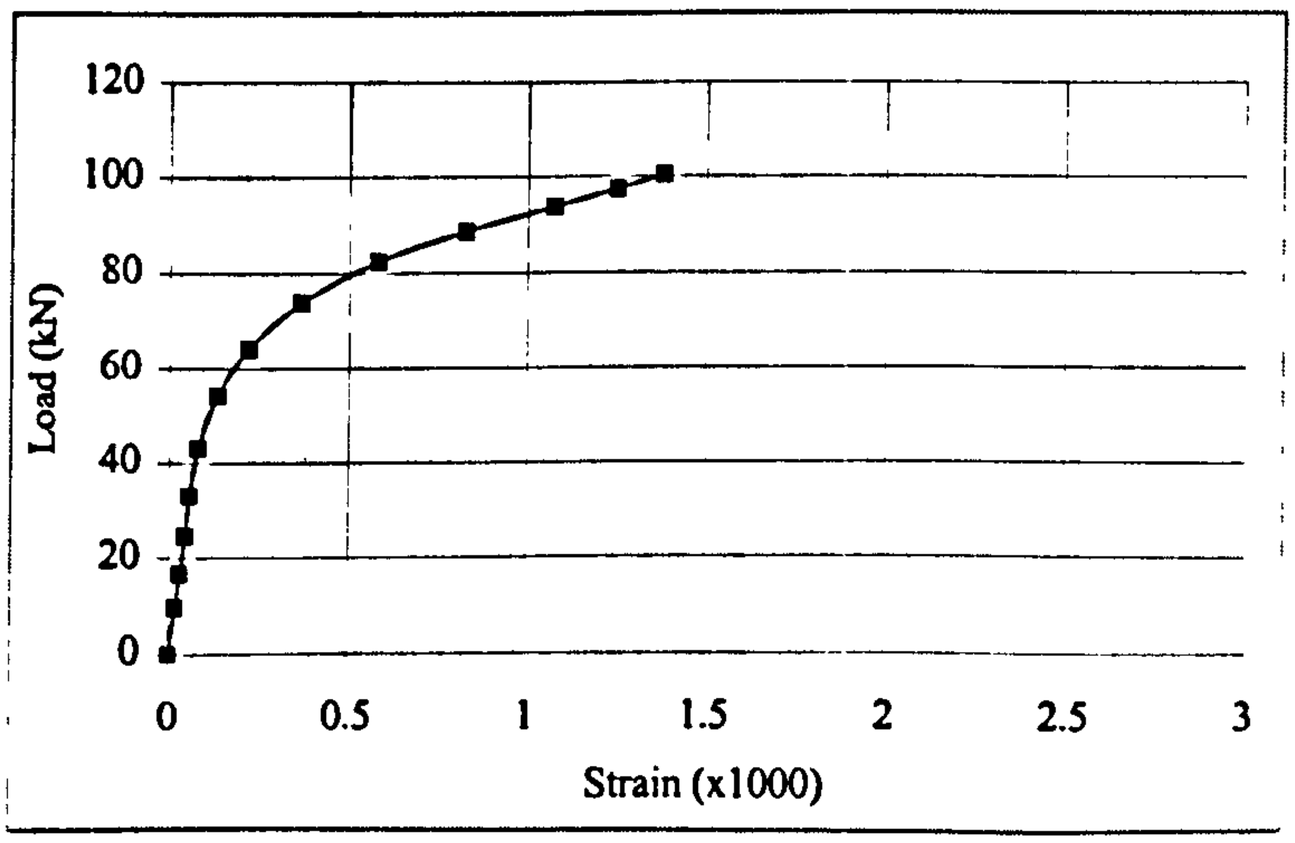

Figure 4.15 Load-strain curve of transverse reinforcement for test T 16-C30-200-80

Also, following the contour stress distribution at different load levels in figure 4.16 shows that for higher depth of precast units, 200mm, the surface remains unremarkably affected with maximum stresses. The conical failure of concrete is mainly concentrated in the entire depth of the cast in situ and precast concrete and hence thin cracks on the outer surface are expected.

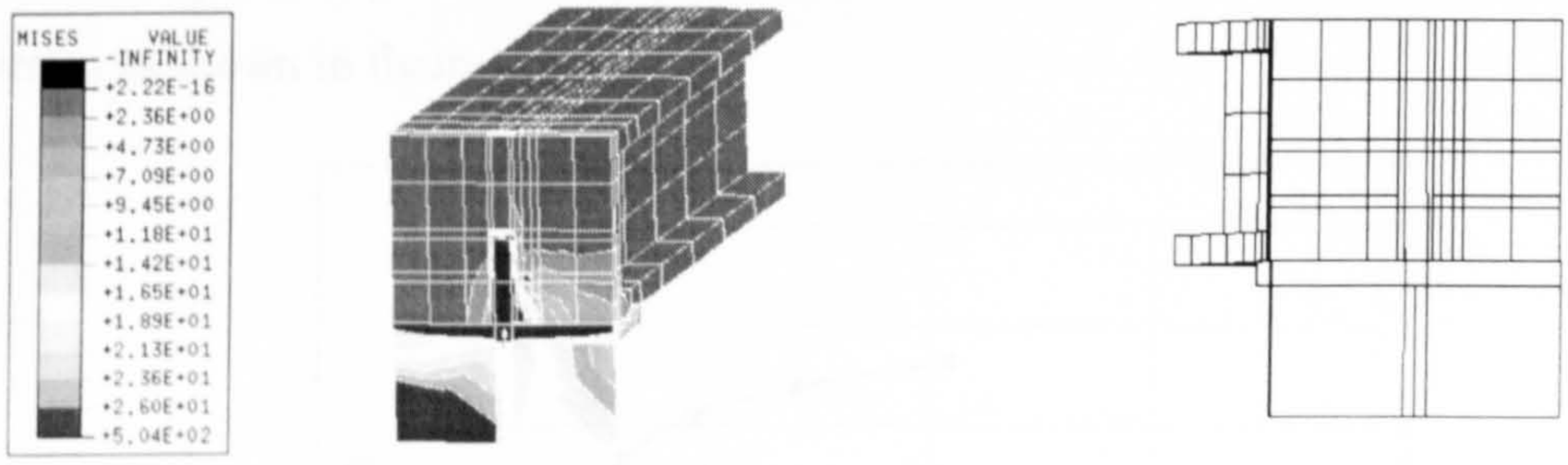

Fig. 4.16.a Load level of 33kN

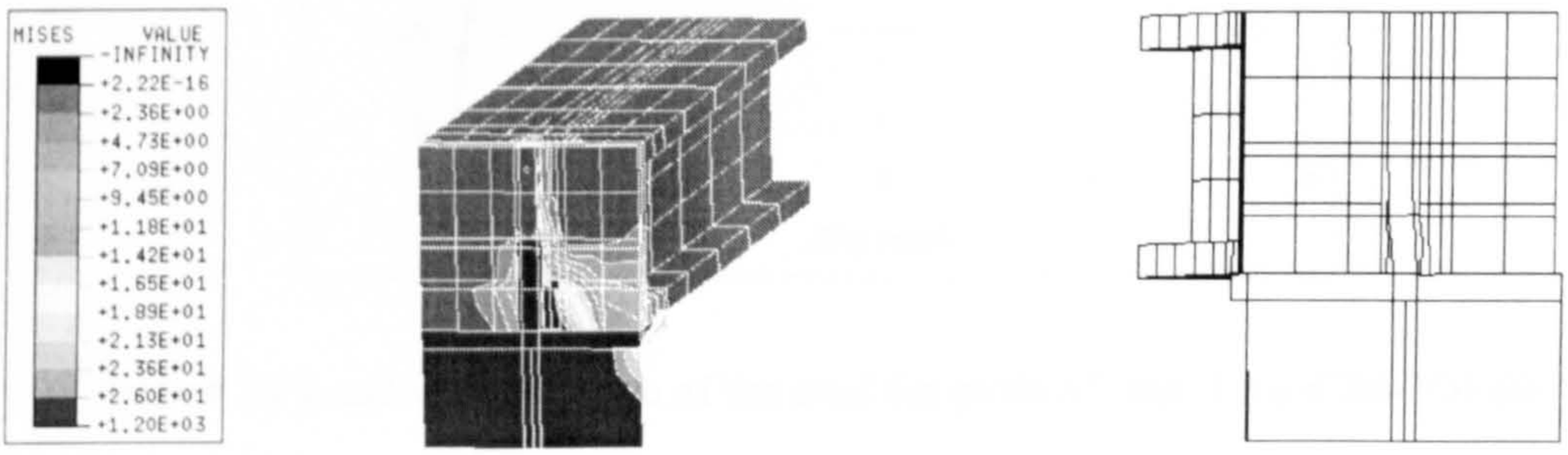

Fig. 4.16.b Load level of 64kN

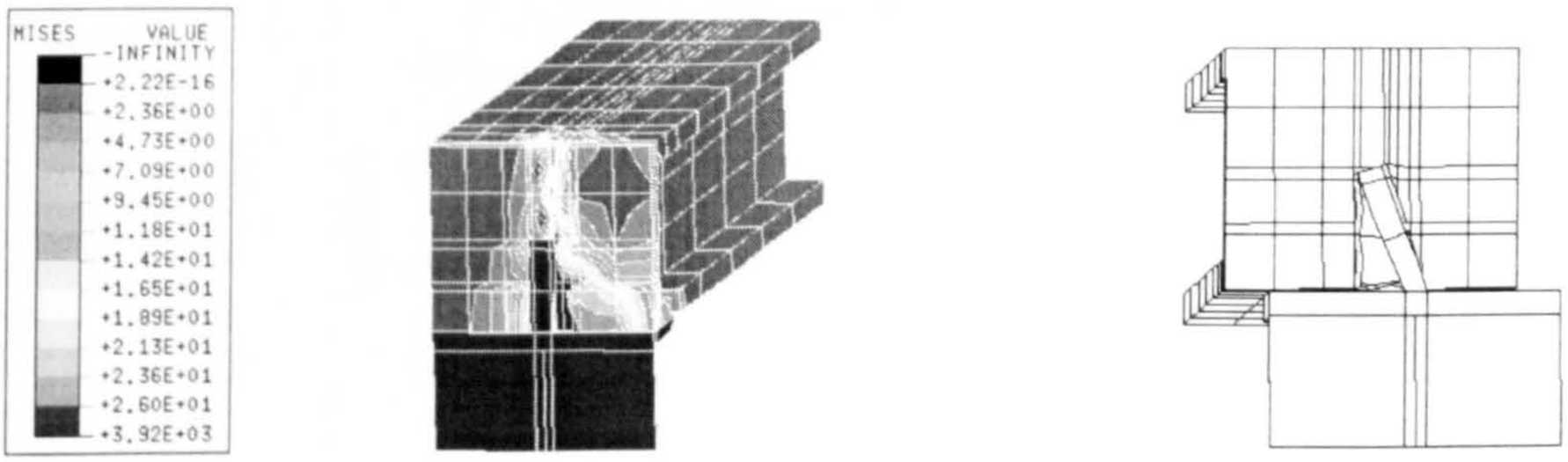

Fig. 4.16.c Load level of 97kN

Figure 4.16 Stress contours and deformed shapes of T16-C30-200-80 at various load levels

4.5.4 Test T 16-C30-200-60

In this test specimen, the same reinforcement bar of 16mm, in-situ concrete strength of 30N/mm^2 and depth of precast hollow core of 200mm like the previous specimen, were used. The only difference is in the gap size, which is taken 60mm. Figure 4.17 shows the load-slip curve of the stud for T 16-C30-200-60. The maximum failure load was 92.72kN at a slip of 4.18mm obtained by FE analysis. The failure is mainly reached by yielding of the stud since the 16mm reinforcement did not reach its yield stress as shown in figure 4.18.

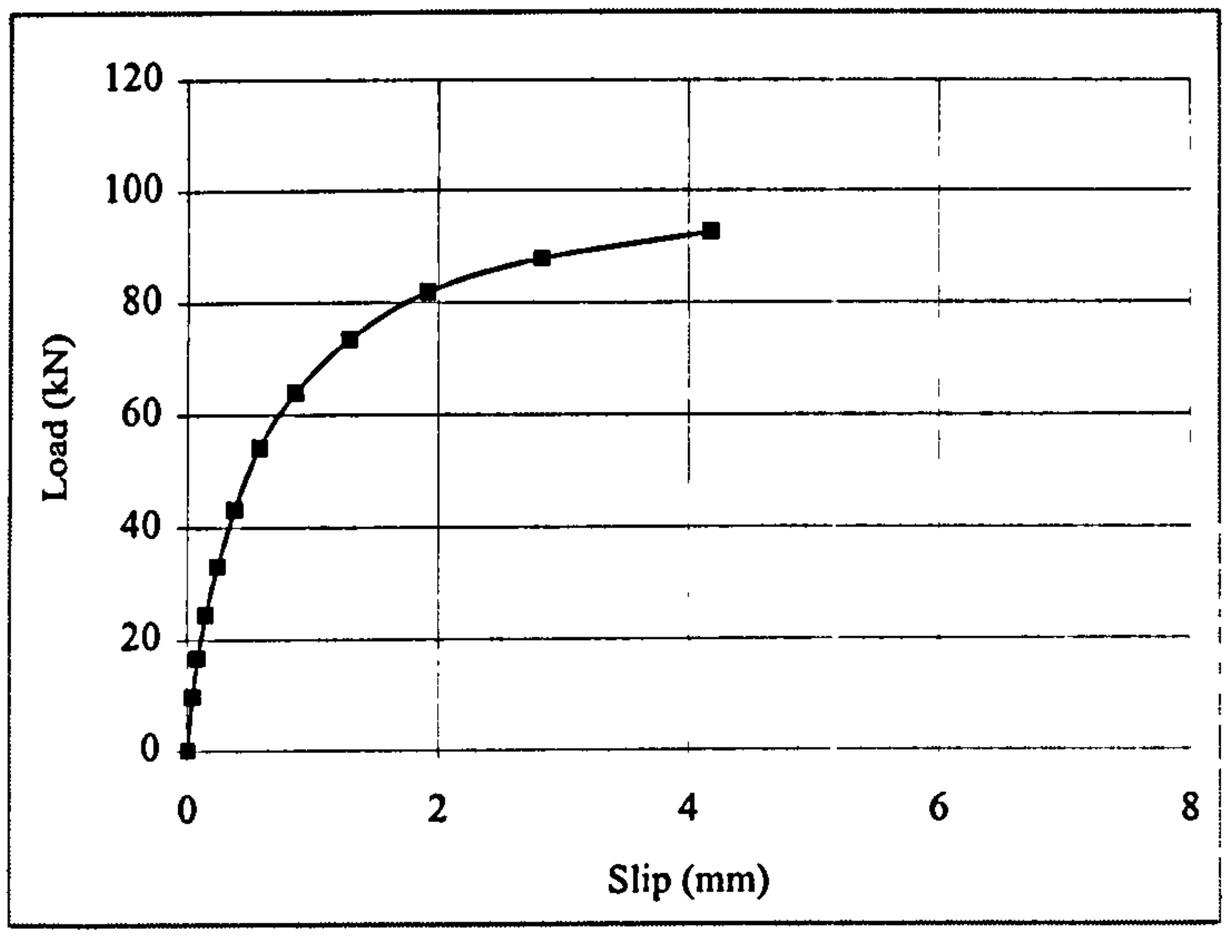

Figure 4.17 Load vs. slip curve of the stud for push-off test T 16-C30-200-60

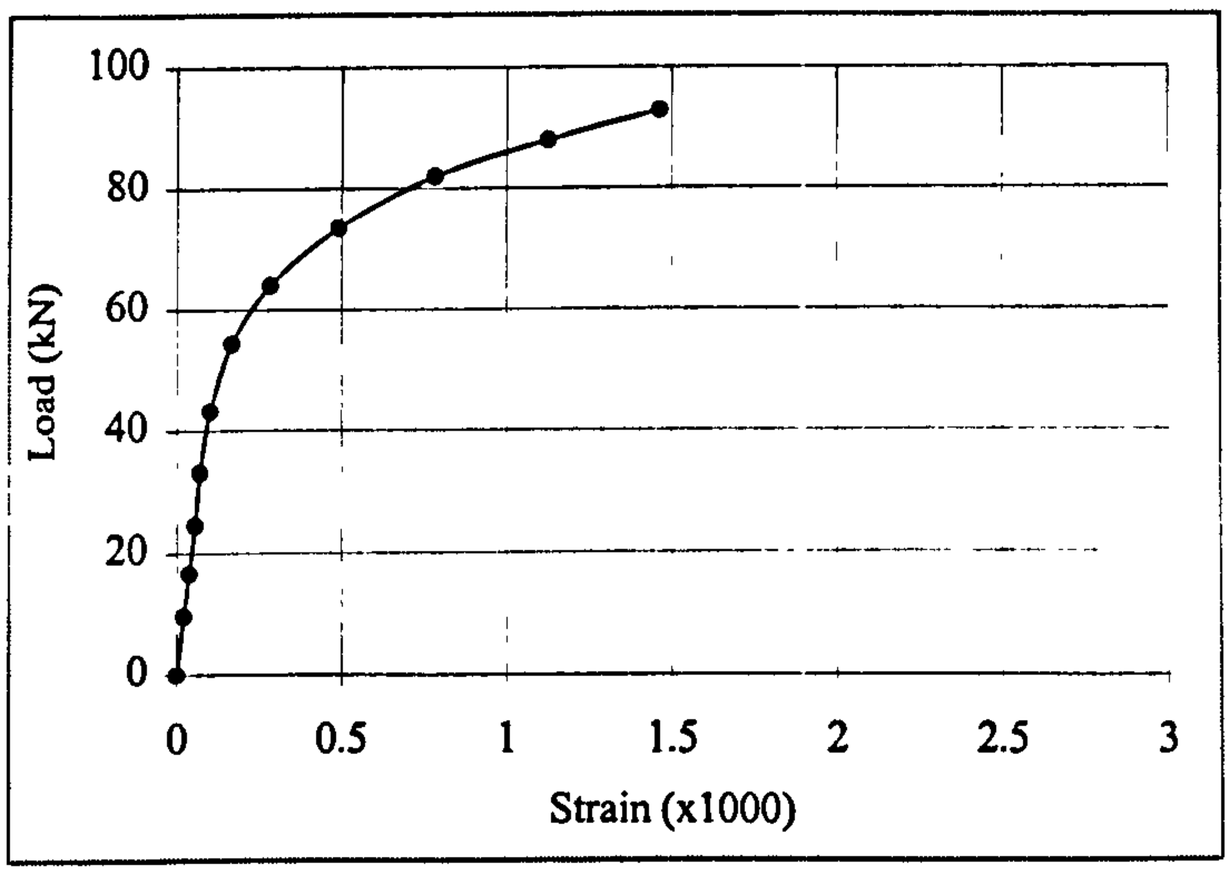

Figure 4.18 Load-strain curve of transverse reinforcement for test T 16-C30-200-60

Figure 4.19 shows the contour stress distribution and deformed shapes at different load levels. It can be seen that the conical failure did not reach the top surface of the in-situ and precast concrete because of higher depth of hollow core unit as for the previous test.

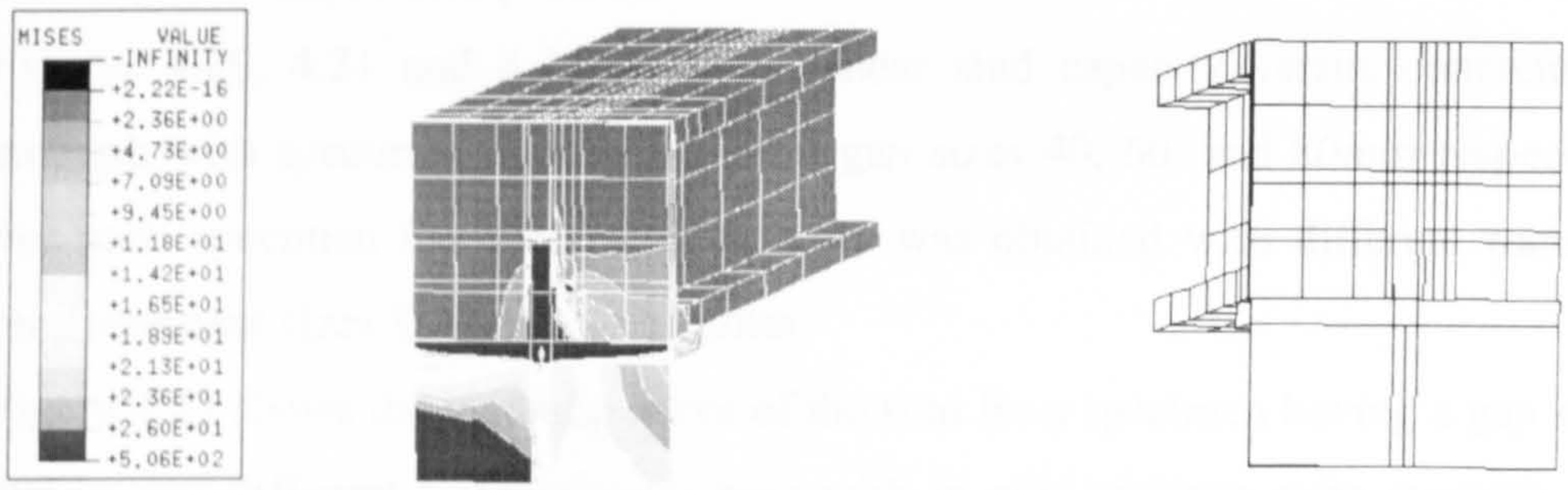

Fig. 4.19.a Load level 33kN

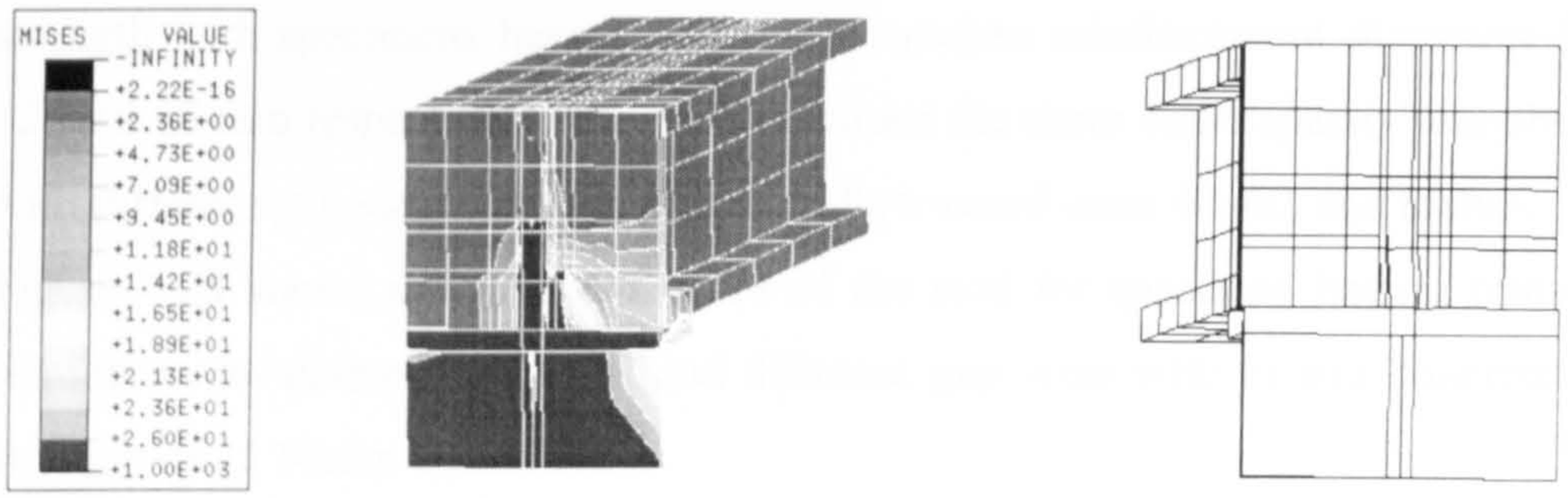

Fig. 4.19.b Load level 54kN

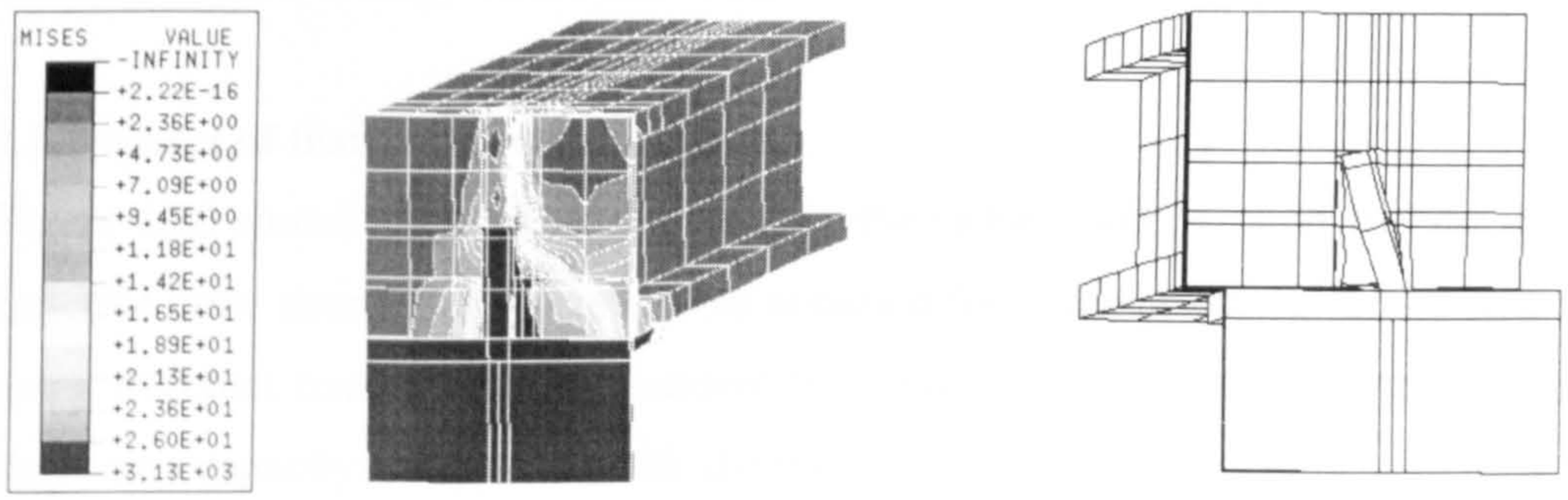

Fig. 4.19.c Load level 92kN

Figure 4.19 Stress contours and deformed shapes of T16-C30-200-60 at various load levels

4.6 Parametric study

Parametric studies were carried out using the present finite element model to investigate the effect of variations in transverse reinforcement diameter, insitu concrete cube strength and gap size between 150mm deep HCUs on both the shear stud capacity and load-slip curve.

Figures 4.20, 4.21 and 4.22 show the shear stud capacity versus concrete cube strength with specimens having different gap sizes 40, 60, and 80mm respectively. For each specimen the shear stud capacity was obtained with different transverse reinforcement sizes 8, 10, 12, and 16mm.

Figure 4.23 shows the load-slip curve of the stud for a specimen having a gap size of 40mm and different reinforcement bars with in situ concrete cube strength of 25 N/mm^2.

Figures 4.24 to 4.27 show the shear stud capacity versus in situ concrete cube strength with specimens having different transverse reinforcement diameters 8, 10, 12, and 16 mm respectively. For each specimen the shear stud capacity was obtained with different gap sizes between precast hollow-cored units 40, 60, and 80mm.

Figure 4.28 shows the load-slip curve of the stud for specimen having transverse reinforcement diameter of 8mm and different gap sizes with in situ concrete cube strength of 25 N/mm^2.

Figures from 4.29 to 4.30 show the load-slip curves of the stud at different in situ concrete cube strengths with certain gap 40mm and different reinforcement diameters 8mm, 10mm, 12mm and 16mm respectively.

4.6.1 Effect of transverse reinforcement

Figure 4.20 shows the relationship between the failure load per stud and the in situ concrete cube strength. The curves are obtained for a gap width 'g' of 40 mm and using different transverse reinforcement bar diameters 'bs'. It can be seen that the shear stud capacity is increased with the increase in bar diameter. This is because the transverse reinforcement bars enhance the in-plane shear resistance of the composite slab by crossing the precast and the in situ concrete interface. By increasing the bar cross section area, the assistance of the precast concrete to the in situ concrete increases in resisting transverse forces from shear connectors. When the reinforcement bar reaches the yield stress, the concrete around the stud fails leading to earlier failure of connection. This is because the presence of the transverse bar

controls the longitudinal splitting of the slab by carrying tensile splitting forces. The use of 16mm diameter in this test specimen provides shear capacity for the connection close to that one of adequately reinforced solid slab of the same strength as the in situ concrete and has the same depth. In another meaning if a small gap is used in the precast slab specimen, the bar diameter should be increased to obtain shear stud capacity close to that one of solid slab. Also, it can be seen that effect of the reinforcement size decreases with the increase of in-situ concrete strength.

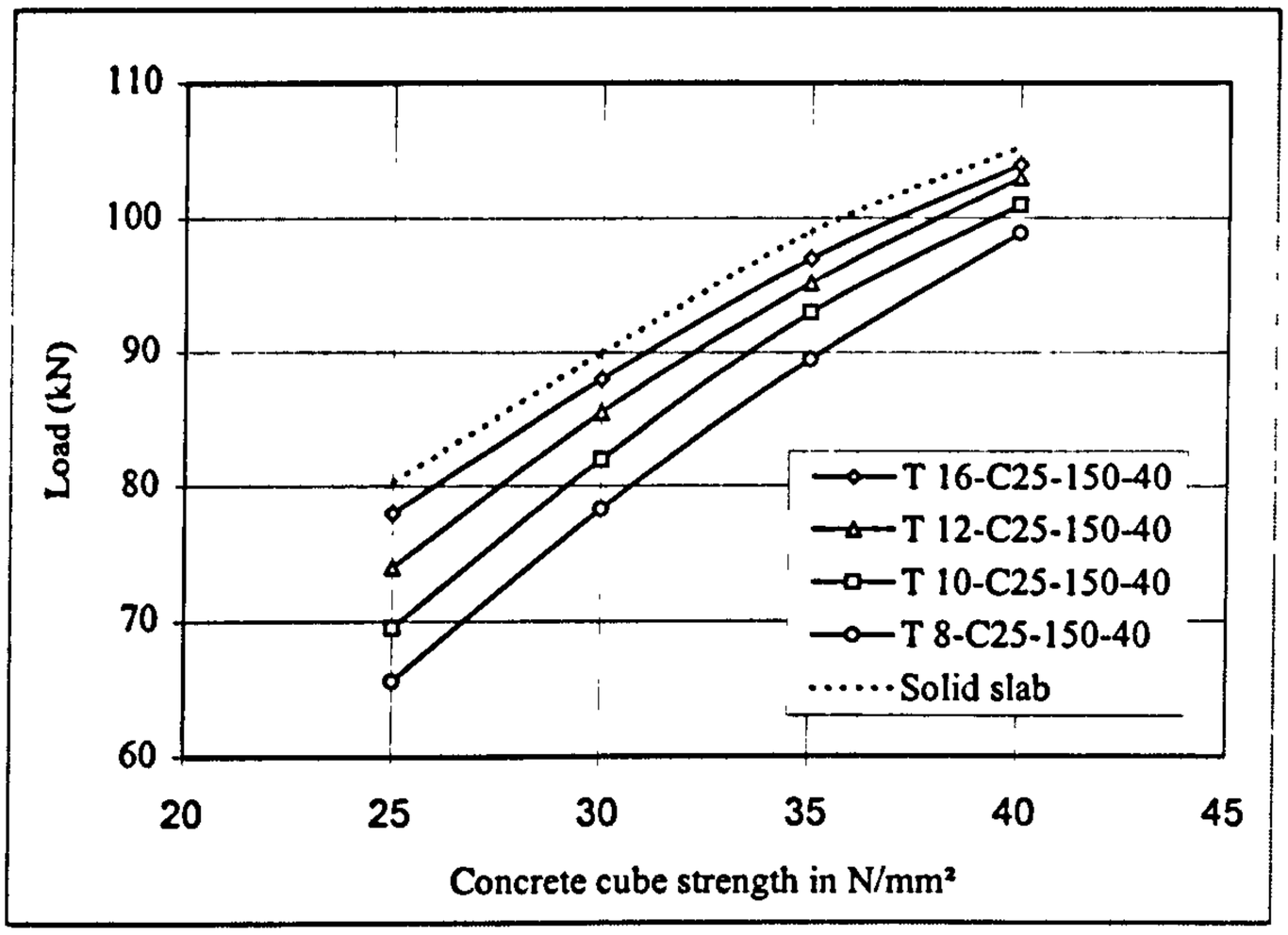

Figure 4.20 Effect of 'bs' change on load per stud-in situ concrete cube strength curve

The same curves between the load per stud and the concrete cube strength are obtained in figures 4.21 and 4.22 for 'g' equals 60 and 80 mm respectively. It can be seen from figure 4.21 that the increase in the gap size, the decrease in the effect of the reinforcement bar diameters on the shear stud capacity. Also, it can be noticed that the curves obtained for the bar diameters 12 and 16 mm are close. This means that, for a gap of 60 mm, the required reinforcement diameter that provides approximately the same stud capacity in solid slab specimen may be reduced to 12 mm. Also figure 4.22 shows that for a gap 80 mm, the effect of change in transverse reinforcement size on the shear stud capacity is reduced. A gap of 80mm may provide a good composite action between the precast and cast concrete with a small reinforcement ratio. The shear stud capacity will be very close to that one obtained from a solid concrete slab of the same cast concrete strength.

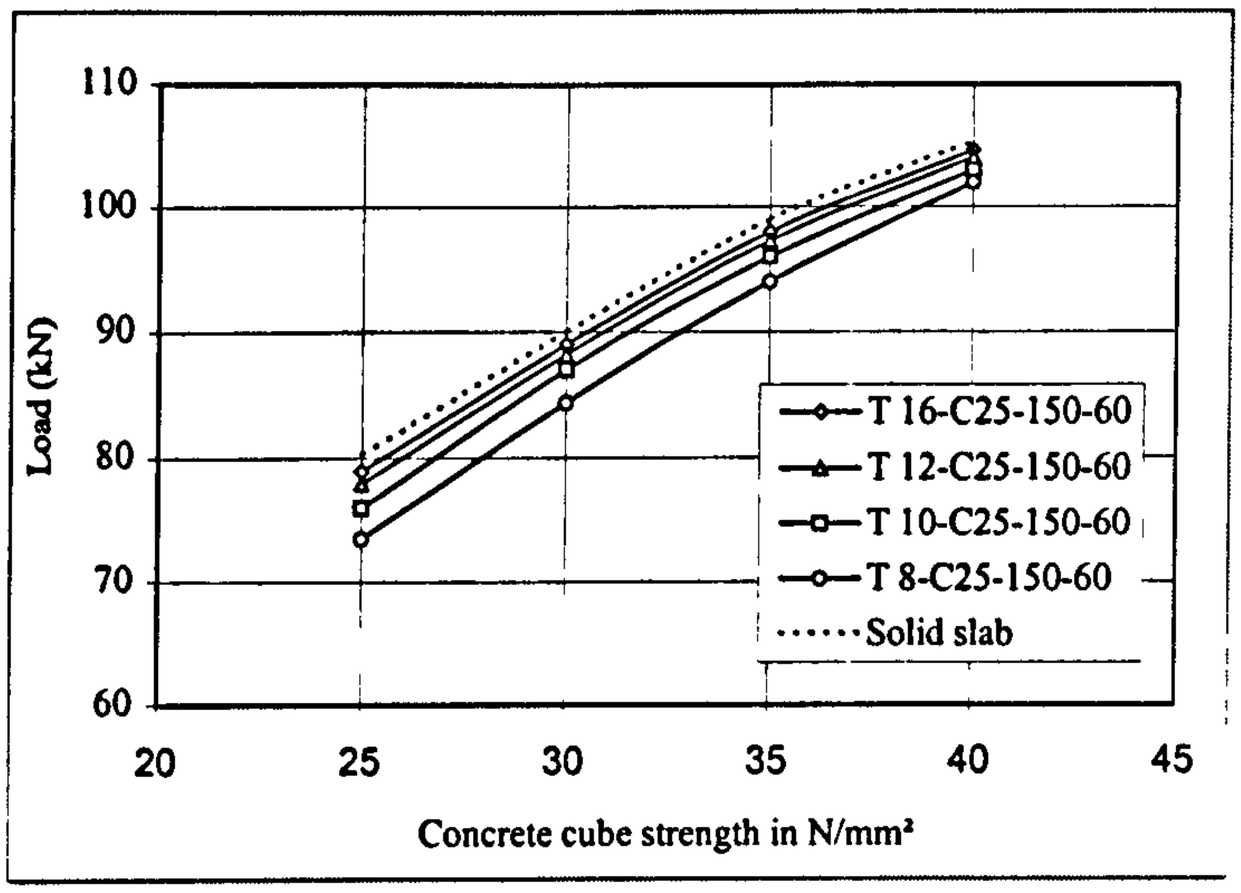

Figure 4.21 Effect of 'bs' change on load per stud-in situ concrete cube strength curve

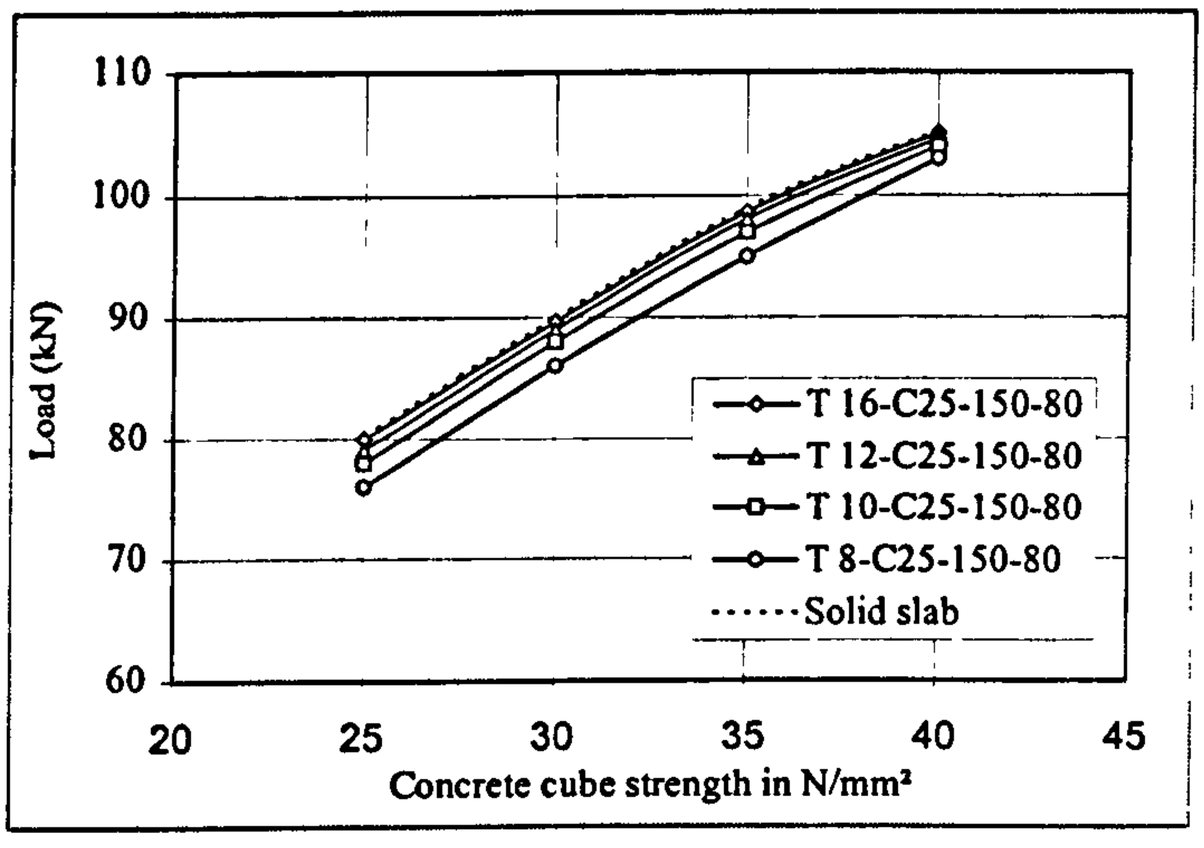

Figure 4.22 Effect of 'bs' change on load per stud-in situ concrete cube strength curve

Figure 4.23 shows the load-slip curve of the stud for a gap size of 40mm. The curves are obtained using different bar diameters with in situ concrete strength of 25 N/mm^2. It can be seen that the change in the transverse reinforcement diameter has no significant effect on the shear capacity of the connection. It affects the load-slip behaviour of the stud and hence the connection ductility.

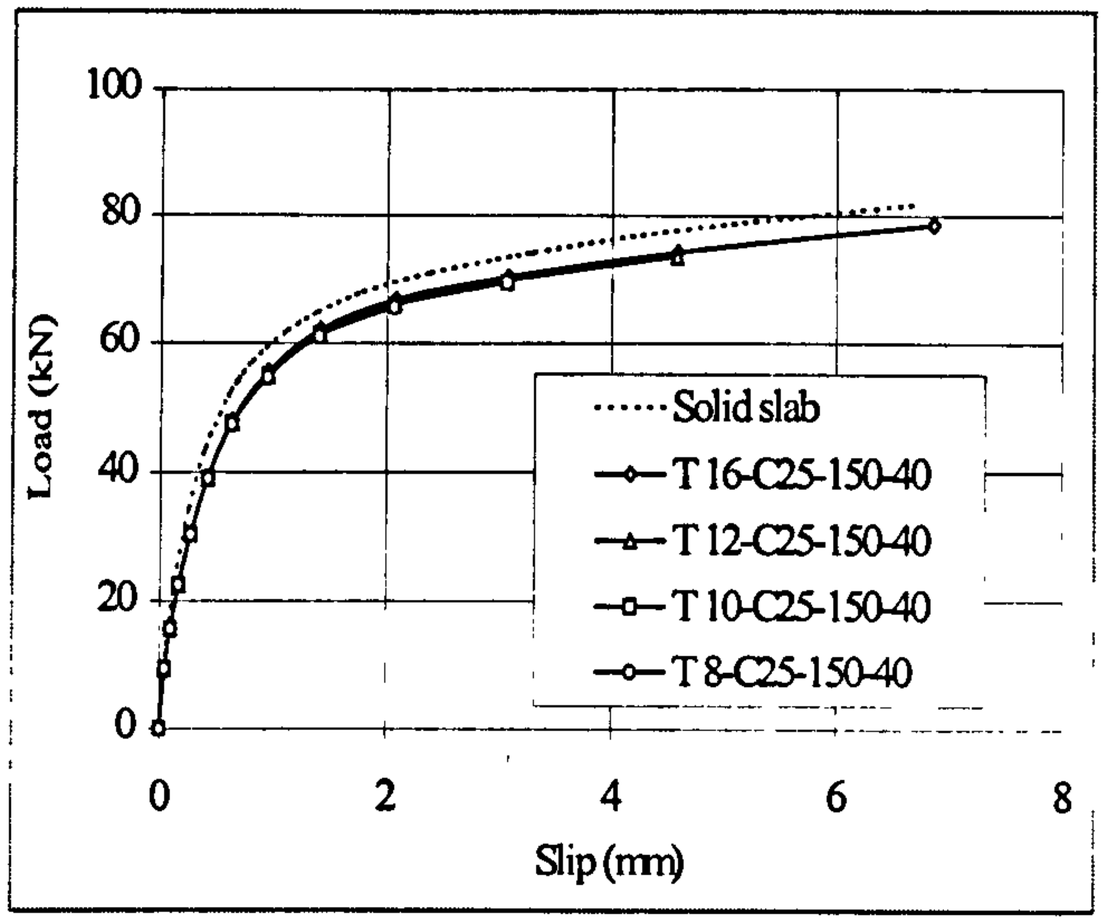

Figure 4.23 Effect of 'bs' change on the load-slip curve

4.6.2 Effect of gap width

Figure 4.24 shows the failure load per stud versus in situ concrete cube strength for a precast composite specimen using 'bs' equals 8 mm and different gap sizes. It can be seen that the shear stud capacity is increased with the increase in gap size for the same reinforcement bar diameter. This is attributed to the increase of stresses in the in situ concrete for smaller gap sizes. This leads to crushing of concrete around the stud. Also it can be seen that for gaps 60 and 80 mm, the shear stud capacities are close using the same 8mm bar. This means that the increase in the gap size leads to reducing the effect of reinforcement size and this effect is clear in smaller gap sizes.

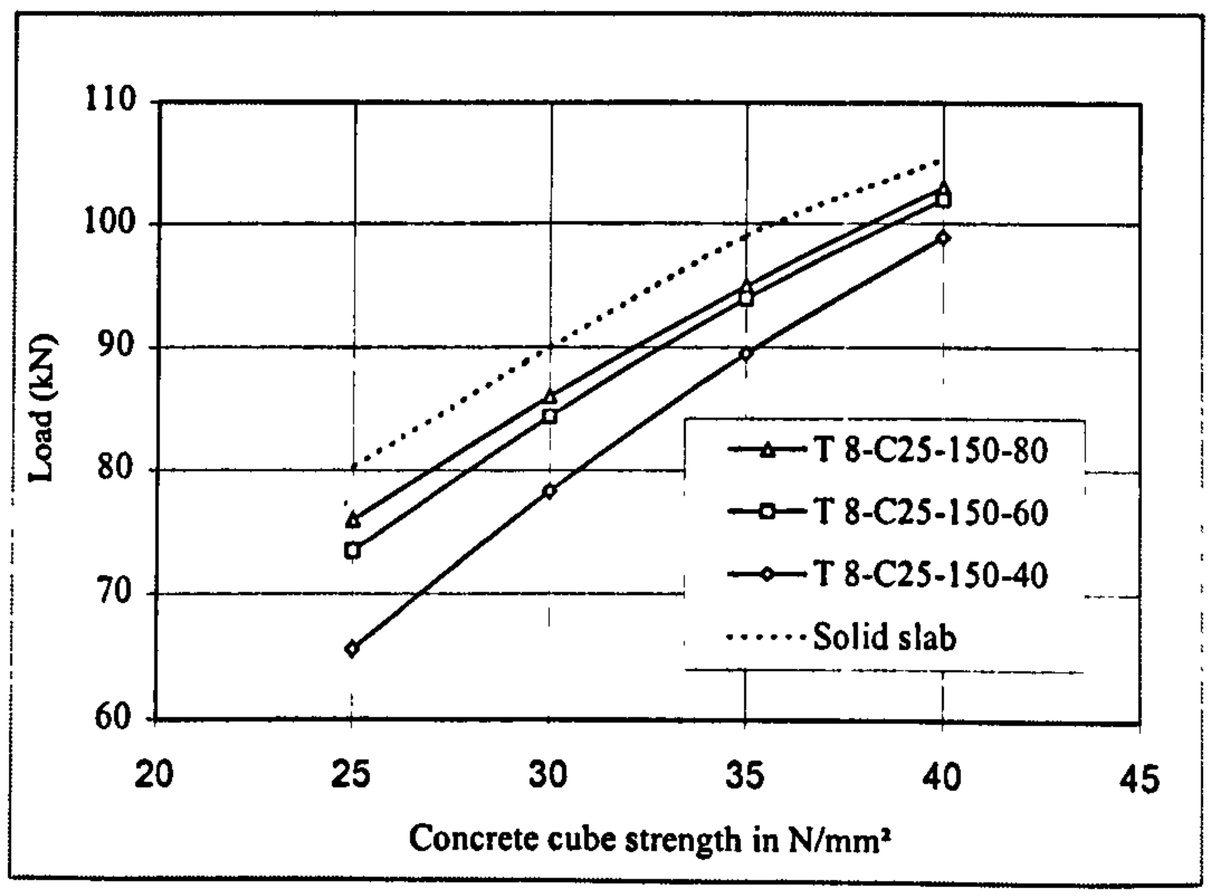

Figure 4.24 Effect of 'g' change on load per stud-in situ concrete cube strength curve

The same curves between the failure load per stud and concrete cube strength are obtained in figures 4.25, 4.26 and 4.27 using different 'bs' equals 10, 12, and 16 mm respectively. It can be seen from figures 4.25 and 4.26 that the increase in reinforcement bar diameter, the decrease in the effect of gap size change on the shear stud capacity. Also it can be noticed that the difference between the obtained curves at 60 and 80 mm is decreased by the increase in reinforcement bar diameter. Figure 4.27 shows that for 16mm bar diameter, the effect of change in gap size on the shear stud capacity is not significant.

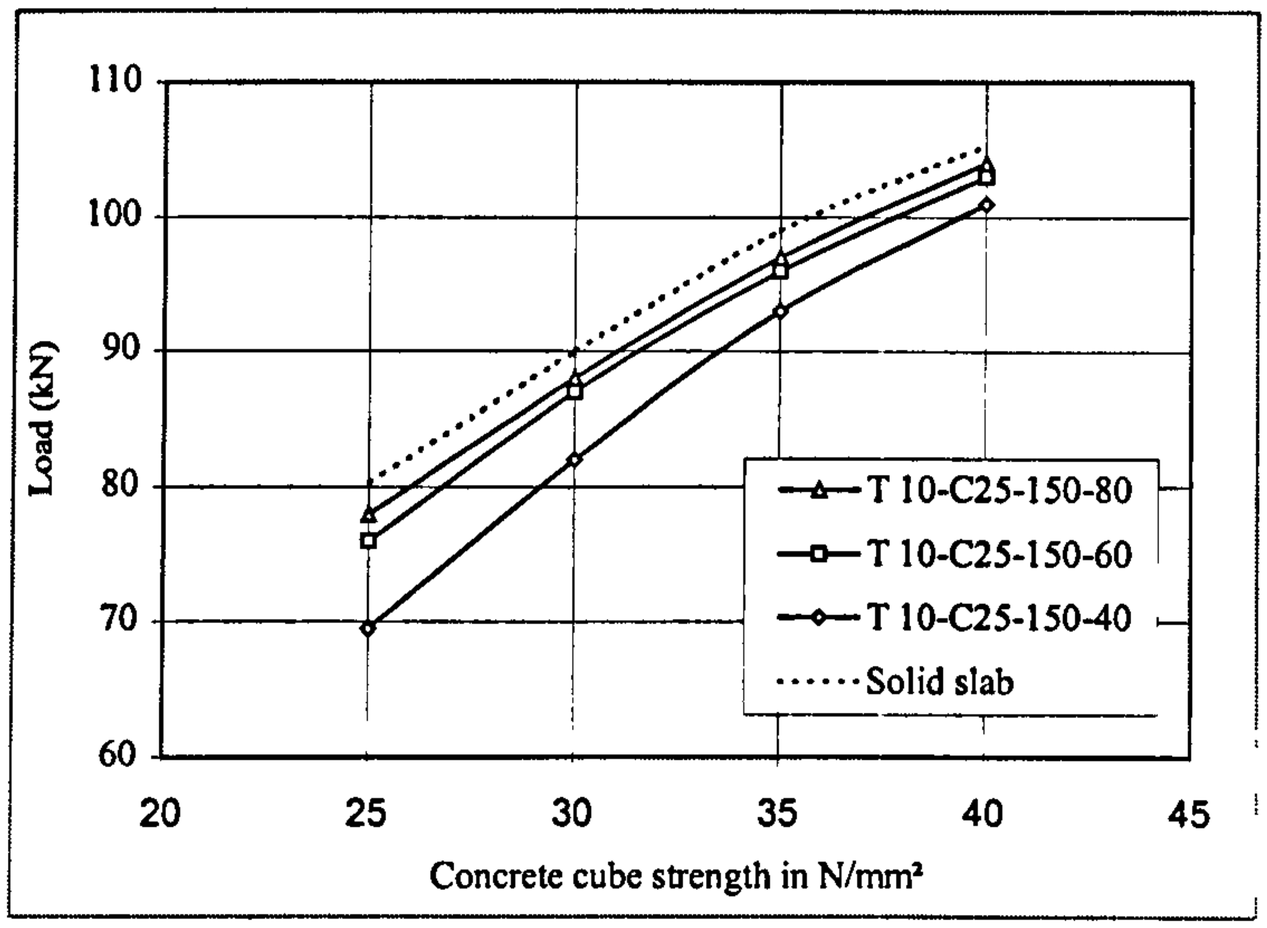

Figure 4.25 Effect of 'g' change on load per stud-in situ concrete cube strength curve

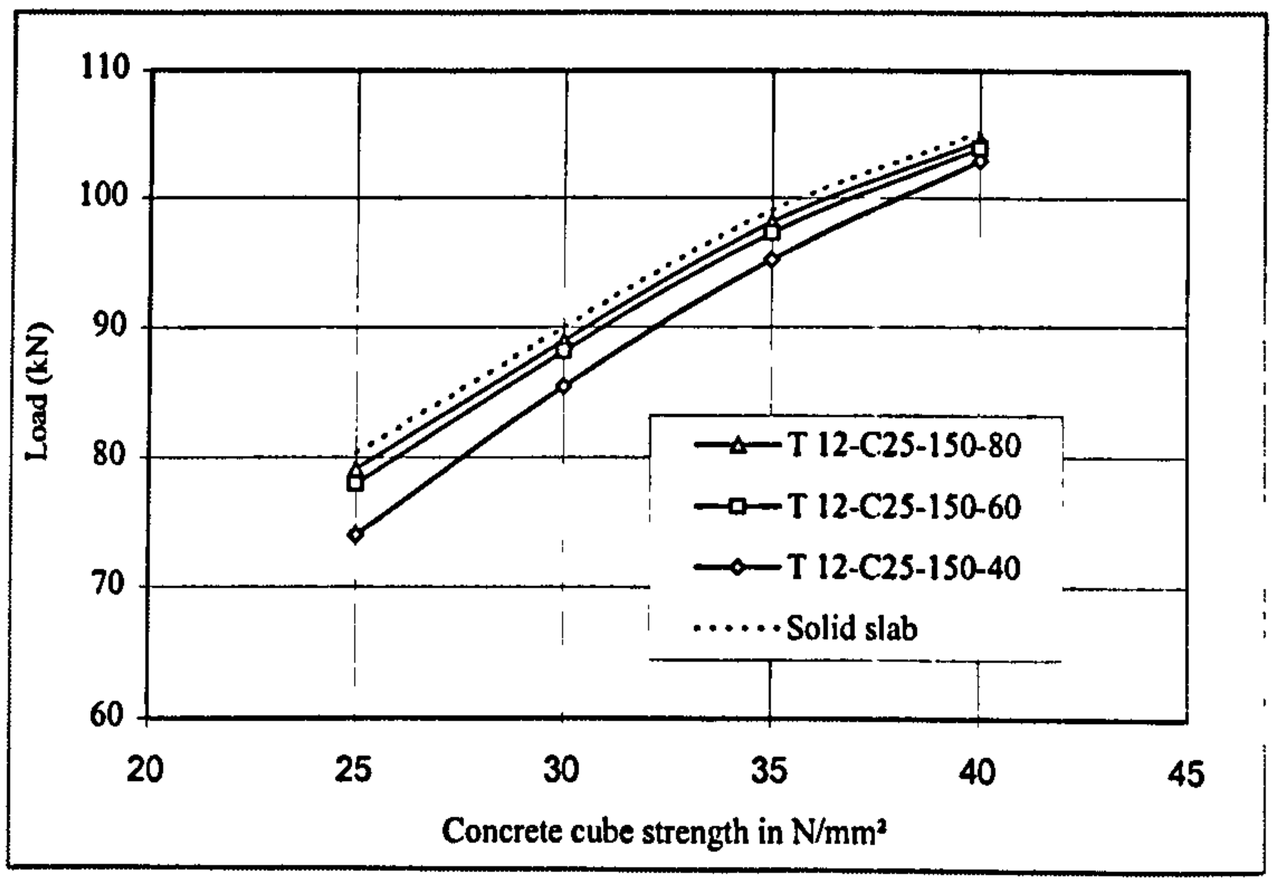

Figure 4.26 Effect of 'g' change on load per stud-in situ concrete cube strength curve

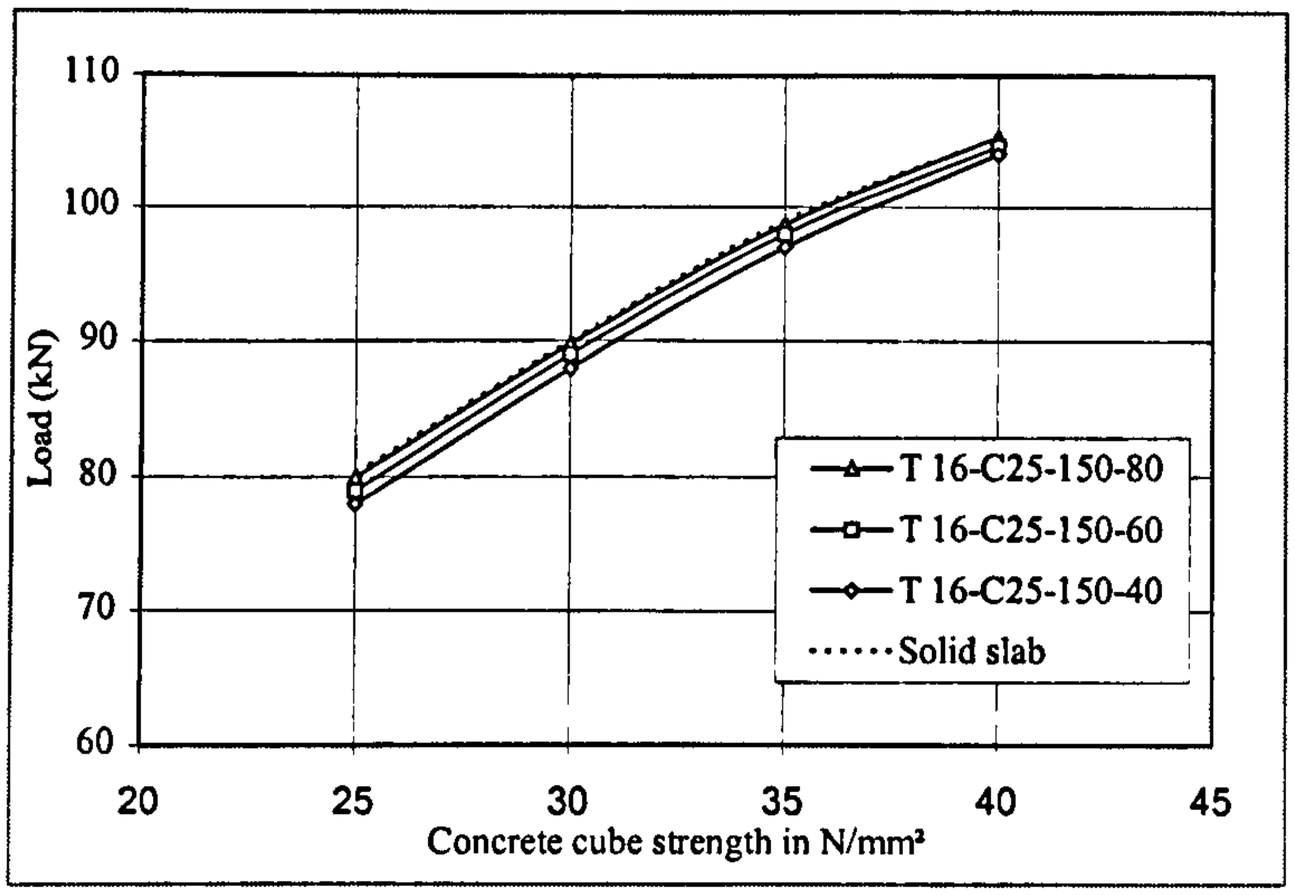

Figure 4.27 Effect of 'g' change on load per stud-in situ concrete cube strength curve

Figure 4.28 shows the load-slip curve of the stud using a certain transverse reinforcement diameter of 8mm. The curves are obtained using different gap sizes and using in situ concrete cube strength of 25 N/mm^2. It can be seen that the change in the transverse gap width has no significant effect on the shear capacity of the connection. It affects only the load-slip behaviour.

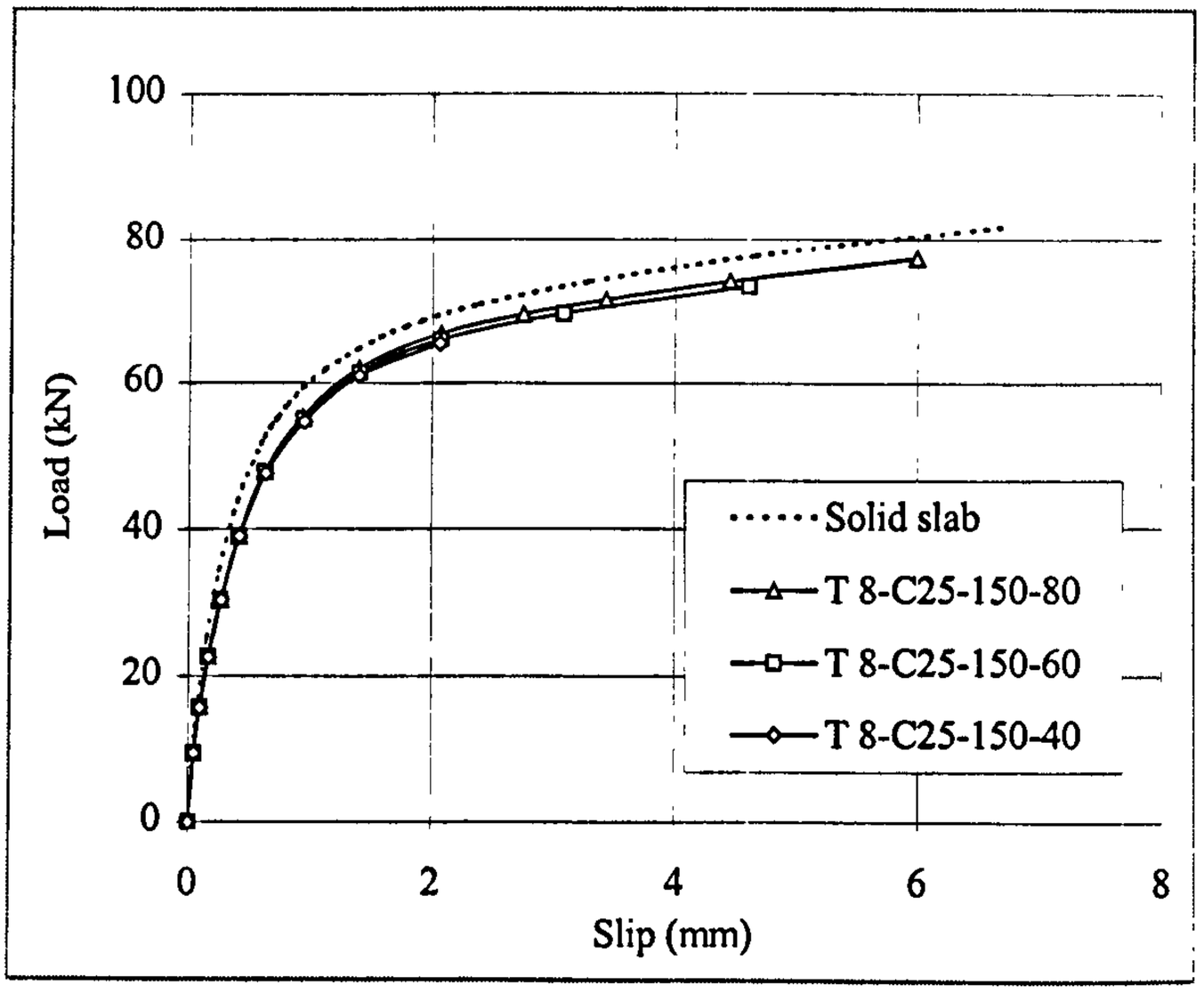

Figure 4.28 Effect of 'g' change on the load-slip curve

4.6.3 Effect of strength of in-situ in-fill

Figures from 4.29 to 4.32 show the load-slip curves of the stud using different in situ concrete cube strengths for 'g' equals 40mm and different reinforcement sizes 8, 10, 12 and 16mm respectively. It can be seen that both the load-slip behaviour and the shear stud capacity are affected remarkably by the change in the in situ concrete strength. The shear stud capacity and the stiffness of the stud is increased with the increase of in situ concrete strength.

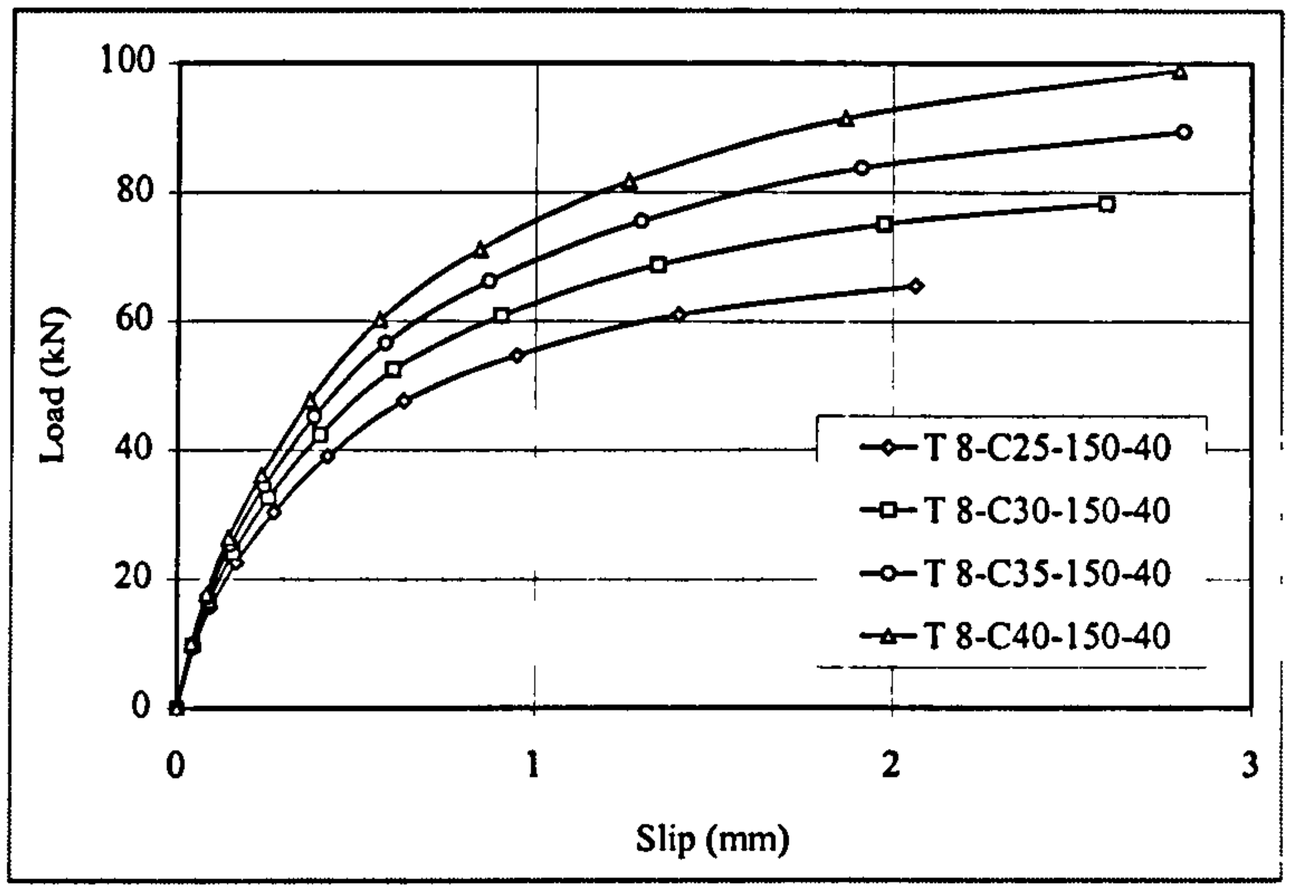

Figure 4.29 Effect of insitu concrete strength change on the load-slip curve (bs 8mm)

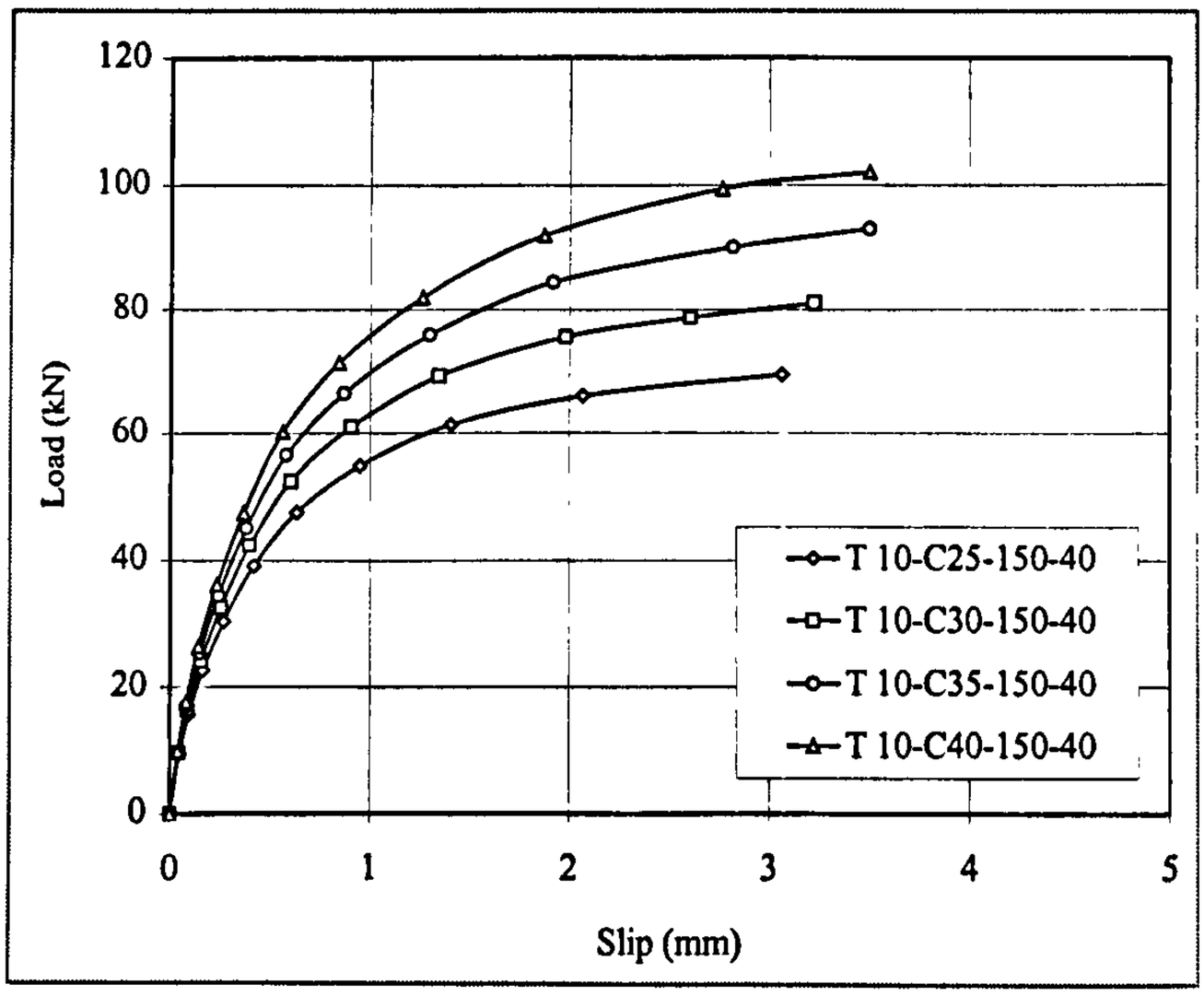

Figure 4.30 Effect of insitu concrete strength change on the load-slip curve (bs 10mm)

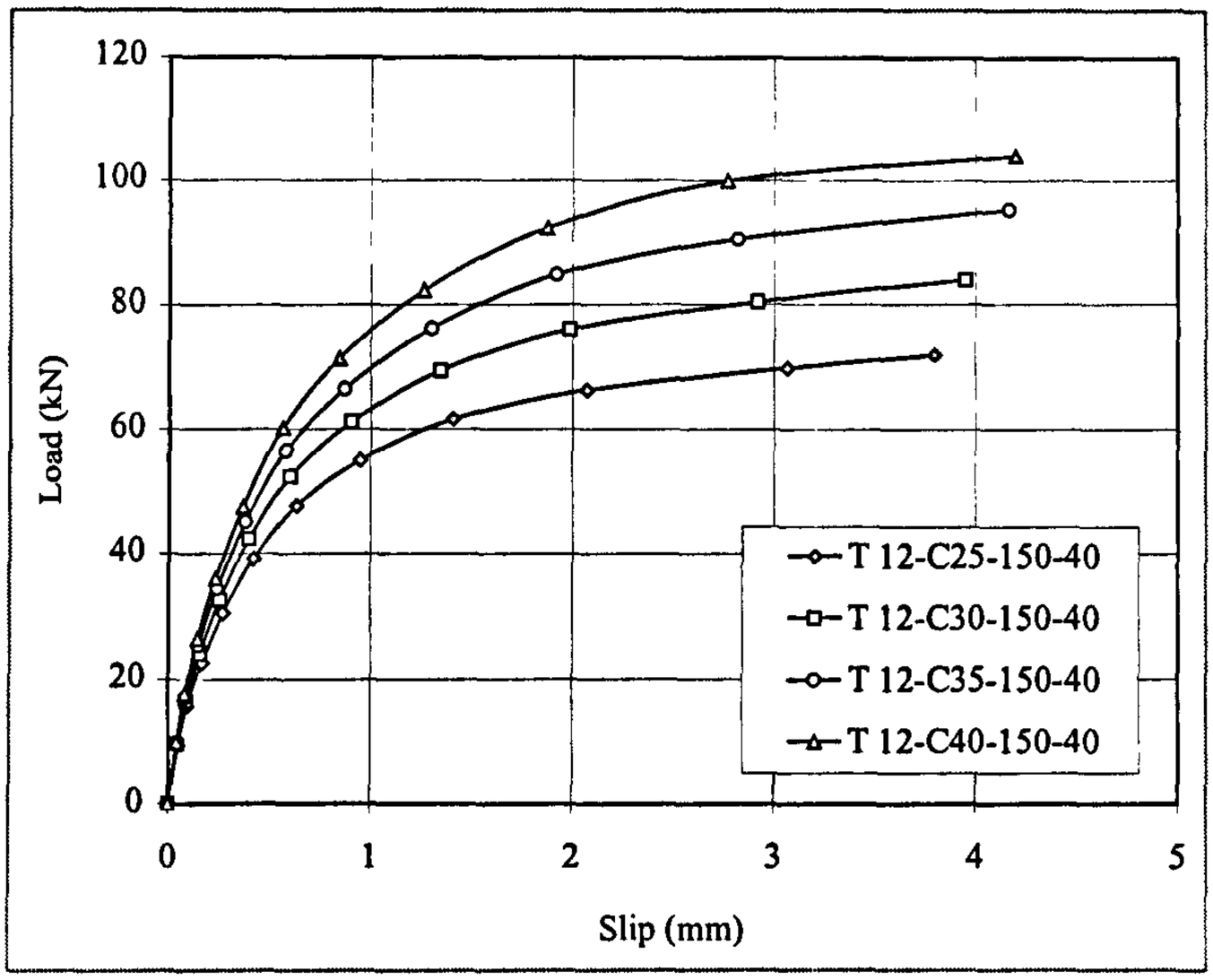

Figure 4.31 Effect of insitu concrete strength change on the load-slip curve (bs 12mm)

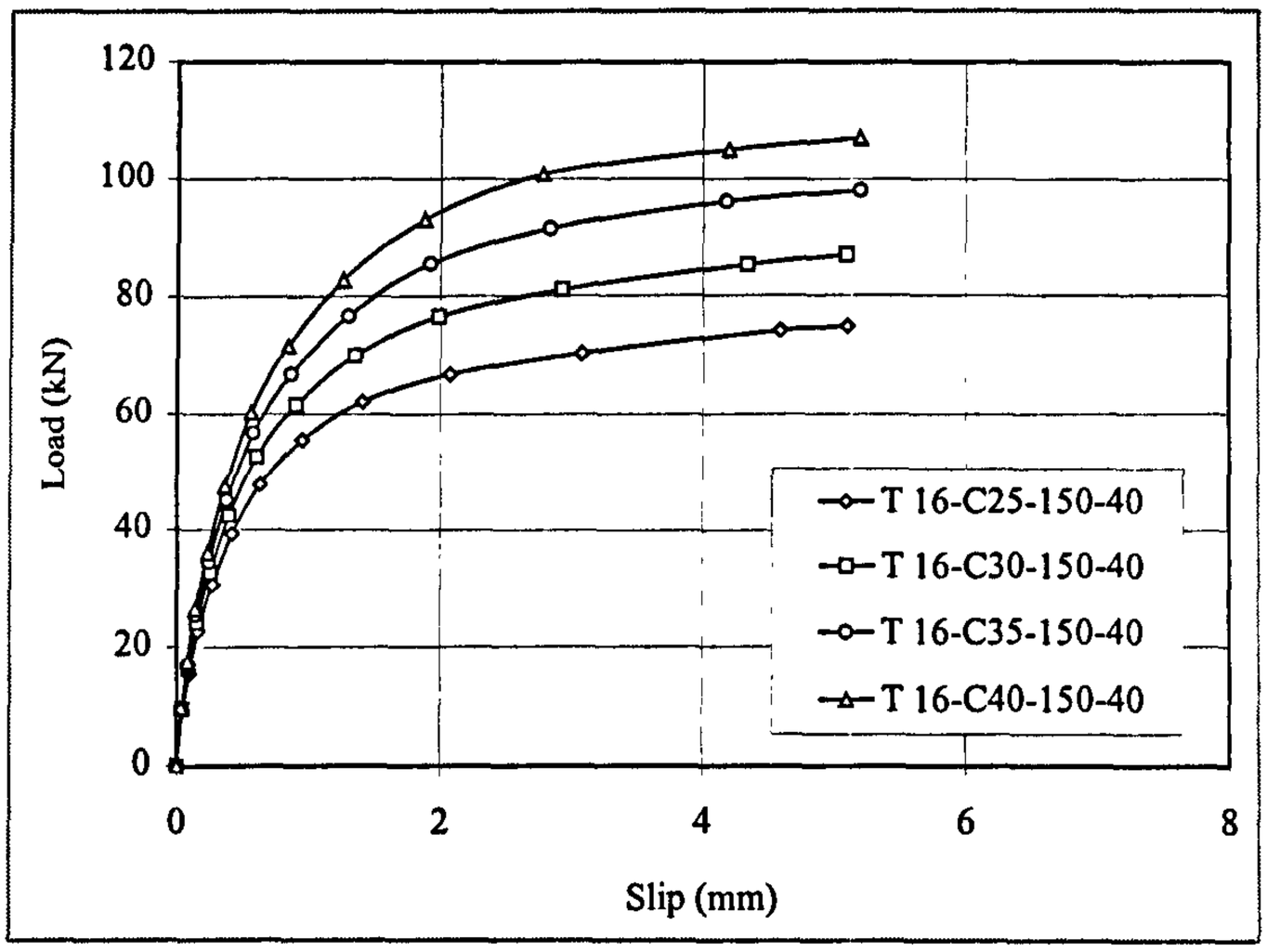

Figure 4.32 Effect of insitu concrete strength change on the load-slip curve (bs 16mm)

4.7 Modelling of a full precast hollow-cored units with three studs

To investigate the behaviour of a row of studs within steel-precast push-off test, it is decided to simulate the highlighted part of the push-off test in the rectangle B shown in figure 4.5. The shown part represents a push-off test specimen consisting of two HCUs 600mm width and three studs welded in each flange of the steel beam. The same procedures, used in the push-off test specimen containing one stud in each flange, will be followed.

4.7.1 Finite element mesh of the model

Figures 4.33.a and 4.33.b show the finite element FE mesh used to represent the quarter of a steel-precast concrete push-off test specimen. This specimen consists of two 600mm-width x 150mm-deep HCUs with square ended profile. These units are attached to each flange of the steel beam which has three 19x100mm welded studs, 150mm distance between each other, in each flange. The 65mm gap between the precast units is filled with cast in-situ concrete. One 10mm reinforcement bar is put in each milled slot, 500mm long filled with cast in-situ concrete, to connect the precast units with the cast in-situ concrete.

Each precast concrete unit is divided into 19 elements along X-direction, 7 elements along Y-direction and 3 elements along Z-direction. The half of the cast in situ concrete is modelled with 25 elements in X-direction, 2 elements in Y-direction, and 5 elements in Z-direction. All precast and cast concrete are C3D8 elements except the cast concrete around the shear stud, which are C3D15 and C3D20 elements. The half of the shank of each shear connector consists of one C3D15 element in X-direction, one element in Y-direction and two elements along Z-direction. The half of the stud connector head consists of one C3D15 element and two C3D20 elements along X-direction and one element in Y-direction and one element in Z-direction. The flange half of the steel beam is divided into 18 elements along X-direction, 3 elements along Y-direction and one element in Z-direction. The web quarter of the steel beam is divided into 18 elements along X-direction, one element in Y-direction and 3 elements in Z-direction. The half of each transverse reinforcement bar is divided into one element along X-direction, 7 elements along Y-direction and one element along Z-direction.

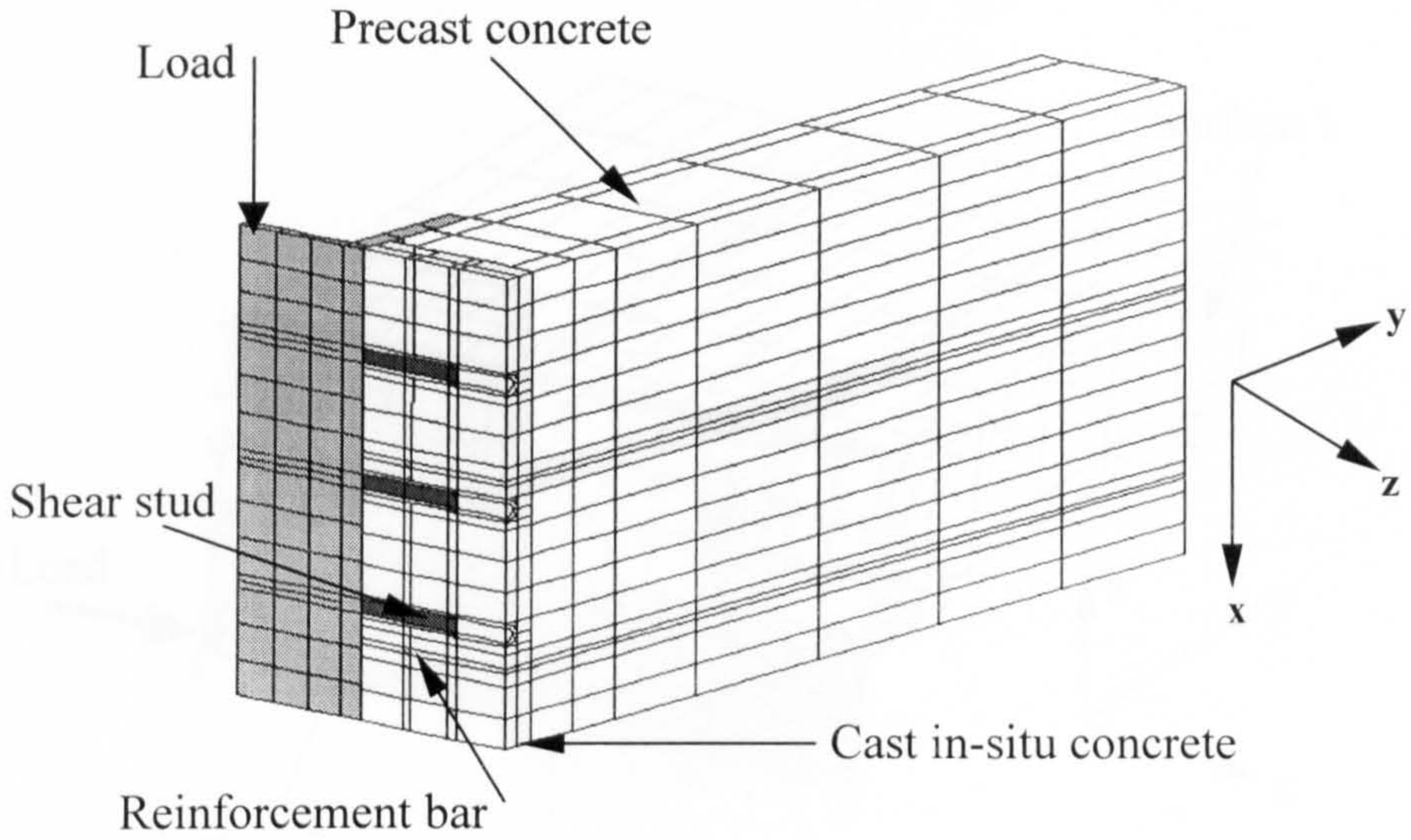

Figure 4.33.a Finite element mesh of the 3-stud model

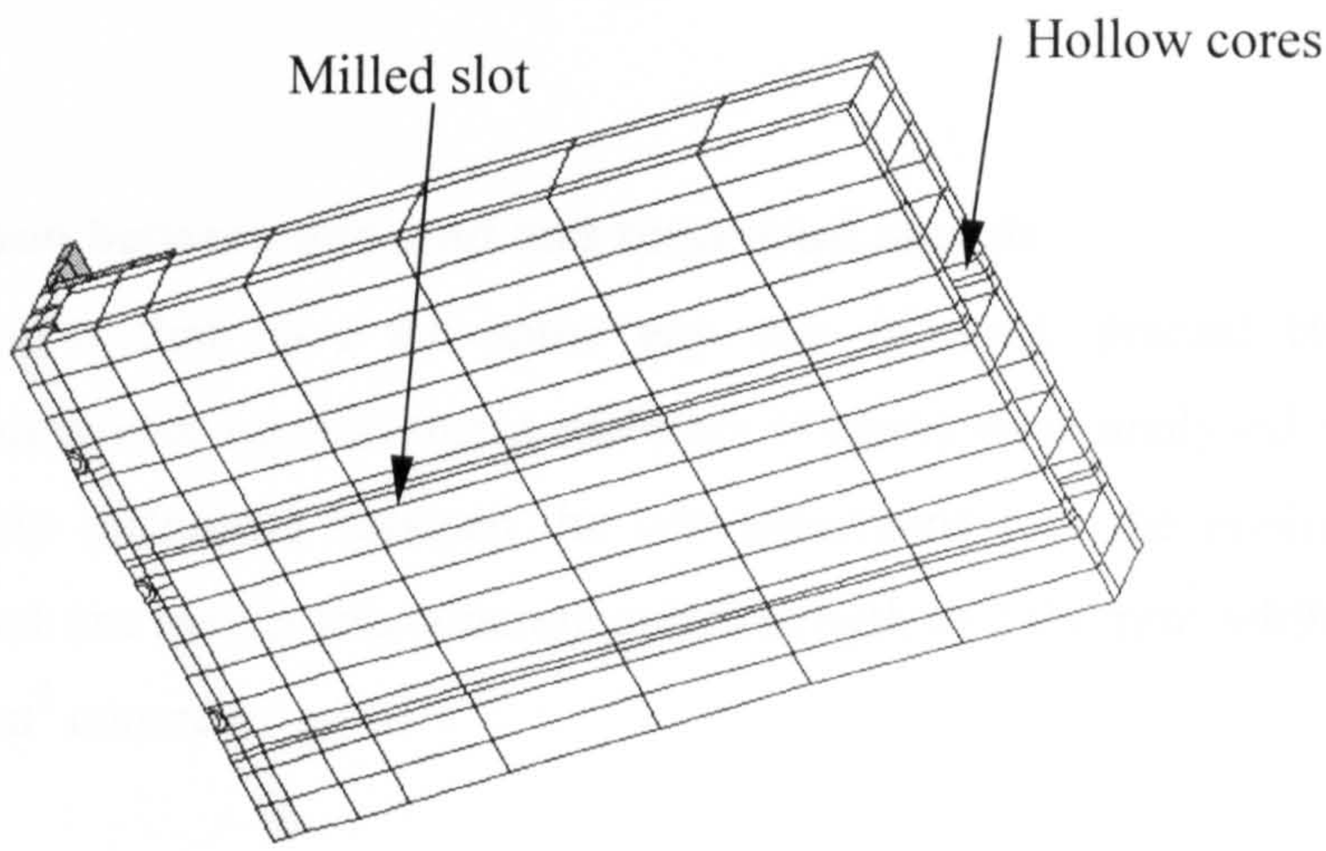

Figure 4.33.b Finite element mesh of the 3-stud model

4.7.2 Boundary conditions and load application

The same boundary conditions and load are used with the same procedures used with the one stud model as shown in figure 4.34.

4.7.3 Material modelling of the components

The precast hollow-cored concrete, cast in situ concrete, studs, steel beam, and reinforcement bars are represented with the same stress-strain curves mentioned earlier in the one stud model.

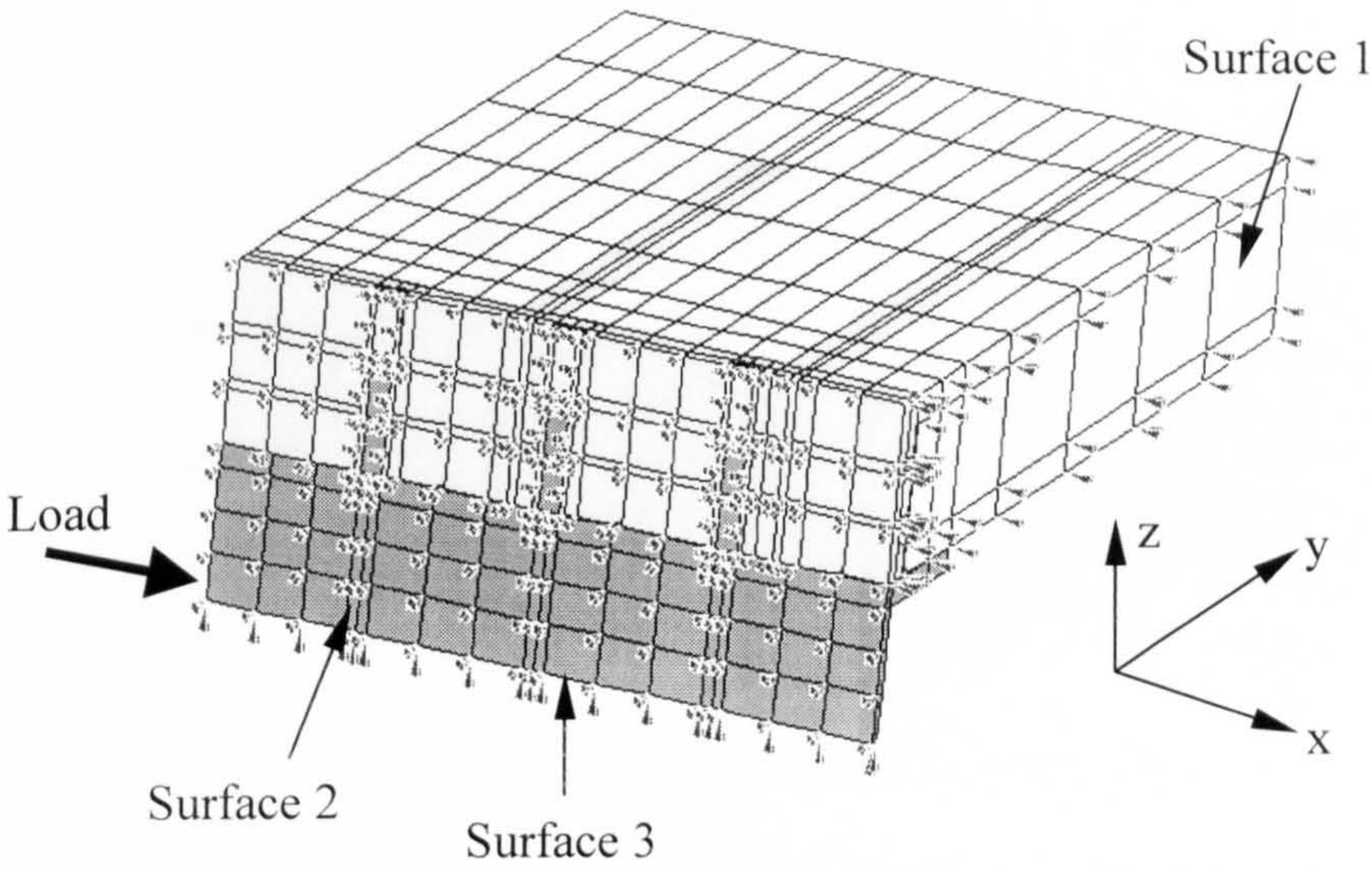

Figure 4.34 Application of load and boundary conditions on the 3-stud model

4.7.4 Comparison between one-stud and three-stud models

Two push-off tests that have the same gap size (65mm), precast HCU depth (150mm) and transverse reinforcement diameter (10mm) were analysed using both models. The only difference between the two specimens was the in-situ concrete strength. The first one had in-situ concrete cube strength of 25N/mm^2 while the other one had 40N/mm^2 concrete.

Results of push-off test T 10-C25-150-65

Figure 4.35 shows a comparison between the load-slip curve of the headed stud, in the model containing one stud in each flange (1-stud model), with that curve of the stud, in the model containing three studs in each flange (3-stud model). The shear capacity of the stud in the 1-stud model is 68kN compared with 71kN of that in the 3-stud model. The difference between both is about 4% as a percentage of the capacity in the 3-stud model. This is expected since the redistribution of stress among the studs after yielding allows for carrying slightly additional load and hence increasing the shear stud capacity. The cause of failure is yielding of the 10mm reinforcement bar same as it is detected from the 1-stud model.

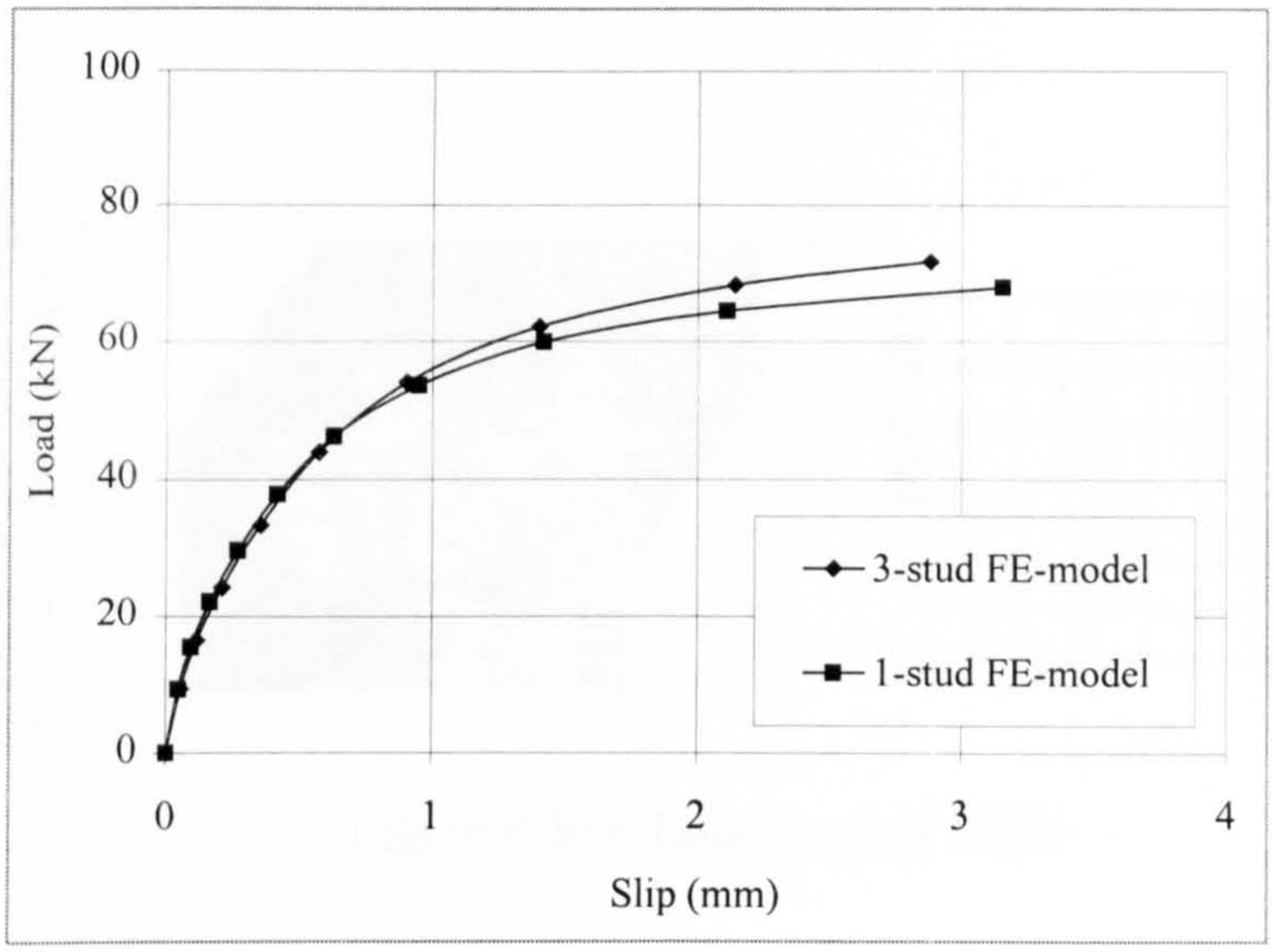

Figure 4.35 Load-slip curves of push-off test T 10-C25-150-65

Figure 4.36 shows the distribution of contour Von Mises stresses and deformed shape at different load levels. It can be seen that, at low load levels, the concrete elements remain in contact with the stud and the stresses in concrete do not reach the yield values. The failure occurred when the reinforcement bar yielded and consequently the concrete reached its yield values forming conical failure zones. The conical shape extended to cover the full depth of concrete especially for this low concrete strength. Also, it can be seen that the stud undergoes single curvature bending because of the low concrete strength.

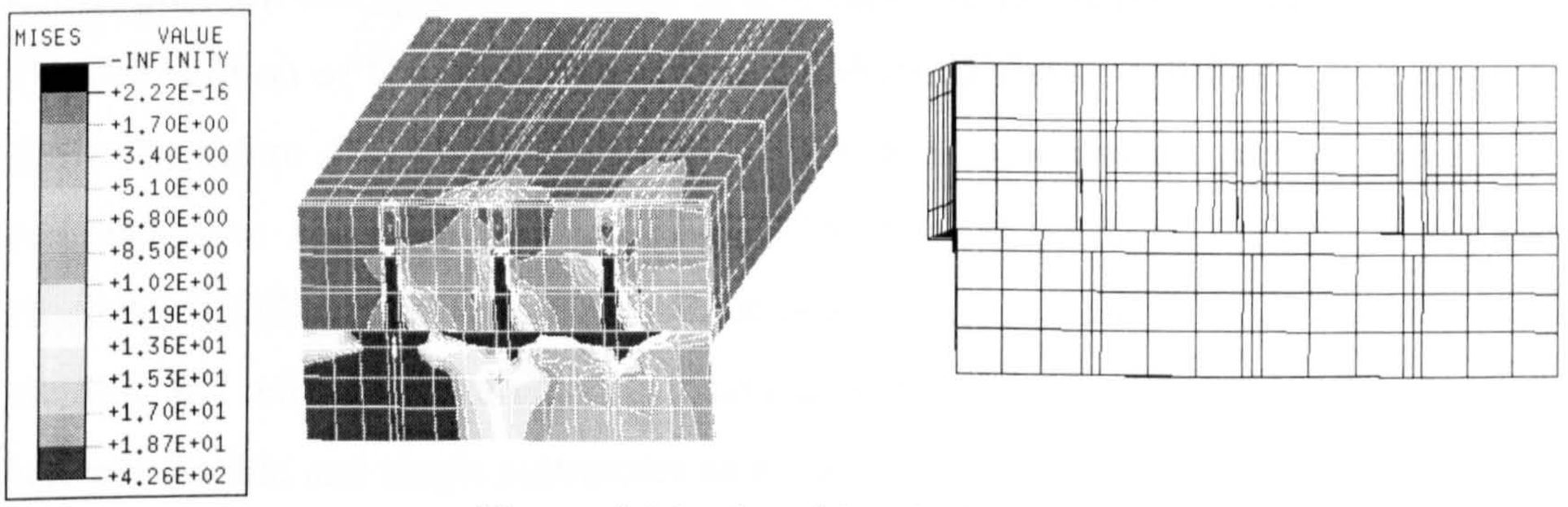

Figure 4.36.a Load level of 24kN

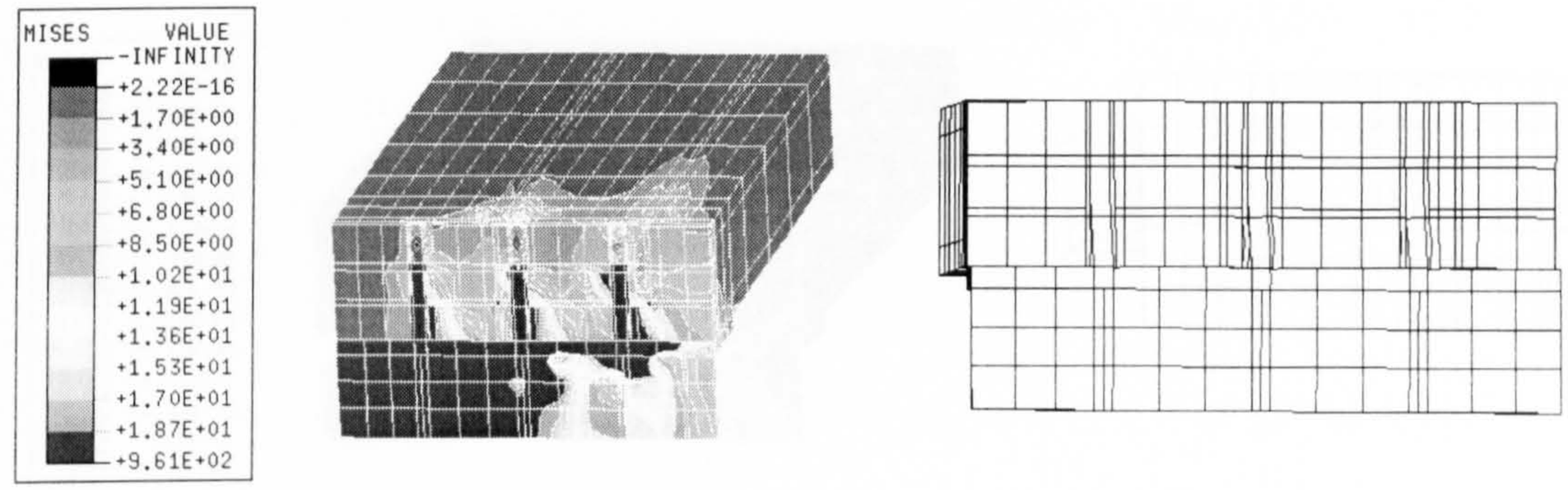

Figure 4.36.b Load level of 44kN

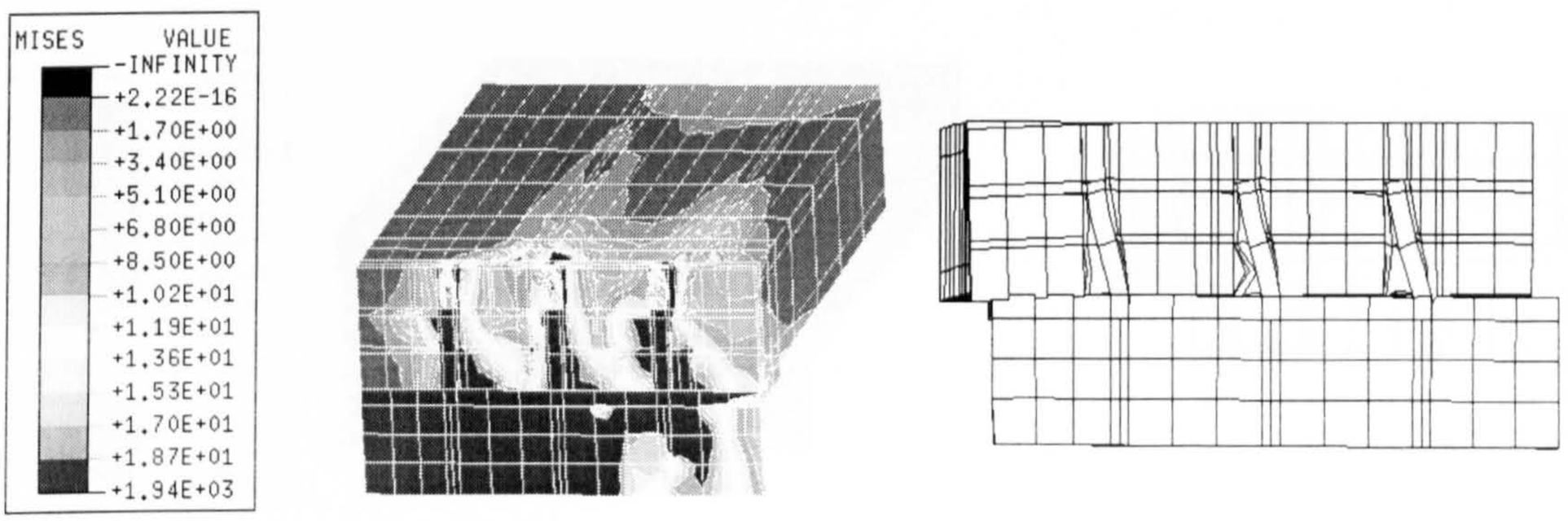

Figure 4.36.c Load level of 72kN

Figure 4.36 Contour stresses and deformed shape of T10-C25-150-65

Results of push-off test T 10-C40-150-65

In this push-off test specimen, higher in-situ concrete strength of 40N/mm^2 was used. The distribution of Von Mises stresses and deformed shape at different load levels is shown in figure 4.37. It can be seen that the stresses across the precast and in-situ concrete were less than that in T10-C25-150-65 and no clear conical failure was obtained at failure. The mode of failure is a combined failure mode between stud yielding and reinforcement yielding. The stud yielded in combined curvature bending between double and single curvatures as shown in figure 4.37.c.

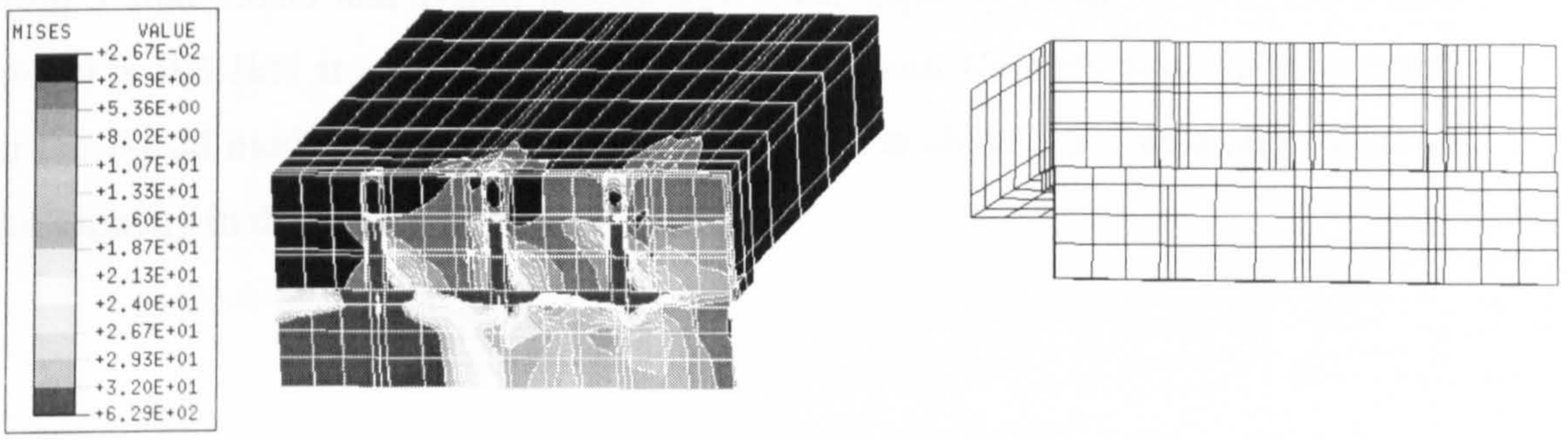

Figure 4.37.a Load level of 40kN

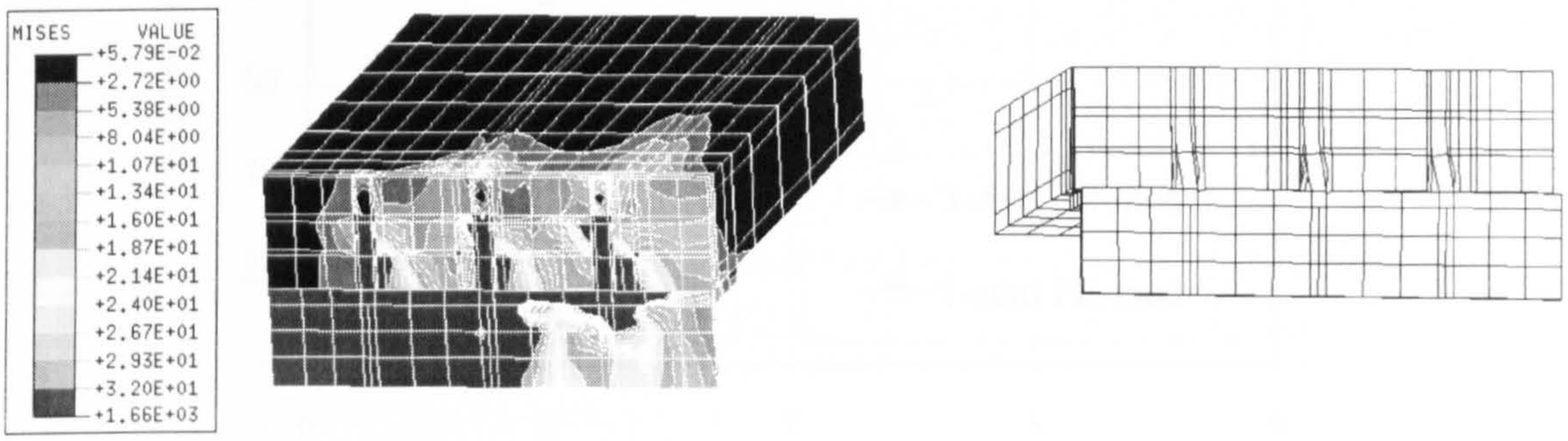

Figure 4.37.b Load level of 82kN

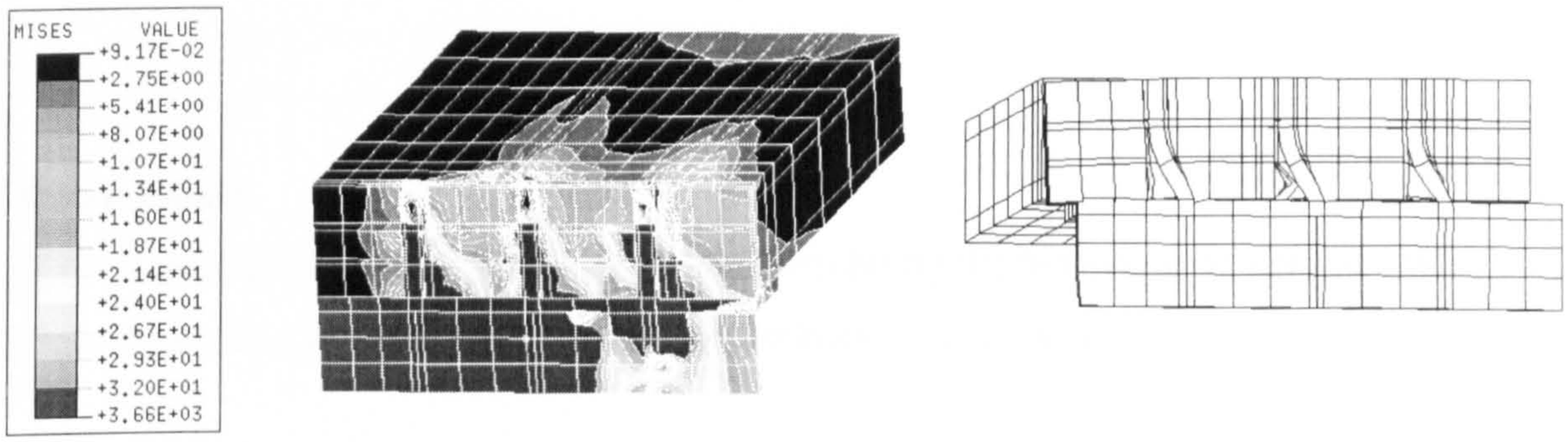

Figure 4.37.c Load level of 103kN

Figure 4.37 Contour stresses and deformed shape of T10-C40-150-65

Figure 4.38 shows a comparison between the load-slip curves of the stud obtained from 3-stud model and 1-stud model. The shear capacity of the stud in the 3-stud model is 103.1kN at a slip of 2.696mm compared with 100.6kN at a slip of 2.73mm in the 1-stud model. The difference between both is about 2.5% as a percentage of the capacity in the 3-stud model.

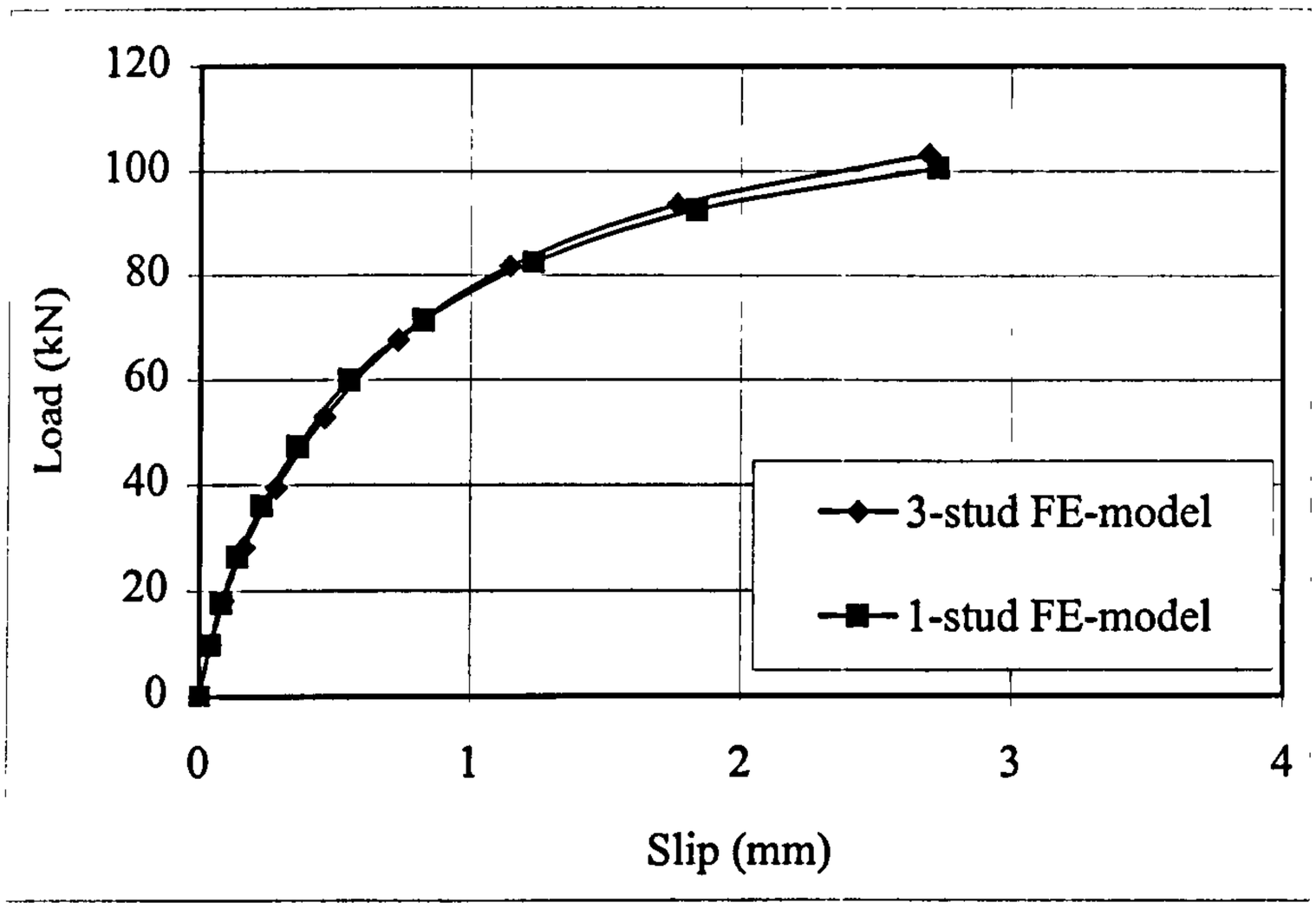

Figure 4.38 Load-slip curves of push-off test T 10-C40-150-65

4.8 Summary

This chapter described the numerical model simulating the behaviour of headed stud shear connectors in push-off tests with precast hollow core slabs.

In composite construction with hollow core slabs, it is not possible to always provide adequate transverse reinforcement to eliminate its failure. Therefore, additional mode of failure is investigated using the finite element analyses. Transverse reinforcement bars enhance the in-plane shear resistance by crossing the precast and the in-situ

concrete interface. It limits the longitudinal splitting of the concrete by carrying tensile splitting forces. Transverse bars of small diameters are likely to yield, because of concentrations of in-plane and longitudinal stresses in the bar elements at the interface between precast and in-situ concrete, causing premature failure of the concrete around the stud and hence transverse bar failure mode. Specimens with higher sizes of transverse bars have shown higher ductility in terms of the load-slip behaviour of the stud than that of lower sizes.

Parametric studies carried out using the finite element model have shown that transverse gap size, transverse reinforcement diameter and in-situ concrete strength had significant effect on the behaviour of shear connectors in composite beams with precast hollow core slabs. It was found that:

a. The shear stud capacity is increased with the increase of the gap size between HCUs using transverse reinforcement bars of diameter less than 16mm theoretically. This increase is obtained for gap sizes up to 80mm. For gap sizes greater or equal to 80mm, there is no effect on the shear stud capacity and it may be taken as the similar solid slab one that has the same thickness and strength of the in situ concrete.
b. The shear stud capacity is increased with the increase of the transverse reinforcement diameter with gap sizes less than 80mm. This increase is obtained for reinforcement bar diameters up to 16mm. For bar diameters higher or equal to 16mm, there is no effect on the shear stud capacity and it may be taken as the similar solid slab one that has the same thickness and strength of the in-situ concrete.
c. Both of the increase in bar diameters or gap sizes increased the ductility of shear connection and hence the load-slip behaviour of the headed stud shear connector.
d. As composite beams with solid slabs, the in situ concrete strength had significant effect on the shear stud capacity and load-slip behaviour of the stud in push-off tests with precast hollow core slabs if the mode of failure due to transverse reinforcement is eliminated.

Although, review of previous experimental research carried out on push-off tests with precast hollow core slabs has paved the way in developing the present finite element model, the number of the published push-off tests is still limited in this new type of composite construction. The only equation found in the literature dealing with evaluation of the headed shear stud capacity in push-off tests with precast hollow core slab is Equation 2.7, presented in chapter 2, given by Lam, Elliott and Nethercot[23]. This equation represents an empirical equation containing 2 new reduction factors and 1 new magnifying factor, derived from the statistical analysis of 10 push-off tests carried out by the authors. The concrete cylinder strength is the average strength of the precast and in-situ concrete and modulus of elasticity is the average modulus of precast and in-situ precast concrete. The push-off tests had constant in-situ concrete strength of 25N/mm^2, different transverse reinforcement bar sizes 8, 16 and 25mm, two widths of HCUs 600mm and 1200mm, and different gap sizes 40, 65 and 120mm. Looking into the factors affecting this equation it can be seen that, maximum capacity can be obtained when both of the 2 reduction values become 1.0 and this happens when the diameter of transverse bar becomes 20mm and the transverse gap becomes 70mm. On the other hand, the magnifying factor varies from 1-1.5 for HCU widths 600mm and 1200mm respectively. This means that this equation ignores the interaction between the above mentioned parameters which is proved by this study. For example, present parametric study has shown that the increase in transverse reinforcement or in-situ concrete strength improves the shear connection capacity of push-off tests with smaller gap sizes. Also investigation for the effect of increase in transverse reinforcement diameter and gap sizes has shown that the maximum capacity can be obtained by using diameter 16mm bar and by using 80mm gap size. Table 4.2 shows the comparison of finite element solution and calculated values using the modified equation by Lam et al.[23].

The results showed that the finite element model can accurately predict the behaviour of headed studs in push-off tests with precast hollow core slabs, it offers a reliable and cost-effective alternative to laboratory testing. It can reduce the number of future push-off tests in this new type of composite construction.

Gap size (mm)	Bar size (mm)	In-situ concrete cube strength (N/mm^2)			
		C25	C30	C35	C40
40	8	66 (58)	78 (60)	90 (63)	99 (66)
	10	70 (62)	82 (65)	93 (68)	101 (71)
	12	74 (66)	85 (69)	95 (73)	103 (76)
	16	78 (74)	88 (78)	97 (82)	104 (85)
60	8	74 (68)	84 (72)	94 (75)	102 (78)
	10	76 (73)	87 (77)	96 (81)	103 (84)
	12	78 (78)	88 (82)	97 (86)	104 (90)
	16	79 (88)	90 (92)	98 (97)	105 (101)
80	8	76 (74)	86 (77)	95 (81)	103 (84)
	10	78 (79)	88 (83)	97 (87)	104 (90)
	12	79 (84)	89 (88)	98 (92)	105 (96)
	16	80 (95)	90 (99)	99 (104)	105 (107)

( ) [$P_R=0.29\alpha\beta\varepsilon d^2(\omega f_{cp}E_{cp})^{1/2}$] Lam et al.[23]

Table 4.2 Ultimate shear capacity (kN) of headed studs in push-off tests with precast HC slabs

5. Experimental Investigation

5.1 Introduction

In this chapter, experimental investigations for the behaviour of headed stud shear connector in composite girders with solid and precast HCU slabs are described. Push-off tests with both types of slabs were carried out to validate and check the accuracy of the FE models discussed in chapters 3 and 4. The shear connection capacity, load-slip curves and modes of failure were detected from the present experimental investigation. Comparison between both FE and experimental results will be discussed in chapter 6.

5.2 Push-off tests on studs used with solid reinforced concrete slab

Four full-scale push-off tests with different concrete grades were tested to validate the present finite element model. The FE modelling and testing of headed studs in solid concrete slabs may be considered as control tests before extending that to FE modelling and testing of headed studs in hollow core slabs. The specimens were prepared and tested horizontally similar to those conducted by Lam et al[23]. The general arrangements and material properties of these tests are presented in this chapter.

5.2.1 Description of test specimen

The test specimen shown in figure 5.1 consists of a full scale concrete slab cast on the top flange of a short steel universal column (UC) which has pre-welded headed stud connectors. The dimensions of the concrete slab are 1680x1200x150mm. The test set up is shown in figure 5.2. The concrete slab was cast horizontally according to the requirements of the EC 4[8]. Compaction was done using a poker vibrator of 30mm diameter. Curing was done under a wet hessian covered by polythene sheeting until the time of testing. The slab was reinforced longitudinally and transversely with two layers of reinforcement. Each layer consists of six longitudinal and six horizontal bars. All bars were 10mm diameter according to the requirements of the EC 4.

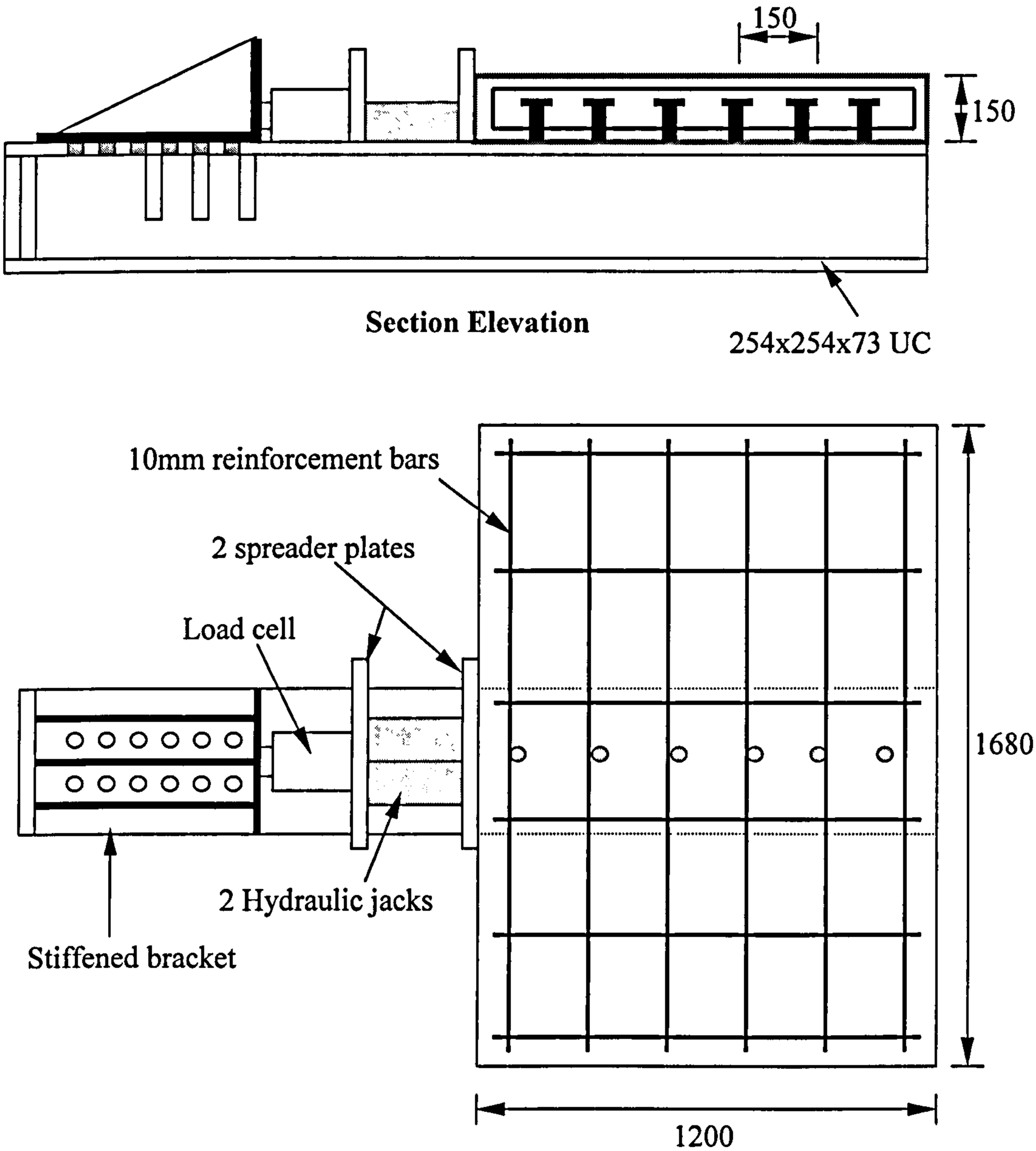

Figure 5.1 Dimensions of slab and details of the test

The steel beams used in the tests were a 254mm x 254mm x 73kg universal columns. The flanges of the steel beams were not greased so natural adhesion is not prevented. Each beam had six studs with 150mm spacing between each other of 150mm and

welded onto the beam as shown in Figure 5.2. The studs were TRW Nelson studs, 19mm diameter by 100 mm long and the as-welded height is 95 mm.

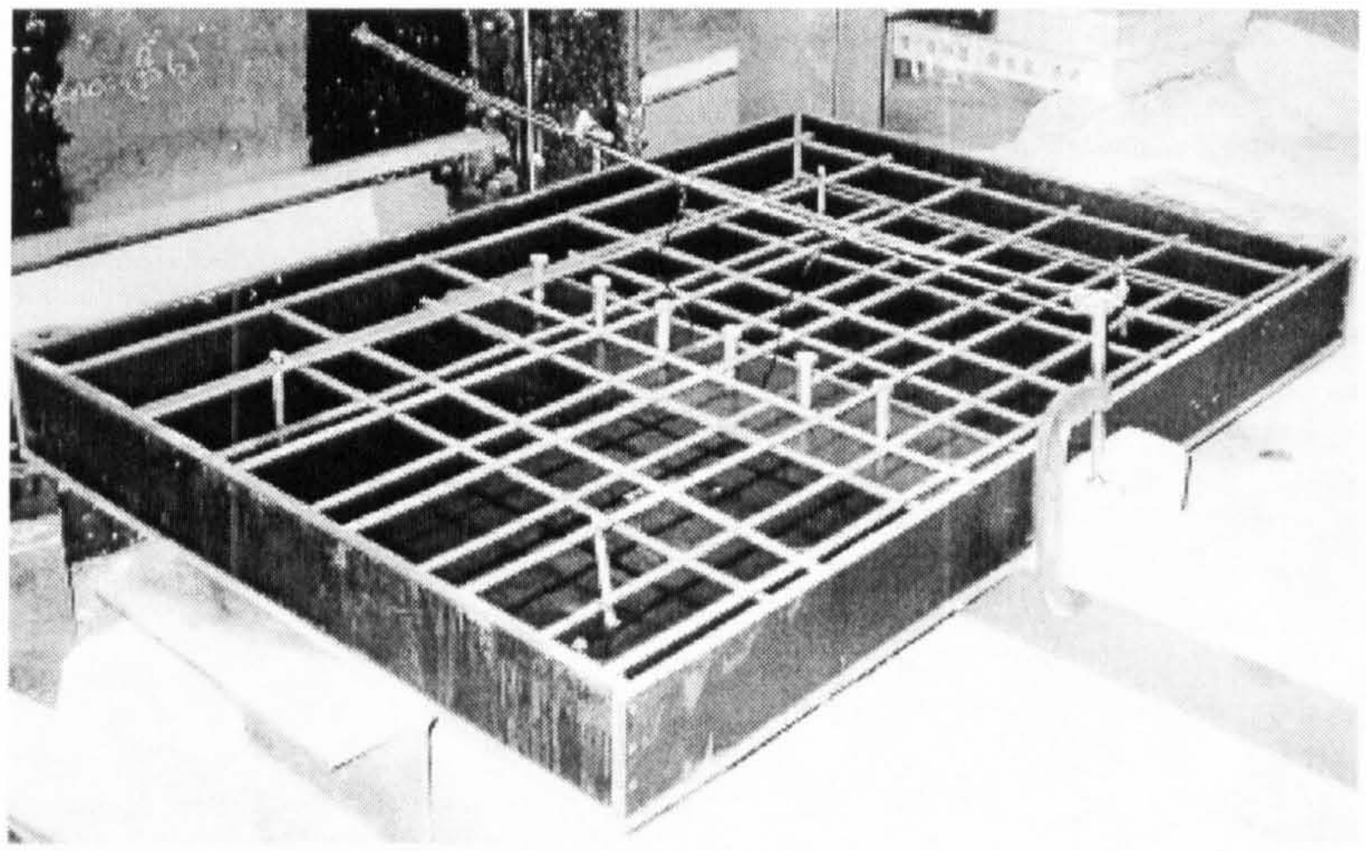

Figure 5.2 General arrangement of test specimen before casting of concrete

5.2.2 Loading frame

The main components of the test rig consisted of 2 no. 500kN hydraulic jacks bracketed onto the steel beam. A single hydraulic pump, Enerpac PAE16000 shown in figure 5.3, was used for both jacks so the loading is applied simultaneously. The load was applied and measured using a 3000kN load cell. To improve distribution of load, a spreader beam, 50mm thickness, was placed between the load cells and the specimen so that the load was equally distributed along the slab edge. A second spreader plate was placed between the jacks and the load cell, see figure 5.1.

5.2.3 Instrumentation

5.2.3.1 Displacement recordings

In each test, two linear voltage displacement transducers (LVDTs) were positioned in the arrangement indicated Figure 5.6. At each load increment, the LVDT's were used to monitor the relative longitudinal slip between the concrete slab and the steel beam.

5.2.3.2 Strain gauges

Strain gauges were fixed to each transverse reinforcement bar, and covered with plastic tubing, for protection against concrete leaking onto the gauges, to monitor the strain, see

figure 5.4. The final strain was taken as the average value of the two readings of the strain gauges.

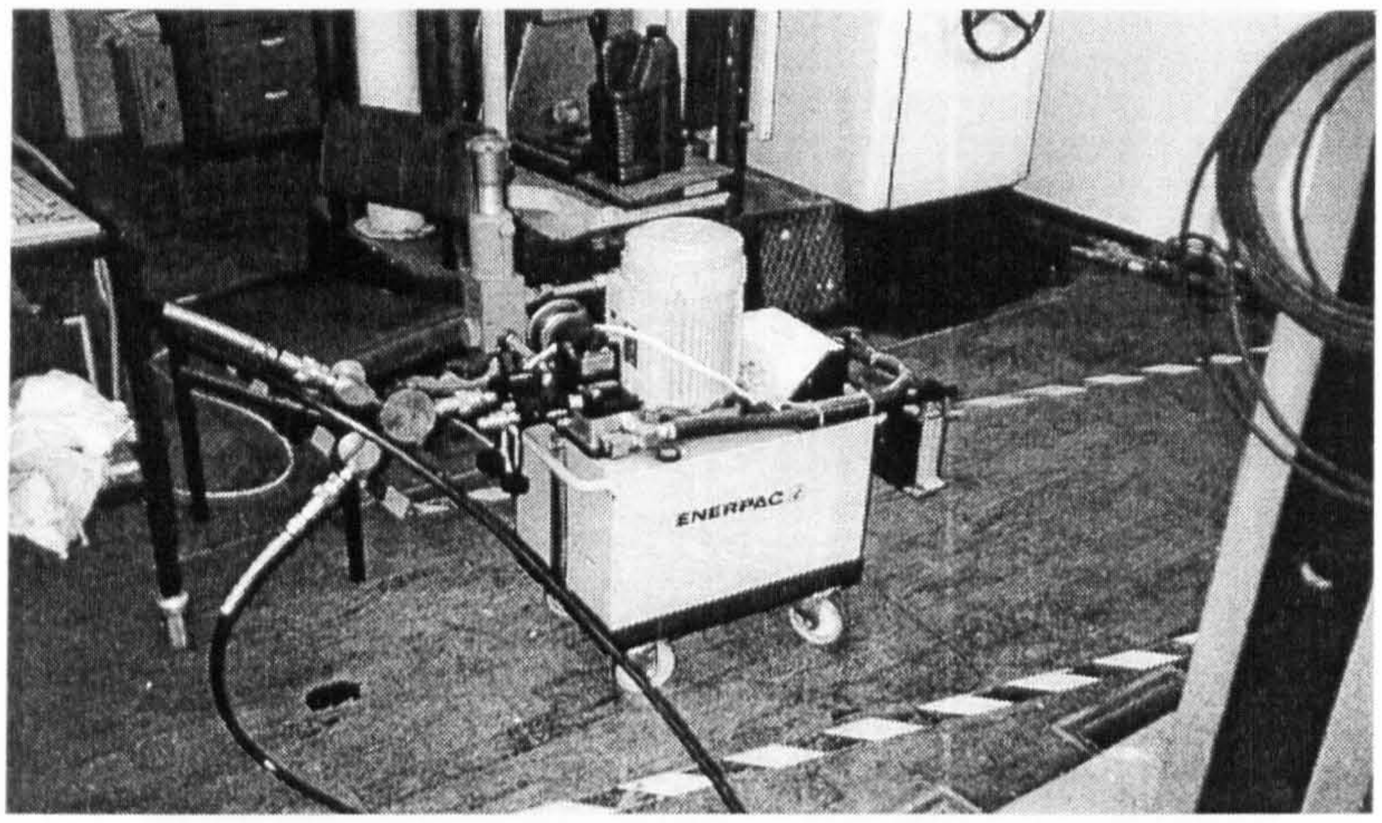

Figure 5.3 Hydraulic pump used in the push-off tests

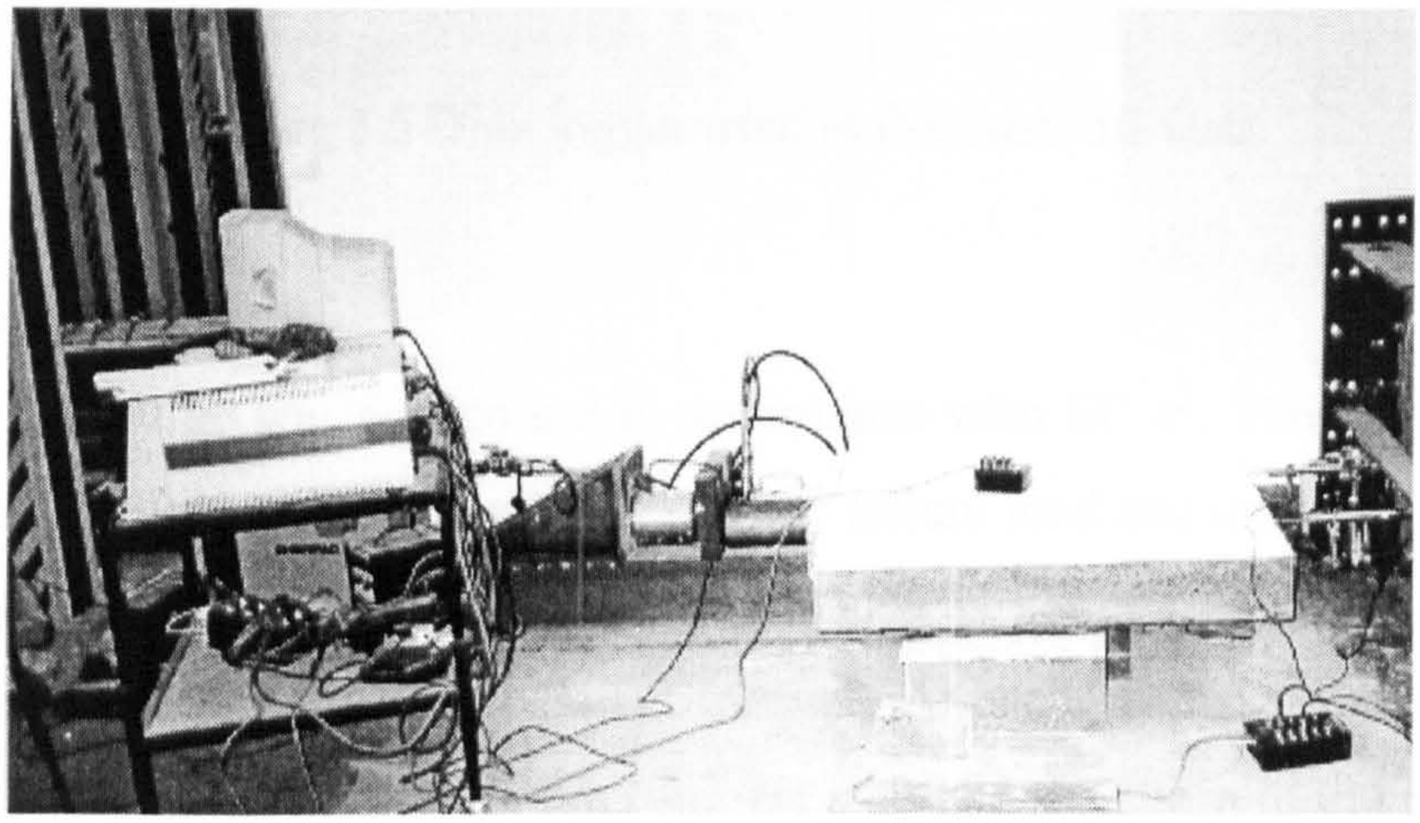

Figure 5.4 Arrangement of push-off test specimen before testing

5.2.3.3 Data logger

The readings of the load cell, LVDTs and the strain gauges were read directly with Schulmberger 3530 model data logger shown in figure 5.5. The readings were printed

directly, and also recorded on disc for later transfer on computer disc storage for the preparation of load vs. slip and load vs. strain curves.

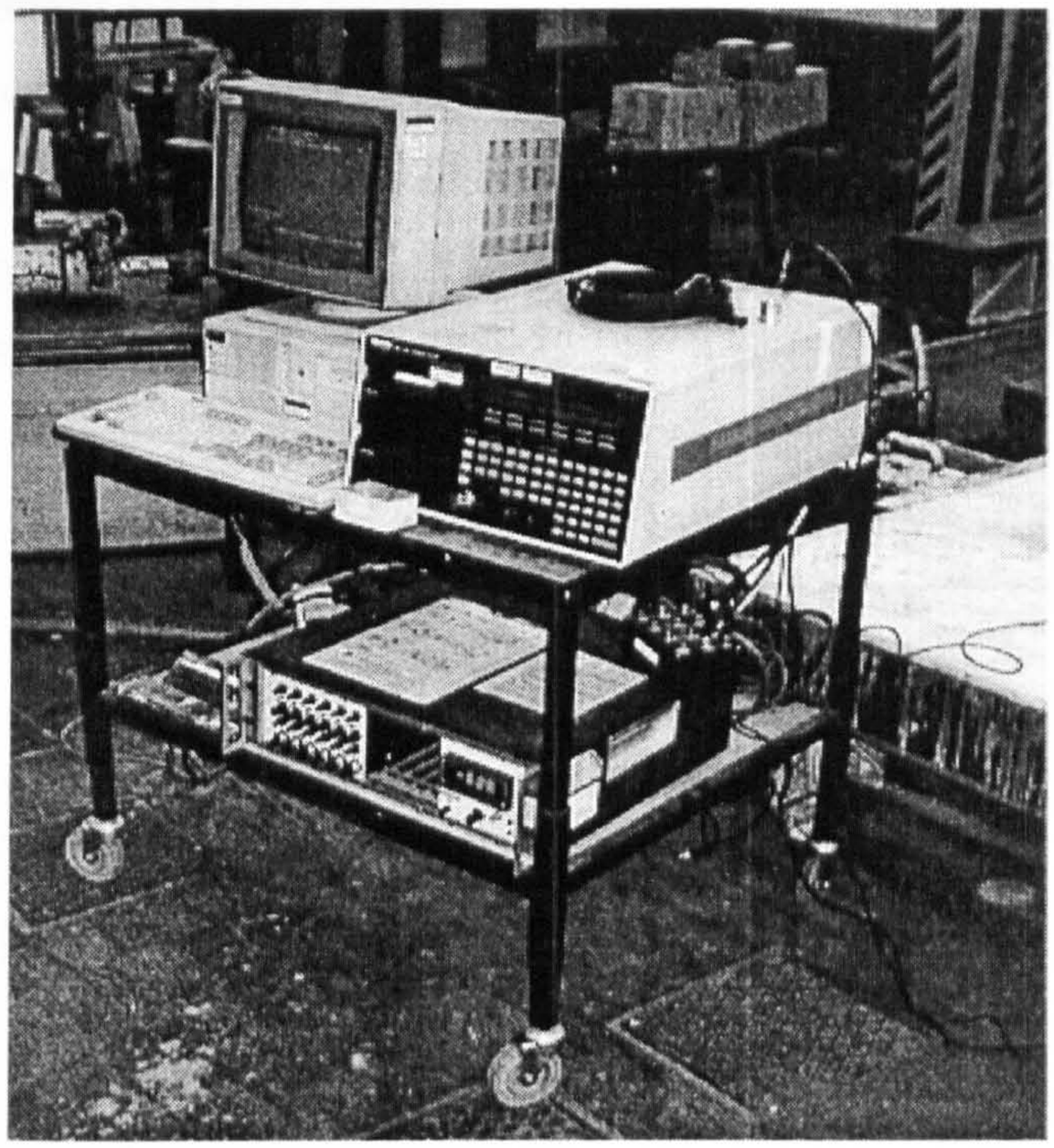

Figure 5.5 Data logger used in the push-off tests

5.2.4 Loading procedure

The loading procedure was carried out in accordance with EC 4[8]. The load was applied in increments of 20kN up to 40% of the expected failure load and unloaded. The process was repeated 25 times. After this stage, the load was applied up to the failure with smaller load increments until failure was observed. At each load increment, readings of the slip between the steel beam and the concrete slab and the strain in the reinforcement bars were recorded on the data logger.

5.2.5Material testing

5.2.5.1 Concrete testing

In-situ concrete was cast in the laboratory. To monitor the in-situ concrete strength, twelve (100x100x100mm) cubes and five cylinders (100x200mm), per specimen, were

cast at the same time as the specimens. The cube tests were carried out in accordance with BS 8110[65].

5.2.5.2 Reinforcement steel bar testing

To establish the mechanical properties of the 10mm diameter reinforcement bars, tensile tests on three specimens were conducted. Figure 5.6 shows the stress-strain curves of the three test specimens. The average yield stress was 460N/mm^2 and the average modulus of elasticity was 200000 N/mm^2.

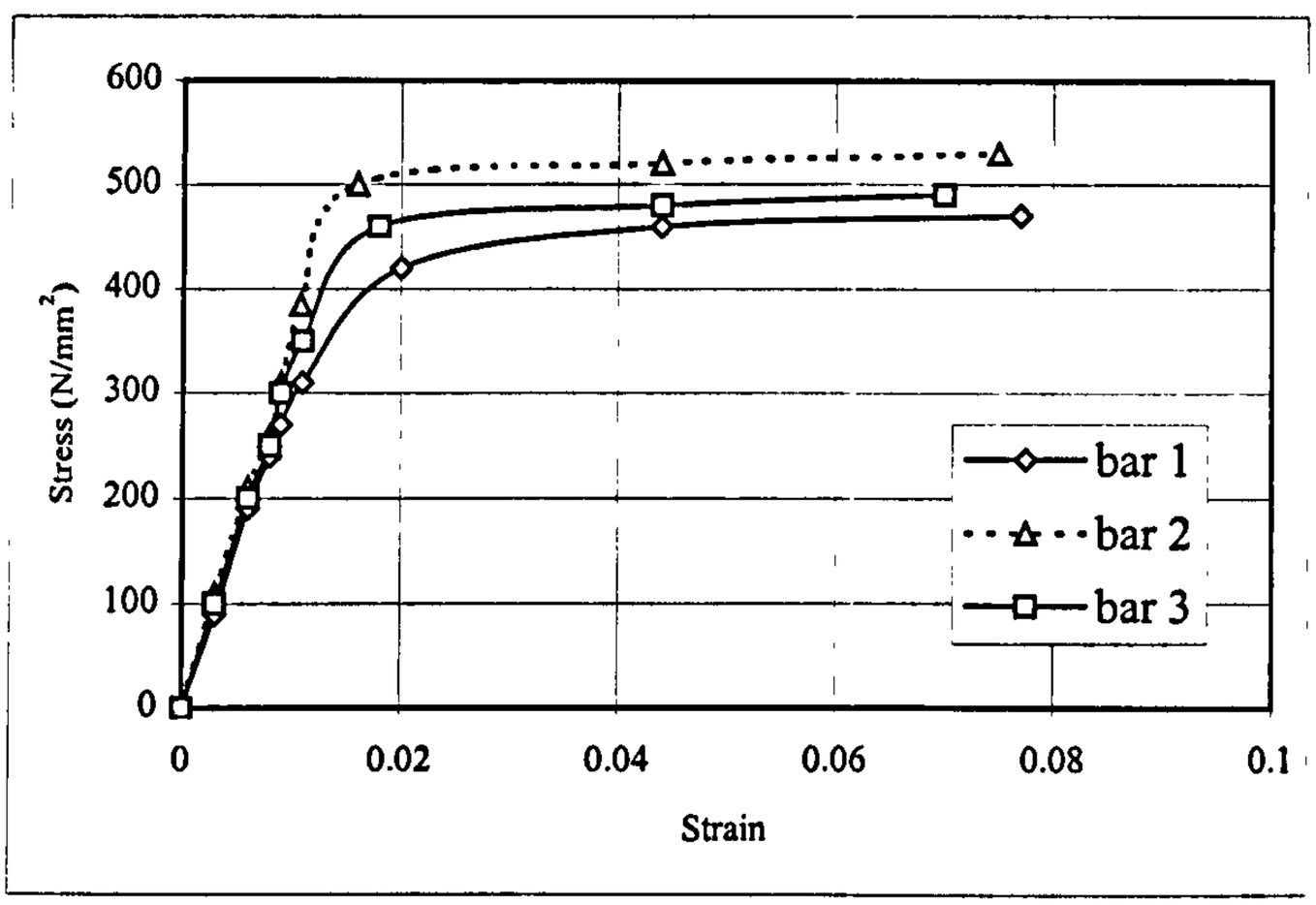

Figure 5.6 Stress-strain curve for 10mm reinforcement bars used in push-off tests

5.2.5.3 Shear stud connectors

The headed shear stud connector (19mm diameter x 100mm height) used in the push-off tests was manufactured by TRW Nelson Stud Welding Ltd. To determine the mechanical properties of the stud material, three coupons were machined from finished studs. Tensile tests were conducted for the three coupons to evaluate the stress-strain characteristic. The stress-strain curves are plotted in Figure 5.7. From these plots, the following average properties of the stud were found:

f_u = 470.8 N/mm^2, f_y = 400.0 N/mm^2 and elongation = 28%.

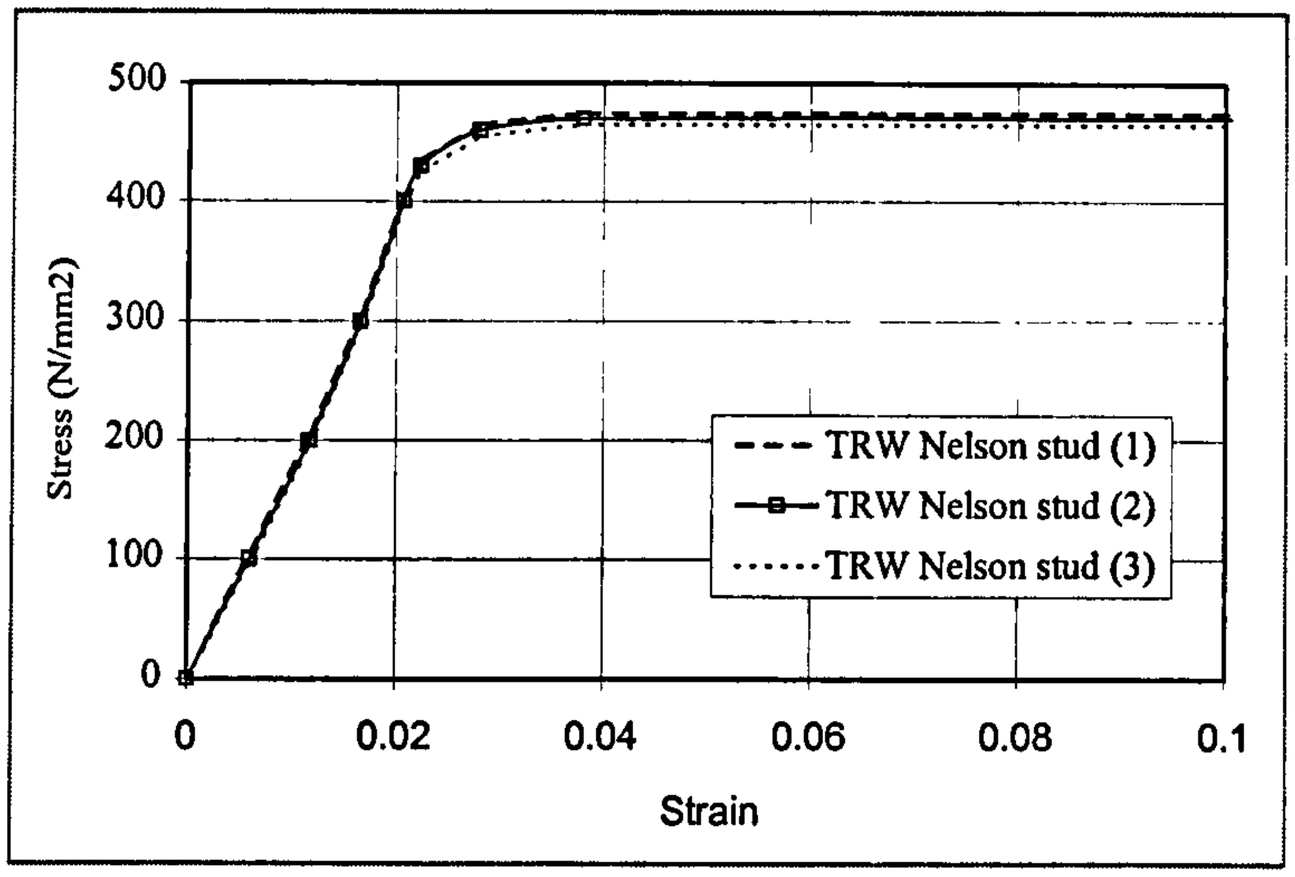

Figure 5.7 Stress-strain curve for headed stud used in push-off tests

5.2.6 Test results:

The main objective of the push-off tests was to determine the horizontal shear capacity and the load-slip behaviour of the shear connector in solid slabs. The variable test parameter was the concrete cube strength. Load vs. slip curve was plotted for each test. The maximum shear capacity, modes of failure and cracks in concrete were observed throughout the test.

5.2.6.1 Test S1 (C50):

Test specimen S1 had concrete cube strength of approximately 50N/mm^2 at the time of testing. The load was applied in small increments of 20kN per six studs to accurately measure the load-slip curve of the headed stud shear connector. The testing procedures were the same as specified in the EC 4[8]. The loading ended when the slab separated from the steel beam. The first and the last studs in the group sheared off while the other 4 studs bent in the direction of loading. No crack on the surface of the concrete slab was formed during loading. After the test, several small cracks were found at the concrete surface perpendicular to the direction of loading as shown in figure 5.8.

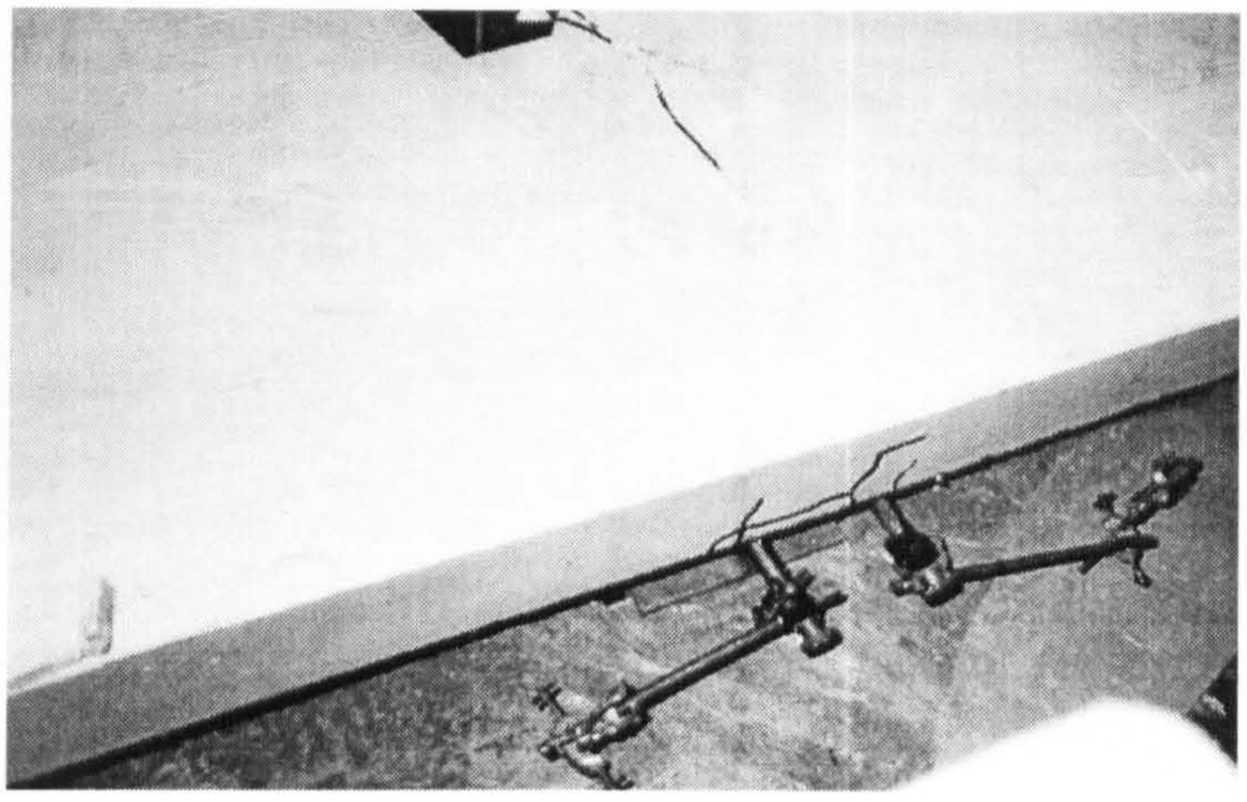

Figure 5.8 Cracks at the end of concrete slab of test specimen S1

Cracks formed around the studs and in the longitudinal direction forming small overlapping conical surfaces. The interaction between the concrete and the studs was partially lost. Measured strain in the bottom reinforcement was greater than that of the top reinforcement at the corresponding positions. This indicated that the bottom reinforcement carries more loads than the top reinforcement. Figure 5.9 shows the deformations in the lower surface of concrete slab after lifting it at the end of the test. The mode of failure is stud yielding. Two of the studs sheared off during the test in the welding zone and others bent in a double curvature shape as shown in figure 5.10.

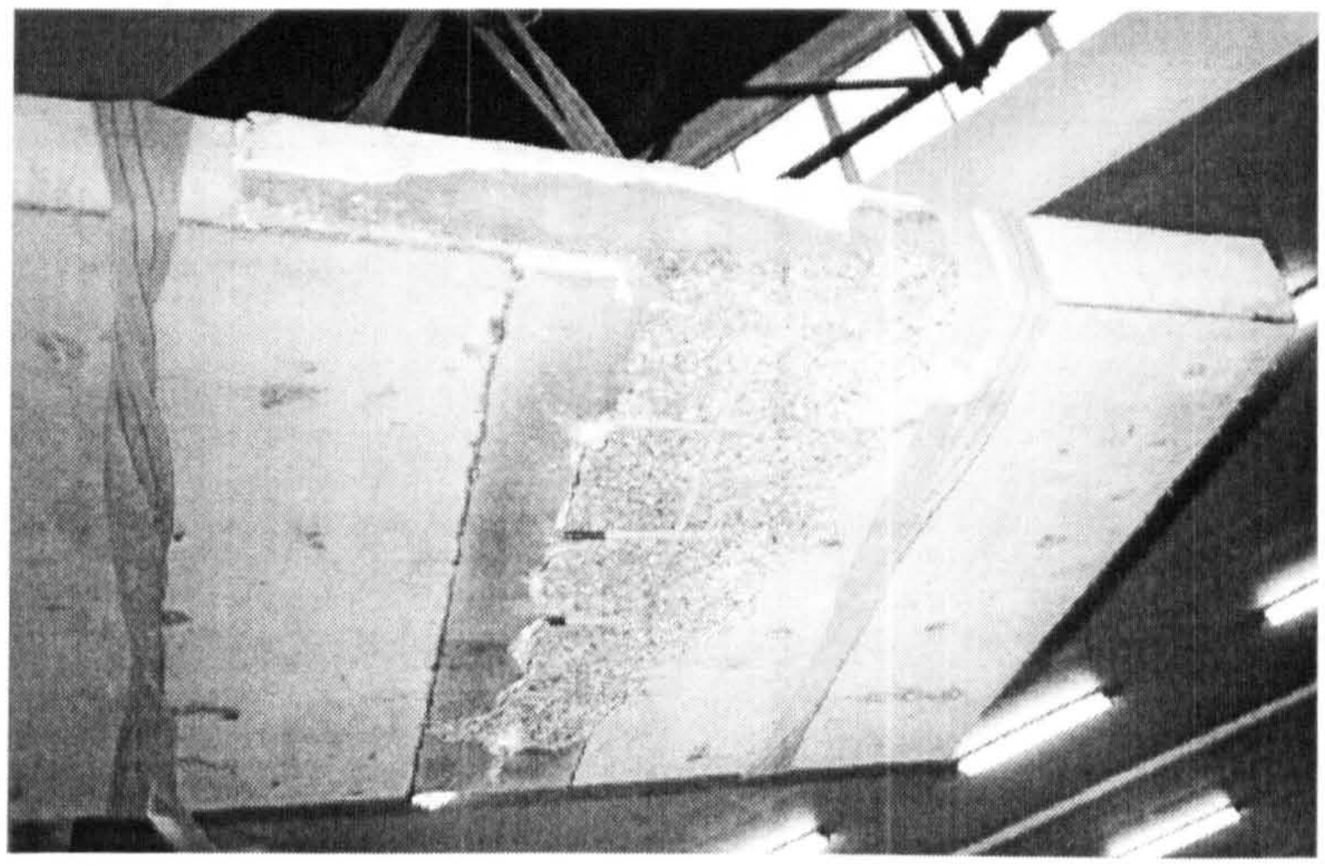

Figure 5.9 Distortion of lower surface of concrete slab of test specimen S1

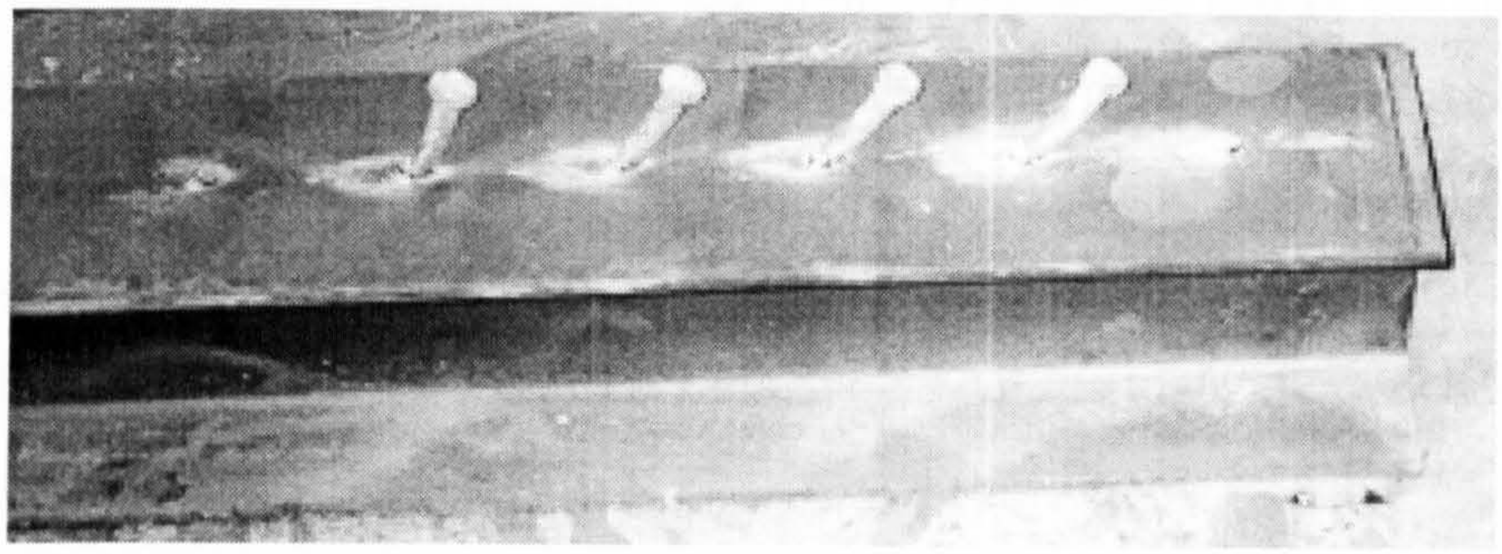

Figure 5.10 Shear studs for test specimen S1 after termination of test

Figure 5.11 shows the load vs. slip curve of the stud for test specimen S1. At a load level of 129kN per stud with a slip of 3.8mm the specimen started to fail and the load was maintained approximately at this level with continuous slip. The maximum load was 130.4kN per stud at a slip of 9.3mm.

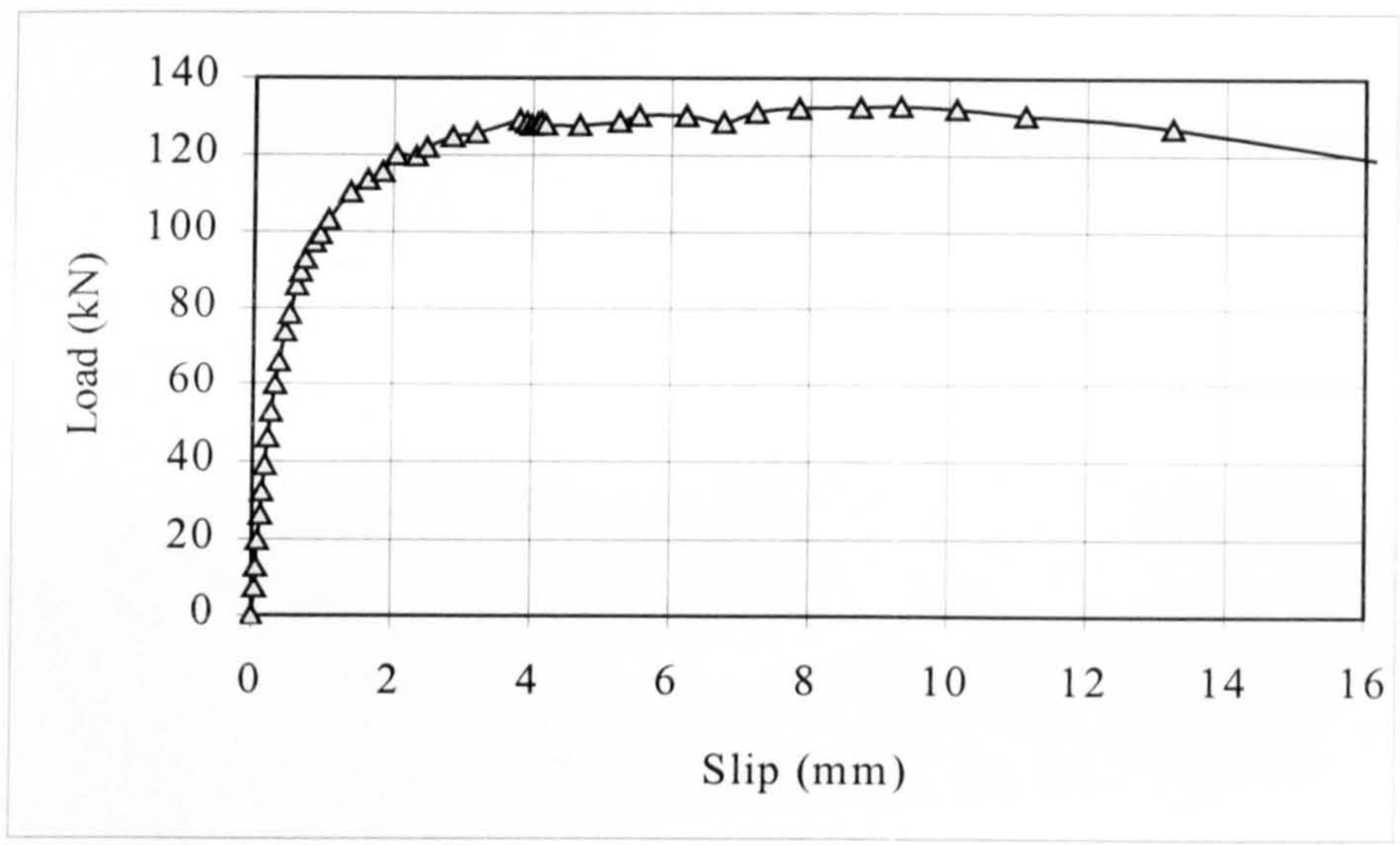

Figure 5.11 Load vs. slip curve of the stud for test specimen S1

5.2.6.2 Test S2 (C20):

In the test specimen S2, the test terminated when the slab separated from the steel beam. The first crack was observed at a load of 66.5kN per stud with 2.4mm slip at the steel-beam-concrete slab interface. Some small cracks followed during loading till failure on

the upper surface of the concrete slab, see figure 5.12 which shows the crack pattern distribution on the top surface of concrete slab at failure. The concrete around the stud formed attached conical failure surfaces along the gauge line of the six studs, approximately with the full depth of the stud, and separated from the surrounded concrete as shown in figure 5.13. All the six studs bent in single curvature shape in the direction of loading but none of the studs sheared off. Figure 5.14 shows the headed studs after the test.

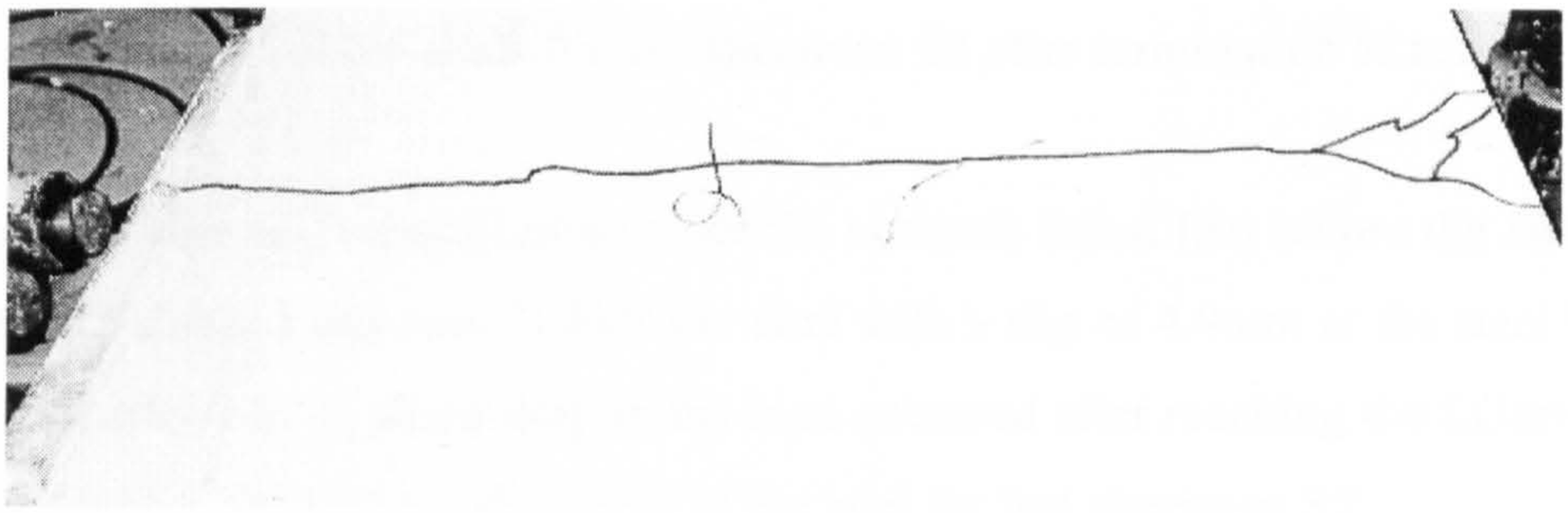

Figure 5.12 Cracks at middle upper surface of concrete slab for test specimen S2

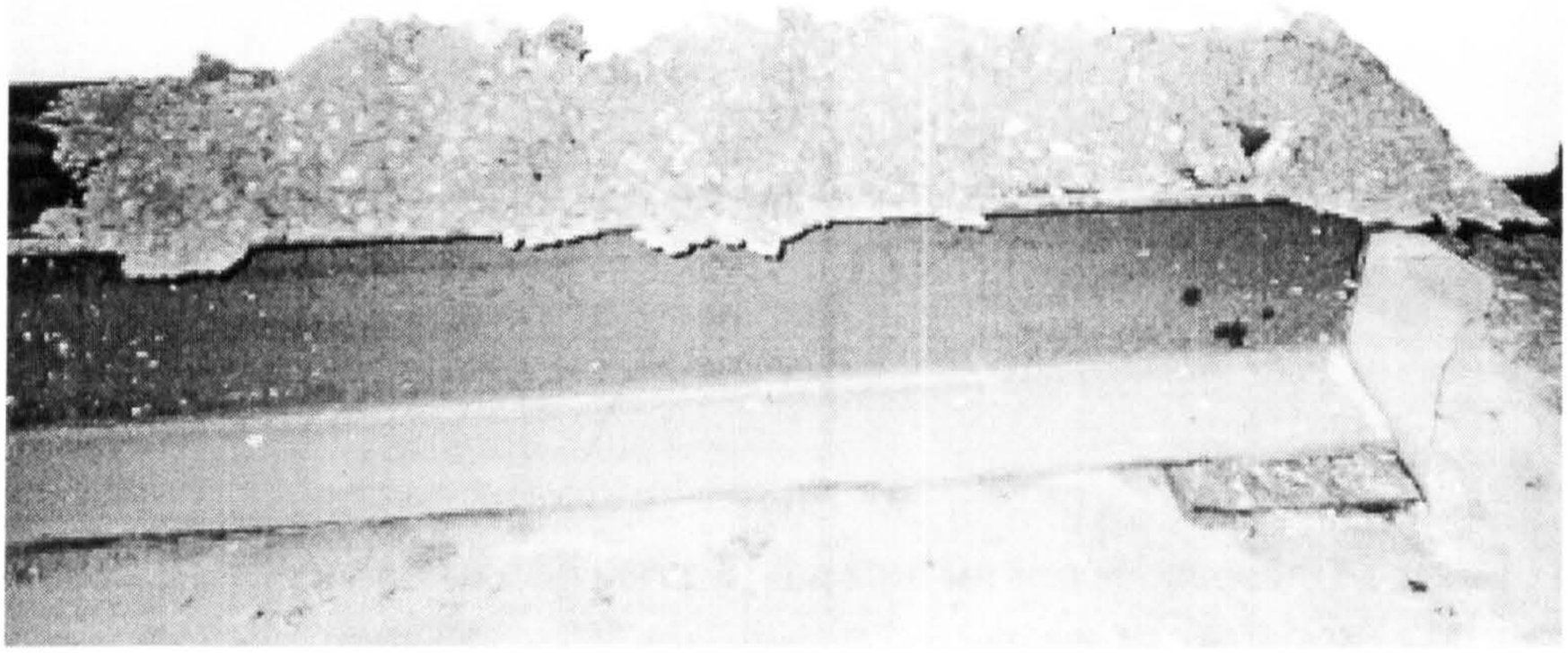

Figure 5.13 Conical failures of concrete around the studs for test specimen S2

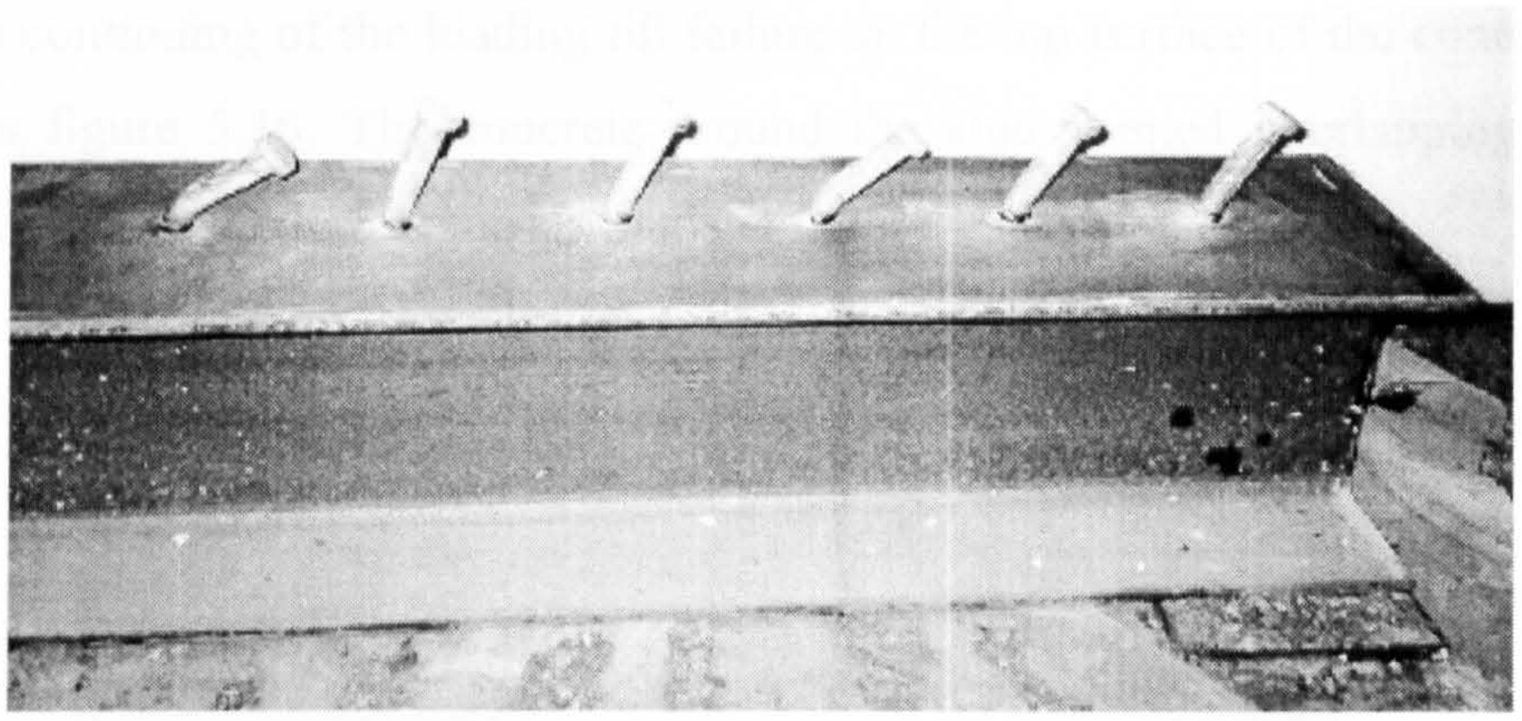

Figure 5.14 Shear studs for test specimen S2 after termination of test

The mode of failure is concrete failure since the concrete failed first before the failure of studs. The maximum Load was 71.6kN per stud with a slip of 4.9mm at the steel beam-concrete slab interface. A sharp drop in the load occurred after reaching the failure load. Figure 5.15 shows the load vs. slip curve of the stud for test specimen S2.

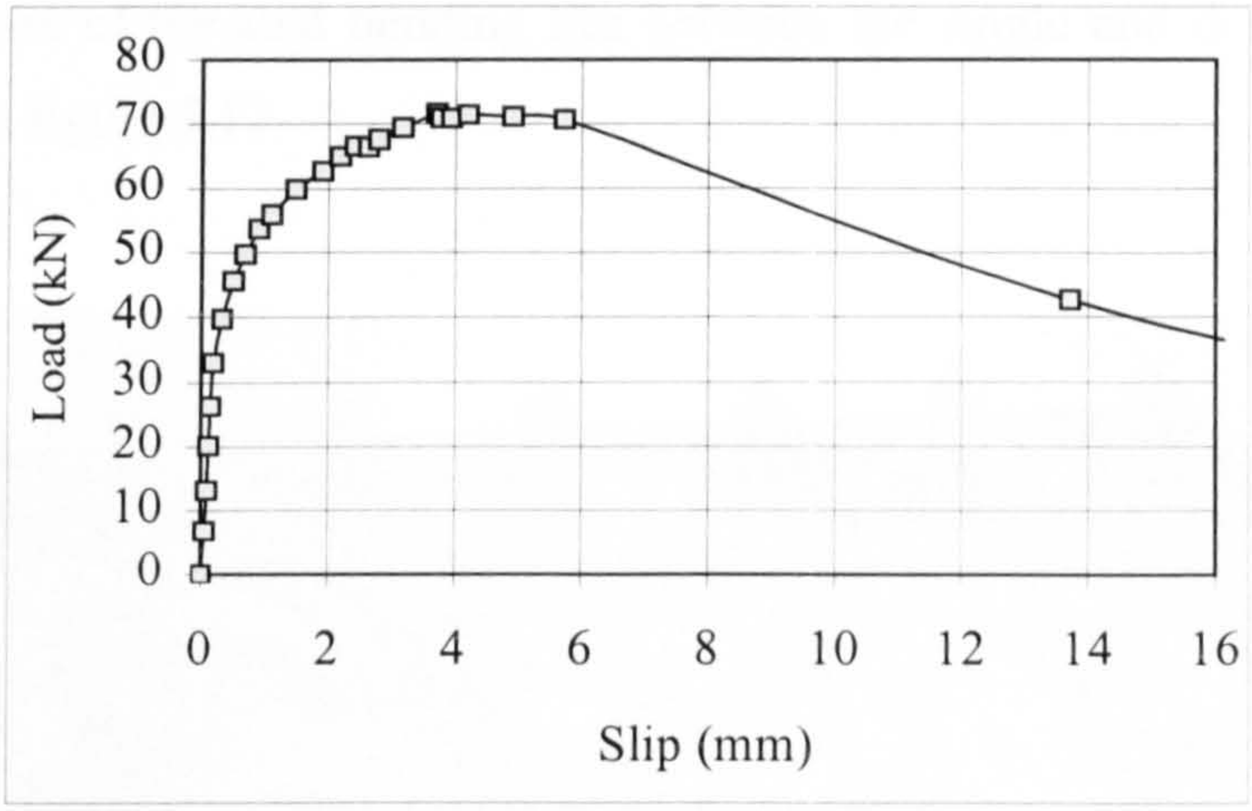

Figure 5.15 Load vs. slip curve of the stud for test specimen S2

5.2.6.3 Test S3 (C30):

In the test specimen S3, the loading ended when the slab separated from the steel beam. The first crack was observed at a load level of 87kN per stud accompanied with a slip of

2.4mm at the interface between steel beam and concrete slab. Some small cracks were formed with continuing of the loading till failure on the top surface of the concrete slab as shown in figure 5.16. The concrete around the stud formed overlapping conical surfaces along the gauge line of the six studs at failure.

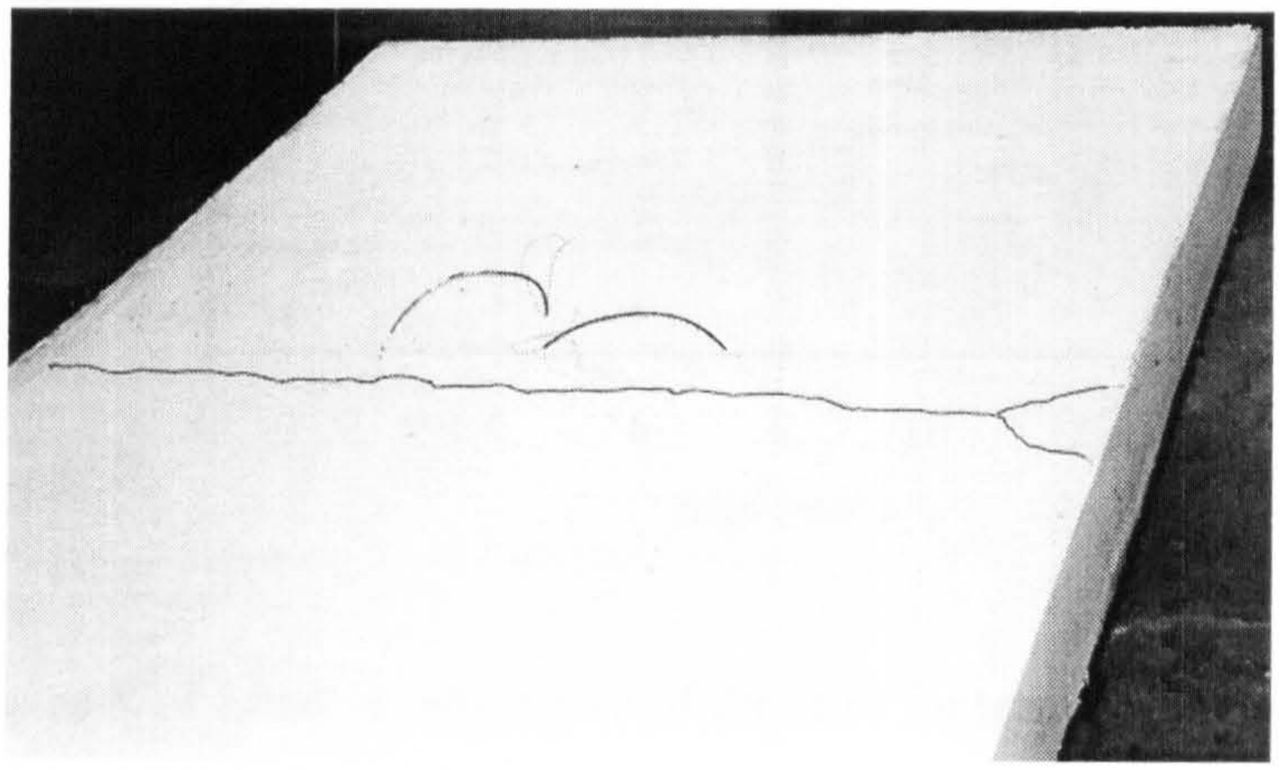

Figure 5.16 Cracks at middle upper surface of concrete slab for test specimen S3

The mode of failure is a combined mode between concrete failure mode and stud failure mode. The curvature of the stud bending lies between the single and double curvature shapes as shown in figure 5.17.

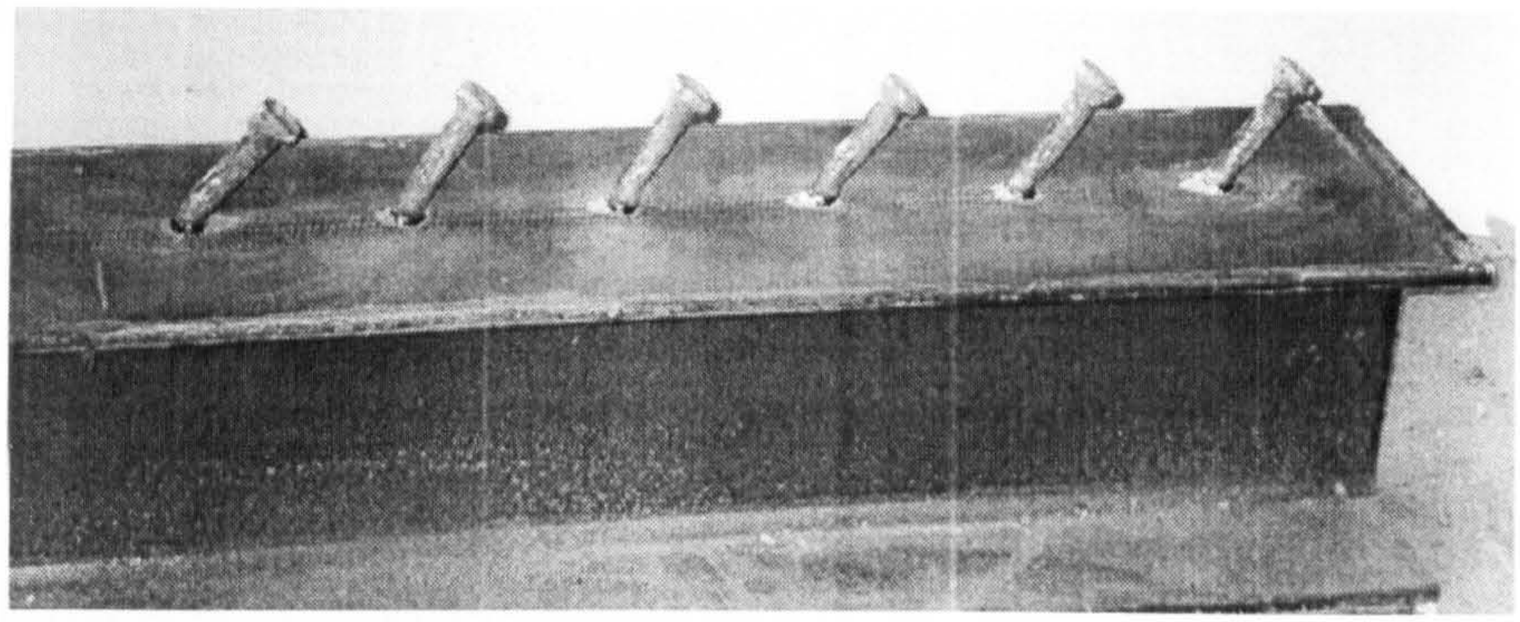

Figure 5.17 Shear studs for test specimen S3 after termination of test

Figure 5.18 shows the load vs. slip curve of the stud for test specimen S3. The maximum Load was 93kN at a slip of 5.96mm.

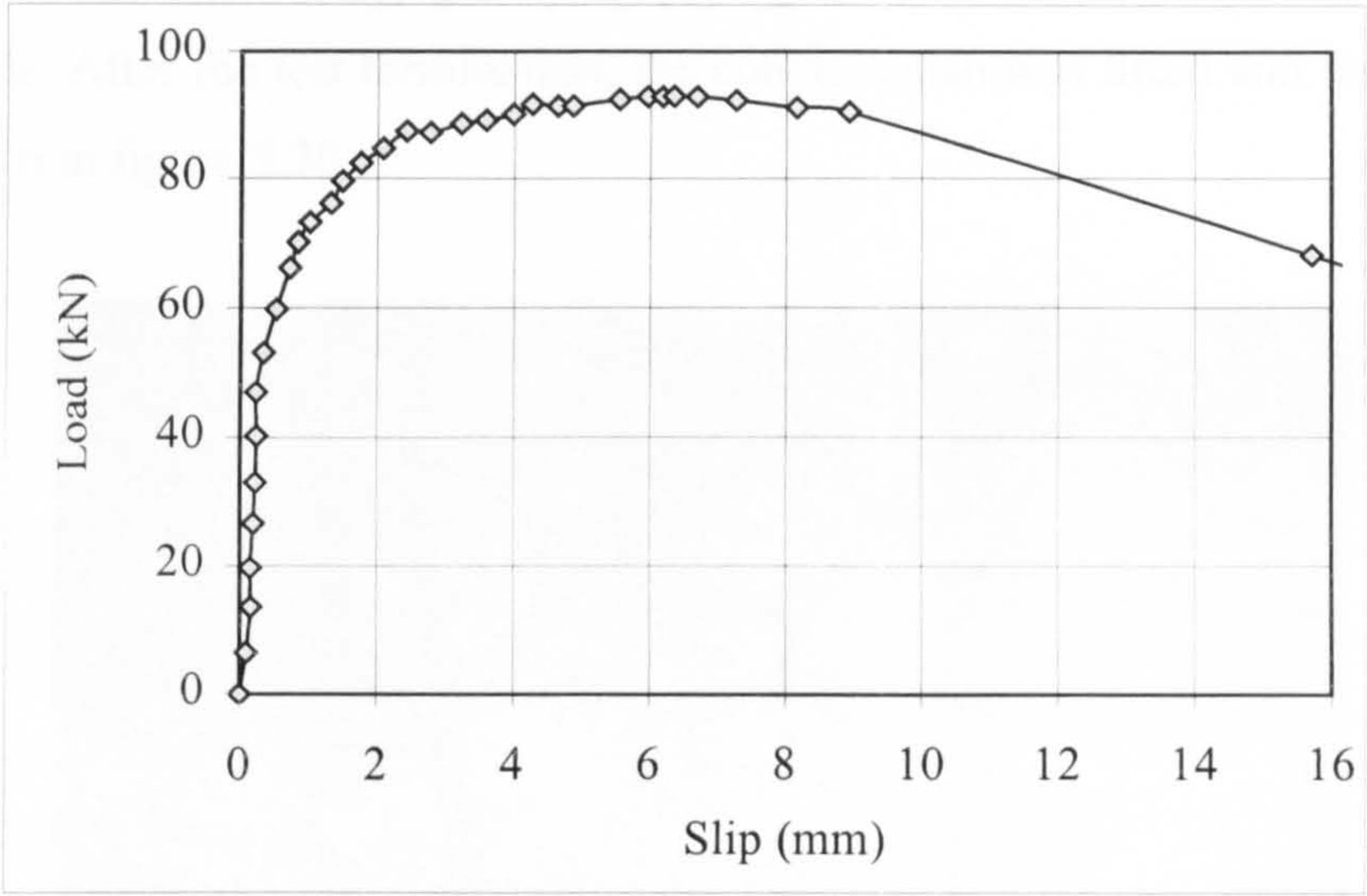

Figure 5.18 Load vs. slip curve of the stud for test specimen S3

5.2.6.4 Test S4 (C35):

In the test specimen S4, the loading ended by separation of the concrete slab from the steel beam. The first and the last studs in the group sheared off in the welding zone as shown in figure 5.19. While the other four were applied to bending in the direction of loading due to the yield of the stud material at the maximum stress zones. The bending curvature is between the double and single curvatures obtained for specimens S1 and S2 respectively.

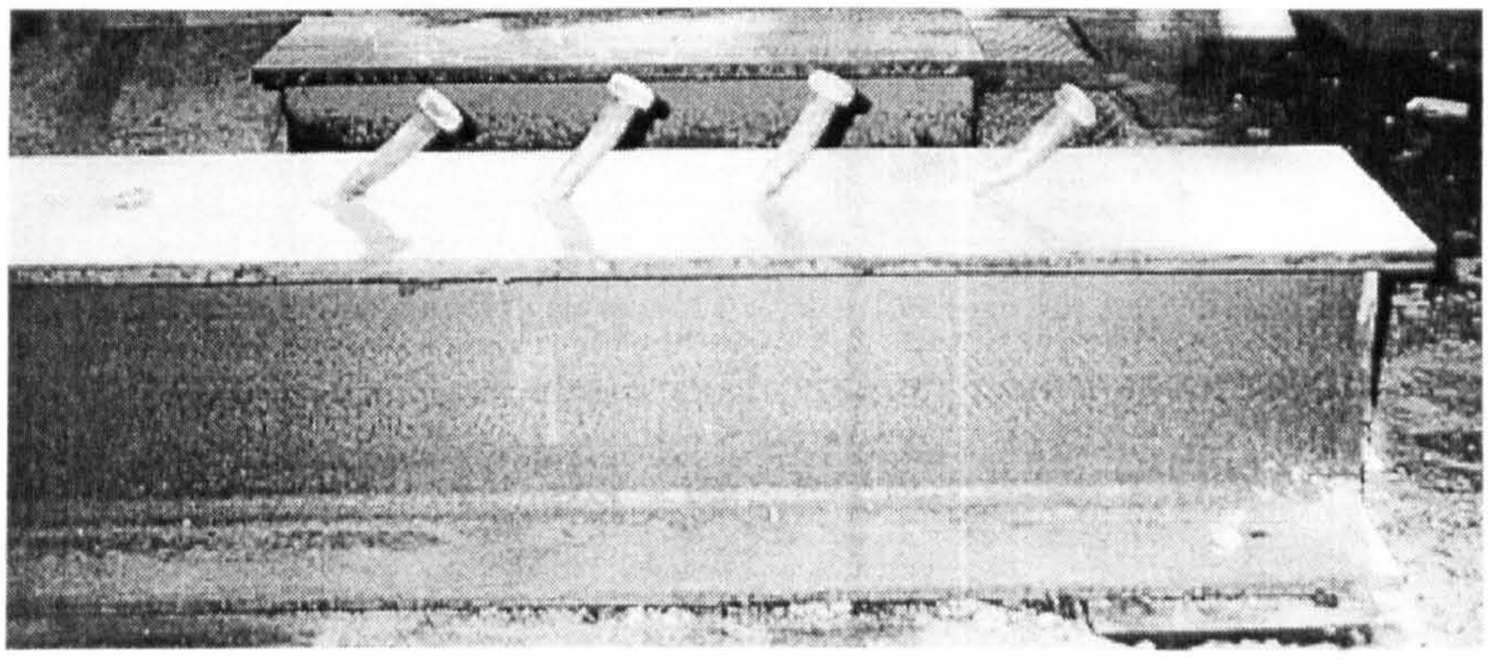

Figure 5.19 Shear studs for test specimen S4 after termination of test

The first crack appeared at loading of 80kN per stud and more thin cracks were observed at higher loads. After the test termination, the concrete slab was lifted and the distortion shape is shown in figure 5.20.

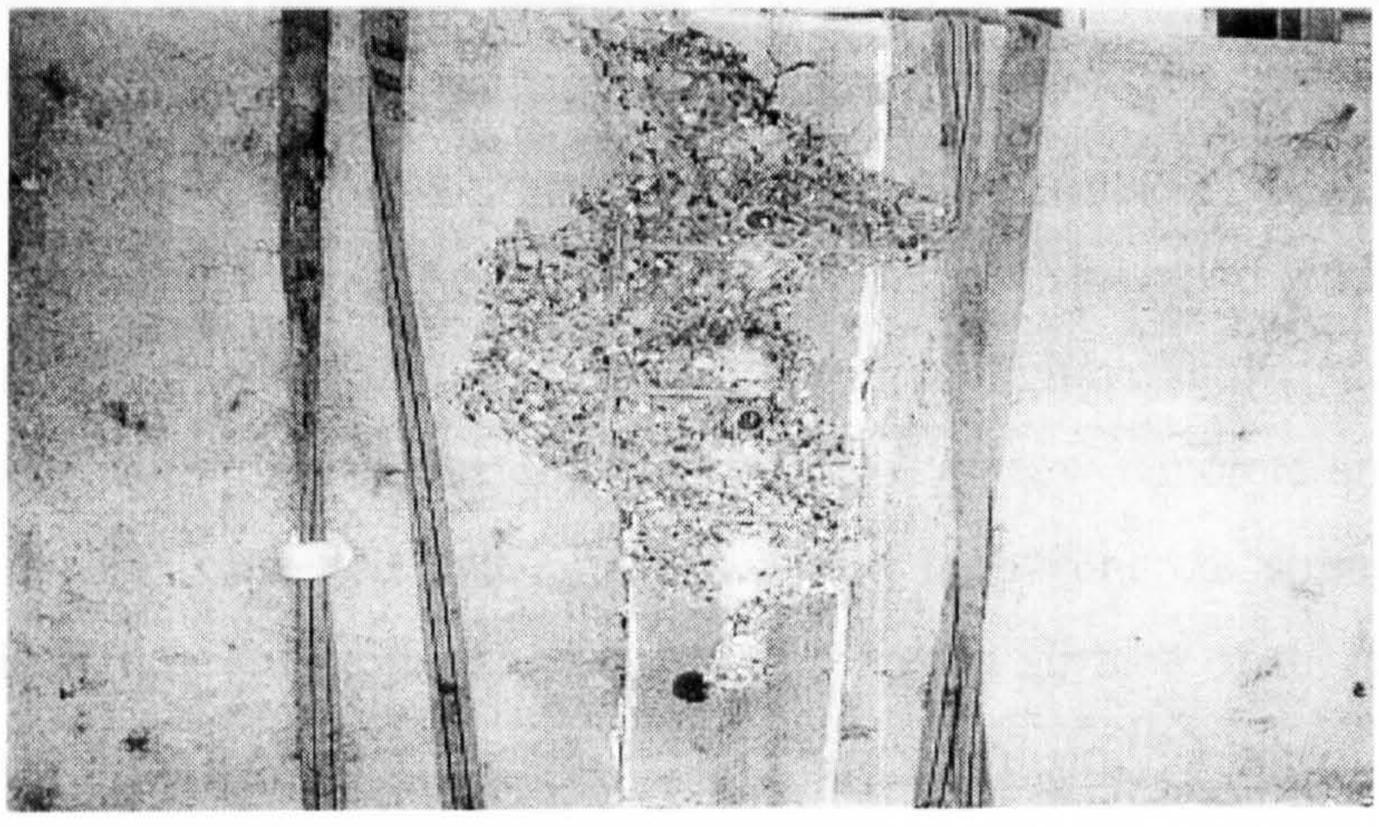

Figure 5.20 Distortion of lower surface of concrete slab of test specimen S4

The mode of failure is combined failure mode between the stud yielding failure mode and the concrete failure mode but the tendency to the first one is higher. The maximum load was 102.0kN per stud at a slip of 6.1mm. Figure 5.21 shows the load-slip curve of the stud for test specimen S4.

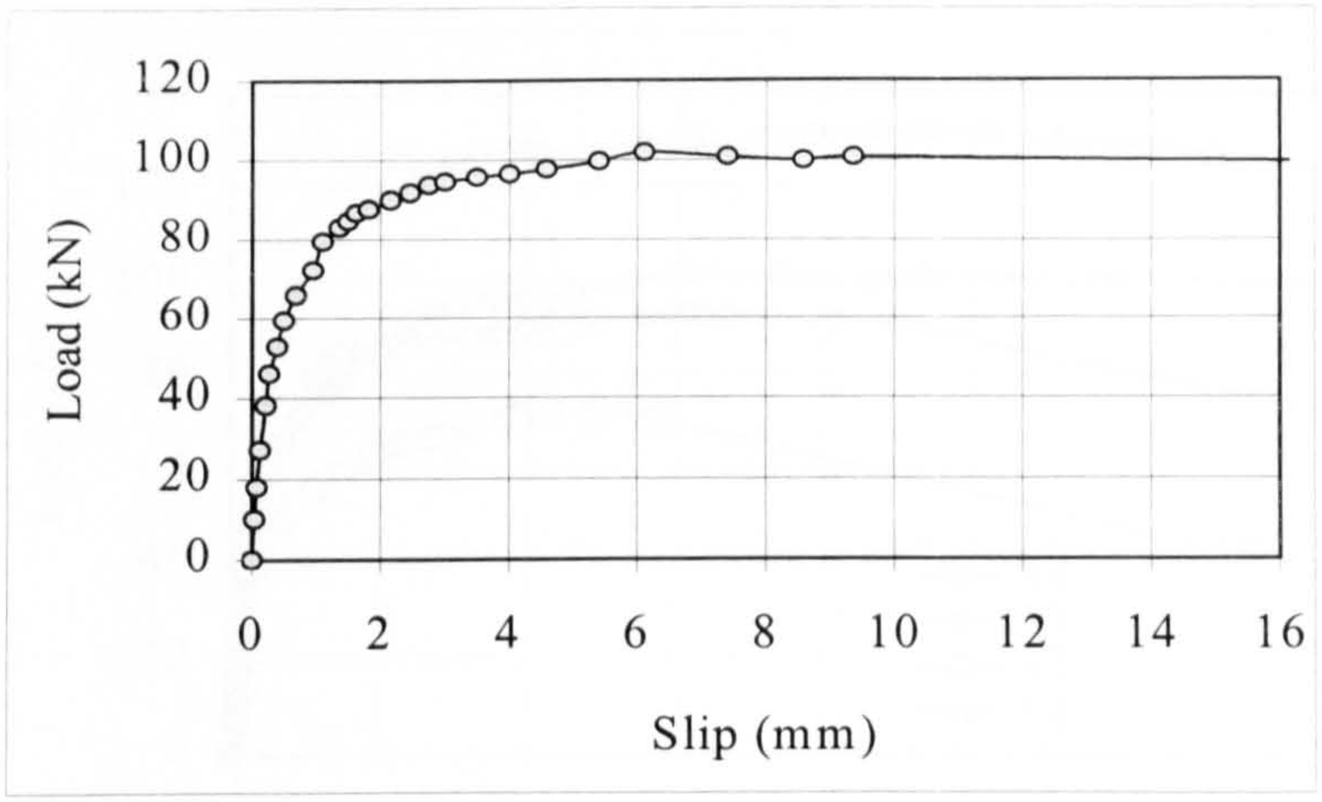

Figure 5.21 Load vs. slip curve of the stud for test specimen S4

5.2.7 Summary of results

Four full-scale push-off tests with solid slabs were carried out in this study using an established technique used by Lam, Elliot and Nethercot[23].

The main purpose of carrying these tests was to validate and check the accuracy of the present finite element modelling results. Since the main variable parameter in the tests was the concrete strength, it was observed that concrete cube strength had a considerable effect on shear connection capacity, load–slip behaviour of the headed stud and finally modes of failure. Specimens with high concrete cube strength have shown more ductility in the load-slip behaviour of the headed stud than that of low concrete strengths, see figure 5.22. It is also observed that specimens with high concrete strength did not achieve concrete failure before the stud shear off. The top surface of these specimens remained un-cracked at the end of the test. The failure was mainly obtained by shearing of studs. On the other hand, specimens with low concrete strengths formed overlapping concrete cone failures along the gauge line of the studs. None of the studs sheared–off and few cracks formed at the top surface of the concrete slab at the end of the test. Figure 5.22 shows the load-slip curves of the 19mm diameter x100mm height stud for the four tests carried out in this study. A comparison will be made in chapter 6 between these curves and those previously obtained in chapter 3 from FE element analyses.

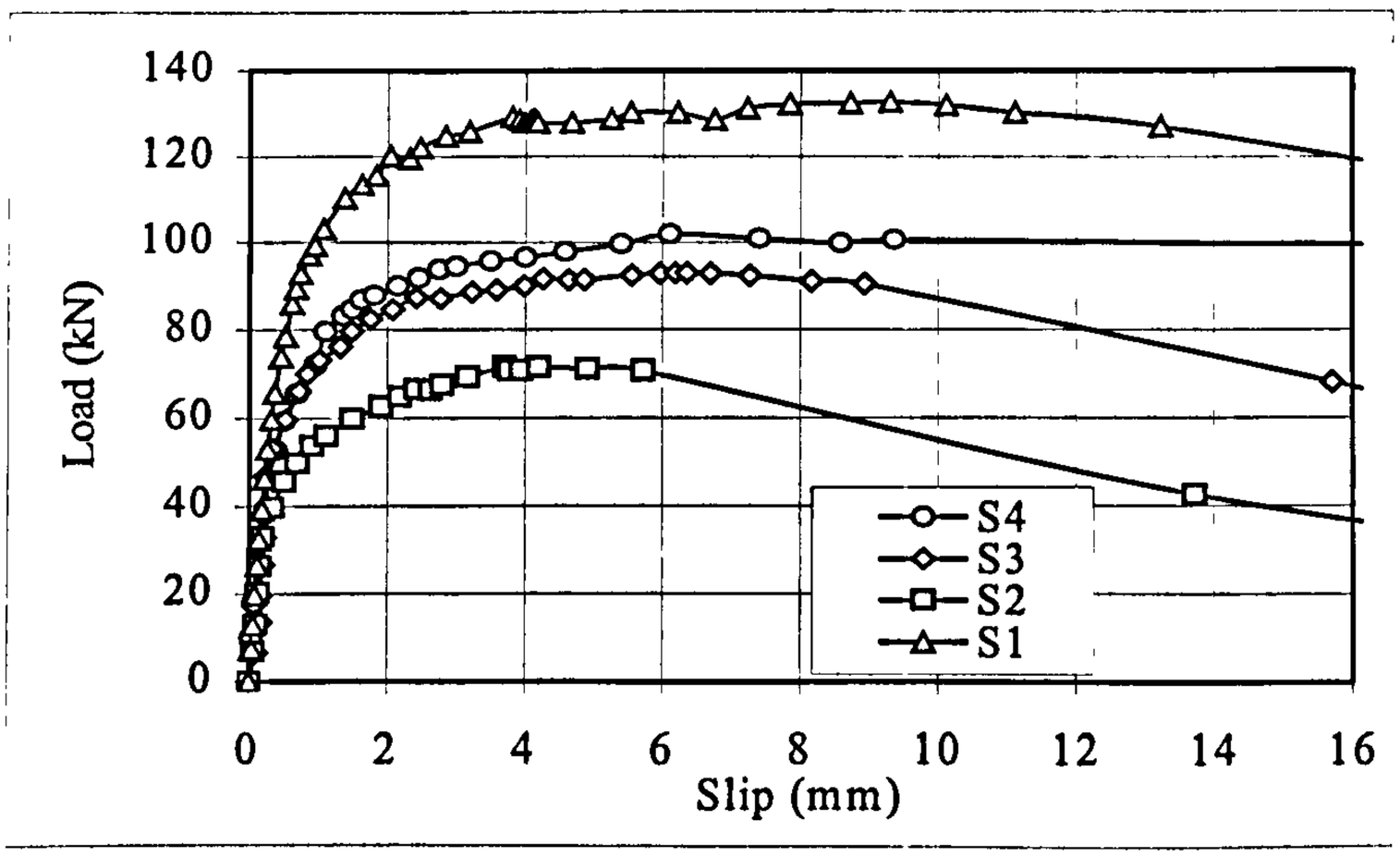

Figure 5.22 Load versus slip curves of the stud for solid slab push-off tests

The behaviour of headed stud in push-off tests with solid slabs is related to the confinement of the concrete around the stud. The concrete bearing stress, resulting from the application of the shear load, on the shaft of the stud allows for the bending of the stud assuming that rigid connection is made to the steel beam. The deformation of the stud causes the head to rotate, which cause the concrete to crack in the region behind the stud. The tensile cracks will allow further rotation of the head and increase the stresses at the critical element of the stud at its collar. Three different curvatures of bending behaviour were predicted from present push-off tests. Push-off test specimens with higher concrete strength, like specimen S1 with concrete strength C50 N/mm^2, had higher resistance to tensile cracking in the region behind the stud and consequently formed an obstacle for the stud to rotate freely and forced the stud to bend in a double curvature mode at failure. On the other hand, push off test specimen S2 with concrete strength of C20 N/mm^2 were weak enough in terms of tensile cracking resistance in the region behind the stud and formed concrete cone failure allowing the stud to bend in a single curvature mode. Other specimens failed in a combined failure mode allowing the stud to bend in a curvature lies between single and double curvatures.

The shear connection capacity is also affected by the concrete strength as observed by many researchers. Push-off tests with high concrete strength resulted in higher shear connection capacity provided tensile splitting is controlled by adequate transverse reinforcement. Table 5.1 which shows summary of the shear connection capacity for the four push-off tests carried out in this study on headed studs with solid reinforced concrete slabs.

Test Ref.	Diameter of Headed stud (mm)	Concrete Grade (N/mm^2)	Shear capacity (kN)
S1	19	50	130.4
S2	19	20	71.6
S3	19	30	93
S4	19	35	102

Table 5.1Summary of results for push-off tests with solid slabs

5.3 Push-off tests on studs used with precast hollow core concrete slab

Experimental investigation of headed shear stud capacity in composite girders with precast hollow core units is a current research area, as described in chapter 2. Present push-off tests on this type of shear connections are designed to verify the FE modelling of the same connections previously discussed in chapter 4. This chapter includes the details and results of four full size push-off testing using the standard precast square-end hollow core units. The modes of failure, the load vs. slip curves, the load vs. strain curves, and the failure load are presented. A comparison between the FE results with the experimental results will be held in chapter 6.

5.3.1 Test arrangement and details of the specimen

The same loading frame, instrumentation, loading procedure and material testing used with push-off tests with solid slabs are used in present push-off tests with precast HCU concrete slabs. The only difference is the test specimen arrangements and components. A detailed description of the push-off test specimen was previously given in section 4.2.1 as introduction to the FE modelling of push-off tests with precast HC slabs investigated in chapter 4.

5.3.2 Test results

The main objective of the present push-off tests is to validate and compare with the FE modelling of this type of composite construction previously described in chapter 4. The horizontal shear capacity of the headed stud connector, load vs. slip characteristic of the stud and load vs. strain curve for the transverse reinforcement bar were obtained for each test. The variable test parameters were the area of transverse reinforcement, in-situ concrete strength and the gap of the in-situ in-fill. These parameters proved influential from research conducted by Lam[23] and Nip[32]. Cracks in concrete and modes of failure were observed throughout the test.

Test specimens are given a reference of the following format T bs-C-t-g where:
T: test specimen, bs: bar size, C: grade of in-situ concrete, t: the concrete slab thickness and g: the gap size. So, T 10-C25-150-65 is a test specimen that has 10mm transverse

reinforcement diameter, concrete cube strength of 25N/mm^2, concrete slab thickness of 150mm and a gap size of 65mm.

5.3.2.1 Test specimen T 10-C25-150-65

This test specimen had a small transverse reinforcement diameter of 10mm size, a gap of 65mm and the depth of the precast HCU and the in-situ concrete were 150mm. The in-situ concrete cube strength was 25N/mm^2 as evaluated from experimental material testing at the time of testing. No cracks were observed for load up to 66kN per stud. The first crack was found longitudinally along the specimen and also transversely between the joints as the applied load reached 67kN per stud. Tensile cracks were observed after maximum load was achieved. The test was terminated due to excessive cracking longitudinally along the specimen. Figure 5.23 shows the crack pattern of T 10-C25-150-65 after the test.

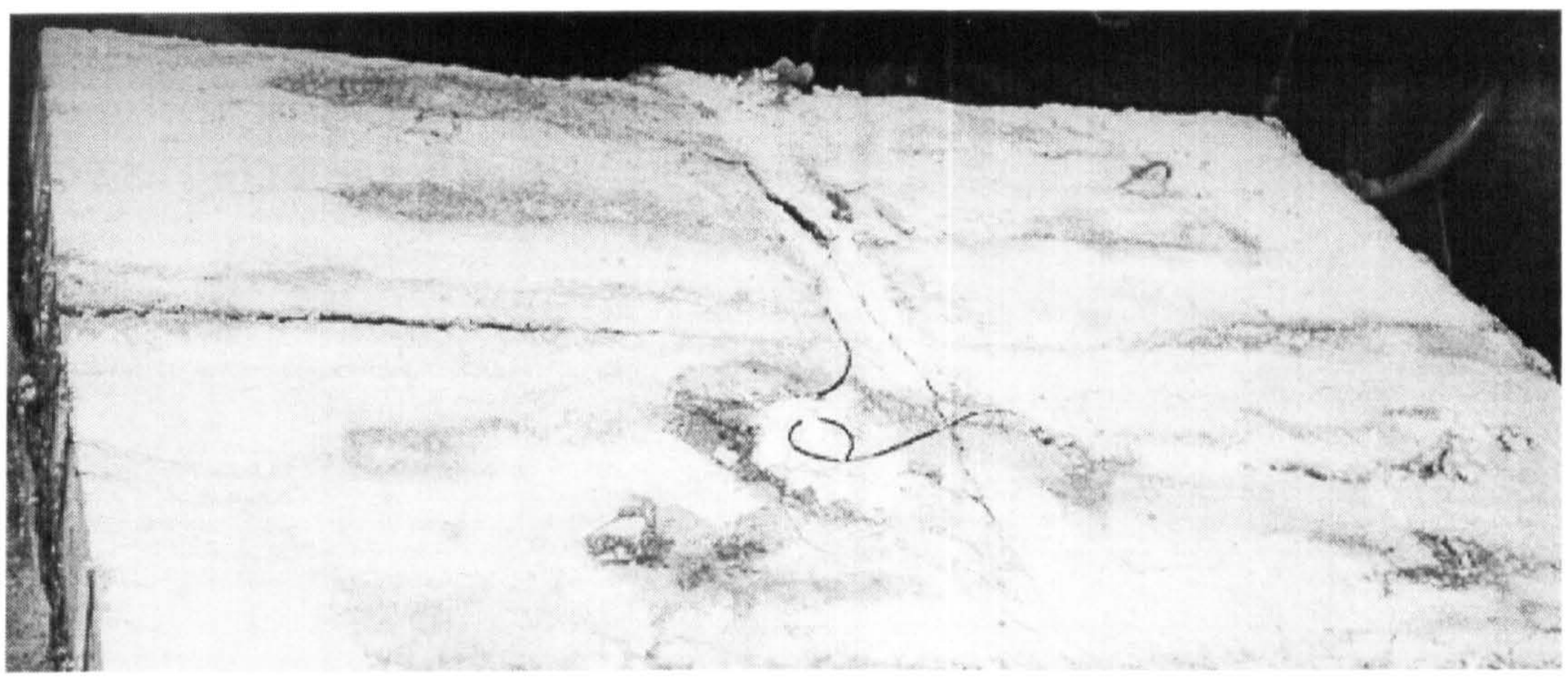

Figure 5.23 Crack pattern of T 10-C25-150-65 after the test

Mode of failure is yielding of transverse reinforcement and subsequently tensile splitting of in-situ in-fill concrete around the shear studs. None of the studs sheared off at the end of the test as shown in figure 5.24.

Load reduction occurred as the applied load reached the maximum of 68kN per stud, with crack widths up to 1mm as a high tensile strain was occurred in the transverse reinforcement. Slip at maximum load was 2.63mm. The applied load gradually reduced as the transverse reinforcement becomes fully yielded. The load vs. slip curve of the stud is shown in figure 5.25.

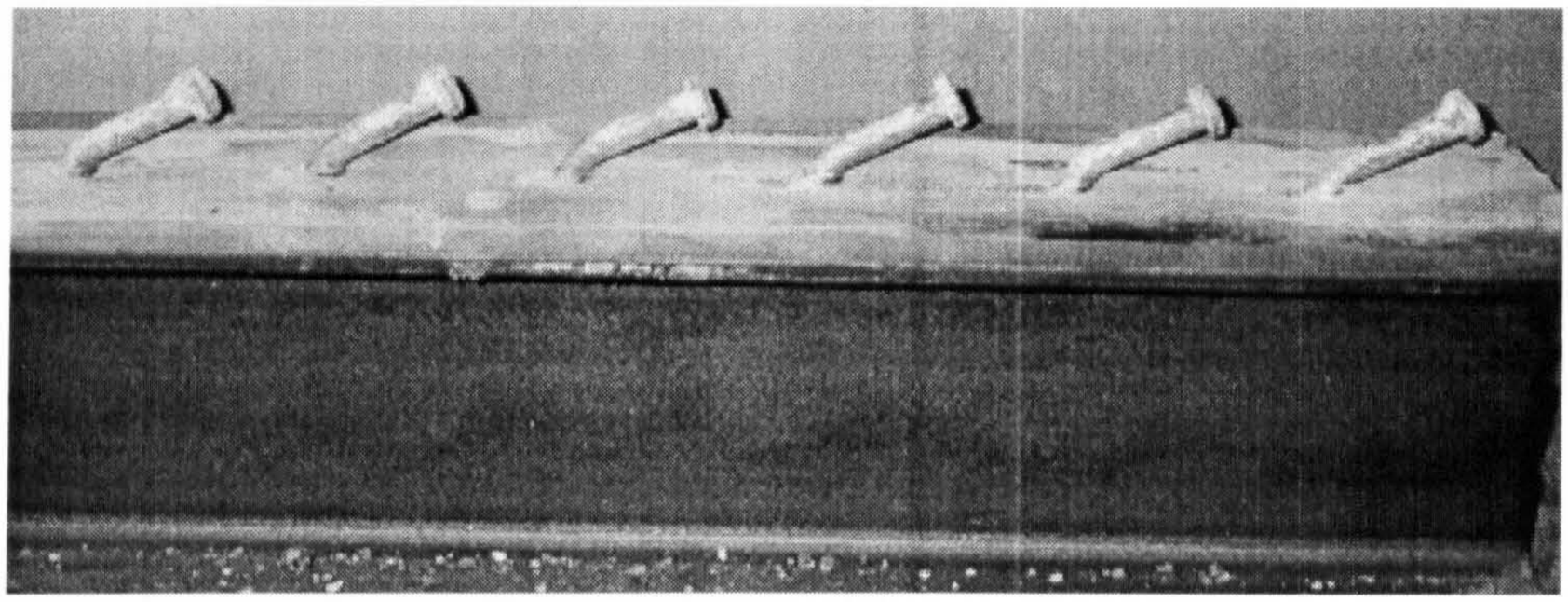

Figure 5.24 Shear studs for test specimen T 10-C25-150-65 after testing

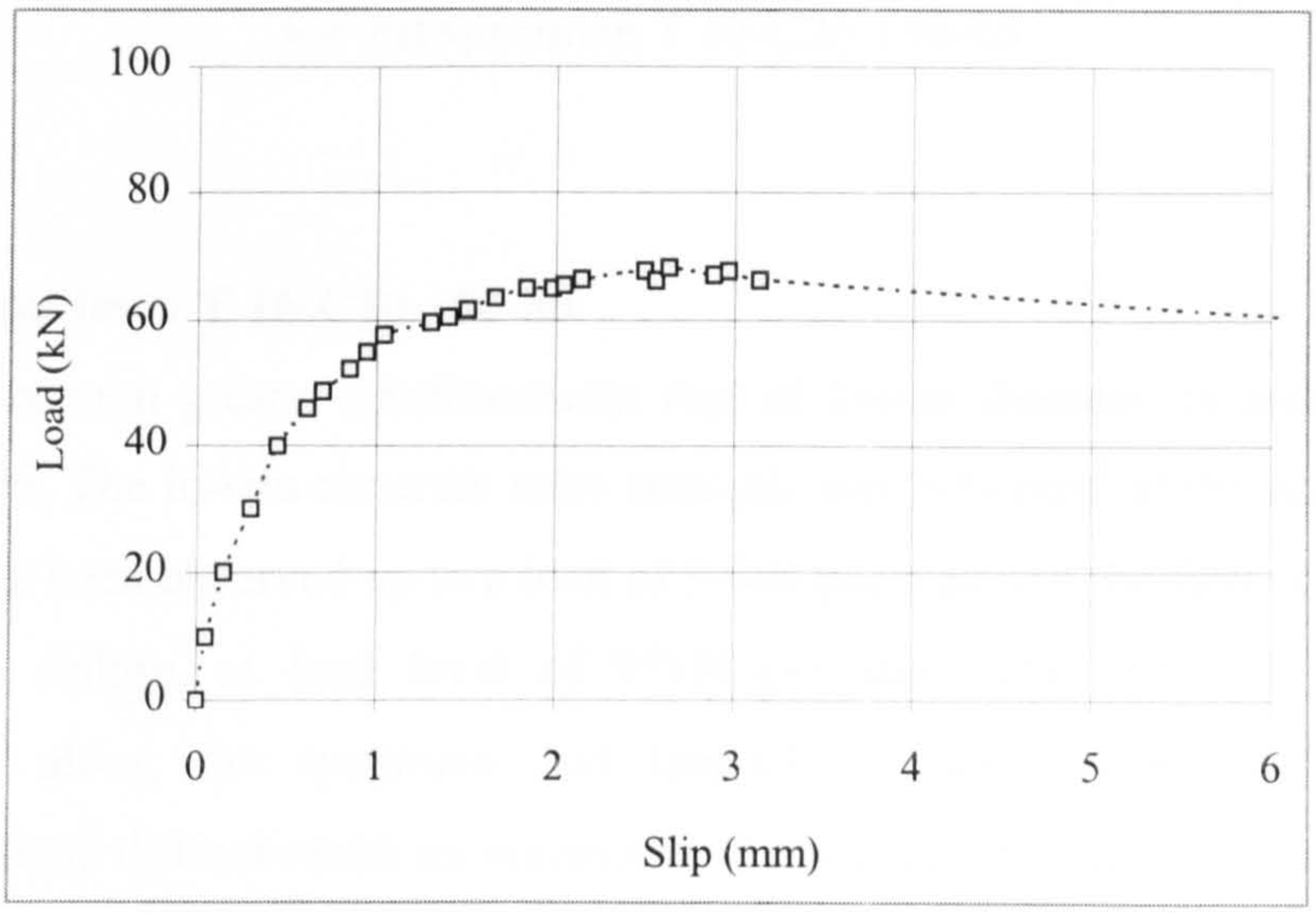

Figure 5.25 Load vs. slip curve of the stud for test specimen T 10-C25-150-65

The relationship between the load per stud and the strain in the reinforcement bar is plotted in figure 5.26. It can be seen that, the reinforcement bar reached its ultimate strain at failure although none of the studs has sheared off.

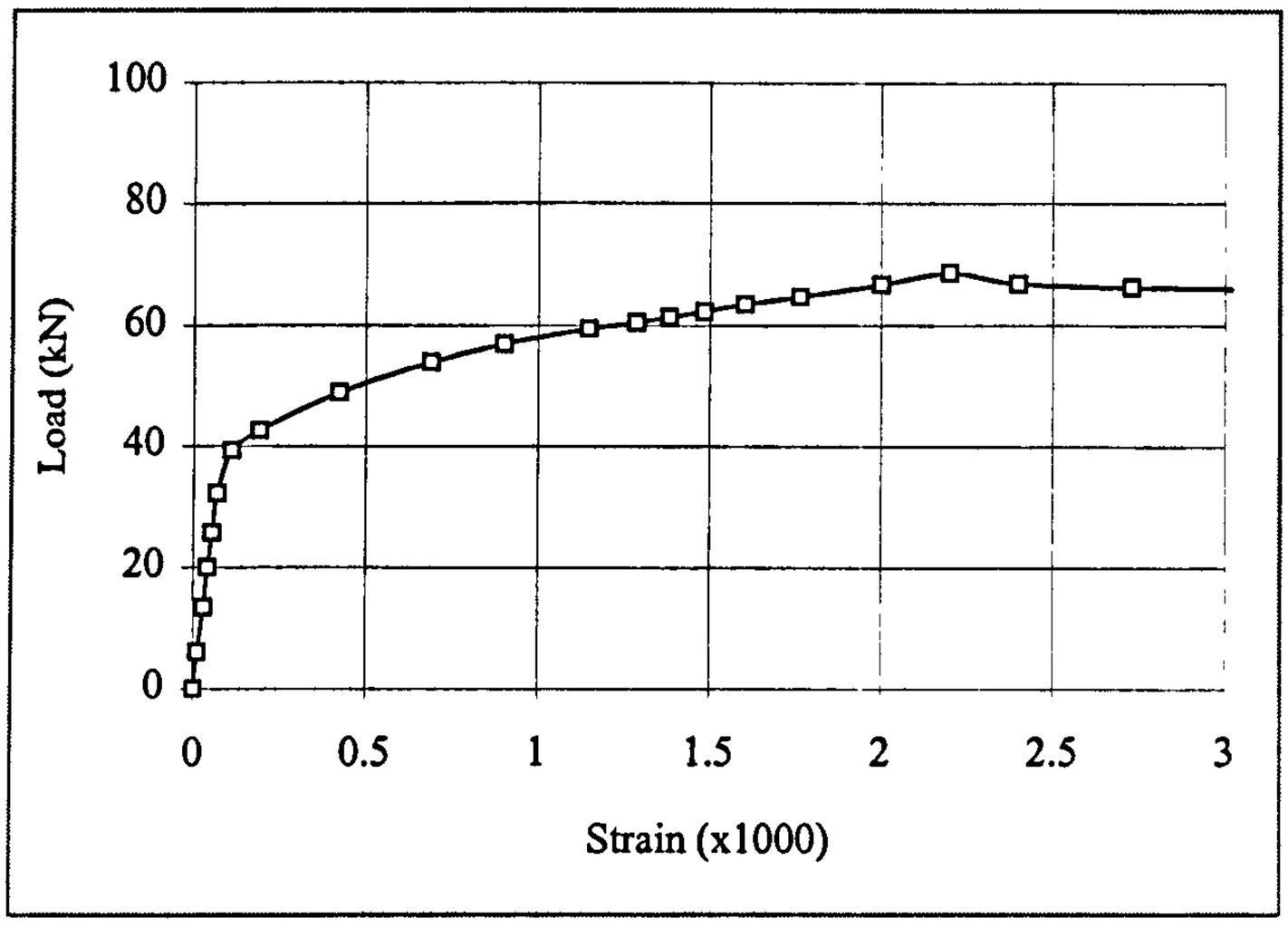

Figure 5.26 Load vs. strain curve of the reinforcement bar
for test specimen T 10-C25-150-65

5.3.2.2 Test specimen T 16-C30-150-80

In this test specimen greater reinforcement size of 16mm diameter is used with a gap width of 80mm. The in-situ concrete cube strength was 30N/mm^2 at the time of testing. No cracks have been observed up to a load of 93kN per stud and the first crack observed was, close to failure, at load level of 95kN per stud. The observed cracks were longitudinally along the specimen and laterally at the position of joints. The reinforcement bars did not reach its maximum strain as failure occurred because of stud yielding. The test was terminated because of studs shearing off and splitting of concrete due to tensile cracks observed nearly at failure. Figure 5.27 shows the crack distribution over the specimen after failure.

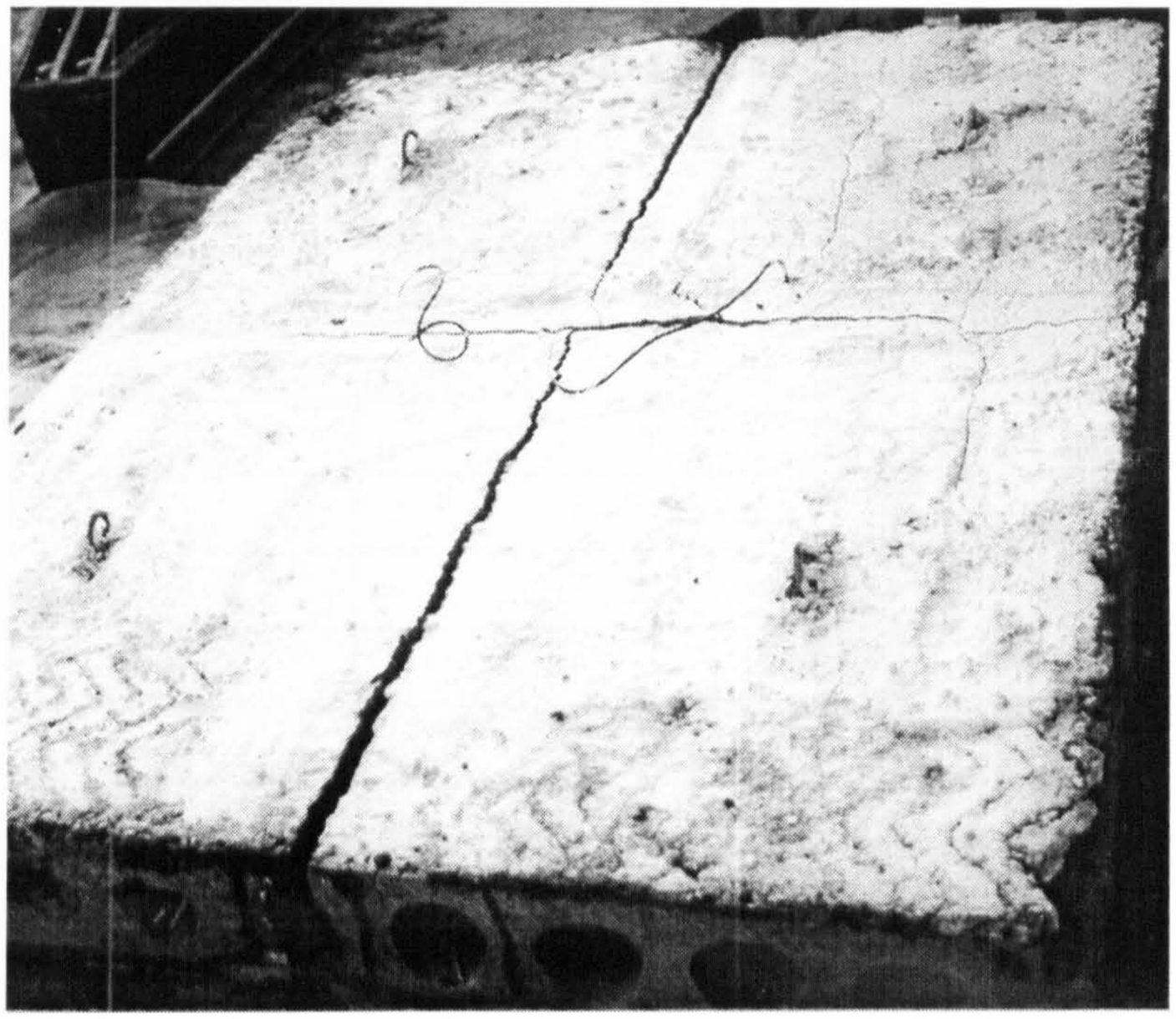

Figure 5.27 Crack pattern of T 16-C30-150-80 after the test

The mode of failure is a stud yielding since four studs sheared off at failure as shown in figure 5.28. The reinforcement bars did not reach its ultimate strength at failure as printed from the data logger. Splitting of concrete around the studs at failure happened due to the load transfer from the failed four studs to the remaining two studs.

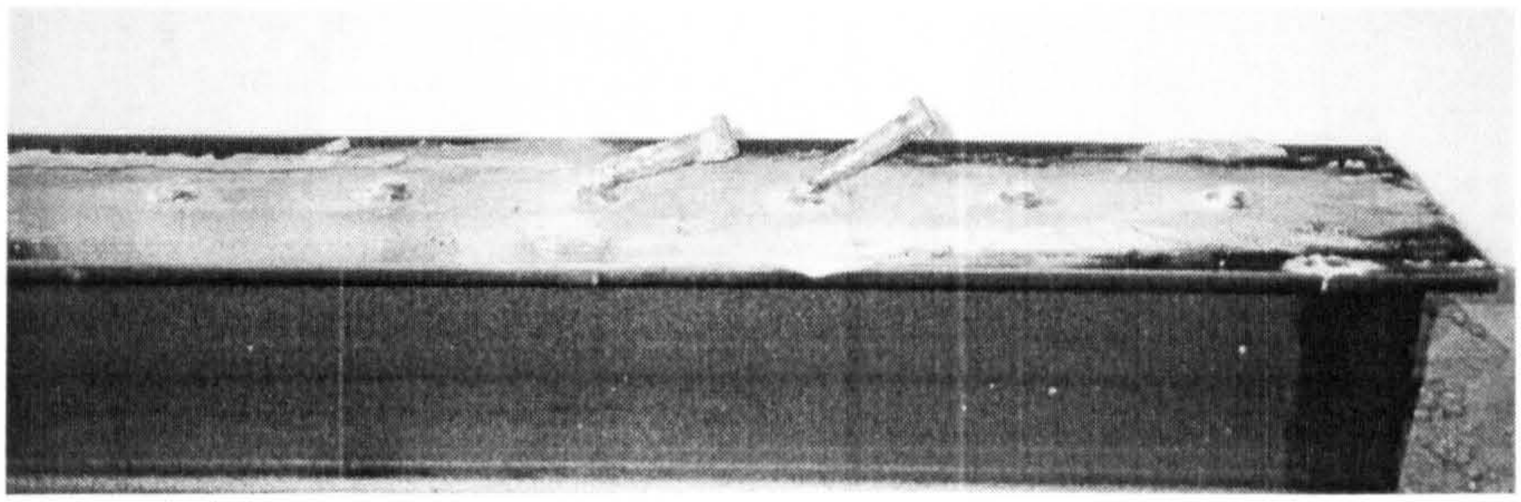

Figure 5.28 Shear studs for test specimen T 16-C30-150-80 after testing

The maximum observed load for this test was 97.3kN at a slip of 5.1mm. Load reduction occurred after reaching the maximum load due to failure of studs. The load vs. slip curve of the stud is shown in figure 5.29.

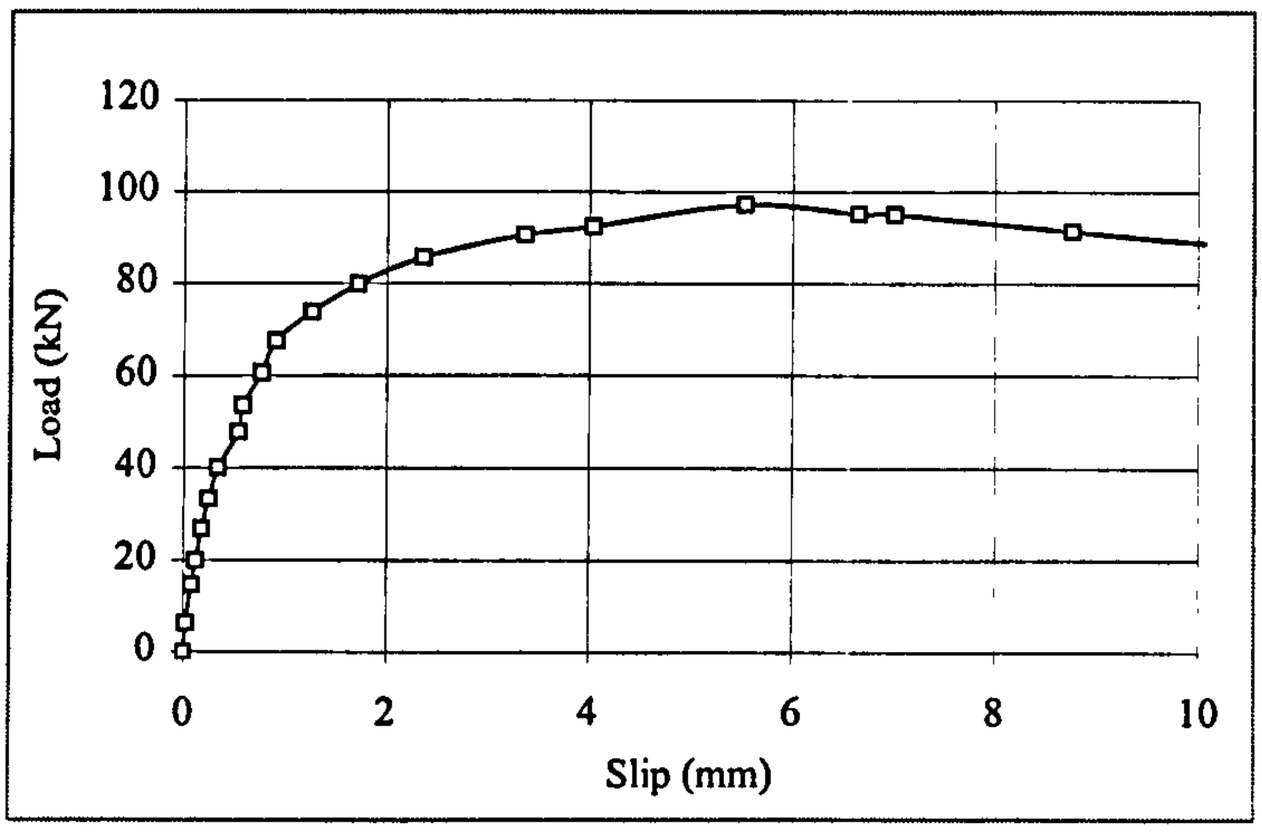

Figure 5.29 Load vs. slip curve of the stud for test specimen T 16-C30-150-80

Figure 5.30 shows the load-strain curve of the stud for T 16-C30-150-80. It can be shown that although four studs have already yielded and sheared off, the reinforcement bar did not reach its yield stress and consequently its yield strain.

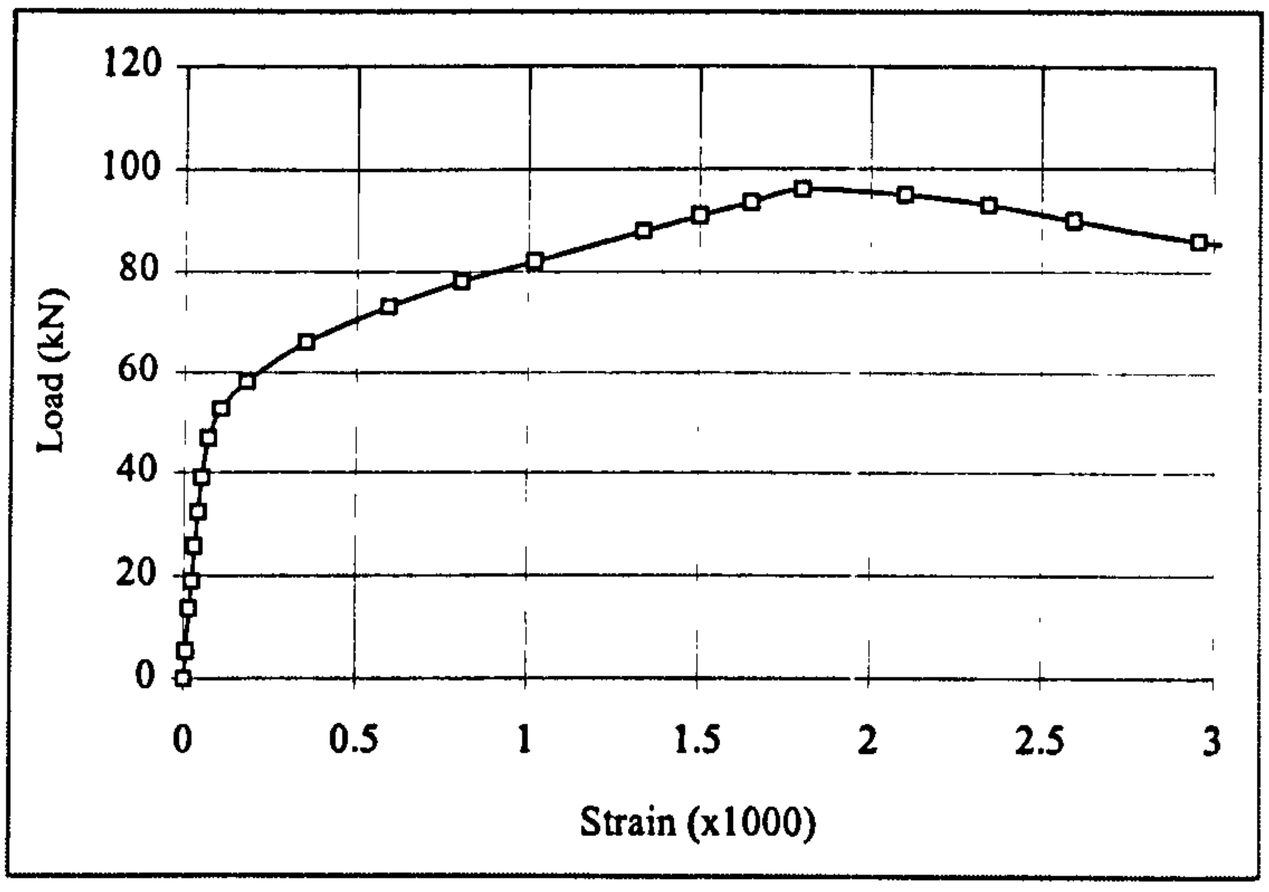

Figure 5.30 Load vs. strain curve of the reinforcement bar for test specimen T 16-C30-150-80

5.3.2.3 Test specimen T 16-C30-200-80

The only difference between this test specimen and T 16-C30-150-80 specimen is the HCU depth and consequently the cast concrete depth. The same 16mm diameter reinforcement bar size was used with 80mm gap and the in-situ concrete strength at the time of testing was 30N/mm^2. The purpose of this test was to study the effect of the increase in HCU depth on the shear stud capacity. As it was expected from the previous test, the cracks developed along the longitudinal direction and in the adjacent hollow core to the lateral joint. It was noticed that the longitudinal crack on the top surface was very thin and didn't reach the specimen borders as seen from figures 5.31.a and 5.31.b that shows two different views of the specimen. This means that the increase in hollow core depth leads to decreasing tensile stresses at the top surface. The reinforcement bar did not reach its ultimate strength at failure. The test was ended because of separation of concrete from the beam after the failure of five studs.

The mode of failure is stud failure mode. The greater reinforcement size enhances the concrete strength around the stud especially with greater depth of the HCU. The reinforcement bar failure was not reached at failure. Figure 5.32 shows that five studs from total of six studs sheared off at the end of test.

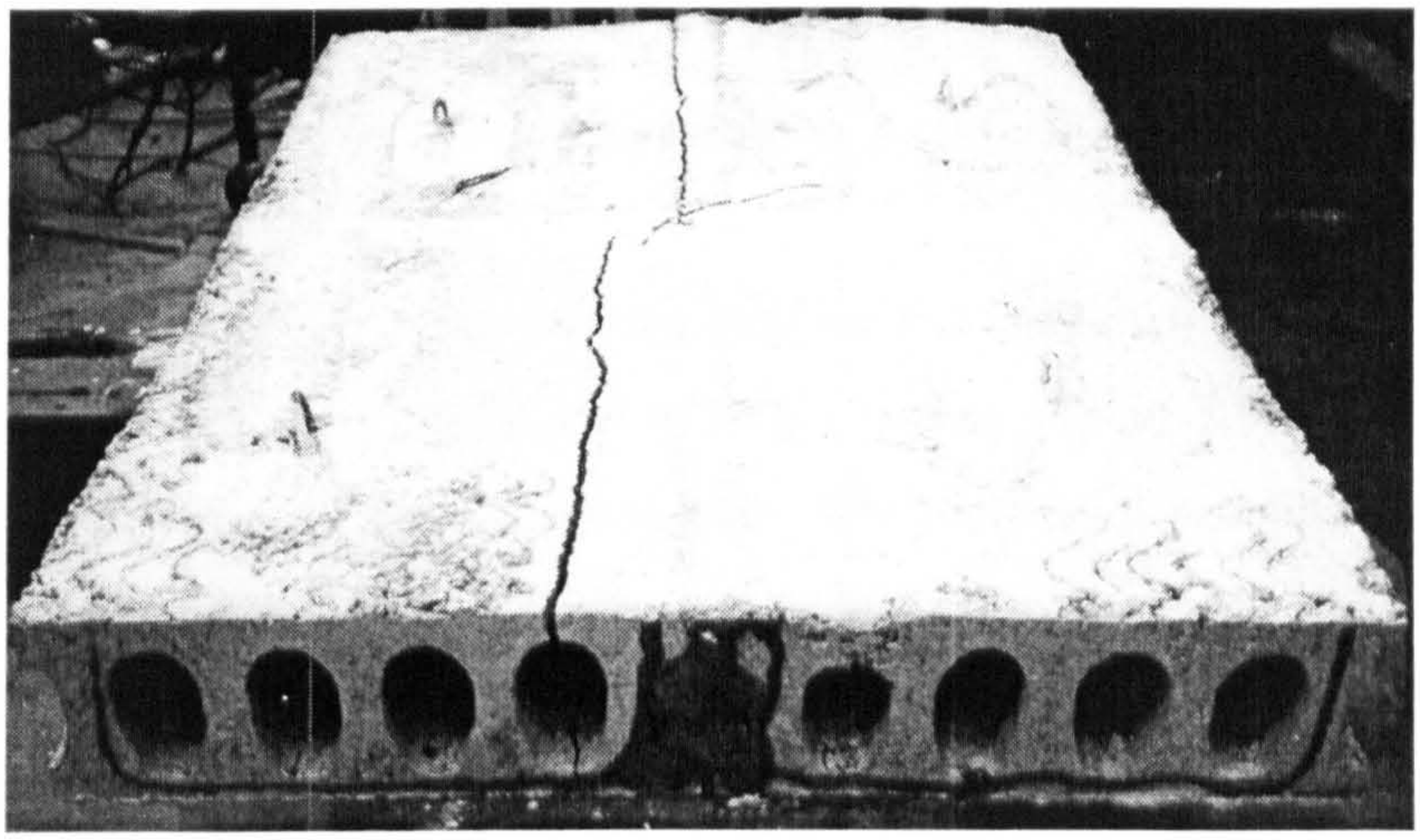

Figure 5.31.a

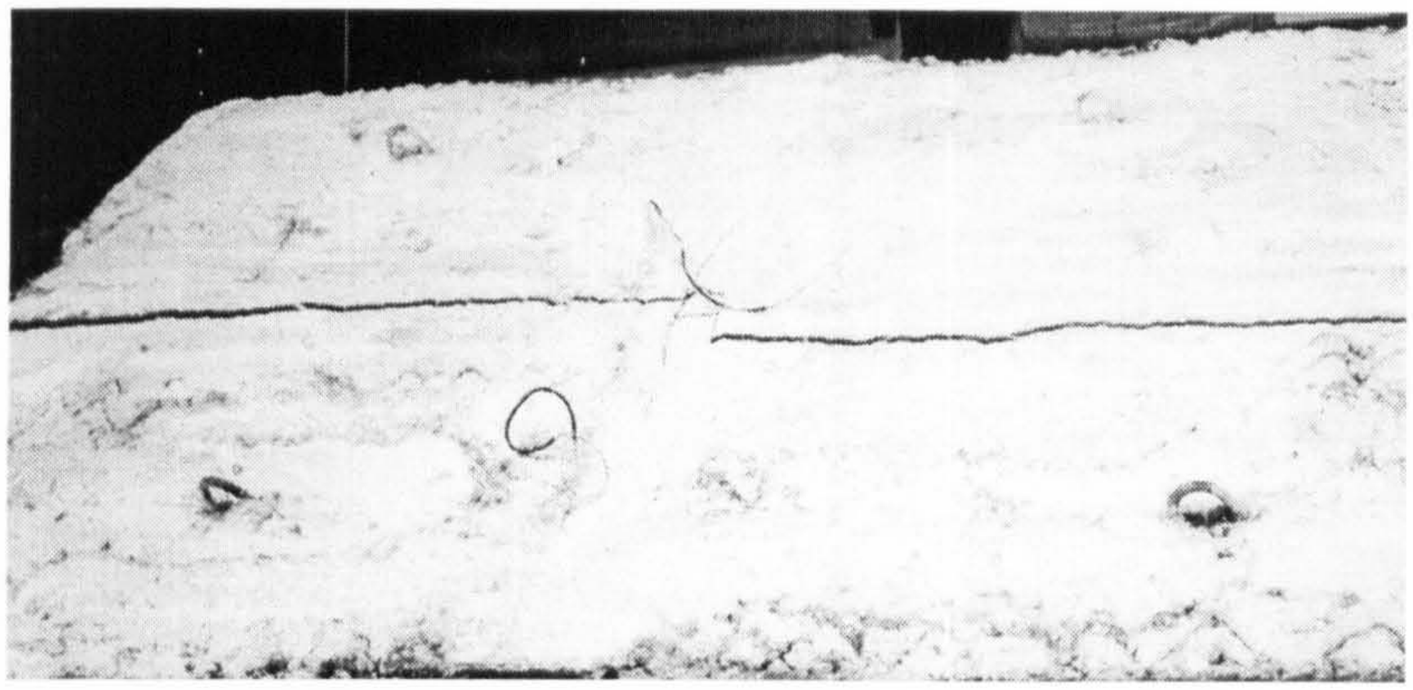

Figure 5.31.b

Figure 5.31 Crack pattern of T 16-C30-200-80 after the test

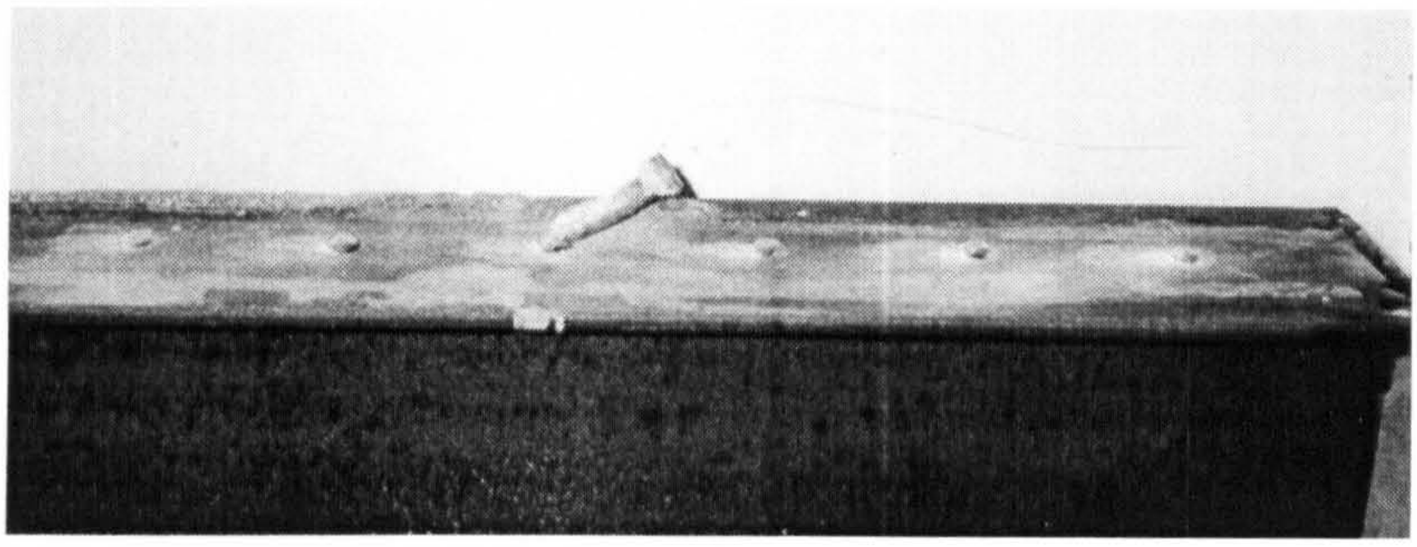

Figure 5.32 Shear studs for test specimen T 16-C30-200-80 after testing

Figure 5.33 shows the load vs. curve of the stud for test specimen T 16-C30-200-80. The specimen started to fail at a load level of 96kN with a slip of 3.9mm at the interface between the steel beam and the concrete slab. The load level remained approximately constant with an increase in deflection up to the failure load. Reduction of the load occurred after reaching the failure load. The failure load at the end of the test was 99.53kN at a slip of 5.93mm compared with 97.3kN at a slip of 5.53mm obtained for test specimen T16-C30-150-80. This means that there is a slightly increase of 2.5% in the stud shear capacity due to the increase in the HCU depth.

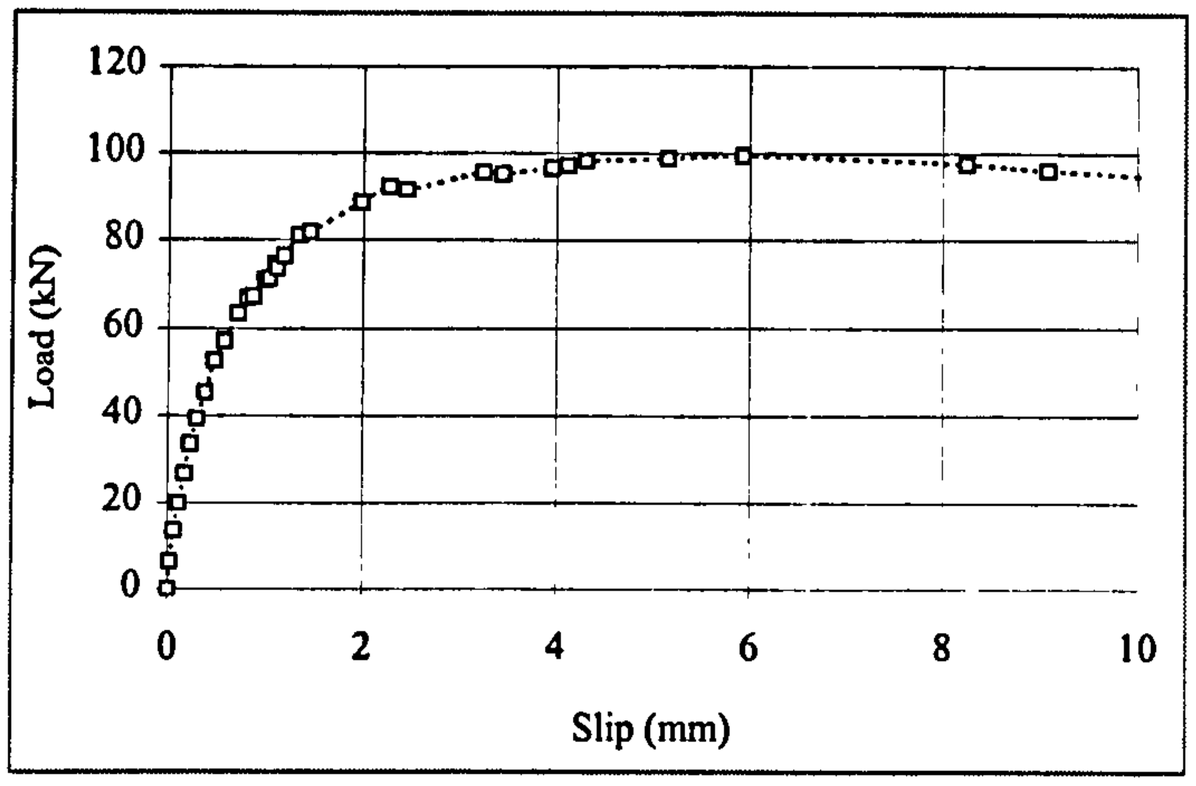

Figure 5.33 Load vs. slip curve of the stud for test specimen T 16-C30-200-80

Figure 5.34 shows that the 16mm reinforcement bar did not reach its ultimate stress at failure, although 5 studs have already failed and sheared off at failure. This indicates that the failure is mainly caused by stud failure.

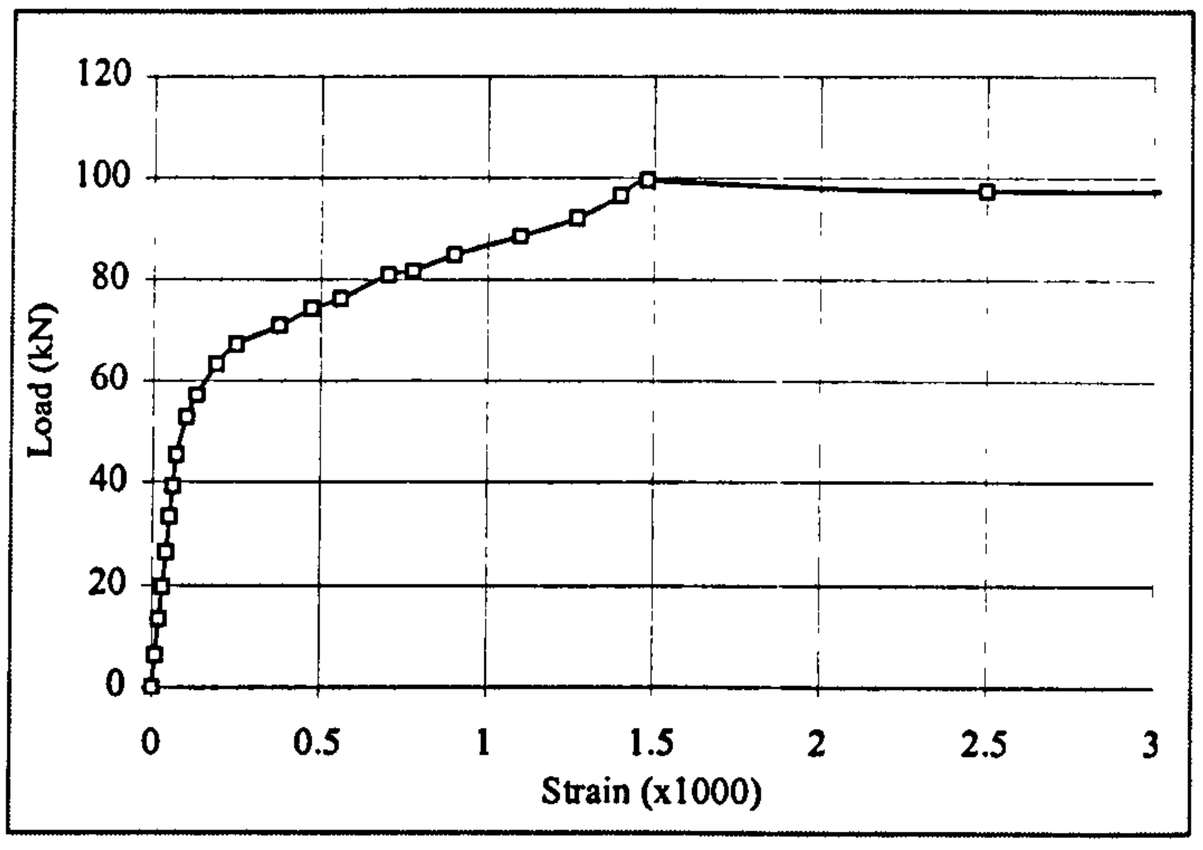

Figure 5.34 Load vs. strain curve of the bar for test specimen T 16-C30-200-80

5.3.2.4 Test specimen T 16-C30-200-60

In this test specimen a 16mm transverse reinforcement bar is used with the same HCU 200mm depth used in T 16-C30-200-80 and the same in-situ concrete strength of 30N/mm^2. The difference between the two test specimens is in the gap width since the present test specimen has a gap width of 60mm instead of 80mm. The purpose of this

test is to study the effect of change in gap width on the shear stud capacity. As it was expected for this greater HCU depth of 200mm the crack developed mainly through the lateral joints and through the adjacent hollow core to the lateral joints. A thin crack developed longitudinally in the middle top surface of the specimen. Figures 5.35a and 5.35b show the crack distribution over the test specimen.

The mode of failure is a stud failure mode since two studs sheared off because the high reinforcement size used that enhances the concrete strength around the shear stud. Figure 5.36 shows the remaining shear studs after failure.

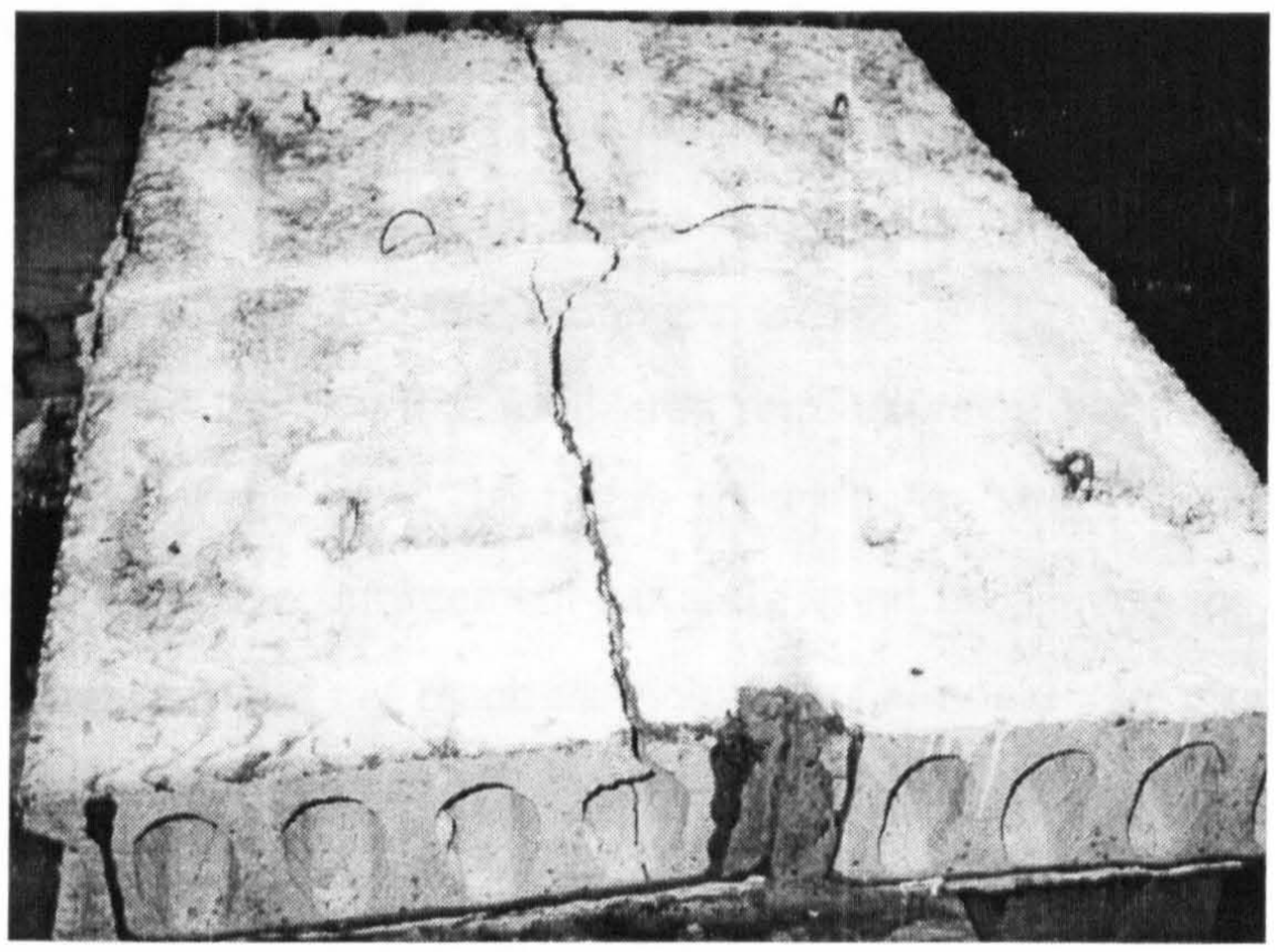

Figure 35.a

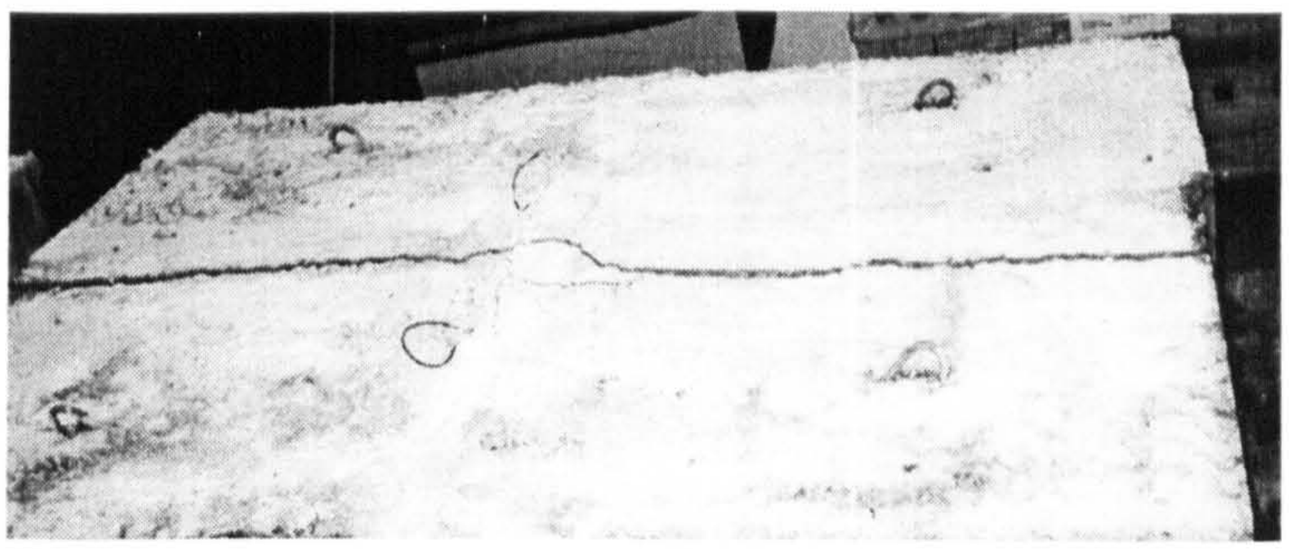

Figure 35.b

Figure 5.35 Crack pattern of T 16-C30-200-60 after the test

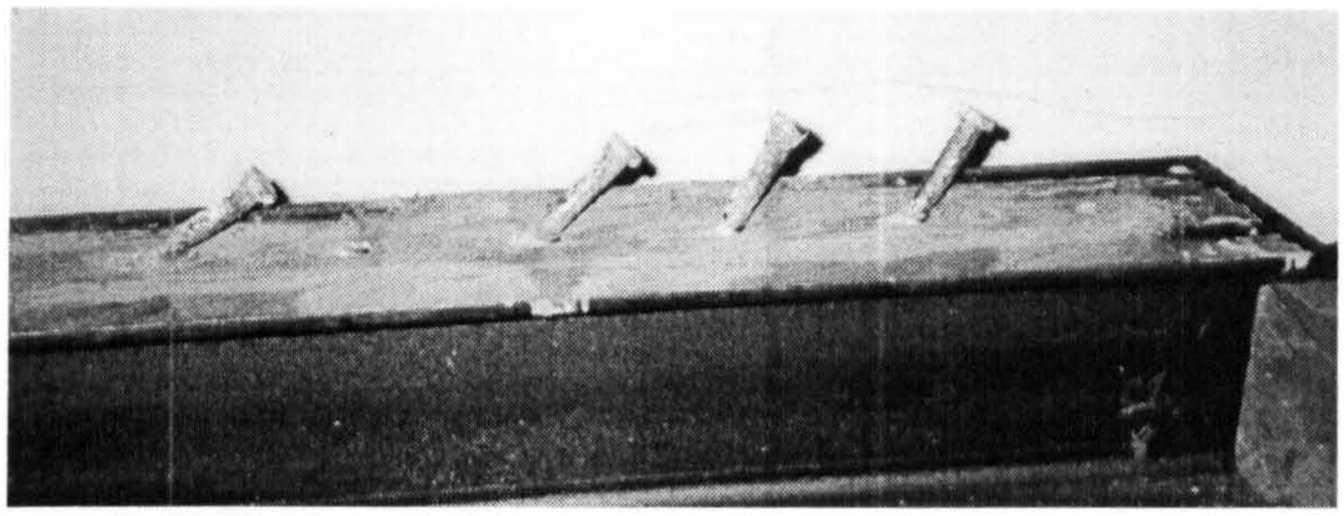

Figure 5.36 Shear studs for test specimen T 16-C30-200-60 after testing

Figure 5.37 shows the load vs. slip of the stud of this test specimen. The maximum failure load was 91.8kN at a slip of 3.71mm compared with 99.7kN at a slip of 5.93mm compared with T 16-C30-200-80. This means a reduction of 7.9% of the shear stud capacity is occurred due to the decrease in the gap size.

Also, figure 5.38 stresses the fact that for 16mm reinforcement bar the failure is mainly caused by the yielding of the stud. The figure shows the relationship between the load per stud and the strain in the reinforcement bar at different load levels for T 16-C30-200-60. The reinforcement bar did not reach its yield stress although two studs have already sheared off at failure.

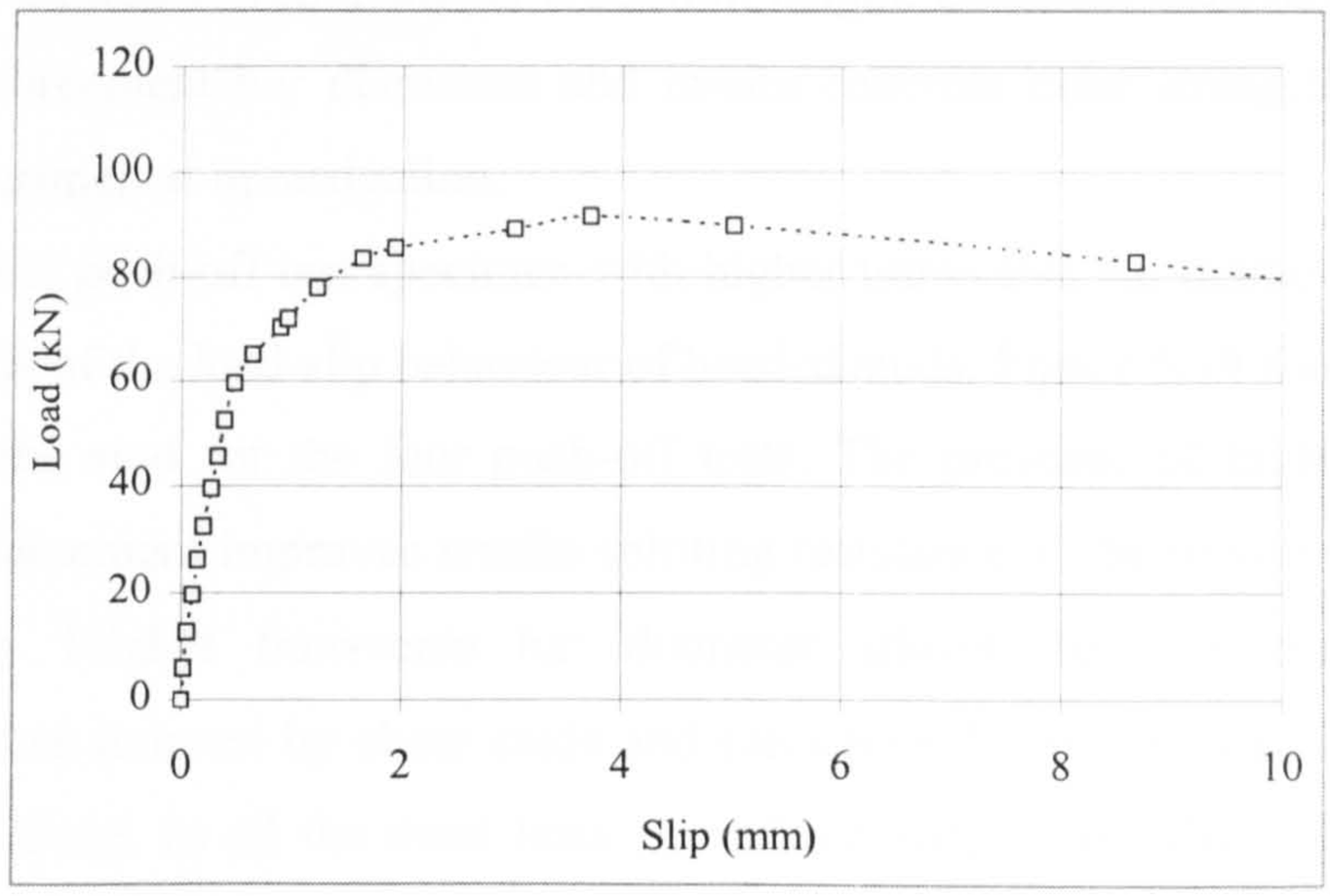

Figure 5.37 Load vs. slip curve of the stud for test specimen T 16-C30-200-60

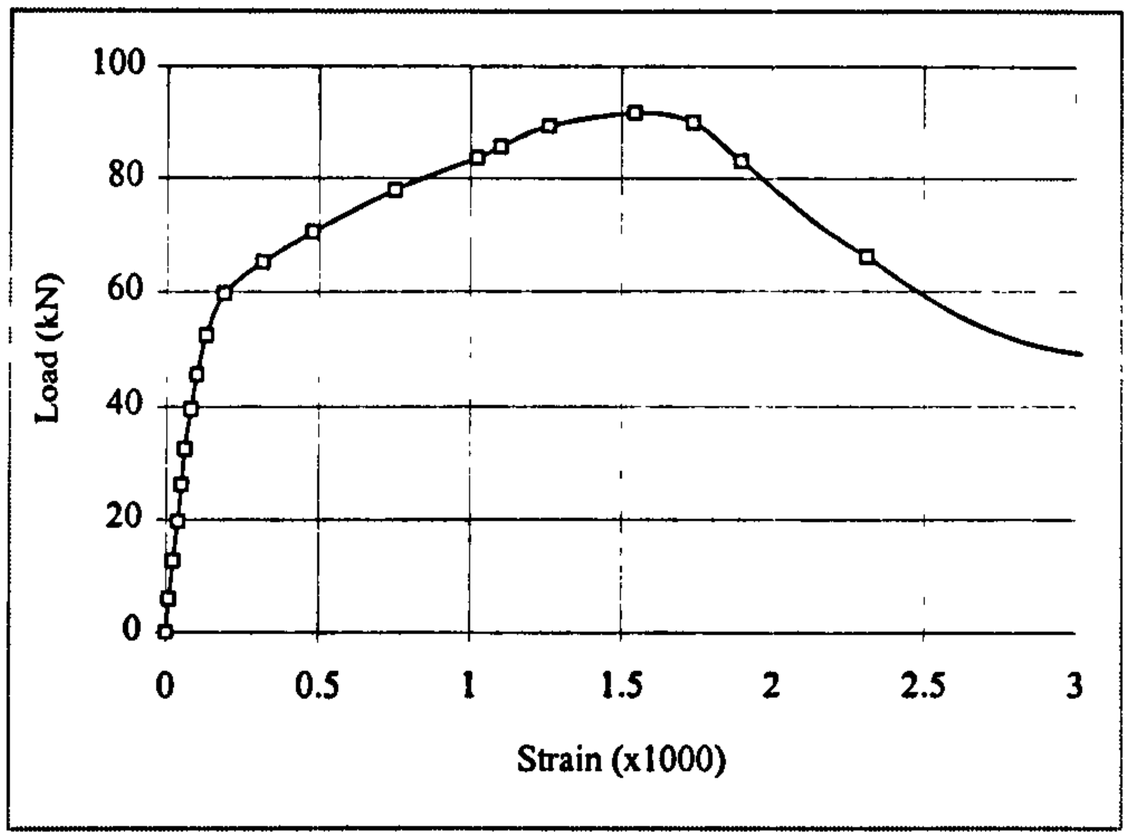

Figure 5.38 Load vs. strain curve of the reinforcement bar
for test specimen T 16-C30-200-60

5.3.3 Summary of results

This chapter described the details of four new push-off tests with precast hollow core slabs. The push-off tests investigated the effect of hollow core units height on the behaviour of headed studs in this new type of construction, which was not previously studied. The hollow core units used in the experimental investigation had square ends and the studs used had 19mm diameter x 100mm height. Different transverse gap sizes, transverse reinforcement bar diameters and in-situ concrete cube strengths have been used in the experimental investigation.

It is observed that push-off test specimen with higher transverse bar diameters had high ductility in terms of the load-slip behaviour of headed studs. Figure 5.39 shows the load-slip curves of the stud for the four push-off tests. The presence of higher degree of transverse reinforcement improves tensile splitting resistance of the in-situ concrete and limits cracking. Higher transverse bar diameter allows the concrete to sustain longitudinal forces induced by shear studs and can cause the stud to yield before clear concrete cone failure. In all the three tests carried out with 16mm diameter transverse reinforcement, stud failure was observed, the stresses and consequently strains in the reinforcement bars did not reach its ultimate values. Figure 5.40 shows the load-strain

curves of the transverse reinforcement bars in the four push-off tests with precast hollow core slabs carried out in this study.

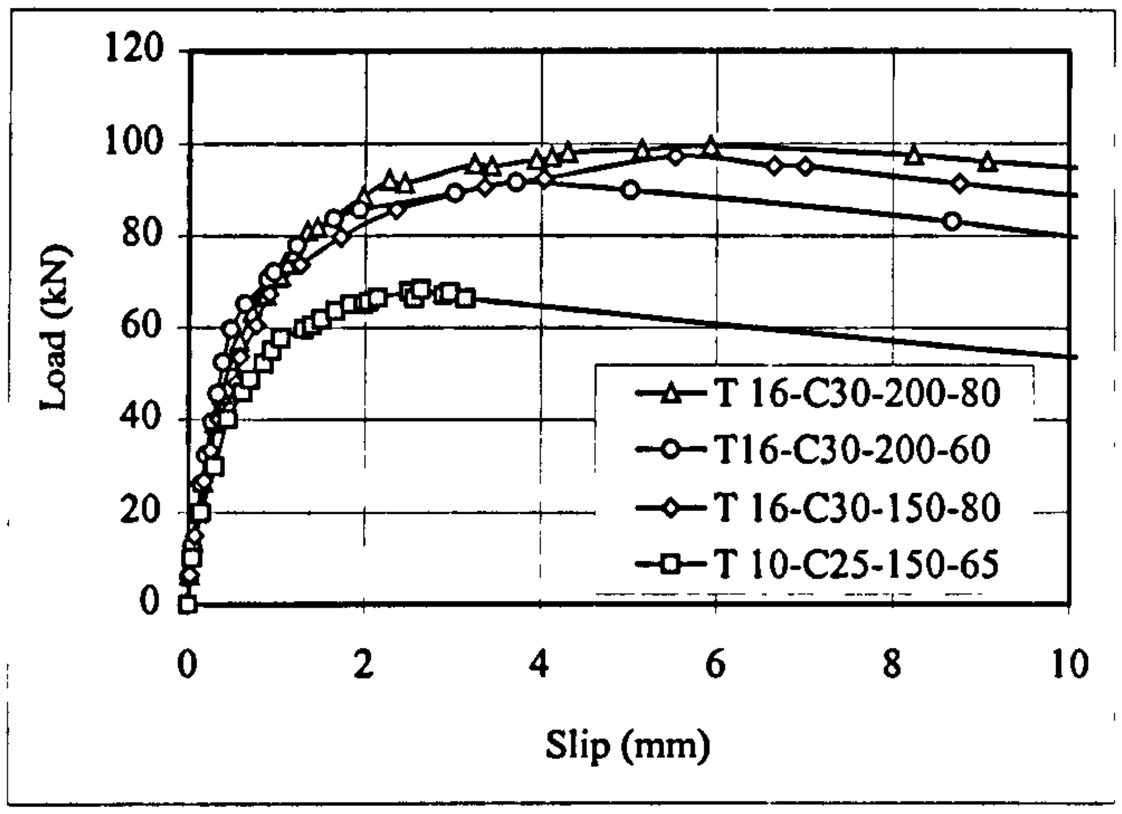

Figure 5.39 Load-slip curves of the stud for push-off tests with precast HC slab

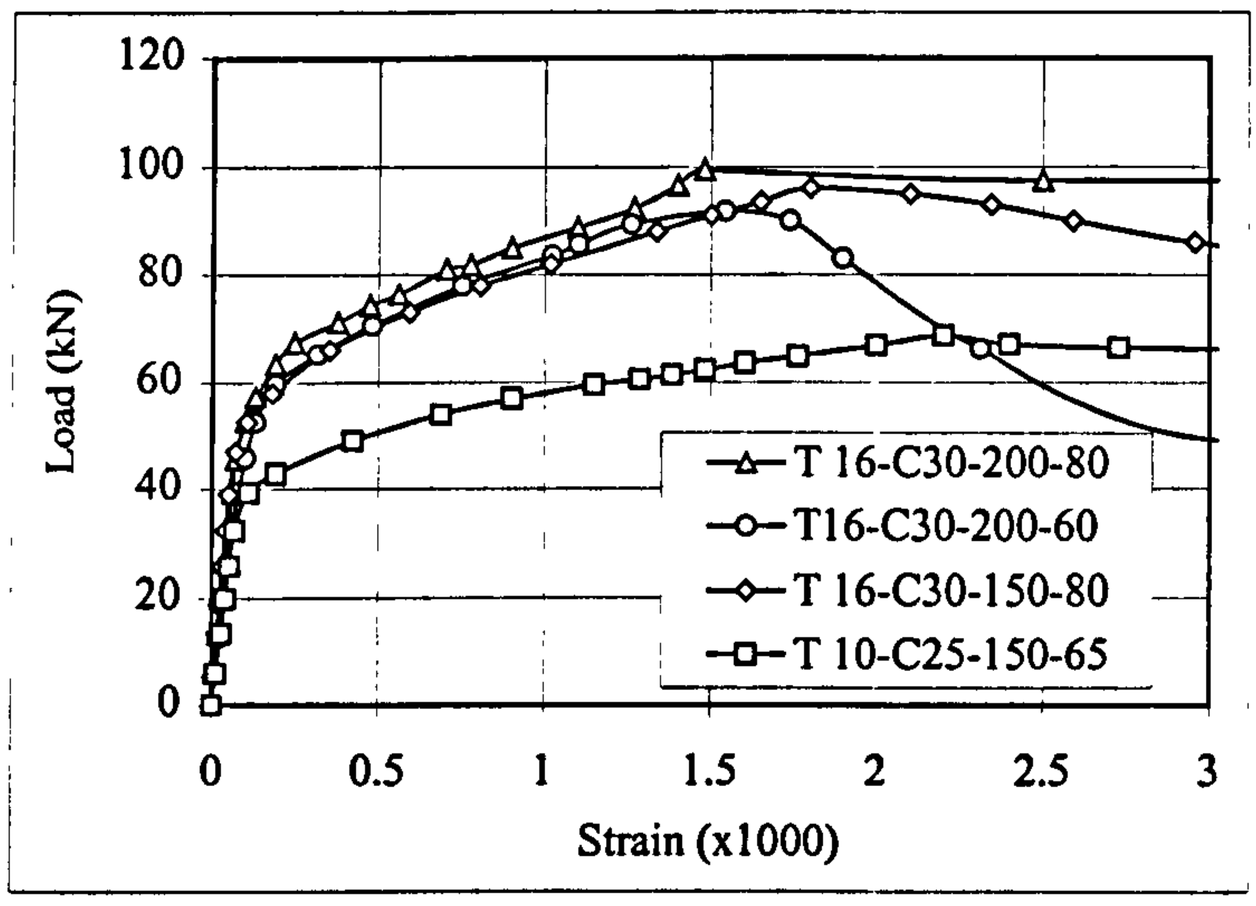

Figure 5.40 Load-strain curves of transverse reinforcement bar for precast hollow core slab push-off tests

Push-off test with 10mm transverse bar had less ductility in the load-slip behaviour of the stud and the bar reached its yield stress causing concrete cone failure around the studs. None of the studs sheared off compared with specimens with 16mm transverse

bars in which some of the studs sheared off. Many cracks have been observed on the top surface and in the lateral and longitudinal gaps between the hollow core units.

It was also observed that, the shear connection capacity was increased with the increase in hollow core unit depth and consequently the increase in the depth of in-situ concrete around the stud, for the same reinforcement diameter, same gap width and the same in-situ concrete strength. The choice of the 600mm hollow core unit width was intended so that the effect of the edge joint was included in a test length of 1200mm. The observed shear connection capacities for the push-off tests, summarised in table 5.2, can be considered the least shear capacity may be observed and this increases the safety in the observed values. Also, the shear connection capacity was increased by the increase in the gap size, for the same reinforcement diameter, same hollow core unit height and same in-situ concrete strength.

Test ref.	Diameter of headed stud (mm)	In-situ concrete grade (N/mm^2)	Shear capacity (kN)
T 10-C25-150-65	19	25	68
T 16-C30-150-80	19	30	97.3
T 16-C30-200-80	19	30	99.5
T 16-C30-200-60	19	30	91.8

Table 5.2 Summary of results for push-off tests with precast HC slabs

6. Comparison between Experimental Investigation and FE Modelling

6.1 Introduction

This chapter describes the comparison between the FE results previously discussed in chapters 3 and 4 with experimental results presented in chapter 5. The comparison includes verifications of load-slip curves, shear capacity of connections and modes of failures. The aim of these comparisons is to increase the understanding of the behaviour of these connections and to check the accuracy and efficiency of the FE models.

6.2 Comparison of FE results with tests on headed shear studs in solid slabs

The results of the four push-off tests with solid slabs investigated experimentally will be presented in comparison with FE results. The variable parameter in the push-off tests was the concrete cube strength. The headed stud shear connector used in the full-scale push-off tests was the 19mm diameter x100mm height and the depth of the concrete solid slab was 150mm.

6.2.1 Test S1 (C50)

Figure 6.1 shows the load-slip curve obtained from experimental data in comparison with the finite element solution for test specimen S1. The maximum load in the test was 130.4kN per stud at slip of 9.3mm compared with 133.4kN at slip of 9.26mm obtained from the present FE solution at the same concrete strength. The experimental failure load is less than that obtained from FE solution by 2.2%. The curve shows good agreement between both experimental results and FE solution.

Because of higher concrete strength, the mode of failure was stud yielding failure mode. The concrete slab upper surface remained with no cracks and separation happened in the lower surface connected with the steel beam through the studs as shown from the stress contour distribution, see figure 6.2. The stud yielded in a double curvature mode using FE analysis and that was noticed experimentally as shown in figure 6.3.

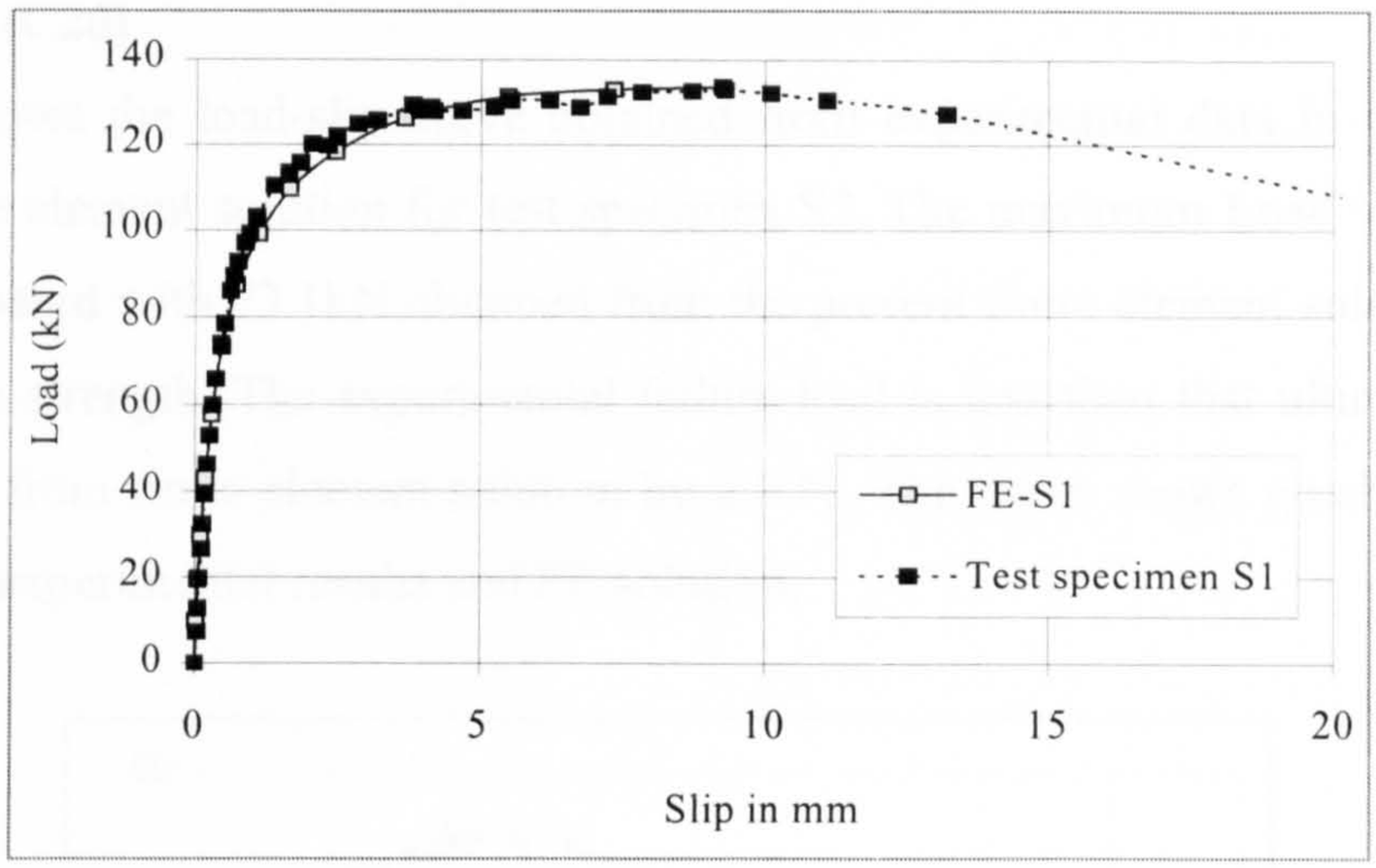

Figure 6.1 Comparison between experimental results and F.E. solution for S1 specimen

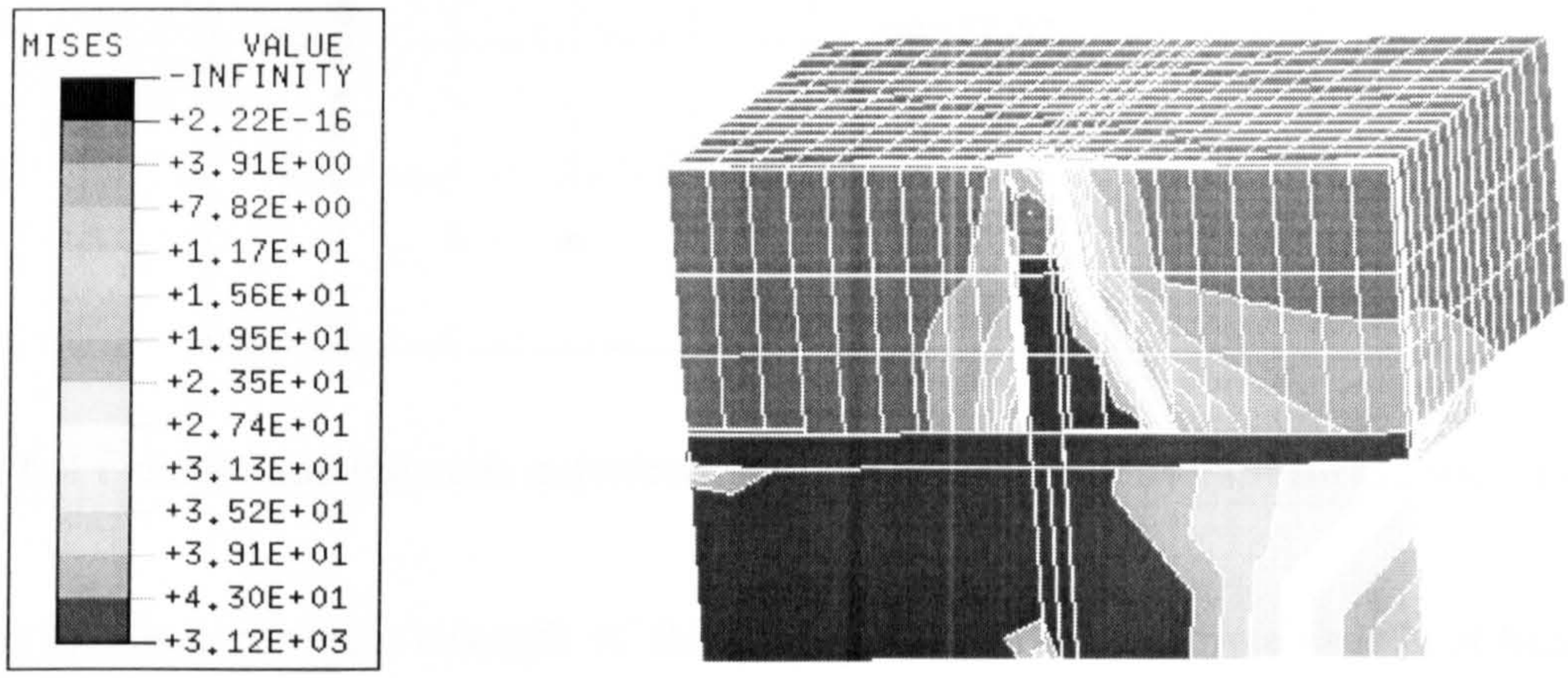

Figure 6.2 Mises stress contour distribution over FE-S1 at failure

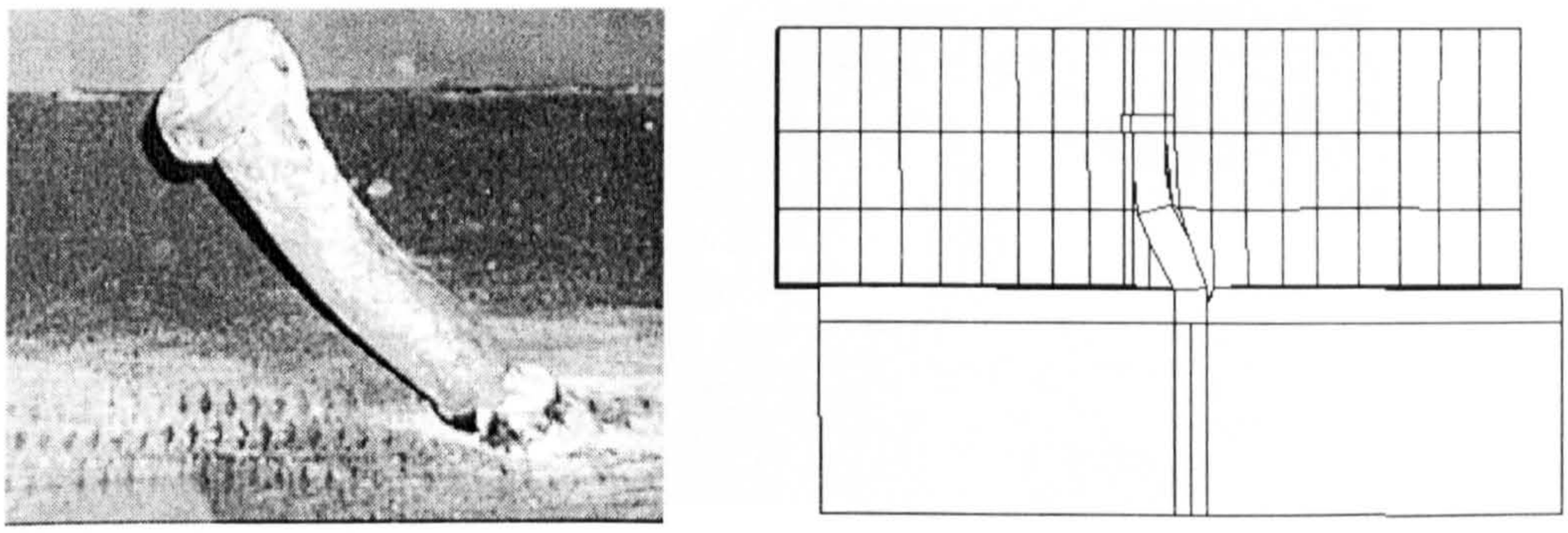

Figure 6.3 Comparison between experimental and FE deformed shape of the stud

6.2.2 Test S2 (C20)

Figure 6.4 shows the load-slip curve obtained from experimental data in comparison with the finite element solution for test specimen S2. The maximum Load was 71.6kN per stud compared with 73.1kN obtained from the present finite element solution at the same concrete strength. The experimental failure load is less than that ultimate failure load obtained from finite element solution by 2.2 %. The curve shows good agreement between both experimental results and FE solution.

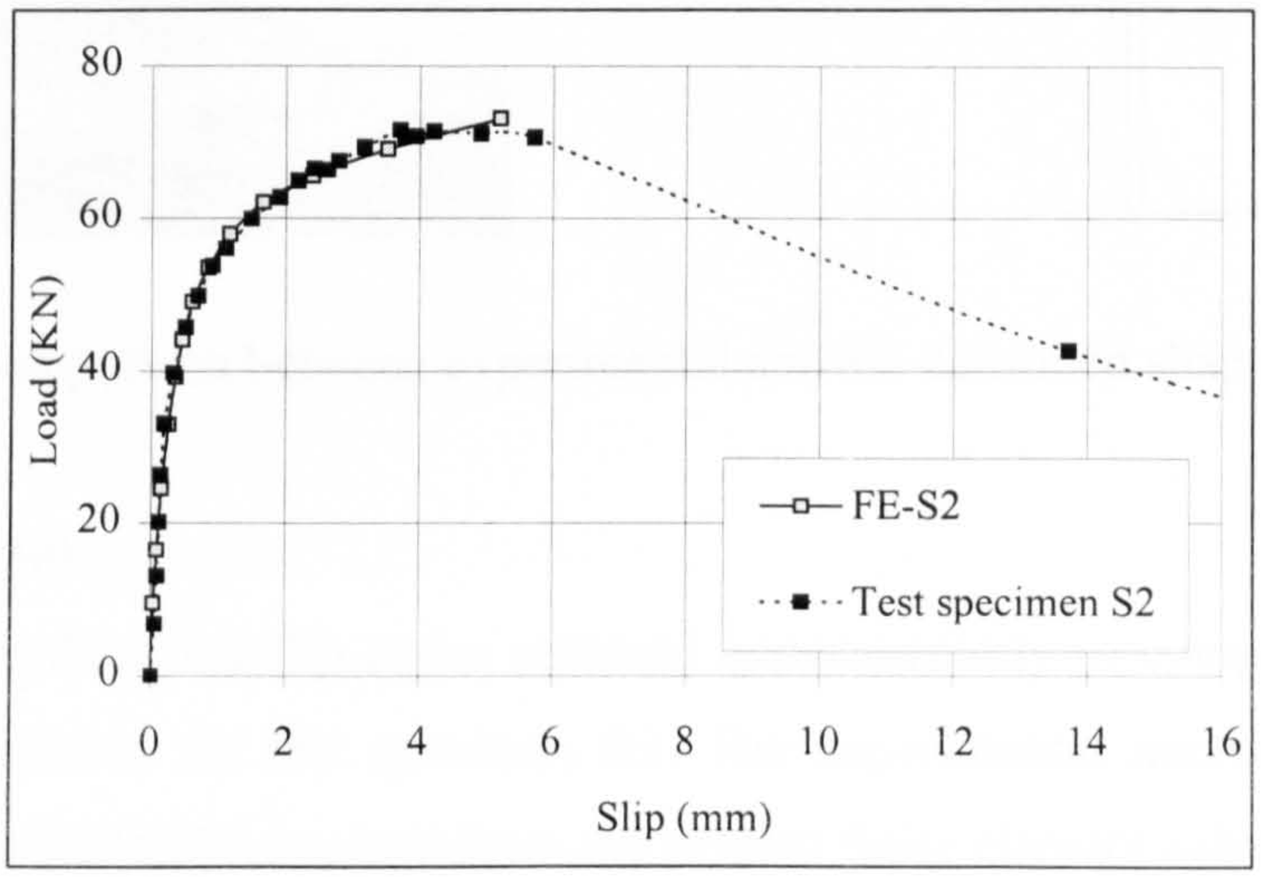

Figure 6.4 Comparison between experimental results and F.E. solution for S2 specimen

Because of lower concrete strength of this test specimen, the concrete fails first before the stud causing concrete failure mode. The conical failure of concrete around the stud extended to cover the full thickness of the slab, see figure 6.5.

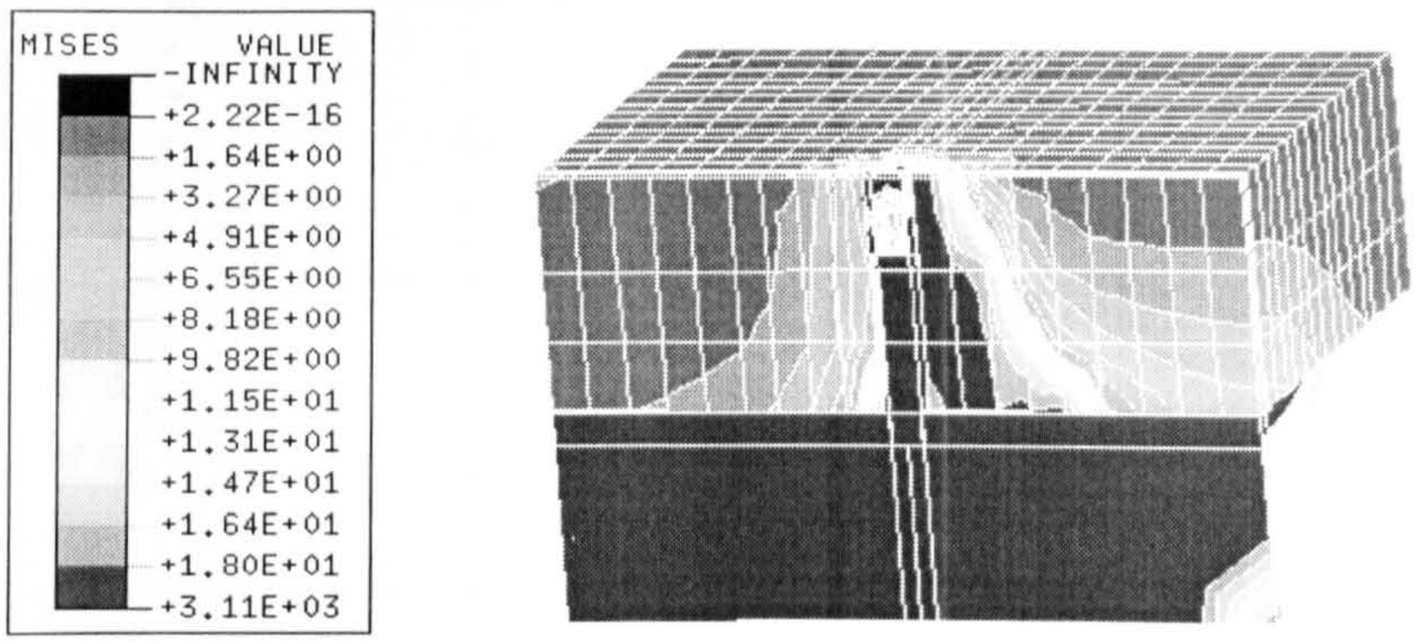

Figure 6.5 Mises stress contour distribution over FE-S2 at failure

The stud bent in a single curvature shape as shown in figure 6.6 which shows good agreement between the deformed shape after failure obtained experimentally with that obtained from FE analysis.

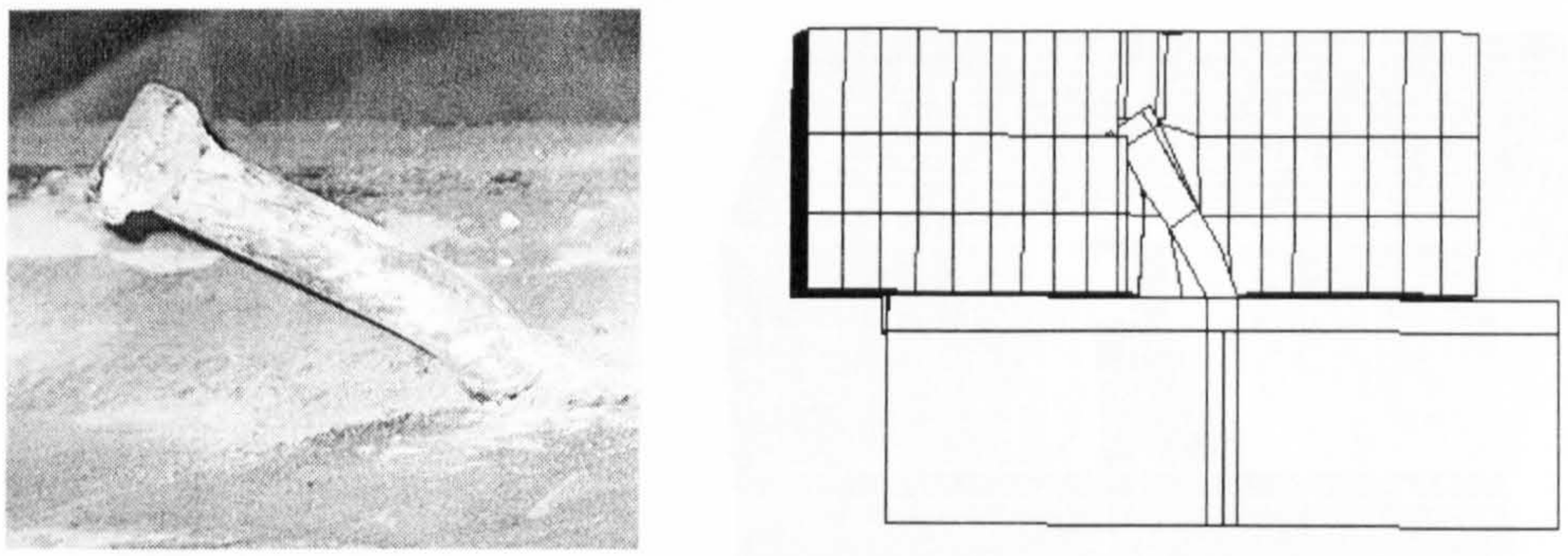

Figure 6.6 Comparison between experimental and FE deformed shape of the stud

6.2.3 Test S3 (C30)

Figure 6.7 shows the Load-slip curve obtained experimentally in comparison with the finite element solution for test specimen S3. The experimental maximum Load was 93kN compared with 90kN obtained from the present finite element solution at the same concrete strength. The experimental failure load is greater than that load obtained from the finite element solution by 3.3 %.

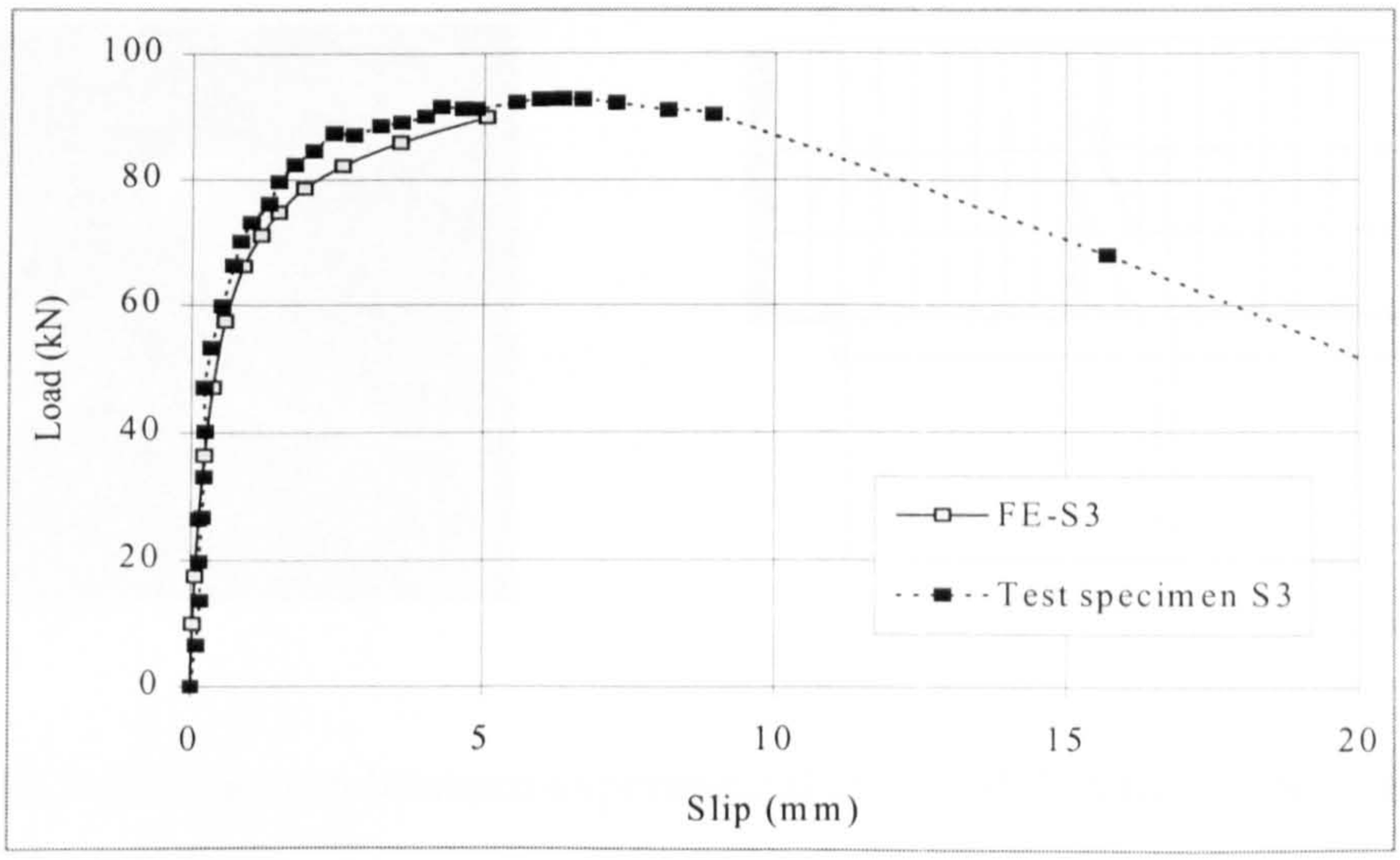

Figure 6.7 Comparison between experimental results and F.E. solution for S3 specimen

In this test specimen, the mode of failure is combined failure mode between concrete failure and stud yielding. The concrete slab around the stud formed a conical failure shape at failure as shown in figure 6.8 using the FE analysis.

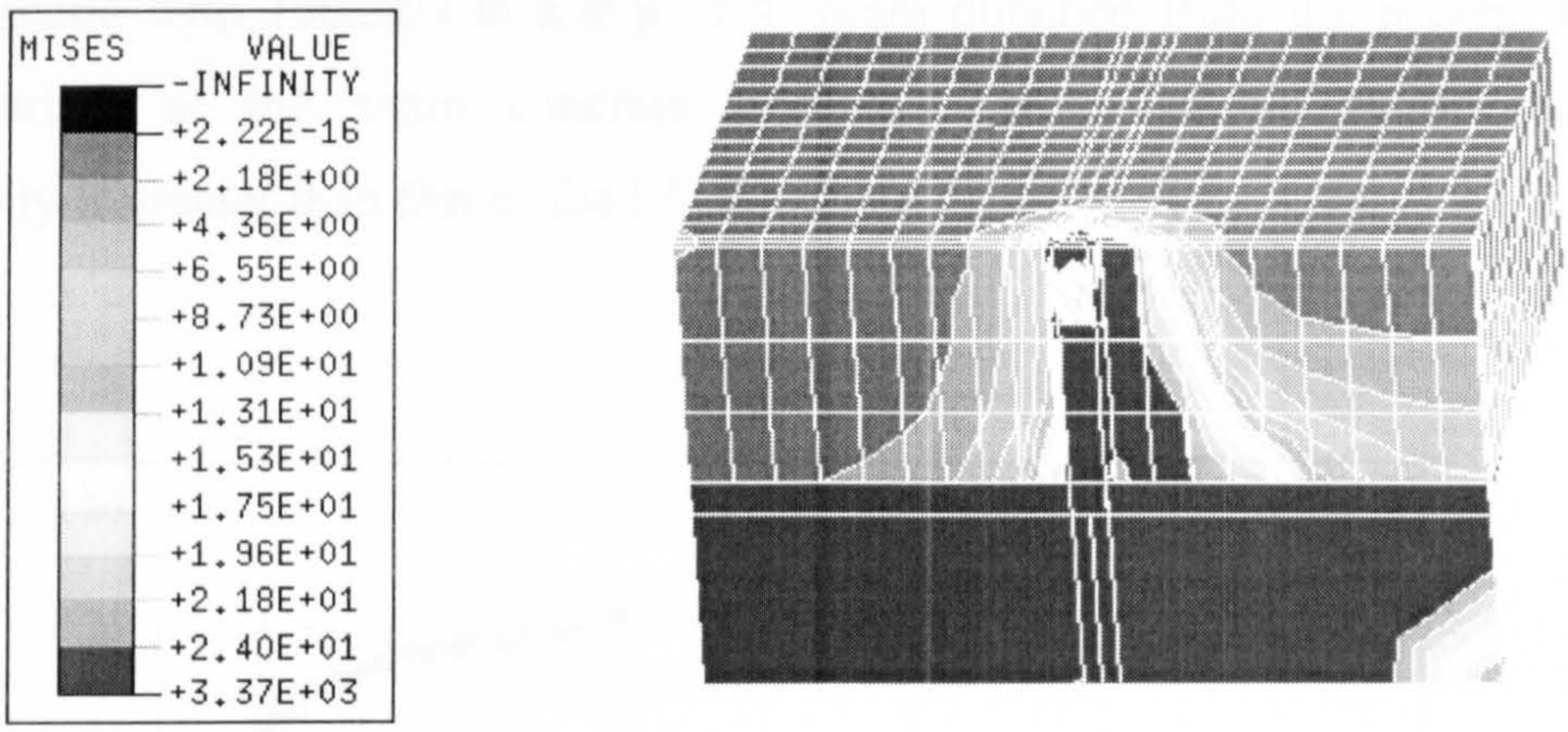

Figure 6.8 Mises stress contour distribution over FE-S3 at failure

Also, the studs bent as noticed experimentally and numerically. The bending curvature is between the double and single curvatures discussed earlier for test specimens S1 and S2 respectively, see figure 6.9.

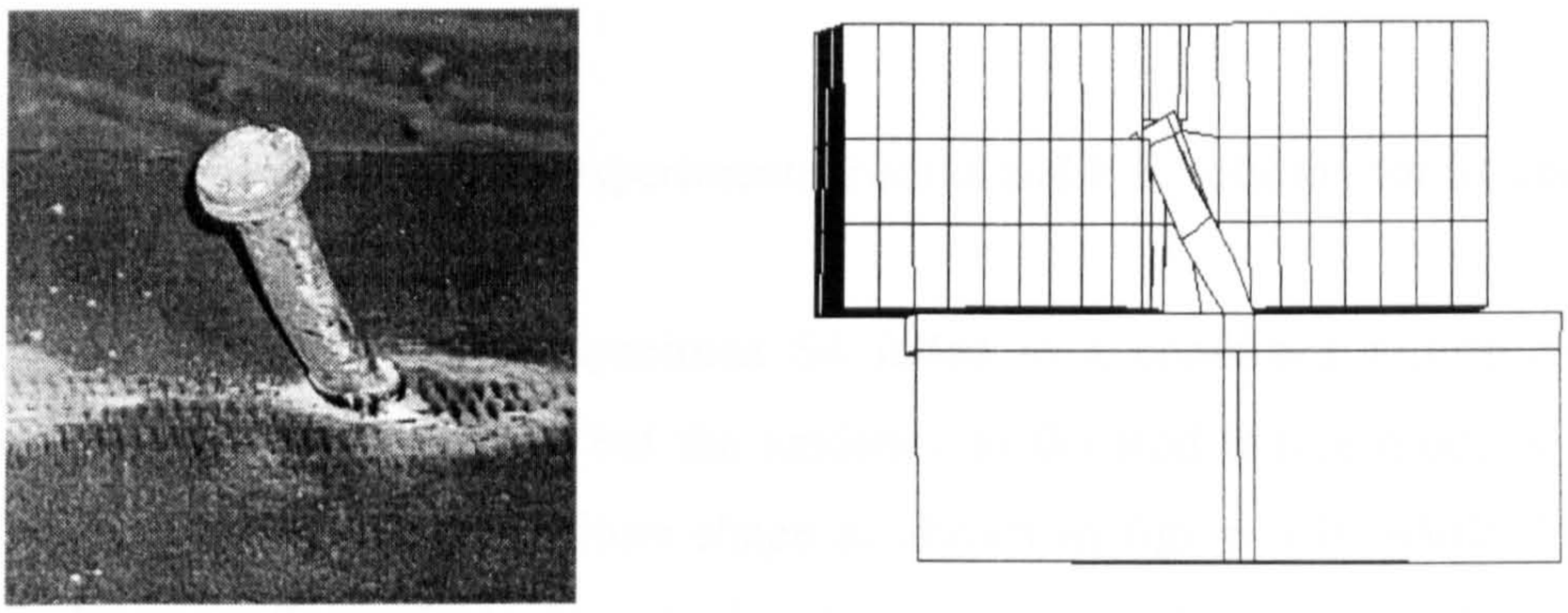

Figure 6.9 Comparison between experimental and FE deformed shape of the stud

6.2.4 Test S4 (C35)

The load vs. slip curve obtained from experimental investigation is compared in figure 6.10 with that obtained numerically using the FE method. The figure shows good agreement between the two curves. The maximum load was 102.0kN per stud at a slip of 6.1mm compared with 100.2kN at a slip of 4.76mm obtained from the present finite element solution at the same concrete strength. The maximum load obtained experimentally is greater than that of the FE solution with 1.8%.

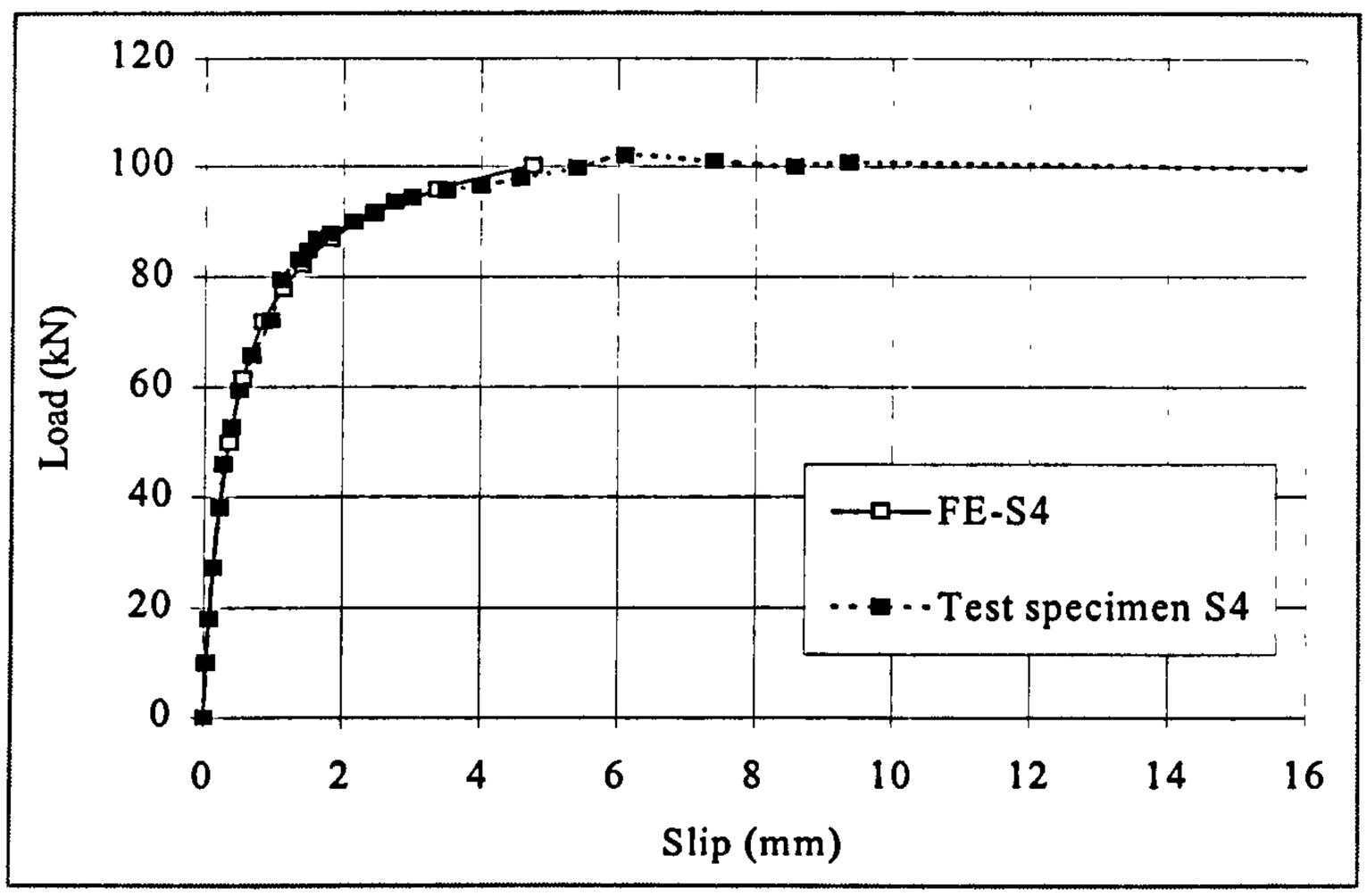

Figure 6.10 Comparison between experimental results and F.E. solution for S4 specimen

Like test specimen S3, the test specimen S4 failed in a combined failure mode of concrete failure and stud yielding but the tendency to the stud failure mode is higher. The concrete formed a conical failure shape as shown in figure 6.10 while the studs bound as shown in figure 6.11. Also the bending curvature of the studs is between the double and single curvatures shapes explained earlier for specimens S1 and S2 respectively.

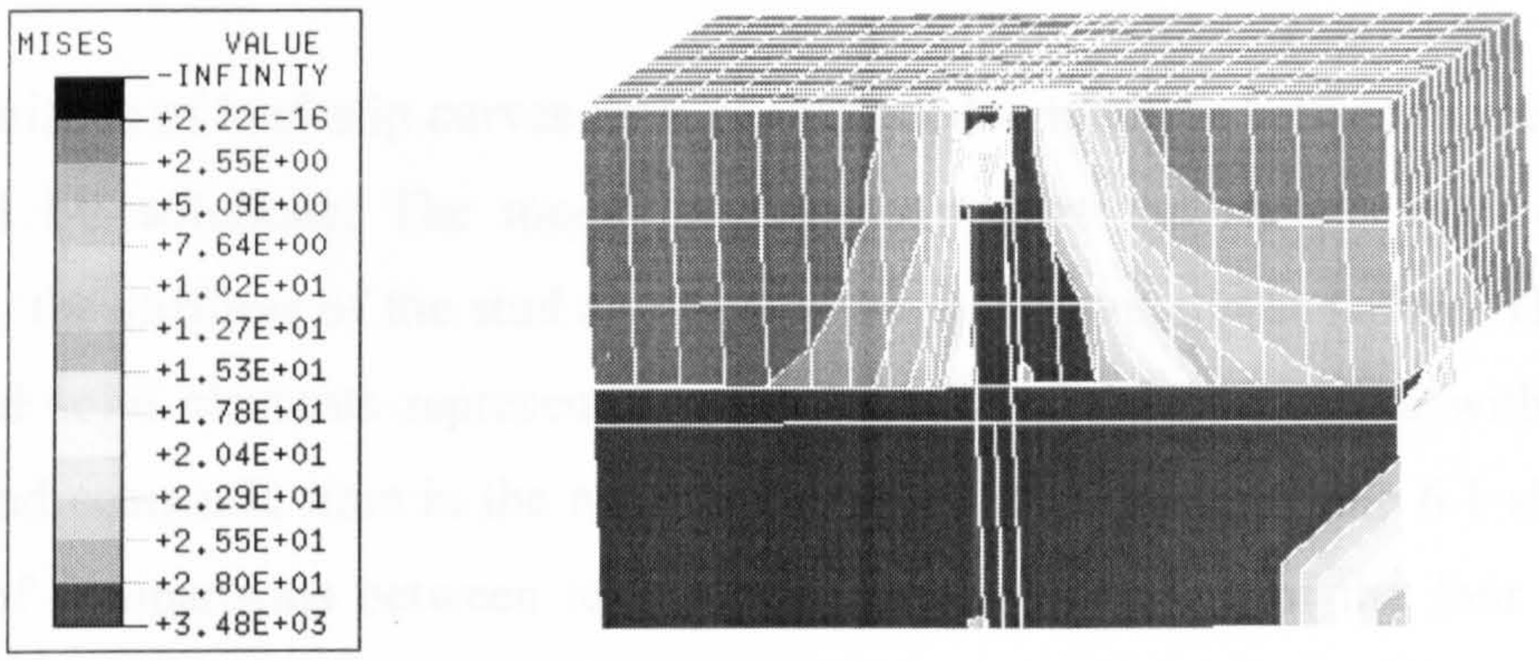

Figure 6.10 Mises stress contour distribution over FE-S4 at failure

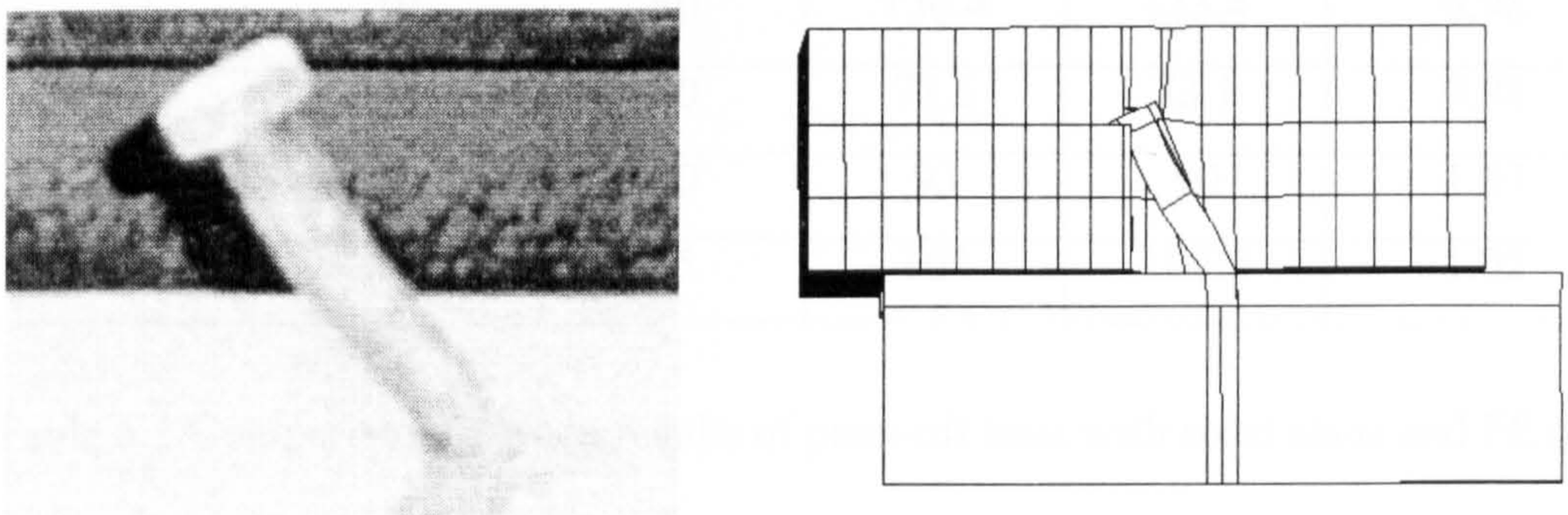

Figure 6.11 Comparison between experimental and FE deformed shape of the stud

6.2.5 Summary

This chapter described the comparison between FE modelling and experimental investigation of headed stud behaviour in push-off tests with solid slabs. The main objective of this comparison was to check the accuracy and the validity of the finite element model. The comparison between the numerical and experimental investigations

included comparisons of shear connection capacity, load-slip behaviour of the stud and the modes of failure.

The comparisons of load-slip curves have shown good agreement between experimental results and FE solutions. The model is able to predict the shear capacity of the connection, the stiffness of the stud and finally the maximum slip at failure. The three-dimensional solid elements represented the behaviour of the connection with enough accuracy and economic time in the analysis process of the model. Table 6.1 shows the summary of comparisons between test results and FE modelling of the four push-off tests carried out in this stud on headed studs in composite girders with solid slabs.

Test ref.	Diameter of headed stud (mm)	Concrete grade (N/mm^2)	Push-off test results (kN)	FE model results (kN)	Push-off test/FE model
S1	19	50	130.4	133.4	0.98
S2	19	20	71.6	73.1	0.98
S3	19	30	93	90	1.03
S4	19	35	102	100.2	1.02

Table 6.1 Comparison between results of push-off tests with solid slabs and FE model

In principal, three modes of failure were observed from present push-off tests and verified numerically by present FE model. The first mode of failure is the concrete cone failure where no stud failure is observed. For this mode of failure, the concrete around the stud started to fail before the stud was yielded, the failure progresses through the thickness of the concrete forming a conical shape around the stud. The second mode of failure is that the stud connector was fully yielded and no concrete failure is observed. This mode of failure is identified as stud failure mode where the yield stress is reached in the stud elements while maximum concrete stress of the concrete elements is not

reached. Finally, the third mode of failure is the combined failure of stud and concrete slab when maximum stresses are reached in stud and concrete elements.

The general conclusion could be drawn from comparisons between experimental and numerical modelling is that good agreement is achieved in the behaviour of headed stud shear connectors in composite beams with solid slabs gives. The reliability of the numerical modelling could eliminate the need for future laboratory testing. The finite element model is simple and can be used in future research if the following procedures were followed in any future study:

1. *Modifications in the input file*: The main geometrical variables in present finite element model simulating the behaviour of headed stud in push-off tests with solid slabs are diameter of the stud, stud height and concrete slab dimensions. The modification is required only in case of studying any new parameters, which were not covered in this study. The other variables are the material properties of the components which are mainly, ultimate strength of shear stud connector, modulus of elasticity of the shear stud, concrete slab design strength and modulus of elasticity of the concrete slabs. Guidelines of calculating these material variables are presented in chapter 3.

2. *Evaluation of the shear stud capacity, load-slip behaviour and modes of failure*: From the ABAQUS data files, all the stress and strain values are tabulated for each element in column form at each increment. To evaluate the failure modes, the critical element should be investigated, i.e. stud element near the collar and concrete elements around the stud. The mode of failure could be determined when one of the conditions is exceeded. Also by post ABAQUS processing, stress contours and deformed shapes can be plotted.

6.3 Comparison of FE results with tests on headed shear studs in hollow core slabs

Four push-off tests with precast HC slabs were also investigated experimentally and numerically using the FE model. The push-off tests included different gap sizes, different HCU heights, different transverse reinforcement bars and two different in-situ concrete strengths. This gives a variety to check the FE model by comparing both experimental and FE results. The shear connection capacity, the load-slip curve of the headed stud and the load-strain curves of the bars evaluated from both approaches will be presented.

6.3.1 Test T 10-C25-150-65

Figure 6.12 shows a comparison between the load-slip curve obtained from FE modelling with that obtained from experimental investigation. It can be seen that good agreement was achieved between both results. The maximum experimental failure load was 68.4kN at a slip of 2.63mm compared with 67.9kN at 3.16mm. This means that the FE failure load is less than that experimental one by 0.8%.

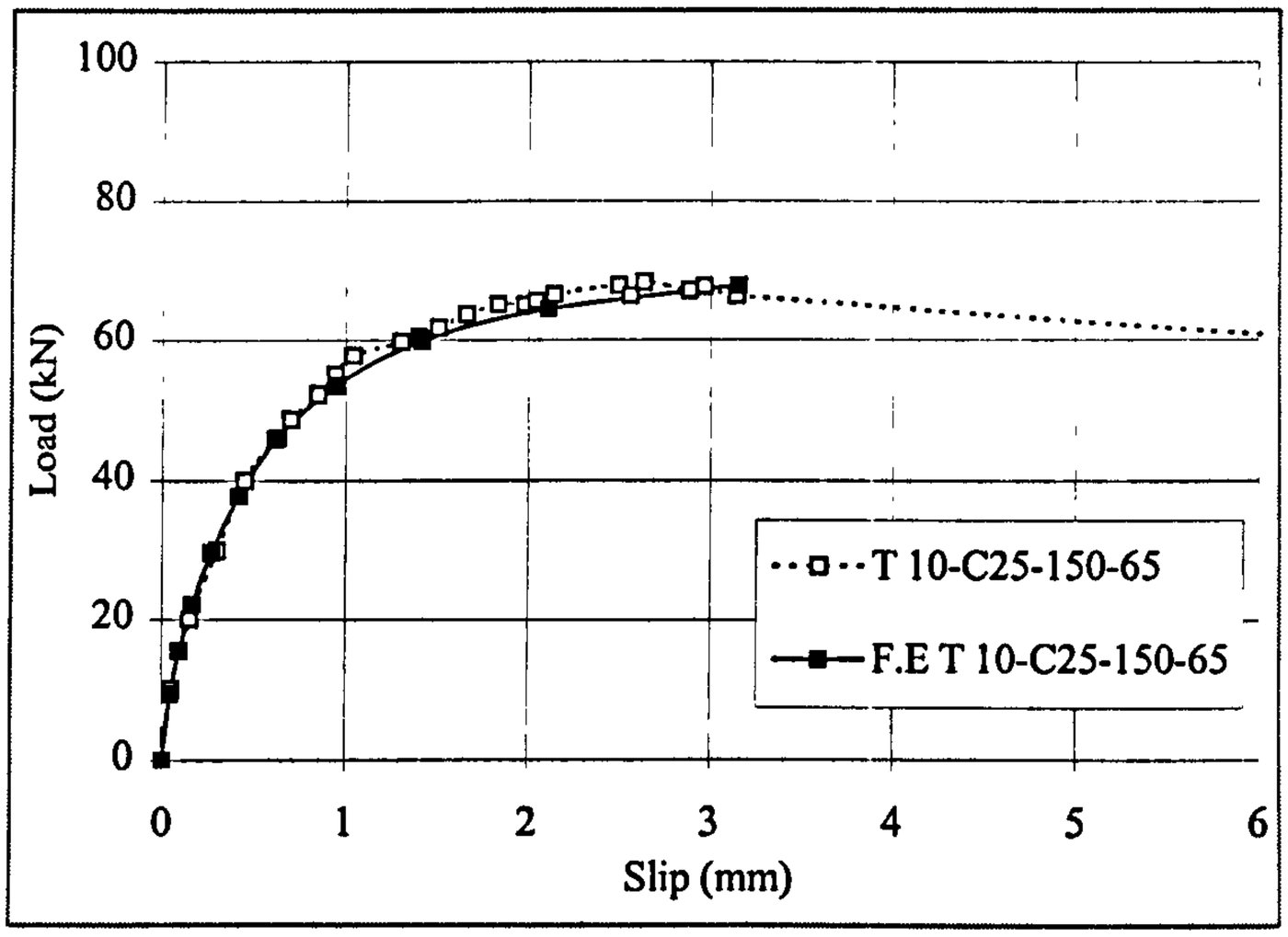

Figure 6.10 Load vs. slip curve of the stud for push-off test T 10-C25-150-65

As explained earlier, for that lower reinforcement size (10mm), the transverse reinforcement failure mode is likely to occur. The reinforcement bar yields first leading

to concrete failure around the stud, which has not reached its full yielding yet. Figure 6.11 shows both curves of load vs. strain, of the transverse reinforcement bars, obtained from FE element modelling and experimental investigation. The figure shows good agreement between both curves. It can be seen that the reinforcement bar reaches its ultimate strain and consequently ultimate stress at the failure load in both plots.

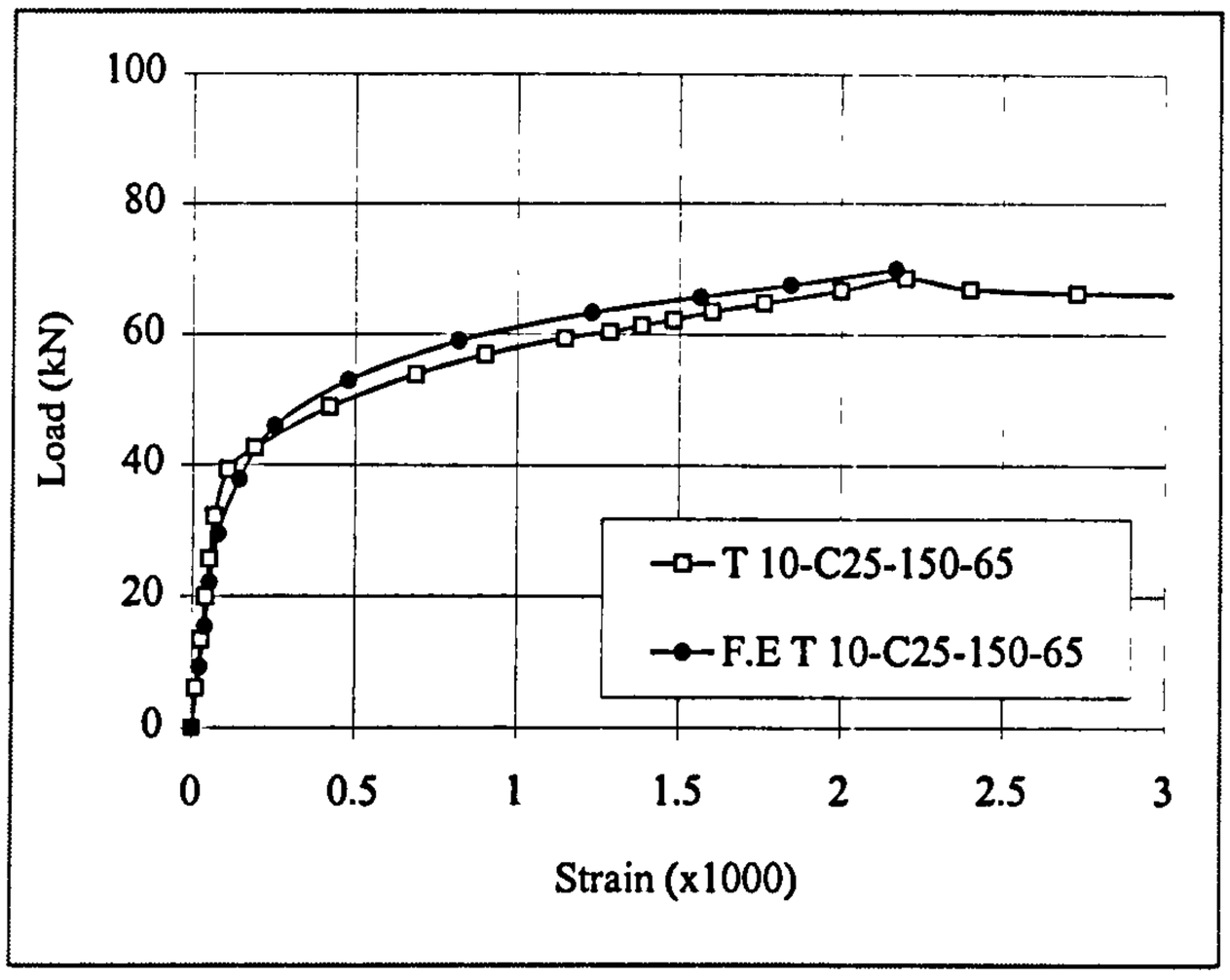

Figure 6.11 Load-strain curve of transverse reinforcement for test T 10-C25-150-65

6.3.2 Test T 16-C30-150-80

In this push-off test, the load vs. strain curve is plotted in figure 6.12 for larger transverse reinforcement bar diameter (16mm) compared with (10mm) diameter in the previous test. The curve contains comparison between both FE solution and experimental results. It can be seen that although failure has occurred and four studs have already sheared off, as previously observed in chapter 5 for this push-off test specimen, the transverse reinforcement bar did not reach its ultimate strength in both FE modelling and experimental investigation. This stresses the fact that for higher transverse reinforcement sizes, the mode of failure is likely to be because of stud failure instead of reinforcement bar and consequently concrete failure. Figure 6.12, as well, shows good agreement between FE solution and experimental investigation.

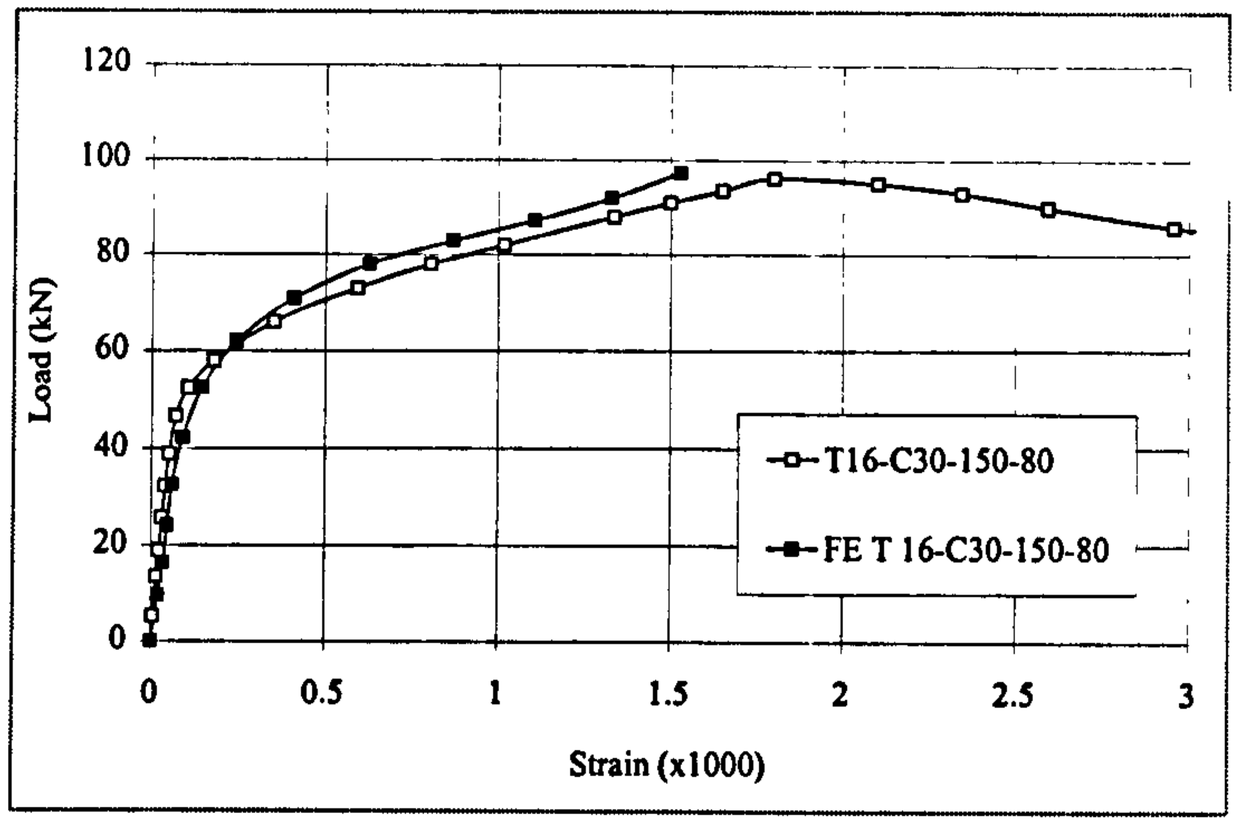

Figure 6.12 Load-strain curve of transverse reinforcement for test T 16-C30-150-80

Figure 6.13 shows good agreement between the load vs. slip obtained from FE solution and that obtained experimentally. The maximum experimental load was 97.3kN at a slip of 5.53mm compared with 95.5kN at a slip of 6.9mm obtained from FE modelling. The FE failure load is less than that experimental load with 1.9%.

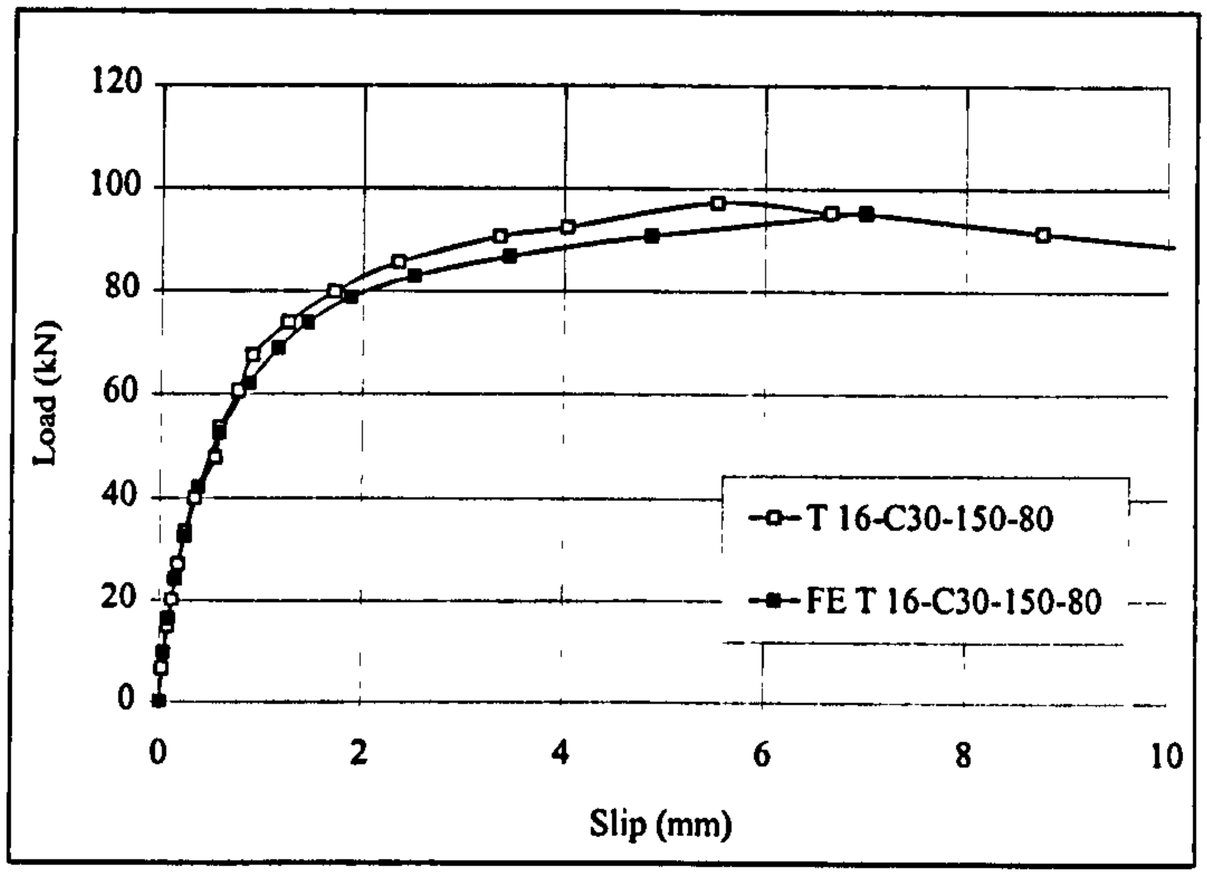

Figure 6.13 Load vs. slip curve of the stud for push-off test T 16-C30-150-80

6.3.3 Test T 16-C30-200-80

Figure 6.14 shows the load-slip behaviour of the stud for push-off test T 16-C30-200-80. The curve compares FE solution with experimental results. It can be shown that there is

good agreement between both of them. The experimental failure load was 99.53KN at a slip of 5.93mm compared with 100.3KN at a slip of 6.85mm from FE analysis. The FE maximum load is greater than experimental failure load with about 0.8%.

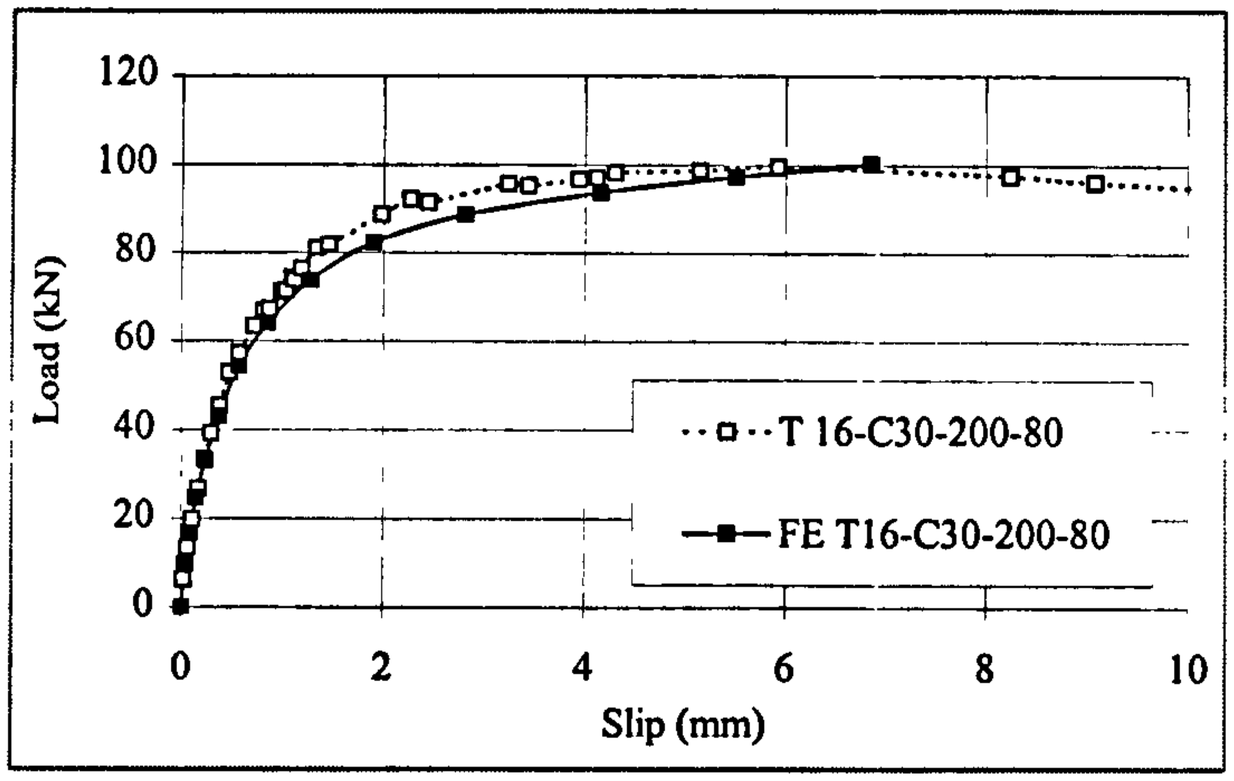

Figure 6.14 Load vs. slip curve of the stud for push-off test T 16-C30-200-80

A comparison between the resulted load-strain curves numerically by FE modelling and experimentally by push-off test T 16-C30-200-80 for the 16mm bar is shown in figure 6.15. The figure shows good agreement between both approaches and clears the fact that, for 16 reinforcement diameter doesn't reach the ultimate strength and failure of connection is governed by the failure of the stud.

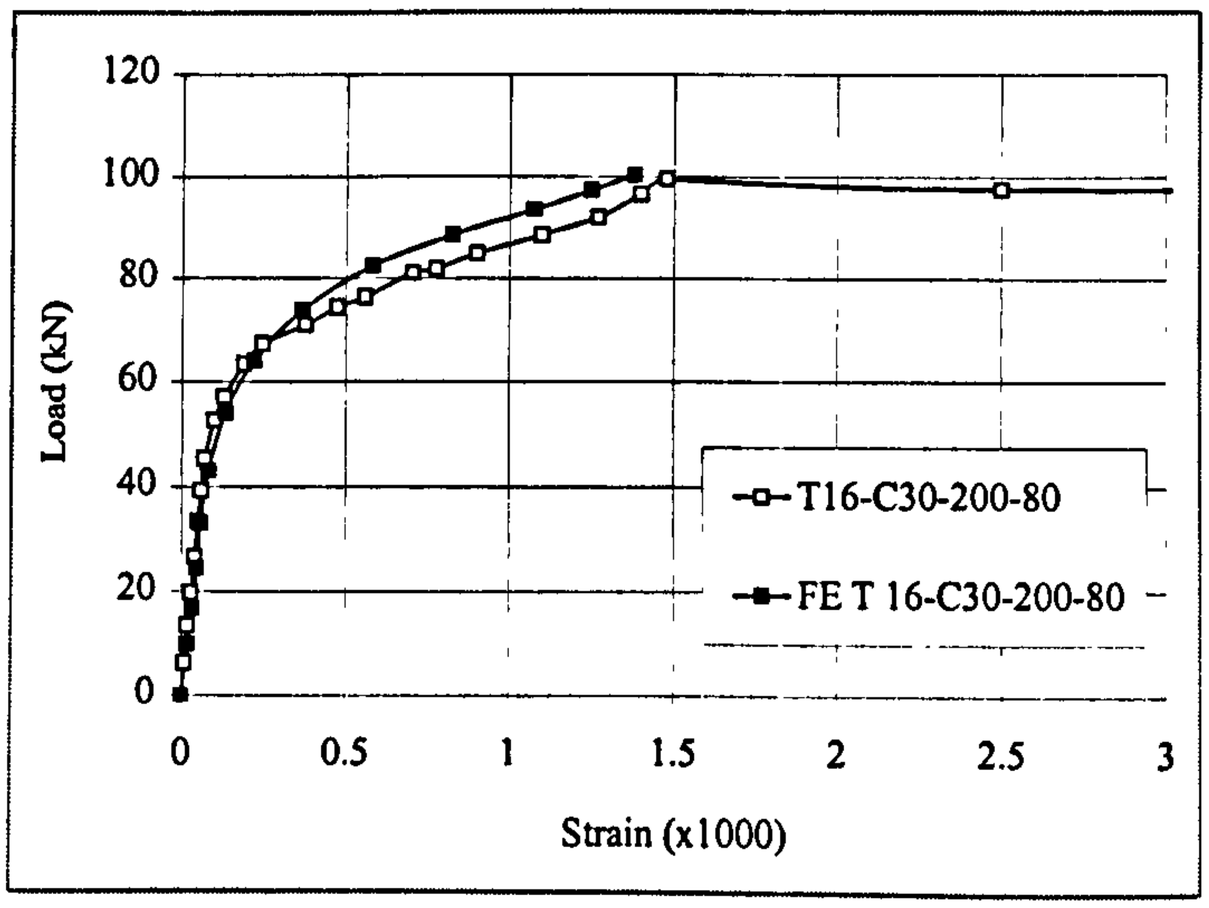

Figure 6.15 Load-strain curve of transverse reinforcement for test T 16-C30-200-80

6.3.4 Test T 16-C30-200-60

A comparison between the load-slip curves obtained from both FE solution and experimental results held in figure 6.16 for push-off test specimen T 16-C30-200-60. The curve shows good agreement between numerical and experimental results. The experimental failure load was 91.78KN at a slip of 3.71mm compared with 92.72KN at a slip of 4.18mm from FE analysis. The FE maximum load is greater than experimental failure load with about 1.02%.

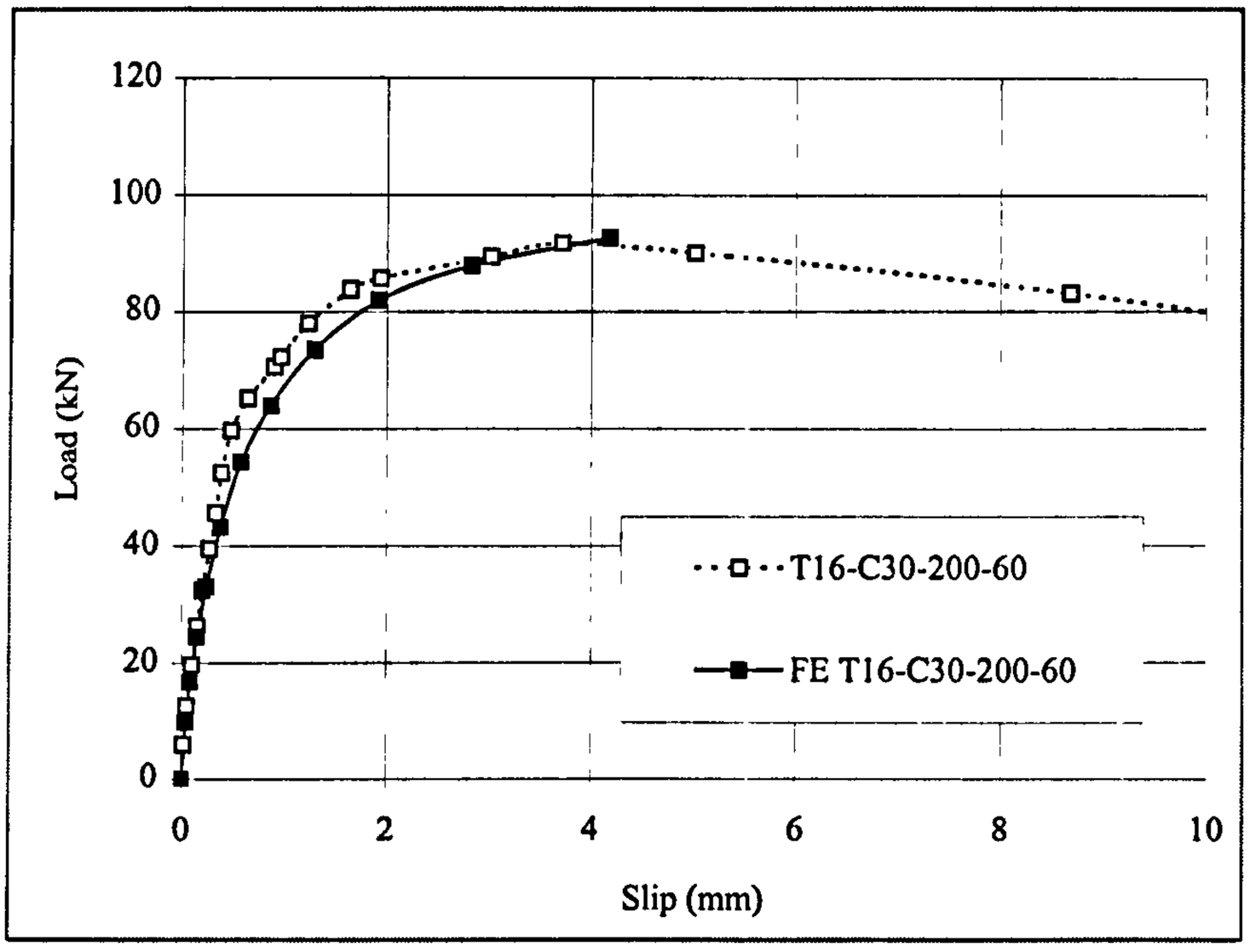

Figure 6.16 Load vs. slip curve of the stud for push-off test T 16-C30-200-60

Also, figure 6.17 shows that the 16mm reinforcement bar did not reach its ultimate strength in both FE and experimental results. The figure shows good agreement between both of them. The failure of connection occurred by the yielding of the stud elements in the numerical analysis. The same happened experimentally since two of the six studs sheared-off while others bent in the direction of loading at failure while the strain gauges reading showed that the reinforcement bar did not reach its ultimate strain and consequently ultimate strength was not reached.

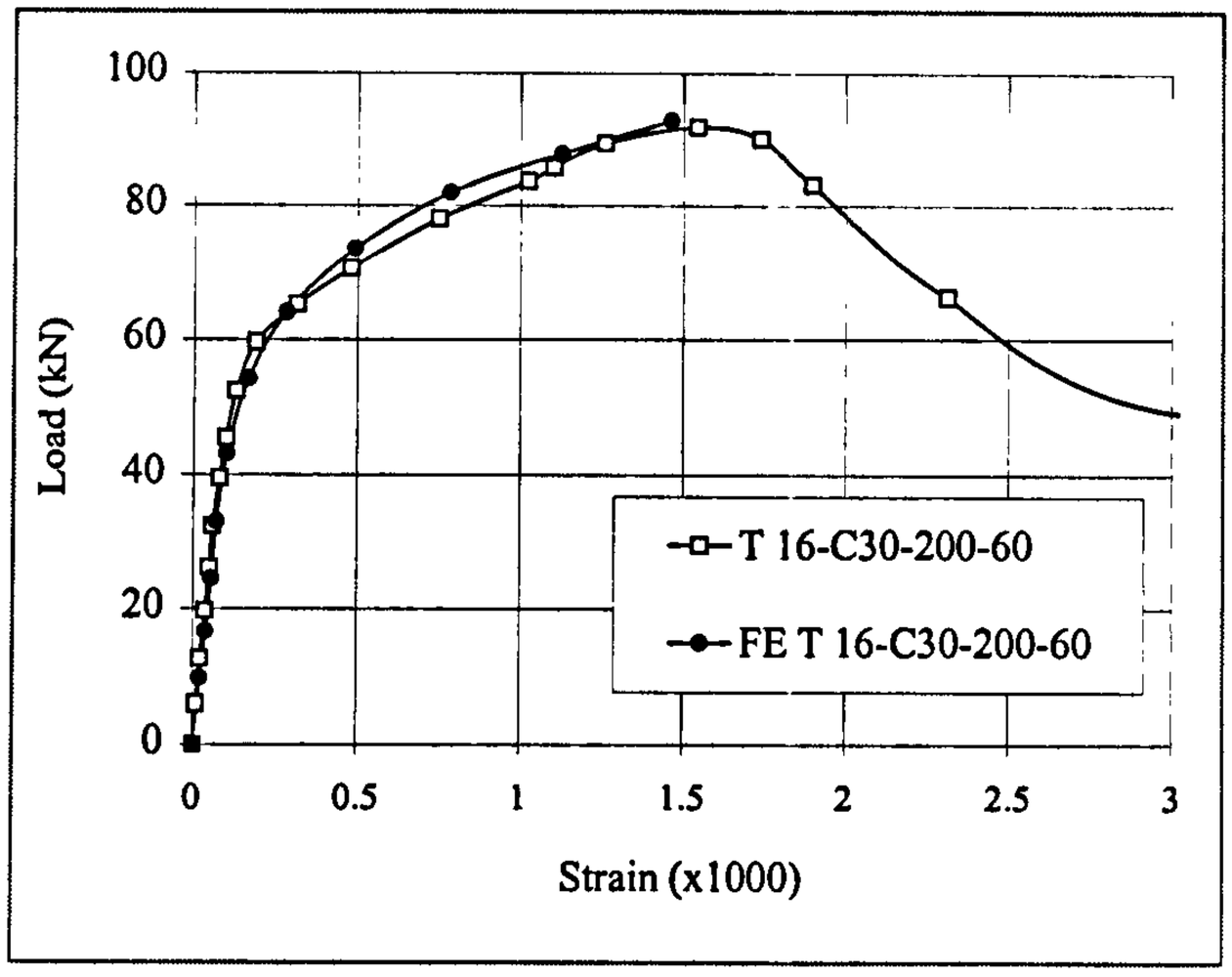

Figure 6.17 Load-strain curve of transverse reinforcement for test T 16-C30-200-60

6.3.5 Summary

This chapter described the comparison between experimental investigation and FE modelling of headed studs in push-off tests with precast hollow core slabs. The main objective of this comparison was to check the accuracy and the validity of the finite element model.

Comparison between experimental and numerical evaluation of shear connection capacity, load-slip behaviour of headed stud and load-strain behaviour of transverse reinforcement bar was presented and good agreement has been achieved. Table 6.2 shows summary of the four push-off test results conducted in chapter 5 in comparison with the FE results evaluated in chapter 4. It can be seen that a very close correlation is noted between the test results and the FE analyses in evaluating the shear capacity of connection.

Test Ref.	Diameter of headed stud (mm)	Concrete grade (N/mm^2)	Push-off test results (KN)	FE model results (KN)	Push-off test/FE model
T 10-C25-150-65	19	25	68.4	67.9	1.01
T 16-C30-150-80	19	30	97.3	95.5	1.02
T 16-C30-200-80	19	30	99.5	100.3	.99
T 16-C30-200-60	19	30	91.8	92.7	.99

Table 6.2 Comparison between results of push-off tests with precast HC slabs and FE model

It was also observed from the parametric studies conducted by the FE modelling and considered as well in the experimental investigation that, the transverse gap width and the HCU depth had considerable effect on the shear connection behaviour. Curves 6.18 and 6.19 show that the increase in gap size leads to an increase in the shear stud capacity numerically and experimentally respectively. The increase in gap width reduces the stresses in the in-fill concrete around the stud. These stresses can cause concrete failure, either directly by crushing or indirectly due to increased splitting forces. The increase in the capacity of shear connection due to the increase in gap size depends on many factors, especially the transverse reinforcement size used in the test, as previously explained in chapter 4 and becomes negligible at certain gap width after which the shear capacity is not affected. Figure 6.18 shows an increase of 8.2% of the shear capacity of T 16-C30-200-60 due to an increase of 20mm in the gap size obtained from FE analysis. Figure 6.19 as well shows an increase of 8.4% of the shear capacity of T 16-C30-200-60 due to an increase of 20mm in the gap size obtained from experimental investigation. Both curves show that the increase in gap size has a small effect on the stiffness of the stud but it affects remarkably the ductility of the connection.

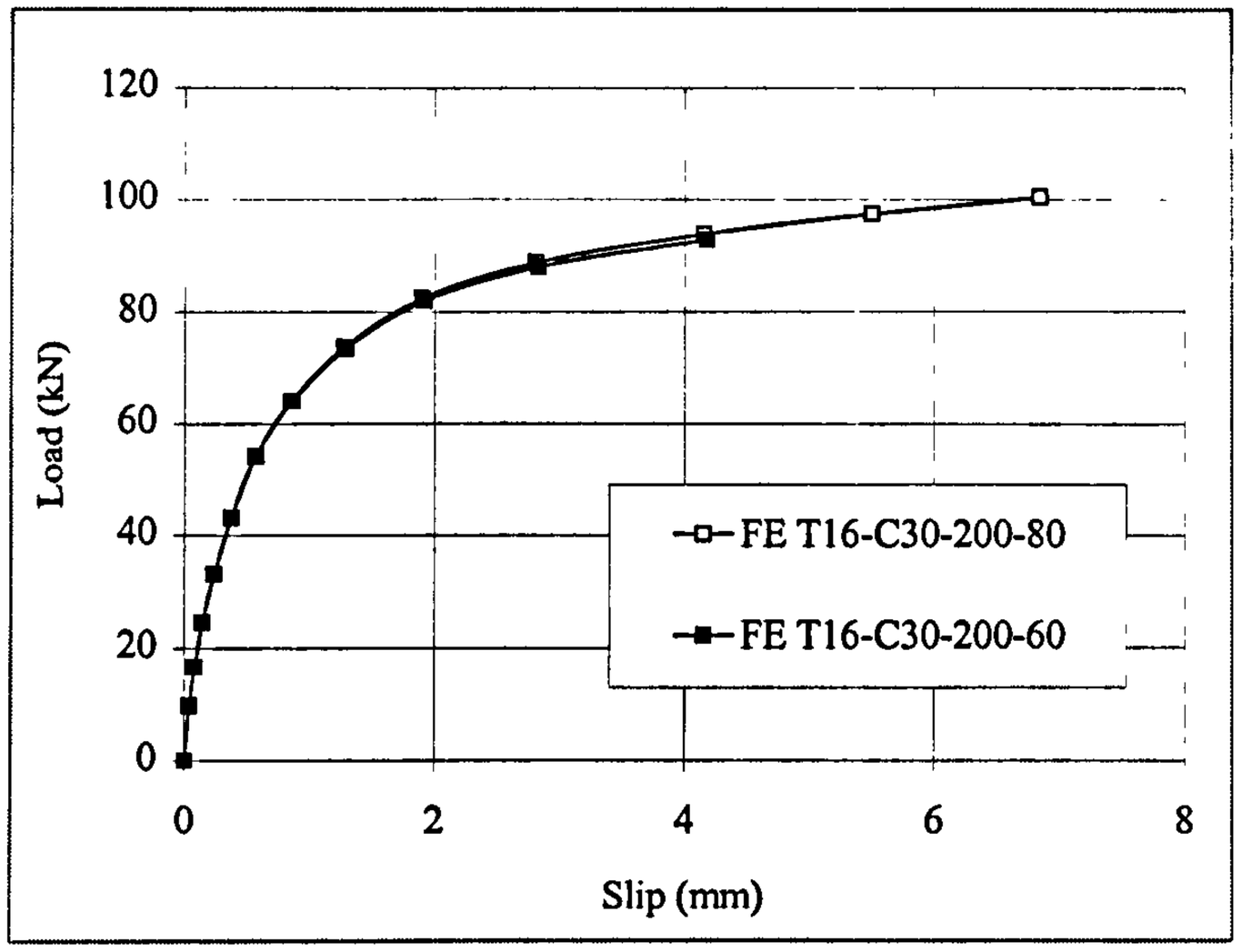

Figure 6.18 Effect of change of the gap size on the Load-slip curve numerically

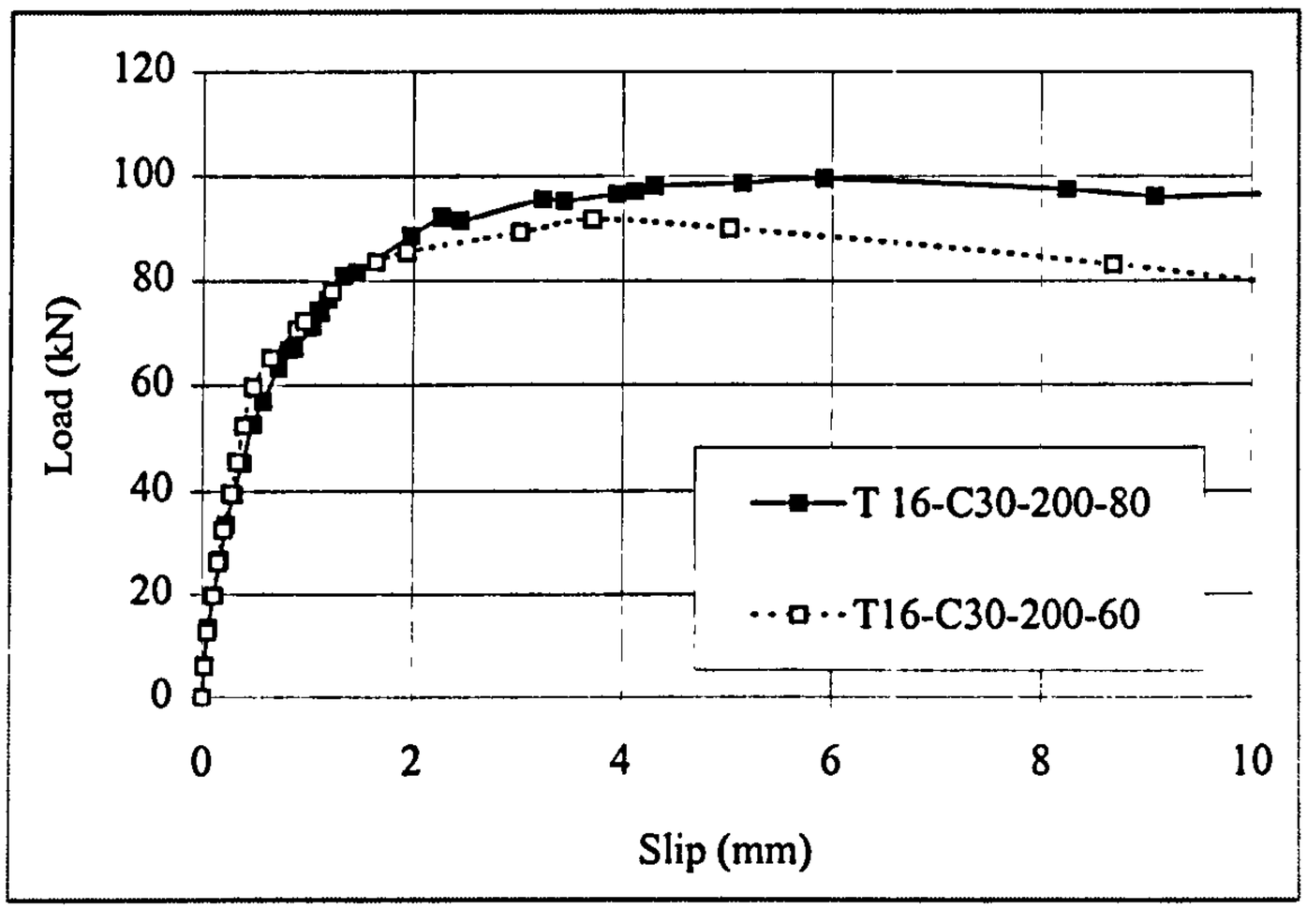

Figure 6.19 Effect of change of the gap size on the Load-slip curve experimentally

Figures 6.20 and 6.21 show that the increase in HCU depth increases the shear capacity of the connection numerically and experimentally respectively. Figure 6.20 shows an increase of 5.1% in the shear stud capacity due to an increase of 50mm in the HCU depth of the push-off test specimen T 16-C30-150-80 as obtained from FE modelling. Also, figure 6.21 shows an increase of 2.3% in the shear stud capacity due to an increase of 50mm in the HCU depth of the push-off test specimen T 16-C30-150-80 as obtained from experimental investigation.

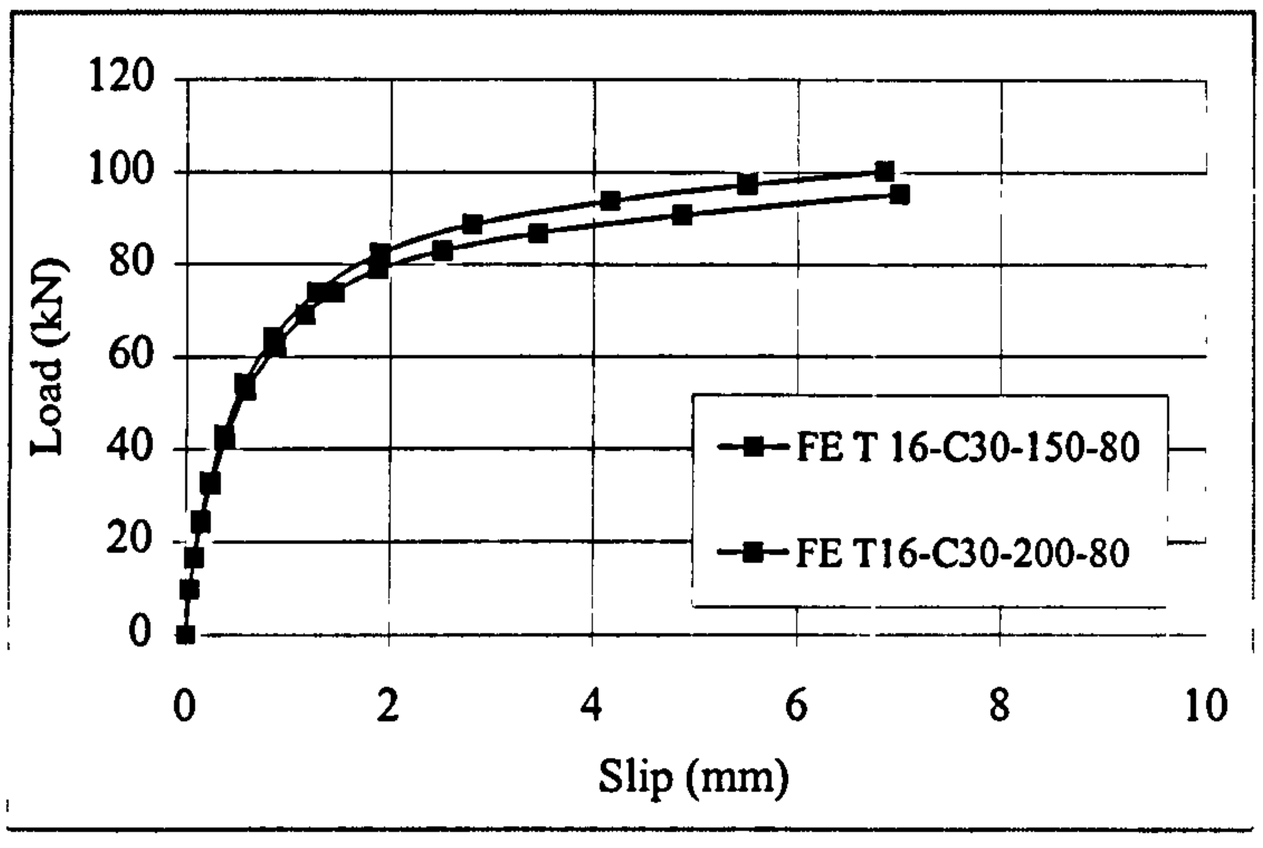

Figure 6.20 Effect of change of the HCU depth on the Load-slip curve numerically

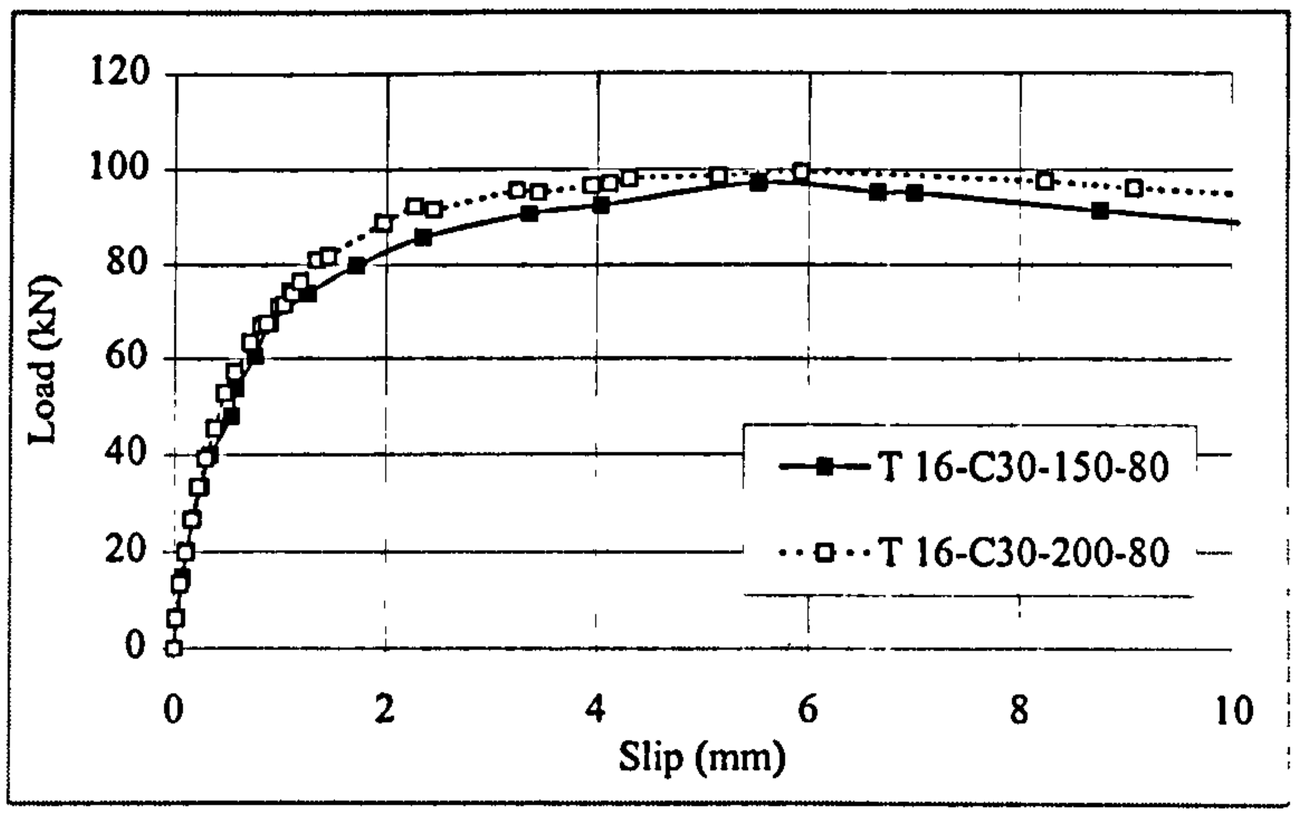

Figure 6.21 Effect of change of the HCU depth on the Load-slip curve experimentally

Good agreement is achieved experimentally and numerically in the behaviour of headed stud shear connectors in composite beams with precast hollow core slabs. The reliability of the numerical modelling could eliminate the need for future laboratory testing. The simplicity and efficiency of the developed finite element model make it useful for future research if the following procedures were followed in any future study:

3. *Modifications in the input file*: The main geometrical variables in present finite element model simulating the behaviour of headed stud in push-off tests with precast hollow core slabs are diameter of the stud, stud height, hollow core slab dimensions, transverse reinforcement size and transverse gap size. The modification is required only in case of studying the effect of the change in any of these parameters. The other variables are the material properties of the components, which are ultimate strength of shear stud connector, modulus of elasticity of the shear stud, in-situ concrete design strength, modulus of elasticity of the in-situ concrete, precast HCU design strength, modulus of elasticity of the precast HCU, ultimate strength of the transverse reinforcement bar and finally the modulus of elasticity of the transverse reinforcement bar. Guidelines of calculating these material variables are presented in chapter 4.

4. *Evaluation of the shear stud capacity, load-slip behaviour and modes of failure*: From the ABAQUS data files, all the stress and strain values are tabulated for each element in column form at each increment. To evaluate the failure modes, the critical element should be investigated, i.e. stud element near the collar, concrete elements around the stud and transverse reinforcement bar. The mode of failure could be determined when one of the conditions is exceeded. Also by post ABAQUS processing, stress contours and deformed shapes can be plotted.

7. Finite element modelling of the behaviour of both steel-solid slab and steel-precast HC slab composite girders

7.1 Introduction

The results obtained from FE modelling of headed studs in composite girders with solid slabs or precast hollow core slabs, discussed in chapters 3 and 4 respectively, are used to model steel-solid slab concrete and steel-precast HC slab composite girders in this chapter. A finite element model is presented for the analysis of each type. The model takes into account the non-linear behaviour of concrete, steel beam and shear connectors. The non-linear load-slip relationship of the shear stud is taken from numerical modelling of push-off tests. The accuracy and efficiency of the model are demonstrated by comparing the present finite element (FE) results with available published experimental and numerical researches. An effective parametric study for the effective width of steel-precast concrete slab composite girders is presented.

7.2 Basic layout of composite girders

Composite construction has been taken a remarkable interest in the last few decades because of development in materials, construction techniques, and computation capabilities. Because of its construction advantages, the steel-concrete composite section is commonly used in bridges and buildings. These advantages are obtained by maintaining interaction between the concrete slab and the structural steel girders with shear connectors. The use of precast solid slabs or composite slab with profiled steel sheeting in composite girders has the advantage, over cast in place concrete slabs, of avoiding the use of form-work and the fact that it can be completed very quickly. Composite construction of steel frames with profiled steel decking to support the floor slabs is now common in UK multi-storey construction, but the use of precast, prestressed concrete hollow-core units (HCUs) in conjunction with the steel frame to provide composite action is relatively new. The main advantage in using HCUs is their excellent structural capacity with remarkably reduced self-weight since the hollow-cores account for up to 50% of the cross section.

In steel-HCU composite construction, the commonly used headed stud connectors are welded to the steel beam and the HCUs are positioned on the top flange of the steel beam. A gap, 'g' in Figures 7.1.a and 7.1.b, between longitudinal edges of the HCUs is taken to allow for correct compaction of cast in situ concrete around the headed studs. Transverse tie steel reinforcement bar is placed in an opened core, between two closed cores to limit the longitudinal splitting. The gap 'g', the opened cores, and the key joints between HCUs along the beam length are filled with in situ concrete.

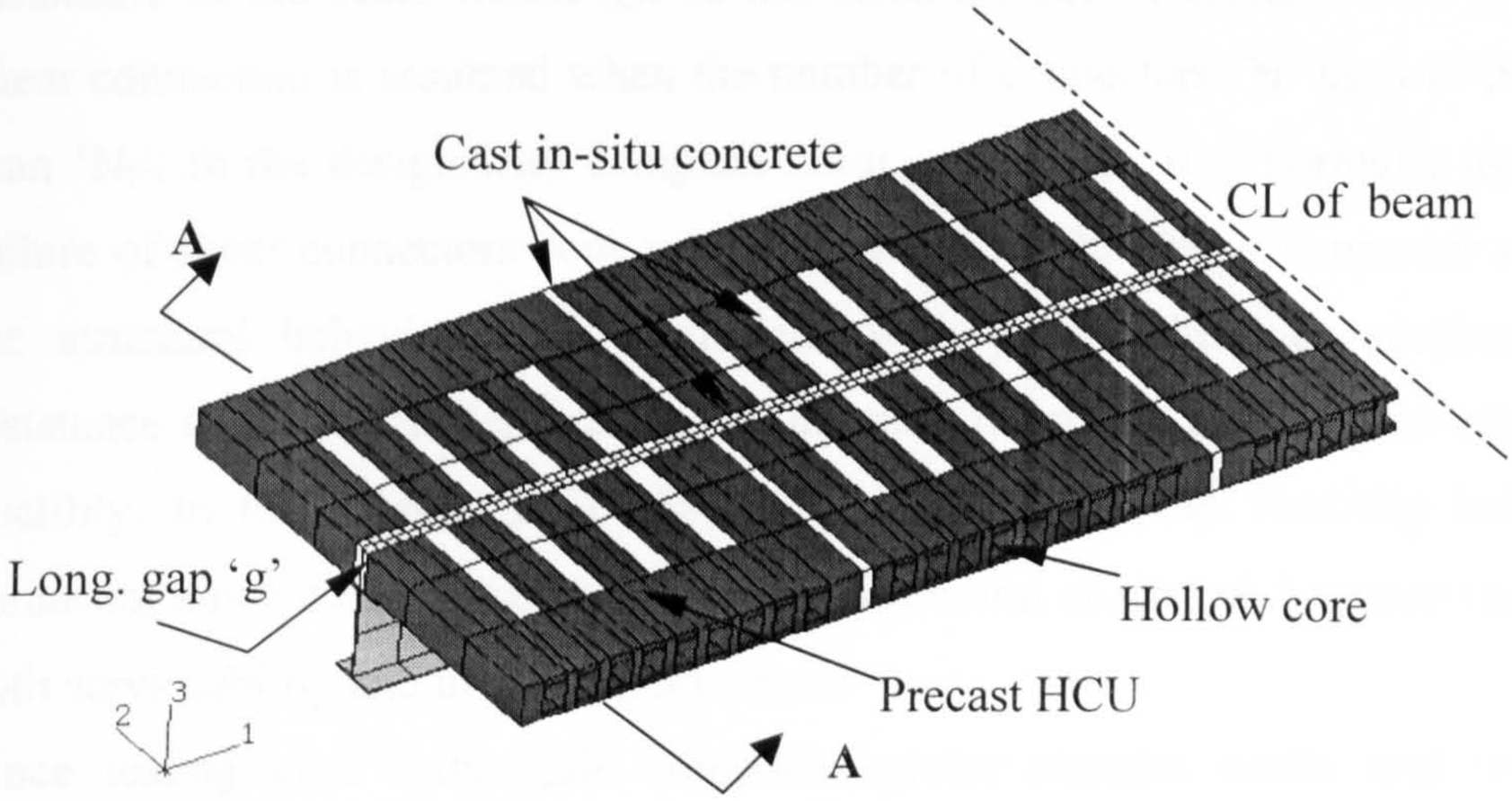

Figure 7.1.a General Layout of steel-precast HCU slab composite girder

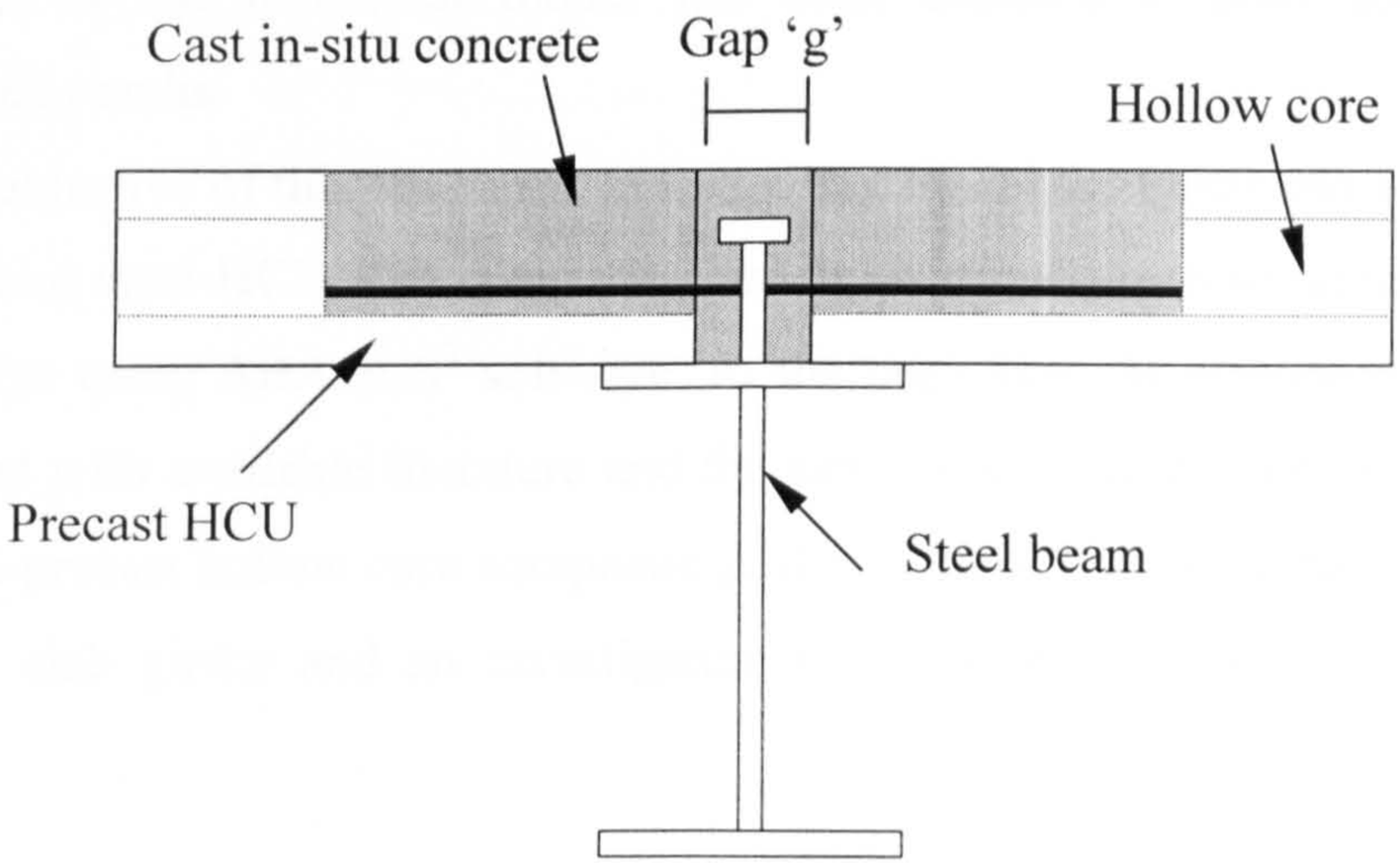

Figure 7.1.b Cross section A-A through steel-precast HCU slab composite girder

Recent researchs[66,36], part from this study, have been carried out using the FEM to investigate the load-slip behaviour and ultimate strength of the headed stud connector in both steel-solid slab and steel-HCU slab. The results obtained were validated against test results and compared with current codes of practice BS5950[7] and EC4[8]. These results are used in the present study to identify the behaviour of the non-linear spring representing the shear stud in the composite girder. For a given beam, loading and design method, complete shear connection is defined as the least number of the connectors 'N_f' such that the bending resistance of the beam would not be increased if more connectors were provided. Partial shear connection is assumed when the number of connectors 'N' used in the beam is less than 'N_f'. In the design with complete shear connection, it is normally assumed that the failure of shear connectors does not occur and the influence of connector deformation on the structural behaviour was neglected. With partial shear connection, the ultimate resistance of the beam depends on the ultimate resistance of the shear connector and its ductility. In these cases, it is important to use the correct load-slip behaviour of the connector since it can cause significant redistribution of stresses between the connectors in both serviceability and ultimate limit states.

Since testing of a fully scale composite girder remains costly and time-consuming, numerical methods that can predict the non-linear behaviour and the ultimate load capacity of the girder are developed to replace most of the experiments. This is ensured once verification of the numerical model has been established from selective controlled experimental results.

The main objective of this chapter is to accurately model the behaviour of composite steel-solid slab and steel-HCU slab composite girders. A three dimensional model is developed for each type using ABAQUS[2] software. At the beginning the steel-solid slab is modelled and verified with available literature and the same modelling procedures will be extended to the steel-precast hollow core composite girders. Concentration is made on the composite steel-HCU slab girder and an investigation of the effective width of the HCU slab is presented.

7.3 Finite element modelling

The main components of a composite beam are the concrete slab, the steel beam and the shear connector, which is the headed shear stud connector chosen for this study. To model the composite girder efficiently, it is important to accurately simulate the actual behaviour of the material of each component. ABAQUS material library contains effective material models that can simulate the actual behaviour of each component accurately.

7.3.1 Material modelling of a reinforced concrete slab

The stress-strain curve for the concrete is modelled through the *CONCRETE option. To define the shape of the failure surface, *FAILURE RATIOS option is used. The ratio of the ultimate bi-axial compressive stress to the uni-axial compressive ultimate stress is selected as 1.16. The absolute value of the ratio of the uni-axial tensile stress at failure to the uni-axial compressive stress is taken as 0.15. The reinforcement is introduced through a special command (*REBAR) available in the ABAQUS software. It is mentioned in the user guide for the software that this command can simulate some interaction between the concrete and the reinforcement. To define the retained tensile stress normal to a crack as a function of the deformation in the direction normal to the crack, *TENSION STIFFENING parameter is used, see Figure 7.2 which shows the stress-strain curve representing this model as given in the manual of ABAQUS theory. Following the BS 8110: part 1, 2 1997[65], Average values of ultimate strain at failure 'ε_u', the ultimate compression stress of concrete 'f_{uc}', the initial Young's modulus 'E_{co}' can be calculated from the following relations:

$$\varepsilon_u = .00024(f_{cu})^{0.5} \quad \text{.....(7.1)}$$

$$f_{uc} = 0.67\, f_{cu} \quad \text{.....(7.2)}$$

$$E_{co} = 5500\,(f_{cu})^{0.5} \quad N/mm^2 \quad \text{.....(7.3)}$$

where:

f_{cu} : the cube strength of concrete

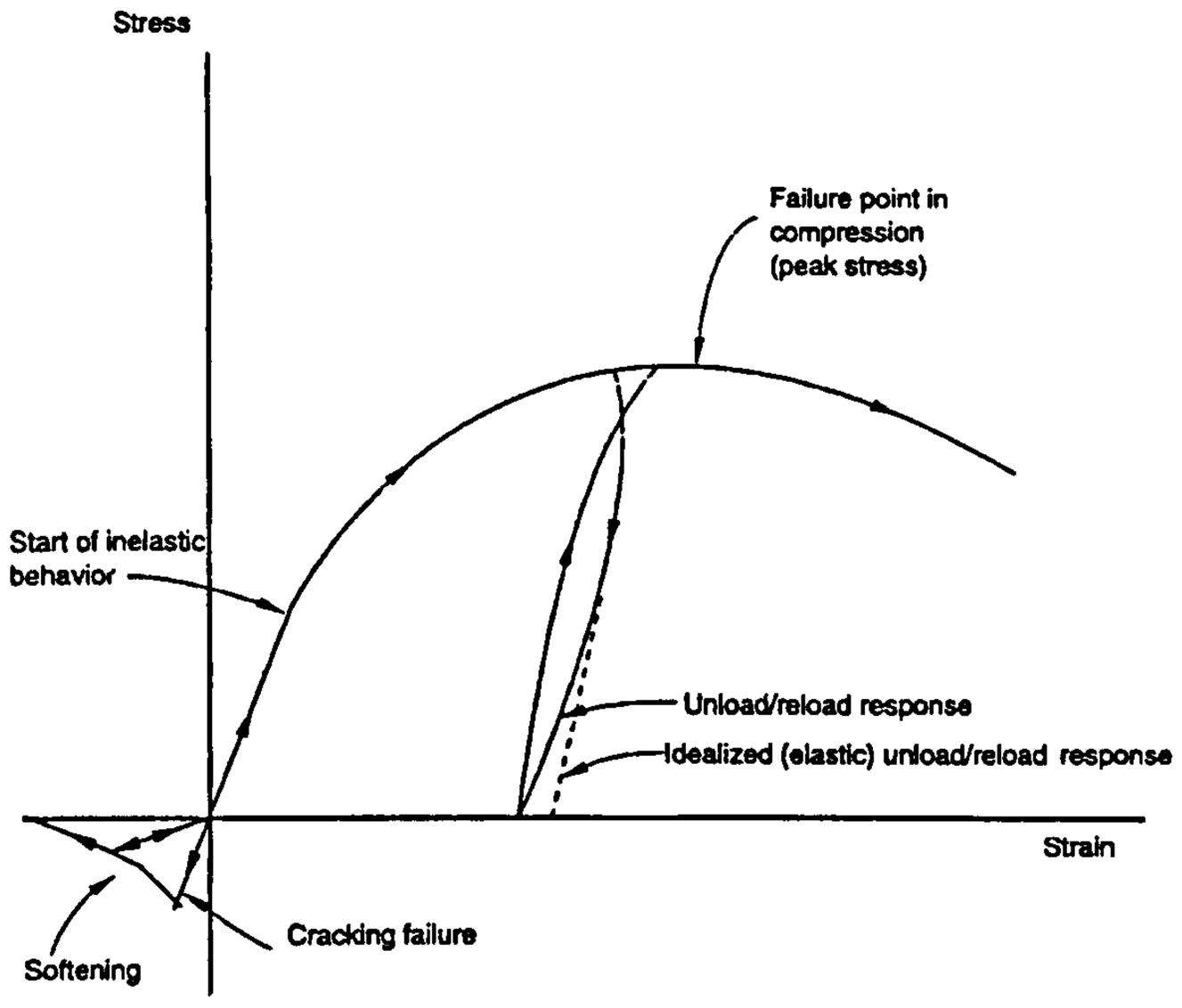

Figure 7.2 Uniaxial stress-strain curve for concrete (ABAQUS model)

7.3.2 Material modelling of steel beam

The simulated material model of the steel beam treats the steel material as elastic-plastic material, i.e. it behaves as linear elastic material with Young's modulus E_s up to the yield stress of steel f_{ys}. After this stage it becomes fully plastic. In the present study, E_s is taken equal to 206000 N/mm^2 f_{ys} is taken 270N/mm^2 for flange and 300 N/mm^2 for web.

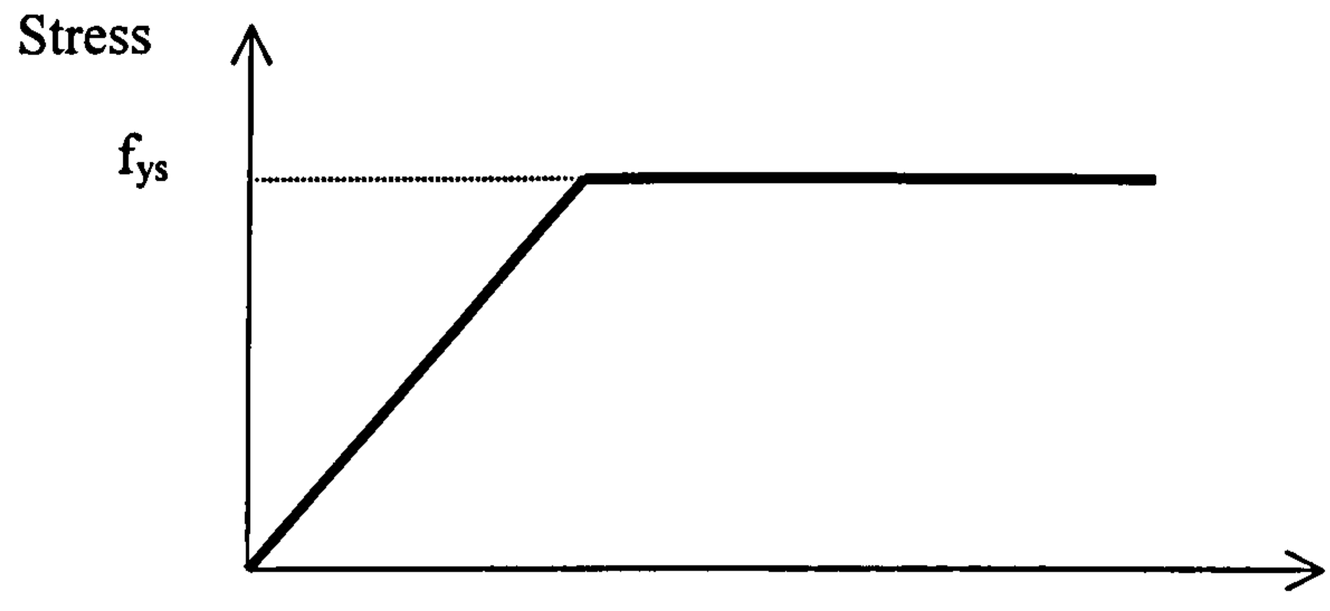

Figure 7.3 Bilinear stress-strain curve for steel (elastic-plastic model)

7.3.3 Modelling of shear stud connector

In a composite steel and concrete beam, shear connectors must be provided throughout the length of the beam. The shear connectors transmit the longitudinal shear force between the steel beam and the concrete slab ignoring the effect of frictional bond between the two materials. The shear connector is modelled and defined in ABAQUS using a non-linear spring element (*SPRING). The spring element is of zero length that bears only shear force, and obeys the load-slip characteristic of the shear connector used. The positions of the spring elements coincide with the positions of the shear connectors used in the composite beam. Because the load-slip characteristic of the shear connector is non linear, the force is assumed to be a function of relative displacement in the spring and is defined by giving a table of force values in ascending values of relative displacement. The load-slip characteristic of the shear connector is obtained from the corresponding FE modelling of push-off test.

7.3.4 Modelling of reinforcement bars

Reinforcement in elements is defined by using the *REBAR option in ABAQUS manual. It can be defined as individual reinforcing bars in the elements or as layers of uniformly spaced reinforcing bars. The material properties of the bars are distinct from those of the underlying elements and are defined separately. In the present study,
the same bilinear simulated curve shown in figure 7.3 for steel beam is used in modelling the reinforcement bar steel material but with a yield stress f_{ys} equals to 320N/mm^2.

7.4 FE modelling of steel-solid slab composite girders

The main objective of modelling steel-solid concrete composite girders is to check the accuracy of the modelling procedure used in this research before extending it to the proposed modelling of steel-precast HCU slab composite girders. Two simply supported beams (B1 and B2) tested by Chapman[53] are modelled in this research. Beam B1 is subjected to a concentrated load at the middle of the beam as shown in figure 7.4 and has a uniformly distribution of studs in pairs with a distance of 115 mm between any two pairs. The studs are 12.7mm (diameter) x 50mm (height) and are welded to a 305x152x65 UB. The cross section of the concrete slab is 1220mm (width) x 152mm (depth) and has a

compressive strength of 32.7 N/mm^2 and tensile strength of 3.07 N/mm^2. The slab is reinforced longitudinally with four top bars and four bottom bars 8mm diameter each.

Beam B2 is subjected to a uniformly distributed load but it has the same concrete cross section, reinforcement bars, and steel beam. The concrete compressive strength is 33.8 N/mm^2 and the tensile strength is 3.14 N/mm^2. The studs are 19mm (diameter) x 102mm (height) and are distributed in pairs in a triangular distribution as shown in figure 7.4.

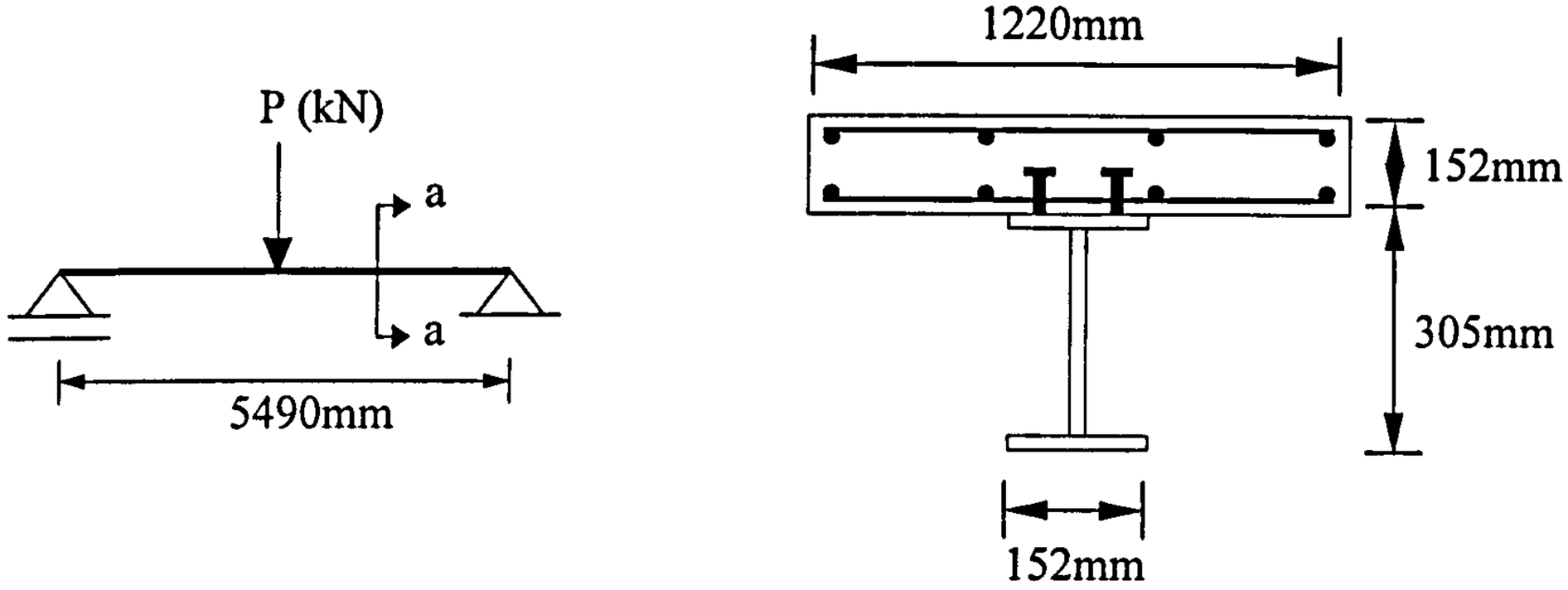

Figure 7.4.a Layout and cross section of beam B1

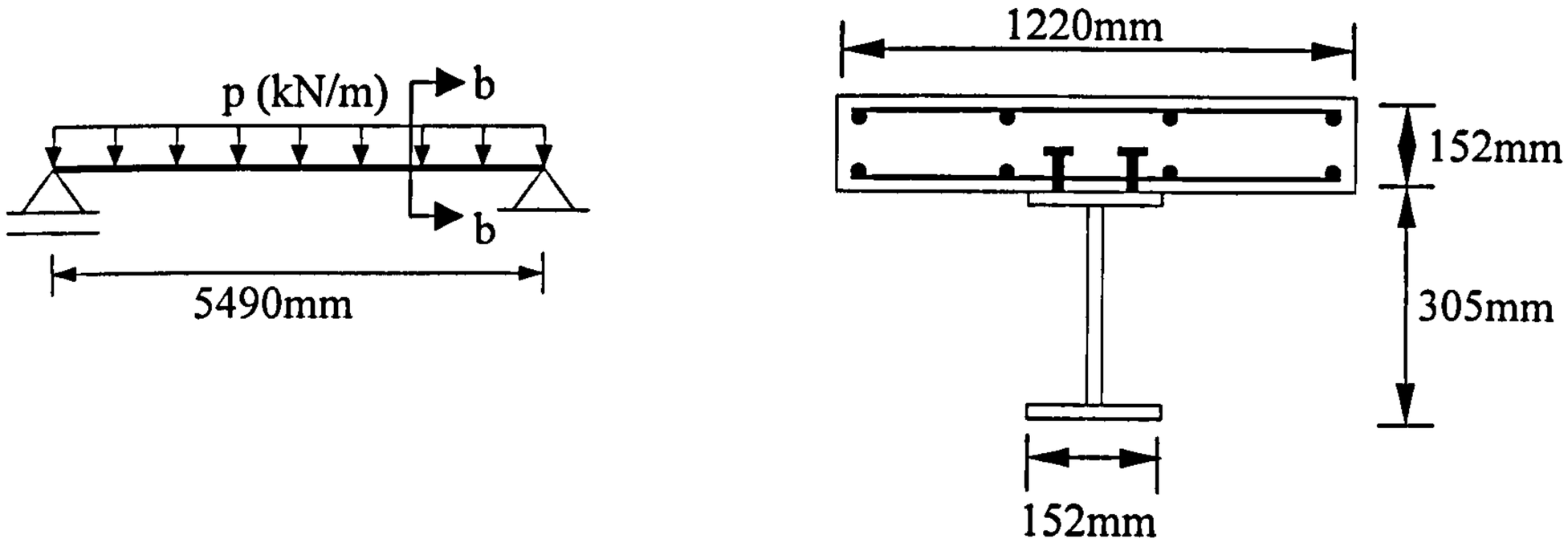

Figure 7.4.b Layout and cross section of beam B2

7.4.1 Finite element mesh Beams B1 and B2

Figure 7.5 shows the finite element mesh used to represent the composite girders B1 and B2. The three-dimensional eight-node solid element (C3D8), available in ABAQUS element library and shown in figure 7.5, is used to model both steel beam and concrete slab elements. At the beginning different finite element meshes were examined to chose the most appropriate one that gives adequately accurate results and takes less time in the solution process. Because of symmetry, only half of the beam is modelled. The concrete slab is divided into 24 elements along X-direction, 8 elements along Y-direction and 1 elements along Z-direction to avoid local failure. The shear connector is represented by a non-linear spring as explained earlier with a load-slip relationship taken from the FE modelling of push-off test with the same stud diameter. The flange of the steel beam is divided into 24 elements along X-direction, 6 elements along Y-direction and one element in Z-direction. The web of the steel beam is divided into 24 elements along X-direction, 2 elements along Y-direction and 2 elements in Z-direction.

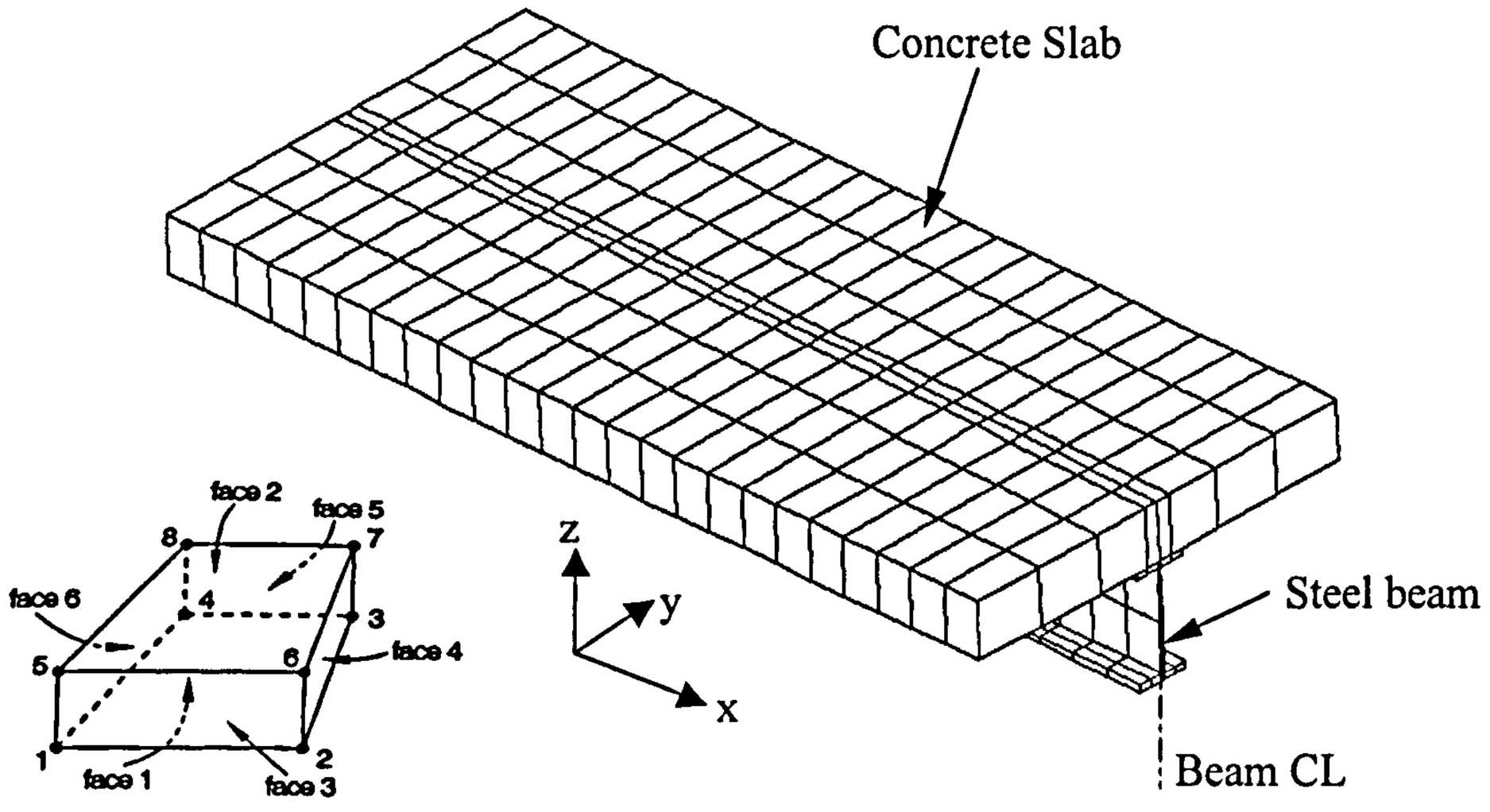

C3D8 element

Figure 7.5 Finite element mesh of beams B1 and B2

7.4.2 Boundary conditions

For the application of the supports and boundary conditions on beams B1 and B2, all nodes of concrete slab and the steel beams in the symmetry surface passing through the middle of

beams are restricted to move in X and Y directions as shown in figures 7.6 and 7.7. The support is allowed to move in X-direction and prevented to move in Y and Z directions.

7.4.3 Application of load

A static concentrated load is applied at the middle of the composite girder B1 as shown in Figure 7.6. Uniformly distributed loads are applied at the middle surface of the concrete slab of the composite girder B2 as shown in figure 7.7. The loads are applied using the modified RIKS method available in the ABAQUS[2] software. The basic algorithm of this method is Newton method in which, the solution is obtained as a series of increments with iterations to obtain equilibrium within each increment. The RIKS method is generally used to predict unstable and non-linear collapse of a structure. It uses the load magnitude as an additional unknown and solves simultaneously for loads and displacements. Therefore, another quantity must be used to measure the progress of the solution. ABAQUS[2] uses the arc length along the static equilibrium path in load-displacement space. An initial increment of displacement is given on the data line and the initial load proportionality factor is equal to this initial increment using the automatic incremental scheme. This initial increment will be adjusted if the increment fails to converge. From then on, the value of load after each increment is computed automatically. The solution ends either by specifying the maximum value of the load or a maximum displacement value at a specified degree of freedom.

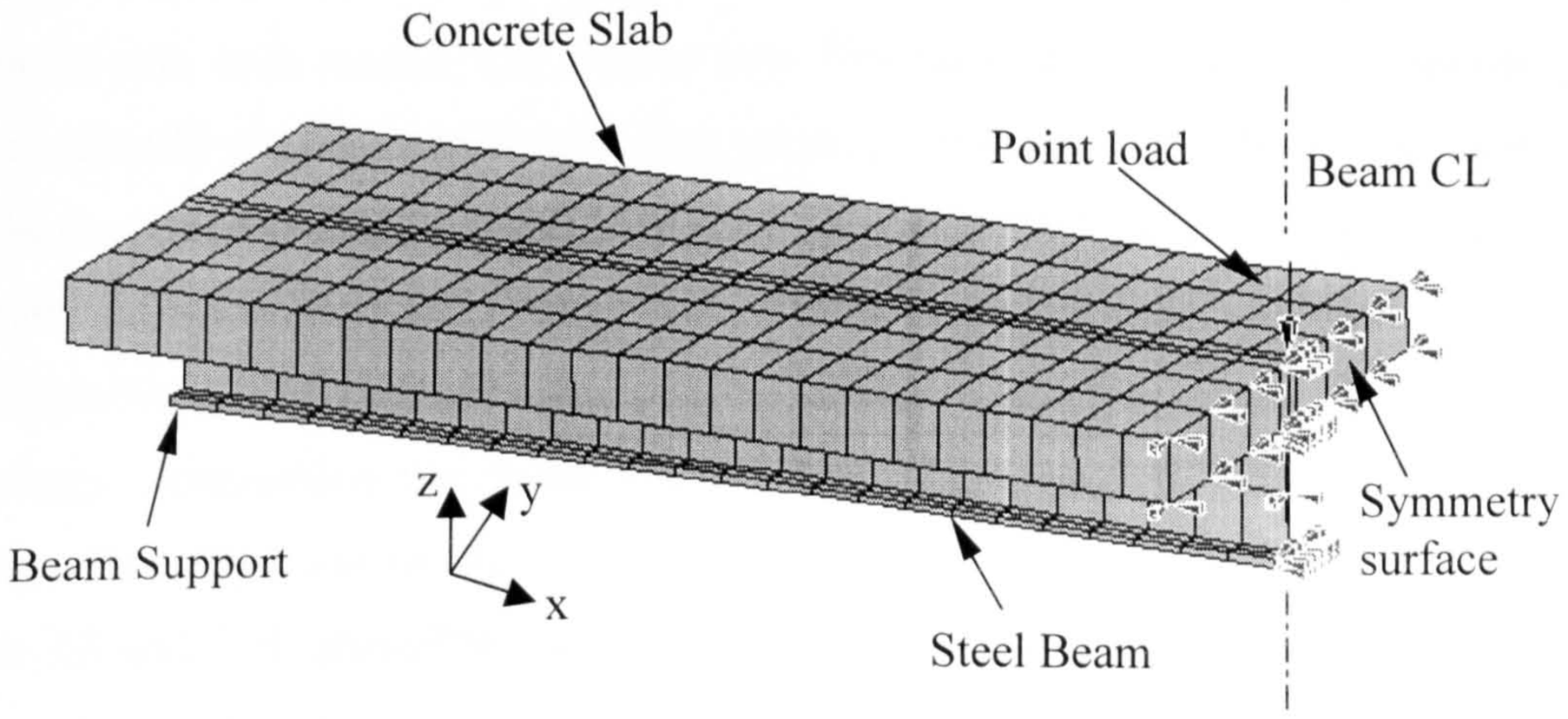

Figure 7.6 Application of load and boundary conditions on beam B1

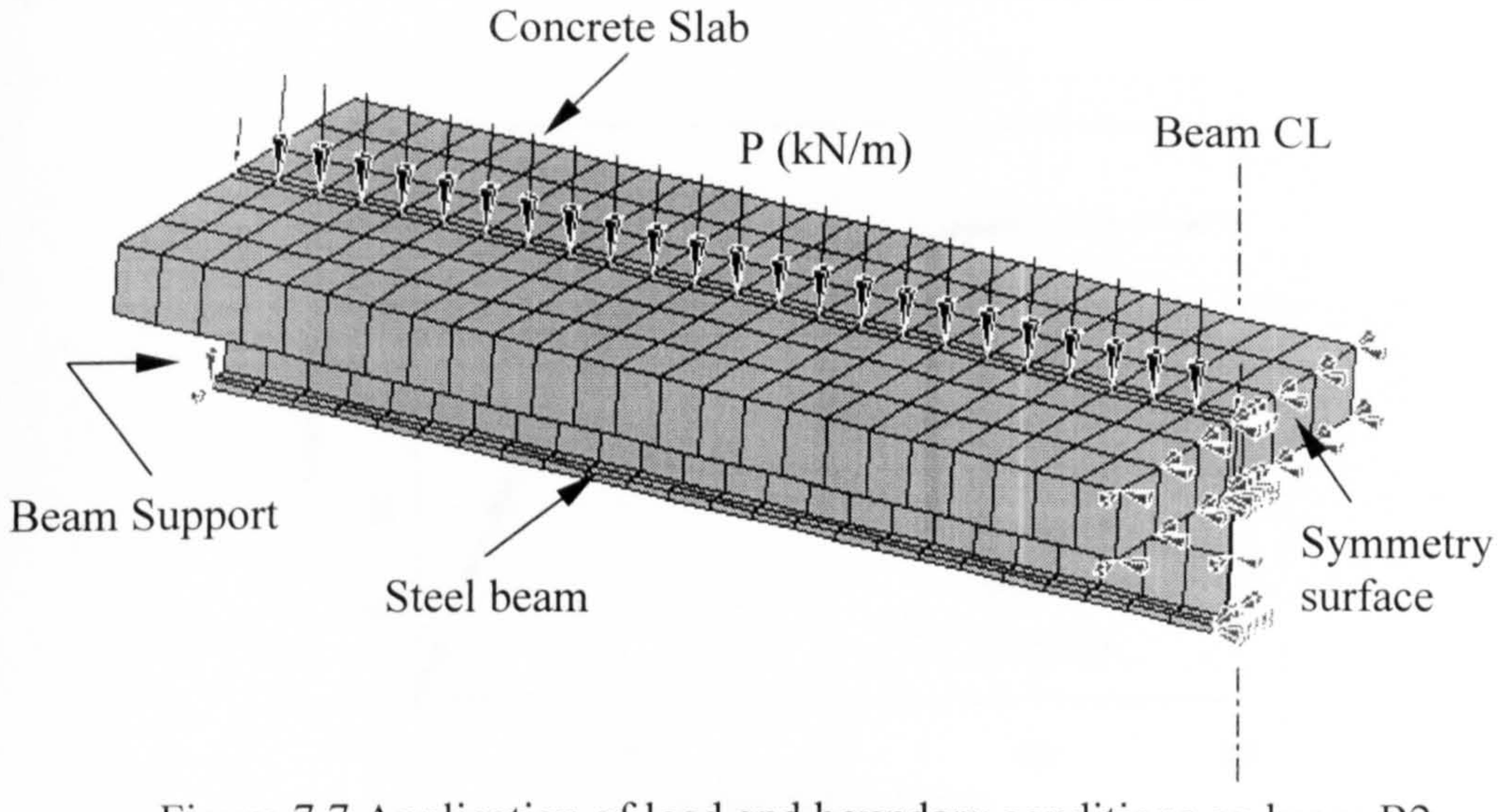

Figure 7.7 Application of load and boundary conditions on beam B2

7.4.4 Results and discussions

The present load versus mid-span deflection curves of beams B1 and B2 are compared with the earlier experimental results carried by Chapman[53] and with the analytical solution of Gattesco[52] as well. Also the bending stress distribution over the beam at failure and the displaced shape obtained from the present FE solution are presented.

7.4.4.1 Simply supported beam B1

Figure 7.8 shows the load-deflection curve at the mid-span of beam B1 obtained from the present FE solution. The results are plotted in comparison with the experimental results published by Chapman[53] and the analytical solution of Gattesco[52]. The figure shows good agreement with both results. The output data files have shown that the composite girder behaved linearly elastic up to 213kN with mid-span deflection of 8.5mm. The first tensile crack in the concrete elements occurred at a load of 316.72kN with mid span deflection of 13.09mm. At a load of 496kN maximum stress of concrete slab was reached. The steel beam elements at mid span did not reach its yielding stress. The maximum shear force in the springs representing the studs was 42.3kN (approximately 86% of the maximum capacity of the shear stud used).

Figures 7.9 and 7.10 show the distribution of bending stresses and the displaced shape at failure respectively. The stress distribution is plotted in a range from ($+32N/mm^2$) to ($-32N/mm^2$) to show the contour stresses within the concrete slab. It can be shown that the top surface of concrete slab elements at the middle of the composite beam reached its maximum strength. Mode of failure was concrete failure.

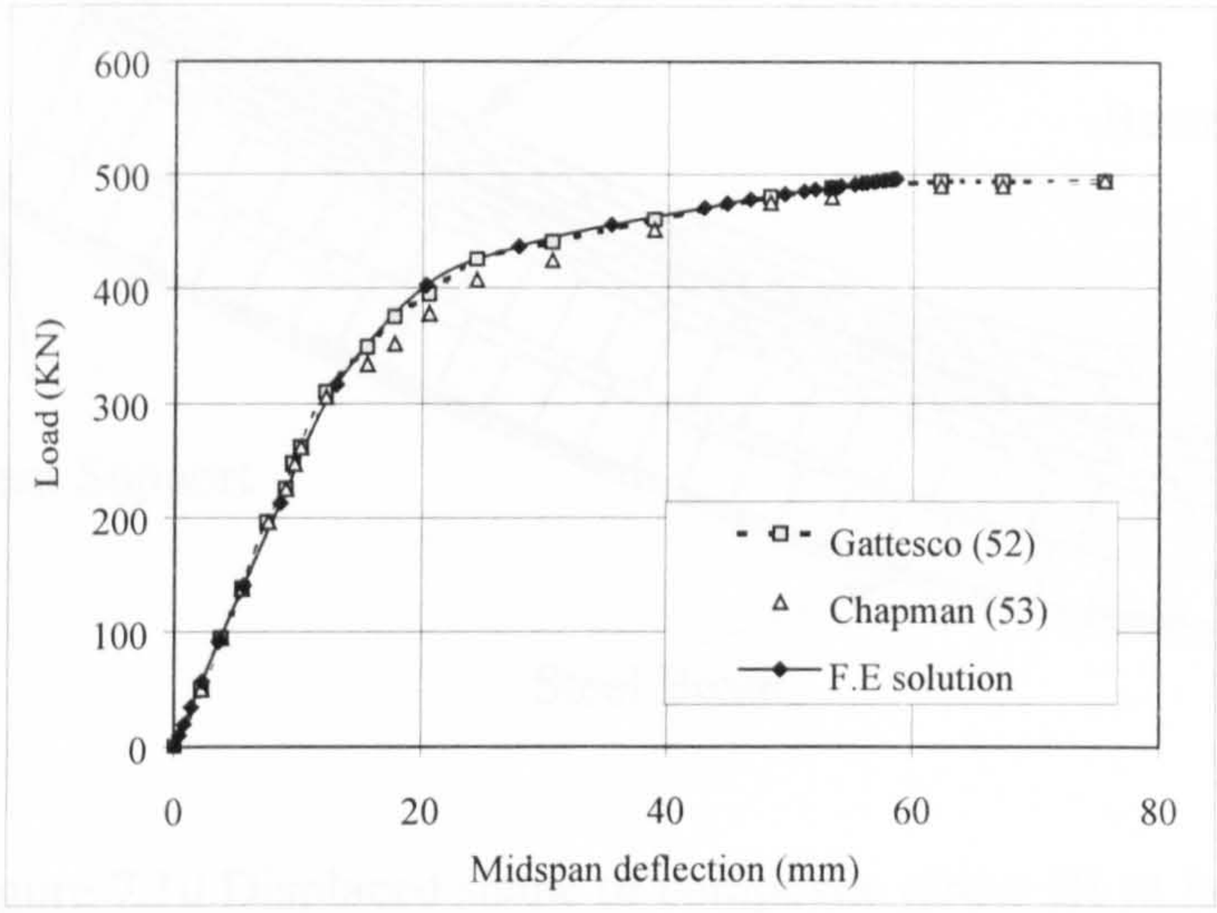

Figure 7.8 Load versus mid-span deflection of composite girder B1

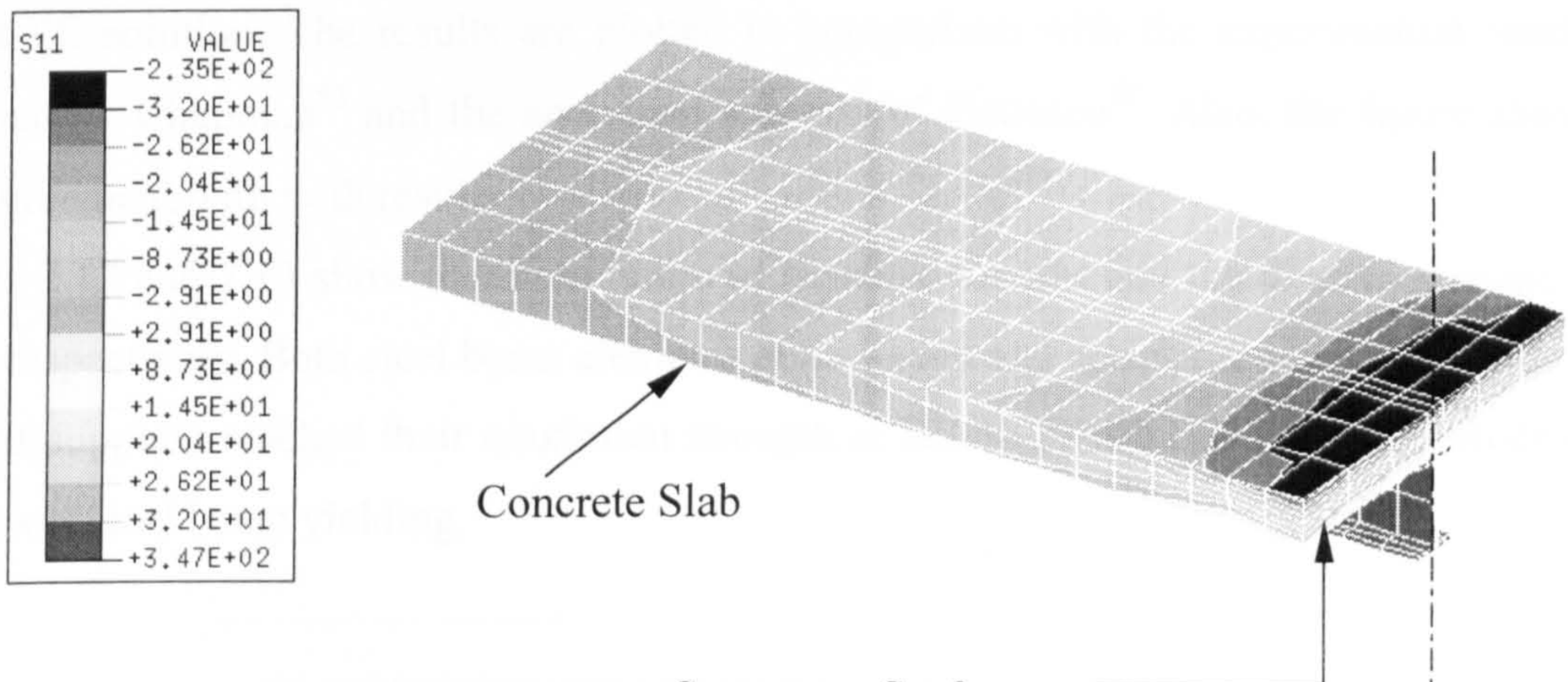

Figure 7.9 Distribution of bending stresses over composite girder B1 at failure

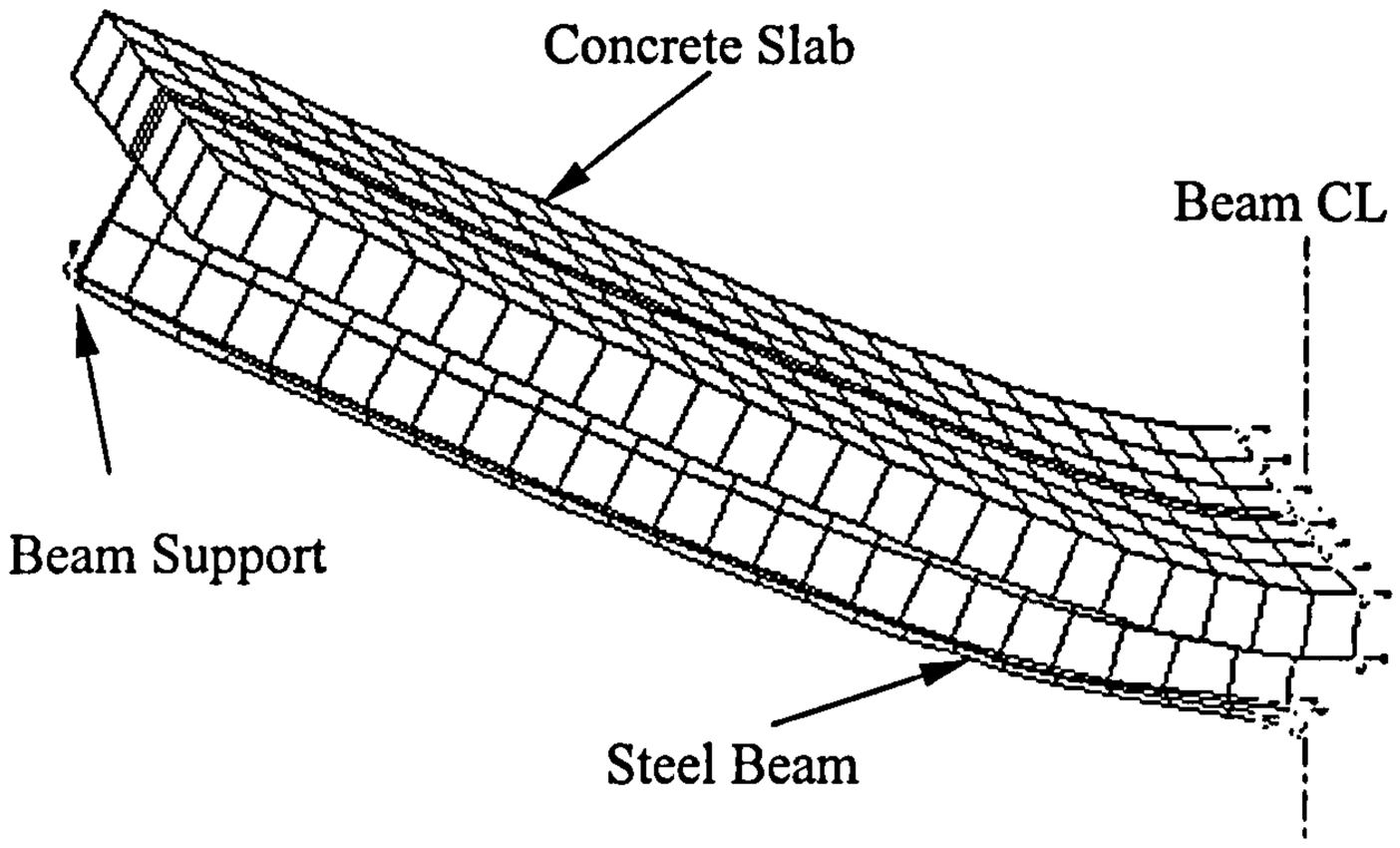

Figure 7.10 Displaced shape of composite girder B1 at failure

7.4.4.2 Simply Supported beam B2

Figure 7.11 shows the load-deflection curve at the mid-span of beam B2 obtained from the present FE solution. The results are plotted in comparison with the experimental results published by Chapman[53] and the analytical solution of Gattesco[52]. Also, the figure shows good agreement with both results.

Figures 7.12 and 7.13 show the distribution of bending stresses and the displaced shape at failure respectively. Both steel beam elements at mid-span and springs representing studs at and near supports reached their maximum strength at failure before concrete slab. Mode of failure was steel beam yielding.

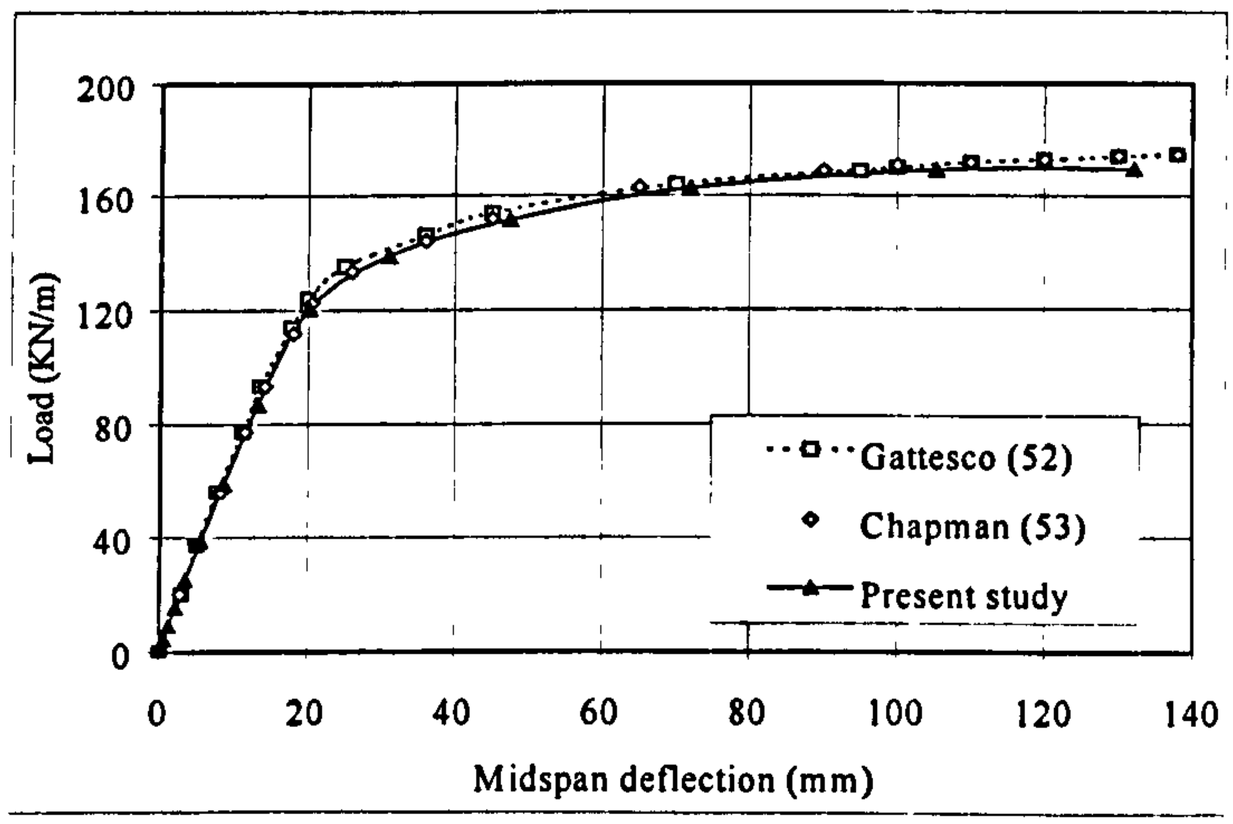

Figure 7.11 Load versus mid-span deflection of composite girder B2

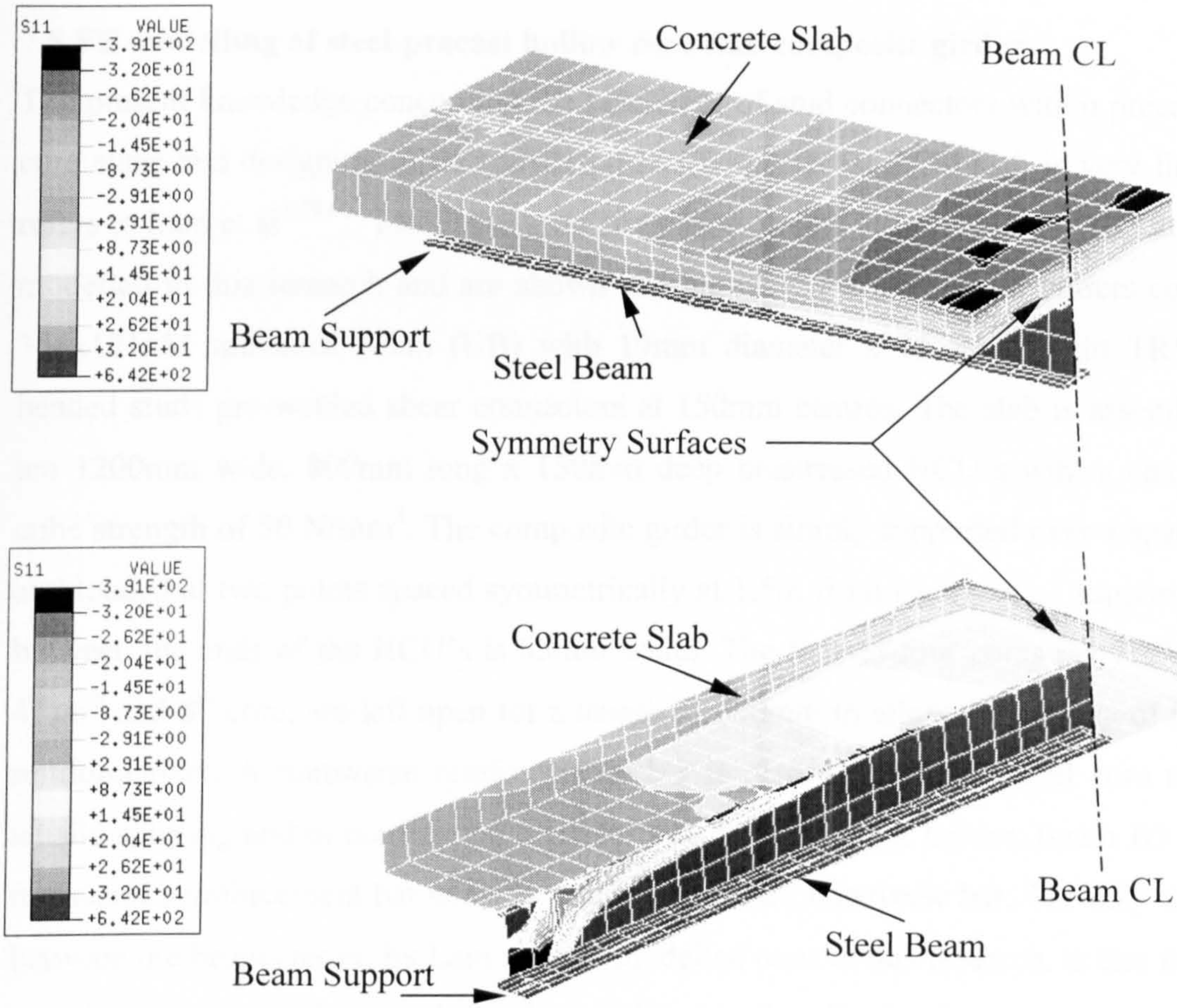

Figure 7.12 Distribution of bending stresses over composite girder B2 at failure

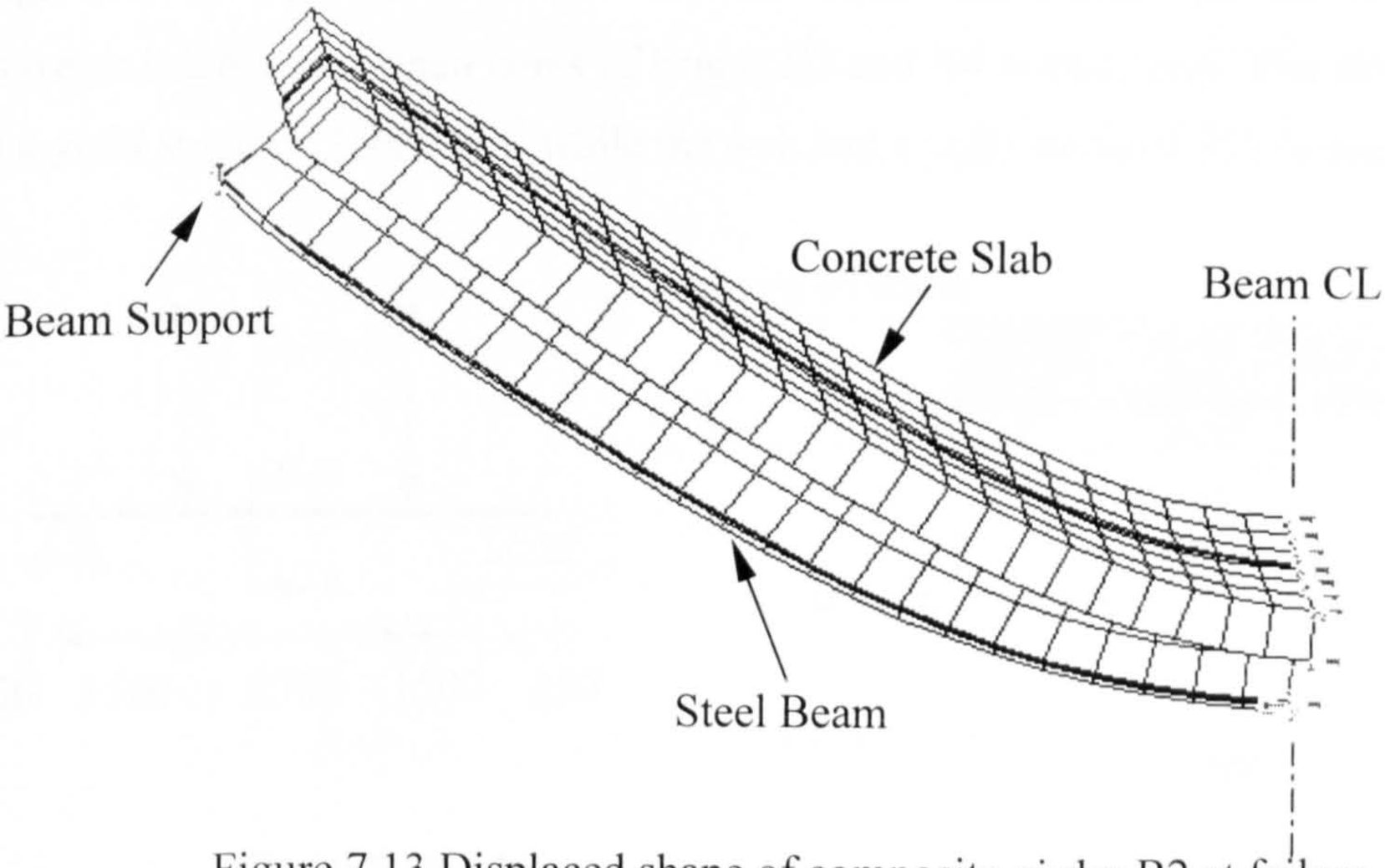

Figure 7.13 Displaced shape of composite girder B2 at failure

7.5 FE modelling of steel-precast hollow core slab composite girders

The present knowledge concerning the behaviour of stud connectors within precast hollow core slabs and designing of composite girders with precast HCU slab is very limited and refers to Lam et al[1,59,60]. Two 6.0m span composite girders tested by Lam[59] (B3 and B4) are modelled in this research and are shown in figure 14. The composite girders consist of a 356x171x51 universal beam (UB) with 19mm diameter x 125mm height TRW-Nelson headed studs pre-welded shear connectors at 150mm centres. The slab is assembled from ten 1200mm wide, 800mm long x 150mm deep prestressed HCU's with a characteristic cube strength of 50 N/mm^2. The composite girder is simply supported over a span of 5.7m and loaded at two points spaced symmetrically at 1.5m from each end of support. The gap between the ends of the HCU's is 65mm width. The tops of four cores per HCU, i.e. 2nd, 4th, 6th and 8th core, are left open for a length of 500mm to allow the placing of transverse reinforcement. A transverse reinforcement bar is placed in each opened core to prevent tensile splitting and to confine the concrete slab from splitting failure. Beam B3 has 8mm transverse reinforcement bar while beam B4 has 16mm transverse bar. The only difference, between the beams tested by Lam and the modelled ones in this research, is that the HCU's used in present modelling of the girder are those used earlier by the authors in Ref. 59 with square ends and 9 cores instead of tapered ends with 11 cores. Figure 7.14 shows a typical HCU, supplied by Bison Floor Ltd., simulated in the present study. In-situ concrete with design cube strengths of 26N/mm^2 and 32 N/mm^2 are placed into the longitudinal and transverse joints and opened cores of beams B3 and B4 respectively. The steel beam flange had a yield stress of 310N/mm^2 while the web had a yield stress of 355 N/mm^2.

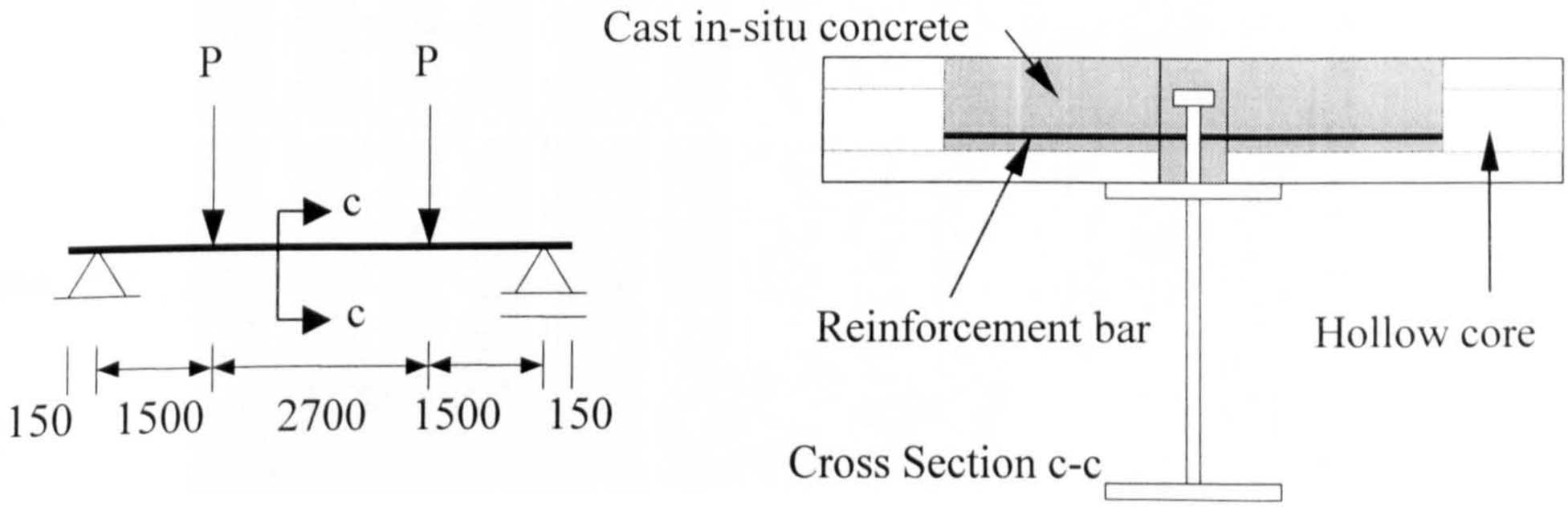

Figure 7.14.a Layout and cross section of beams B3 and B4

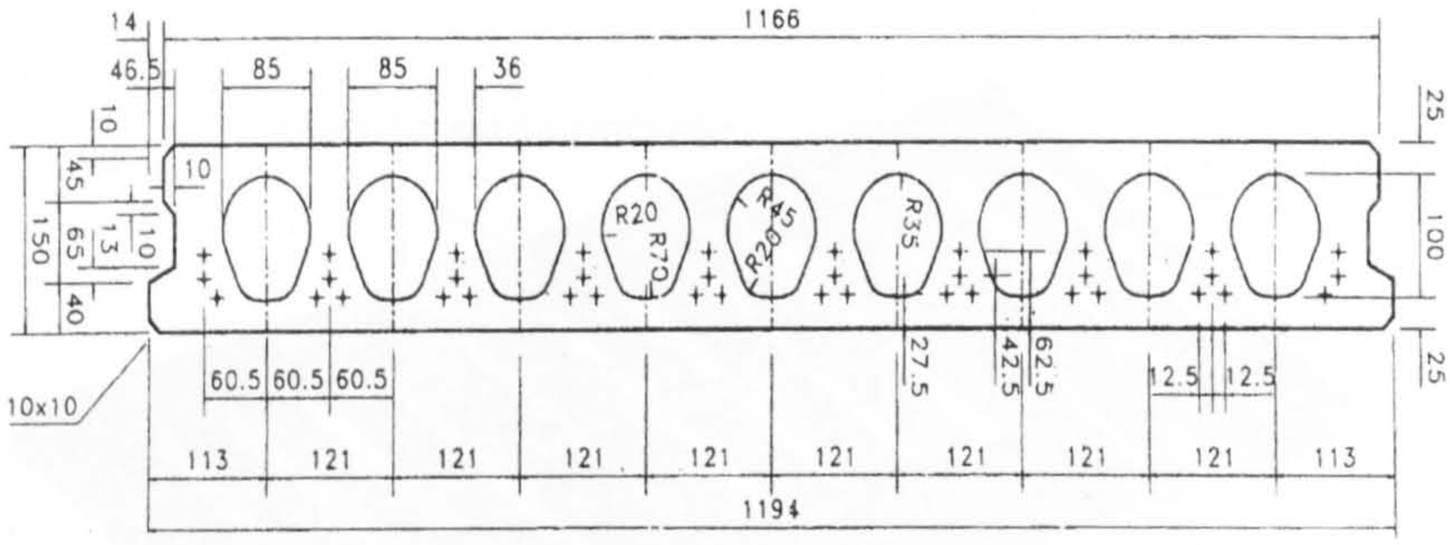

Figure 7.14.b Details of a typical 1200mm length HCU

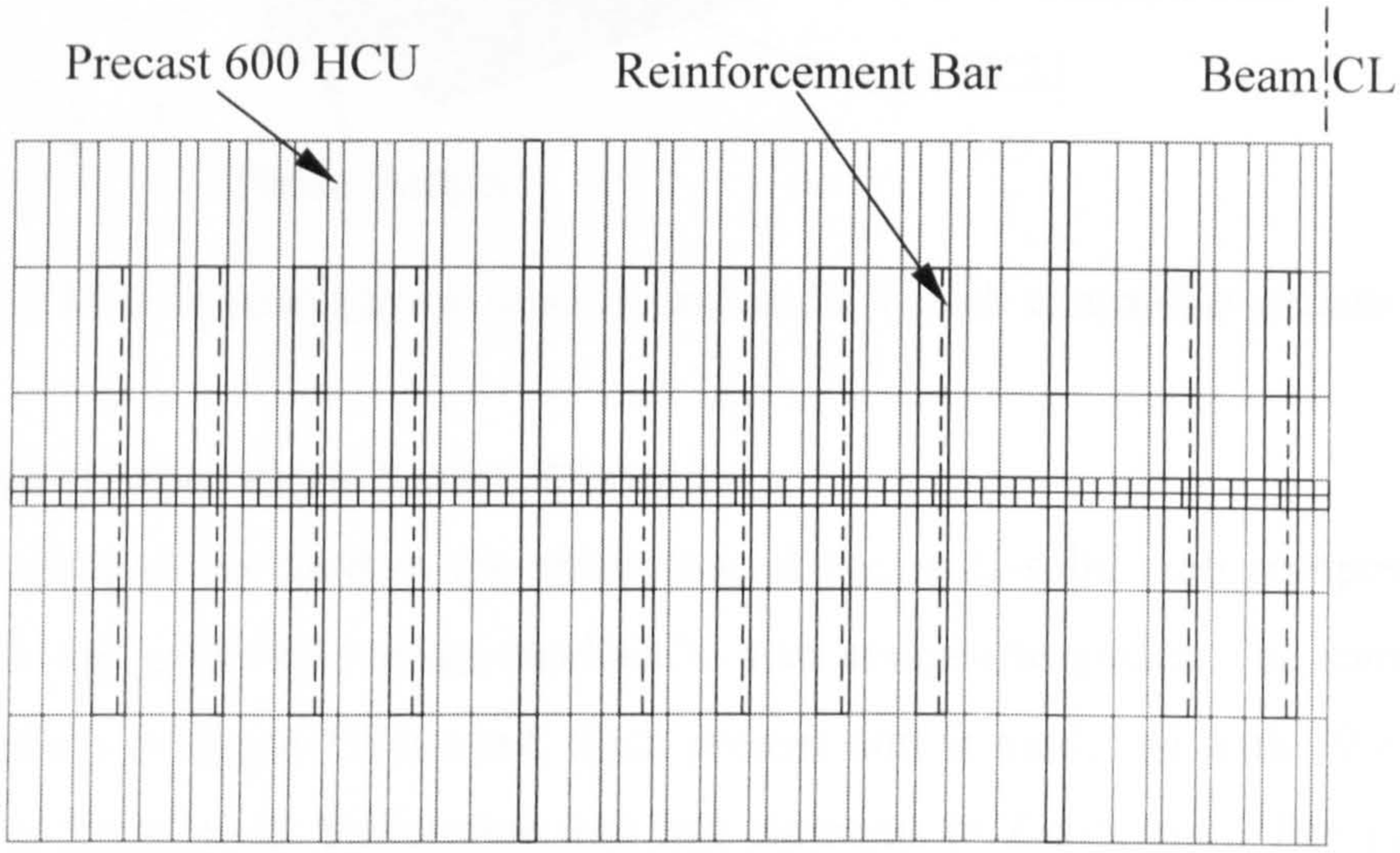

Figure 7.14.c Plan view of the FE mesh with reinforcements for beams B3 and B4

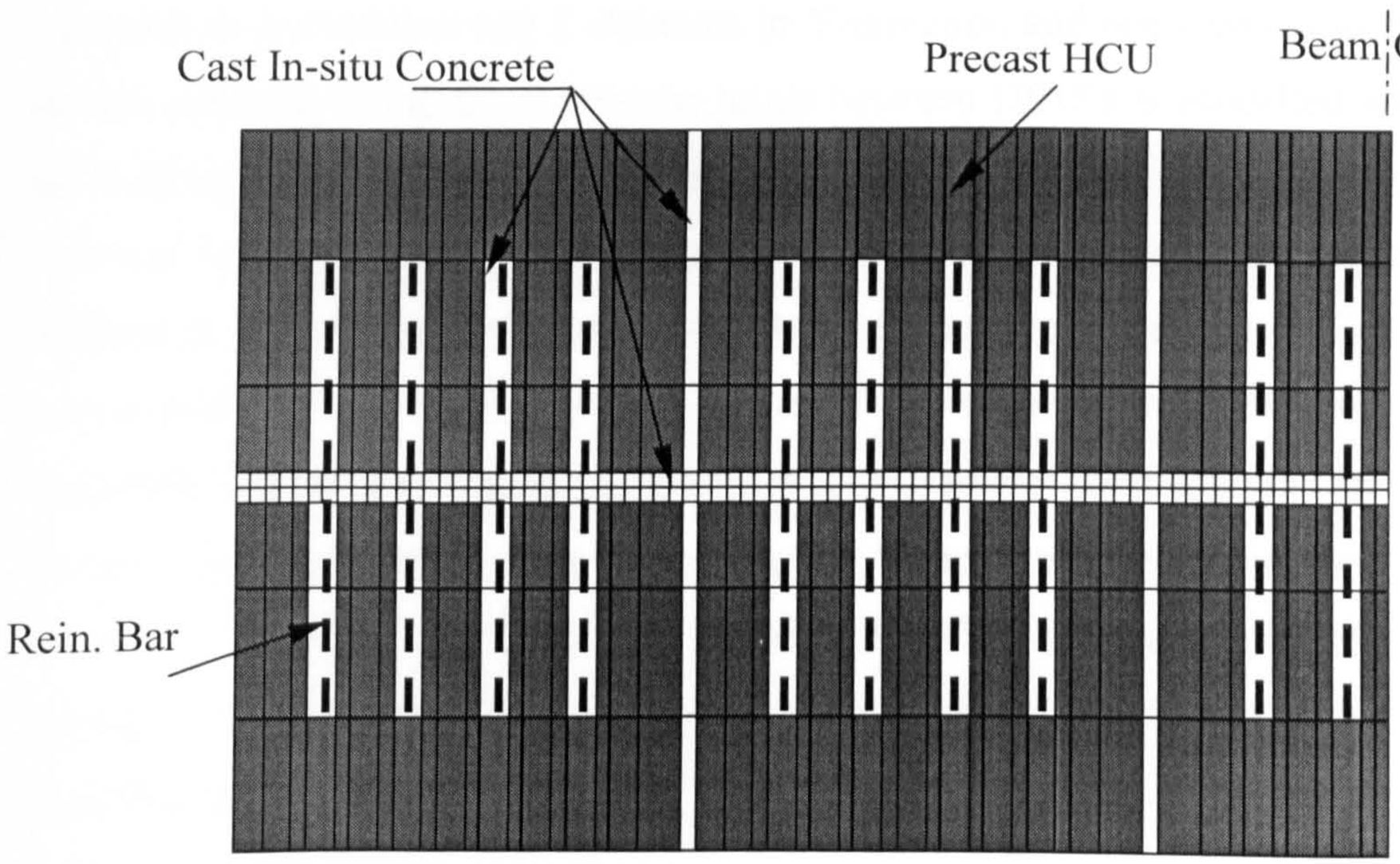

Figure 7.14.d Plan view of the elements of beams B3 and B4

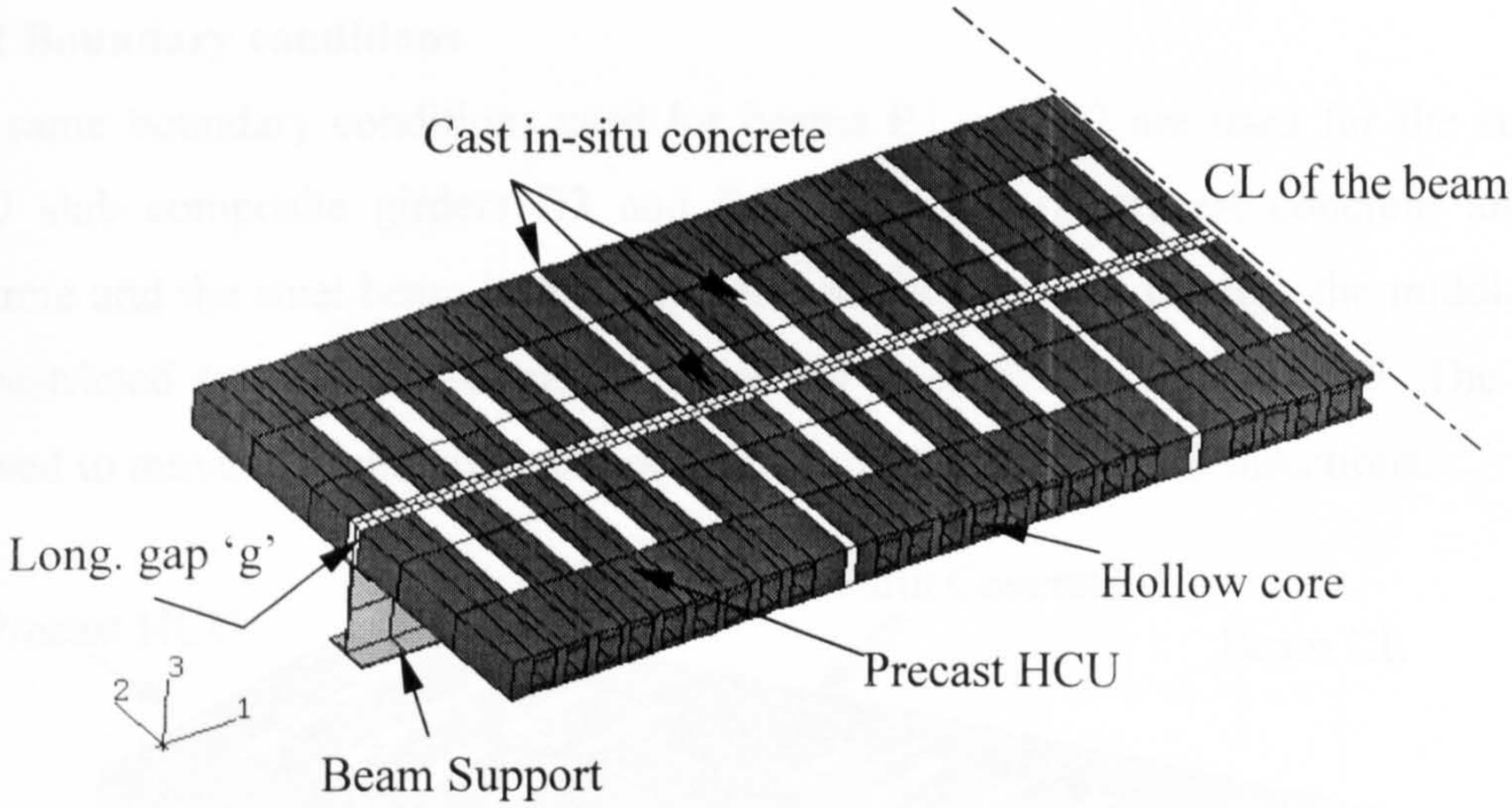

Figure 7.14.e General Layout of steel-precast HCU slab composite girders B3 and B4

7.5.1 Finite element mesh Beams B3 and B4

The same procedures used in the modelling of the steel-solid slab composite girder are followed in the modelling of the steel-HCU slab composite girder. The same FE element (C3D8) shown in figure 7.5 is used. Each precast unit is modelled with 19 elements in X-direction, 3 elements in Y-direction and two elements in Z-direction. The in-situ concrete filling the gap 'g' between the HCU's in the longitudinal direction is modelled with 80 elements in X-direction and 2 elements in Y-direction and one element in Z-direction. The in-situ concrete filling the transverse joints between HCU's is modelled with one element in X-direction, 6 elements in Y-direction and one element in Z direction. The in-situ concrete filling each opened core and contains the reinforcement bar is modelled with one element in X-direction, two elements in Y-direction and one element in Z-direction. Figures 7.14.d and 7.14.e show the general layout of the beam mesh. Each reinforcement bar is modelled individually using the (*REBAR) parameter available in ABAQUS element library. The reinforcement bar is crossing the in-situ concrete within the opened core and the gap 'g' as shown in figures 7.14.c and 7.14.d. The studs are modelled with non-linear springs as explained earlier and the positions of each stud coincide with their actual positions in the beam test carried by Lam[59]. The non-linear load-slip behaviour of the stud, for both beams of 8mm and 16mm transverse reinforcement bars, are taken from modelling of stud connectors explained in chapter 4.

7.5.2 Boundary conditions

The same boundary conditions used for beams B1 and B2 are used for the steel-precast HCU slab composite girders B3 and B4. All nodes of precast concrete units, in-situ concrete and the steel beam in the symmetry surface passing through the middle of beams are restricted to move in X and Y directions as shown in figures 7.15. The support is allowed to move in X-direction and prevented to move in Y and Z directions.

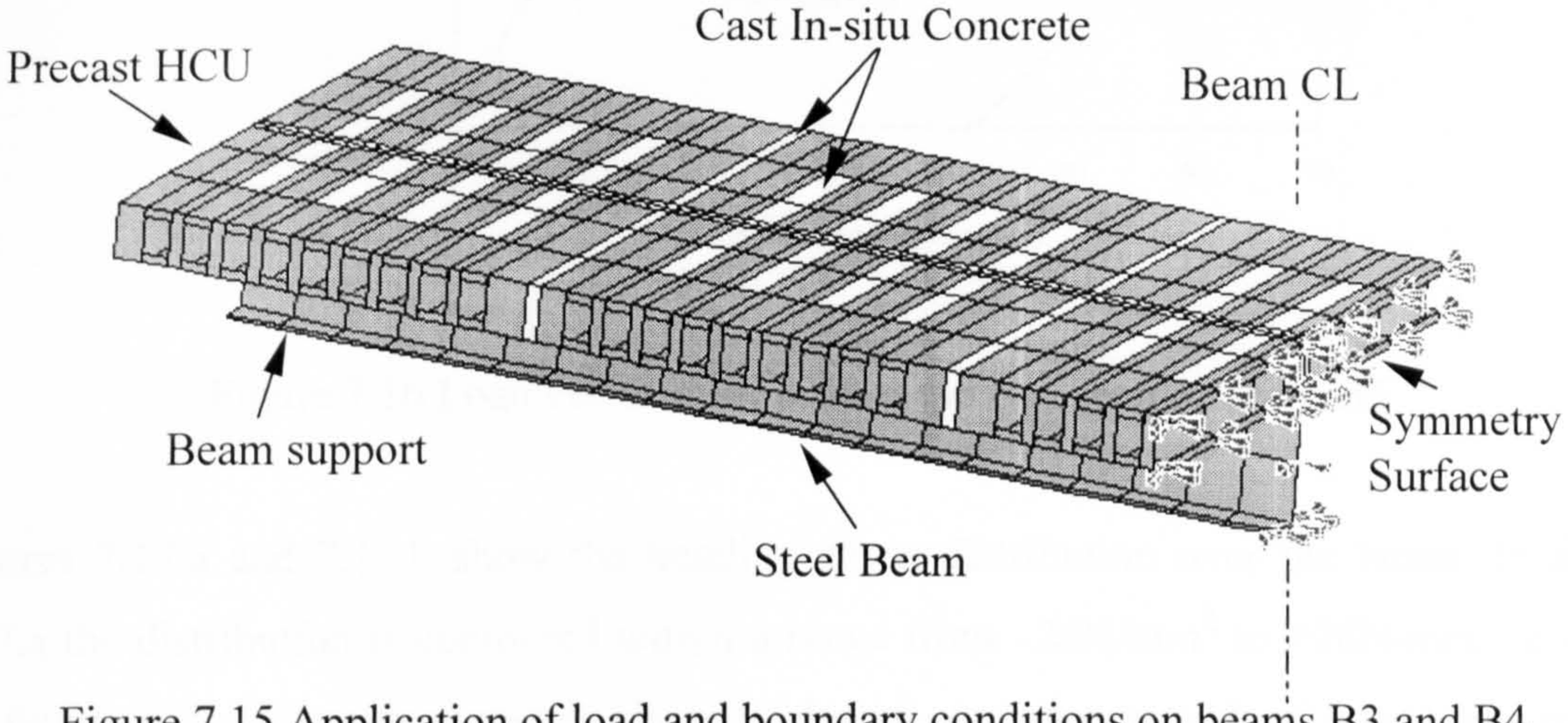

Figure 7.15 Application of load and boundary conditions on beams B3 and B4

7.5.3 Application of load

Also, the same load procedures used with beams B1 and B2 are followed and a static concentrated load is applied at the same position of the tested beam using the RIKS method available in the ABAQUS software.

7.5.4 Results and discussions of Beam B3

The load versus mid-span deflection curve obtained from the present FE study for beam B3 is compared with the experimental results obtained by Lam[59] as shown in figure 7.16. The curve shows good agreement between both FE solution and experimental results. The FE solution shows that the composite beam remained elastic up to 167kN with a mid-span deflection of 10.8mm compared with 170kN and 11.0mm respectively in Lam results. The experimental maximum load was 315kN with 33.7mm deflection at mid span compared with 321.8kN load with 33.35mm deflection obtained from finite element solution.

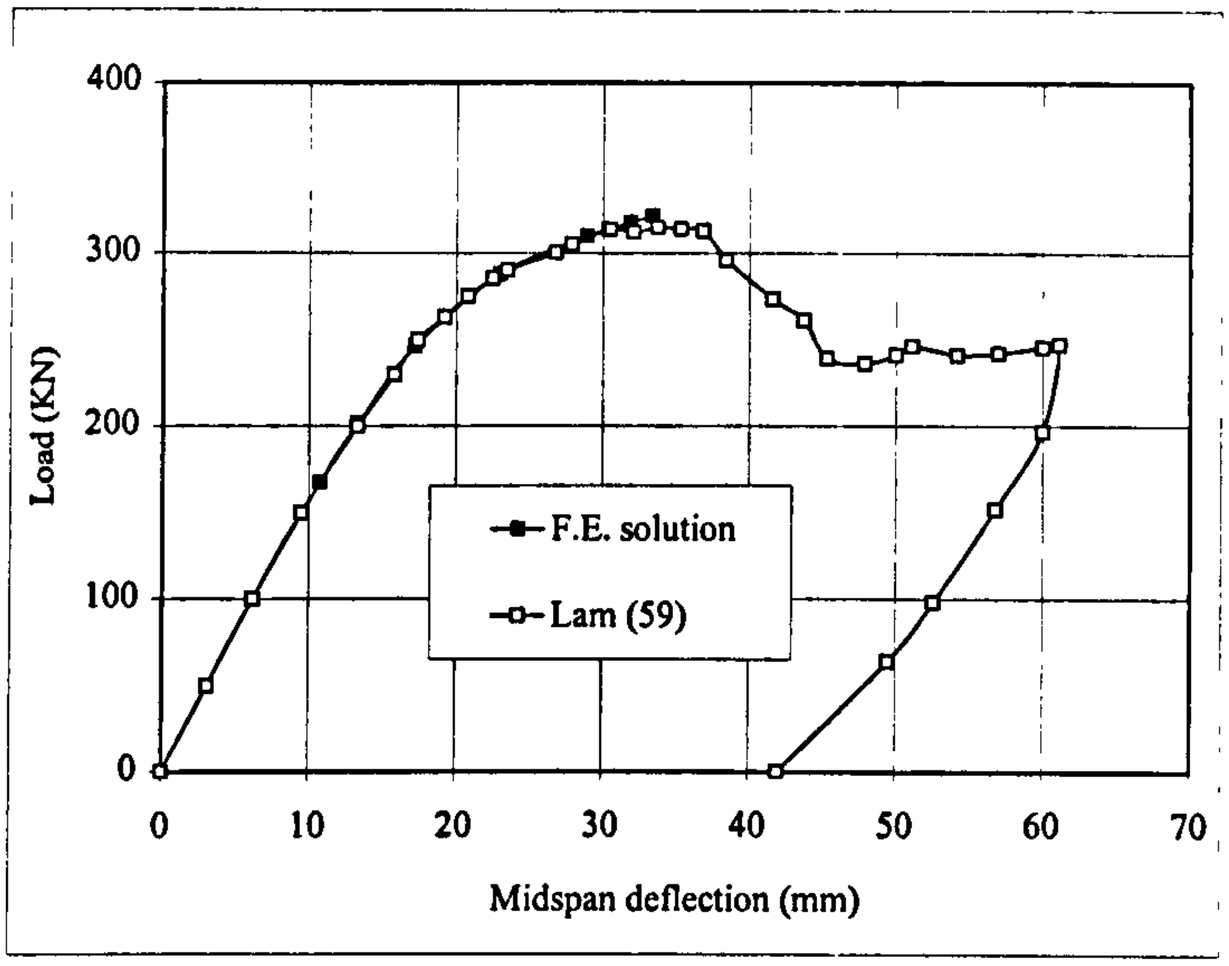

Figure 7.16 Load versus deflection at the mid span of beam B3

Figures 7.17.a and 7.17.b show the bending stress distribution over the beam. In figure 7.17.a the distribution is contoured within a range from $-26N/mm^2$ to $+26N/mm^2$ to show the failure in the concrete elements since the design concrete strength of in-situ concrete in the tested beam was $26N/mm^2$. On the other hand, figure 7.17.b shows the distribution over a range from $-26N/mm^2$ to $+310N/mm^2$ to show the failure in the steel beam elements since the ultimate tensile strength of the flange is $310N/mm^2$. At a load of 246kN with a mid-span deflection of 17.2mm, the data files have shown that the concrete elements in the middle of the beam developed some tensile cracks at bottom surface of concrete elements. By increasing the load, maximum compressive stress of concrete elements was reached at top surface as shown from figure 7.17.a. Failure of concrete elements was recorded at a load of 321.8kN. This was accompanied by yielding of the steel beam elements at the middle of the beam since the steel beam carried the applied load after concrete failure. The maximum shear load in the springs representing the studs was ~ 68kN (which is approximately 97% of the maximum shear capacity of the stud) in the springs between the loading point and the supports. The maximum slip in the springs was 1.6mm near supports at failure. Mode of failure is concrete yielding mode.

Figure 7.18 shows the deformed shape of the beam B3 at failure as plotted from the ABAQUS post processing.

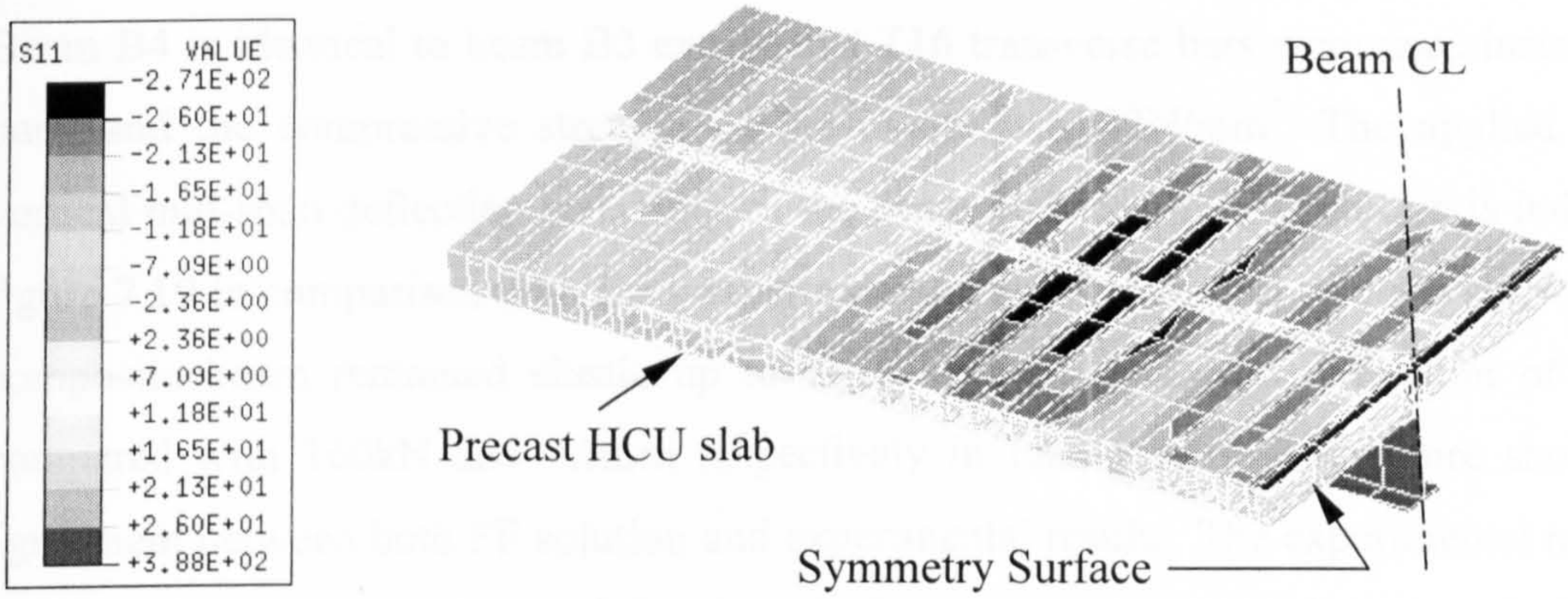

Figure 7.17.a Distribution of bending stresses over composite girder B3 at failure

(Stress ranges from $-26N/mm^2$ to $+26N/mm^2$)

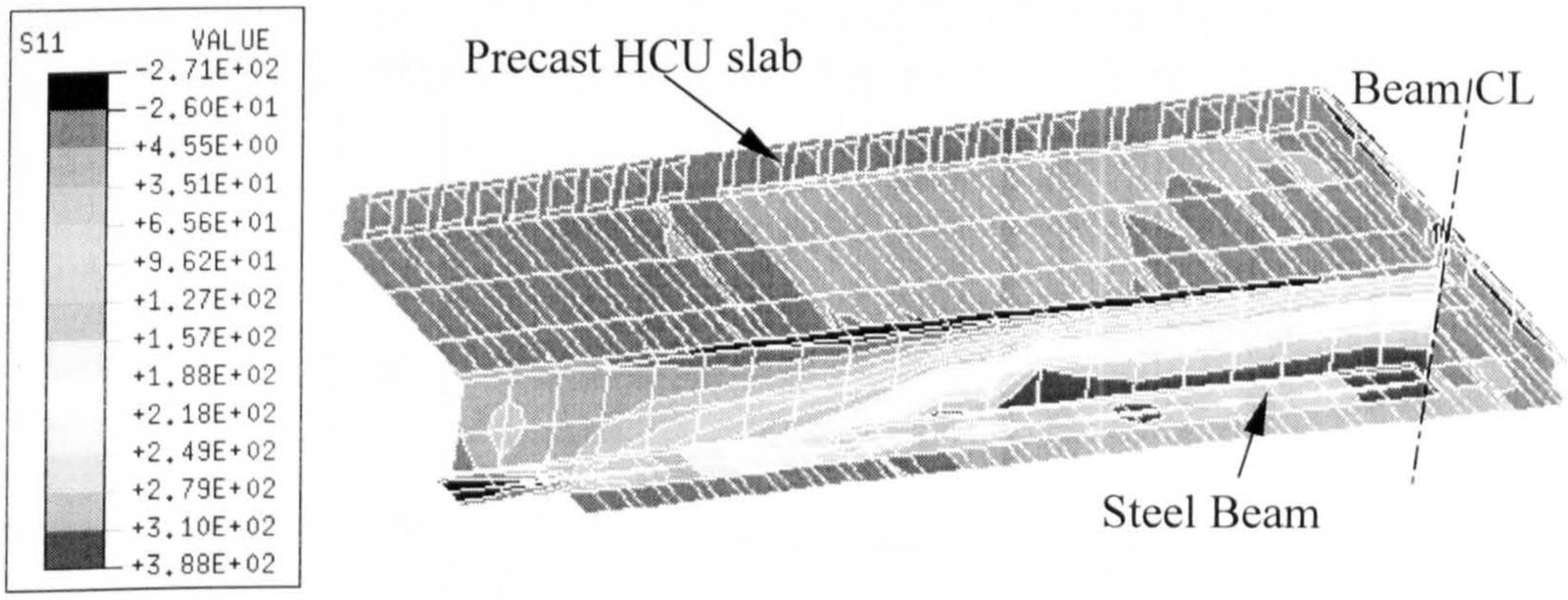

Figure 7.17.b Distribution of bending stresses over composite girder B3 at failure

(Stress ranges from $-26N/mm^2$ to $+310N/mm^2$)

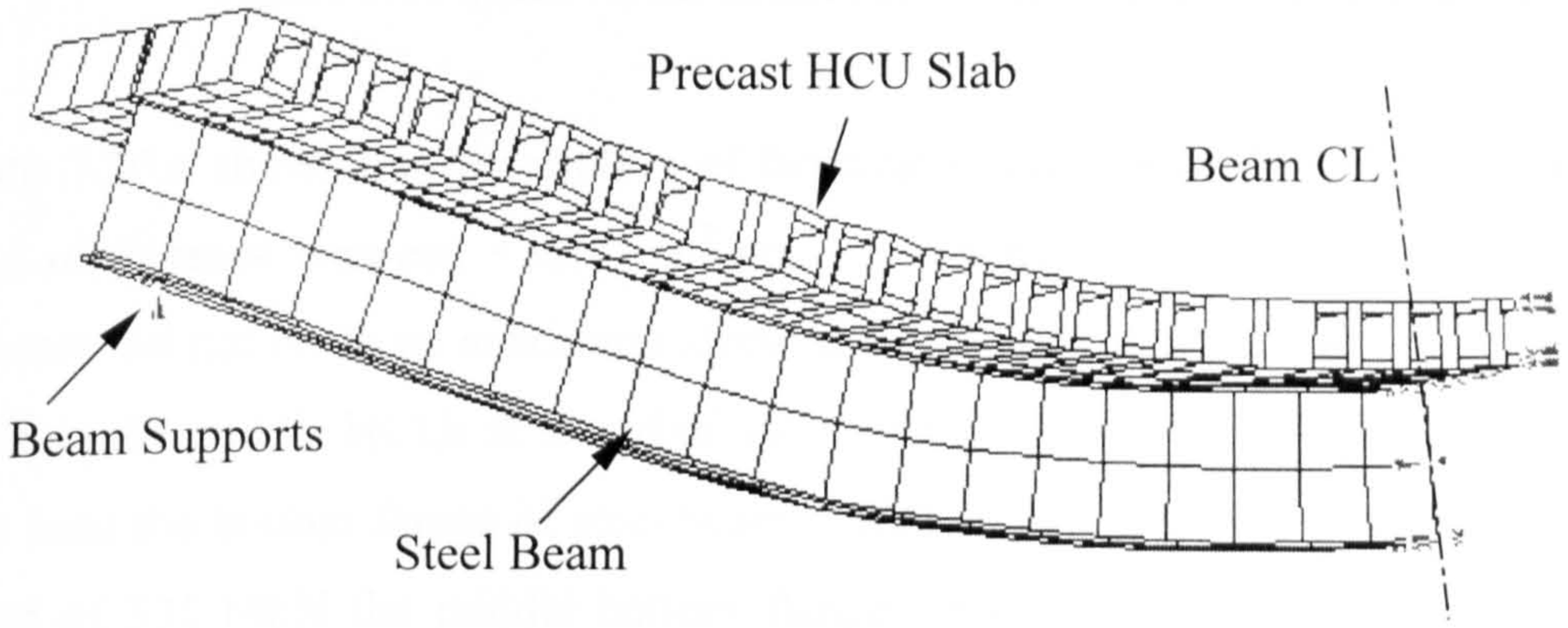

Figure 7.18 Displaced shape of composite girder B3 at failure

7.5.5 Results and discussions of Beam B4

Beam B4 is identical to beam B3 except that T16 transverse bars were used instead of T8 bars, and the compressive strength of the in-situ was 32N/mm^2. The applied load vs. vertical mid-span deflection behaviour of the beam obtained by FE solution is indicated in figure 7.19 in comparison with Lam experimental results[59]. The FE solution shows that the composite beam remained elastic up to 167kN with a mid-span deflection of 10.5mm compared with 160kN and 9.0mm respectively in Lam results. The figure shows good agreement between both FF solution and experimental results. The experimental maximum load was 330kN at a mid-span deflection of 32.8mm while the FE failure load is 331.14kN at deflection of 34.1mm.

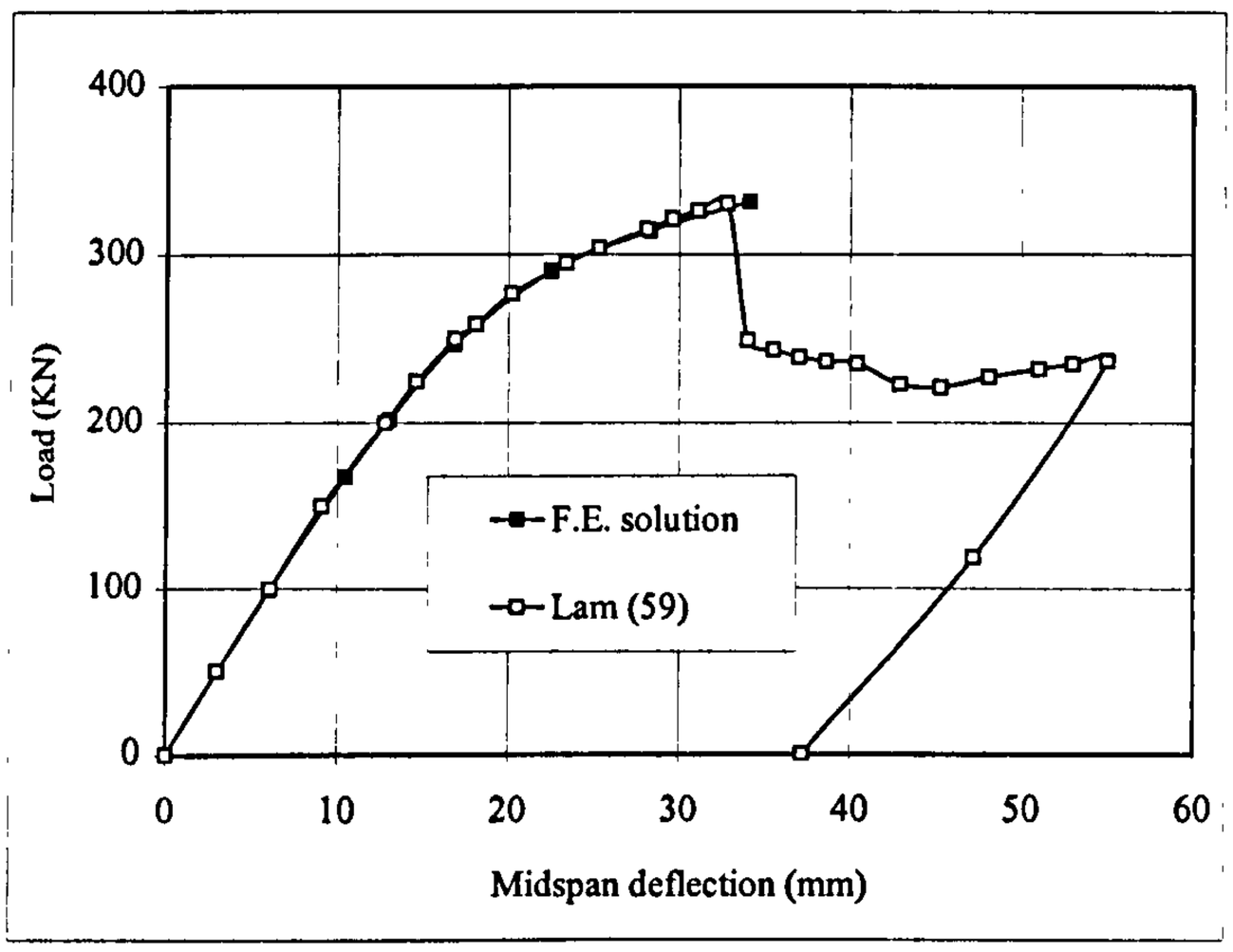

Figure 7.19 Load versus deflection at the mid span of beam B4

Figure 7.20.a shows the distribution of bending stresses over the composite girder for a range of stresses between +32N/mm^2 and –32N/mm^2. It can be seen that the concrete elements did not reach its maximum stress at failure although the data files indicated some cracks in the middle HCUs at a load of 247kN with a mid-span deflection of 17mm. At the same load the bottom flange of steel beam reached its yield stress, which is 310N/mm^2. At a load of 331.14kN the middle bottom flange elements completely yielded as shown in figure 7.20.b. The maximum stress in reinforcing bars was 55N/mm^2 which is far from its

maximum tensile stress. The maximum shear load in the springs representing the studs was ~ 80kN (which is approximately 90% of the maximum shear capacity of the stud) in the springs between the loading point and the supports. The maximum slip in the springs was 0.8mm at failure. Mode of failure is steel beam yielding mode.

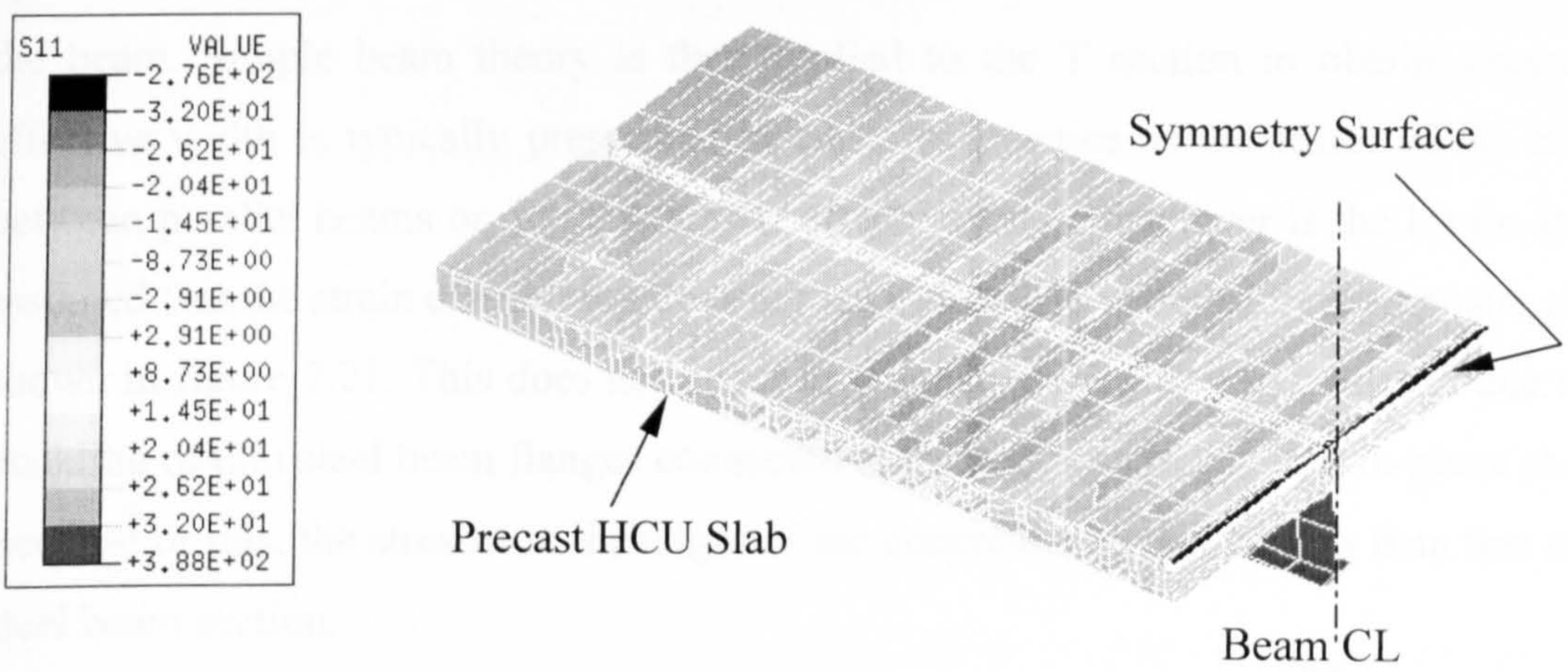

Figure 7.20.a Distribution of bending stresses over composite girder B4 at failure
(Stress ranges from $-32N/mm^2$ to $+32N/mm^2$)

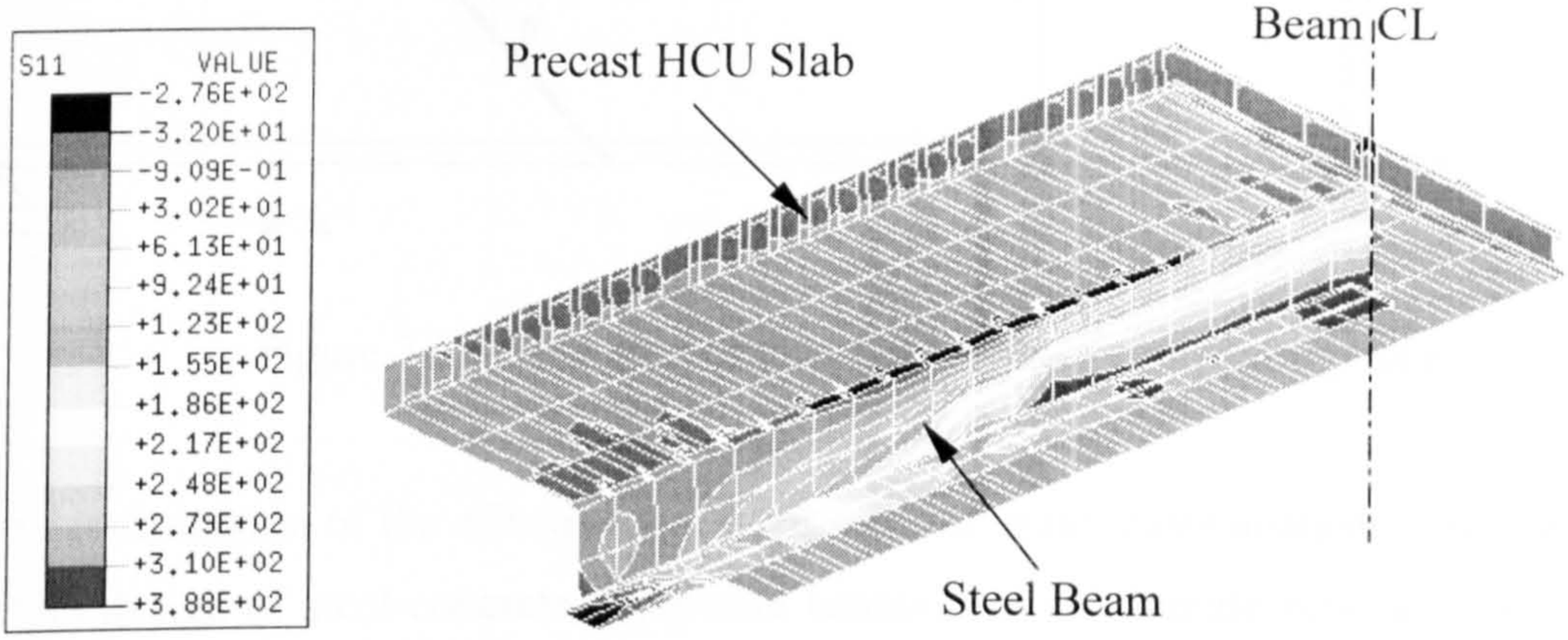

Figure 7.20.b Distribution of bending stresses over composite girder B4 at failure
(Stress ranges from $-32N/mm^2$ to $+310N/mm^2$)

7.6 Evaluation of the effective width of composite steel-HCU slab girders

7.6.1 Introduction

In design practice, composite action between the steel beam and the solid reinforced concrete slab is normally treated by the approximate method of assuming a T beam formed by the beam and an effective width of slab, usually assumed constant for the full length of the beam. Simple beam theory is then applied to the T section to obtain stresses. The effective width is typically prescribed in codes of practice as the lesser of the distances between parallel beams or one quarter the effective span whichever is the lesser. It is also assumed that the strain distribution does not vary along the width of the composite girder as shown in figure 7.21. This does not occur in practice, owing to nonlinearities due to post-buckling of thin steel beam flanges connected to the concrete slab and to in-plane shear lag. Because of this, the stresses at the edges of the concrete slab will be less than that over the steel beam section.

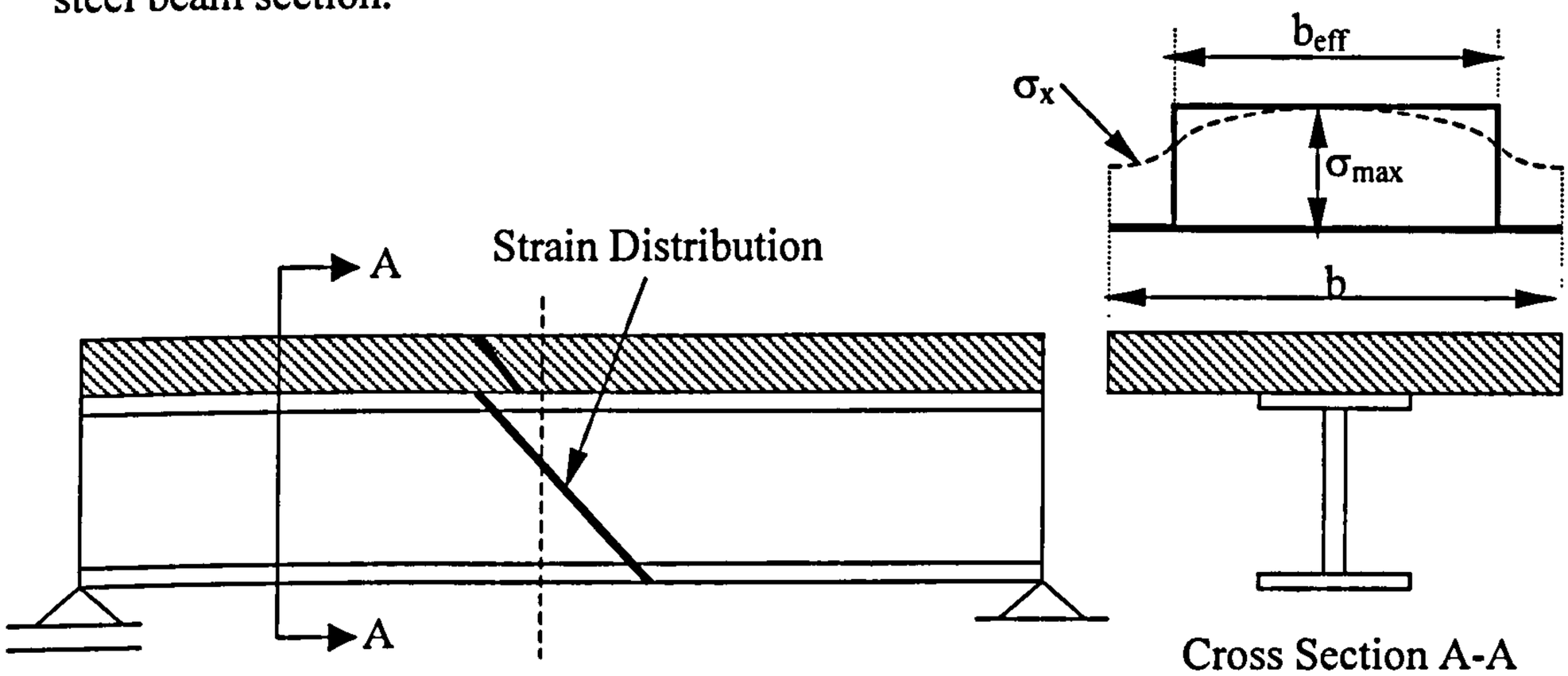

Figure 7.21 Definition of effective width of composite girder

The determination of the effective width for ultimate limit states analysis is on the basis of correct design of steel-concrete composite beams. For an ultimate state analysis, codes in general propose to use the same effective width as computed for an elastic analysis. In particular, Eurocode 4 expresses the effective width for elastic or plastic analysis as a function of the distance (L_o) between the points of zero bending moment ($b_{eff}=L_o/4$). This represents an evident approximation since when plastic phenomena advance in the slab, normal stresses tend to become uniform in the cross section involving an increment of the

effective width. So it is important for a non-linear analysis to take into consideration cracking of concrete and plastic behaviour of steel beam.

The evaluation of the effective width of composite steel-precast HCU slab composite girders is very complicated due to the presence of two concrete materials and the presence of holes. In this thesis, the same FE modelling procedure used in analysing beams B3 and B4 in this chapter will be used in carrying out a parametric study on 27 beams with different spans, different depths of HCUs and different steel beam cross sections to establish the effective slab width. All material nonlinearities of precast concrete, cast in situ concrete and steel beam will be taken into account. The load-slip characteristic of the shear stud will be also taken into consideration as explained in section 7.3.3 in this thesis.

7.6.2 Effective width for elastic analysis

In an elastic analysis, the effective width of the slab b_{eff} is theoretically defined as the width of slab that develops the actual total horizontal force in the slab when the stress is assumed constant at the peak value and this can be represented mathematically by:

$$b_{eff} = \frac{\int_{-b/2}^{b/2} \sigma_x dy}{\sigma_{max}} \qquad \text{.....(7.4)}$$

where:

σ_x : the longitudinal axial stress

b : the slab width

σ_{max} : the peak value of the longitudinal axial stress over the width b

In a non-linear step-by-step incremental load procedure, the stresses and strains at the end of the first increment are obtained based on elastic material properties. So, by integrating the longitudinal axial stresses over the width 'b' at the end of the first increment and dividing the result by the peak value of the longitudinal stress, the elastic effective width can be calculated easily. The same approach will be used in the present parametric study to evaluate the elastic effective width of composite girders with precast HC concrete slab.

7.6.3 Effective width for plastic analysis

The elastoplastic analysis of composite girders under study was accomplished by a step by step load incremental procedure. The (*RIKS) method available in the ABAQUS FE package was used in the analysis of the composite steel-precast HC concrete girders. Initially the composite girder is solved by an elastic analysis and the stresses at the end of the first increment are calculated based on this assumption. The minimum value of the load that will cause any point in the structure to plastify is then determined. The elastic equations are then modified so that the equations at the yielded points obey the plastic condition. Loads are then applied to the structure in increments to form additional yield points. For each load increment, it is necessary to solve the equilibrium equations and to find the distribution of incremental stresses in equilibrium with the increments of loads. Therefore, at any load stage, the internal stress field will always satisfy the equations of equilibrium and the yield condition, together with the boundary conditions. The procedure is repeated until the yielding has spread to a stage when equilibrium may no longer be maintained or convergence during the iteration procedure can no longer be obtained. The von Mises' yield criteria available in the ABAQUS software is adopted in this study to govern the equilibrium at the plastic stage for the steel beam, in situ concrete and precast HCUs.

When the slab in a composite girder reaches the plastic stage, normal stresses tend to become uniform along the width of the cross section involving an increment of the effective width. The theoretical effective width, calculated from equation 7.1, will cover the part that has uniform normal stress (maximum uni-axial compressive stress, in addition to two parts that represent the transfer of stresses from the yielded part to the unyielded one of the cross section, see figure 7.22. Taking into consideration the cracking of concrete at failure, the transfer of stresses from the yielded part of the cross section to the unyielded can not be ensured. So, for design safety, the plastic effective width in this study will be considered as the width that has uniform maximum longitudinal axial stress over the width of the cross section at failure, as shown in figure 7.22. Unlike the theoretical effective width, the plastic effective width is independent on the slab width used (with a condition that it is greater than the effective width). It is dependent on the elastic-material properties of the composite girder components.

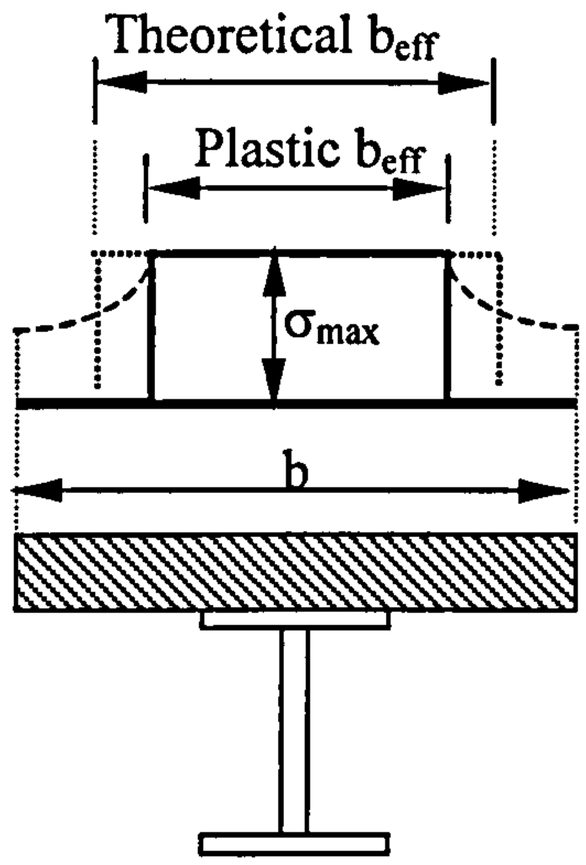

Figure 7.22 Definition of the plastic effective width of composite girder

7.6.4 Parametric study for the evaluation of the effective width of composite steel-precast HCU slab girders

The summary of the 27 composite steel-precast HC slab beams analysed in this parametric study is shown in table 7.1. The beams are loaded with uniformly distributed load up to failure and the distribution of longitudinal axial stresses is plotted on the top surface of the concrete slab at failure. The beams are classified into 9 main groups depending on the used steel beam cross section and the precast HCU depth. Each group contains three different beam spans 6, 9 and 12m that have the same steel beam cross section and the same HCU depth. The width of the concrete slab is chosen so that the ratio of the slab width 'b' (spacing between girders) to the beam span 'L' remains constant. The b/L ratio is chosen (b/L~1/3) and the effect of the change in this ratio on the calculation of the effective width will be followed later on. The width of the concrete slab is taken as 2065mm (1000mm HCU width each side + 65mm gap width between HCU ends) for 6m span beams, 3065mm for 9m span beams and 4065mm for 12m span beams.

The HCU precast slab has characteristic cube strength of 50N/mm^2 while the cast in situ concrete has a design concrete strength of 26N/mm^2. The steel beam has a yield stress of 275N/mm^2. 8mm transverse reinforcement bars are placed in the 500mm slots and kept constant for all the 27 beams to make the results comparable. The load-slip characteristic of the 19mm diameter x 100mm height used with HCU concrete slab, 26N/mm^2 cast in situ concrete and 8mm transverse reinforcement is taken from the previous FE study discussed in chapter 4.

Group	Beam	Steel Beam Cross Section (mm)	HCU Depth (mm)	Span (m)
G1	S1	UB 356x171x51	150	6
	S2	UB 356x171x51	150	9
	S3	UB 356x171x51	150	12
G2	S4	UB 406x178x60	150	6
	S5	UB 406x178x60	150	9
	S6	UB 406x178x60	150	12
G3	S7	UB 457x191x67	150	6
	S8	UB 457x191x67	150	9
	S9	UB 457x191x67	150	12
G4	S10	UB 356x171x51	200	6
	S11	UB 356x171x51	200	9
	S12	UB 356x171x51	200	12
G5	S13	UB 406x178x60	200	6
	S14	UB 406x178x60	200	9
	S15	UB 406x178x60	200	12
G6	S16	UB 457x191x67	200	6
	S17	UB 457x191x67	200	9
	S18	UB 457x191x67	200	12
G7	S19	UB 356x171x51	250	6
	S20	UB 356x171x51	250	9
	S21	UB 356x171x51	250	12
G8	S22	UB 406x178x60	250	6
	S23	UB 406x178x60	250	9
	S24	UB 406x178x60	250	12
G9	S25	UB 457x191x67	250	6
	S26	UB 457x191x67	250	9
	S27	UB 457x191x67	250	12

Table 7.1 Summary of the modelled beams in the parametric study

Elastic and plastic evaluation of effective width of composite steel-precast HC slab girders

The adopted approach to evaluate the elastic effective width (the effective width is calculated based on elastic material properties) and the plastic effective width (the effective width is calculated based on elastic-plastic material properties) is the same one previously discussed in sections 7.6.2 and 7.6.3 respectively. The procedures are explained in detail for steel-precast HC slab girders of group one (G1), see table 7.1, and then will be applied for the other eight groups aimed by this study. The beams are loaded up to failure with a uniform distributed load and with the same details previously mentioned.

Elastic effective width

The stress distribution through the cross section has been plotted at different sections over the span after the first increment that represents the elastic stresses on the section. The integration equation 7.1 has been carried out numerically using the trapezoidal rule to evaluate the elastic effective width at different sections for the beams (S1, S2 and S3) that have spans (6, 9 and 12m) and have the same (b/L) ratio. Figures 7.23, 7.24 and 7.25 show the distribution of the effective width over the span for beam S1, S2 and S3 respectively. The elastic (b_{eff}/L) ratio calculated at centre line of the beams was approximately the same and equals to 0.288 (for b/L ratio=0.34).

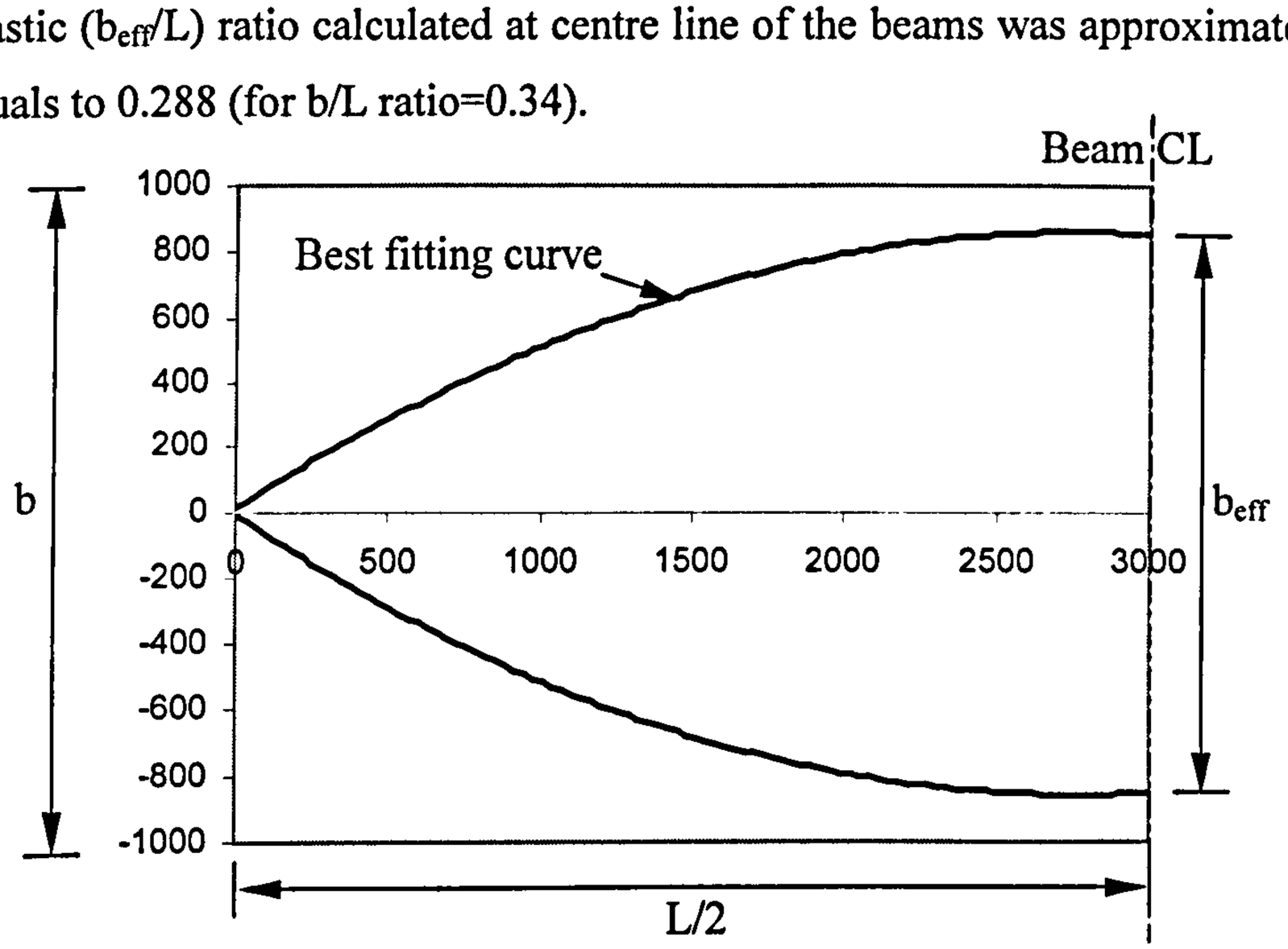

Figure 7.23 Distribution of the elastic b_{eff} over the 6m span composite girder S1

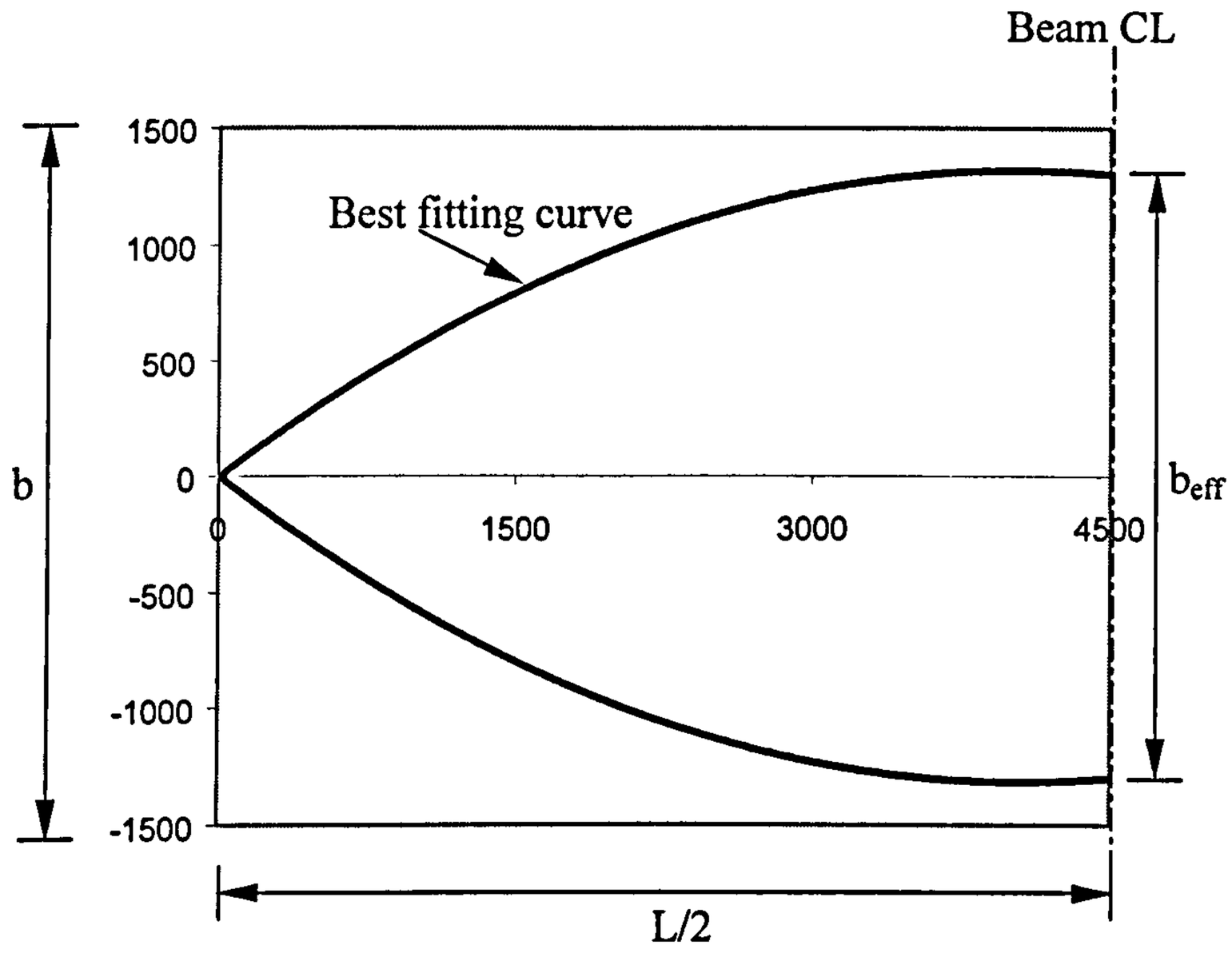

Figure 7.24 Distribution of the elastic b_{eff} over the 9m span composite girder S2

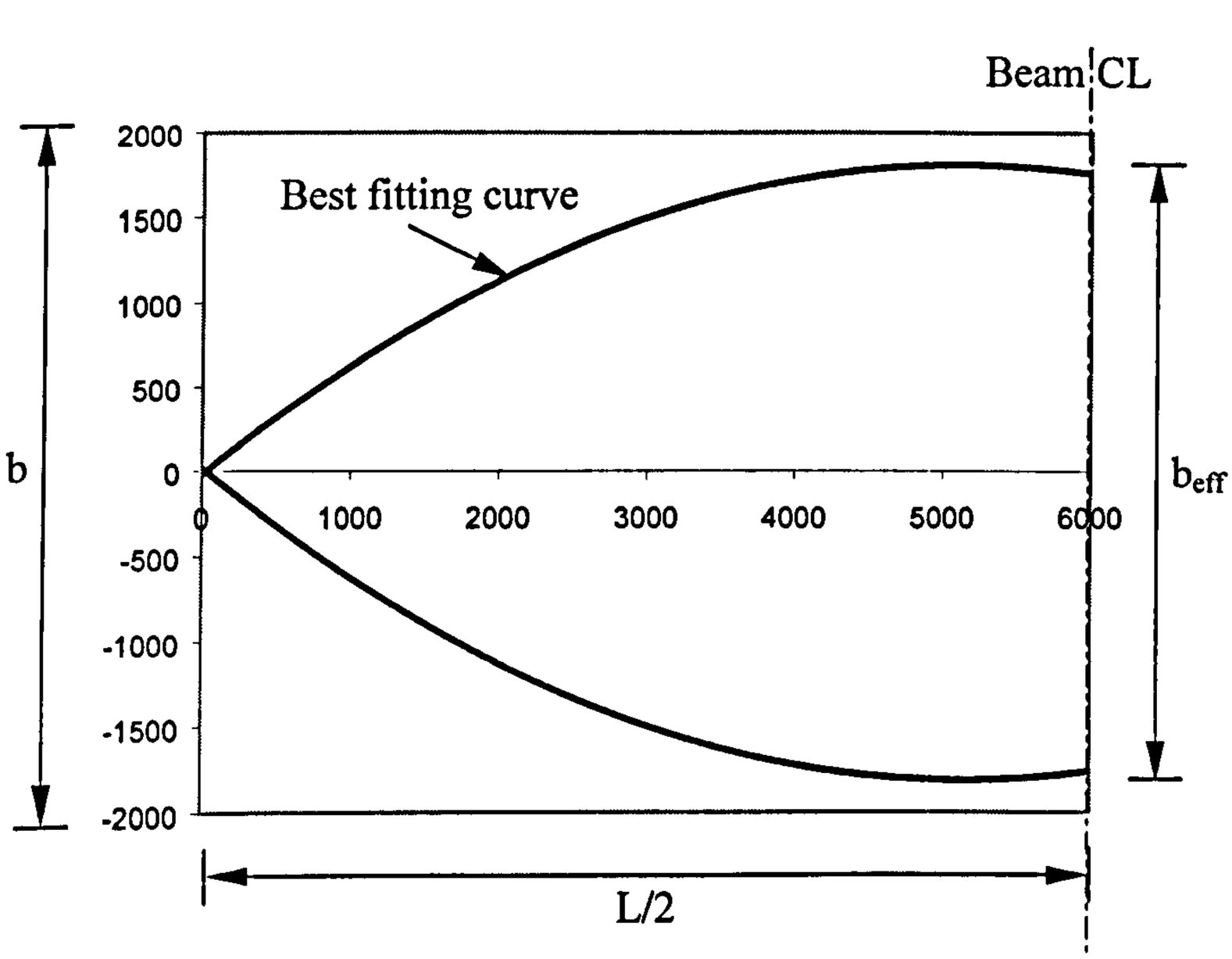

Figure 7.25 Distribution of the elastic b_{eff} over the 12m span composite girder S3

Plastic effective width

Figures 7.26, 7.27 and 7.28 show the distribution of longitudinal axial stresses at failure on the top surface of the composite girders S1, S2 and S3 respectively. Since the critical compressive stress is the design compressive strength of the in situ concrete, the contour stress limits were taken from -26N/mm^2 to +26N/mm^2. It can be seen that the distribution of axial stress over the section at failure is uniform over the yielded elements of the concrete slab and decreases at the edges as previously explained in section 7.6.3. The constant width of the precast HC–in situ concrete slab represents the actual width that interacts with the steel beam in carrying longitudinal axial stresses (plastic effective width). This width remains approximately the same even if greater width of concrete 'b' was used as will be explained later on.

Table 7.2 shows the summary of the plastic effective width calculated at failure of the composite girders S1, S2 and S3 representing group1. The average plastic (b_{eff}/L) ratio calculated at centre line of the beams is 0.237 (for b/L ratio=0.34). This means that the calculation of the effective width based on elastic material properties may lead to a misleading value. In order to justify this conclusion the present parametric study has been carried out over a variety of composite steel-precast HC slab that have different steel cross sections and different HC slab depth and has the same (b/L=0.34) ratio.

The average elastic (b_{eff}/L) for the 27 beams remained approximately the same value of 0.29 and the average plastic (b_{eff}/L) for the same beams based on ultimate state is 0.22. These values are calculated at the middle span of the composite girders.

Figures 7.26-7.34 show the distribution of longitudinal axial stresses for the 27 beams at failure. Also, tables from 7.2 to 7.10 show the summary of the calculated plastic effective width for the 27 beams separately.

Group 1 (UB 356x171x51, 150mm slab)

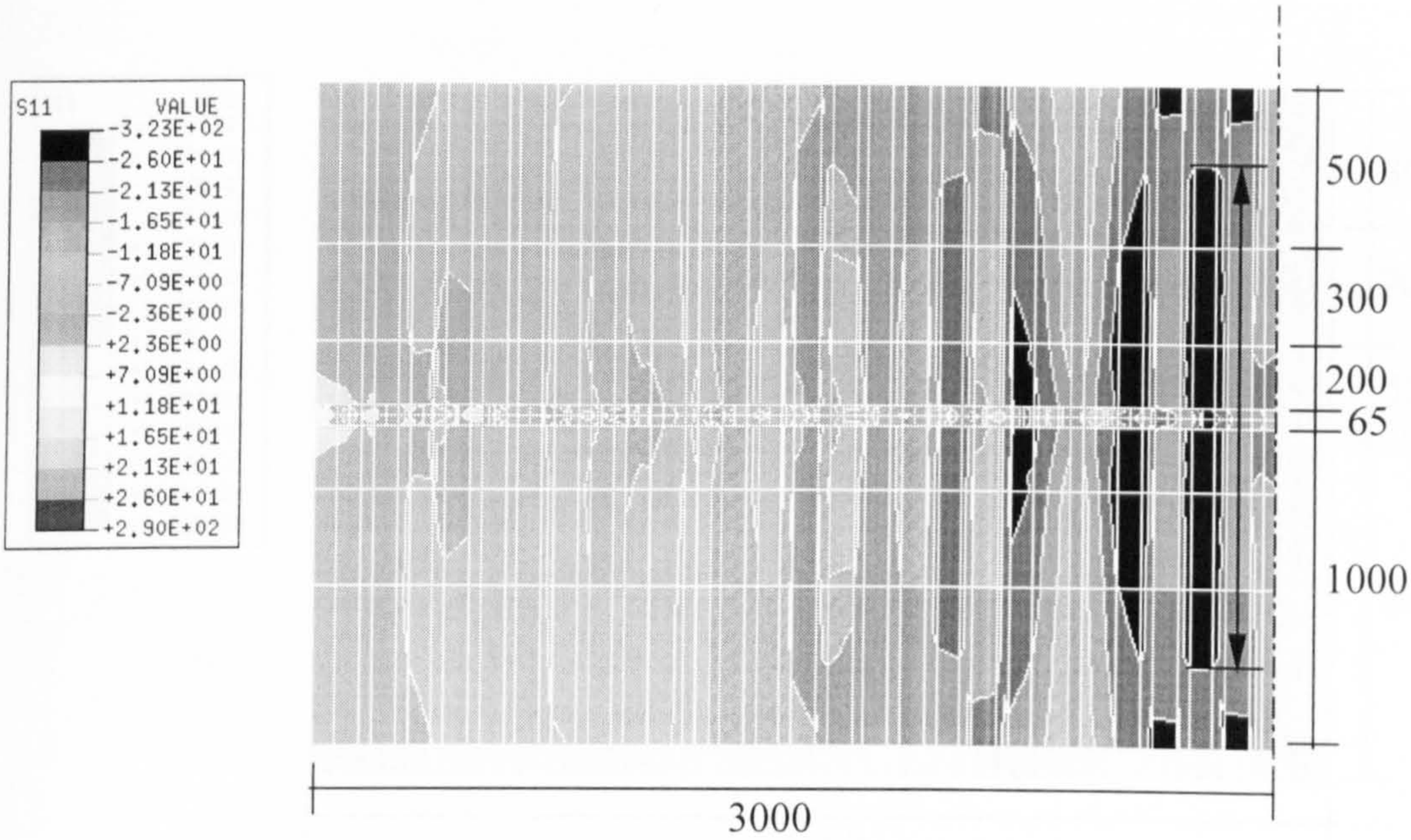

Figure 7.26.a Contour stresses plan of 6m span beam S1

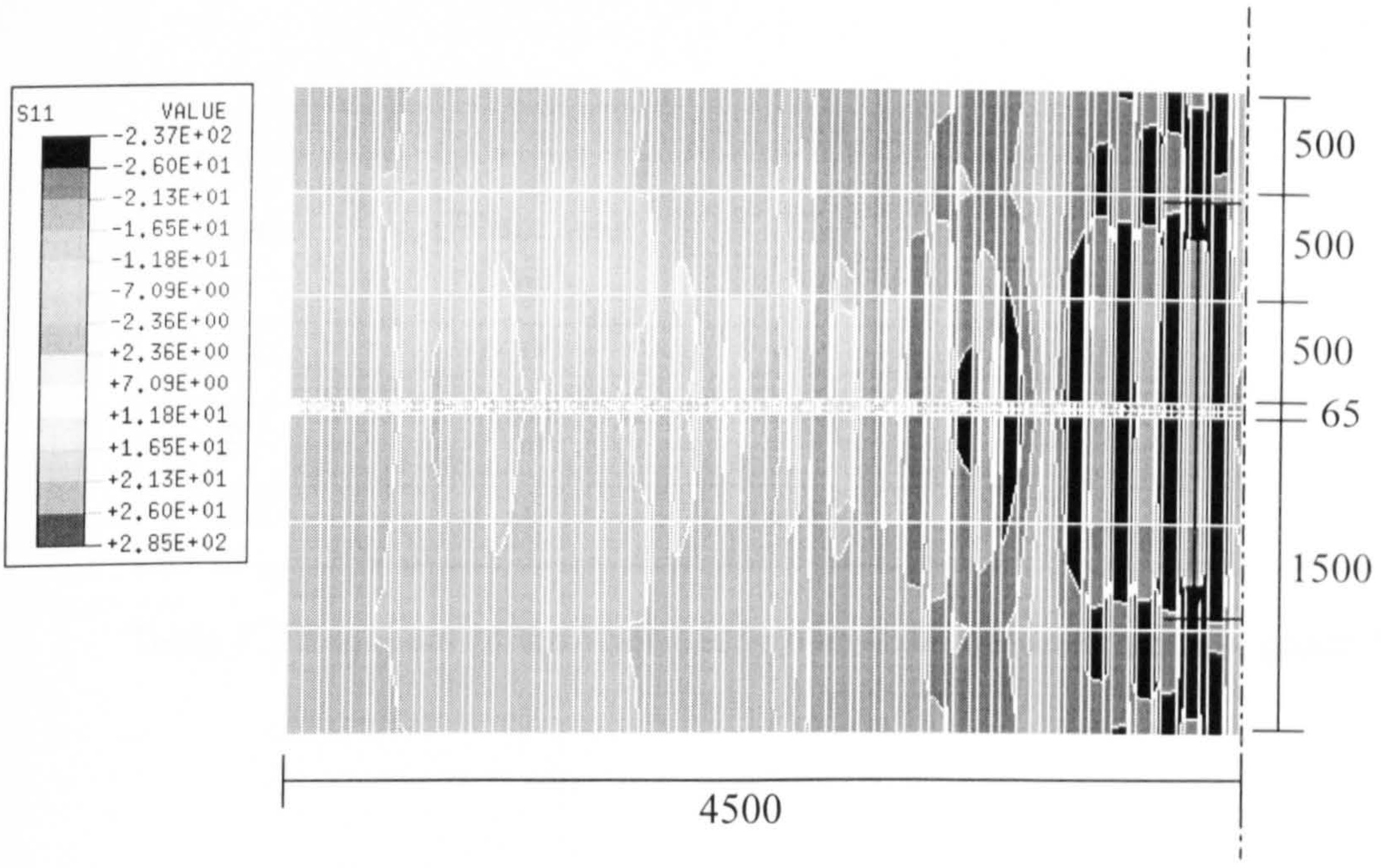

Figure 7.26.b Contour stresses plan of 9m span beam S2

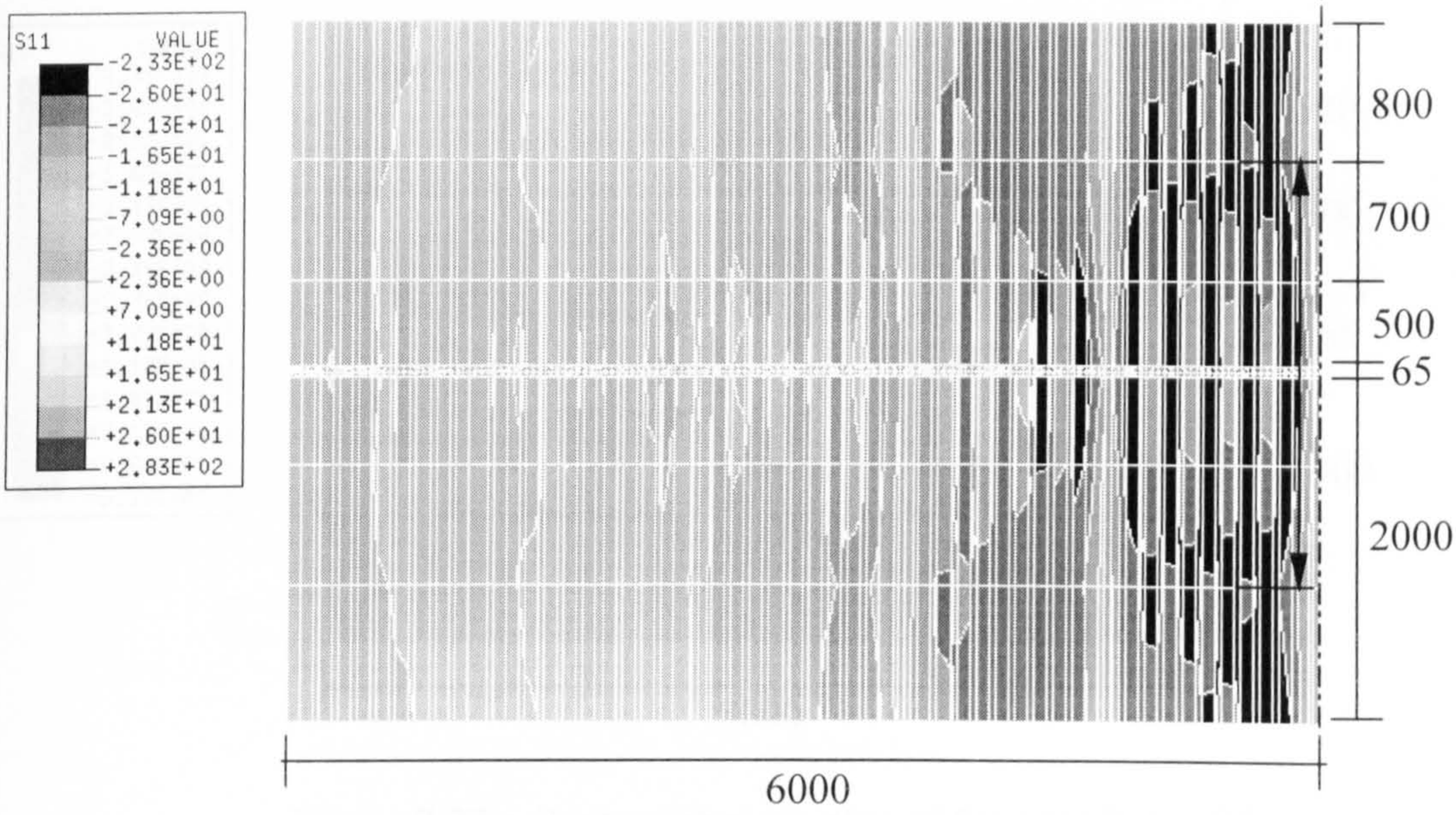

Figure 7.26.c Contour stresses plan of 12m span beam S3

Beam	L (Beam span) (mm)	b_{eff} (mm)	b_{eff}/L (mm)
S1	6000	1692	0.282
S2	9000	2008	0.223
S3	12000	2465	0.205

Table 7.2 Summary of the Plastic effective width per span ratio for group 1

Group 2 (UB 406x178x60, 150mm slab)

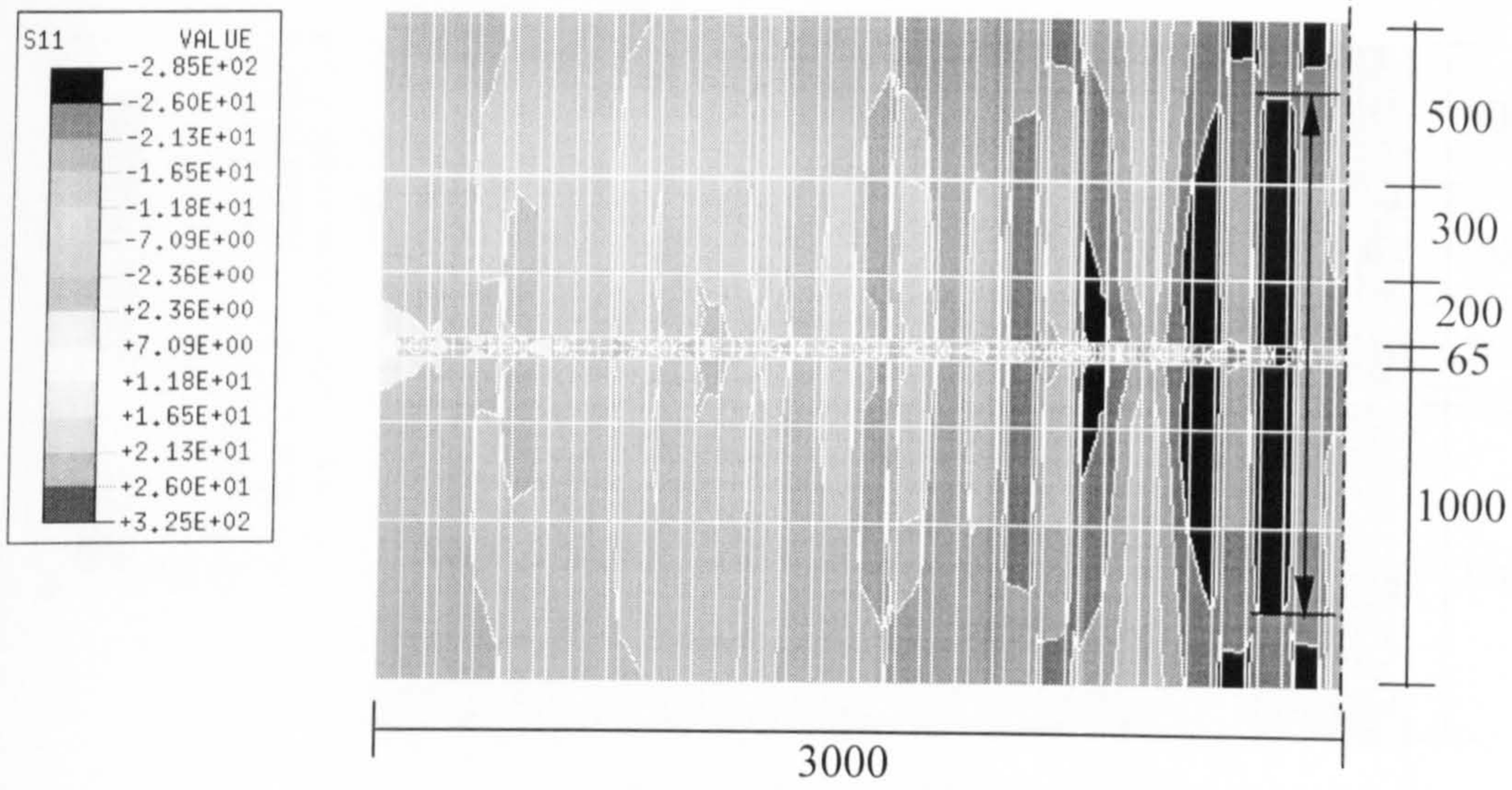

Figure 7.27.a Contour stresses plan of 6m span beam S4

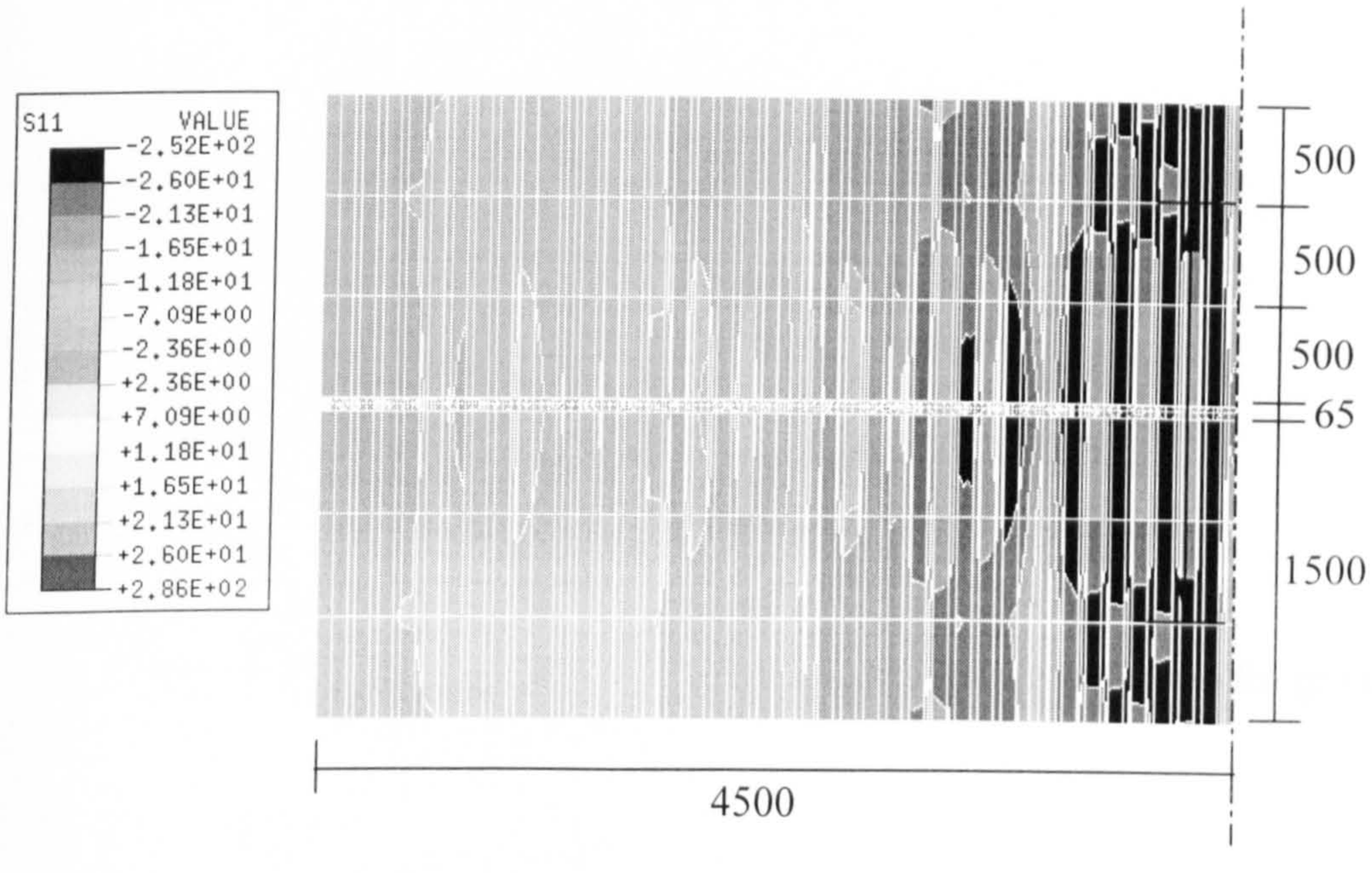

Figure 7.27.b Contour stresses plan of 9m span beam S5

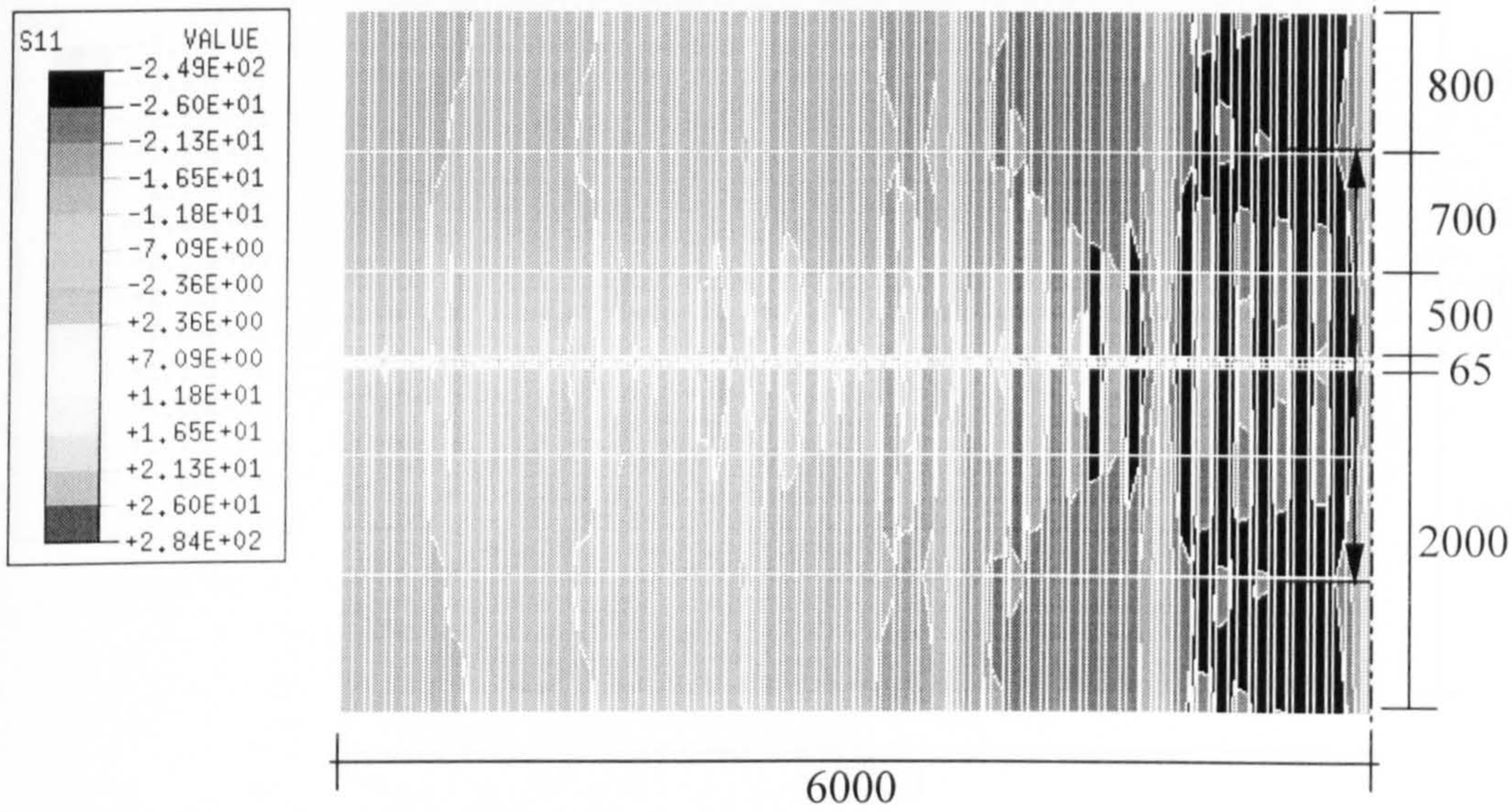

Figure 7.27.c Contour stresses plan of 12m span beam S6

Beam	L (Beam span) (mm)	b_{eff} (mm)	b_{eff}/L (mm)
S4	6000	1591	0.265
S5	9000	2065	0.229
S6	12000	2465	0.205

Table 7.3 Summary of the plastic effective width per span ratio for group 2

Group 3 (UB 457x191x67, 150mm slab)

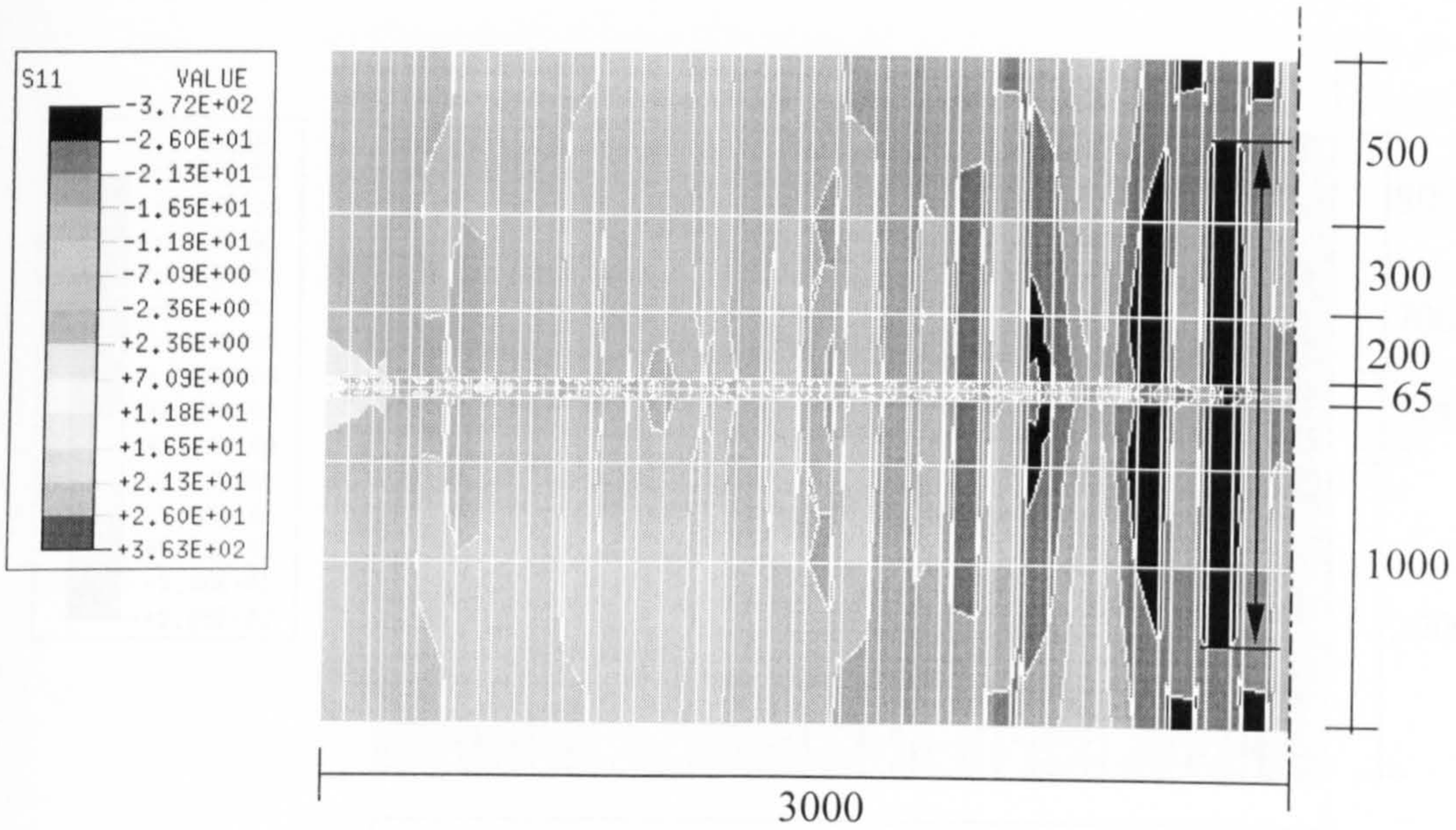

Figure 7.28.a Contour stresses plan of 6m span beam S7

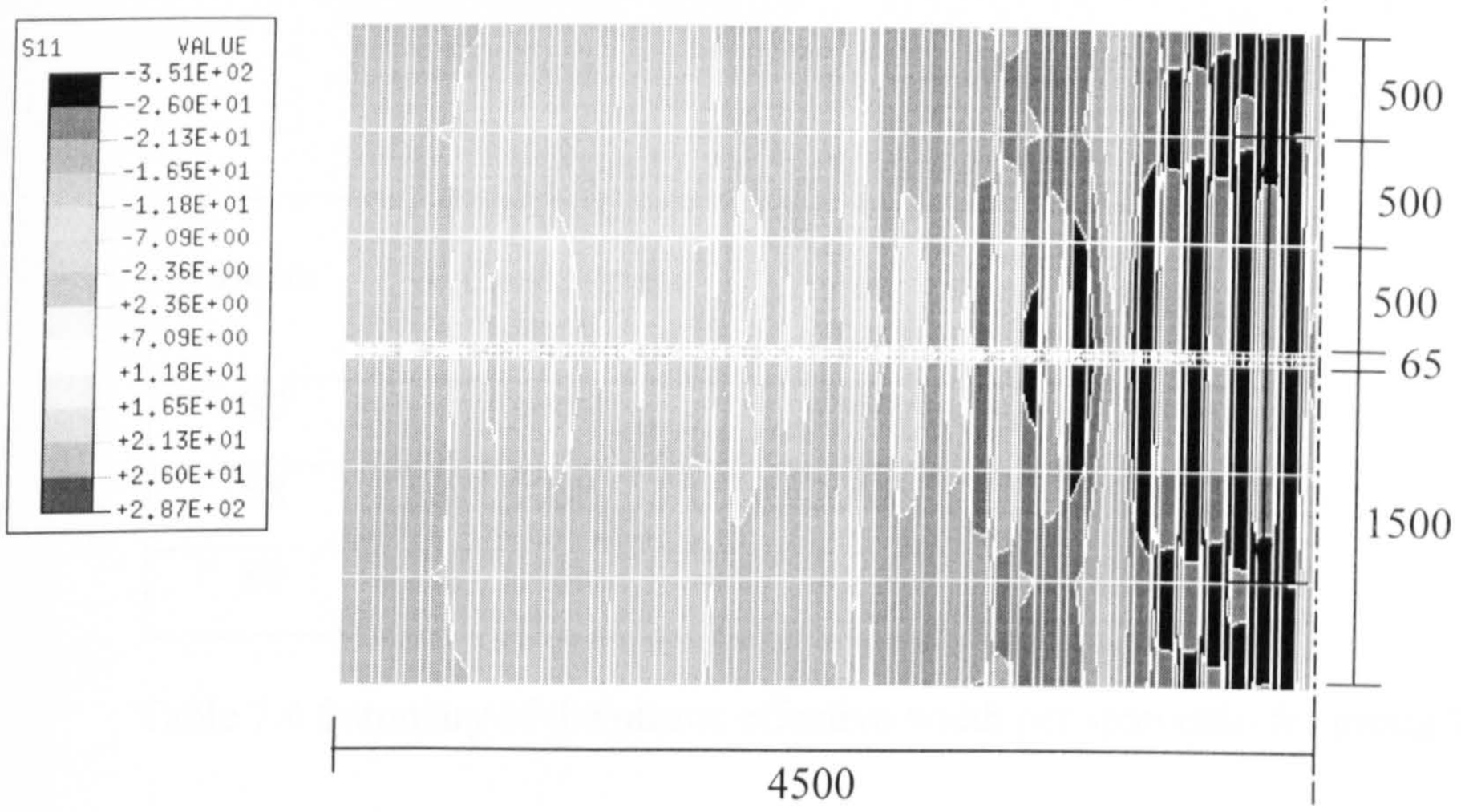

Figure 7.28.b Contour stresses plan of 9m span beam S8

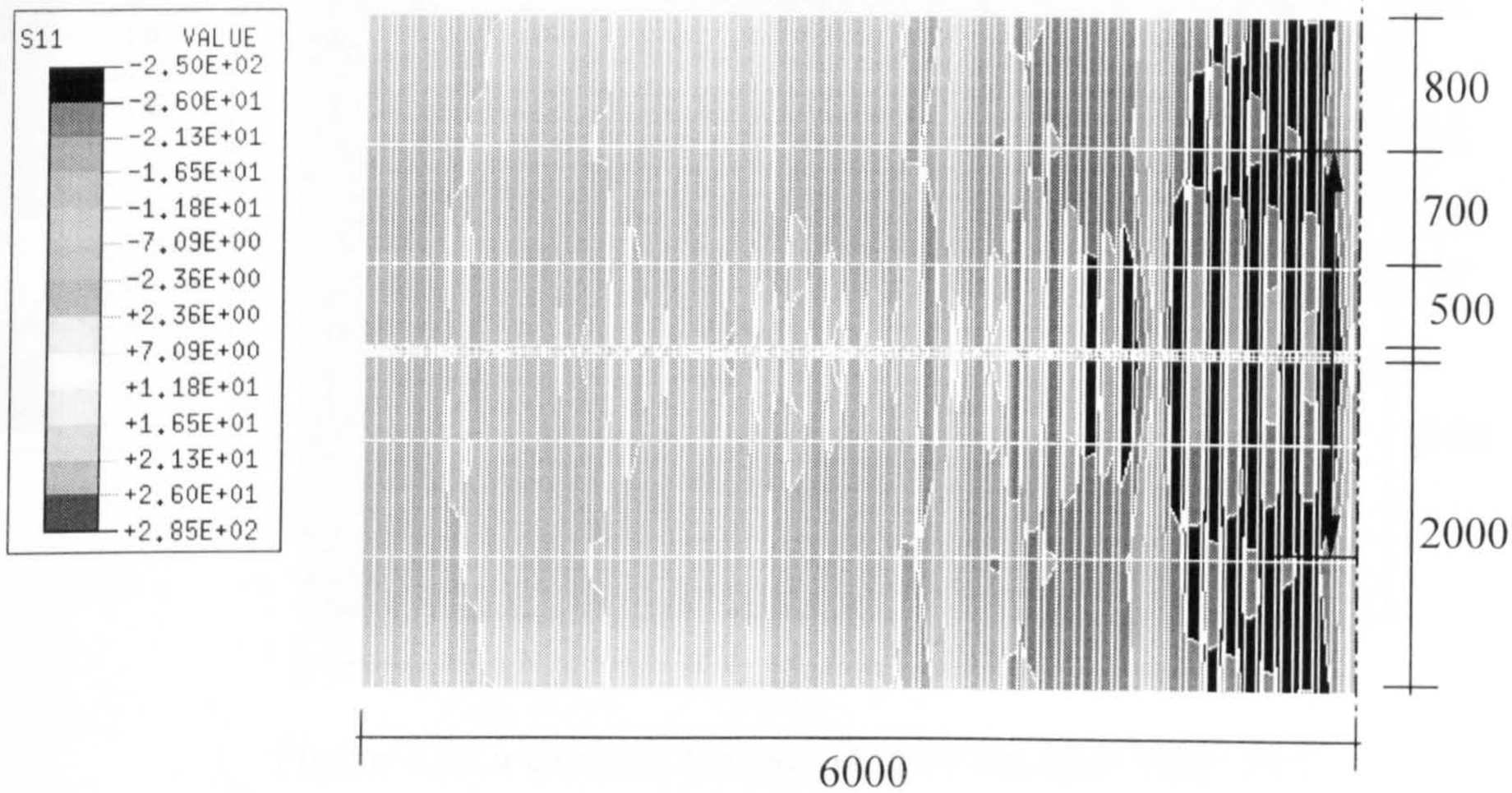

Figure 7.28.c Contour stresses plan of 6m span beam S9

Beam	L (Beam span) (mm)	b_{eff} (mm)	b_{eff}/L (mm)
S7	6000	1557	0.259
S8	9000	2065	0.229
S9	12000	2465	0.205

Table 7.4 Summary of the plastic effective width per span ratio for group 3

Group 4 (UB 356x171x51, 200mm slab)

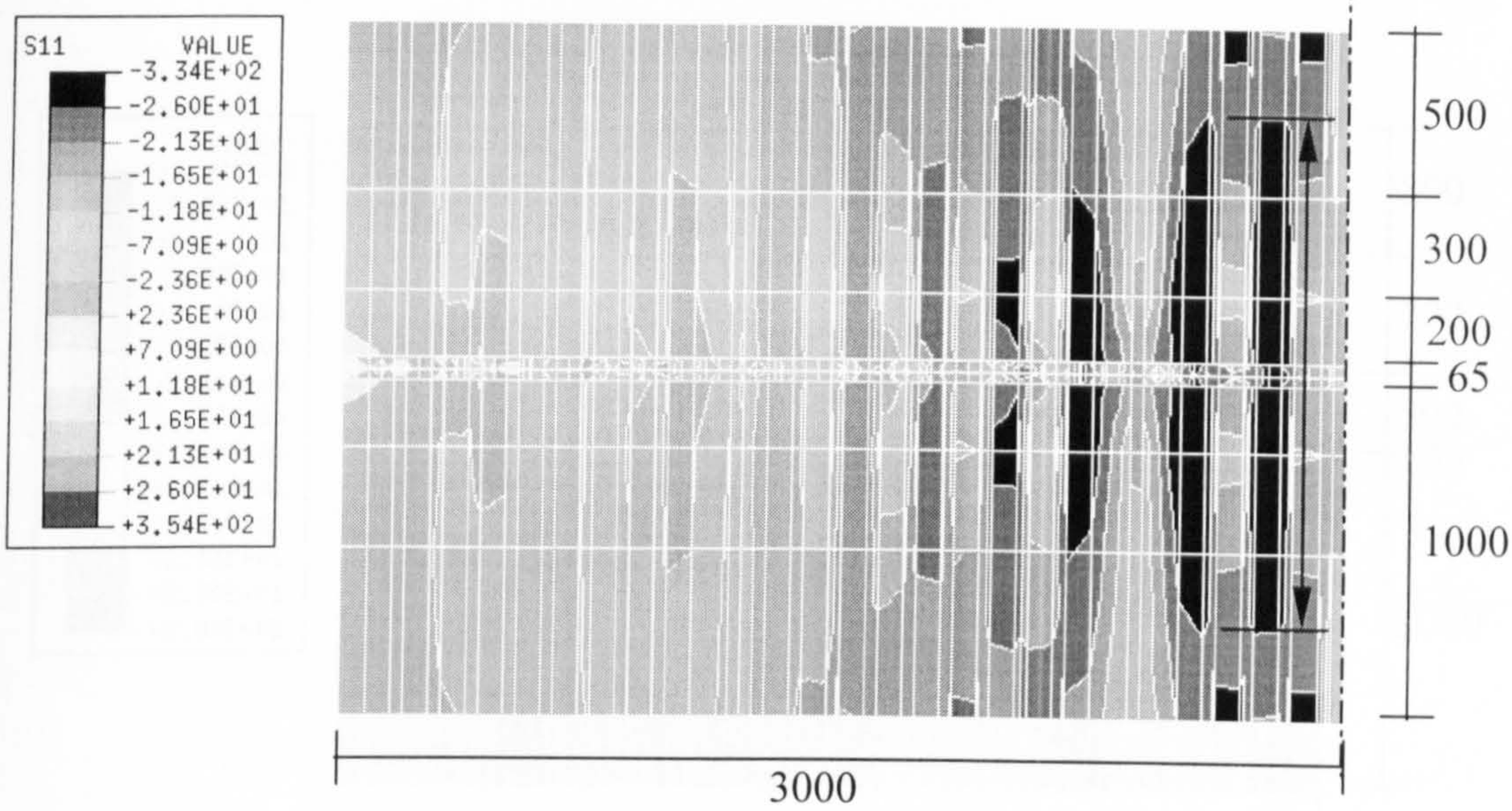

Figure 7.29.a Contour stresses plan of 6m span beam S10

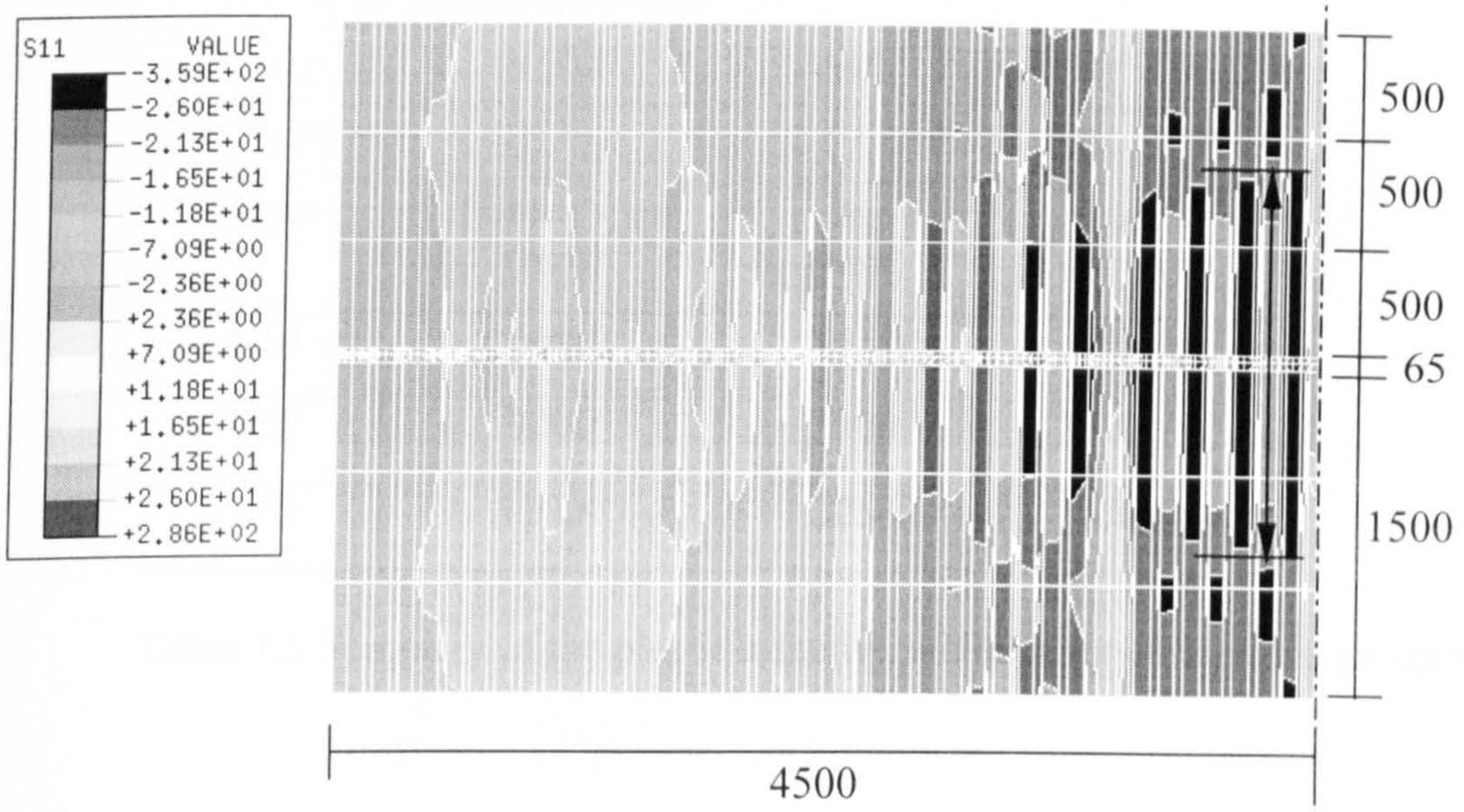

Figure 7.29.b Contour stresses plan of 9m span beam S11

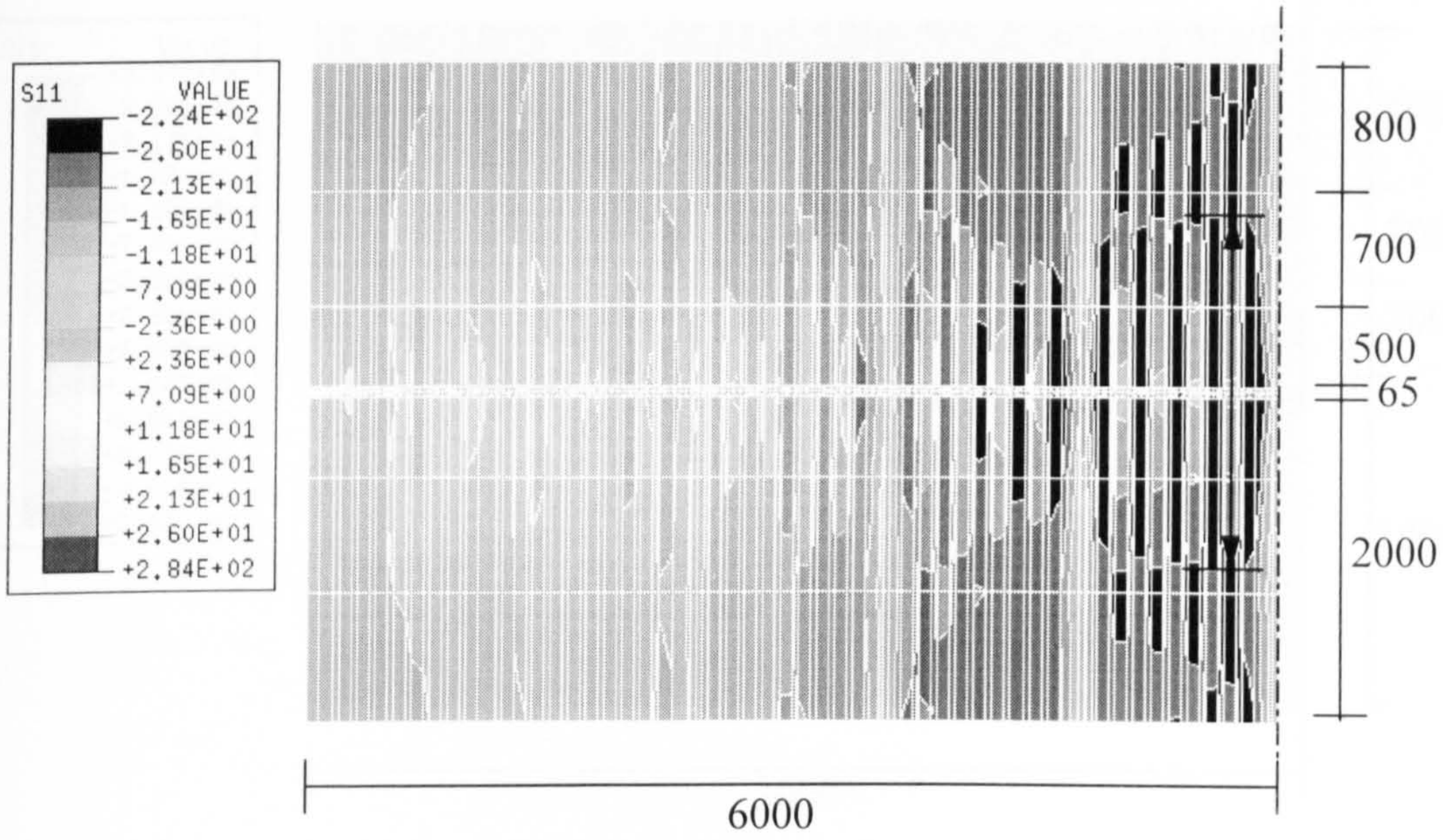

Figure 7.29.c Contour stresses plan of 12m span beam S12

Beam	L (Beam span) (mm)	b_{eff} (mm)	b_{eff}/L (mm)
S10	6000	1557	0.259
S11	9000	1800	0.2
S12	12000	2258	0.188

Table 7.5 Summary of the plastic effective width per span ratio for group 4

Group 5(UB 406x178x51, 200mm slab)

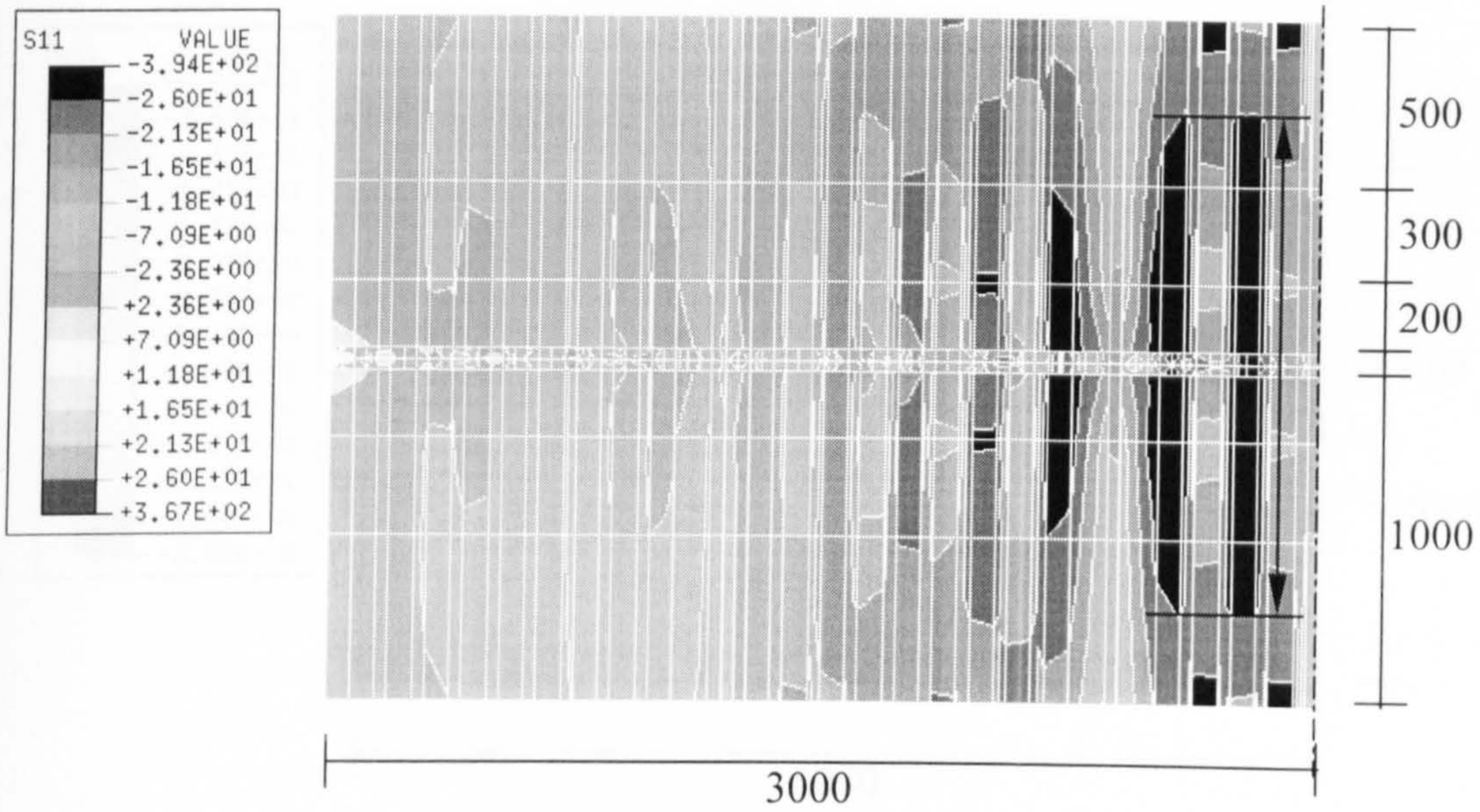

Figure 7.30.a Contour stresses plan of 6m span beam S13

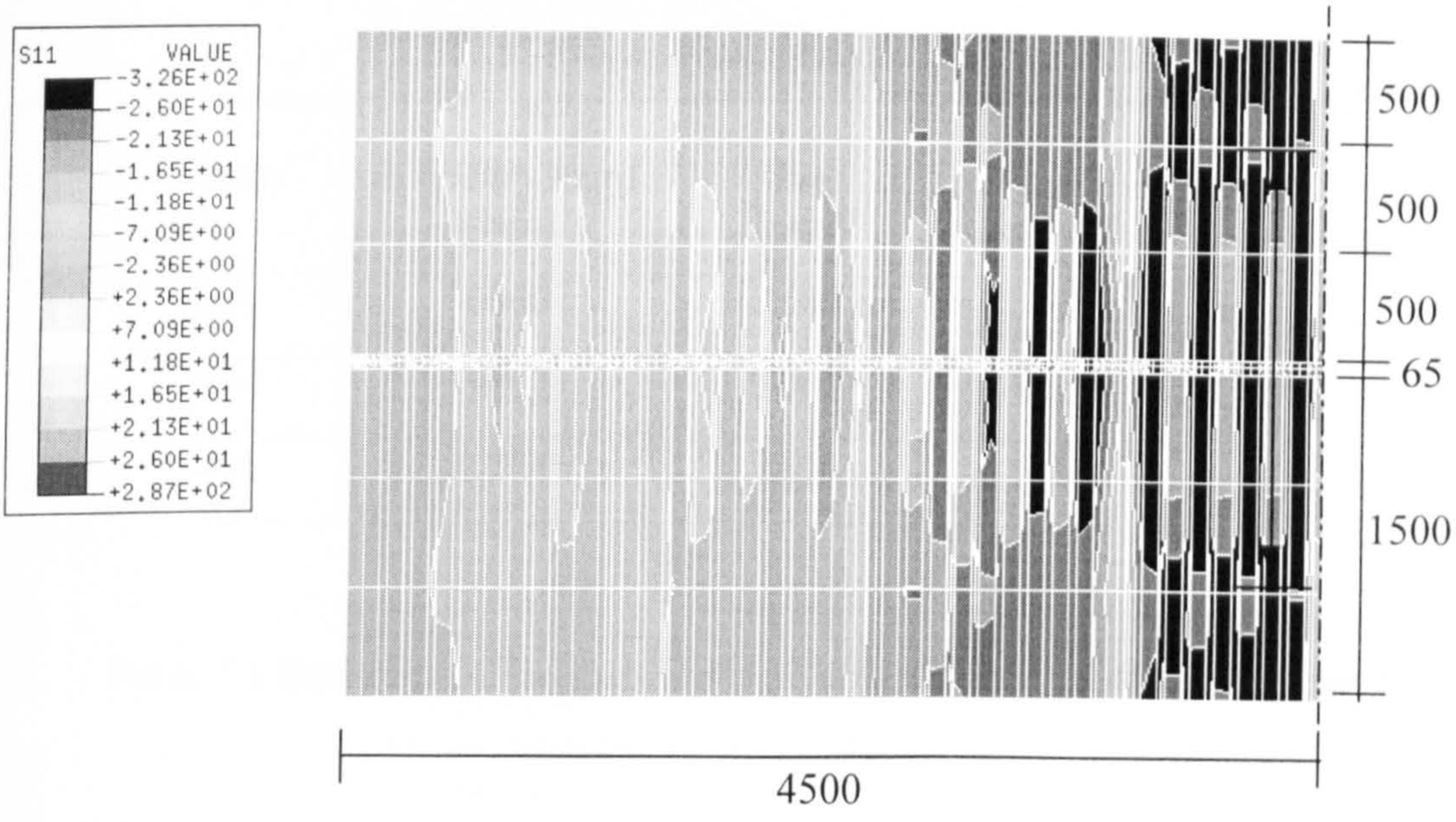

Figure 7.30.b Contour stresses plan of 9m span beam S14

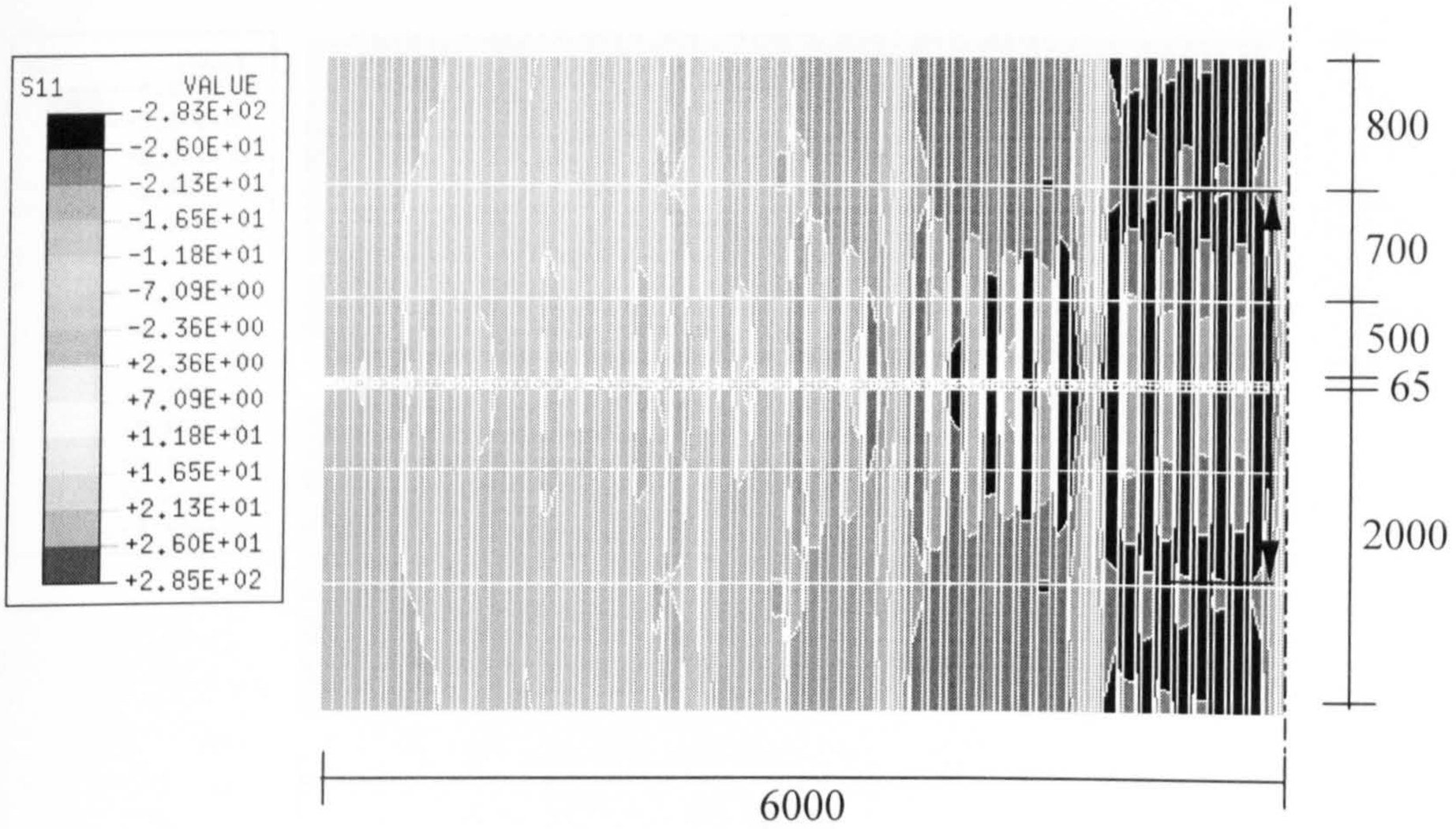

Figure 7.30.c Contour stresses plan of 12m span beam S15

Beam	L (Beam span) (mm)	b_{eff} (mm)	b_{eff}/L (mm)
S13	6000	1502	0.25
S14	9000	2065	0.229
S15	12000	2465	0.205

Table 7.6 Summary of the plastic effective width per span ratio for group 5

Group 6 (UB 457x191x67, 200mm slab)

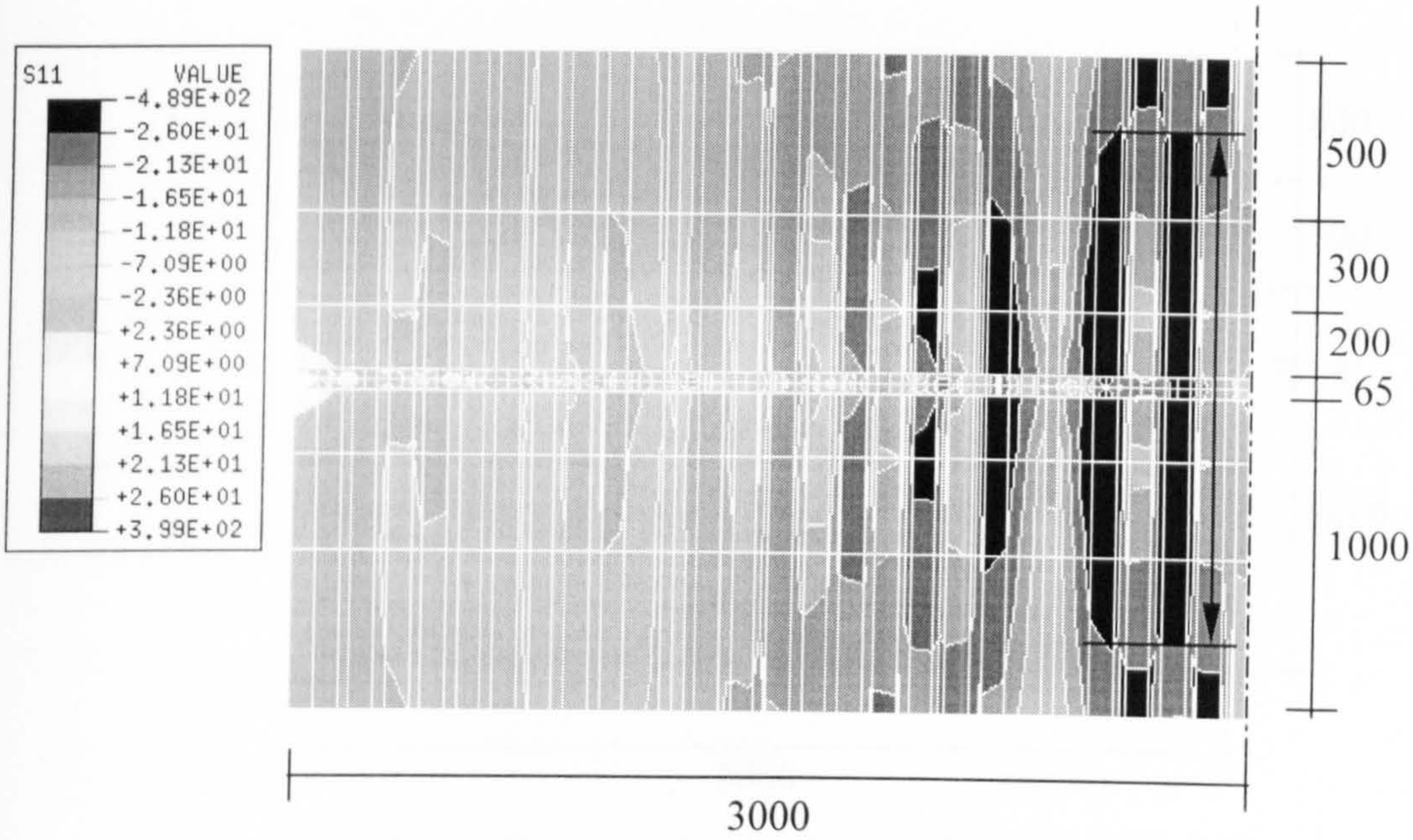

Figure 7.31.a Contour stresses plan of 6m span beam S16

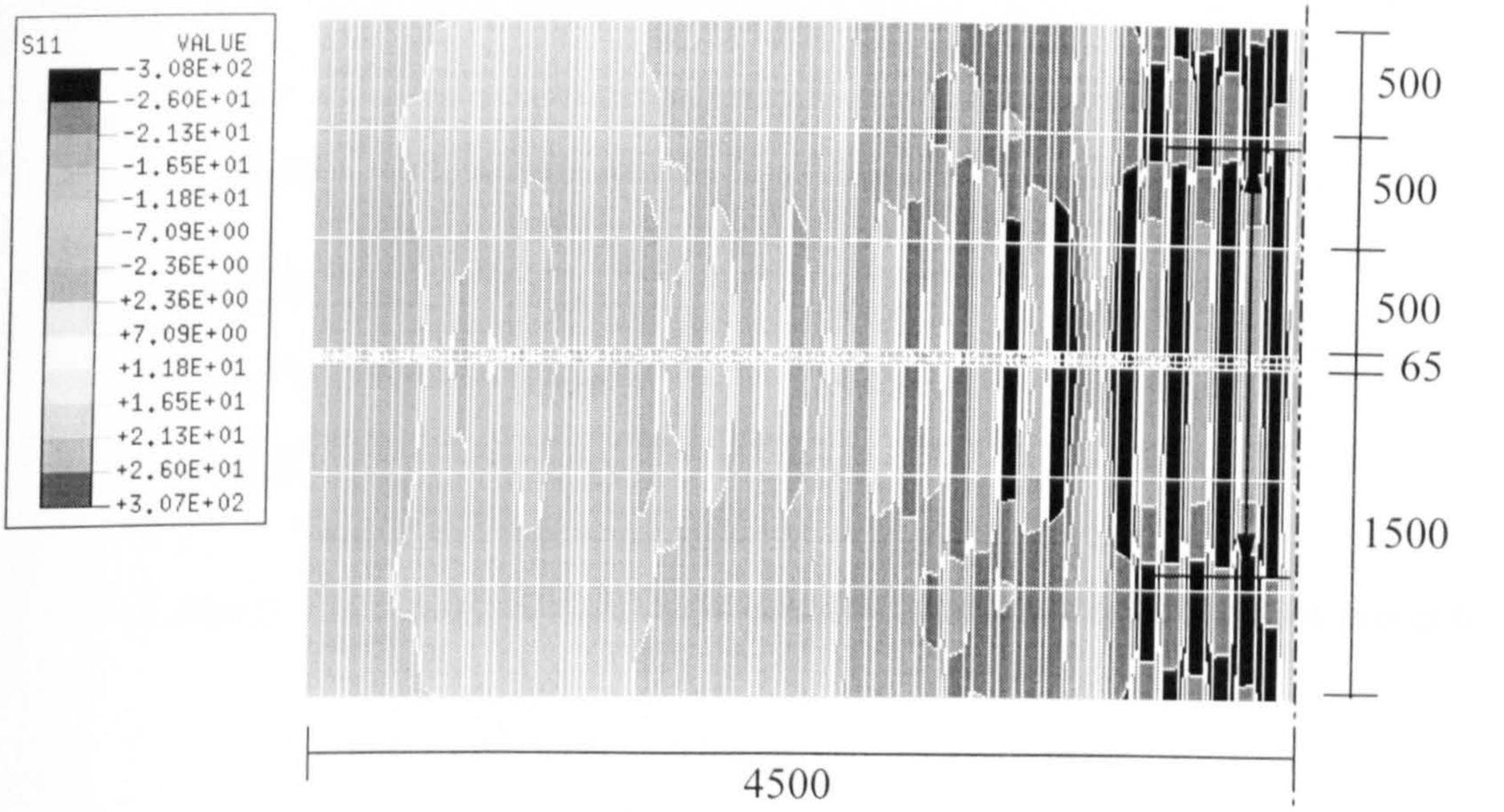

Figure 7.31.b Contour stresses plan of 9m span beam S17

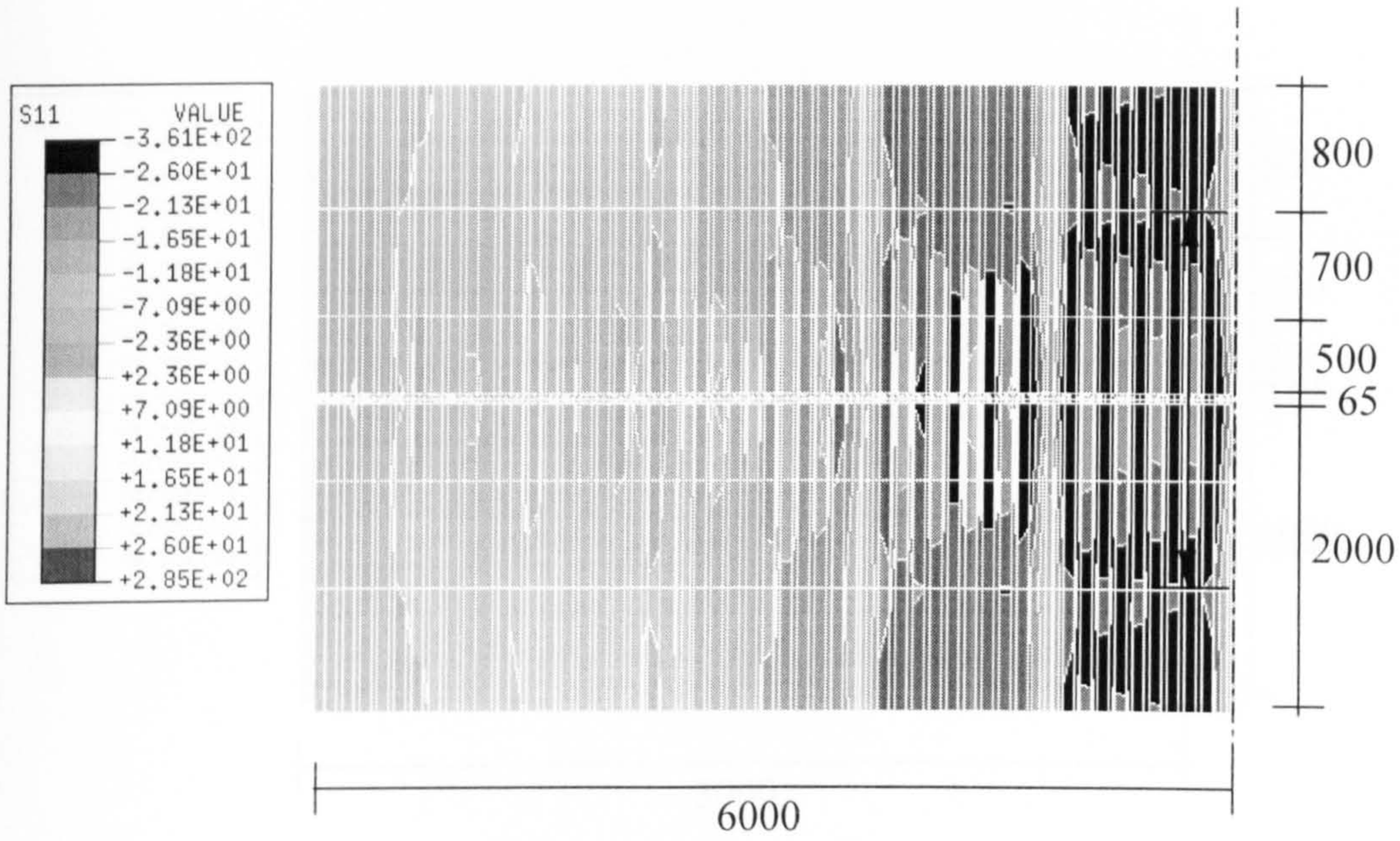

Figure 7.31.c Contour stresses plan of 12m span beam S18

Beam	L (Beam span) (mm)	b_{eff} (mm)	b_{eff}/L (mm)
S16	6000	1620	0.27
S17	9000	1964	0.218
S18	12000	2465	0.205

Table 7.7 Summary of the plastic effective width per span ratio for group 6

Group 7 (UB 356x171x51, 250mm slab)

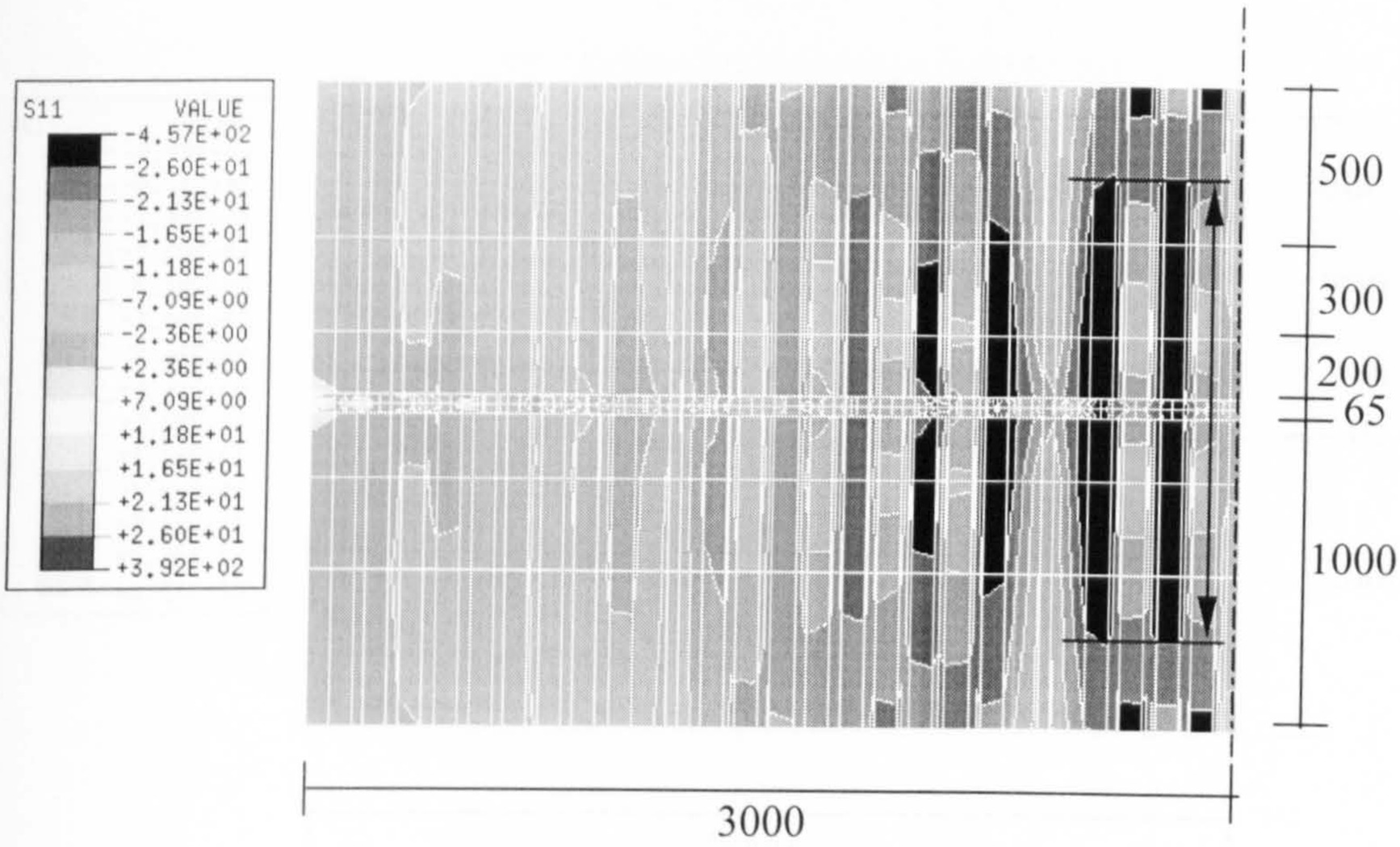

Figure 7.32.a Contour stresses plan of 6m span beam S19

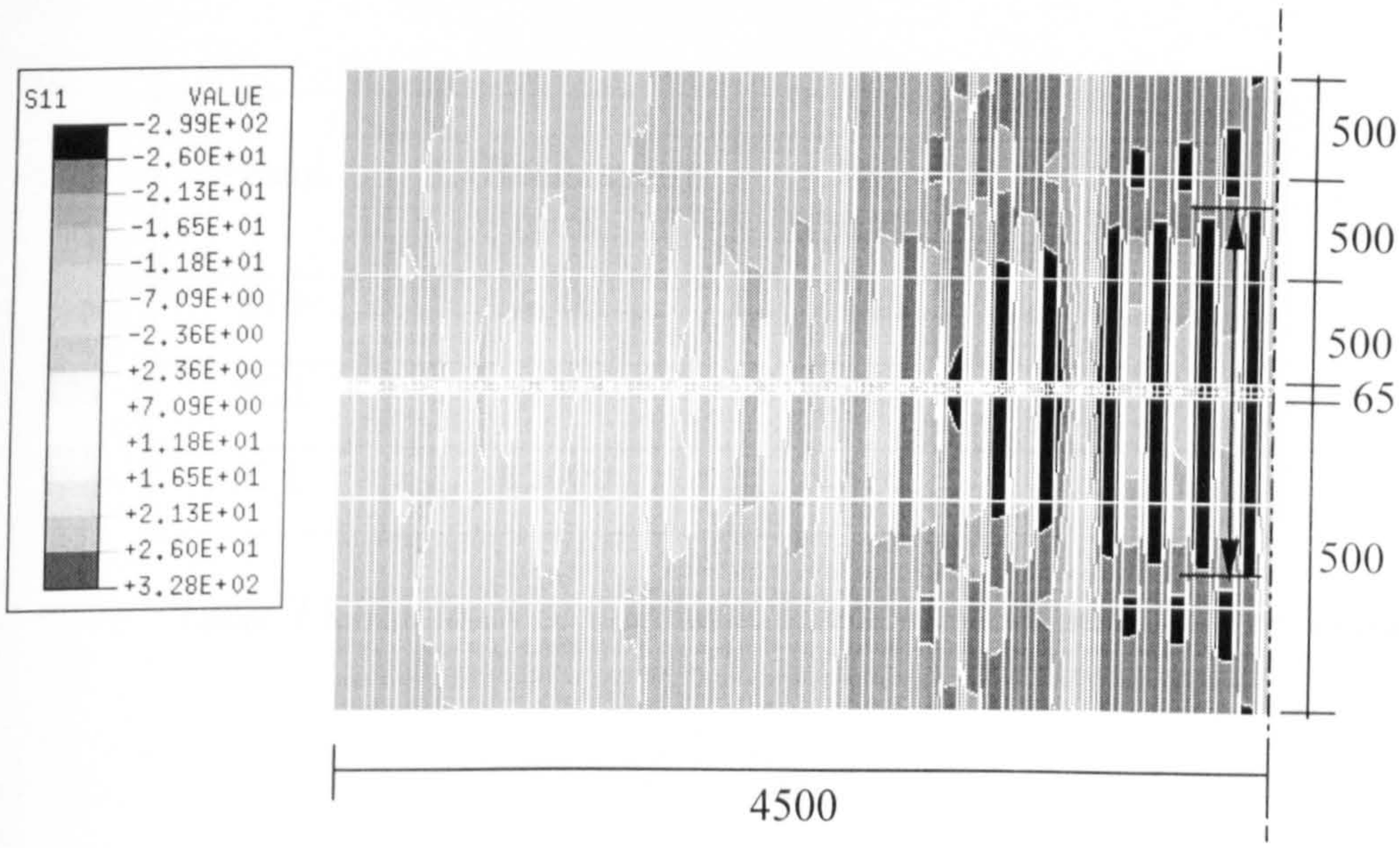

Figure 7.32.b Contour stresses plan of 9m span beam S20

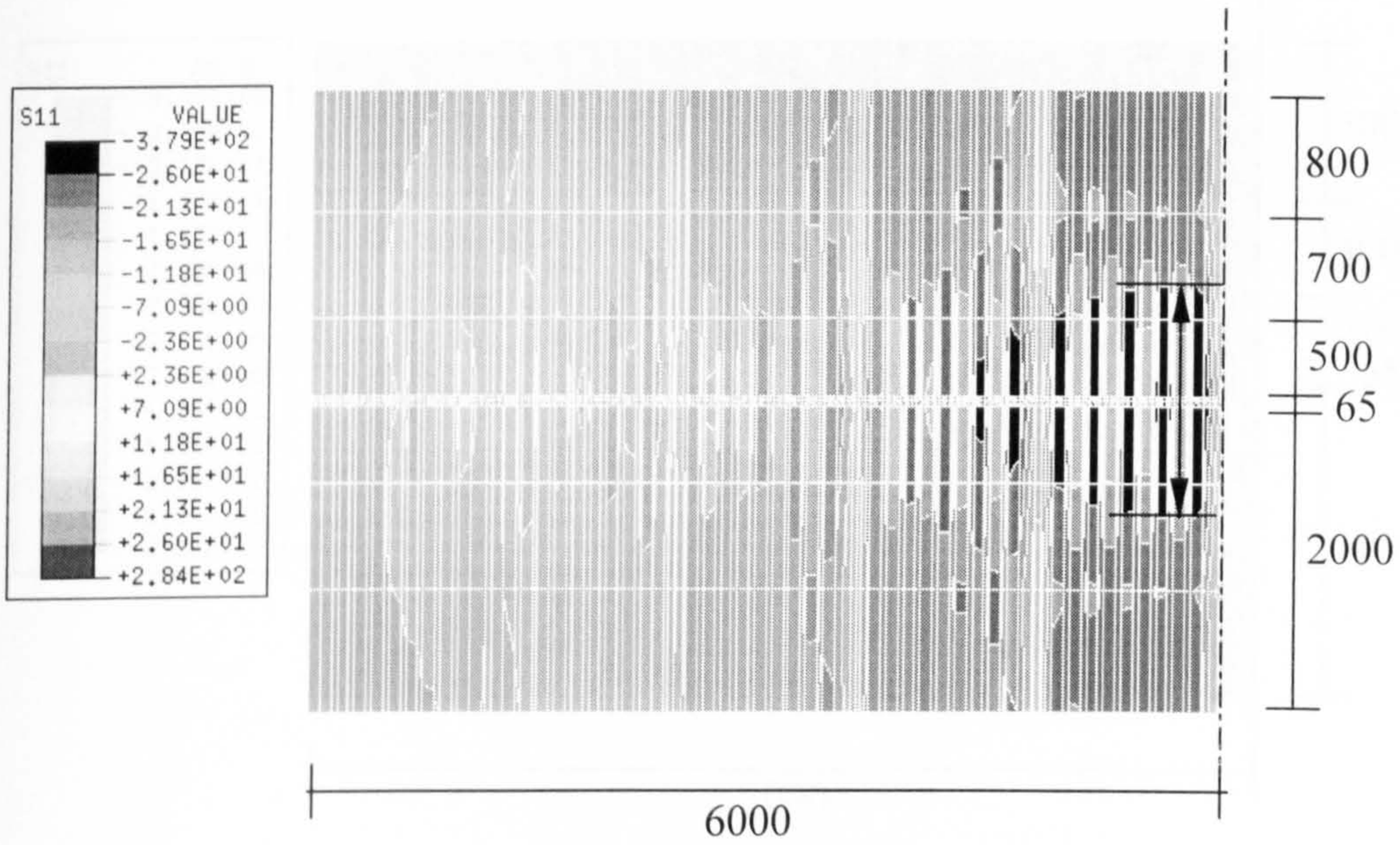

Figure 7.32.c Contour stresses plan of 12m span beam S21

Beam	L (Beam span) (mm)	b_{eff} (mm)	b_{eff}/L (mm)
S19	6000	1490	0.248
S20	9000	1792	0.199
S21	12000	1516	0.126

Table 7.8 Summary of the plastic effective width per span ratio group 7

Group 8 (UB 406x178x60, 250mm slab)

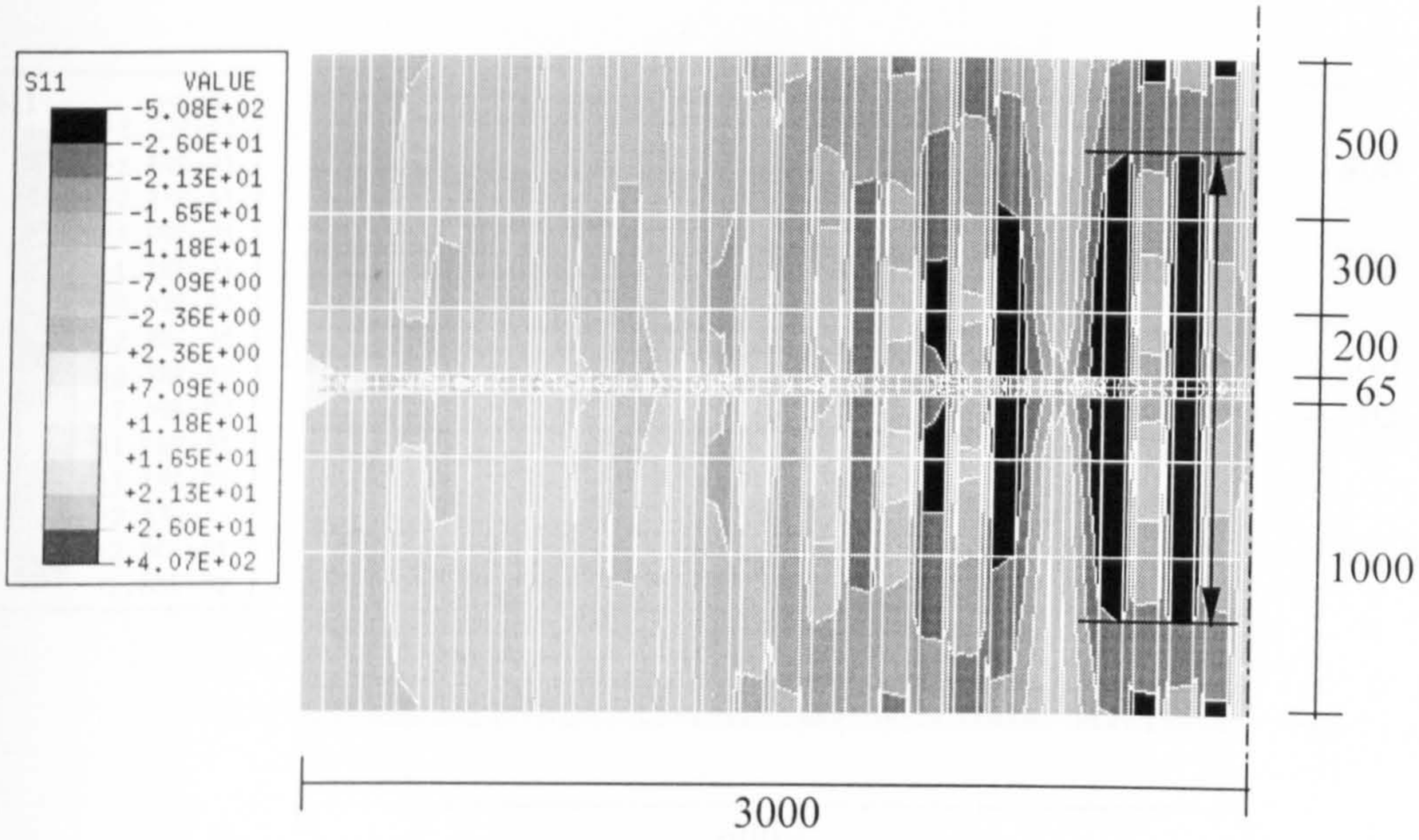

Figure 7.33.a Contour stresses plan of 6m span beam S22

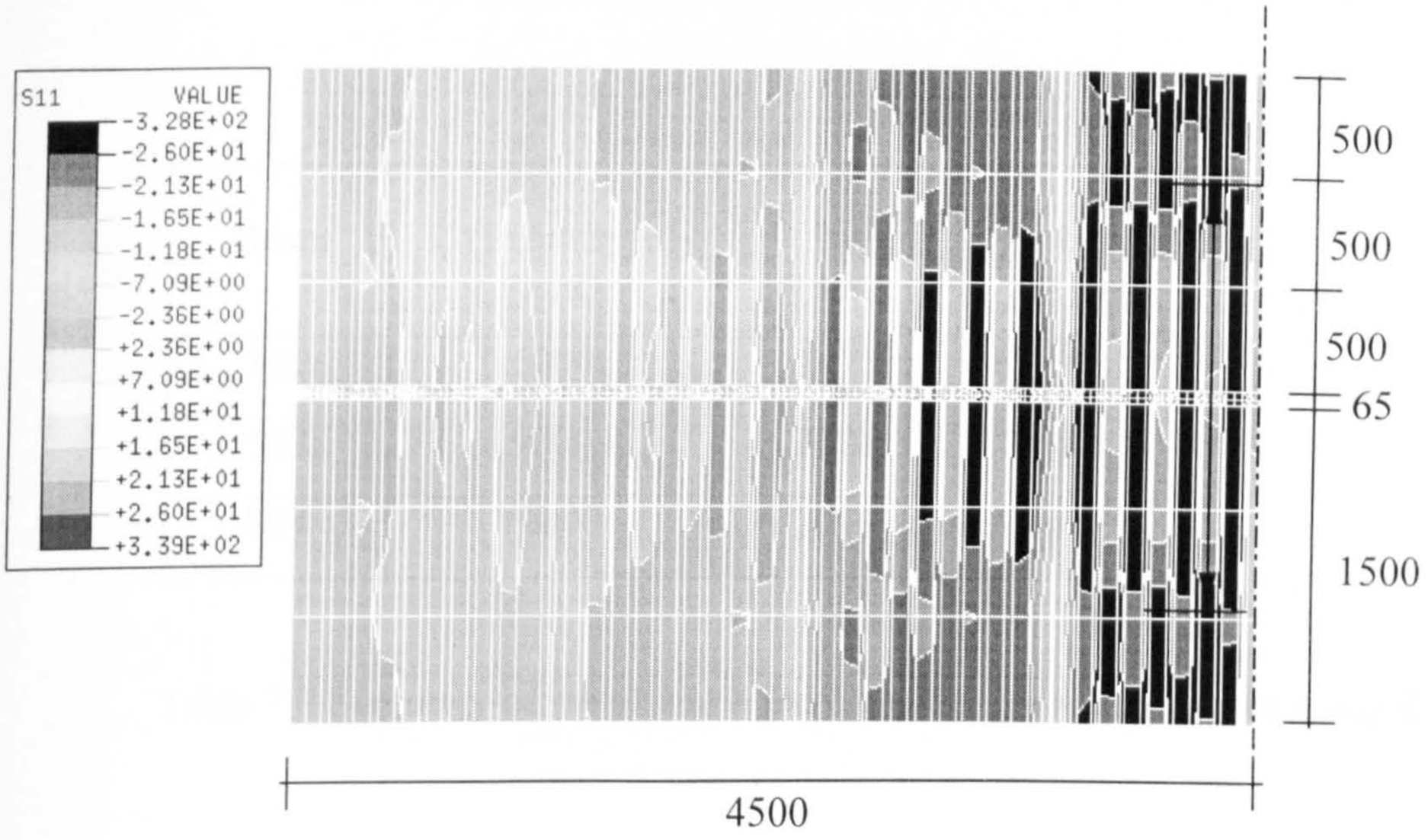

Figure 7.33.b Contour stresses plan of 9m span beam S23

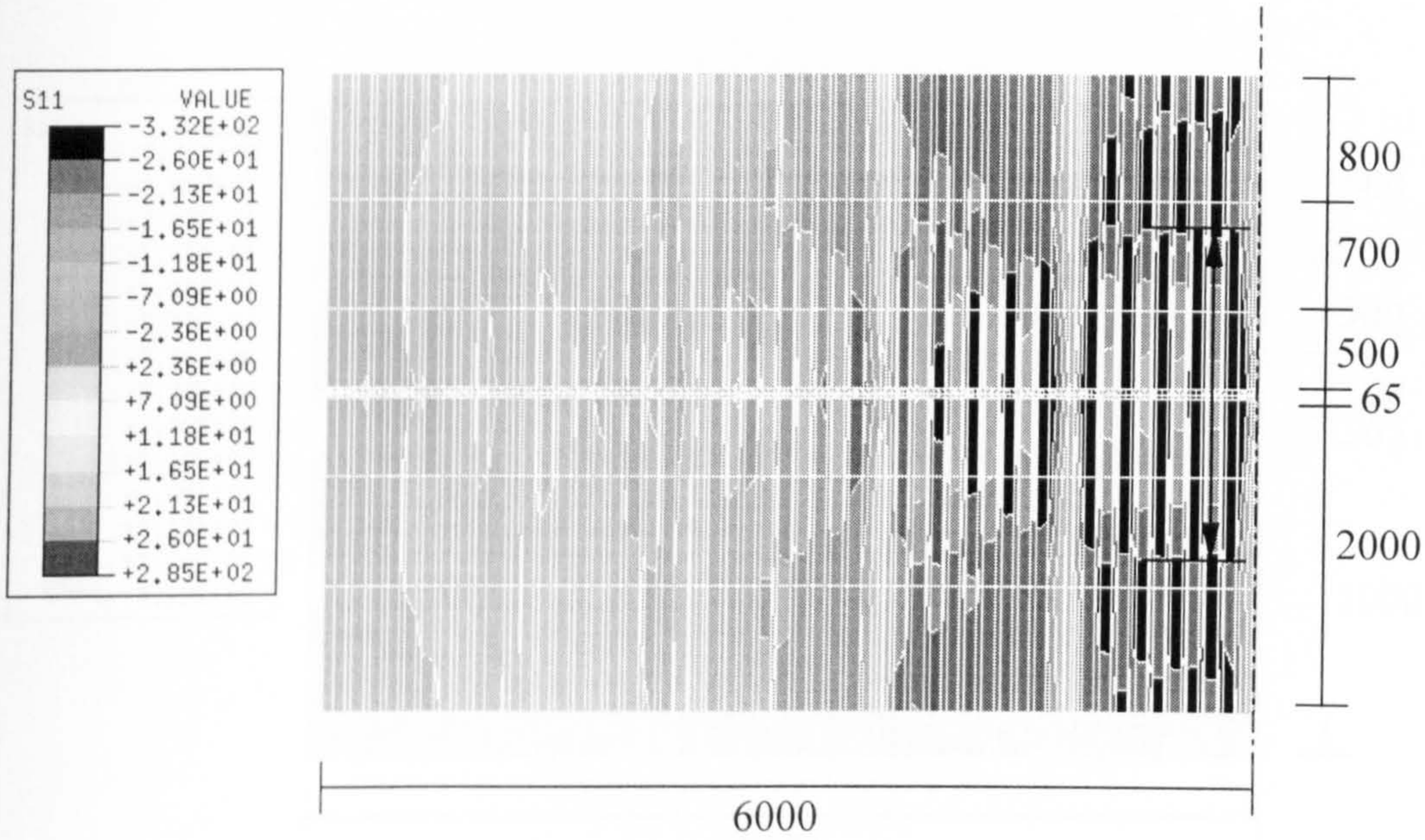

Figure 7.33.c Contour stresses plan of 12m span beam S24

Beam	L (Beam span) (mm)	b_{eff} (mm)	b_{eff}/L (mm)
S22	6000	1475	0.246
S23	9000	2028	0.225
S24	12000	2098	0.175

Table 7.9 Summary of the plastic effective width per span ratio for group 8

Group 9 (UB 457x191x67, 250mm slab)

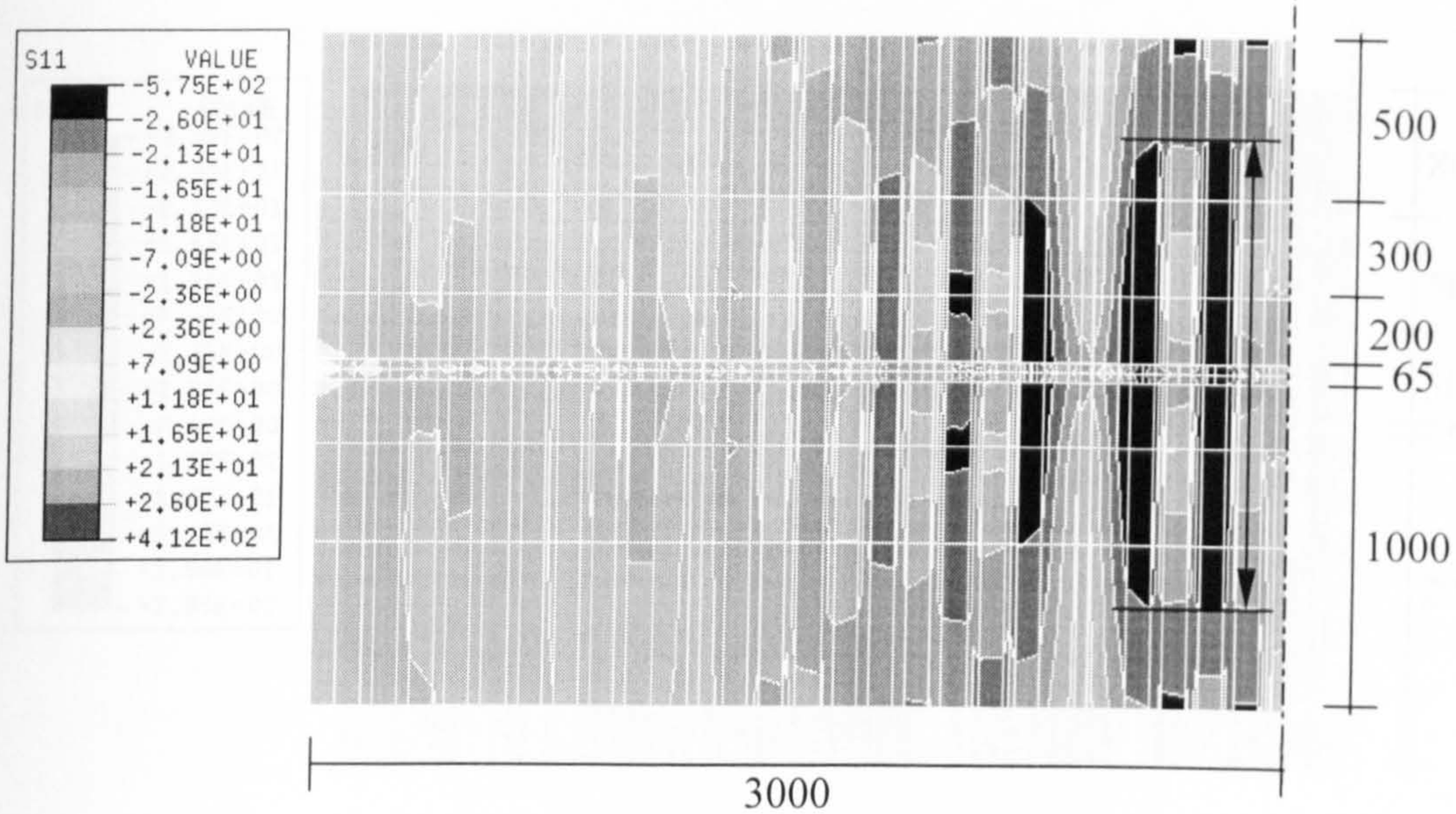

Figure 7.34.a Contour stresses plan of 6m span beam S25

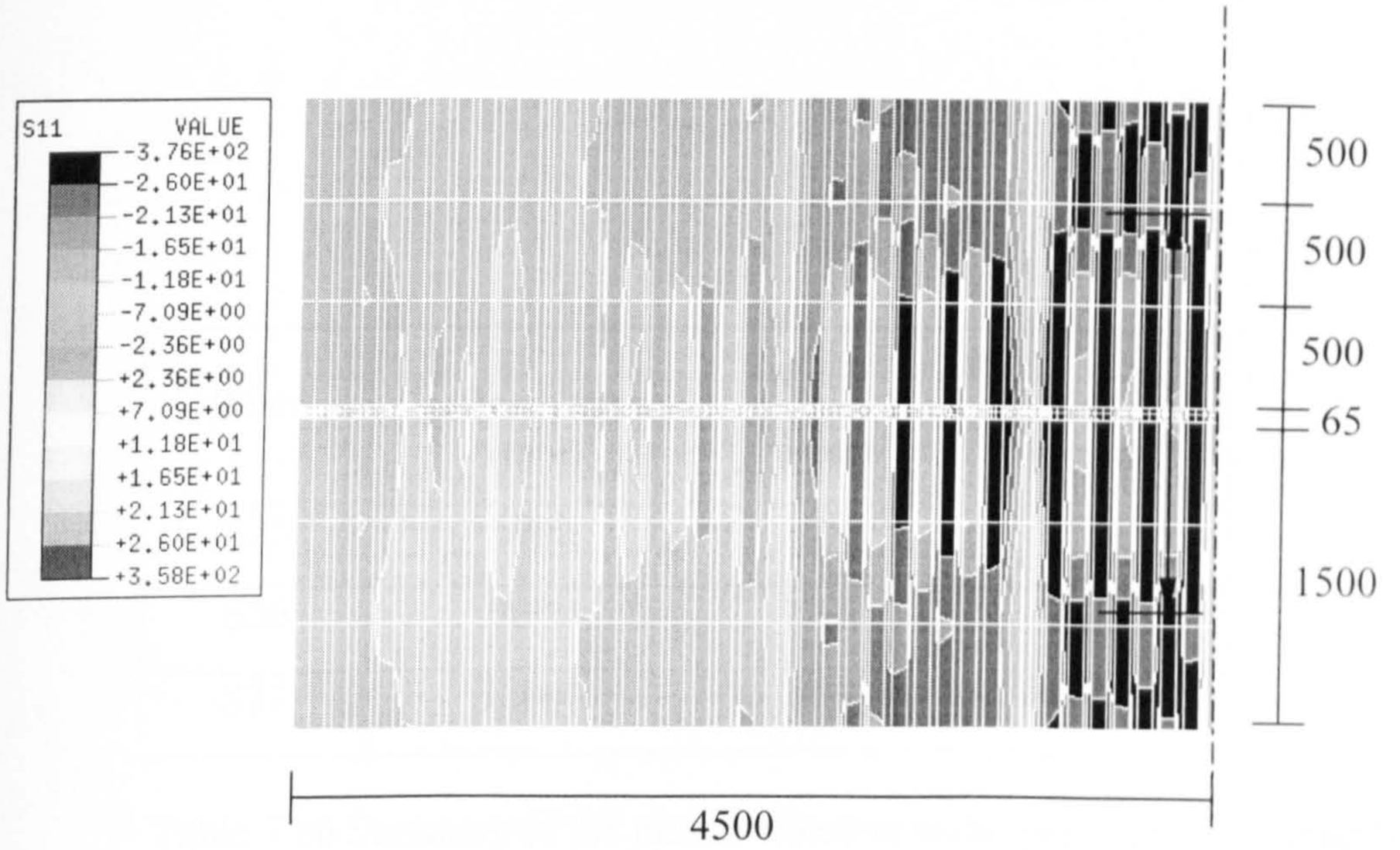

Figure 7.34.b Contour stresses plan of 9m span beam S26

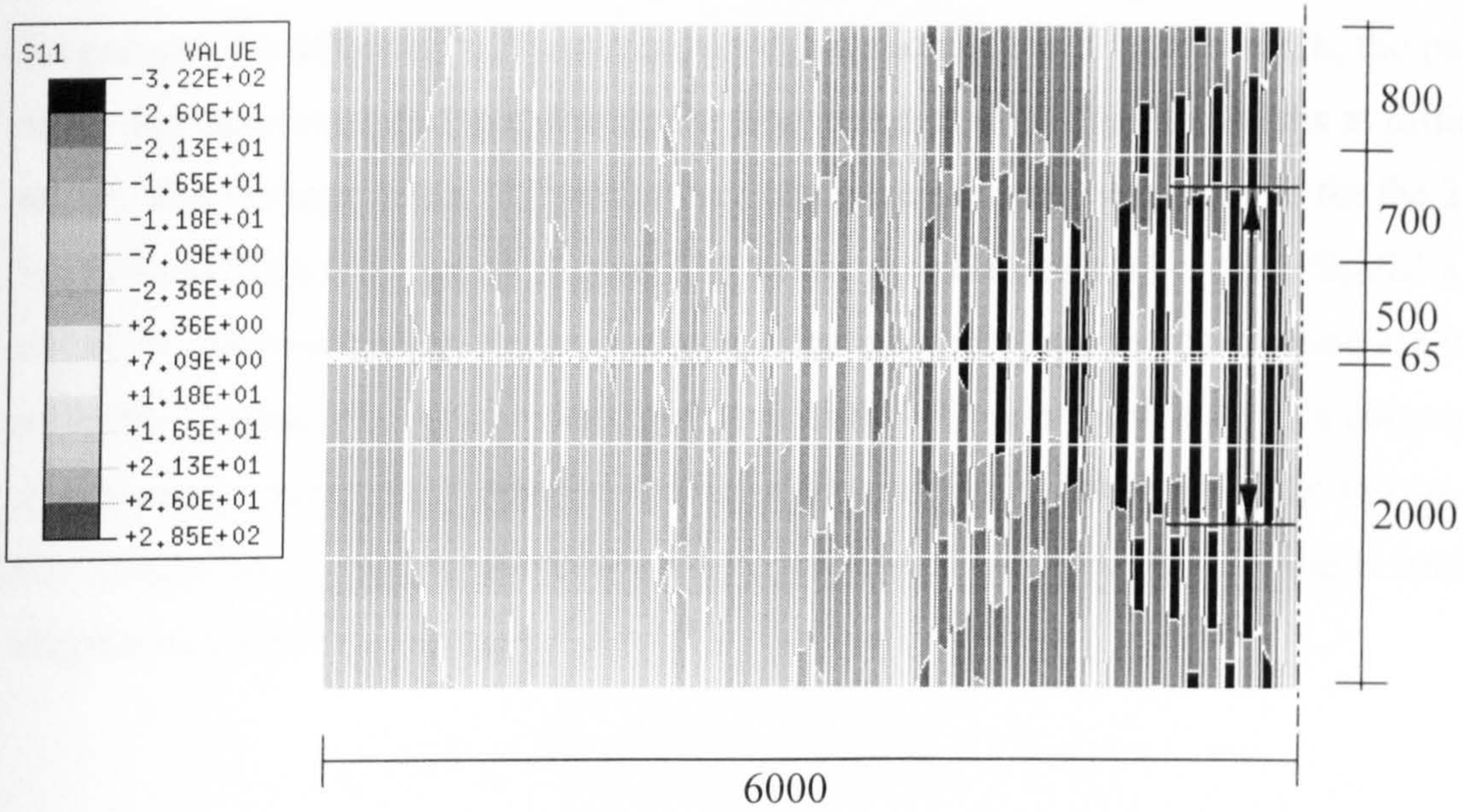

Figure 7.34.c Contour stresses plan of 12m span beam S27

Beam	L (Beam span) (mm)	b_{eff} (mm)	b_{eff}/L (mm)
S25	6000	1452	0.242
S26	9000	1950	0.217
S27	12000	2064	0.172

Table 7.10 Summary of the plastic effective width per span ratio group 9

7.6.5 Effect of 'b/L' ratio on the calculation of the effective width

The parametric study on a variety of composite steel-HC slab girders has shown that, for a 'b/L' ratio equals to 0.34 the effective width calculated based on elastic material properties is greater than that one calculated based on elastic-plastic material properties. To investigate the effect of 'b/L' ratio on the calculation of the effective width, the parametric study has been extended to calculate the elastic and plastic effective widths at different b/L ratios. The 9m span beam 'S2' is analysed using the same procedures used for the 27 beams but with different b/L ratios. Figure 7.35 shows the relationship between 'b_{eff}/L' and 'b/L' ratios. It can be seen that both the elastic effective width and the plastic one are increased with the increase of the slab width until the plastic effective width reaches a constant value. The average value of the effective width is equal to 0.22L for most of the beams that has $b \geq 0.26L$. This value is calculated at the middle of the span and decreases towards the support as shown from figures 7.23-7.25.

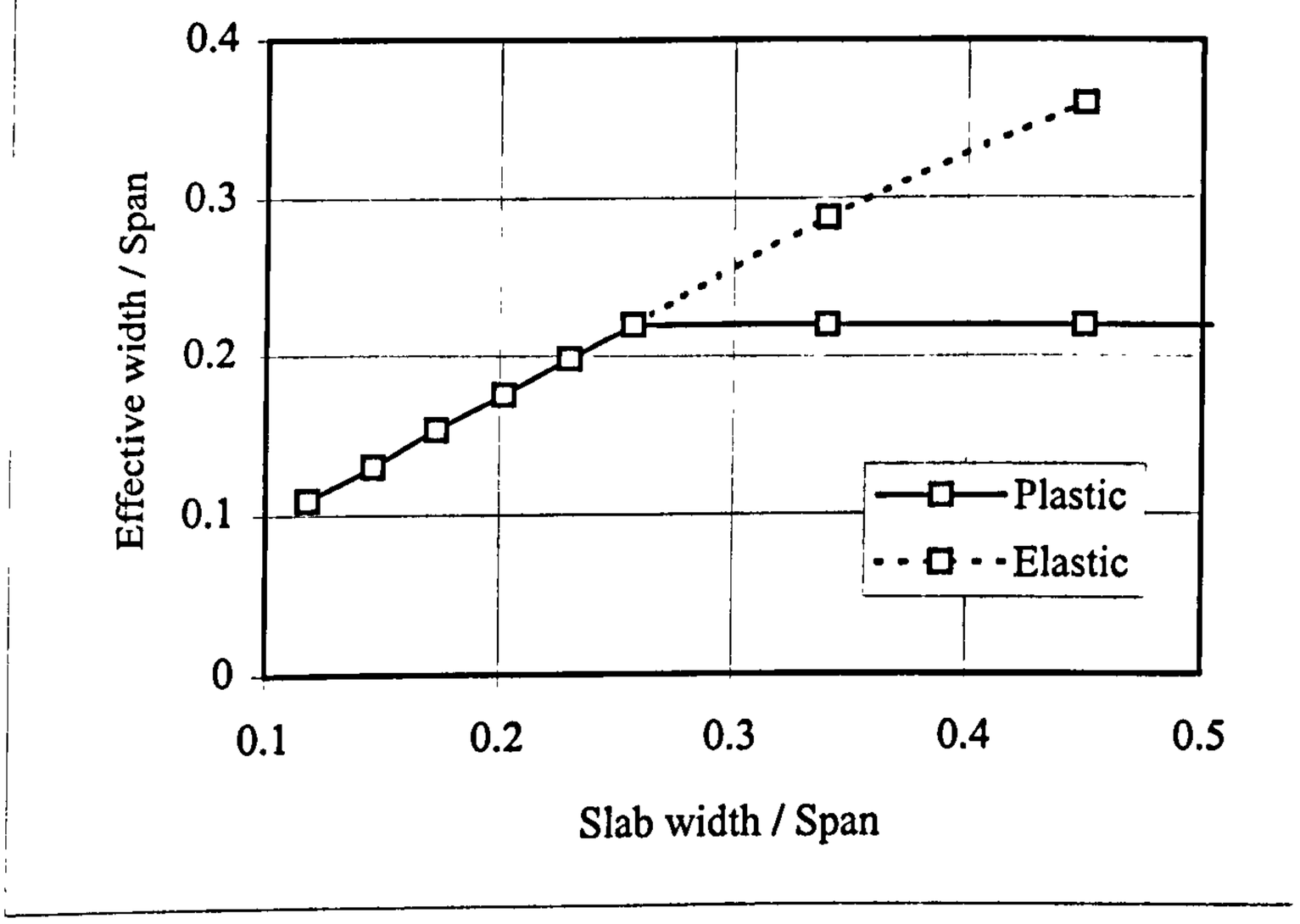

Figure 7.35 Effective width of composite steel-precast HC slab girders

7.6.6 Moment-deflection curves of composite steel-precast HC slab girders

The previous parametric study carried out to evaluate the effective width of composite steel-precast HC slab girders is used to give the designers some important information about the moment vs. mid-span deflection curves.

Figures 7.36, 7.37 and 7.38 show the moment-deflection curves of composite steel-precast HC slab girders that have HC slab depth of 150mm and different steel beam cross sections for beam spans 6, 9 and 12m respectively. Also, figures 7.39, 7.40 and 7.41 show the moment-deflection curves of composite steel-precast HC slab girders that have HC slab depth of 200mm and different steel beam cross sections for beam spans 6, 9 and 12m respectively. Finally, figures 7.42, 7.43 and 7.44 show the moment-deflection curves of composite steel-precast HC slab girders that have HC slab depth of 250mm and different steel beam cross sections for beam spans 6, 9 and 12m respectively. The predicted effective width is used in calculating the moment capacity.

Three failure modes have been checked to determine the failure point of composite girders (1. yielding of steel beam, 2. failure of headed studs, and finally 3. compressive failure of top surface of concrete slab). Generally, the elastic neutral axis was close to the interface between the steel beam and the concrete slab for most of the beams. By increasing loading beyond the elastic stage, the moment acting on the composite section increased. This resulted in yielding of the bottom flange of the steel beam and moving of the neutral axis towards the compression zone. As the moment acting on the composite section was further increased, the load carried by the composite section remained constant and the yielding of the concrete slab was likely to occur. Failure of the shear connectors occurred between yielding of the steel beam and yielding of the concrete slab. Failure of shear connectors resulted in reduction in load carrying capacity of the composite section.

The ductility of the beams decreased with the increase of the HCU depth for the same span and the same steel beam cross section. The deflection was increased and the moment capacity was decreased with the increase of the span for the same steel beam cross section and the same HCU depth.

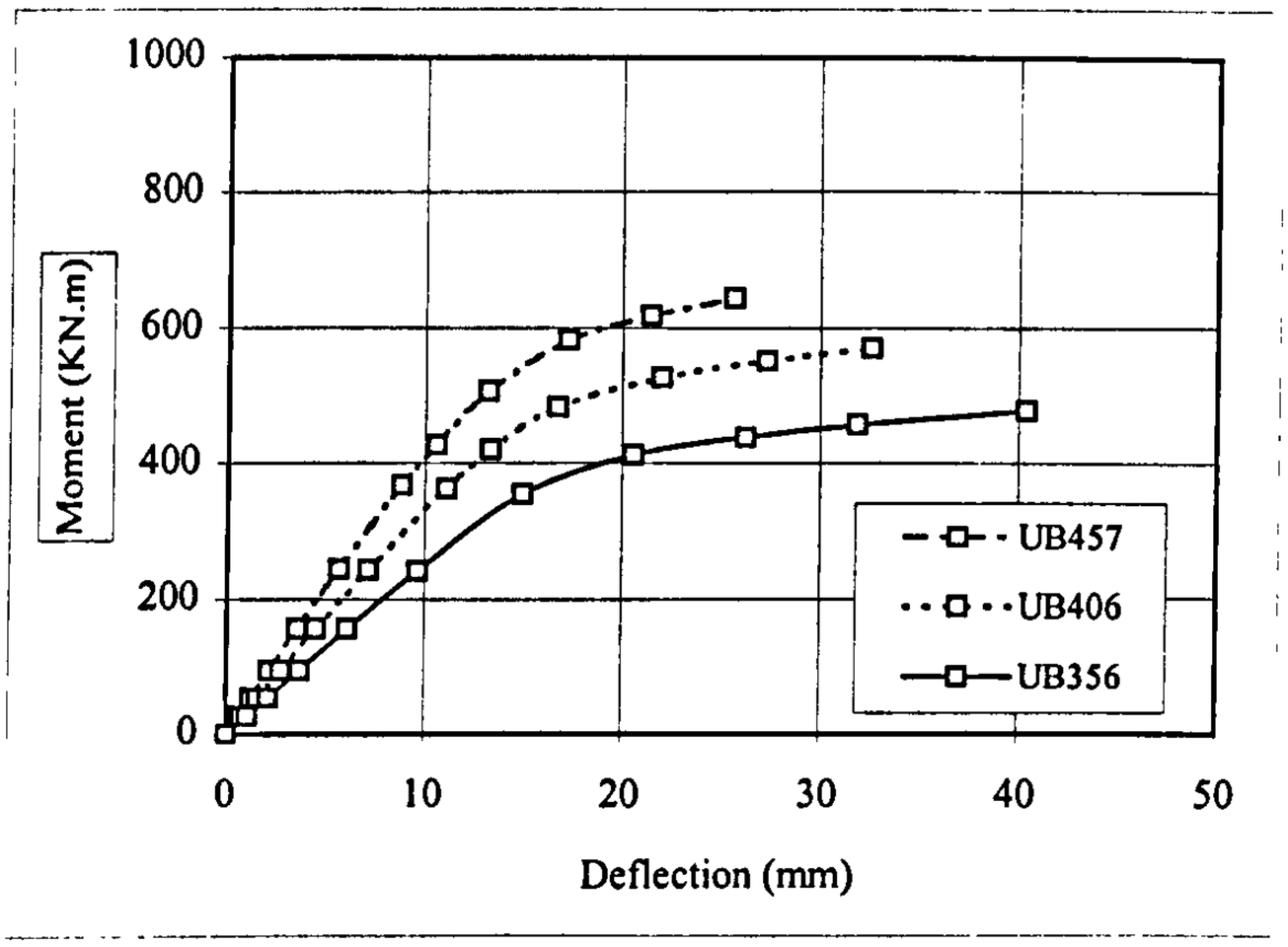

Figure 7.36 Moment vs. mid-span deflection curves of 6m span composite girders with 150mm deep HCUs

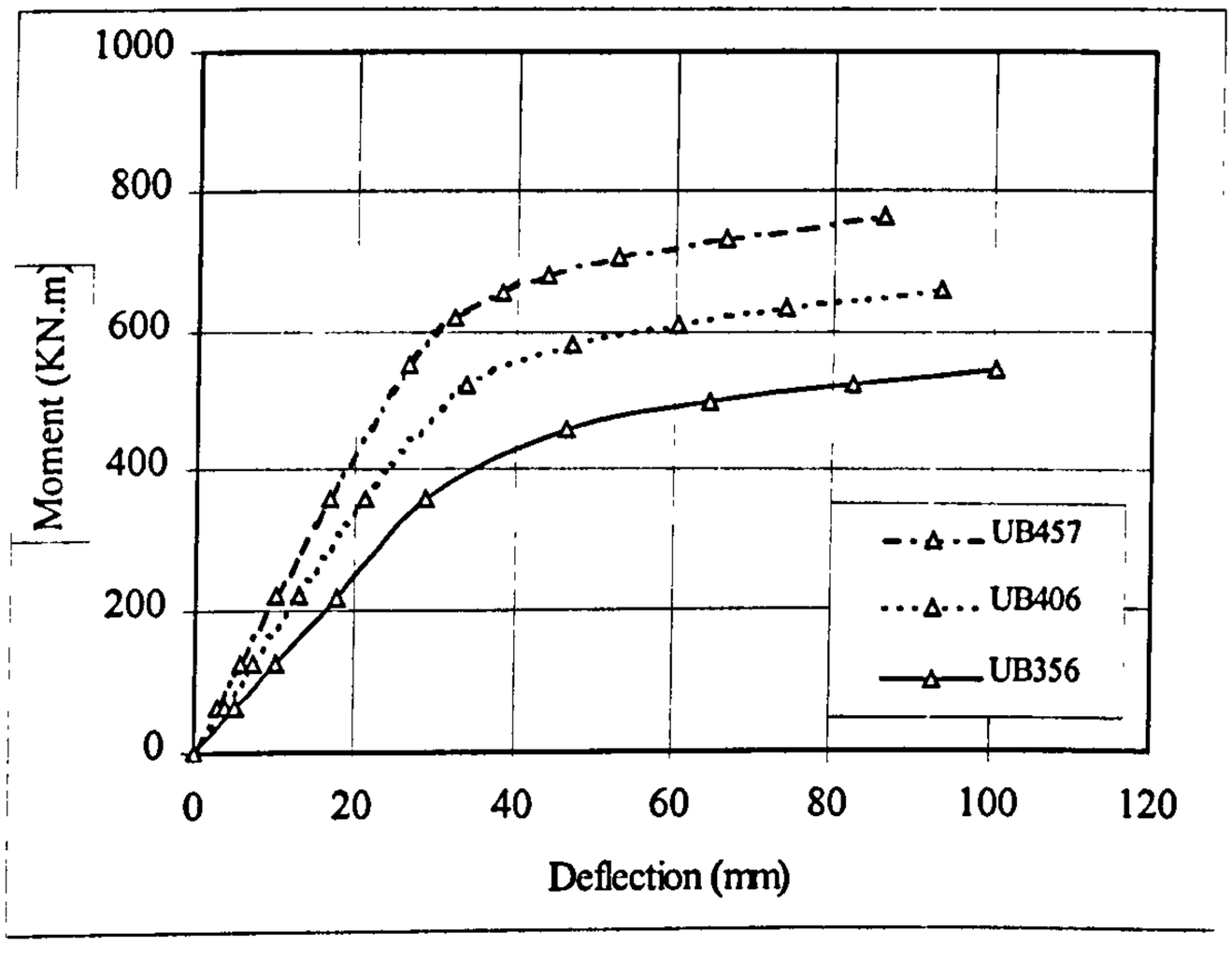

Figure 7.37 Moment vs. mid-span deflection curves of 9m span composite girders with 150mm deep HCUs

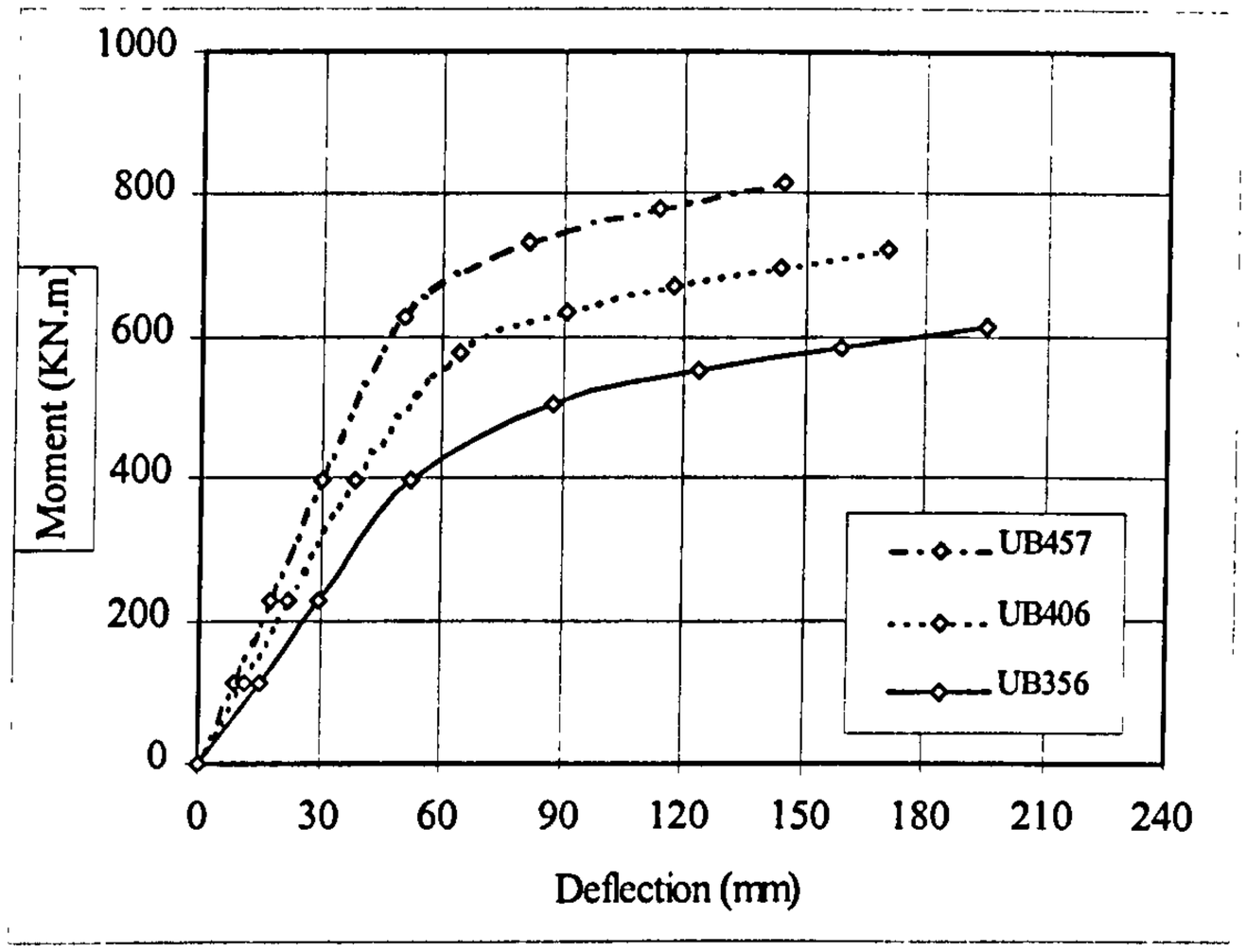

Figure 7.38 Moment vs. mid-span deflection curves of 12m span composite girders with 150mm deep HCUs

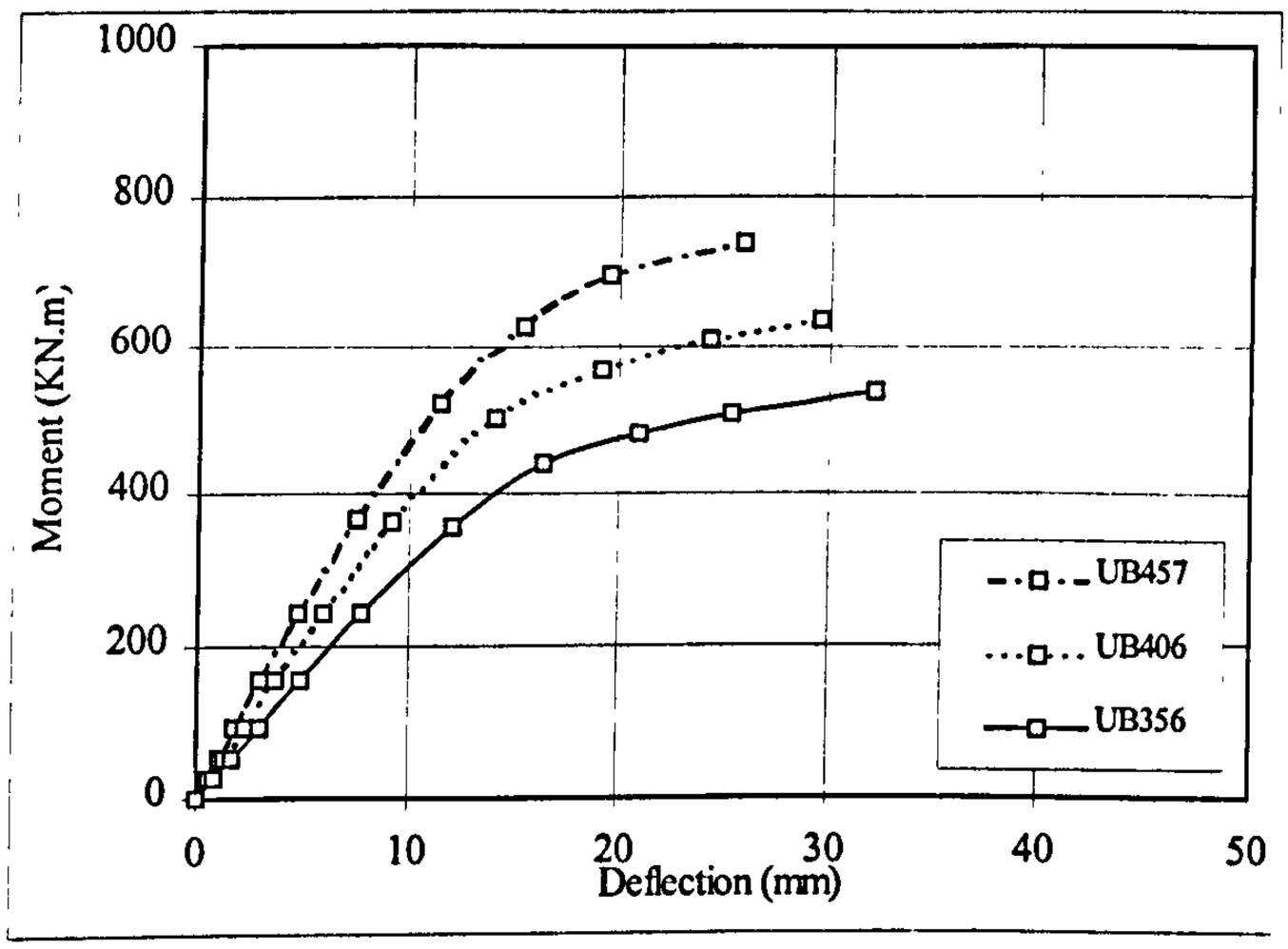

Figure 7.39 Moment vs. mid-span deflection curves of 6m span composite girders with 200mm deep HCUs

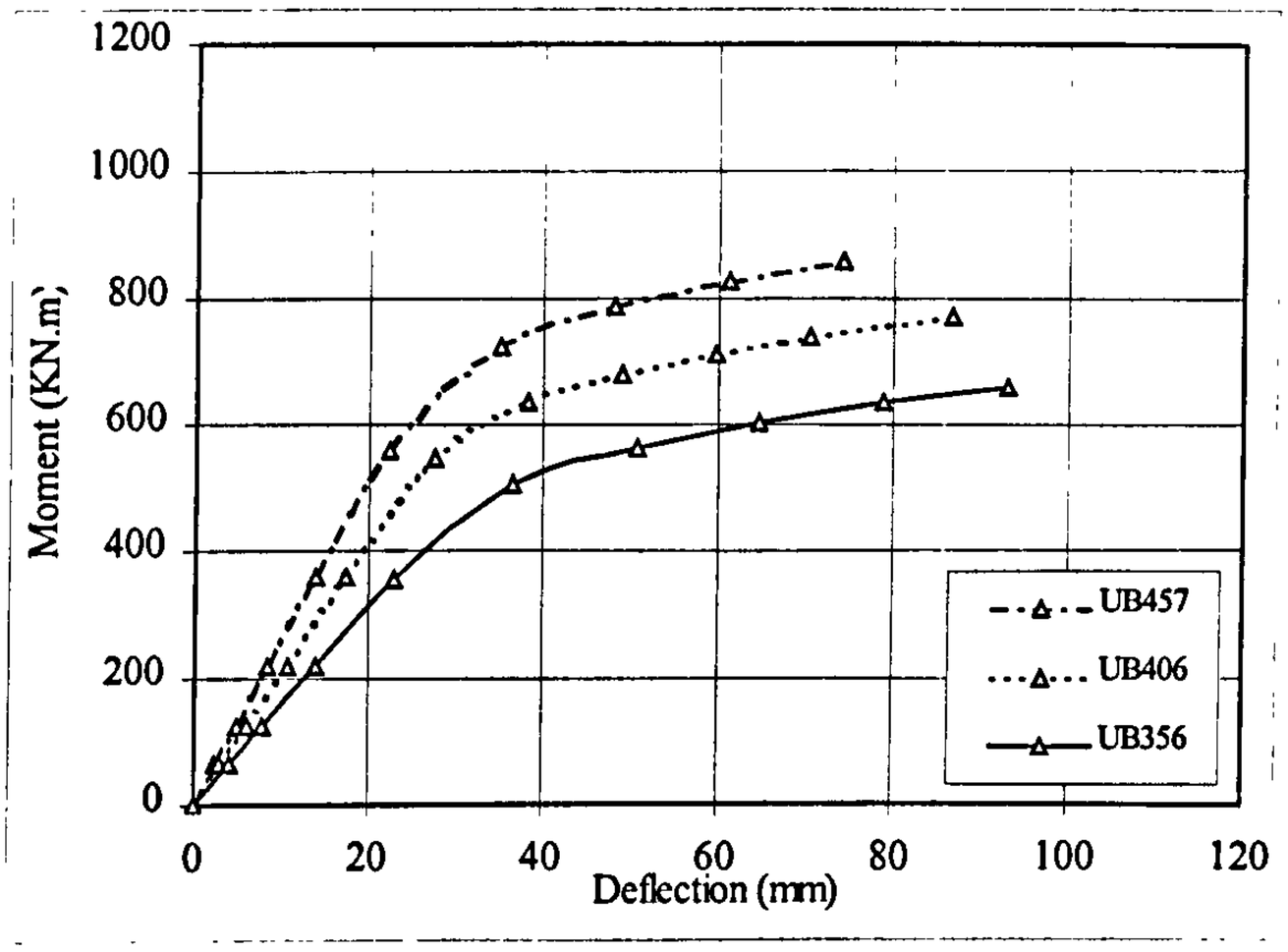

Figure 7.40 Moment vs. mid-span deflection curves of 9m span composite girders with 200mm deep HCUs

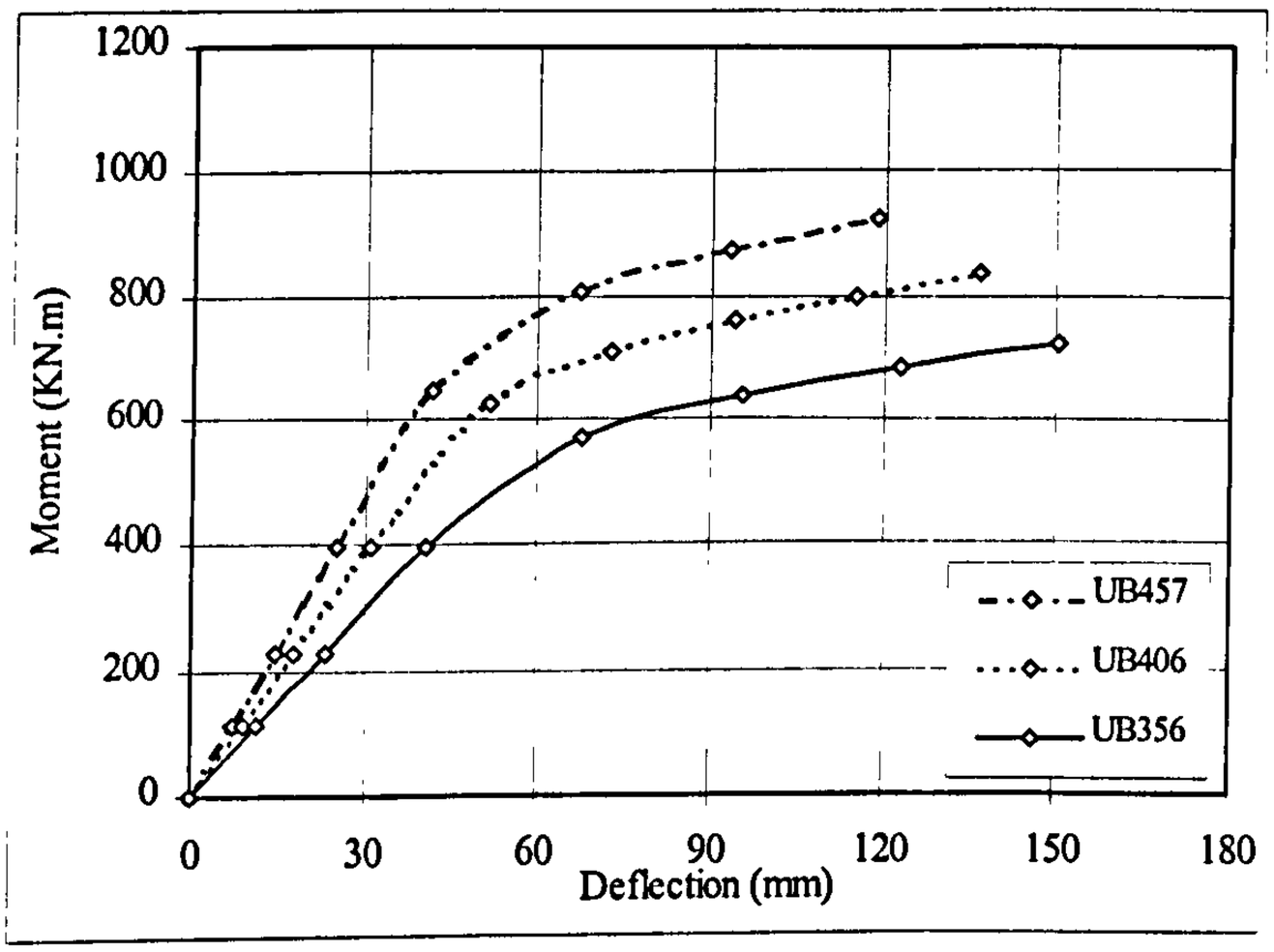

Figure 7.41 Moment vs. mid-span deflection curves of 12m span composite girders with 200mm deep HCUs

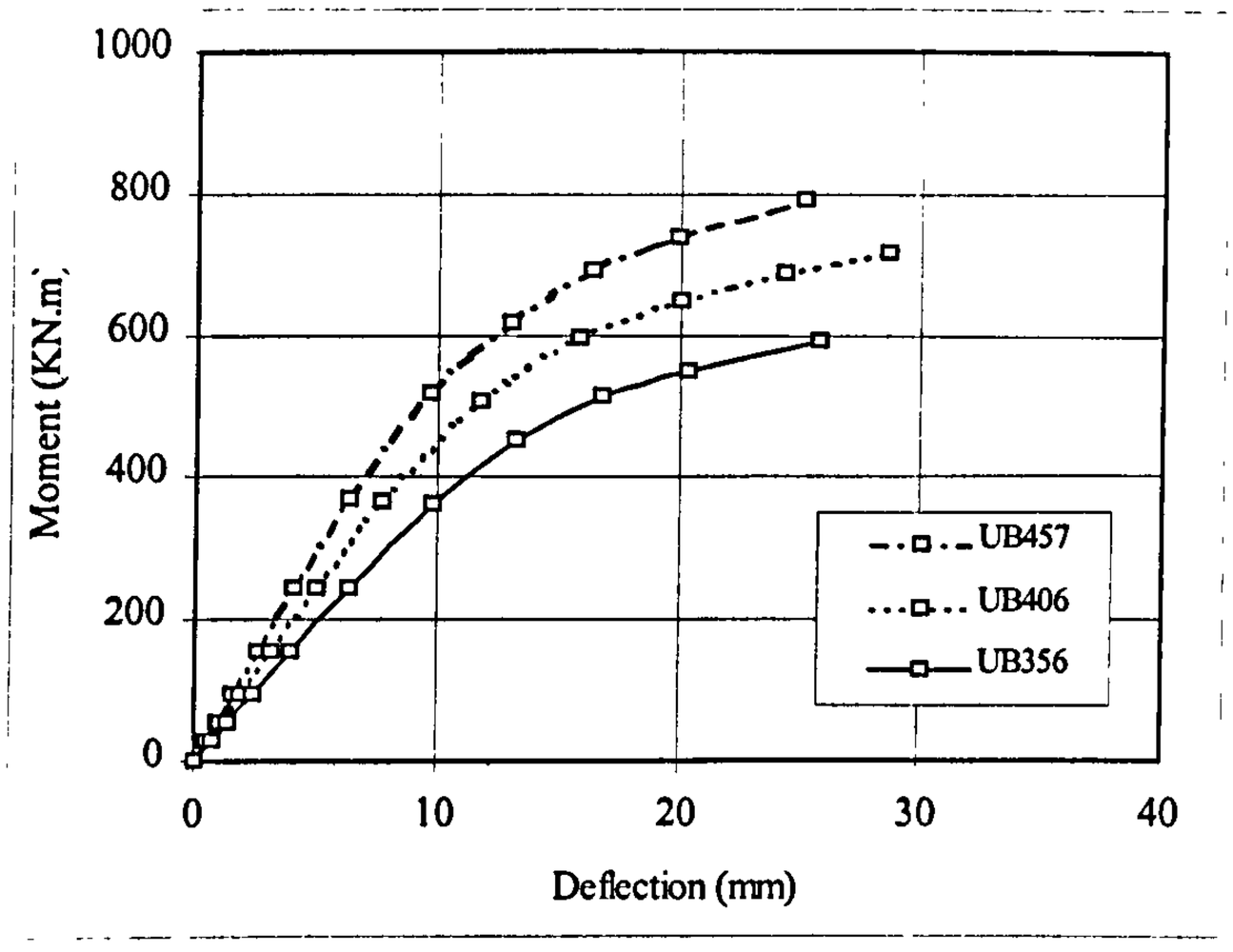

Figure 7.42 Moment vs. mid-span deflection curves of 6m span composite girders with 250mm deep HCUs

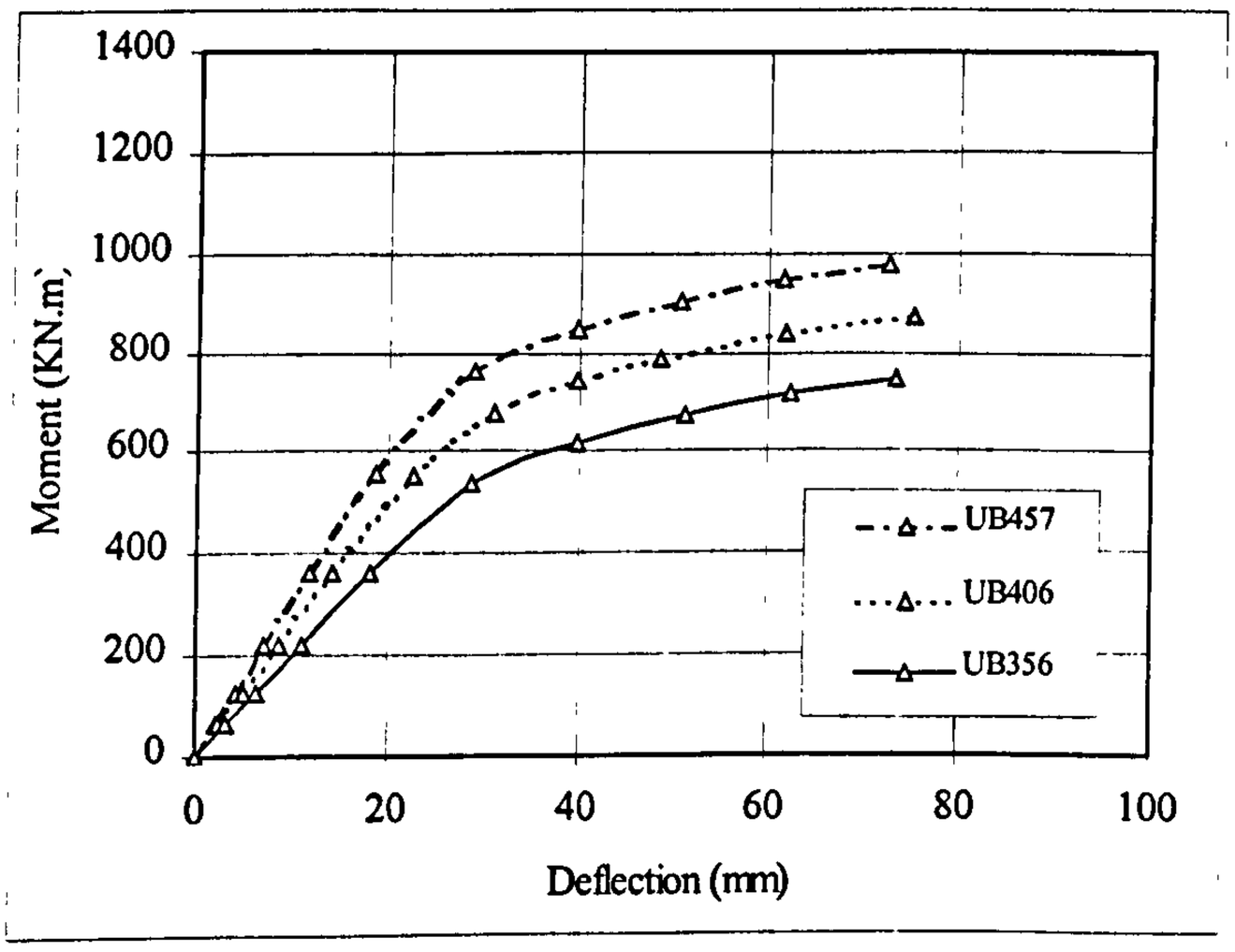

Figure 7.43 Moment vs. mid-span deflection curves of 9m span composite girders with 250mm deep HCUs

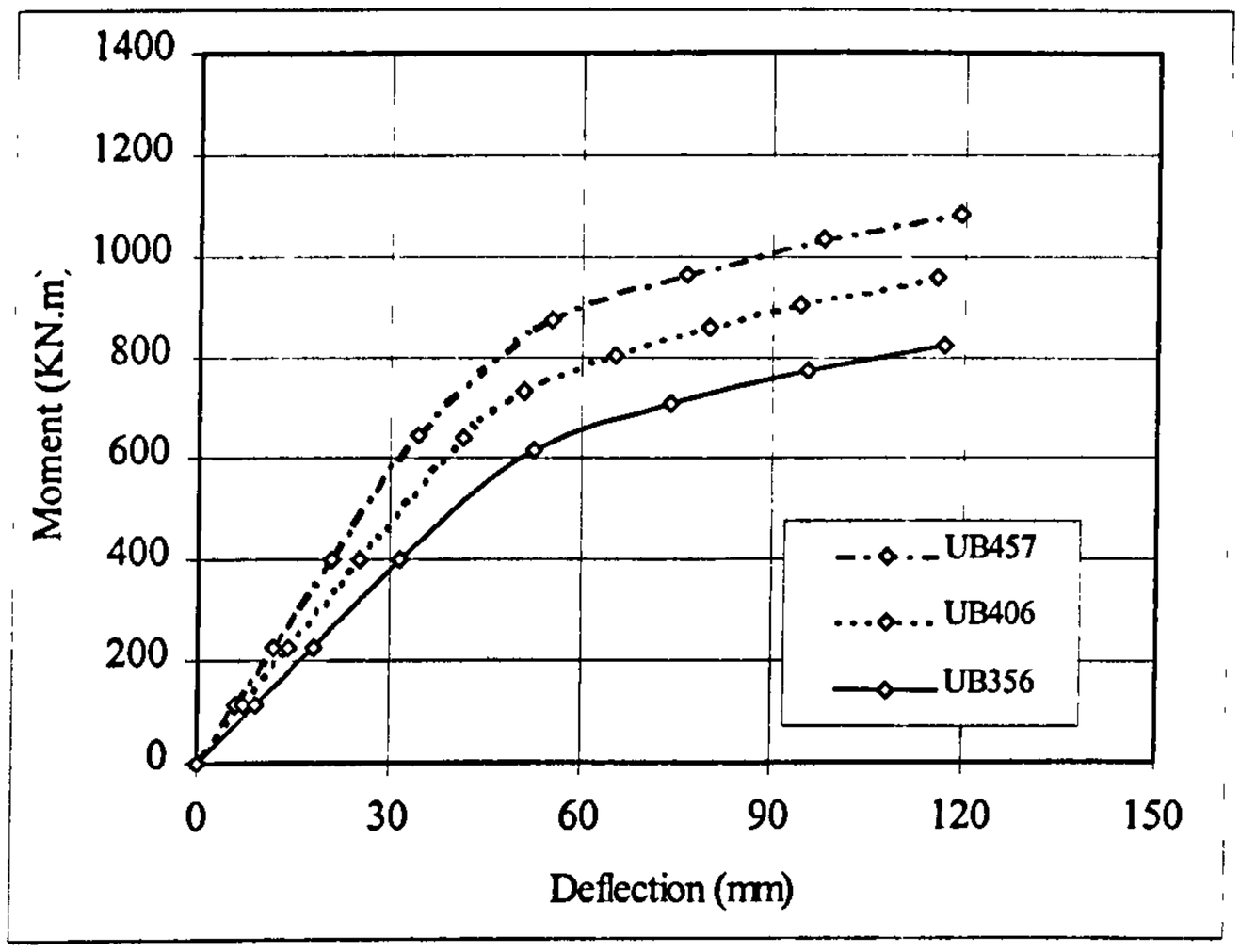

Figure 7.44 Moment vs. mid-span deflection curves of 12m span composite girders with 250mm deep HCUs

7.7 Summary and discussions

This chapter described finite element modelling of composite beams with solid slabs and with precast hollow core slabs. The literature review carried out in chapter 2, explained that no complete finite element modelling has been developed so far. Previous numerical modelling for the behaviour of composite beams either neglected the behaviour of shear connections by assuming rigid links between the steel beam and the concrete slabs or used values from push-off test results to input in the numerical model. This chapter introduced two complete finite element models for the structural behaviour of composite beams with solid slabs and with precast hollow core slabs. The shear connection capacity and the load-slip behaviour of the stud were predicted from previous numerical modelling of push-off tests with both types of slabs.

Good agreement has been achieved between the results of the finite element models and previous published experimental and numerical researches dealing with the structural behaviour of composite beams with solid slabs and with precast. Both models took into account the non-linear load-slip characteristics of the headed stud shear connector. The material non-linearity for all components of the composite girders has been taken into consideration accurately. This offers a reliable and valid finite element model for replacing laboratory tests on composite beams. It could be used to carry out effective and comprehensive parametric studies.

This chapter also introduced an effective parametric study for the evaluation of the effective width of composite beams with precast hollow core slabs. The study has analysed 27 composite beams with different hollow core depths, steel cross sections and different spans. The effective width has been evaluated in both elastic and plastic ranges. It is observed that the calculated moment capacity based on the elastic effective width overestimated the capacity of the composite beam. It is found that the effective width calculated at the mid-span can be taken as 0.22 x the span for (slab width/beam span) ratio equals or greater than 0.26. For (slab width/beam span) ratios less than 0.26, the effective width can be calculated based on elastic behaviour from Figure 7.35. The moment capacities obtained using the finite element analyses are shown in Table 7.11.

To show the practical significance of the predicted effective width and moment-deflection curves, the moment capacity obtained from finite element modelling is compared with results from the rigid plastic analysis. This comparison would give designers confidence in the uses of rigid plastic analysis principles and confirmed the reliability of the developed finite element models. Following the same approach explained by Lam et al.[62], the ultimate moment capacity of the beams under investigation can be calculated. The concrete slab is assumed to be stressed with a stress equals to $0.45f_{cu}$ over its effective width see figure 7.45. The resistance of the concrete flange F_{conc} is given by:

$$F_{conc} = 0.45 f_{cu} b_{eff} d_p \qquad \text{.....(7.5)}$$

where f_{cu} is the compressive concrete cube strength of the in-situ concrete that is equals to 26N/mm^2, b_{eff} is the effective width calculated from present parametric study as 0.22 the span of the beam, and d_p is the depth of the HCU.

The resistance of the steel beam F_{steel} is given by:

$$F_{steel} = A_{steel} f_{ys} \quad \text{.....(7.6)}$$

Where A_{steel} is the cross sectional area of the steel beam and f_{ys} is the yield stress of the steel beam that is equal to 275N/mm^2 for structural steel grade S275.

Composite beam with full shear interaction

For composite beam with full shear interaction (i.e. sufficient number of shear connectors is used to transfer the longitudinal shear forces at the steel-concrete interface), F_{con} (the resistance force of the shear connectors) is greater than the smaller of F_{conc} or F_{steel}. F_{con} is is given by:

$$F_{con} = nP_R \quad \text{.....(7.7)}$$

where n is the number of shear connectors spaced at S in a half span L/2 ($n = \frac{L}{2S} + 1$) and P_R is the resistance of the shear connector obtained from previous FE analysis investigated in Ref. 7 and equals to 70kN for the 19mm diameter x 100mm height headed stud in push-off test with HC slab at in-situ concrete strength of 26N/mm^2 and transverse reinforcement diameter 8mm.

For a plastic neutral axis in the concrete flange ($F_{conc} > F_{steel}$), the calculated ultimate moment capacity of the composite beam is given by:

$$M_{comp} = F_{steel} \left(\frac{D}{2} + d_p - \frac{F_{steel}}{F_{conc}} \frac{d_p}{2}\right) \quad \text{.....(7.8)}$$

where D is the overall depth of the steel beam.

For a plastic neutral axis in the steel section ($F_{steel} > F_{conc}$), the calculated ultimate moment capacity of the composite beam is given by:

$$M_{comp} = F_{steel}\frac{D}{2} + F_{conc}\frac{d_p}{2} - \frac{(F_{steel} - F_{conc})^2}{F_{flange}}\frac{T}{4} \qquad \text{.....(7.9)}$$

where F_{flange} is the axial capacity of one steel flange of thickness T and breadth B ($F_{flange} = TBf_{ys}$).

Composite beam with full shear interaction

For composite beam with partial shear interaction, F_{con} is less than the smaller of F_{conc} or F_{steel}. The calculated ultimate moment capacity of the composite beam is given by:

$$M_{comp} = M_s + F_{con} \times (d_p - \frac{F_{con}}{F_{conc}}\frac{d_p}{2}) - \frac{(F_{steel} - F_{con})^2}{F_{flange}}\frac{T}{4} \qquad \text{.....(7.10)}$$

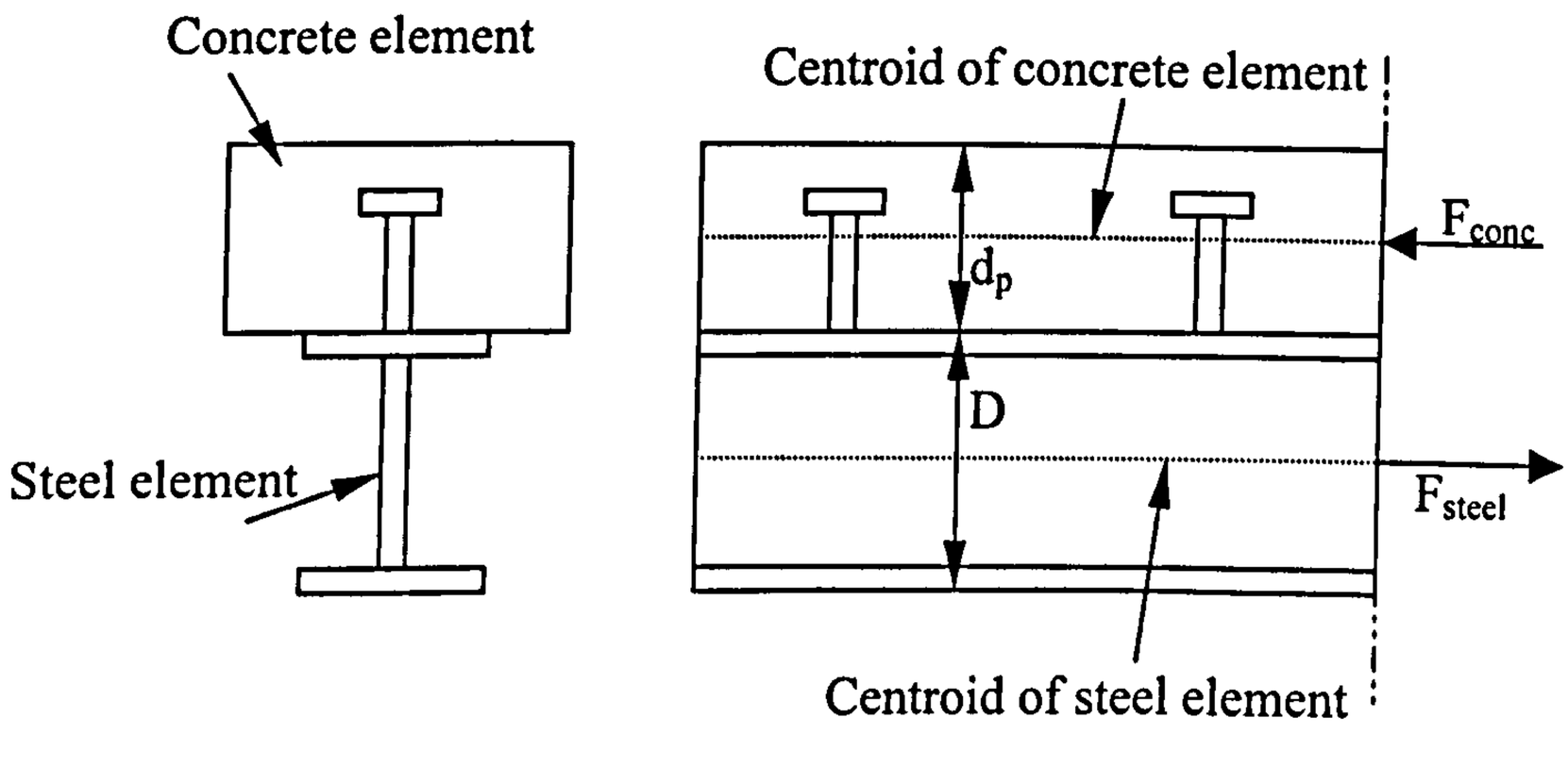

Figure 7.45 Force distribution of composite beam

Table 7.11 contains the summary of the calculations of the ultimate moment capacity obtained from both plastic design principles in comparison with that obtained from present

FE solution. It can be shown that good agreement between both results has been achieved in most of the beams. This confirms the validity of the finite element model to predict effectively the moment capacity of the composite beams with hollow core slabs.

A further study has been carried out to show the practical significance of the predicted elastic and plastic effective widths. Figure 7.35 shows that for b/L ratio equals to 0.4, the elastic effective width is equal to 0.33L while the plastic effective width is equal to 0.22L. The moment capacities of the composite beam sections using elastic effective width were evaluated and summarised in Table 7.12. The values are compared with that previously obtained using plastic effective width in table 7.11. Table 7.12 shows that the calculated moment capacity based on elastic effective width overestimated the moment capacity of the composite beams by an average of 15%.

Table 7.11 Summary of the calculations of the ultimate moment capacity

Group	Beam	UB	b_{eff} (mm)	d_p (mm)	A_s (cm^2)	D (mm)	T_{flange} (mm)	B_{flange} (mm)	Z_{pl} (cm^3)	M_s (kN.mm)	F_{flange} (kN)	F_{conc} (kN)	F_{steel} (kN)	F_{con} (kN)	Failure Mode	M_{comp} cal. (kN.m)	M_{comp} FE (kN.m)	$\frac{M_{comp}\ cal.}{M_{comp}\ FE}$
	S1	356x171x51	1320	150	64.9	355	11.5	171.5	896	246400	542.4	2316.6	1784.75	1470	Concrete	396	478	0.83
G1	S2	356x171x51	1980	150	64.9	355	11.5	171.5	896	246400	542.4	3474.9	1784.75	2170	Concrete	516	546	0.95
	S3	356x171x51	2640	150	64.9	355	11.5	171.5	896	246400	542.4	4633.2	1784.75	2870	Concrete	533	612	0.87
	S4	406x178x60	1320	150	76.5	406.4	12.8	177.9	1199	329725	626.2	2316.6	2103.75	1470	Steel beam	478	570	0.84
G2	S5	406x178x60	1980	150	76.5	406.4	12.8	177.9	1199	329725	626.2	3474.9	2103.75	2170	Steel beam	648	660	0.98
	S6	406x178x60	2640	150	76.5	406.4	12.8	177.9	1199	329725	626.2	4633.2	2103.75	2870	Steel beam	671	720	0.93
	S7	457x191x67	1320	150	85.5	453.4	12.7	189.9	1471	404525	663.2	2316.6	2351.25	1470	Steel beam	551	644	0.86
G3	S8	457x191x67	1980	150	85.5	453.4	12.7	189.9	1471	404525	663.2	3474.9	2351.25	2170	Steel beam	628	763	0.82
	S9	457x191x67	2640	150	85.5	453.4	12.7	189.9	1471	404525	663.2	4633.2	2351.25	2870	Steel beam	796	814	0.98
	S10	356x171x51	1320	200	64.9	355	11.5	171.5	896	246400	542.4	3088.8	1784.75	1470	Concrete	469	538	0.87
G4	S11	356x171x51	1980	200	64.9	355	11.5	171.5	896	246400	542.4	4633.2	1784.75	2170	Concrete	605	658	0.92
	S12	356x171x51	2640	200	64.9	355	11.5	171.5	896	246400	542.4	6177.6	1784.75	2870	Concrete	622	724	0.86
	S13	406x178x60	1320	200	76.5	406.4	12.8	177.9	1199	329725	626.2	3088.8	2103.75	1470	Steel beam	552	636	0.87
G5	S14	406x178x60	1980	200	76.5	406.4	12.8	177.9	1199	329725	626.2	4633.2	2103.75	2170	Steel beam	753	770	0.98
	S15	406x178x60	2640	200	76.5	406.4	12.8	177.9	1199	329725	626.2	6177.6	2103.75	2870	Steel beam	777	835	0.93
	S16	457x191x67	1320	200	85.5	453.4	12.7	189.9	1471	404525	663.2	3088.8	2351.25	1470	Stud	625	740	0.84
G6	S17	457x191x67	1980	200	85.5	453.4	12.7	189.9	1471	404525	663.2	4633.2	2351.25	2170	Stud	737	859	0.86
	S18	457x191x67	2640	200	85.5	453.4	12.7	189.9	1471	404525	663.2	6177.6	2351.25	2870	Stud	914	925	0.99
	S19	356x171x51	1320	250	64.9	355	11.5	171.5	896	246400	542.4	3861	1784.75	1470	Concrete	543	592	0.92
G7	S20	356x171x51	1980	250	64.9	355	11.5	171.5	896	246400	542.4	5791.5	1784.75	2170	Concrete	694	748	0.93
	S21	356x171x51	2640	250	64.9	355	11.5	171.5	896	246400	542.4	7722	1784.75	2870	Concrete	711	825	0.86
	S22	406x178x60	1320	250	76.5	406.4	12.8	177.9	1199	329725	626.2	3861	2103.75	1470	Steel beam	625	718	0.87
G8	S23	406x178x60	1980	250	76.5	406.4	12.8	177.9	1199	329725	626.2	5791.5	2103.75	2170	Steel beam	858	872	0.98
	S24	406x178x60	2640	250	76.5	406.4	12.8	177.9	1199	329725	626.2	7722	2103.75	2870	Steel beam	882	958	0.92
	S25	457x191x67	1320	250	85.5	453.4	12.7	189.9	1471	404525	663.2	3861	2351.25	1470	Stud	698	793	0.88
G9	S26	457x191x67	1980	250	85.5	453.4	12.7	189.9	1471	404525	663.2	5791.5	2351.25	2170	Stud	845	978	0.86
	S27	457x191x67	2640	250	85.5	453.4	12.7	189.9	1471	404525	663.2	7722	2351.25	2870	Stud	1031	1083	0.95

Group	Beam	FE analysis		
		M_{comp} (Pl.)	M_{comp} (El.)	(Pl.)/(El.) %
G1	S1	478	538	0.89
	S2	546	639	0.85
	S3	612	722	0.85
G2	S4	570	652	0.87
	S5	660	756	0.87
	S6	720	852	0.84
G3	S7	644	744	0.86
	S8	763	867	0.88
	S9	814	960	0.85
G4	S10	538	646	0.83
	S11	658	796	0.83
	S12	724	863	0.84
G5	S13	636	749	0.85
	S14	770	910	0.85
	S15	835	1010	0.83
G6	S16	740	846	0.87
	S17	859	1011	0.85
	S18	925	1128	0.82
G7	S19	592	729	0.81
	S20	748	911	0.82
	S21	825	965	0.85
G8	S22	718	824	0.87
	S23	872	1058	0.82
	S24	958	1154	0.83
G9	S25	793	908	0.87
	S26	978	1164	0.84
	S27	1083	1320	0.82

Table 7.12 Summary of the composite beam moment capacities

8. Conclusions and future work

8.1 Conclusions

The work presented in this thesis has investigated the behaviour of headed stud shear connector in composite girders with solid and precast HC slabs. This has been carried out in two stages. In the first stage, combination of FE modelling and experimental investigation of the behaviour of headed stud in push-off tests, with both types of slabs, has been carried out. In the second stage, the obtained results from the first stage have been used in modelling the longitudinal structural behaviour of composite girders with both types of slabs.

8.1.1 Conclusions related to the FE modelling and experimental investigation of the behaviour of headed studs in push-off tests:

The following conclusions are extracted from the present research:

In push-off tests with solid slabs

1. Since the predicted finite element model can accurately represent all the main features of the behaviour of headed stud in push-off tests with solid slabs, it offers a reliable and very cost-effective alternative to laboratory testing as a way of generating results. Also comparison of finite element results with previous experimental research and with values of current codes of practice indicated that the use of the shear stud capacities predicted in this study is more reliable than that of the tabulated values in BS 5950[7].

2. From the literature review presented in this study, limited success has been achieved in the numerical modelling of push-off tests with solid slabs due to inappropriate choice of finite elements. The three-dimensional solid elements used in this study represented effectively the shear connection with reasonable finite element meshes and less solution time.

3. Good agreement has been achieved between finite element analyses and experimental investigations carried out in present study. It has been observed that the concrete cube strength, stud diameter and stud height significantly affect load-slip behaviour of headed stud shear connector, shear connection capacity and modes of failure.

4. Three modes of failure were observed from present push-off tests and verified numerically by present FE model. The first mode of failure is the concrete cone failure where no stud failure is observed. For this mode of failure, the concrete around the stud started to fail before the stud was yielded, the failure progresses through the thickness of the concrete forming a conical shape around the stud. The second mode of failure is that the stud connector was fully yielded and no concrete failure is observed. This mode of failure is identified as stud failure mode where the yield stress is reached in the stud elements while maximum concrete stress of the concrete elements is not reached. Finally, the third mode of failure is the combined failure of stud and concrete slab when maximum stresses are reached in stud and concrete elements.

5. Although, there is good agreement between the present finite element results with that predicted from Eurocode 4[8] equations, the reduction in shear connection strength due to the reduction in stud height seems to be ignored in the factor (α) given in the Eurocode 4[8] equation, clause 6.3.2.2. A suggested modification for that factor based on the present finite element modelling to include the effect of the stud height on the shear connection capacity may be given as [$\alpha=0.2(h/d+0.5) < 1.0$], where h is the overall height of stud and d is the diameter. Although, further finite element study may be required to investigate the effect of stud height on the shear connection capacity, the suggested value at least ensures good representation of Eurocode 4[8] shear stud capacity for the studs tabulated in BS 5950[7]. It is also

observed from the finite element analyses that BS 5950[7] over-estimated the shear capacity of the headed studs.

6. The review of previous experimental research on push-off tests with solid slabs has shown the lack of push-off tests carried out on headed studs with 22mm diameter x 100mm height and headed studs with 25mm diameter x 100mm height. This suggests that the predicted shear stud capacity from the present finite element solutions may be more accurate than that tabulated in the BS 5950[7] and the Eurocode 4[8].

In push-off tests with precast hollow core slabs

1. The general conclusion to be drawn from present study that since the finite element model can accurately study the behaviour of headed studs in push-off tests with precast hollow core slabs, it offers a reliable and very cost-effective alternative to laboratory testing as a way of generating results. It can at least reduce the number of future push-off tests in this new type of composite construction.

2. Good agreement has been achieved between experimental investigations and present finite element modelling of the behaviour of headed studs in push-off tests with precast hollow core slabs. In addition to the failure modes predicted in case of push-off tests with solid slabs, the transverse reinforcement bar failure mode is investigated using the finite element analyses. It has been observed that transverse reinforcement bars enhance the in-plane shear resistance by crossing the precast and the in-situ concrete interface. Also, it limits the longitudinal splitting of the concrete by carrying tensile splitting forces. Transverse bars of small diameters in push-off tests with precast hollow core slabs are likely to yield because of concentrations of in-plane and longitudinal stresses in the bar elements at the interface between precast and in-situ concrete. Failure of transverse reinforcement bar causes premature failure of the concrete around the stud. Specimens with higher sizes of transverse bars have

shown higher ductility in terms of the load-slip behaviour of the stud than that of lower sizes.

3. Parametric studies carried out using the finite element model have shown that transverse gap size, transverse reinforcement diameter and in-situ concrete strength had significant effect on the behaviour of shear connectors in composite beams with precast hollow core slabs. It was found that:

a. The shear stud capacity is increased with the increase of the gap size between HCUs using transverse reinforcement bars of diameter less than 16mm theoretically. This increase is obtained for gap sizes up to 80mm. For gap sizes greater or equal to 80mm, there is no effect on the shear stud capacity and it may be taken as the similar solid slab one that has the same thickness and strength of the in situ concrete.
b. The shear stud capacity is increased with the increase of the transverse reinforcement diameter with gap sizes less than 80mm. This increase is obtained for reinforcement bar diameters up to 16mm. For bar diameters higher or equal to 16mm, there is no effect on the shear stud capacity and it may be taken as the similar solid slab one that has the same thickness and strength of the in-situ concrete.
c. Both of the increase in bar diameters or gap sizes increased the ductility of shear connection and hence the load-slip behaviour of the headed stud shear connector.
d. The in situ concrete strength had significant effect on the shear stud capacity and load-slip behaviour of the stud in push-off tests with precast hollow core slabs if adequate transverse reinforcement is provided.

8.1.2 Conclusions related to the FE modelling of composite girders with solid and precast hollow core slabs:

1. Present literature review explained that no complete finite element modelling has been developed so far. Previous numerical modelling for the behaviour of composite beams as general either neglected the behaviour of shear connections by assuming rigid links between the steel beam and the concrete slabs or used values form push-

off test results to input in the numerical model. This study introduced two complete finite element models for the structural behaviour of composite beams with solid slabs and with precast hollow core slabs. The shear connection capacity and the load-slip behaviour of the stud were predicted from previous numerical modelling of push-off tests with both types of slabs.

2. Good agreement has been achieved between the results of the finite element models and previous published experimental and numerical researches dealing with the structural behaviour of composite beams with solid slabs and with precast. Both models took into account the non-linear load-slip characteristics of the headed stud shear connector. The material non-linearity for all components of the composite girders has been taken into consideration accurately. This offers the reliability and the validity of the finite element models in replacing laboratory tests on composite beams. It could be used to carry out effective and comprehensive parametric studies.

3. This study introduced an effective parametric study for the evaluation of the effective width of composite beams with precast hollow core slabs. The study has analysed 27 composite beams with different hollow core depths, steel cross sections and different spans. The effective width has been evaluated in both elastic and plastic ranges. It is observed that the calculated moment capacity based on the elastic effective width would overestimate the capacity of the composite beam. From the parametric study carried out to investigate the effective width of composite steel-precast HC slab girders, it is found that the effective width is equal to 0.22 x the span for (slab width/span) ratio greater or equal to 0.26. This value is obtained at the middle of the composite girder. For values of (slab width/span) ratio less than 0.26, the effective width can be calculated based on elastic behaviour from Figure 7.35.

4. Good agreement has been achieved in the comparison between the moment capacity obtained from finite element modelling, for composite girders with precast hollow core slabs, and the moment capacity based on rigid plastic analysis. This would give

designers confidence in the uses of rigid plastic analysis principles and confirmed the reliability of the developed finite element models.

8.2 Recommendation for future work

On the basis of the results of this study, the following recommendations are proposed for future work:

1. *Experimental investigations on composite girders with precast hollow core units with square ends and headed stud shear connectors.* All studies carried out in this research program were based on FE modelling of these girders and comparing results with previous experimental and numerical results published in the available literature. The experimental tests will increase the validity of the FE model and result in accurate design equations that increase the understanding of the behaviour of this type of construction. Previous experimental investigations of composite girders with precast hollow core slab were carried out by using 19mm diameter x 125mm height studs and hollow core units with tapered ends and were mainly concentrated on 6m spans. Although finite element analyses discussed in this study have shown that the structural behaviour of composite girders has not been considerably affected by the end conditions of the hollow core units or the height of the stud, experimental investigations will verify the reliability of the finite element modelling and result in substantial saving both in manufacturing and construction.

2. *Finite element modelling of the behaviour of headed stud shear connector in push-off tests with profiled steel sheeting composite flooring.* The accuracy and reliability of present finite element modelling of push-off tests with solid slabs and precast hollow core slabs could be applied to model push-off tests with profiled steel sheeting composite slabs. Present literature review has shown that, no detailed FE models have been found dealing with the behaviour of headed stud in this type of construction. Most equations found in the literature concern this type of construction were empirical formulae based on the statistical analysis of the experimental push-off tests. The only developed equations based on theoretical models obtained from

seven observed modes of failure found in the literature is that given by Johnson and Yuan[21]. The main new parameters to be considered in the finite element modelling are the presence of profiled sheeting, sloping slab edges, position of headed stud shear connector and direction of sheeting either parallel or transverse to the steel beam. From the experience gained from present finite element modelling, accurate investigation for the connection between the headed stud welded on the top flange of the steel beam and profiled steel sheeting composite slab. Also, the modelling of the hole through the decking in which the stud will be positioned and its boundaries with the stud. New modes of failures are expected such as local concrete failure around the foot of the shear connector due to the sloping edges and shearing of the connector just above the weld collar due to high concentration of stresses from the composite slab.

3. *Finite element modelling of composite girders with profiled steel sheeting.* Towards complete finite element representation of the structural behaviour of composite girders with profiled sheeting composite slab, the results obtained from aimed numerical modelling of push-off tests will be used in representing the shear connection in this type of composite construction. The shear connection capacity and the load-slip behaviour of headed stud obtained from numerical modelling will be used in defining the non-linear springs representing the studs in the longitudinal direction. From the experience gained from the finite element modelling of composite girders with solid and precast hollow core slab, the only obstacle in the finite element modelling will be the finite element meshing of concrete inside the profiled sheeting. Since the thickness of profiled sheeting is very small compared with concrete slab, a finite mesh is required to control the aspect ratio within the limits of the finite element package. Having a fine mesh has a lot of difficulties in terms of convergence when using a sophisticated material model of concrete such that one used in chapter 7 of this study. Parametric studies are required to take into consideration different parameters affecting the behaviour of theses composite girders such as thickness of composite slab, effective width of composite girders, steel beam sections and different spans. The findings can be utilised to develop a

comprehensive design procedure for composite girders with profiled sheeting composite slab. This also, will reduce the number experimental tests required since the main disadvantages of this type of composite construction is the increased cost of materials, labour and welding studs through steel sheeting.

4. *Finite Element investigation of complete and partial shear connection in composite girders with precast hollow core concrete floors and with profiled steel sheeting flooring.* Most of previous research surveyed in this study stressed the importance of including the actual behaviour of shear connection in the longitudinal structural behaviour of composite girders. Although the effect of the degree of shear connection on the structural behaviour of composite girders with HCU slabs has been studied by Lam, Elliot and Nethercot[1] by carrying out parametric studies taking into consideration different spacing between studs, the two dimensional element used is not capable for presenting the stress distribution in the transverse direction. Having well established three dimensional finite element models for composite girders with HCU slabs and profiled sheeting composite slabs, parametric studies showing the effect of the shear connection degree on both the composite beam moment capacity, stress distribution along the beam and modes of failure can be easily studied. In this aimed study the non-linear load-slip characteristic of the stud will be taken from finite element modelling of the behaviour of headed stud shear connector in push-off tests with both types of slab. Results from the numerical study can form the basis of design procedures for composite beams with different degrees of shear connection.

References

1. Lam, D., Elliott, K. S., Nethercot, D. A. 'Parametric study on Composite Steel Beams with Precast Concrete Hollow Core Floor Slabs'. *Journal of Constructional Steel Research*, Vol. 54, pp. 283-304, 2000.
2. ABAQUS, User's Manual, Ver. 5.8, Hibbitt, Karlson and Sorensen, Inc., 1998.
3. Viest, I. M. : 'Investigation of Stud Shear Connectors for Composite Concrete and Steel T-Beams'. *ACI Journal*, Vol. 27, Title No.52-56, pp.875-891, April 1956.
4. Thurlimann, B.: 'Fatigue and Static Strength of Stud Shear Connectors', *ACI Journal*. Vol. 30, No. 12, pp.1287-1302, June 1959.
5. CP 117: Part 1. *Composite Construction in Structural Steel and Concrete: Simply Supported Beams in Building*. London, British Standards Institution, 1965.
6. CP 117: Part 2. *Composite Construction in Structural Steel and Concrete: Beams for Bridges*. London, British Standards Institution, 1967.
7. BS 5950: Part 3: Section 3.1 *'Code of Practice for Design of Simple and Continuous Composite Beams'*. British Standards Institution, London, 1990.
8. DD ENV 1994-1-1. Eurocode 4, *Design of Composite Steel and Concrete Structures. Part 1.1, General Rules and Rules for Buildings (with U.K National Application Document)*. British Standards Institution, London, 1994.
9. BS 5400 : Part 5, *Design of Composite Bridges*. British Standards Institution, London, 1979.
10. Johnson, R. P., '*Composite Structures of Steel and Concrete' Vol1, Beams, Slabs, Columns and Frames for Building*', Oxford, Blackwell Scientific Publications, 1971.
11. Johnson, R. P., and Anderson, D., Designers 'Handbook' to Eurocode 4 : Part 1.1, *'Design of Steel and Composite Structures'*. Thomas Telford, London, 1993.
12. ECCS, *Composite Structures*. The construction Press, London, 1981.
13. Johnson, C., 'Deflection of Steel-Concrete Composite Engineering,. *The structural Engineer*, Vol. 124, No. 10, pp. 1159-1165, October 1998.
14. Yam, L. C. P., Chapman, J. C., The Inelastic Behavior of Simply Supported Beams of Steel and Concrete. *Proc. Inst. Civ. Engrs*, Vol. 41, pp. 651-683, 1968.

15. Ollgaard, J. G., Slutter, R. G., and Fisher, J. W., 'Shear Strength of Stud Connectors in Lightweight and Normal-weight concrete'. *American Institute of Steel Construction Engineering Journal*, Vol. 8, No. 2, pp. 651-683, 1968.
16. Menzies, J. B. 'CP 117 and Shear Connectors in Steel-Concrete Composite Beams made with Normal-Density or Lightweight Concrete'. *The Structural Engineer*, Vol. 49, No. 3, pp. 137-153, March 1971.
17. Johnson, R. P., '*Composite Structures of Steel and Concrete' Vol1, Beams, Slabs, Columns and Frames for Building*', Oxford, Blackwell Scientific Publications.
18. Mottram, J.T., Johnson, R.P. 'Push Tests on Studs welded Through Profiled Steel Sheeting'. *The Structural Engineer*, Vol.68, No. 10, pp.187-193, 15 May 1990.
19. Oehlers, D. J., Park, S. M., 'Shear Connection in Haunched Composite Beams with Sloping Sides'. *Journal of Structural Engineering*, Vol. 18, No. 3, pp. 191-207, July 1994.
20. Johnson, R. P., Yuan, H., 'Existing Rules and New Tests for stud Shear Connectors in Troughs of Profiled Sheeting'. *Proc. Instn Civ. Engrs Structs and Bldgs*, Vol. 128, No. 11506, Aug. 1998.
21. Johnson, R. P, Yuan, H., 'Models and Design Rules for Stud shear Connectors in Troughs of Profiled Sheeting'. *Proc. Instn Civ. Engrs Structs and Bldgs*, Vol. 128, No. 11507, Aug. 128.
22. Yuan, H., *'The resistances of Stud Shear Connectors with Profiled Sheeting'*. PhD thesis, University of Warwick, 1996.
23. Lam, D., Elliott, K. S., Nethercot, D. A. 'Push-off Tests on Shear Studs with Hollow-Cored Floor Slabs'. *The Structural Engineer*, Vol. 76, No. 9, pp. 167-174, 5 May 1998.
24. Davies, C., 'Small-Scale Push-out Tests on Welded Stud Shear Connectors'. *Concrete Journal*, Vol. 1, pp. 311-316, September 1967.
25. Davies, C., 'Tests on Half-Scale Steel-Concrete Composite Beams with Welded Shear Connectors'. *The Structural engineer*, Vol. 47, No.1, pp. 20-40, January 1969.
26. Jayas, B. S., Hosain, M. U., 'Behaviour of Headed Studs in Composite Beams: Push-out Tests', *Civil Engrs*, Vol. 15, pp. 240-253, 1987.

27. Oehlers, D. J., 'Splitting Induced by Shear Connectors in Composite Beams'. *Journal of structural engineering*, Vol. 115, No. 2, pp. 341-360, February 1989.

28. Oehlers D. J., and Johnson, R. P., 'The Strength of Stud Shear Connections in Composite Beams'. *The Structural Engineer*, London, England, Vol. 65B, No. 2, pp. 44-48, 1987.

29. Oehlers, D. J., Park, S. M., 'Shear Connection in Haunched Composite Beams with Sloping Sides'. *Journal of Structural Engineering*, Vol. 18, No. 3, pp. 191-207, July, 1994.

30. Johnson, R. P, 'Design of Composite Beams with Deep Haunches', *Proc., Inst. Civ. Engrs*, Vol. 2, No. 51, pp.83-90, Jan. 1972.

31. Li, A. and Krister, C. 'Push-out Tests on Studs in High Strength and Normal Strength Concrete'. *Journal of constructional steel research*, Vol. 36, No. 1, pp. 15-29, 1996.

32. Moy, S. S. J. and Tayler, C., 'The effect of precast concrete planks on shear connector strength'. *Journal of Constructional Steel Research,* Vol. 36, No.3, pp. 201-213, 1996.

33. Shim, C. S., Kim, J.H., Chang S. P. and Chung, C. H., 'The Behavior of Shear Connections in a Composite Beam with a Full-Depth Precast Slab'. *Proceedings of the Institution of Civil Engineers, Structures and Buildings*, Vol. 140, No. 1, pp.101-110, February 2000.

34. Nip, T.F. and Lam, D., 'Effect of End Condition of Hollow Core Slabs on Longitudinal Shear Capacity of Composite Beams'. *First International Conference on Steel and Composite Structures*, pp. 1229-1236, Pusan, Korea, June 2001.

35. Nethercot, D. A., 'The Importance of Combining Experimental and Numerical Study in Advancing Structural Engineering Understanding'. *Structural Engineering, Mechanics and Computation*, Vol. 1, pp. 15-26, 2001.

36. Lam D., El-lobody E., 'Finite Element Modelling of Headed Stud in Composite Steel Beams with Precast Hollow Core Slabs'. *International Conference on Steel and Composite Structures*, Pusan, Korea, June, 2001.

37. Johnson, R. P. and Oehlers, D. J., 'Analysis and Design for Longitudinal Shear in Composite T-beams'. *Proceedings of the Institution of Civil Engineers,* Part 2, No. 71, pp. 989-1021, December, 1981.

38. Oehlers D. J., 'Finite Element Simulation of the Behavior of Concrete Subjected to Concentrated Loads'. *University of Warwick, Technical report CE10*, 1981.

39. Kalfas, C., Pavlidis, P. and Galoussis E., 'Inelastic Behavior of Shear Connection by a Method Based on FEM'. *Journal of constructional steel research*, Vol. 44, Nos 1-2, pp. 107-114, 1997.

40. ABAQUS, User's Manual, Ver. 5.6, Hibbitt, Karlson and Sorensen, Inc., 1996.

41. Ansourian, P., 'An Application of the Method of Finite Element to the Analysis of Composite Floor Systems'. *Proceedings of the Institution of Civil Engineers,* Part 2, Vol. 59, pp. 699-726, 1975.

42. Moffat, U.R., Dowling, P.J, 'The Longitudinal Bending Behaviour of Composite Box Girder Bridges Having Incomplete Interaction'. *The structural Engineer*, Vol. 56B(3), pp. 53-60, 1978.

43. Balakrishnan S., *'The behaviour of Composite Steel and Concrete Beams with Welded Stud Shear Connectors'*, PhD thesis, University of London, 1963.

44. Dabaon, M., Tschemmernegg, F., Hassan, K. and Abdel Lateef, T., 'Load Carrying Capacity of Composite Beams under Partial Shear Interaction'. *Stahlbau*, Vol. 62, No. 1, 1993.

45. Mistakidis, E.S., Thomopoulos, K., Avdelas, A., Panagiotopoulos, P.D., 'Shear Connectors in Composite Beams : A New Accurate Algorithm'. *Thin-walled Structures*, Vol. 18, No. 3, pp. 191-207, 1994.

46. Oehlers, D. J., Tguyen, N. T., Ahmed, M. and Bradford, M. A., 'Partial Interaction in Composite Steel and Concrete Beams with Full Shear Connection'. *Journal of Constructional Steel Research,* Vol. 41, No. 2/3, pp. 235-248, 1997.

47. Oven, V. A., Burgess , I. W., Plank, R. J. and Abdul Wali, A. A., 'An Analytical Model for the Analysis of Composite Beams with Partial Interaction'. *Computer and Structures*, Vol. 62, No. 3, pp. 493-504, 1997.

48. El-Zanati, M. H., Murray, D. W., and Bjorhovde, R., 'Inelastic Behavior of Multi-Storey Steel Frames'. *Structural Engineering Report*, No. 83, Department of Civil Engineering, University of Alberta, Canada, 1980.
49. Cai, C.S., Zhang, Y., and Nie, J., 'Composite Girder Design of Cable-Stayed Bridges'. *Practice Periodical on Structural Design and Construction, Proceedings of an Engineering Foundation Conference*, pp. 158-163, Nov. 1998.
50. Youn, S.G. and Chang, S.P., 'Behaviour of Composite Bridge Decks subjected to Static and Fatigue Loading'. *ACI Structural Journal*, Vol. 95, No. 3, May-June 1998.
51. ABAQUS, User's Manual, Ver. 5.7, Hibbitt, Karlson and Sorensen, Inc., 1997.
52. Gattesco N., 'Analytical Modelling of Nonlinear Behaviour of Composite Beams with Deformable Connection'. *Journal of Constructional Steel Research*, Vol. 52, pp. 195-218, 1999.
53. Chapman, J. C. and Balakrishnan, S., 'Experiments on composite beams'. *Structural engineers*, Vol. 42, pp. 369-383, 1964.
54. Kwak, H. G., and Seo, Y. J., 'Long-term Behaviour of Composite Girder Bridges'. *Computer and Structures*, Vol. 74, pp. 583-599, 2000.
55. Thevendran, V., Shanmugam, N. E., Chen, S. and Liew J. Y. R., 'Experimental Study on Steel-Concrete Composite beams Curved in Plane'. *Engineering Structures*, Vol. 22, pp. 877-889, 2000.
56. Amando, C., and Fragiacomo, M., 'Effective Width Evaluation for Steel-Concrete Composite Beams'. *Journal of Constructional Steel Research*, Vol. 58, pp. 373-388, 2002.
57. ABAQUS, User's Manual, Ver. 4.9, Hibbitt, Karlson and Sorensen, Inc., 1994.
58. Faella, C., Maeinelli, E., and Nigro, E., 'Steel and Concrete Composite Beams with Flexible Shear Connection: 'Exact' Analytical Expression of the Stiffness Matrix and Applications'. *Computers and Structures*, Article in press, 2002.
59. Lam, D., *'Composite Steel Beams Using Precast Concrete Hollow Core Floor Slabs'*, PhD thesis, University of Nottingham, 1998.
60. Lam, D., Elliott, K. S., Nethercot, D. A. 'Experiments on Composite Steel Beams with Precast Concrete Hollow Core Floor Slabs'. *Proceedings of the Institution of Civil Engineers, Structures and Buildings*, Vol. 140, pp. 127-138, May 2000.

61. ABAQUS, User's Manual, Ver. 5.3.1, Hibbitt, Karlson and Sorensen, Inc., 1994.

62. Lam, D., Elliott, K. S., Nethercot, D. A. 'Designing Composite Steel Beams with Precast Concrete-Hollow Core Slabs'. *Proceedings of the Institution of Civil Engineers, Structures and Buildings*, Vol. 140, pp. 139-149, May 2000.

63. Shim, C. S., Kim, J.H., Lee, P. G. and Chang, S. P., 'Design of Shear Connection in Composite Steel and Concrete Bridges with Precast Decks'. *Journal of Constructional Steel Research*, Vol. 57, pp.203-219, 2001.

64. MacMackin, P.J., Slutter, R.G. and Fisher, J.W. ' Headed Steel Anchor under Combined Loading'. *Engineering Journal, American institute of Steel Construction,* second quarter, 43-53, 1973.

65. BS 8110: Parts 1,2, *'Code of Practice for Design of Simple and Continuous Composite Beams'*. British Standards Institution, London, 1997.

66. Lam D., El-lobody E., 'Finite Element Modelling of Headed Stud Shear Connectors in Steel-Concrete Composite Beam'. *Proceedings of the International Conference on Structural Engineering, Mechanics and computation,* Cape Town, south Africa, pp 401-408, April, 2001.